654 100-9-F

CHARACTERIZATION AND EVALUATION OF A PROTOTYPE FORWARD-LOOKING AUTOMOTIVE RADAR (FLAR)

FINAL REPORT

SEPTEMBER 1997

R.K. Gilbert
P.K. Zoratti
R. Becker
G. Brumbaugh
T. Chaplin
M. Harrison
M. Hawks
K. Gondoly

Prepared for:
National Highway Traffic
Traffic Safety Administration
Office of Crash Avoidance Research
NRD-5 1, Room 6220
400 Seventh Street S.W.
Washington, D.C. 20590

Contract Number: DTNH22-94-Y-17016

P.0. Box 134008 Ann Arbor, MI 48113-4008 313-994-1200
http://www.erim-int.com

ERIM-320

REPORT DOCUMENTATION PAGE

Form Approved
OMB No. 0704-0188

1. AGENCY USE ONLY *(LeaveBlank)*	2. REPORT DATE	3. REPORT TYPE AND DATES COVERED
	March 1997	Final, from 1 March 1994 through 28 February 1997

4. TITLE AND SUBTITLE
Characterization and Evaluation of a Prototype Forward-Looking Automotive Radar Final Report

5. FUNDING NUMBERS
DTNH22-94-Y- 17016

6. AUTHOR(S)

R.K. Gilbert, P.K. Zoratti, R. Becker, G. Brumbaugh, T. Chaplin, M. Harrison, M. Hawks, and K. Gondoly

7. PERFORMING ORGANIZATION NAME(S) AND ADDRESS(ES)

Environmental Research Institute of Michigan (ERIM)
P.O. Box 134001
Ann Arbor, MI 48 113-4001

8. PERFORMING ORGANIZATION REPORT NUMBER
654100-9-F

9. SPONSORING/MONITORING AGENCY NAME(S) AND ADDRESS(ES)
National Highway Traffic Safety Administration
Office of Crash Avoidance Research
NRD-51 , Room 6220
400 Seventh Street, S.W.
Washington, D.C. 20590

10. SPONSORING/MONITORING AGENCY REPORT NUMBER

11. SUPPLEMENTARY NOTES

12a. DISTRIBUTION/AVAILABILITY STATEMENT
Limited Distribution

12b. DISTRIBUTION CODE

13. ABSTRACT *(Maximum 200 words)*

This is the final report for a three-year Discretionary Cooperative Agreement with the National Highway Traffic Safety Administration (NHTSA Grant DTNH22-94-Y-17016), "Characterization and Evaluation of a Forward-Looking automotive Radar Sensor." The Environmental Research Institute of Michigan (ERIM) and TRW were the industrial partners in this Cooperative Agreement. The goal of this research program was to increase the knowledge and understanding of radar sensing in the roadway environment by conducting structured testing of TRW's prototype automotive radar sensor, or FLAR, in real-world freeway settings. To achieve this goal, the following program objectives were established:

- to fully characterize TRW's FLAR in a controlled laboratory setting
- to measure radar cross-sections of representative automobiles and roadway objects
- to measure the performance of the FLAR in a variety of freeway settings
- to provide data to TRW for refining its prototype sensor design
- to begin developing methodologies to test, evaluate, and certify sensors for collision avoidance system

14. SUBJECT ITEMS
Automotive Radar Sensor, FLAR, Collision Avoidance System

15. NUMBER OF PAGES

16. PRICE CODE

17. SECURITY CLASSIFICATION OF REPORT	18. SECURITY CLASSIFICATION OF THIS PAGE	19. SECURITY CLASSIFICATION OF ABSTRACT	20. LIMITATION OF ABSTRACT
UNCLASSIFIED	UNCLASSIFIED	UNCLASSIFIED	Same as report

CONTENTS

CONTENTS (CONTINUED)

FIGURES

FIGURES (CONTINUED)

FIGURES (CONTINUED)

FIGURES (CONTINUED)

TABLES

1.0 EXECUTIVE SUMMARY

This document is the final report for a three-year Discretionary Cooperative Agreement with the National Highway Traffic Safety Administration (NHTSA Grant DTNH22-94-Y-17016), "Characterization and Evaluation of a Forward-Looking Automotive Radar Sensor." The goal of this research program was to increase the knowledge and understanding of radar sensing in the roadway environment by conducting structured testing of TRW's prototype forward-looking automotive radar sensor, or FLAR, in real-world freeway settings. To achieve this goal, the following program objectives were established:

- to fully characterize TRW's FLAR in a controlled laboratory setting,
- to measure radar cross-sections of representative automobiles and roadway objects,
- to measure the performance of the FLAR in a variety of freeway settings,
- to provide data to TRW for refining its prototype sensor design, and
- to begin developing methodologies to test, evaluate, and certify sensors for collision avoidance systems.

The findings and recommendations from this research program have national significance from several perspectives, including improved traffic safety and increased competitiveness of the United States Intelligent Transportation System (ITS) industry. The successful deployment of effective sensor-based systems obviously requires a foundation of reliable and low-cost enabling technologies. These results can be used by NHTSA to further its understanding of currently available technologies and to assess system reliability in benefits analyses for crash-avoidance applications. Finally, the radar supplier can use the results of this research effort to further the commercial development of these sensor technologies (Thrust Number 4 of NHTSA's Five-Thrust ITS Strategy).

The various results of this research effort are available in the following:

- This final report summarizes all of the results of the program including discussions of the roadway tests.
- The "Catalog of Radar Scattering Characteristics for Common Roadway Objects" contains radar cross-section plots and images for a number of different objects.
- The raw radar cross-section data is also available for downloading from the ERIM Web server: www.erim.org/Trans/roadobj/.

The key results and conclusions for the program are now briefly summarized.

1.1 CHARACTERIZATION OF VEHICLES AND ROADWAY OBJECTS

This program established an initial database for the radar scattering characteristics of a number of common roadway objects. This database begins to define the environmental framework in which an automotive radar must operate. Under this program four different "classes" of vehicles were characterized along with a motorcycle, human, stop sign, and cinder block wall.

Radar data for each object was collected using a 94 GHz Inverse Synthetic Aperture Radar (ISAR) test facility. The ISAR supported the creation of two-dimensional images for each object at a number of different aspect angles. The aspect angle refers to the relative orientation between the radar and the object. For example, a 0 degree aspect angle of a vehicle corresponds to viewing the vehicle head-on with the radar and a 180 degree aspect angle corresponds to viewing the vehicle from the rear. The two-dimensional images are color-coded to indicate intensity of the radar returns caused by each section of the object.

These images are useful in identifying the various radar scattering attributes of the object. For example, the impact of side-view mirrors, wheel housings, under-body structures, and body panel seams is evident in the images. Knowledge of the distribution of radar scattering centers across various objects could prove to be beneficial to radar processing and threat assessment algorithm developers.

In addition to the images, the characterization procedure produced radar cross-section (RCS) values for each object. The RCS is a quantitative value related to the object's level of radar reflectivity. The RCS of each object can be analyzed as a function of aspect angle or a function of range across the object.

For the objects characterized in this program, it was observed that the RCS value can range from a maximum of approximately +40 dBsm for a 90 degree aspect angle of a Jeep Wrangler, down to -10 dBsm for a 45 degree aspect angle of a stop sign. The primary factors which account for an object's RCS level are the material from which the object is made, the aspect angle between the radar and the object, and the geometric shape of the object. Square objects with flat surfaces, such as a Jeep Wrangler or a cinder block wall, exhibited relatively sharp peak RCS values for aspect angles which resulted in specular returns and much lower returns for aspect angles which deviated from specular orientations. On the other hand, more rounded objects such as a Geo Metro or a human being resulted in RCS values which were not as dependent on aspect angle.

The RCS data is critical in defining the dynamic operating envelope of the radar sensor. For example, from the measurements made in this program, it can be concluded that to detect a human being within its field-of-view, the radar sensor must have enough sensitivity to identify returns from an object with an RCS of around -5 dBsm at the systems desired operating range. Furthermore, the radar sensor must maintain this level of sensitivity when an object with a +40 dBsm RCS is also located within the radar field-of-view.

1.2 ROADWAY TESTS

The FLAR sensor was subjected to a number of orchestrated and non-orchestrated tests for evaluating its performance under a variety of roadway scenarios. The primary focus of these tests was to evaluate how the radar sensor itself interacted with the roadway environment. The TRW FLAR sensor was designed for an Adaptive Cruise Control (ACC) application, and therefore care must be taken in differentiating between the raw radar sensor performance and the TRW processing performance associated with the ACC application. To effectively evaluate the radar sensor, TRW provided access to the raw intermediate frequency (IF) radar signal prior to any TRW processing of the data. This allowed the raw radar data corresponding to any specific roadway scenario to be captured for subsequent processing and analysis.

To support the roadway data analysis, ERIM developed a testbed vehicle with data acquisition capabilities and a data playback software tool. The testbed vehicle provided a means of collecting raw radar data, TRW-processed radar data (range, range rate, etc.), video of the roadway, and vehicle position data from a GPS receiver. The GPS position data was combined with position data from other vehicles to serve as a "truthing" mechanism to assess the accuracy of the FLAR sensor. All of the data was collected and stored for each test scenario. The data playback software was then used to review the data and identify areas for further processing and analysis.

The roadway collections were designed to address some pre-defined sensing scenarios of concern, such as background induced false alarms, vehicle clutter induced falser alarms, tracking as a function of roadway geometry, and tracking in dynamic traffic of varying density. Appendix E of this report contains the program test plan.

Post-collection processing and analysis identified several scenarios as being potentially problematic for the FLAR sensor in terms of generating false alarms or missed detections. These scenarios are summarized below:

- **Roadside vehicles on a straight roadway** were observed to generate-returns in the raw radar data at certain geometries which could be interpreted as objects within the host vehicle's lane.
- **Adjacent lane vehicles on a straight roadway** viewed by the FLAR side beam antennas can generate multiple returns with significant range separation.
- **Guard rails and other roadside objects on curved roadways** generated significant returns which could cause false alarm problems.
- **Tracking vehicles around curved roadways** could prove to be problematic without knowledge of the roadway geometry in front of the sensor.
- **Near-range cut-ins and tracking of narrow vehicles** such as motorcycles could cause missed detections due to limited radar field-of-view.
- **Low RCS vehicles located between radar and large RCS** vehicles could cause missed detections.
- **Bridge or other roadway** overpasses were observed to generate significant returns in the raw radar data under certain circumstances.

In general, the radar sensor itself performed very well in the roadway tests. Somewhat counter-intuitive was the fact that the FLAR performed better under heavier traffic densities than under very light traffic densities. The response time of the raw radar data signal was virtually instantaneous. Two areas of the sensor system design were identified as critical to achieving adequate roadway performance: (1) antenna design and control, and (2) receiver gain control.

1.3 TESTING, EVALUATION AND CERTIFYING METHODOLOGIES

In addition to increasing the general knowledge and understanding of radar sensing in the roadway environment, the FLAR program has established empirical data and identified procedures to support the development of methodologies to test, evaluate, and certify sensors for collision avoidance/warning and adaptive cruise control systems. The program has identified three primary levels at which the testing should occur:

1. Laboratory testing to characterize and baseline the sensor's performance.
2. Environmental testing to identify the range of conditions under which the sensor can perform effectively.
3. Controlled roadway testing to verify algorithmic robustness in specific scenarios of interest to the intended application.

The objective of the laboratory characterization is to validate the standard performance specifications of the sensor. These specifications include ranging accuracy, range rate accuracy, range resolution, transmitted power, and field-of-view. The accuracy and stability of these performance specifications are innately linked to the sensor electronic circuitry. For example, it was discovered during the characterization of the FLAR sensor that the modulation rate was not exactly equal **to** that specified. This error was manifested in a reported "range to target" error which increased with higher ranges. It will be necessary for some quality control inspection of manufactured sensors to be performed to verify fundamental electronic performance. This is especially critical since the cost constraints for automotive-based equipment forces tradeoffs in sensor design and circuitry utilization.

The objective of the environmental testing is to identify sensor performance degradation susceptibility in terms of precipitation interference, material occlusion, and radome/target contamination.

Precipitation tests conducted with the FLAR sensor showed that 94 GHz energy was only marginally affected by various types of airborne precipitation (e.g., rain, snow, and fog). In particular, the precipitation did not induce any observable return levels in the raw radar data, and the attenuation levels were low (in most cases <1 dB/10 m for two-way travel). Of course these attenuation levels are dependent upon precipitation density and particulate size. The most significant outcomes of the precipitation tests were that the radar detected objects within its field-of-view even though the objects were partially or totally visually obscured. Furthermore, material tests indicated that while items such as plastic and glass may cause significant attenuation, 94 GHz energy does exhibit material penetration capabilities which will allow for concealment of the sensor within the automobile structure. The key to environmental testing is to insure that the sensor system operates appropriately under all likely conditions, or that the system can detect when its ability to perform has deteriorated and notify the operator.

The objective of the "controlled" roadway testing is to validate operation at a systems level. This takes into account not only the raw sensor performance, but also the processing and threat assessment or vehicle tracking algorithms for the ACC and CWS applications. This program has identified a number of scenarios which could prove to be problematic for an automobile-based radar sensor. The scenarios which have been cited are by no means exhaustive, but they do provide a starting point around which specific standard testing procedures can be developed. Repeatability of these standard testing procedures is necessary to allow both developers and OEM's to verify acceptable system operation under the same conditions. The vision of this testing process is to define a roadway scene in terms various objects, vehicles, and calibrated radar reflectors positioned to recreate a real-world roadway scenario of interest. The host vehicle can then drive a predetermined trajectory through this scene and the sensor system performance can be evaluated. Both the roadway and RCS data collected as part of this FLAR program will support the definition of the standard roadway scenes discussed above.

1.4 CONCLUDING REMARKS AND SUGGESTED FUTURE EFFORTS

In summary, this FLAR program has:

- Increased the general knowledge and understanding of vehicle-based radar sensing of the roadway environment.
- Established a radar cross-section database for a number of common roadway objects. This database begins to defme the operational envelope in which a vehicle-based radar sensor must operate. The database also supports advance simulation of the roadway environment.
- Identified a number of roadway scenarios which could be problematic for a vehicle-based sensor system. Empirical data on these scenarios will support the creation of standardized repeatable roadway testing procedures.
- Evaluated the weather performance and material penetration characteristics of a 94 GHz radar sensor.
- Established criteria for the baseline characterization and testing of the vehicle-based radar sensors.

The program results are available to interested parties in the form of this final report, an RCS catalog, and data on the world-wide web.

The results of this program serve to aid system developers and evaluators in terms of a more clearly defined operating environment and criteria for meaningful testing procedures. However, the successful deployment of radar technology in vehicle-based applications requires more work in many areas including:

. Mutual Interference Issues

- Manufacturing, Installation, and Calibration Issues
- Use of Simulation to Refine Sensor Design and Algorithm Implementation
- Human Factors and Response to Nuisance Alarms
- Human Factors and Response to Avoidance Maneuvers

2.0 INTRODUCTION

The goal of this research program was to increase the knowledge and understanding of radar sensing in the roadway environment by conducting structured testing of TRW's prototype automotive radar sensor, or FLAR, in real-world freeway settings. To achieve this goal, the following program objectives were established:

- to fully characterize TRW's FLAR in a controlled laboratory setting,
- to measure radar cross-sections of representative automobiles and roadway objects,
- to measure the performance of the FLAR in a variety of freeway settings,
- to provide data to TRW for refining its prototype sensor design, and
- to begin developing methodologies to test, evaluate, and certify sensors for collision avoidance systems.

The results and findings from this research effort are summarized by program objective. Feedback to TRW regarding the performance of its FLAR was provided throughout the program, and was not executed as a specific task. Testing and evaluation methodologies were addressed as part of each testing task. The Annual Reports provide a chronological summary of the Program's activities over the first two years. The third year was dedicated to roadway testing. Most of the test data, results, and supporting information can be found in the appendices.

2.1 TRW FORWARD-LOOKING AUTOMOTIVE RADAR (FLAR)

TRW provided two prototype automotive radars and technical support for test and evaluation. The first prototype, a single-beam radar, was only used during the first year of the program. At the start of the second year, TRW provided a radar with a greater azimuth field-of-view and multiple beams within this field-of-view. The integration of this higher performing radar into the test program greatly enhanced the value of the experimental results. There was a cost, however. Roadway tests were delayed for almost one year because the data acquisition system to had to be changed significantly to accommodate the radar upgrades. ERIM conducted a characterization procedure on each radar sensor to baseline performance. Much of the characterization parameters served to verify TRW's measurements as well as indicate areas where design improvements could increase sensor performance. Section 4 of this report provides a discussion of the characterization procedures and a description of the FLAR's baseline performance.

2.2 MATERIALS AND THE ENVIRONMENT

The Materials Tests were performed in a controlled, off-roadway setting in which all the test objects were stationary. The intent was to quantitatively assess the effect on the quality of the received signal produced by the environment in which these systems will be deployed and by typical materials used in cars and roadway construction. Baseband, time-domain data [i.e., before any signal processing such as the Fast Fourier Transform (FFT)], were collected and stored for off-line analysis. The following materials were evaluated: glass, plastic composite, Plexiglas, cardboard, wood, and rubber. The environmental test conditions included dry, raining, snowing, fog, contamination of radome, and contamination of target. Test data is provided in Appendix B.

2.3 RADAR CROSS-SECTION

The rnauner in which vehicles and other roadway objects interact with electromagnetic energy emitted by a radar is characterized by the object's radar cross-section, or RCS. The radar model presented in Appendix A explains the role of RCS in the overall performance of a radar for this application. RCS measurements were included in this program for two reasons: (1) to provide diagnostic data to support the analysis and evaluation of roadway tests; and (2) to initiate the development of a radar signatures database. The results of this effort were presented at the SPIE Conference in 1995[1] and at a meeting of the AVCS Committee held during the 1996 Annual Meeting of ITS America. While the RCS portion of the FLAR program effort was relatively small, response to the data produced was quite high on the part of automotive sensor developers.

2.4 ROADWAY TESTS

The Roadway Tests were conducted in both structured (on test tracks) and unstructured (on freeways) settings. To support these tests a data acquisition and analysis system had to be developed, and then upgraded when the prototype radar was upgraded (see Appendix C). This system was demonstrated at the 1995 Annual Meeting of ITS America, and at the AVCS Committee Meeting and Vehicle Demonstrations held at the Transportation Research Center (TRC) Inc., in East Liberty, Ohio in August, 1996. In addition, a differential GPS system was developed (see Appendix D) as atruthing tool. The structured tests (see Appendix E) were conducted at the TRC in October and November, 1996 according to a test plan developed in cooperation with NHTSA. The detailed test results of the structured test can be found in Appendix F and results from the unstructured tests found in Appendix G.

2.5 SUMMARY

This final report concludes with a summary of our findings, conclusions, and recommendations, focused on the use of a forward-looking radar for Adaptive Cruise Control Applications.

1"Millimeter Wave Scattering Characteristics and Radar Cross Section Measurements of Common Roadway Objects," P.K. Zoratti, J.J. Ference, R. Majewski, and R.K. Gilbert, SPIE Proceedings on Collision Avoidance and Automated Traffic Management Sensors, Vol. 2592, Philadelphia, PA, 25-26 October 1995.

3.0 MEASUREMENT OF TARGET CHARACTERISTICS/SIGNATURES

3.1 INTRODUCTION

This section summarizes ERIM's activities and findings for Task 3: Measurement of Target Characteristics/Signatures. The objective of Task 3 was to measure the radar scattering characteristics (e.g., the radar cross-section, or RCS) of representative roadway objects, using ERIM's Fine Resolution Rotary Platform Imaging Facility. This imaging approach is valuable because it provides system developers not only with calibrated radar data, but also with two-dimensional radar images. From these, information about individual point scatterers within a single target can be extracted. This information on scattering characteristics can be used to refine processing algorithms for threat assessment, guide the design of automotive radar hardware, and supplement automotive radar simulation programs.

To create a database of radar scattering characteristics for roadway objects, radar data was collected for the following objects:

- 1990 Chevy Corvette ZR-1
- 1995 Ford Taurus
- 1991 Jeep Wrangler
- 1993 Geo Metro EFI
- Honda Motorcycle
- 180 lb. person
- Stop Sign with a square post
- Cinder Block Wall

The entire set of data collected on these objects has been processed and organized into a "Catalog of Radar Scattering Characteristics for Common Roadway Objects." The NHTSA-OCAR has a version of this catalog containing black-and-white images. A catalog with full color images is available from ERIM at a nominal price to cover reproduction costs. Also, the data which constitutes the plots in the catalog can be downloaded from ERIM's Web server: www.erim.org/Trans/roadobj/.

The remainder of this section will discuss:

- background on the need for radar scattering characteristic data;
- methods for making the radar measurements;
- techniques for reducing the measurements to RCS data; and
- general descriptions of the various data output products, with guidelines for interpreting the data.

The section concludes with some general observations and conclusions based on the RCS data. This includes summary information on the variation of return levels and the RCS dependency on aspect angle.

3.2 BACKGROUND

Well-characterized radar RCS data will be essential for developing the guidelines and standards that will affect all phases of a radar-based product's lifecycle, from inception through installation on a vehicle. It begins with the design of both the hardware and the signal processing algorithms, includes methodologies for test and evaluation, and finally, certification that the devices meet specific

performance standards. The need for performance certification will be driven by the need to provide some legal protection against liability claims. At some point, crash avoidance systems will be offered to the public as features that wil1 make the automobile safer to operate. The possible causes for a "failure" are many, and suppliers will want a basis for demonstrating that their products perform as advertised.

This Radar Signatures Database is a mechanism for sharing information. As it is developed, it will eliminate redundant measurement activities on the part of developers to make their own measurements. This should reduce development costs, which in turn should reduce time-to-market and cost to the consumer.

For a given radar, the return from a roadway object will vary as a function of many parameters. These parameters include, but certainly are not limited to, the range and azimuth angle to the target, the target's geometry and materials, the weather, and surrounding roadway environment, which includes other vehicles and non-moving roadway objects. Each of these parameters can take on many values. The problem is further compounded by the number of radar parameters that can be varied. This literally results in a combinatoric explosion in the number of possible test conditions. Clearly such a problem must be approached in a structured and orderly manner. Creation of the Radar Signatures Database will be one method for bringing this problem under control.

3.3 RADAR MEASUREMENTS

The data for the Radar Signatures Database were collected on ERIM's Fine Resolution Rotary Platform Facility. The radar system is based on an HP85 10 Network Analyzer. The objective of the RCS collection task was to collect 94 GHz radar data for a number of roadway objects at various aspect angles. ERIM's Rotary Platform Facility (RPF) was well suited for the task. The RPF consists of a radar antenna pedestal mounted on the outside wall of ERIM's building and 22-foot diameter turntable located 135 feet from the pedestal. The turntable is capable of supporting up to 20,000 lbs and provides a convenient way to vary target aspect angles.

There are two important issues regarding the RCS measurements. The first deals with near-field/far-field effects. Radar cross section (RCS) is normally defined when the incident radar wave is a plane wave; consequently, RCS is normally a "far-field" RCS. The normal requirement for being in the far-field is that the phase deviation from planar is less than 22.5 degrees which translates to a range of at least $2D^2/h$ where D is the target diameter and h is the wavelength. For example, a target with a 2-meter diameter being illuminated by a 77 GHz radar would have to be 2053 meters away to be in the far-field; consequently, automotive radars certainly can operate in the "near-field" when considering objects the size of vehicles. With the collection set-up utilized on ERIM's RPF, the illumination pattern from the 94 GHz radar would be considered to be in the far-field (based on the size of the transmit antenna and range to the platform); however, scatterers which are larger than 0.2 meters may exhibit near-field reflection characteristics. For example, in the far-field, a simple target like a flat plate has a reflection characteristic with a $(\sin X/X)^2$ pattern. As the range to the flat plate decreases below the far-field range, the nulls in the pattern fill in and the sidelobes increase. The overall effect of operating in the "near-field" is that the RCS patterns are range dependent and not constant. The RCS measurements provided in this report correspond to a specific range (40 meters). This should not be considered a significant limitation in analyzing the data for peak return levels and aspect angle characteristics.

The second issue is related to the radar illumination frequency. The measurements were made at 94 GHz to correspond to the TRW FLAR unit operating frequency. The TRW FLAR design is based on military radar technology; however since the inception of this program, the FCC has approved the 76 to 77 GHz band for automotive radar applications. The question therefore arises as to what effect the change in frequency will have on the RCS measurements which were made. The frequency change from 77 to 94 GHz is only 22 percent, so the changes in the RCS pattern for a simple reflector such as a flat

plate will be minor. However, with a complex object like a vehicle, the RCS is the vector summation of the contributions from a large number of individual scatterers distributed across the target. These individual scattering centers act independently of one another and as the range to the object changes, the phases of the contributions from the individual scattering centers will be different for 77 and 94 GHz. The locations of the peaks and nulls of the RCS pattern will vary with frequency; however the mean value of the RCS will not change significantly, and essential characteristics of the target RCS will be the same.

3.3.1 Experimental Setup

Figure 3-l illustrates the physical set-up for the data collection. The Network Analyzer based radar operates in a linear-FM (chirp) pulse mode. The Network Analyzer creates a baseband signal with 2 GHz of bandwidth, centered at 10 GHz. This signal is then amplified and sent to the RF plate, where it is up-converted from a 10 GHz to a 94 GHz center frequency and radiated at the target on the rotary platform using a standard gain horn antenna. The standard gain horn has an approximately 9 degree azimuth beamwidth which illuminates the entire platform. Signals reflected back from the target to the radar are captured by the RPF's receiver and down-converted to baseband and input to the network analyzer. The radar system preserves both the amplitude and the phase of the reflected signals. This information is downloaded from the network analyzer to a PC-based data acquisition system via an IEEE-488 communications bus.

In addition to storing the radar data, the PC also interfaces with an optical shaft encoder mounted on the rotary platform. The turntable must be driven at a very slow speed (e.g., 0.02 degrees/sec), due to the low PRF of the HP8510 and high image resolution requirements. The shaft encoder allows the table position to be exactly correlated with the collected radar data.

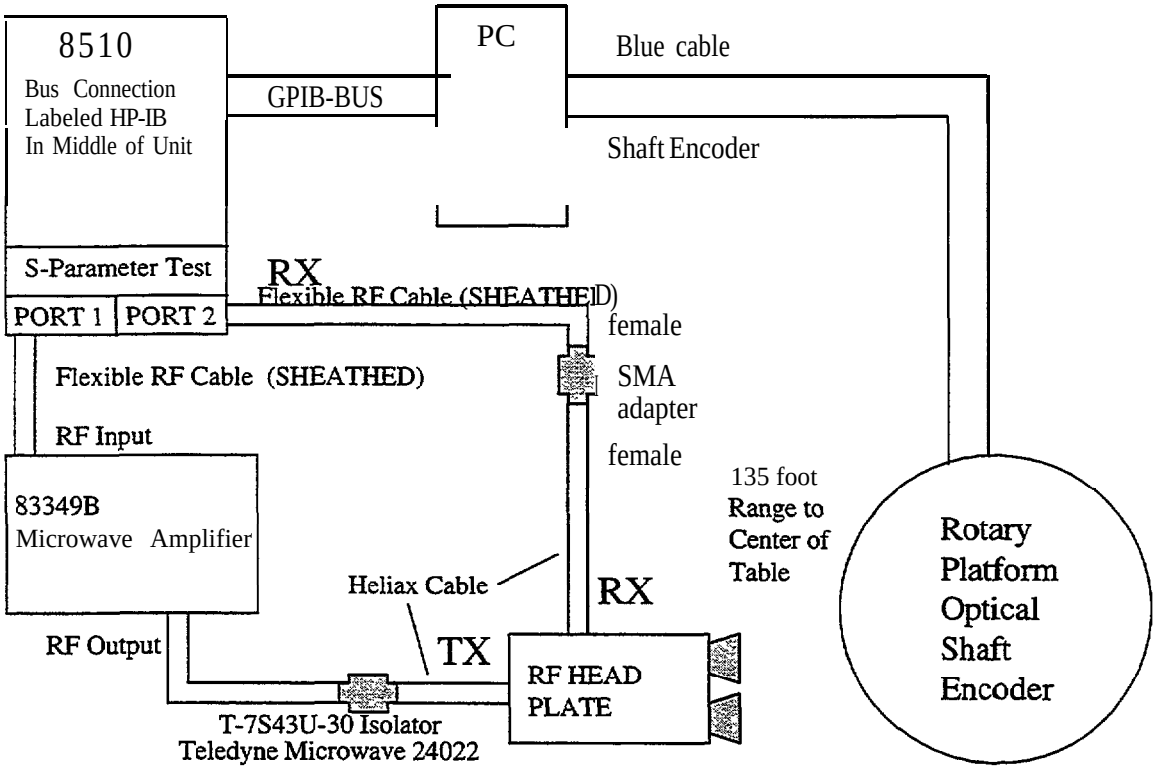

Figure 3-l. Data Collection Set-up

3.3.2 Data Collection

The table was rotated at a fixed rate to illuminate the objects from a continuum of aspect angles, so that Inverse Synthetic Aperture Radar (ISAR) processing techniques could be implemented, as described below, to produce fine azimuthal measurements of the target.

The radar collection system was calibrated prior to each measurement using a series of reference reflectors located on the platform. The reference reflectors have known radar cross-section (RCS) values. The calibration procedure produces a +3 dB accuracy across the rotary platform surface. Higher accuracies can be achieved by compensating for actual target range in the processing software, but this technique was not used here.

The vehicular objects and cinder block wall were located on the center of the table during the collection process. The human and the stop sign were located approximately 3 feet off-center to avoid any obscuration from stationary clutter fold-in. The surface between the collection radar and the rotary platform is fairly level, grass-covered ground. No multipath fences were employed during collections of the roadway objects, but they were used during the calibration procedure.

Table 3-1 summarizes the radar parameters used for these data collections.

Table 3- 1. Radar Parameters

Radar Parameter	Specification
Mode of Operation	Linear-FM Pulsed
Center Frequency	94 GHz
Bandwidth	2 GHz
Transmitted Power	@ 100 mW
Polarization	H/H
Pulse Repetition Frequency	@ 2 Hz

3.4 DATA PROCESSING

The collected radar reflections were downloaded from the collection PC to a Sun/UNIX workstation. The radar data (pulses) are floating point vectors that contain 801 arithmetically complex samples; that is, the samples have both a real and an imaginary part, which are thematically combined to represent the amplitude and phase of the radar returns.

The first processing operation suppresses the stationary clutter. Stationary clutter is energy reflected by all illuminated radar scatterers that were not a part of the rotating platform, such as the earth immediately surrounding the rotating table. To suppress the clutter, the processing software computes the coherent average of all pulses from the collection run. Because the energy reflected by scatterers on the platform averages approximately zero over the course of a complete platform rotation, the averaging operation produces an estimate of the return from only the stationary scatterers. The processing software then subtracts the average from each pulse, thereby suppressing the stationary clutter.

Following clutter suppression, the processing software performs a forward FFT on each pulse, mapping the data to the range-frequency (image) domain. The 801 samples cover a range swath that is about 60 meters wide. The center 120 samples are then extracted to provide a range subswath that is about 9 meters wide and centered on the platform. An inverse FFT is performed on the subset of 120 samples to map the data back to the time domain for subsequent processing.

The signal data next passes to the image formation processing software, where the image formation processor (IFP) produces two-dimensional images of the target by applying the polar format algorithm (PFA). The radar data could be processed directly into imagery with a two-dimensional FFT. However, FFT-based processing provides little control over image aspect ratio and it does not compensate the radar signal history for nonuniformities in the rotation rate of the platform. These nonuniformities can lead to azimuthal resolution variations in the final image. Because the PFA requires range and azimuth resampling of the signal history data, the processor provides the user with a ready mechanism for setting and maintaining both image resolution and aspect ratio.

The PFA also offers a mode of operation known as stabilized scene processing. Stabilized scene processing holds the orientation of the target constant from image to image, at an orientation angle specified by the user. When viewing a sequence of stabilized scene images, the radar appears to rotate around the target. Stabilized scene processing permits the processing software to form an additional output product known as a noncoherently integrated image, which is the sum of the magnitudes from a sequence of stabilized scene images. If the sequence of images covers 360 degrees of aspect angle change, the noncoherently integrated image will be a picture of the aggregate radar scattering of the illuminated target.

3.5 DATA OUTPUT PRODUCTS AND INTERPRETATION

Through informal discussions with parties interested in the RCS data, it became evident that the end-users would like the data processed and presented in a variety of ways. Therefore, we have created five different data output products:

1 Maximum Return Level versus Aspect Angle (Aspect Profile) Plot

2. Return Level versus Range (Range Profile) Plot

3. Two-Dimensional Image "Movie"

4. Two-Dimensional Image--Single Aspect Angle

5. Two-Dimensional Image--Integration of Multiple Aspect Angles

The following subsections describe these five data output products, how they should be interpreted, their potential utility, and current availability. Examples from the "Catalog of Radar Scattering Characteristics for Common Roadway Objects" are used in the explanation of each data type.

3.5.1 Maximum Return Level Versus Aspect Angle (Aspect Profile) Plot

Figure 3-2 is an example of a Maximum Return Level versus Aspect Angle Plot for the 1991 Jeep Wrangler. The aspect profile data indicates the maximum return level of the target as a function of aspect angle for a 360 degree rotation. The y-axis of the plot is the maximum return level (given in dBsm) for the corresponding aspect angle given on the x-axis. Note that the data reports the maximum return level, and not the total RCS of the object. The maximum return level corresponds to the highest power level observed in any given range cell (range cells for this data are approximately 7.5 cm). The maximum return levels are given in dBsm, corresponding to the radar cross-section of the most reflective scatterer on the object. Aspect angle values have been defined such that a 0 degree aspect angle corresponds to illuminating the object from a head-on orientation, a 90 degree aspect angle corresponds to illuminating the object from the left side (or driver side for a vehicle), a 180 degree aspect angle corresponds to illuminating the object from the rear, and a 270 degree aspect angle corresponds to illuminating the object from the right side (or passenger side for a vehicle)

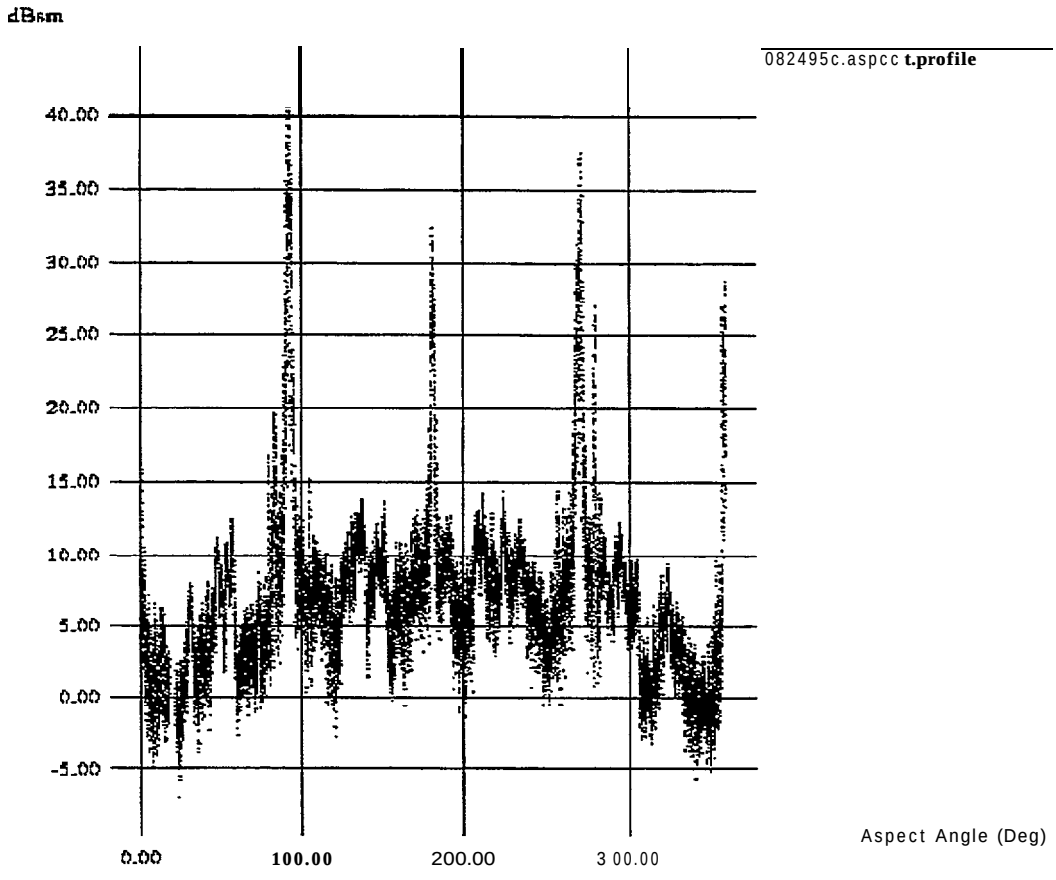

Figure 3-2. Example of Aspect Profile Plot

These data plots are useful for defining the dynamic operating envelope under which an automotive radar must operate. For example, the maximum return levels for the targets measured in this effort ranged from -12 dBsm (a stop sign at its lowest return aspect angle) to +42 dBsm (the Jeep at its highest return aspect angle). This means that the radar must be able to handle returns from targets of this size over its operating range. Another use for this type of data is in high-level simulation programs which do not require high fidelity in the radar models. One could use the data in these types of plots as a look-up table for expected reflectivity, given a specific aspect angle as generated under a particular scenario in the simulation program. The return level is provided in dBsm so that the user can scale expected power level returns according to individual radar configurations and range to target. The user should note, however, that since many automotive radars operate in the near-field, radar cross-section (RCS) is range dependent rather than constant (see Section 3.3).

These types of plots are available in both hard copy and electronic forms. Hard copies of these plots for each target are included in "Catalog of Radar Scattering Characteristics for Common Roadway Objects" which is provided as an appendix to this report in a black-and-white version. A color version is available from ERIM ($400). The data for these plots can also be downloaded at no charge from ERIM's Web server: www.erim.org/Trans/roadobj/.

3.5.2 Return Level Versus Range Plot (Range Profile) for a Given Aspect Angle

Figure 3-3 is an example of a Return Level versus Range Plot for the BMW motorcycle, at a 180 degree aspect angle. The y-axis of the plot is the return for the corresponding range given on the

x-axis. The return levels are given in dBsm, which corresponds to the radar cross-section of the scatterer(s) which constitute the return from that particular range. The range values correspond to the distance across ERIM's rotary platform table. The table itself is approximately 6.7 meters across. Therefore, a range of 0 corresponds to the edge of the platform nearest to the-radar, and a range 6.66 meters corresponds to the edge of the platform farthest from the radar. Each object (except the human and the stop sign) was positioned near the center of the table. Aspect angle values follow the definition provided in the previous section.

These types of data plots are useful for observing how the individual scatterers on the target are distributed as a function of range. Knowledge of scatterer distribution may be helpful in developing algorithms which group multiple scatterers together as a single target, to reduce the burden on tracking algorithms. Another use for this data type is in more advanced simulation programs which can utilize the range profiles to simulate targets at a given aspect angle in a particular scenario. The return level is provided in dBsm to allow the user to scale expected power level returns according to individual radar configurations and range to target, however the user should note that since many automotive radars operate in the near-field, radar cross-section (RCS) is range dependent, and is not constant.

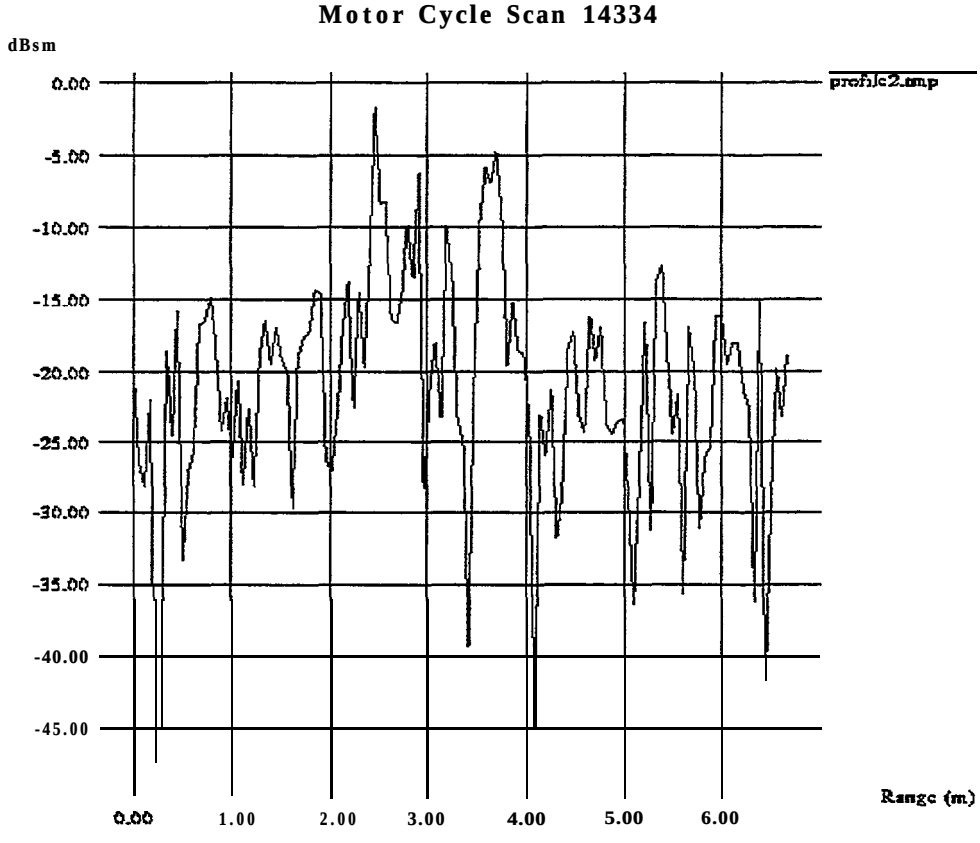

Figure 3-3. Example of Range Profile Plot

3.5.3 Two-Dimensional Image "Movie"

Since the radar data was collected and processed using Inverse Synthetic Aperture Radar (ISAR) techniques, a two-dimensional image of the illuminated object can be formed. A series of images can be linked together to create a dynamic "movie." The movie is a sequence of radar images taken at various

aspect angles and illustrates how the radar return levels vary as the vehicle is rotated. ERIM has a movie of a Ford Taurus available on its world-wide web server: www.erim.org/Trans/roadobj/.

The images in the movie are oriented such that the radar is illuminating from the right side and the observer is looking straight down at the vehicle. Therefore, range is in the horizontal direction and cross-range (i.e., azimuth) is in the vertical direction. The images in the movie are also color-coded, so that low level returns are represented by dark colors (e.g., blue and green) and higher Ievel returns are shown as brighter colors (e.g., orange and yellow). The movie indicates how very high-level returns occur when the front, rear, or sides of the vehicle are perpendicular to the radar illumination. This is due to specular (mirror-like) reflections of the radar energy. As the vehicle rotates away from the0,90, 180, or 270-degree aspect angles, the return levels drop off significantly.

Viewing the data in a movie-type format visually illustrates the dynamic changes in radar return levels with changing aspect angle. Aspect angles which correspond to low return levels can be easily identified for further analysis using the other forms of data output.

Production of these movies was achieved using ERIM's proprietary image manipulation software. Therefore, the movies are not publicly available. Organizations which have special requirements and are interested in viewing movies of other roadway objects can contact ERIM directly.

3.5.4 Two-Dimensional Image-Single Aspect Angle

Figure 3-4 shows black-and-white radar images and corresponding range profile plots of a 1990 Chevy Corvette at 170 and 180 degree aspect angles, respectively. The images are oriented such that the radar is illuminating from the left side and you are looking straight down at the vehicle. Therefore, range is in the horizontal direction and cross-range (i.e., azimuth) is in the vertical direction. The resolution cell of each image is approximately 7.5 by 7.5 centimeters. The images are coded with grey-shades to represent the radar return levels as designated in the scale on each image. The corresponding range profile plot is included below each image to illustrate how a vehicle-based radar might "view" this object.

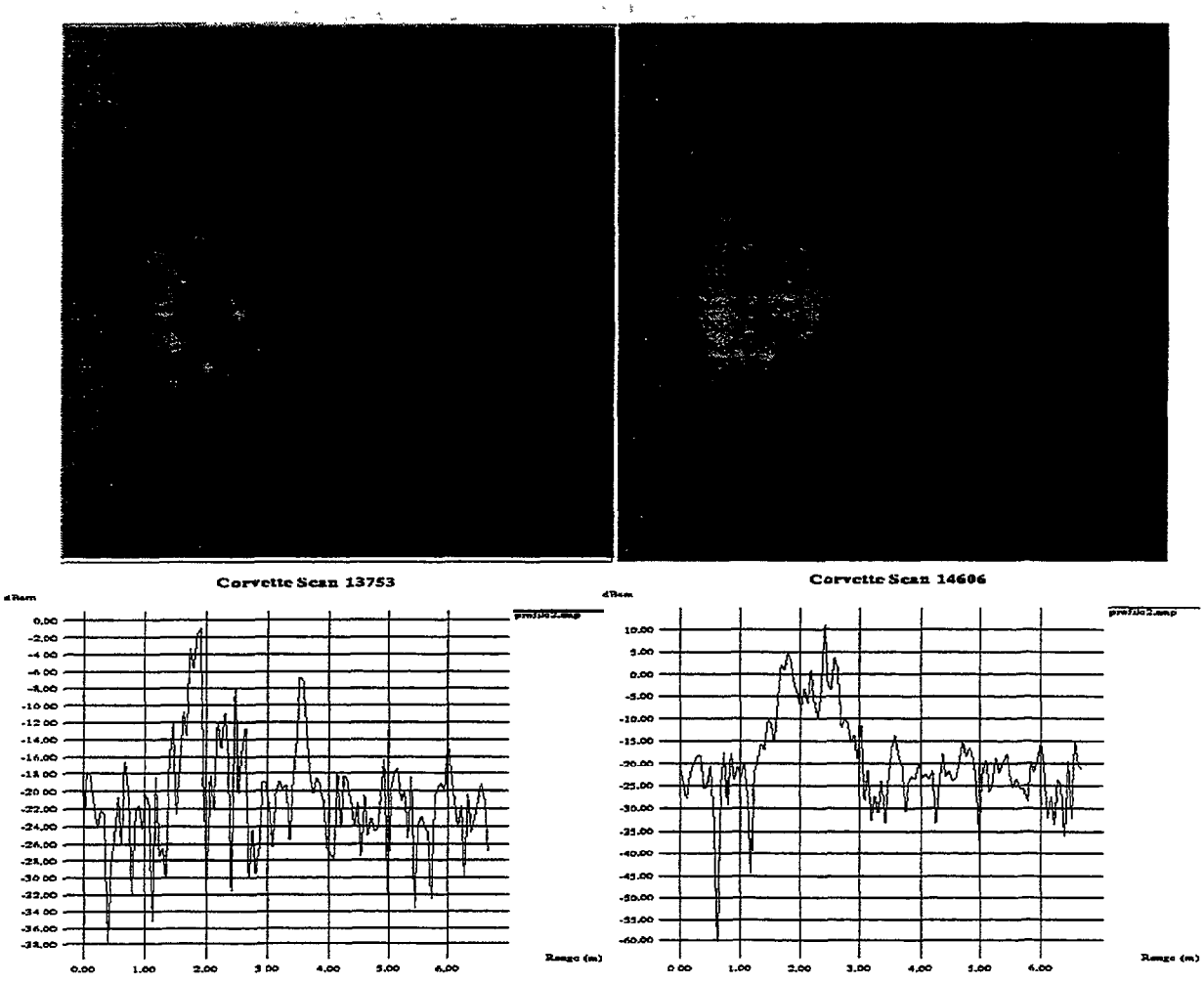

170 Degree Aspect Angle **180 Degree Aspect Angle**

Figure 3-4. **Examples of Single** Aspect Angle **Images**

These images allow the observer to identify individual scattering centers on the object which are active at a given aspect angle. This information can help to explain observations during static or roadway testing of vehicle-based radar sensors. For example, the range profile plot for the 180 degree aspect angle exhibits a "double hump" in the return which may puzzle some researcher. However, the image clearly shows that the second hump is due to a multipath return off the transmission housing underneath the vehicle.

3.5.5 Two-Dimensional Image--Integrated from Multiple Aspect Angles

A noncoherently integrated radar image of a 1993 Geo Metro is shown in Figure 3-5. This image was created by integrating the returns from multiple aspect images, like those discussed in the previous section, spaced at 5-degree increments. The image appears as though the object was being illuminated from all aspect angles simultaneously and you are looking straight down at the vehicle. Therefore, range is in the horizontal direction and cross-range (i.e., azimuth) is in the vertical direction. The resolution cell of the image is approximately 7.5 by 7.5 centimeters.

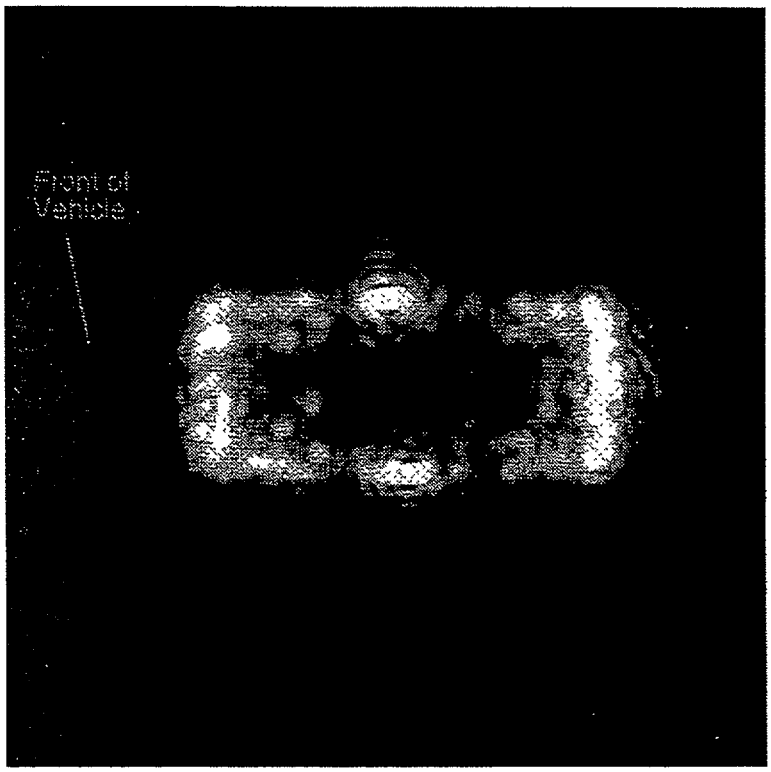

Figure 3-5. Example of Noncoherently Integrated Radar Image

The noncoherently integrated image allows the observer to identify all of the individual scattering centers on a given object. This information can help to explain observations during static or roadway testing of vehicle-based radar sensors. These types of images have been made for all of the vehicles on which data has been collected.

Hard copies of these plots for each target are included in "Catalog of Radar Scattering Characteristics for Common Roadway Objects" which is provided as an appendix to this report in a black-and-white version. A color version is available from ERIM ($400).

3.6 INITIAL OBSERVATIONS AND CONCLUSIONS

It is anticipated that the various data output products described above will find great utility in future automotive radar simulation programs and as guidelines for future designs and testing. Analysis of the RCS data has yielded a number of observations which will now be discussed.

Maximum and Minimum RCS Values

Observations of the RCS data indicate that reflectivity of common roadway objects can vary from over +40 dBsm for the broadside view of a Jeep-type vehicle to below -2 dBsm for a motorcycle or even -10 dBsm for an irregularly shaped sign post. This means that in order to detect these various objects in a given roadway scenario, the automotive radar must have a dynamic range greater than 50dB. In addition, the noise floor of the receiver must be low enough to reliably detect targets with RCS values as low as -5 to -10 dBsm at the maximum operating range of the system.

Return Levels From Aspect Angles Around 180 Degrees

Two of the primary applications of automotive radar will be for Intelligent Cruise Control purposes and for mitigating rear-end collisions. Therefore, the return levels from vehicles when illuminated from the rear (i.e., a 180 degree aspect angle) are critical. In evaluating the aspect profiles of the various vehicles measured in this effort, it was observed, as expected, that all of them except the motorcycle provided a significant return at 180 degrees due to specular reflections from the rear structure of the vehicles. It was also observed that as one deviated from the 180 degree view, the return level dropped off at various rates, based on the geometric shape of the vehicle. Table 3-2 shows the minimum angular departure from a 180 degree aspect at which the RCS of the vehicle drops below the specified value. For example, the reflectivity of a Taurus was observed to drop below 5 dBsm when the aspect angle was below 170 degrees or above 190 degrees.

Table 3-2. Characteristic RCS Fall-Off

Vehide	Angle of Departure From 180 at Which RCS >0 dBsm	Angle of Departure From 180 at Which RCS >5 dBsm	Angle of Departure From 180 at Which RCS >10 dBsm
Jeep	±180	±180	±5
Taurus	±20	±10	±5
Geo Metro	±40	±30	±5
Corvette	±30	±10	0
Motorcycle	±2	0	0

Looking at these numbers indicates that the reflectivity of certain classes of vehicles will drop below 0 dBsm at aspect angles which can be expected to be incurred during normal driving. Obviously the motorcycle poses the largest problem, but even the Taurus and the Corvette will fall below 0 dBsm in road curves. The effects of low RCS levels at common aspect angles will be tested during the road tests planned for this program.

Distribution of Scatterers Across Targets

The range profile plots, single aspect images, and radar image movies demonstrate that the radar energy scatterers are distributed across the extent of the target; they include side-view mirrors, wheels, under-body structures, in-vehicle components, body panel seams, and so forth. The relevance of this attribute to automotive radar is that tracking the returns from each individual scattering center will place an enormous burden on the radar processing and threat assessment electronics. The ability to group these returns into a single object is highly desirable. However, the RCS data indicates that this will not be a trivial task as the object's signature can change significantly with a minute change in aspect angle. This is due to the highly dynamic scintillation effects induced by the small wavelength of automotive radar energy. These effects were observed repeatedly during the roadway tests of this program, in which the returns from a vehicle being tracked by the FLAR varied over a wide range on a pulse-to-pulse basis.

Non-Vehicular Objects

One concern for automotive radars is the interpretation of returns from objects other than vehicles. These objects may be considered clutter if they are off to the side of the roadway (like a stop sign), or a legitimate threat (a pedestrian crossing the roadway). The RCS data collected under this program indicates that a human being can have a reflectivity between +4 and -6 dBsm. Stop signs have a large

specular return at a 0 degree aspect angle but can quickly fall below -5 dBsm. Also, like the stop sign, a block wall (used to simulate a bridge abutment) exhibits a large specular reflectivity which falls off rapidly as the aspect angle departs from 0 degrees.

Many more observations can be made from the data alone, but as mentioned above, the real utility of the data will be in its application for simulation programs. We expect to expand on this initial database during future projects.

It is interesting to note at this point that many of these conclusions, based on the analysis of the RCS data, were actually observed during the road testing phase of this program (see Section 6).

4.0 TRW FORWARD LOOKING AUTOMOTIVE RADAR (FLAR)

4.1 INTRODUCTION

Most of the radar testing in this program, excluding the RCS measurements of common roadway objects, was made using a TRW Forward Looking Automotive Radar (FLAR) The FLAR was provided by TRW and integrated into ERIM's testbed vehicle collection system. Its purpose was to serve as a "generic" automotive radar sensor and provide the basic signals from which ERIM could evaluate the interaction between the radar and its surrounding environment. It should be emphasized that the purpose of the experiments conducted in this program was NOT to test the hardware configuration or algorithms employed in TRW's design. On the contrary, the measurements were designed to isolate the results (as much as possible) from specific attributes of the TRW radar implementation.

This section will first describe the configuration and operation of the TRW radar and then present the results of basic tests conducted to determine baseline performance characteristics. These characteristics were used in subsequent roadway testing of the unit.

4.2 SENSOR CONFIGURATION

The TRW FLAR, model AICC-3B, utilizes 94 GHz radar technology originally developed for military purposes. The FLAR has 3 electronically switched transmit beams and 1 receive beam. Each transmit beam has 3 dB widths of 3 degrees in azimuth and 3 degrees in elevation. The receive beam is approximately 9 degrees in azimuth and 3 degrees in elevation. With this configuration, the sensor's field-of-view is adjusted by directing the signal to be transmitted to the appropriate transmit antenna.

The TRW AICC-3B FLAR consists of two elements (Figure 4-l): the RF head, which contains the transmit/receive antennas and the analog circuitry, and the DSP module which contains the processing unit and the interfaces to the host system (the test computer in the testbed vehicle). The DSP communicates to the RF head via three cables: one for the power connection, one for the radar data, and one for the beam selection bits. The DSP communicates with the host system via three cables: one cable for primary power and the other two for data communication.

In the ERIM testbed vehicle, the RF head is located on a hard mount in front of the vehicle grill, providing a field-of-view uncontaminated by any vehicle structural members. The DSP is located in the vehicle cabin along with the test computer rack.

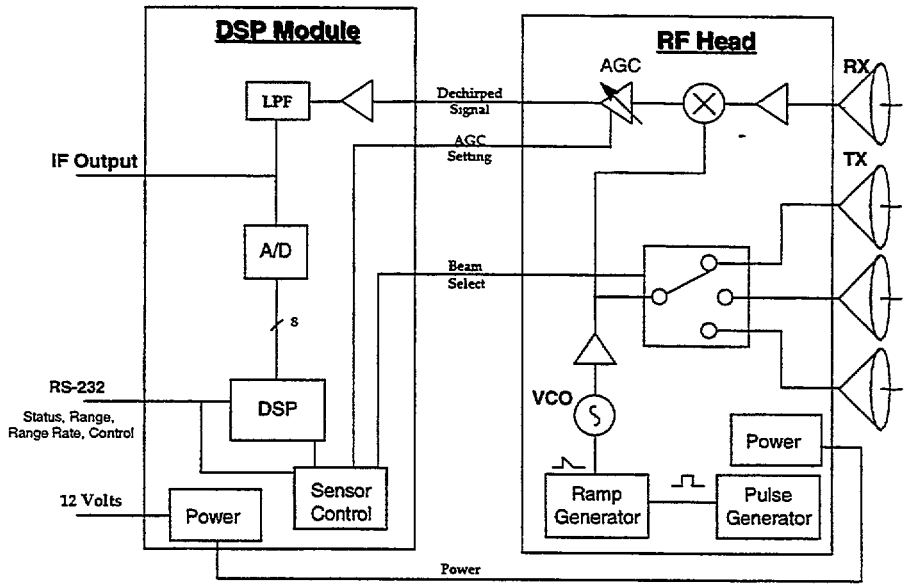

Figure 4-1. TRW's AICC-3B FLAR

4.3 SENSOR OPERATION

4.3.1 General Overview

The TRW FLAR employs a pulsed frequency-modulated, continuous wave (FMCW) radar front-end to determine the distance to objects located in its field-of-view (FOV). A high-level functional block diagram of the TRW radar sensor is shown in Figure 4-1. The following sequence of events describes the process to generate, transmit, and receive a single radar pulse:

1. The pulse generator within the RF head generates a modulation signal which dictates the fundamental timing of the radar.
2. The modulation signal (a square wave) drives the ramp generator, which creates a linearized voltage ramp during the active phase of the modulation signal.
3. The voltage ramp drives the voltage-controlled oscillator (VCO) which outputs a linear frequency modulated signal referred to as a chirp. The chirp bandwidth is at 375 MHz centered at 94 GHz and the chirp rate is at 3 MHz/usec.
4. The chirp signal is amplified and divided into 2 identical signals. One version of the signal is fed to one of the transmit antennas and emitted into the atmosphere. The other version of the chirp is input to the de-chirp mixer (discussed below).
5. A portion of the transmitted energy reflects off objects in the radar's FOV and is intercepted by the receive antenna.
6. The received energy is amplified and input to the de-chirp mixer. The de-chirp mixer subtracts the frequency of the received signal from that of the transmitted signal. Therefore, the de-chirp mixer output signal frequency is proportional to the range of the object which reflected the energy. (This is a fundamental concept of FMCW radar.)
7. The de-chirped signal is fed to the Automatic Gain Control (AGC) amplifier which adjusts the signal level to keep it within the dynamic range of the analog-to-digital (A/D) converter. The AGC control signal is generated by the sensor control circuitry located in the DSP Module.

8. The IF signal is further amplified and low-pass filtered before the A/D converter digitizes the de-chirped signal so it can be processed by the FLAR's DSP circuitry.
9. The DSP circuitry uses frequency-domain analysis to determine range to deteeted objects and sequential range differentiation to determine relative range rate.

The radar pulse has a signal bandwidth of 375 MHz centered at 94 GHz. The received signal is de-chirped and down-converted to a base band signal with a bandwidth of 2 MHz.

The description above corresponds to the sequence involved in processing a single radar pulse. The TRW FLAR integrates the energy from multiple pulses to improve the signal-to-noise ratio and therefore increases the sensor's detection capability. Depending on the mode, the TRW DSP electronics will integrate the returns from five or six pulses.

The ERIM interface with the radar IF signal occurs prior to any digitization, as illustrated in Figure 4-l. Therefore, the ERIM data collection system A/D converter has an input signal similar to that of the TRW DSP Module (see Appendix C). ERIM's processing algorithms can analyze both individual and groups of pulses.

4.3.2 Timing Specifications

As mentioned above, the FLAR processor integrates a number of pulses together to improve the signal-to-noise performance of the radar. Each group of pulses is fully processed and an update provided over the RS232 interface before the next group of pulses is transmitted. A radar frame consists of one set of pulses and the processing time before the next set of pulses is transmitted-this also corresponds to the data update rate of the sensor. The rate at which pulses are sent out is known as the pulse repetition frequency (PRF). The number of pulses within a group is dependent on the operating mode. The sensor timing parameters for the FLAR are shown in Table 4- 1.

Table 4-l FLAR Timing Parameters

Parameter	Value	Description
Pulse Duration	123 mS	Length of each transmitted pulse
Pulses/Group	6	Acquisition Mode
	6	Tracking Mode
	5	Surveillance Mode
Pulse-pulse Time	1.87 mS	Equivalent PRF of 535 Hz
Frame Time/Update Period	50.2 mS	Equivalent Frame PRF 20 Hz

The timing diagram in Figure 4-2 illustrates the radar timing parameters for the tracking and acquisition modes. The tests conducted during this program used only the acquisition and tracking modes of the FLAR and, therefore, always had 6 pulses per radar frame.

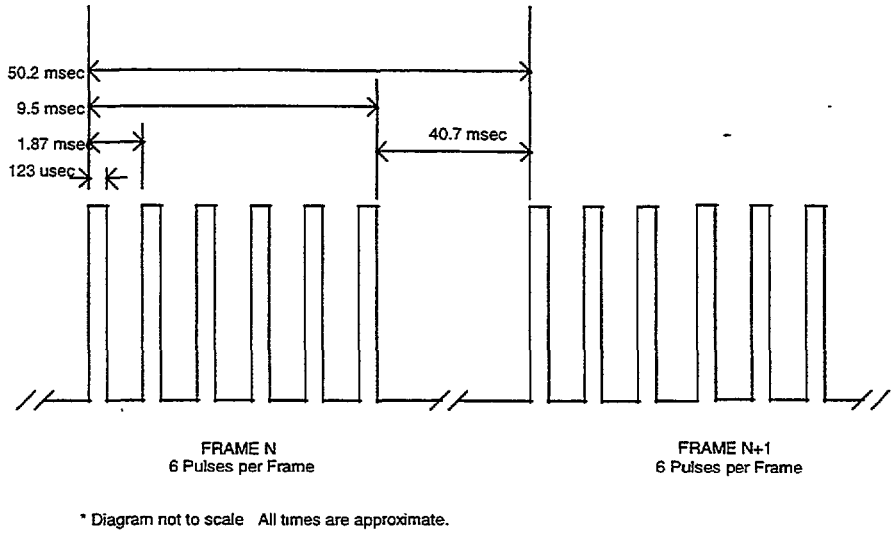

Figure 4-2. FLAR Transmit Pulse Timing

4.3.3 Automatic Gain Control (AGC) Amplifier

As described earlier, the FLAR's automatic gain control (AGC) amplifier keeps radar return levels within the dynamic range of the A/D converter. The plot below illustrates the attenuation (reference to maximum amplifier gain) of the AGC amplifier. The x-axis corresponds to the control voltage applied to the AGC amplifier and the y-axis is the corresponding attenuation in dB.

It was critical that the ERIM collection system monitor the AGC control voltage being sent from the DSP module to the RF head, so that the analysis procedures could account for effects of the AGC on the signal return levels observed during the tests.

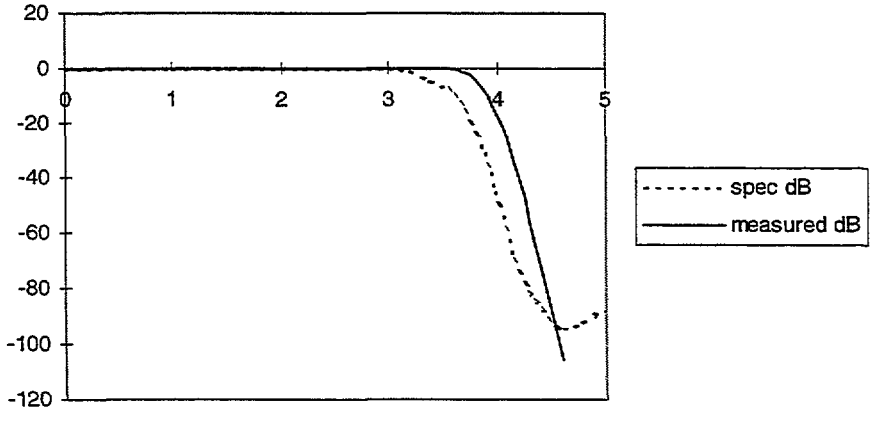

Figure 4-3. AGC Attenuation (dB) Versus Voltage (Volts)

4.3.4 Transmitted Waveform

The FLAR generates a linear FM signal referred to as a chirp. Both time and frequency domain representations of a chirp signal are provided in Figure 4-4.

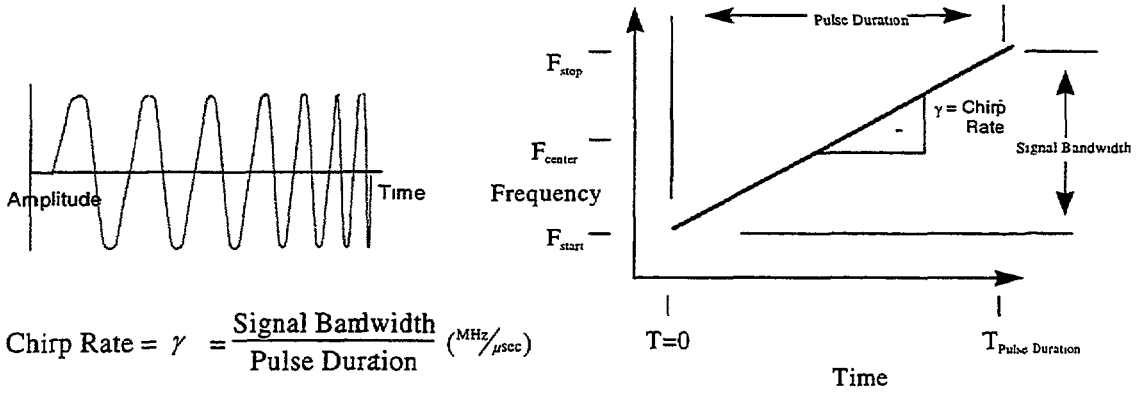

Figure 4-4. Graphical Representations of a Chirp Waveform

This form of signal is typical in FMCW-type radars. It is the frequency modulation of the transmitted signal which allows the range-to-targets within the sensor's field-of-view to be calculated. As shown in Figure 4-5, using a chirp signal results in the range being proportional to frequency.

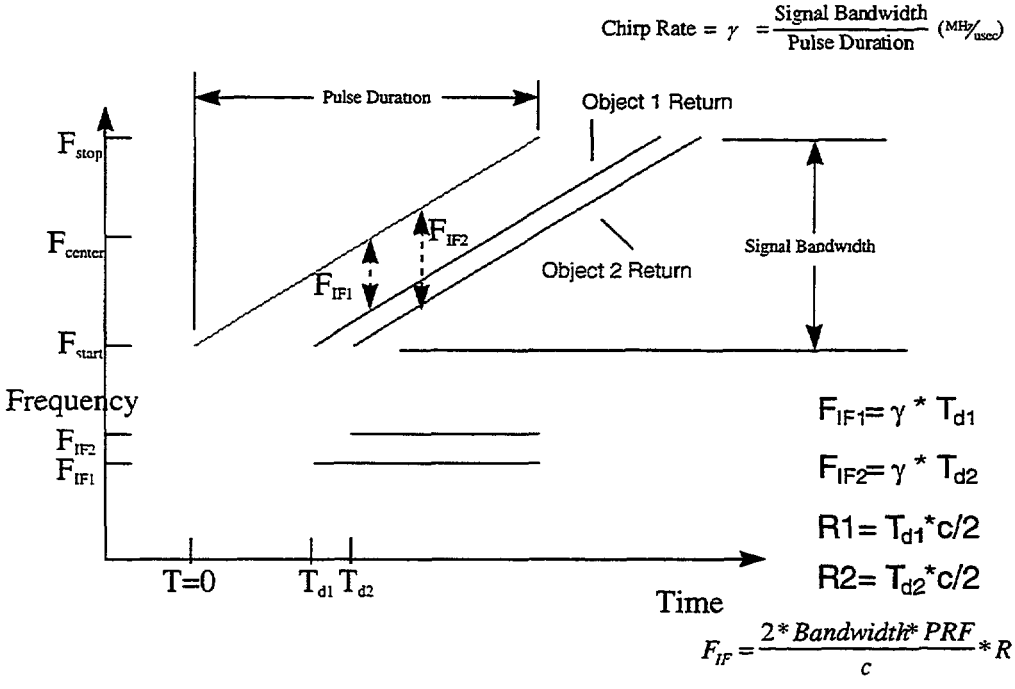

Figure 4-5. Range in Proportion to IF Frequency

The frequency which a remote sensor uses (e.g., 77 GHz or 94 GHz) determines how the energy interacts with objects in the environment. For example, lower frequency emissions tend to penetrate materials more than higher frequencies. The bandwidth of the transmit signal determines the range resolution for FMCW sensors such as the TRW FLAR.

For the purposes of this program, measuring the transmit waveform parameters served to verify both FLAR stability and the frequency and bandwidth specifications reported by TRW. Also, the bandwidth value was used in conjunction with the transmit time (discussed in the previous section) to determine the chirp rate. The chirp rate allowed the frequency domain analysis of the return signals to be correlated

with the actual range to objects in the sensor field-of-view. The transmit waveform parameters are summarized in Table 4-2.

Table 4-2. Transmit Waveform Parameters

Parameter	Value
Center Frequency	94.165 GHz
Bandwidth	375 MHz
Chirp Rate (calculated)	3.048 MHz/usec

4.3.5 Intermediate Frequency Signal

The TRW FLAR intermediate frequency (IF) waveform parameters correspond to the signal which is input to the sensor receiver A/D converter. The IF signal was considered the raw FLAR sensor output and all the digital signal processing was performed on this signal. The parameters of concern for the IF signal are frequency, bandwidth, and voltage level. These parameters dictated the required specifications of the A/D converter and any signal conditioning (e.g., amplification) required prior to the A/D. The FLAR IF signal parameters are summarized in Table 4-3.

Table 4-3. IF Signal Parameters

Parameter	Value
Frequency	DC to 2 MHz
Bandwidth	2 MHz
Voltage Range	-1 volt to + 1 volt

4.3.6 Power Measurements

The transmit power level of a radar affects the signal-to-noise ratio of the return echoes in the sensor's receiver. The higher the transmitted power, the stronger the return echoes from objects in the scene. Therefore, from a signal-to-noise perspective, the higher the transmit power the better. However, implementation, cost, and safety issues limit the transmit power level.

The results of direct measurements of the FLAR transmitted waveform are given below:

- Left Beam: 21.7 mW
- Center Beam: 26.6 mW
- Bight Beam: 22.3 mW

These values correlate with the antenna beam pattern measurements made on ERIM's rotary platform. Figure 4-6 indicates that the left and right transmit beam power emissions are down slightly from the center beam.

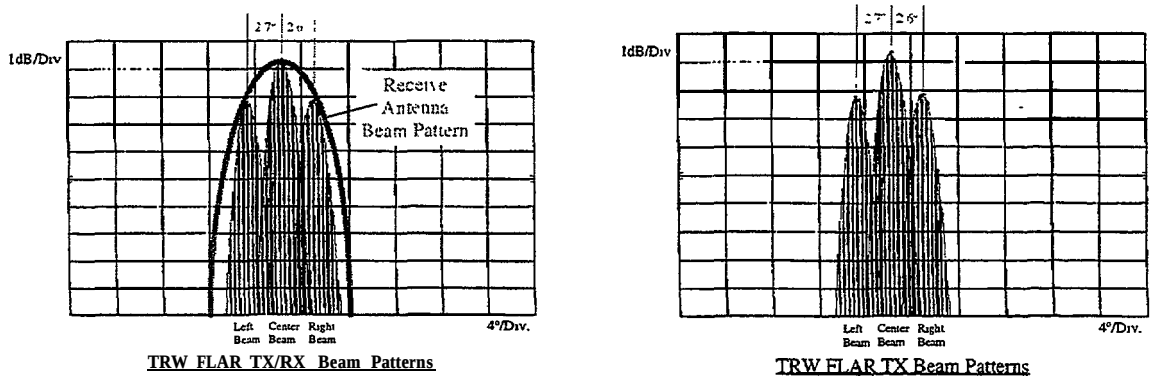

Figure 4-6. FLAR Beam Patterns

4.3.7 Antenna Beam Patterns

The FLAR sensor uses three beams pointed to the left, center, and right of the sensor boresight (i.e., the vehicle center line). Figure 4-3 illustrates the FLAR beam patterns and their orientation with respect to each other. TRW uses the three-beam approach in order to implement a search and track algorithm for an Automated Cruise Control (ACC) application.

Because the goal of this program was to view the FLAR as a generic radar sensor, the TRW beam switching algorithm was not employed in the testing. An override switch was used to manually select an active transmit beam during any particular test.

4.3.8 Beam Switch Isolation

As described earlier, the TRW FLAR uses a switch to direct the transmit signal to one of three separate antennas. The isolation between the different ports of this switch are provided in Table 4-4.

Table 4-4. Beam Switch Isolation

	Right Beam (dB)	Left Beam (dB)	Center Beam (dB)
Left Beam	18.7	I 0	16.2
Center Beam	34.3	30.3	0
Right Beam	0	15.9	18.6

4.4 BASELINE PERFORMANCE CHARACTERISTICS

4.4.1 Radar Field-of-View

The radar's field-of-view is directly related to the antenna beam patterns discussed above. Several tests were conducted to determine the basic field of view of the sensor (see Appendix A). These tests found, as expected, good correlation between the measured beam patterns and azimuthal detection of targets.

Typically, antenna beam widths are specified in terms of their 3 dB points, which correspond to locations in the beam pattern where the antenna gain is down 3 dB from its maximum gain. In the case of the FLAR, each transmit beam has a 3 dB width of 3 degrees in both azimuth and elevation. This

corresponds to a beam width of approximately one lane width, at 80 meters from the radar. However, as illustrated in Figure 4-7, the antenna patterns can detect objects well outside their 3 dB points.

The results of measurements taken on ERIM's rotary platform measurements are shown in Figure 4-7. These plots show the mainlobes along with the sidelobes for the center, right, and left antenna beams respectively. A "zoomed" in version on the mainlobes for each antenna was provided in Figure 4-6.

The left and right antenna beams show a sidelobe about 12-15 dB below the mainlobe. The left beam sidelobe is approximately 4.5 degrees from the left beam mainlobe. The right beam sidelobe is approximately 6.5 degrees from the right beam mainlobe. The 3 dB beam width on all three beams is approximately 2.7 degrees wide.

Knowledge of these beam patterns is essential in evaluating the performance of the FLAR during roadway testing. Antenna sidelobe levels can significantly affect the performance of the sensor. For example, a 30 dBsm target azimuthally located within the sidelobe of the left beam would be interpreted by the sensor as a 15 to 18 dBsm target located in the mainlobe of the left antenna.

Taking this issue a step further, a large target located outside the 3 dB point of the center beam (i.e., outside the road lane) could appear to be a somewhat smaller target located inside the road lane.

Several of the roadway tests in this program are designed to address these issues. Using the typical 3 dB point specification, the 3-antenna approach provides the FLAR with an approximately 8.3 degree azimuth field of view.

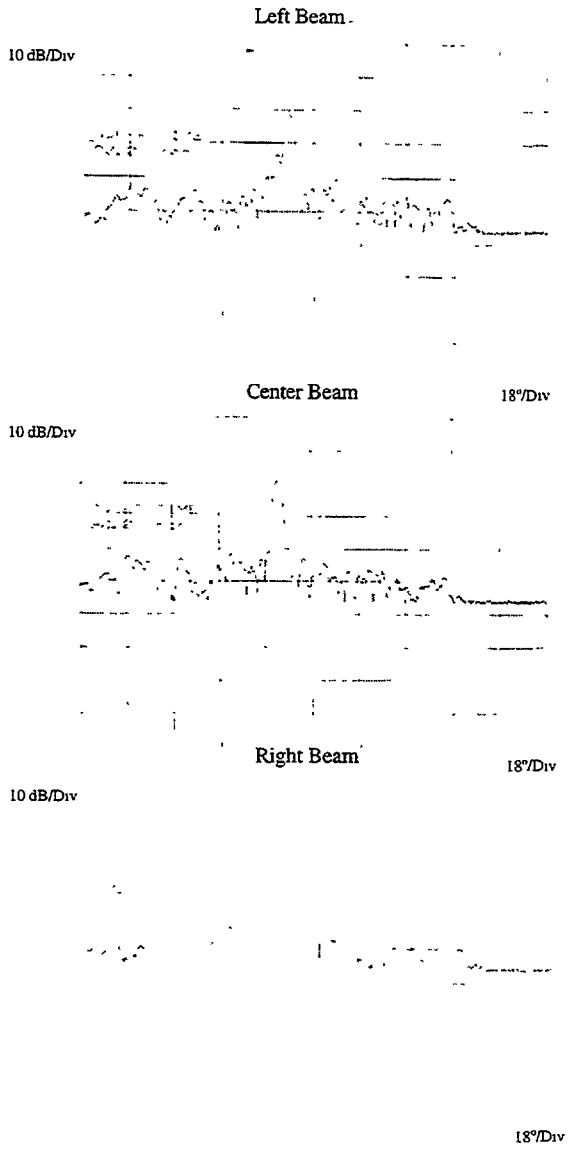

Figure 4-7. FLAR Beam Patterns

4.4.2 Range Accuracy

The range tests are a set of static tests designed to measure the absolute accuracy of the FLAR sensor. Targets were placed at known distances and data was collected for analysis using ERIM-developed processing software (in other words, only the raw radar signal was being considered, to avoid evaluating TRW's particular processing algorithms). The tests were divided into two distinct sets: (1) Far Range Tests and (2) Near Range Tests. This section will discuss the results from both sets and relate the findings to expectations for other automotive radars.

4.4.2.1 Far Range Tests (10 to 100 meters)

Data for these tests was collected by placing a corner reflector at 10 meter increments from 10 to 100 meters from the FLAR sensor. Individual tests were run using a 10 dBsm and 20 dBsm target to evaluate correlation between the results.

Figure 4-8 shows the results for the 20 dBsm and 10 dBsm corner reflectors. The solid line represents the mean detected distance and the dotted lines show one standard deviation from the mean. The dot-dashed line shows the distance reported by the FLAR sensor (which utilizes the TRW processing algorithms).

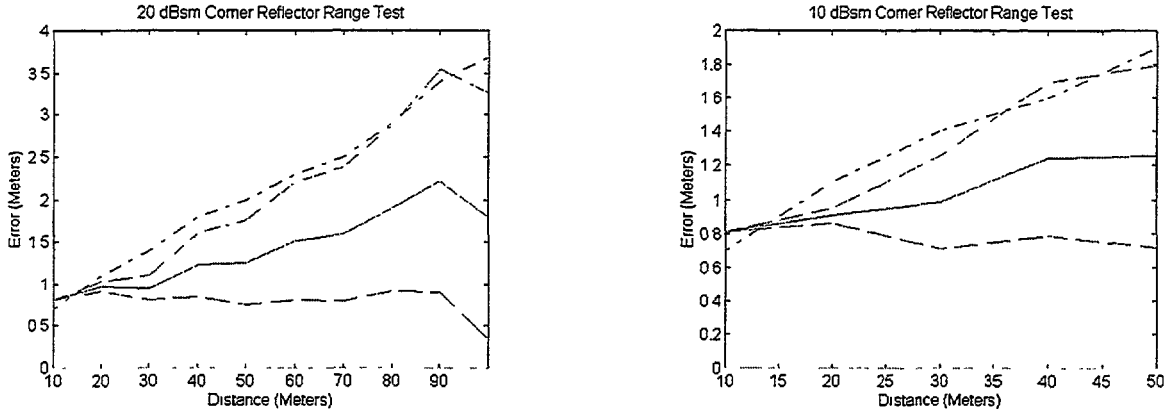

Figure 4-8. Corner Reflector Range Test Results

The figures show both a nonzero slope and a DC offset. The DC offset is an unaccounted for static error in the either the FLAR sensor or the test setup/analysis routine. The slope is due to a chirp rate discrepancy. That is, the chirp rate is not really what the specification says it is. Figure 4-9 shows how a discrepancy in the chirp rate can lead to an error in the reported target range. The vertical lines (Actual/Theoretical Dechirped Frequency) correspond to the sine wave created when the sensor dechirps the return from the target. The frequency of the dechirped sine wave is:

$$f = \frac{d\gamma}{c}$$

where f is the frequency of the dechirped sine wave

d is the distance from the sensor in meters

γ is the FLAR sensor chirp rate in MHz/μs

c is the speed of light in meters/μs

For a given chirp rate there is a unique frequency, for every range. However, if the chirp rate changes, then the one-to-one correspondence between range and frequency also changes.

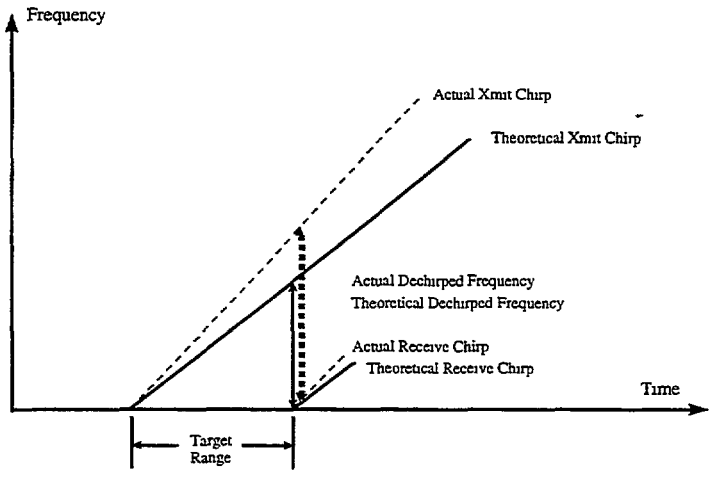

Figure 4-9. Effect of Chirp Rate Error

Using the actual measurements taken in these tests, a true chirp rate was calculated using information from Figure 4-8 as follows. The actual method used was to fit a line to the mean value data on Figure 4-8 and use information from that line to calculate the new values.

Let

$$d_1 = \frac{fc}{\gamma}$$

$$d_2 = \frac{fc}{\gamma + \Delta\gamma}$$

where d_1 is the assumed distance using the TRW numbers

d_2 is the measured distance (from Figure 4-10)

f is the frequency of the dechirped sine wave

c is the speed of light

γ is the chirp rate

$\Delta\gamma$ is the unknown difference in chirp rate to be calculated

The figure shows the error term obtained by subtracting d_1 from d_2. That is, the theoretical chirp rate value was used to calculate the distance given the sine wave data. Therefore the range dependent error (known because the actual distance was measured during the experiment) was caused by using the wrong chirp rate. In equation form the distance error is:

$$\Delta d = d_2 - d_1 = \frac{fc}{\gamma} - \frac{fc}{\gamma + \Delta\gamma}$$

Solving this equation for $\Delta\gamma$ gives the following:

$$\Delta\gamma = \frac{-\gamma^2}{\gamma - \frac{fc}{\Delta d}}$$

where $\gamma = 3.04878$ MHz/μS

$c = 300$ m/μS

f is chosen arbitrarily

Δd is chosen from the best fit line derived from Figure 4-9, given f

Adding in this correction to the chirp rate results in a range error profile that is nearly flat. However there is still a static offset that has to be removed. This was accomplished by noting the y intercept point from the line fit procedure during the chirp calculations. Applying both corrections and re-running the Matlab analysis software yielded the results shown in Figure 4-10. As expected the error was zero mean with a standard deviation proportional to range. The same correction coefficients were then applied to the results from the 10 dBsm corner reflectors; if the error was an effect of the sensor then correction coefficients should work for all test setups. The new chirp rate and offset values were:

$\gamma_{new} = 3.09319$ MHz/μs (Compared to 3.04878 theoretical)

Static Offset = 0.633727 Meters

The results of using these new correction values in the data processing is shown in Figure 4-10 for the 20 dBsm and 10 dBsm reflectors. As expected the range errors now had a zero mean with a standard deviation proportional to range. Since the error was attributed to a chirp rate discrepancy, the corrections were expected to work for all test set-ups. In fact, this proved to be the case, as a comparison of the first 50 meters of the 20 dBsm range test was almost identical to the 10 dBsm range tests. (Note that the 10 dBsm target was not detectable beyond the 50 meter mark.) **Therefore, the new chirp rate parameter and offset were be used throughout the program.**

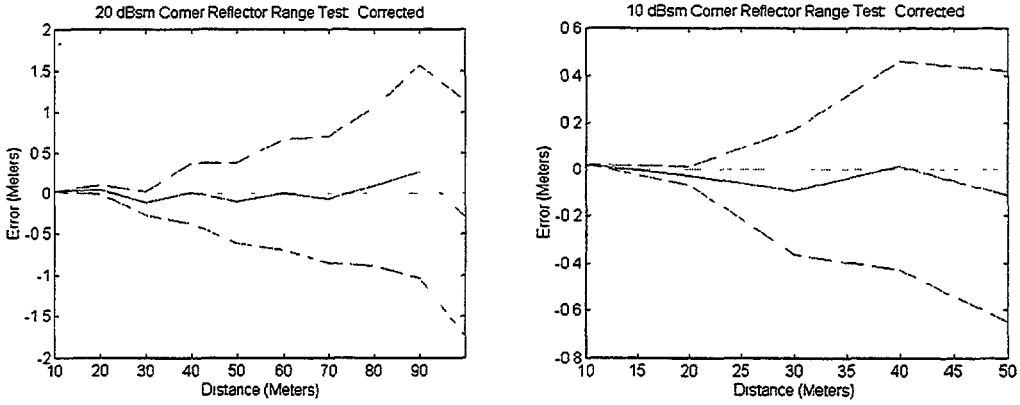

Figure 4-10. Corrected Corner Reflector Range Test Results

In summary, the FLAR sensor showed both a static offset and a range dependent error. These errors can be corrected by calibrating the sensor using radar range measurements to calculate two correction coefficients. In addition, the sensor shows an increase in reported range variations as the range to the target increases. The following section on range resolution provides a detailed discussion on the effects of transmit and receive signal phase errors. These can result in a greater variation of reported target range as the actual range to the target increases.

The actual results of this test are specific to the TRW FLAR sensor. However, it is likely that the 'offset' and 'linear' errors discussed in this section will occur in other radars designed for automotive applications. The methodology for correcting these errors is a calibration process which will determine:

1. Variable signal delays through the radar components, which result in offset errors.
2. Variations (from spec) in the transmit signal FM modulation (Chirp Rate), which results in linear range errors.

The correction of values resulting from such a calibration process can be implemented in the sensor's processing algorithms and require no "fine-tuning" of the hardware. With appropriate instrumentation, this process can be substantially automated.

The magnitude of the offset and linear errors will be dependent on the quality of the components used in the system. Therefore, cost versus performance versus required calibration effort trade-offs will have to be correctly evaluated for production of automotive radar sensors. For example, a common approach to creating a linear frequency modulated signal (i.e., a chirp) is to drive a voltage-controlled oscillator (VCO) with a voltage ramp. The quality (linearity, spectral purity, etc.) of the VCO output signal is proportional to the component cost. Therefore, it is critical that automotive radar design engineers understand the overall radar system performance implications on a component by component basis.

Besides considering the absolute magnitude of the offset and linear ranging errors, the system designer must evaluate a particular system's sensitivity to such errors. This sensitivity evaluation must include the radar processing and threat assessment algorithms employed by the system. For example, a system employing range differentiation to determine range rate (as opposed to Doppler processing) will be highly sensitive to the variations in the range reported by the FLAR sensor in these tests.

4.4.2.2 Near Range Tests (0 to 10 meters)

This next set of tests was aimed at evaluating performance as targets approached the near-field antenna range. It also demonstrates the effects of a physically small target close to the FLAR's two-antenna bistatic arrangement. A bistatic arrangement refers to the fact that the FLAR uses physically separate transmit and receive antennas (some radars use a duplexor to allow a single antenna to function for both transmit and receive).

The issue of near-field versus far-field radar measurements was discussed in Section 3 with regard to the radar cross-section measurements. For these near-range tests, the near-field issues must be considered. In the near field the antenna beam pattern can be assumed to be the same shape as the antenna aperture. The space around an antenna is divided into three regions, the reactive near-field region, the radiating near-field region, and the radiating far-field region. The boundaries between these regions are dependent on the antenna design. However certain criteria are generally used to denote the boundaries between the regions. The reactive near-field region ends at a distance $\lambda/2\pi$ from the antenna, where λ is the transmitted wavelength. The commonly used definition for the boundary between the near-field and far-field regions is:

$$R = \frac{2D^2}{\lambda}$$

where R is the boundary distance from the antenna

D is the largest aperture dimension

λ is the transmitted wavelength

For the FLAR antenna the reactive near-field region is approximately 0.5 mm. This battery of tests never operated in that region. The radiating near-field region extends out to approximately 3 meters.

The FLAR collection system was set up in the ERIM highbay facility. A piece of radar absorbing material was placed between the sensor and the far wall in order to eliminate undesired returns. A 10 dBsm corner reflector was placed in front of the sensor at a range of 10 meters and a set of radar pulses was collected. The reflector was moved one meter closer, and the process was repeated, until the reflector was 1 meter from the sensor. The range data was analyzed using the same analysis routines described the previous section.

Processing of the various data sets resulted in the plots shown in Figure 4-11. The solid line represents the mean detected distance and the dotted lines show one standard deviation from the mean. The dot-dashed line shows the distance reported by the FLAR sensor (which utilizes the TRW processing algorithms). Note that the static offset and chirp rate corrections determined in the far range tests (see discussion above) were employed while processing the near-range data sets.

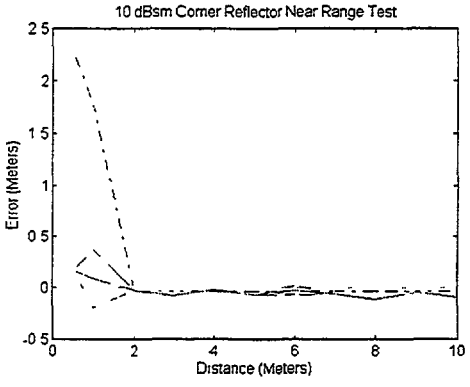

Figure 4-11. 10 dBsm

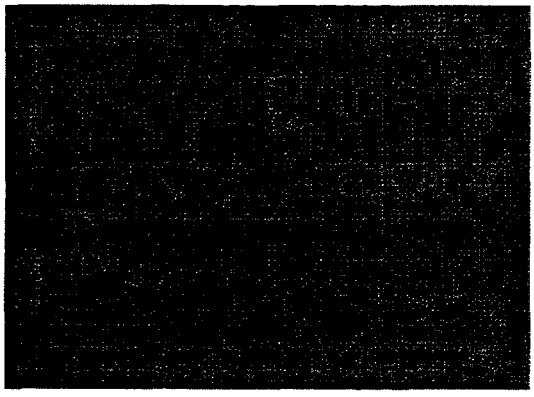

Figure 4-12. 10 dBsm at 1 Meter

The plot indicates that the FLAR accurately measured the target's range until the target was placed closer than 2 meters. The measurement taken at 1 meter shows a significant error in the ERIM processed data (i.e., the raw radar signal); the error is extreme for the TRW processed data.

A single return pulse for the 1 meter distance is shown in Figure 4-12. The figure shows two distinct peaks, one at the target distance and one at roughly twice the distance. The FLAR sensor reported the ghost target (at the further distance) as the real target and ignored the real target. The data shows that the target was detected at the appropriate range. The FLAR sensor software for some reason chooses to detect only the ghost target.

Figure 4-13 shows a plot of 100 consecutive pulses from the FLAR sensor. The second "ghost" target is always present. The second target is caused by one of three effects. First, it could be caused by too much power reflecting back to the FLAR sensor. This could make the RF front end saturate, causing the circuit to operate in the nonlinear region. Second, it could be caused by energy reflecting back into the transmitter, which would also cause the circuits to act in an unpredictable fashion. Third, the target may be an effect of multipath reflections. This would be a case where the radar bounces off the target, then the vehicle, then the target again.

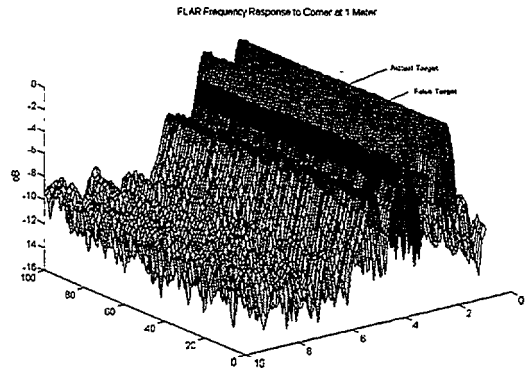

Figure 4-13. FLAR Frequency Response to Comer at 1 Meter

Due to ERIM's limited access to the TRW hardware and processing algorithms, the cause of the double peaks in the radar data could not be experimentally determined.

In summary, the FLAR sensor does not operate reliably at ranges less than 1 meter. The error can cause a target to appear farther away than it really is. This could have disastrous consequences in real world intelligent cruise control or collision avoidance situations.

4.4.3 Range Resolution

The ability to separate signal returns into reflections from distinct targets or objects is described by a radar's range resolution specification. The TRW FLAR has a stated range resolution of 0.5 meters.

The theoretical range resolution of a chirped radar system is given by the following equation:

$$Pr = \frac{C}{2B}$$

where pr is the range resolution in meters

C is the speed of light: $3 * 10^8$ m/s

B is the processed bandwidth

The theoretical resolution of the FLAR system, using the documented bandwidth of 375 MHz, is 0.4 meters.

A typical way of measuring the resolution of a radar system is to measure the IPR 3 dB beam width from a point target. This can be accomplished by using any of the range data collected for the range accuracy tests. The effect of limited resolution is seen as a combining of the peak responses from two physically close targets. This effect can be seen in Figure 4-14.

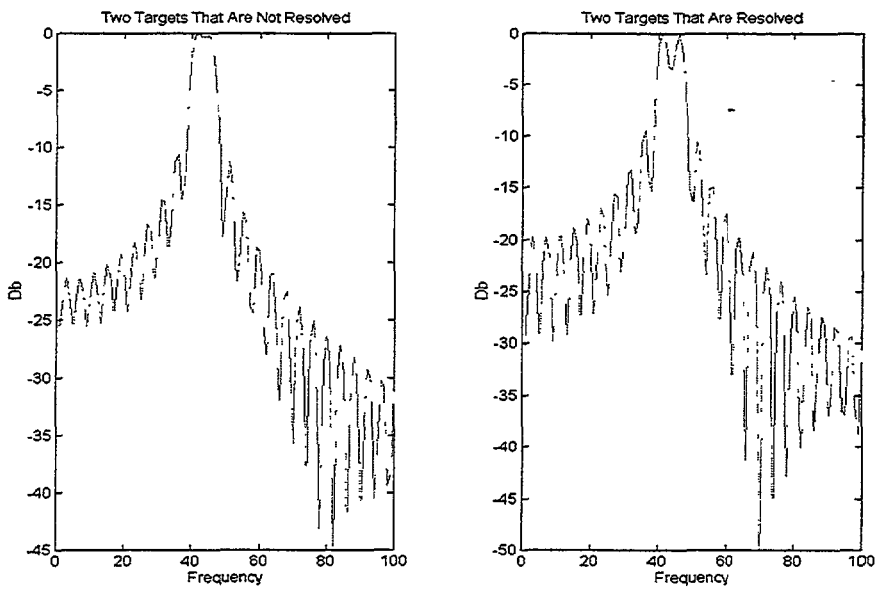

Figure 4-14. Effect of Limited Resolution

The resolution of the sensor system is degraded by nonlinearities in the transmitted chirp signal. If these errors are static pulse-to-pulse then they can be removed either by predistorting the waveform (an expensive alternative) or by post processing of the collected data. If the errors are not the same pulse-to-pulse, the system performance can be only marginally improved by post processing. Correction requires modification of the waveform generation circuit to remove the pulse-to-pulse instabilities.

Two approaches were used to characterize the FLAR range resolution. First was an analytical approach to determine the IPR width of the FLAR's dechirped signal; the second was a physical experiment using two displaced corner reflectors located within the FLAR's field of view.

Analytical Approach

Since the system uses a dechirped approach, only the difference of the phase error between the two chirps is available for study. This is shown in the following discussion.

The phase of a single transmitted chirp is given by:

$$\phi_T(t) = 2\pi\gamma t^2 + 2\pi f_0 t + \phi_E(t)$$

where γ is the chirp rate in MHz/microsecond,

f_0 is the initial starting frequency, and

$\phi_E(t)$ is the unknown phase error on the chirp waveform

(t) denotes a function of time (in microseconds).

Some time later the same signal is received from a target in the scene. The received signal will be a duplicate of the transmitted one, delayed by a time equal to the two-way propagation delay to the target. This assumes a non-moving target and non-moving sensor. The receive phase is given by:

$$\phi_R = 2\pi\gamma[t-\tau_D]^2 + 2\pi f_0[t-\tau_D] + \phi_E(t-\tau_D)$$

where τ_D is the time delay (two-way) from the target, and

[t] denotes straight multiplication.

After dechirping the phase of the receive signal is:

$$\phi_\Delta = 4\pi\gamma t\tau_D - [2\pi f_0 - 2\pi\gamma]\tau_D + \phi_E(t) - \phi_E(t-\tau_D)$$

The first term is the linear phase component of the received sine wave. The second term is a phase delay equal to the round-trip time to the target. The final two terms make up the difference of the phase error.

The plots in Figures 4-15 summarize the analytical results. The figure shows that the 3 dB width of the IPR for a 10 dBsm target located 10 meters from the radar is very close to the theoretical value and within TRW's stated specification. However, there is a substantial degradation in performance for a the same target located 40 meters from the radar.

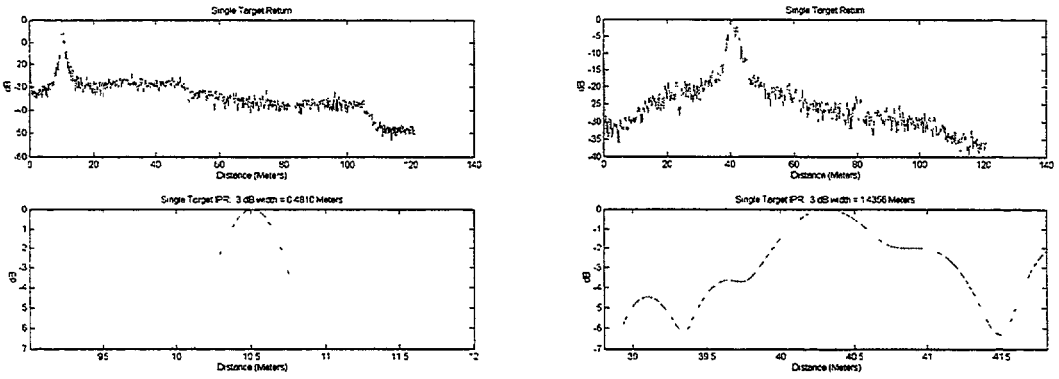

Target at 10 meters

Target at 40 meters

Figure 4-15. Performance With a Single 10 dBsm Target

As the target moves away from the sensor, the main beam starts to broaden as it is corrupted by nonlinearities in the FLAR. The performance degradation is similar to a synthetic aperture radar (SAR) problem ERIM encountered in the early 1980's and is caused by phase errors in the transmitted chirp. At near ranges the errors are small, but as the range increases the error becomes more noticeable.

In the case of the FLAR sensor, the phase errors causing the degraded IPR response were found to be of two different types. First, there is a quadratic phase error caused in part by waveguide dispersion. That is, the waveguide does not have constant phase characteristics over the bandwidth of the transmitted chirp. It could also be caused, in part, by other circuits with nonlinear phase characteristics. However there was no access to the circuit during this test so it is impossible to determine exactly where the error is being introduced.

The quadratic error causes a broadening of the mainlobe of the IPR, which decreases the system resolution. However, it does not explain the mainlobe corruption in Figure 4-18. The corruption resembles a sinusoidal phase error of many cycles per transmit pulse. A thorough signal analysis indicates that the transmitted signal is being distorted by a roughly 40 KHz sinewave within the radar.

A test sine wave was created and a sinusoidal phase error of 40 KHz was added to demonstrate the effects of sinusoidal phase error on a pure tone. The results, along with an actual FLAR sensor return, are shown in Figure 4-16. The middle plot of Figure 4-16 and the right plot are very similar in that they

have a mainlobe with very high sidelobe levels. Also of note is the asymmetry around the mainlobe. Both plots show a similar asymmetry, with the right side (far range) falling off faster than the left side (near range).

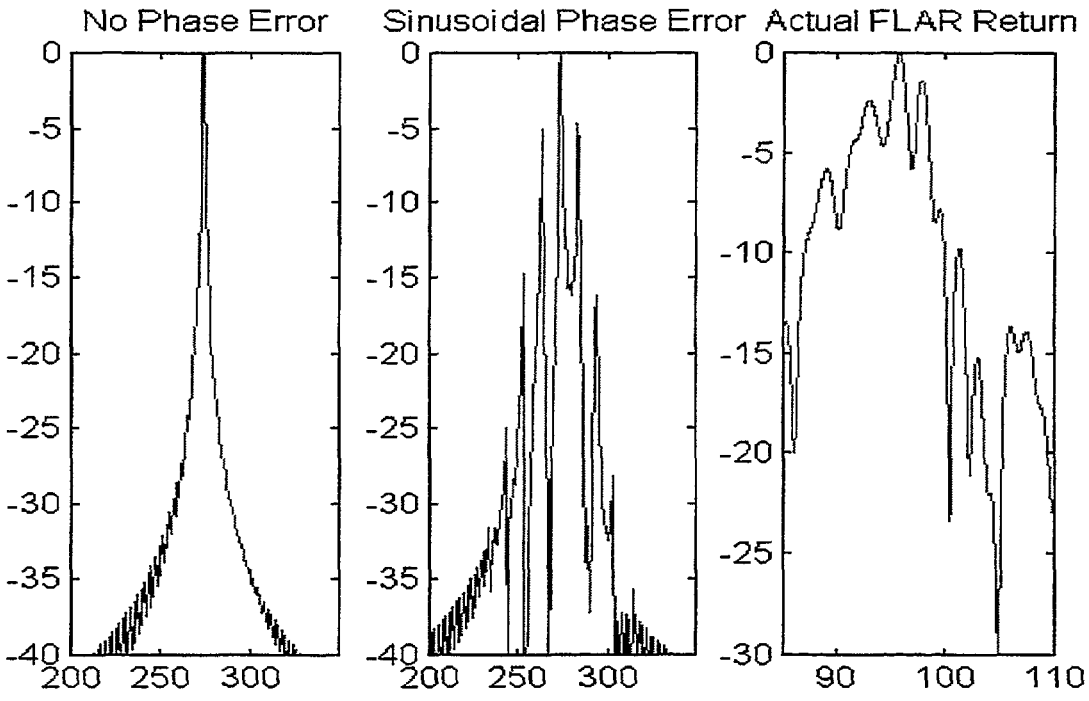

Figure 4-16. Effects of Sinusoidal Phase Error

Sinusoidal phase errors are worse at far ranges than they are at near ranges. This is because the dechirping process shows the phase errors as the difference between the transmitted and received error. Two sine waves with little phase difference (i.e., a small time delay with respect to their period) subtract leaving a small residual. As the phase difference increases the difference becomes larger. When the errors are out of phase the difference can actually be larger than the original phase error (constructive interference).

It is this sinusoidal error within the FLAR transmit chirp which causes the range accuracy deviations identified in the range accuracy tests discussed above.

With this analytical knowledge, the physical tests of FLAR range resolution performance were performed at near ranges to avoid the errors induced by the sinusoidal distortion.

Empirical Approach

This test used data previously collected for the range accuracy tests. However, the analysis differed. Only one set of six pulses was used. This data was heavily up-sampled by zero padding the FFT to 32768 (32K) points. This allowed an accurate measurement of the 3 dB IPR width.

A resolution demo was performed in the ERIM highbay facility using two similar corner reflectors placed close together. The corners were placed approximately 5 meters from the FLAR sensor. The corners were mounted on a low reflectance (cardboard) flat plate marked off in 0.1 meter increments. The flat plate was mounted on a 0.7112 meter (28 inch) high Styrofoam pillar. The corners were

initially set at a distance of 0.6 meters and moved in a tenth of a meter every collection thereafter. The comer reflectors were nominally sized to be 11.6 dBsm.

In these tests, the sensor was able to reliably resolve two similar sized objects placed more than 0.6 meters apart. At relative distances less than 0.6 meters, the sensor would sometimes resolve them and sometimes not. This matches fairly well with the theoretical analysis discussed above.

With regard to a generic automotive radar, the range resolution is important, as it allows the system to track and identify multiple objects. As shown, the quality of the transmit signal plays a major role in the range resolution performance of the radar. This of course relates back to the cost-performance trade-off which must be made by system developers in implementing a specific radar sensor design.

4.4.4 Baseline IF Signal Characteristics

The last baseline characteristic of interest in this program is the typical range profile produced by the FLAR when mounted on the ERIM TBV and presented with an "empty" roadway environment. The "empty" roadway environment refers to being on a typical roadway without any other vehicles or objects to produce a return.

Figures 4- 17 and 4-18 show range profile plots for 160 frames of radar data collected on an empty roadway. Figure 4-17 shows the range profile with the return levels on the y-axis and the corresponding range on the x-axis. Each profile from the 160 frames is overlayed on this plot. Figure 4-18 is a similar plot, except that instead of overlaying the profiles from each frame, a third dimension on the plot is used to position the frames side-by-side to produce a "time-history" of the returns. Both of these plots were made from the same set of data.

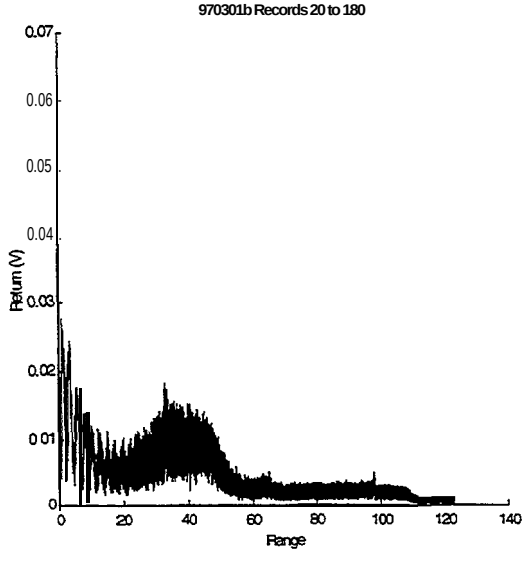

Figure 4-20. Two-Dimensional Range Profile Plot

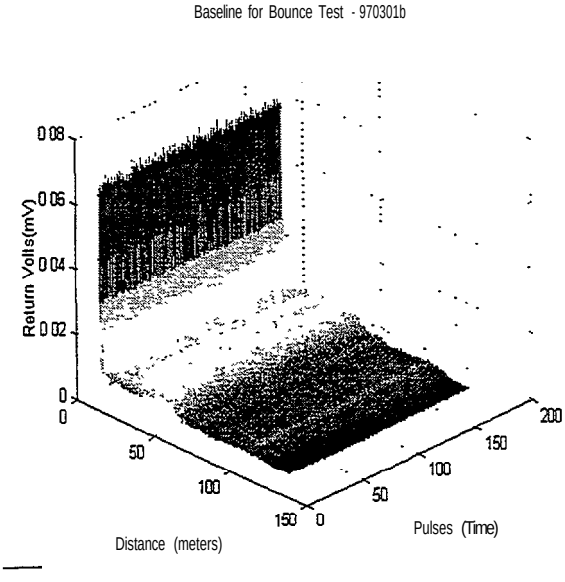

Figure 4-21. Three-Dimensional "Time History" Range Profile Plot

The FLAR exhibits a clear range profile characteristic which has been observed throughout the evaluation of the unit. First is the very-near-range return which is significantly above the noise floor of the sensor. This near-range return is attributed to leak-through of the transmit signal into the receiver circuitry. While this "return" is well above the noise floor, it does not compete with the return levels from any significantly sized objects. The TRW processing algorithm does not recognize this return as a target.

The second characteristic is the "'hump" which appears at ranges between approximately 30 to 45 meters. Initially, this hump was attributed to the range at which the antenna beam pattern intersected with the roadway surface. However, "bounce tests" were found to have no effect on the characteristic hump. Therefore, this hump is attributed to some distortion or response within the FLAR receiver circuitry.

These baseline characteristics of the FUR IF signal were considered in the analysis of data collected on the natural roadway.

5.0 MATERIALS AND THE ENVIRONMENT

This section will present the results of testing designed to quantify the effects of various materials and environmental conditions on FLAR performance. In these tests, the FLAR was being treated as a "generic" 94 GHz radar sensor. That is to say that none of the TRW algorithms associated with the ACC application were employed in arriving at these results.

The tests were conducted by carefully controlling the environment presented to the radar sensor and recording the raw radar signals, to evaluate changes based on the environmental conditions. The tests are divided into three sections: (1) Materials Testing, (2) Precipitation Testing, and (3) Contamination Testing. The results are summarized below and described more completely in Appendix B.

5.1 MATERIALS TESTING

The materials testing experiments were designed to quantify the amount of attenuation experienced by the radar signal when it is transmitted through various types of materials. This testing indicates the types of materials which should be considered for the housing of an automotive radar. The testing also identifies materials which the radar may have a difficult time detecting on the roadway.

The types of materials tested were:

- Plexiglas
- Windshield-type Glass
- Epoxy Glass
- Thin Cardboard
- TPO (a flexible plastic commonly used in automobile bumpers/facia)
- 3/4" Plywood
- RAM (Radar Absorbing Material)

The testing procedure consisted of placing a 5dBsm comer reflector at approximately 20 meters from the FLAR. Data was then collected as a sample of each material was placed between the FLAR and the comer reflector. Appendix B provides a complete description of the testing procedures and analysis. Also included in Appendix B is a brief explanation of the mechanisms which cause conductive and non-conductive materials to reflect energy.

5.1.1 Results

Three effects were observed during the material obstruction tests: (1) target signal strength attenuation, (2) direct reflection from the material being tested, and (3) creation of multipath returns. Each of these effects are discussed below.

Attenuation

Table 5- 1 summarizes the attenuation results of the material tests. The return levels and AGC settings for each collection are provided. These measured parameters were used to calculate the "AGC adjusted voltage" values which were then compared to determine the attenuation levels. The "Baseline" measurement was used as the reference for each attenuation calculation. Note that the attenuation levels provided are for "two-way" propagation. In other words, the radar signal passed through the material under test twice---once on transmission, and once after it was reflected off the target in the scene.

Table 5-1. Attenuation

Material Description	Measured Return Volts	AGC Control Setting (v)	AGC Mag. Attenuation (dB)	AGC Adjusted Return Volts	Two-Way Power Attenuation (dB)
Baseline	0.458	4.154	-19.9034	1.4403	0.0
Clear Plexiglas	0.405	3.956	-5.9292	0.5698	8.1
Thin Cardboard	0.4	3.906	-3.6324	0.4930	9.3
Windshield Glass (15 degrees)	0.381	3.906	-3.6324	0.4696	9.7
Epoxy Glass	0.343	3.906	-3.6324	0.4228	10.6
Thick Cardboard (corrugated)	0.188	3.906	-3.6324	0.2317	15.9
TPO	0.17	3.906	-3.6324	0.2095	16.7
TPO (15 degrees)	0.163	3.906	-3.6324	0.2009	17.1
Plywood (0.75")	0.056	3.906	-3.6324	0.0690	26.4
RAM	0.05	3.906	-3.6324	0.0616	27.4

Figure 5-1 illustrates the relative attenuation levels listed in Table 5-1. The materials are listed from lowest attenuation level to highest. Note that the RAM attenuation level represents the maximum attenuation level for the given test set-up (e.g., size and distance of target). Returns from the reference reflector placed in the scene were always observable in the radar data except for tests with the RAM. Even in tests with the plywood as the obstructing material, the FLAR still detected the 5 dBsm reference target at 20 meters.

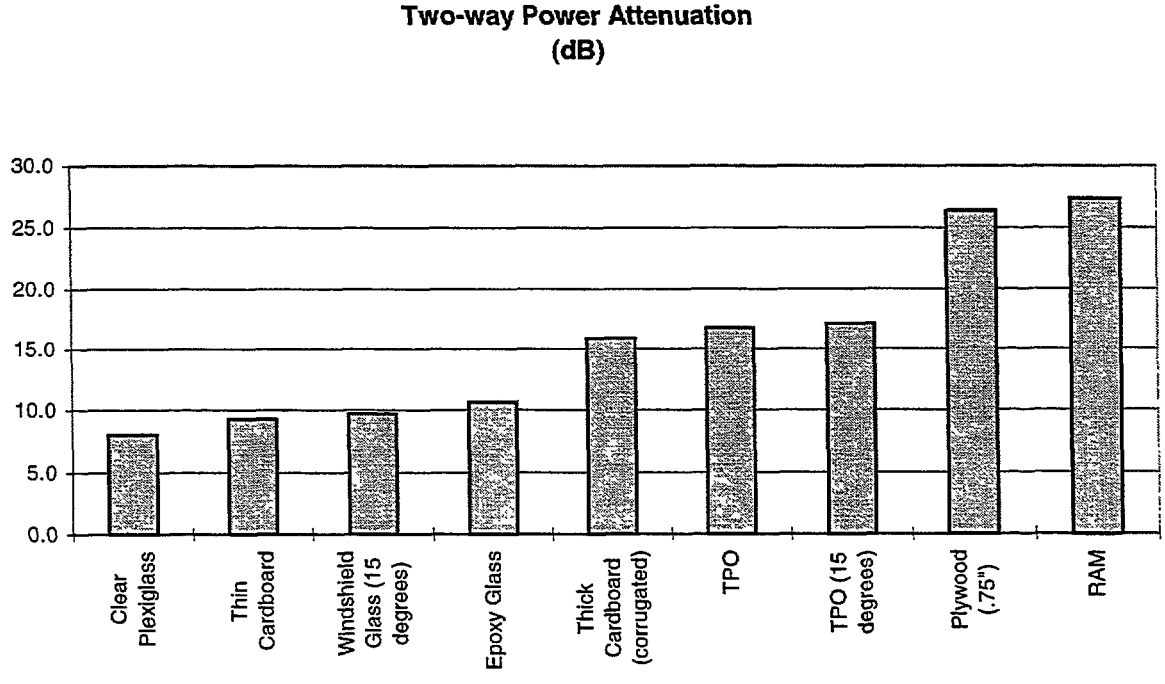

Figure 5-1. Attenuation Levels

The two-way attenuation levels vary from 8.1 dB for the clear Plexiglas to over 17 dB for the TPO (a plastic-type material commonly used for bumpers and facia styling) and over 26 dB for the plywood.

Reflections

In addition to attenuating the return levels from the reference reflector, many of the materials produced a direct radar signal return (i.e., the material reflected the radar energy). The materials producing the largest reflections were the windshield glass and TPO materials. Note that these reflection levels were highly dependent upon the orientation between the FLAR and the material sample. The plots included in Appendix B indicate that these reflection levels can be nearly equal to the return level from the reference reflector. Of course the material samples were at a much closer range than the reference reflector-l to 2 meters for the material samples versus 20 meters for the reference reflector.

Much lower direct reflections were observed from the cardboard, Plexiglas and plywood materials. While these reflections were clearly evident, they were not much above the noise floor of the FLAR.

Multipath

In addition to the reflections and signal attenuation, several of the material samples were observed to produce multipath returns from the reference reflector. Figure 5-2 is a diagram showing how an obstructing material can cause a multipath return. Some level of energy is refracted by the material and directed along an indirect path to the target. Since the distance the radar signal must travel the indirect path is longer than that along the direct path, the resulting range reading from the radar will be greater than the actual direct range to the target.

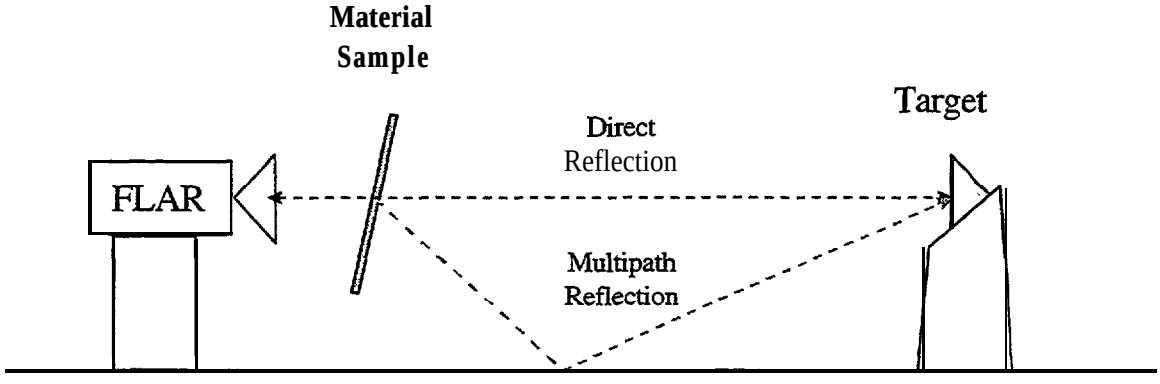

Figure 5-2. Multipath Reflection

Figure 5-3 shows the radar returns collected with a TPO material sample oriented 15 degrees off vertical. The multipath returns from the reference reflector are clearly evident. These effects were also observed for other materials tested. The effect of this phenomenon is that the peak level return from the reference reflector is decreased and false returns are produced. See the plots in Appendix B for more multipath examples.

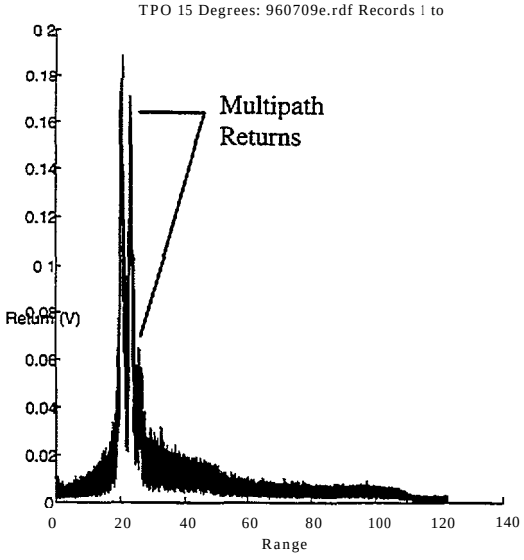

Figure 5-3. Multipath Returns From TPO Material at 15 Degree incident Angle

5.1.2 Conclusions

The tests discussed in this section have evaluated the effects of various materials on the target return levels for a 94 GHz radar. Figure 5-l summarizes the test results. The power attenuation level is provided for each material tested. Again, these attenuation levels correspond to the effects on a 94 GHz radar, but similar results can be expected at 77 GHz. Key observations of the test include:

- All materials tested allowed some portion of the radar signal to pass through the material and attenuated the radar signal to some degree.
- Except for the RAM material, the return from the reference reflector was still observable.
- Some materials reflected observable energy at certain orientations.
- Some materials produced multipath returns at certain orientations.

For styling, automotive radars will have to be integrated into the overall vehicle structure. This means the radar antennas will most likely be covered by some type of material. Knowledge of the absorption, transmitivity, and reflection characteristics of various materials is therefore critical to the successful implementation of automotive radar sensors.

These materials tests identify issues which must be addressed in order to successfully integrate a radar into the automobile. First, if the radar antennas are to be concealed by some material, the signal attenuation resulting from the chosen material must be compensated for to maintain the required radar sensitivity. Increasing the transmit power of the radar is au easy solution which may, however, have serious cost implications. Therefore, the concealing material must be carefully selected. Typically suggested locations for automotive radars would place the sensors either behind the plastic material of the front facia or grill, or behind the glass of the windshield or headlights.

The quantitative data from these tests (see Figure 5-1) indicate that placing the sensor behind a slanted windshield may produce less attenuation than placing it behind TPO-type plastic. An even better solution is to place it behind clear Plexiglas. Another option is to utilize specially fabricated material which exhibits very low attenuation; however, this could add cost to the system implementation.

In orienting the radar with respect to a concealing material, care must be taken not to produce a significant direct reflection which may saturate the radar receiver and “blind” it to other objects. Also,

and perhaps more serious from a threat assessment algorithm perspective, is the danger of having a concealing material generate numerous multipath returns. This could potentially place a large burden on the sensor processing electronics in terms of having to generate track files for objects which do not actually exist in the scene. Some level of multipath is inevitable, due to the complexity of the roadway environment, but inappropriately choosing and orienting a material in front of the radar sensor could severely compound the problem.

Another important issue regarding the attenuation characteristics of materials concerns accurately reporting the range to non-metal roadway targets. As vehicle manufacturers continue to reduce weights, the use of non-conductive plastic materials is expected to increase. As the results of these material tests indicate, the use of non-conductive materials can severely decrease the overall radar cross-section of the vehicle.

5.2 PRECIPITATION TESTS

The purpose of these precipitation tests was to evaluate the effects of snow, rain, and fog on the performance of the FLAR sensor. Since in automotive applications, the role of the radar would be to enhance the human's ability to perform during inclement weather, the sensor's performance capability under various weather conditions is critical to evaluate.

Both natural and simulated precipitation tests were conducted to arrive at the results discussed below. The snow data was derived from natural snow precipitation only. The fog data was collected using an artificial fog machine. The rain data was collected using both natural rain and rain from a high-pressure washer to allow the precipitation rate to be more controlled.

5.2.1 Results

In general, the precipitation tested had little effect on the FLAR's performance. In particular, the precipitation particles were not found to produce any significant returns to the FLAR and the attenuation levels were very small.

Table 5-2 shows the quantitative summary of the tests (see Appendix B for details). The return levels and AGC settings for each collection are provided. These measured parameters were used to calculate the "AGC adjusted voltage" values which were then compared to determine the attenuation levels. The "Baseline" for each collection was used as the reference for each attenuation calculation. Note that the attenuation levels provided are for "two-way" propagation. In other words, the radar signal passed through the precipitation-filled atmospheric medium twice-once on transmission, and once after it was reflected off the target in the scene.

Figure 5-4 illustrates the attenuation levels produced from the various levels and types of precipitation. These attenuation levels have been normalized to 10 meter ranges. These values are not considered substantial; return levels from the FLAR during static collections with precision reference reflectors in a controlled environment have been observed to fluctuate by values approaching these. Note that negative attenuation levels indicate that the peak return from the target in the scene actually increased. This could be due to the wet target causing more of the radar energy to 'be directed back in the direction of the FLAR, or due to the wet ground between the radar and the target causing a higher level of multipath returns.

Table 5-2. Precipitation Test Results

Precipitation Description	Target Range (m)	Measured Return Volts	AGC Control Setting (v)	AGC Mag. Attenuation (dB)	AGC Adjusted Return Volts	Two-Way Power Attenuation (dB)	Two-Way Power Attenuation (dB/10 m)
Light Rain	13	0.492	3.906	-3.6324	0.6064	-0.4	-0.29
Moderate Rain	13	0.441	3.906	-3.6324	0.5436	0.6	0.44
Heavy Rain	13	0.421	3.906	-3.6324	0.5189	1.0	0.75
Moderate Snow	22	0.083	3.906	-3.6324	0.1023	-0.7	-0.30
Heavy Snow	22	0.085	3.906	-3.6324	0.1048	-0.9	-0.39
Fog 1	3	0.366	3.906	-3.6324	0.4511	0.3	1.05
Fog 2	3	0.375	3.906	-3.6324	0.4622	0.1	0.35

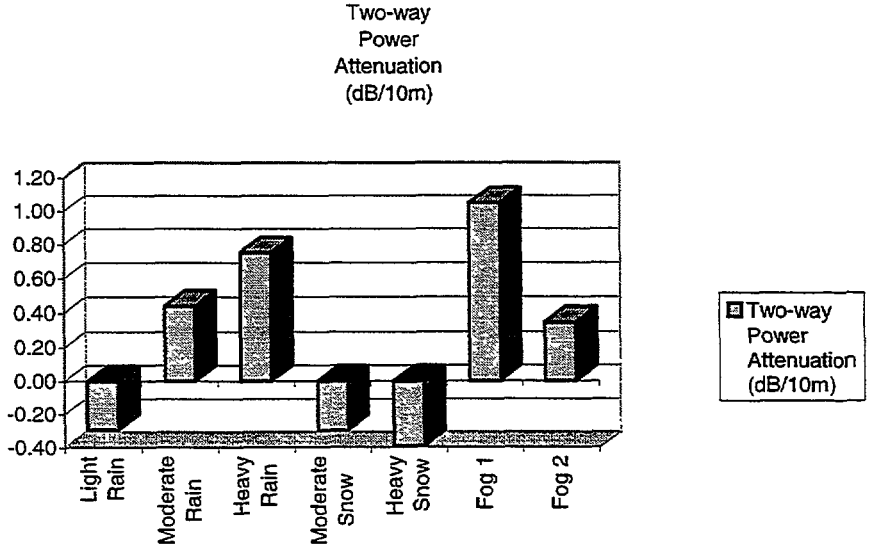

Figure 5-4. Precipitation Attenuation Levels

5.2.2 Conclusions

The primary conclusion of this test is that the FLAR performance was not significantly affected by the various levels and types of precipitation tested. In particular, the precipitation did not produce any observable return levels in the FLAR IF signal, and the attenuation levels were very low. However, the combination of a low RCS target at a far range during heavy rates of precipitation (or heavy fog) could cause a problem for an automotive radar.

The results achieved during this testing correlate well with those in the open literature. There are several papers which have been published on the attenuation of high frequency communication systems as a result of precipitation (see Appendix B). In general, both theoretical and empirical attenuation levels are stated to be about 10 dB per kilometer (one-way). Relating the information obtained in the

open literature to the operating ranges for automotive radars, one could expect power attenuation levels on the order of 1 to 3 dB at 100 meter ranges.

The measurements conducted as part of this program indicate that the actual attenuation levels may be somewhat higher than the 1 to 3 dB values mentioned above. More practical values could range from 2 to 10 dB of power loss at 100 meter ranges. Of course these values are highly dependent upon the rate of precipitation and also particulate size. As the particulate size approaches 1/4 wavelength of the radar frequency, the particulate will begin acting as an antenna.

In practical terms, the most important outcome of this test was the verification that the FLAR was capable of detecting targets within its field-of-view in the presence of significant precipitation. Except for the light rain collections, the target itself was visually obscured from the FLAR's location. During the heavy rain and fog tests, the target was often totally obscured. Despite the visual obscuration, return levels from the target were easily observed in the raw radar signal. These observations provide empirical support to those who cite radar's all-weather performance advantage over infrared or optical sensors for automotive applications.

The surprising phenomenon observed during the testing was the occasional increase in return levels in the presence of precipitation. This was observed during several collections. While the increase was not significant, it was measurable. Possible explanations for this phenomenon are:

- As the precipitation fell, the ground between the radar and the target became wet and a larger multipath return. Theoretically, enhanced multipath returns can increase actual target returns over 10 dB given a particular geometry.
- As the precipitation particles landed in the target, they caused an increase in the non-specular returns due to increased refraction and energy scattering. For tests conducted with reference reflectors, the increase may have come from particles landing on the styrofoam support pedestal.

5.3 CONTAMINATION TESTS

The purpose of these contamination tests was to evaluate how dirt, moisture, and snow would affect the FLAR's performance. The "contamination" could occur either at the target location or at the sensor. For example, the target itself would be considered "contaminated" if it were snow covered, or the sensor could be "contaminated" if its antennas were covered with mud.

The underlying concern for automotive applications is that dirt or other contaminants covering either the target or the sensor itself could severely inhibit the sensor's operation. For example, some laser sensors have had problems tracking targets contaminated with a thick film of dirt.

To evaluate the effect of contaminants on the FLAR, the following contamination scenarios were tested:

- Vehicle target contaminated with snow: In this scenario, the rear portion of the target vehicle (a Pontiac Sunbird) was partially (about 50 percent) covered with fairly dry snow.
- Vehicle target contaminated with water: In this scenario, the target vehicle (a small pick-up truck) was sprayed with water from a hose. Care was taken to perform the baseline test with already wet ground to isolate the vehicle contamination from multipath effects.
- FLAP sensor contaminated with snow: This scenario had approximately 1 inch of snow densely packed on the face of the FLAR sensor.
- FLAB sensor contaminated with semi-dry mud: The mud tests were divided into two levels of contamination- The first level had the glass plate covered with mud, but was still visually translucent. The second level had the glass plate covered with thick mud so that it was visually opaque. This second level is referred to in the tests as "very muddy."

5.3.1 Results

The results of the contamination tests were not what was intuitively expected. Therefore, several data sets were collected/analyzed for each type of test and the results were found to be consistent.

Table 5-3 shows the quantitative summary of the tests. The return levels and AGC settings for each collection are provided. These measured parameters were used to calculate the "AGC adjusted voltage" values which are then compared to determine the attenuation levels. The "Baseline" for each collection was used as the reference for each attenuation calculation. Note that the attenuation levels provided are for "two-way" propagation.

Table 5-3. Contamination Test Summary

Material Description	Measured Return Volts	AGC Control Setting (v)	AGC Mag. Attenuation (dB)	AGC Adjusted Return Volts	Two-Way Power Attenuation (dB)
Water on Truck	0.514	3.906	-3.632	0.634	-0.5
Snow on Car	0.09	3.906	-3.632	0.111	-1.2
Translucent Mud at Sensor	0.197	3.906	-3.632	0.243	-0.7
Opaque Mud at Sensor	0.306	3.906	-3.632	0.377	-4.5
Snow Covered Sensor	0.02	3.906	-3.632	0.025	11.8

Figure 5-5 illustrates the attenuation levels produced from the various types of contamination. Negative attenuation levels indicate that the peak return from the target in the scene actually increased.

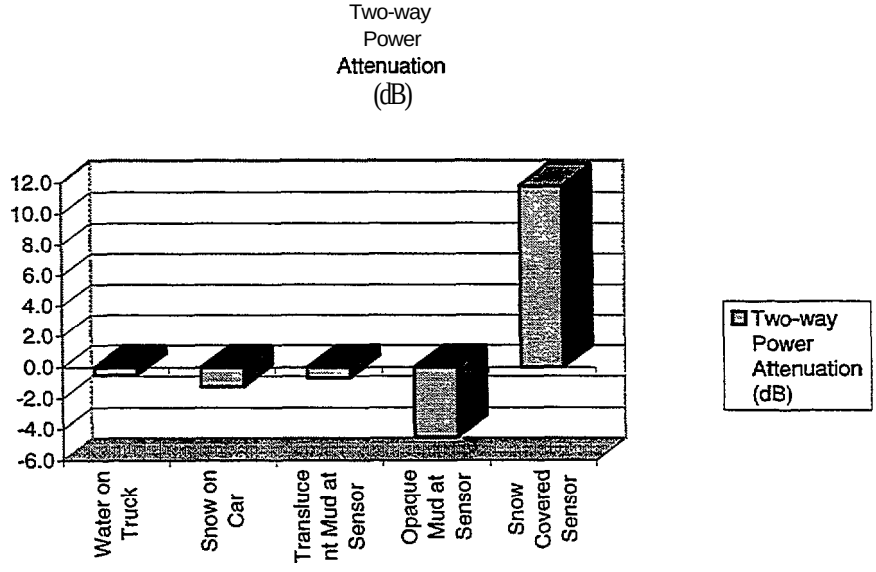

Figure 5-5. Contamination Attenuation Levels

The increases in peak return levels observed in the contaminated vehicle test results correlate with some of the observations made during the precipitation tests. In these cases, a possible explanation is

that the particulate contamination on the vehicle may be enhancing the return level by creating more scattering centers through refraction of the radar energy. See Appendix B for a detailed explanation of this hypothesis.

Results from the contaminated sensor test using semi-dry mud were similar to the contaminated target results. These tests again resulted in 'negative' attenuation, or an observed gain in peak return level. In analyzing the range profiles for the mud contamination tests, it was observed that the contaminated glass plate itself did not reflect energy back to the FLAR. The only difference between the baseline and contamination tests was the peak return level from the reference reflector. A potential cause for this phenomenon is discussed in Appendix B.

Finally, the result of the test in which the FLAR sensor was "caked" with 1 inch of wet snow indicates that the snow did in fact inhibit the sensor from detecting the reference target. Note that the 11 dB signal attenuation caused the reference target return to drop below the system noise level (i.e., the target was not observable).

Special Note: Although these tests indicate a snow-covered vehicle does not pose a detection problem for the radar, the reader should be aware that these results correspond to the specific contamination scenario presented to the FLAR. This scenario was fairly "dry" snow over 50 percent of the rear section of a mid-sized car. We would expect that the heavy "wet" snow which totally covers a vehicle could cause serious detection problems for radar system.

5.3.2 Conclusions

The analyses of the contamination tests have identified some phenomena which were unanticipated. The presence of contamination particulates at both the target and sensor have been observed to cause an increase in the peak return from reference targets in the FLAR's field of view. A potential mechanism for creating this phenomenon is presented in Appendix B. However, it should be noted that this hypothesis has not been thoroughly tested. More research into the phenomenon is required. While the measurement equipment and procedures have been reviewed, the limited access to the FLAR electronics has severely limited our ability to rule out a sensor specific response to the contamination.

The primary conclusion from these tests is that both target and sensor contamination from rain, snow, and mud may cause return levels from targets in the scene to actually increase. This would of course add to the robustness of the automotive radar in detecting objects at non-specular aspect angles. However, the mechanism causing this phenomena needs to be more clearly understood.

Conversely, the snow-covered sensor tests indicate that certain contaminants could also cause severe degradation in sensor performance to the point of missing significant targets within the scene.

6.0 ROADWAY TESTS

The Roadway Tests were conducted in both structured (on test tracks) and unstructured (on freeways) settings. These tests were focused on the sensing issues that might arise in the Adaptive Cruise Control application. To support them a data acquisition and analysis system was developed and upgraded when the prototype radar was upgraded (see Appendix C). In addition, a differential GPS system was developed (see Appendix D) as a truthing tool which provided an independent measurement of the distance between the host vehicle and roadway objects of interest. This system was demonstrated at the 1995 Annual Meeting of ITS America, and at the AVCS Committee Meeting & Vehicle Demonstrations held at the Transportation Research Center (TRC), Inc., East Liberty, Ohio in August, 1996. The structured tests (see Appendix E) were conducted at the TRC in October and November, 1996 in accordance with a test plan developed in cooperation with NHTSA. The detailed test results can be found in Appendix F.

The primary purpose for these tests was to characterize the sensor's measurement performance capabilities in five major categories that are discussed separately in the following sections. Detecting objects, vehicle background, moving or stationary, is a signal processing task that will be addressed from the standpoint of examining the information available from this sensor for detection purposes.

This section will summarize the results and key observations of the structured and unstructured roadway tests. These roadway tests have been grouped into five major categories. The reader should refer to Appendices F and G for more detailed discussion of each of the specific tests.

6.1 BACKGROUND MEASUREMENTS

The issue addressed by these measurements is false alarms that could result from returns induced by "background" objects which include vehicles parked on the roadside, roadside barriers, and vehicles in adjacent lanes.

Table 6- 1 summarizes the results of the various tests which were designed to address the background object/false alarm issue. The information in parentheses following the test title indicates the appendix section in which the tests are discussed in detail. Also, details regarding the test configuration are discussed in the test plan provided in Appendix E.

Table 6- 1. Background Measurements Results and Key Observations

Test Title	Results and Key Observations
Vehicle Induced False Alarms--Straight Roadway-Roadside Vehicle (F.1)	While the FLAR never tracked the roadside vehicles returns from the roadside vehicles were present in the raw radar data at ranges from 50 to 90 meters with the FLAR center beam active. The low return levels (max +3 dBsm for a tractor trailer) are attributed to the orientation between the host and secondary vehicles which causes the roadside vehicle to be illuminated by the low gain fringe of the center beam's mainlobe.
Vehicle Induced False Alarms--Straight Roadway-Adjacent Lane Vehicle (F. 1)	Returns from adjacent lane vehicles were not evident with the FLAR center beam active. Returns in the raw radar data were observed with the left beam active. It was observed that with a tractor/trailer in the adjacent lane, returns were induced by scatterers on both the front and rear portions of the vehicle.
Vehicle Induced False Alarms-Curved Roadway-Roadside Vehicle (F-10)	Guard rails around the outside of a curve induced a characteristic return in the radar as the host vehicle maneuvered through the turn. The returns from the guard rail were significant and the FLAR occasionally "locked-on" to the rail for brief periods of time. Vehicles parked along the curved roadway caused brief returns above those of the guard rail returns *as* the FLAR's center beam scanned across the vehicle. The level of return from the roadside vehicles were significant and varied by type of vehicle. The FLAR processing never "locked on" to any of the roadside vehicles.
Vehicle Induced False Alarms--Curved Roadway-Adjacent Lane Vehicle (F. 10)	Vehicles located in the adjacent lane on a curved roadway were found to induce returns in the raw radar data which are similar to those of a preceding vehicle in the same lane as the host vehicle on a straight roadway. This test scenario clearly indicates that to minimize false alarms, the radar must have some knowledge of the host vehicle dynamics or geometry of the upcoming roadway.
Open Roadway Tests	Bridge overpasses were found to induce substantial returns especially when the issue of vehicle loading was addressed. Tests to evaluate the response to various road surfaces resulted in no observable difference in backsound returns from concrete, asphalt, or dirt roads. Guard rails and roadside signs were observed to induce varying levels of return based on geometric orientation. Hills were found to have little effect in terms of inducing signals in the raw radar data.

6.2 TEMPORAL CHANGES

The issue addressed by these measurements is the ability of the FLAR to respond to traffic changes in terms of the **sensor response time.** Lead vehicle braking either the host or lead vehicle leaving the lane, and cut-ins are all typical roadway events that must be accommodated by the radar sensor. To provide sufficient time for threat assessment algorithm processing driver warning, and driver response, the radar measurement processing latency should be minimized.

Table 6-2 **summarizes** the results of the various tests which were designed to address the temporal change issue. The information in parentheses following the test title indicates the appendix section in which the tests are discussed in detail. Also, details regarding the test configuration are discussed in the test plan provided in Appendix E.

Table 6-2. Temporal Change Measurements Results and Key Observations

Test Title	Results and Key Observations
Braking Secondary Vehicle--Straight Roadway (F.2)	From a system perspective, the FLAR performed-well: accurate tracking of lead vehicle maintained at 20 Hz update rate and the reported range error was consistently < +l meter. From a sensor perspective, the dynamics caused large pulse-to-pulse signal return variations which approached 10 dB.
Intentional Lane Changes--Straight Roadway (F.4)	The radar sensor raw data responded virtually instantaneously to environmental changes. As the host vehicle changed lanes, the returns from the in-lane vehicle did not end abruptly, but dissipated rapidly as the radar beam boresight shifted during the lane change maneuver.
Tracking New Target Vehicle--Straight Roadway (F.5)	During these tests, the FLAR tracking algorithm performed well. As the secondary vehicle changed Ianes, the switch from tracking one vehicle to the other was instantaneous and stable (i.e., no jitter between the tracking of the two vehicles).
Tracking With Cut-In-Straight Roadway (F.6)	The results of these tests were much like those described in F-5 above. The reader is referred to the appendix for a discussion of near range cut-in problems which can occur due to the radar's limited field of view.
Open Roadway Tests	Many temporal changes in medium to heavy traffic scenarios due to dynamic maneuvers, oncoming traffic, and roadside objects were presented to the FLAR. The radar sensor exhibited virtually instantaneous response to the changing conditions, while the FLAR higher-level processing occasionally had some acquisition and tracking latency for new targets. This latency was generally well under 1 second. This illustrates the fact that from a system perspective, the delay in reporting the range to targets and generating track files for threat assessment is highly dependent on filtering and processing algorithms employed.

6.3 RANGE CLUTTER

The issue addressed by these measurements is radar's ability to discriminate between vehicles at various ranges from the host vehicle when the vehicles have significantly different radar cross sections. The vehicle furthest from the host vehicle represents range **clutter** relative to the vehicle immediately in front of the host vehicle (i.e., the secondary vehicle), and could limit the radar's ability to accurately measure the range between the host vehicle and the secondary vehicle.

Table 6-3 summarizes the results of the various tests which were designed to address the range clutter issue. The information in parentheses following the test title indicates the appendix section in which the tests are discussed in detail. Also, details regarding the test configuration are discussed in the test plan provided in Appendix E.

Table 6-3. Range Clutter Measurements Results and Key Observations

Test Title	Results and Key Observations
Strong Vehicle Clutter in Range-Straight Roadway **(F-7)**	The significant observation in this set of tests was that the EAR occasionally lost track of a near range low RCS vehicle (motorcycle) due to the **large** clutter signal from a further range large RCS vehicle (truck). The FLAR was observed to actually start tracking the further range vehicle. This could result in highly undesirable consequences for the ACC application. The range clutter induced errors can be caused by large differences in return levels and reduced radar sensitivity from Automatic **Gain** Control (AGC) activity.
Open Roadway Tests	While the open roadway tests presented the FLAR with a wide variety of traffic scenarios, the FLAR was never observed to lose track of a preceding vehicle due to range clutter returns. Geometries such as those created on the test track were not encountered. This illustrates one of the problems in testing automotive radars, namely, the roadway environment in which the radar must operate is virtually unconstrained with regards to the multitude of geometries and objects which can be encountered. Therefore, careful design and evaluation of potentially problematic scenarios must be carried out under test rack conditions.

6.4 AZIMUTH CLUTTER

The issue addressed by these measurements is radar's ability to discriminate between vehicles in adjacent lanes relative to the host vehicle when the host vehicle is measuring the range to an in-lane secondary vehicle. The vehicles in the adjacent lanesrepresent **azimuth clutter to the** host **vehicle and could** limit the radar's ability to accurately measure the range between the host vehicle and the secondary vehicle. Depending on the nature of the measurement error, the higher-level processing in the ACC system may not be able to reliably track the proper secondary vehicle.

Table 6-4 summarizes the results of the various tests which were designed to address the azimuth clutter issue. The information in parentheses following the test title indicates the appendix **section in** which the tests are discussed in detail. Also, details regarding the test configuration are discussed in the test plan provided **in** Appendix E.

Table 6-4. Azimuth Clutter Measurements Results and Key Observations

Test Title	Results and Key Observations
Out-of-Lane Vehicle Clutter-Straight Roadway, Single Clutter Vehicle (F.3)	Tests conducted with the FLAR center beam activeresulted in no returns from the out-of-iane clutter vehicle. Tests conducted with the FLAR left beam active resulted in low level retnrns from the out-of-lane clutter vehicle. These low level returns did not result in a loss of track on the preceding in-lane vehicle.
Vehicle Clutter in Azimuth-Straight Roadway, Multiple Clutter Vehicles F. 8)	These tests were run with only the FLAR center beam active. No returns from the out-of-lane clutter vehicles were observed. It should be noted that in these tests, the target vehicle maximum range was approximately 50 meters. Higher would result in a wider center beam coverage area which might begin to illuminate adjacent lanes at higher intensities.
Vehicle Clutter in Azimuth-Curved Roadway (F. 12)	Radar returns from both in-lane and adjacent lane vehicles were dependent upon the radius of roadway curvature, range to the vehicles, and boresight of the active antenna. Results showed that instead of tracking the in-lane vehicle, the FLAR tracked the vehicle in the outside lane under commonly encountered geometries. Tests with the left and right FLAR antenna beams active illustrated how "steering" the radar beam while negotiating a curve would enhance the radar sensor's performance with regards to tracking the in-lane vehicle.
Open Roadway Tests	Heavier traffic scenarios actually resulted in few returns from azimuth clutter due to occlusion and AGC sensitivity effects created by near range in-lane objects (heavy traffic density). Tests in lower density traffic showed that azimuth clutter (guard rails, signs, 2-lane oncoming traffic, etc.) cause significant transient returns levels in the raw radar data. The FLAR ACC algorithm never "locked-on" and tracked these returns, however, an algorithm designed for collision avoidance or warning may have false alarm/missed detection problems with these events. It should be noted that systems designed to ignore stationary objects could filter many of these clutter returns out.

6.5 ROADWAY GEOMETRY

Roadway geometry stresses the radar's ability to make range measurements because varying **roadway geometry** essentially requires a wider radar field-of-view to accommodate the angular variations between the host and secondary vehicles. Simply increasing the field-of-view will introduce azimuthal clutter, and thus a basic design trade-off is introduced, that is, simultaneously accommodating varying roadway and traffic conditions.

Table 6-5 summarizes the results of the various tests which were designed to address the roadway geometry issue and its relationship to field-of-view requirements. The information in parentheses following the test title indicates the appendix section in which the tests are discussed in detail. Also, details regarding the test configuration are discussed in the test plan provided in Appendix E.

Table 6-5. Roadway Geometry Measurements Results and Key Observations

Test Title	Results and Key Observations
Merging Traffic-Straight Roadway (F.9)	Roadway geometries associated with merging traffic lanes did NOT induce returns within the FLAR sensor. For these **tests,** the FLAR field-of-view was limited to 3 degrees in azimuth (i.e., the beamwidth of the center transmit antenna). The reader is referred to Section 6.4 ("Azimuth Clutter") for the description of tests which address field-of-view issues for roadside vehicles.
Tracking through a Curve and Vehicle Clutter in Azimuth-Curved Roadway (F.ll and F.12)	These test scenarios are probably the most pertinent to the field-of-view issue. These tests illustrated that the radar sensor field-of-view must be wider than 3 degrees to effectively track in-lane objects beyond a 20 meter **range** on a typical roadway curvature. The reader should also refer to test scenario F. 10 ("Vehicle Induce False Alarms-Curved Roadway") for a discussion on the impact of guard rails around curves and the relationship with sensor field-of-view.
Open Roadway Tests	The open roadway tests in medium to heavy traffic scenarios were somewhat encouraging in that they showed occlusion and AGC sensitivity effects from the higher traffic densities effectively reduced the radar's field-of-view by limiting its range. In these cases, the reduced field-of-view did not inhibit tracking the preceding in-lane vehicle throughout a variety of road geometries and provided the benefit in eliminating much of the out-of-lane clutter. However, light traffic tests showed how azimuthal clutter from numerous objects generate significant transient radar returns which must be addressed by processing algorithms. Many of these returns were from objects such as guardrails and roadside signs located on curved roadways. Also, a variety of hills were encountered in the open roadway tests which were found not to induce any significant returns in the FLAR sensor. The biggest impact on the hills was the loss of track on the preceding in-lane vehicle for low traffic densities.

7.0 SUMMARY

This section will summarize the findings and conclusions of the FLAR program.

7.1 CHARACTERIZATION OF VEHICLES AND ROADWAY OBJECTS

ERIM's Fine Resolution Rotary Platform Imaging Facility was used to create radar images of selected roadway objects. The roadway objects were selected to provide a meaningful set of data across a variety of objects which could be commonly found in a roadway environment. To that end, data was collected on the following objects:

- 1990 Chevy Corvette ZR-1
- 1995 Ford Taurus
- 1991 Jeep Wrangler
- 1993 Geo Metro
- Honda Motorcycle
- Human
- Stop Sign
- Cinder Block Wall

Data for each of the objects listed above was collected by a 94 GHz instrumentation radar. The object was rotated while being illuminated by the radar so that reflection characteristics of the object which are angle dependent could be identified. The radar data was processed to create two-dimensional images of each object. The images are useful in identifying the parts of the object which are and are not reflective to the radar energy for a given aspect angle.

In addition to the images, the radar data was processed to produce radar cross-section values for each object. The radar cross-section, or RCS, is a quantitative value which describes the object's level of radar reflectivity. The data collected supports analyzing RCS both as function of aspect angle and as a function of range across the target.

Section 3 of this final report provides a detailed description of both the image and digital data outputs available as a result of the database creation. The reader is also referred to Appendix A which includes a general discussion of radar cross-section and its dependence on object material, object shape, and aspect angle.

In general, the critical information available in the database can be divided into three categories: (1) maximum and minimum RCS values, (2) dependency of RCS on object shape or aspect angle, and (3) distribution of radar reflectors on a given object.

First, examining the data across all the objects which were measured, indicates that RCS levels vary from around +40 dBsm for a broadside perspective of a Jeep, to -2 dBsm for a motorcycle, down to - 10 dBsm for a stop sign. Furthermore, besides varying from object to object, the RCS can vary greatly for a single object depending upon aspect angle. For example, the RCS for the Jeep ranged from a maximum of +40 dBsm down to well below +5 dBsm. This wide variation plays a significant role in the development of radar sensor hardware which must have enough sensitivity to detect small RCS targets in the presence of large RCS targets.

Second, observations of maximum RCS as a function of aspect angle illustrates how an object's shape affects its radar reflectivity. For example, a relatively square Taurus-type vehicle exhibits a significant decrease in RCS as its aspect angle departs from 180 degrees (180 degrees is defined as

viewing a target from behind-&at is, looking at a vehicle's rear end). On the other hand, a more curved vehicle like a Corvette or Metro, exhibited less of an abrupt fall-off in RCS as the aspect angle departed from 180 degrees. These characteristics can be related to the ability of an automotive radar to track a given vehicle through a roadway curve. Again, knowledge of the extent of RCS changes as a function of aspect angle are valuable to a sensor designer in terms of addressing sensitivity issues.

Third, the images which were produced by the RCS database work provide valuable insight into the attributes of an object which actually cause the radar reflectivity. The images illustrated the distribution of radar reflectors (a.k.a. scatterers) across a target. In particular, the impact of side-view mirrors, wheels, under-body structures (e.g., transmission housing), and even body panel seams are evident. Knowledge of these radar scattering mechanisms is critical for radar processing and threat assessment algorithm developers. For example, the ability to identify multiple scatterers as part of a single object will have a major impact on the load placed on the processing electronics.

In summary, this effort established an initial database which could support the efforts of hardware designers, algorithm developers, and simulation programmers. The database's value to hardware designers and algorithm developers has already been discussed. However, its greatest utility may come in the form of support to collision avoidance system simulation programs. The simulation programs can make use of the data to apply range and aspect angle dependent RCS attributes to objects within the simulation scene.

Since the establishment of the database, information has been made available to interested parties in the form of hard copy images and data plots as well as digital data files. Hard copies of the data images and plots have been compiled into a "Catalog of Radar Scattering Characteristics for Common Roadway Objects." Hard copies of the database information is available through NHTSA-OCAR and the digital data files can be downloaded from ERIM's website (http:\www.erim-int.com).

Finally, additional discussion of the database can be found in the technical paper:

- "Millimeter Wave Scattering Characteristics and Radar Cross Section Measurement of Common Roadway Objects," P.K. Zoratti, J.J. Ference, R. Majewski, and R.K. Gilbert. In ***Proceedings of the SPIE on Collision Avoidance and Automated Traffic Management Sensors,*** Philadelphia, PA, 25-26 October 1995. Vol. 2592

7.2 ROADWAY TESTS

When one considers the number of different types of situations which may be presented to an automotive radar, a combinatoric explosion of possibilities is encountered. Obviously it was not practical to attempt evaluating the FLAR performance under all possible conditions. Instead, a series of tests was designed to evaluate the FLAR performance in some standard roadway settings and also some settings in which it was anticipated that the FLAR performance may be degraded. The primary variables for the tests included: (1) roadway geometry (e.g., straight, curved, sloped); (2) background clutter (e.g., out of path vehicles, guard rails, roadside signs); and (3) location and density of other moving vehicles on the roadway. The complete test plan is provided in Appendix E of this report.

The tests were conducted on both a closed test track and the open roadway. To evaluate the sensor performance during the road tests, the ERIM testbed vehicle acquired a variety of data including the raw radar signal (i.e., the IF signal), the TRW processed data (e.g., range and range rate of object being tracked), and video data of the road scene. In addition, a differential GPS system was used on several of the tests to independently locate the position of a target vehicle with respect to the FLAR sensor. Information on the DGPS truthing solution and its accuracy is provided in a paper in Appendix D of this report.

It is important to note that in interpreting the test results, one must take care in differentiating between the sensor performance and the system performance. The sensor performance pertains to the radar sensor itself and how it interacts with a given roadway environment. The system performance pertains to how the raw radar data is interpreted by the processing electronics and algorithms to depict the actual state of the environment within the sensor's field of view. The FLAR sensor used in these tests was developed by TRW for an Adaptive Cruise Control (ACC) type of application. Therefore, the sensor as well as the processing algorithms was designed specifically for the ACC application which has different requirements than a collision warning application. The real purpose of the tests conducted in this project was to focus on the sensor performance, but when appropriate, the overall TRW FLAR system performance was also analyzed.

The results from the various road scenarios tested are summarized in Section 6. A more complete discussion of each test conducted on the closed test track is provided in Appendix F. The data collections made on the open roadway are discussed in Appendix G. Both appendices include numerous data plots illustrating the sensor response to the specific test scenario. Where appropriate, quantitative calculations are provided. The analysis presented in Appendices F and G are is focused primarily on the radar sensor performance perspective. The objective of this analysis was to identify particular scenarios which could result in a raw radar data response which could prove difficult to interpret by standard processing and threat assessment algorithms.

The scenarios identified as potential problems are summarized below. ***(Note that these results must be taken in the context of the FLAR configuration which had 3 switched antennas with 3 degree azimuth and 3 degree elevation beam widths. Sensors with different configuration can have significantly different performance.):***

- **Roadside vehicles on a straight roadway** were observed to generate returns in the raw radar data at certain geometries which could be interpreted as objects within the host vehicle's lane.
- **Adjacent lane vehicles on a straight roadway** viewed by on the FLAR side beam antennas can generate multiple returns with significant range separation.
- **Guard rails and other roadside objects** on **curved roadways** generated significant returns which could cause false alarm problems.
- **Tracking vehicles around curved roadways** could prove to be problematic without knowledge of the roadway geometry in front of the sensor.
- **Near-range cut-ins and tracking of narrow vehicles** such as motorcycles could cause missed detections due to limited radar field-of-view.
- **Low RCS vehicles located between radar and large RCS vehicles** could cause missed detections.
- **Bridge or other roadway** overpasses were observed to generate significant returns in the raw radar data under certain circumstances.

In general, the radar sensor itself performed very well in the roadway tests. Somewhat counter-intuitive was the fact that the FLAR performed well under heavier traffic densities than under very light traffic densities. This was a result of a decreased amount of clutter returns due to limiting the sensor's field-of-view by the near range traffic. The response time of the raw radar data signal to changes in the roadway environment was virtually instantaneous given the 7 millisecond pulse repetition rate. For example, objects which were present in the radar's field-of-view for only a short duration, such as a parked vehicle on the roadside in a curve, were easily identified in the raw radar data. Two areas of the sensor configuration were identified as critical to achieving adequate roadway performance: (1) antenna design and control, and (2) receiver gain control.

The FLAR radar antenna beam width and side lobe levels define the radar's field-of-view at any given instant. While the side lobe levels were not attributed to any shortcomings in the radar performance, the roadway tests in this program indicated that the FLAR's 3 degree azimuth beam width may be too wide to reduce the effect of azimuth clutter to an acceptable level. For instance, vehicles parked on the roadside on a straight roadway induced radar returns which could possibly be interpreted as a low RCS object located in the center of the roadway. Also, it was identified that the FLAR would have problems tracking the appropriate vehicle around a curve without knowledge of the roadway geometry.

A number of automotive radar developers are addressing these shortcomings by using a narrower beam antenna which is scanned across the desired field-of-view. By correlating the radar response in one scan position with the response to another scan position, objects should be able to be placed much more accurately in a azimuth plane. This will work well for azimuth clutter on a straight roadway, but it appears that some knowledge of the roadway geometry preceding the host vehicle must be available to the processing algorithms in order to adequately handle tracking vehicles through a curve. The ability to "steer" the radar beam in a curve is highly desirable. Of course a scanned narrow beam antenna can add significant cost, real-estate requirements, and processing complexity.

The other area of sensor configuration which was identified as critical was the receiver gain control. The RCS data collected as part of this program indicates that objects may vary by as much as 40 dBsm or more. In order to achieve this dynamic range, the FLAR sensor employs a variable gain amplifier with the receiver electronics. When a large signal level is detected with the FLAR receiver, the gain of the amplifier is decreased. This can lead to the undesired situation where a large RCS target at some medium range, say a truck at 40 meters, can reduce the sensitivity of the radar such that a low RCS target at some near range, say a motorcycle at 20 meters, is not detected.

The extension of the basic radar sensor performance to the higher level system functionality for ACC and CWS applications becomes manifested in "false alarms" and "missed detections." From the tests conducted under this program, it was concluded that except for the limitations sited above, the FLAR sensor performs fairly well from the pure radar perspective. That is, the raw radar data responds to its environment in an acceptable manner. The success of applying the radar sensor to ACC and CWS lies in the interpretation (i.e., processing) of the radar data in such a way as to produce an acceptable level of false alarms and missed detections.

The roadway tests and their resulting data identified a number of scenarios which need to be addressed by the processing algorithms to be employed by ACC and CWS applications. The primary issue is the timely assessment of whether or not a detected object causes a real threat to the host vehicle. Systems which purposely ignore returns from stationary objects will have a much easier task in assessing threats, however, their value as a collision warning sensor will certainly be limited. Assuming that detection and assessment of stationary objects is necessary means that all the returns from the roadway "clutter" must be properly identified.

The returns which result from a guard rail as a vehicle enters a curve is a good example of a scenario which needs to be addressed by the threat assessment algorithm. Analyzing the raw radar data without knowledge of the roadway environment could lead to the conclusion that there is a stopped object within the host vehicle lane. Depending upon the timing thresholds of a CWS, this scenario could generate a false alarm. Data collected under this program shows a characteristic signature which develops from the guard rail as the host vehicle maneuvers through the turn. Knowledge of this signature, combined with information about the road geometry in front of the host vehicle and perhaps some knowledge of the azimuthal extent of the guard rail would allow a much more robust threat assessment algorithm to be employed. The empirical data collected during this program also indicates that roadside signs and oncoming traffic pose similar problems.

7.3 TESTING, EVALUATION AND CERTIFYING METHODOLOGIES

During this program a number of testing and evaluation methods were identified and used to evaluate the FLAR performance. In addition, the empirical data produced by the RCS and roadway measurements will support the creation of future "controlled" test procedures which can be repeated to refine an automotive radar's performance both in terms of configuration and processing.

To begin with the FLAR sensor had to be characterized via laboratory type measurements to support the analysis of roadway data. This laboratory characterization included measuring the range accuracy, range resolution, and field-of-view of the radar sensor. These types of measurements will need to be made to validate the typical performance specifications of the unit as claimed by the manufacturer. Section 4 of this report provides details on the tests conducted and their results.

During the laboratory testing, several anomalies in the FLAR's performance were identified and explained. For example, the range accuracy of the FLAR was found to decrease with increased distance. This error was attributed to the FLAR' s linear FM modulation rate (i.e., chirp rate) being slightly different than that specified by TRW. This was not surprising since the RF electronics within the sensor can have variability due to manufacturing, temperature, and age. The point to make is that procedures for calibrating the operation of automotive radar's must be developed to insure accurate performance.

After characterizing the baseline performance of the FLAR, the sensor was subjected to a number of different environmental conditions in terms of precipitation, material occlusion, and radome/target contamination. The results of these tests are provided in Section 5. The results of these tests is significant in terms of comparing radar technology to other types of remote sensing alternatives. As expected, the radar performed very well under precipitation tests which is the primary advantage of radar over infrared and laser sensing systems- The materials test served to identify the type of material which could be used to house the radar sensor as well as which materials could pose detection problems for radar.

Beyond laboratory calibration procedures and environmental sensitivities of the FLAR sensor, this program identified some common roadway scenarios which could cause erroneous performance. In addition to identifying the scenarios, the data collected also provides quantitative information which can be used to develop measurable and repeatable test procedures for validation of system performance.

For example, the open roadway tests conducted to evaluate the impact of bridge overpasses indicates that for a host vehicle to operate adequately with 5 degrees of tilt due to loading the rear compartment, the sensor must be able to reject the equivalent returns from a 2.5 dBsm object located approximately 14 feet above the roadway with a large azimuthal extent. Note that this problem statement defines several parameters around which a standardized roadway test can be created. With this type of empirical data, a test track can be outfitted with calibrated targets positioned properly to represent a given roadway scenario.

Besides generating the empirical data sited above, this program also validated the use of a differential GPS solution to serve as a truthing mechanism for specially orchestrated dynamic roadway testing.

In addition to actual physical testing of the radar sensor, the data produced by the RCS measurements database created under this program will support the simulation' testing of collision warning sensors. While a number of problematic roadway scenarios were identified during the roadway testing effort of this program, it was not possible to subject the FLAR to the extremely large number of combinatoric roadway scenario possibilities. Also, safety of the test engineers and drivers limited the types of orchestrated maneuvers which could be conducted. For these reasons, simulation testing of well modeled sensors and targets is still necessary.

7.4 CONCLUDING REMARKS

In summary, the foundation for generating a series of tests to validate the performance of an automotive radar has been produced by this program. This series of tests includes laboratory calibration, evaluation of environmental performance, repeatable roadway testing using calibrated reflectors to represent a roadway scenario, and the use of simulation.

To conclude this report, several areas related to collision warning and adaptive cruise control system development which warrant further investigation will be cited.

Expansion of RCS Database

There has been a high level of interest from system developers in the RCS database since its creation. This database consists of a limited number of objects all collected at a single range under benign weather conditions. Expansion of the database to include a more diverse set of objects under varying environmental conditions should be explored to support future sensor development and simulation programefforts.

Mutual Interference

This program focused on the response of the FLAR sensor to a variety of roadway scenarios. However, these roadway scenarios did not have any other radar sensors present. Susceptibility to mutual interference is highly dependent upon sensor confirmation. As these sensors are introduced into the automotive market and their penetration increases, the mutual interference among sensors may become an issue. Both physical and simulation techniques can be used to evaluate what level of impact mutual interference may have on widespread system operational use.

Manufacturing, Installation. and Calibration Issues

If FLAR-type sensors are to be mass produced and factory installed on vehicles, issues regarding sensor calibration must be addressed. For example, to what degree will an installation tolerance of +1 degree of sensor alignment affect system performance? Should the sensor be self-aligning? To what extent will the aging of the signal generation electronics affect system accuracy? If a host vehicle gets bumped in the parking lot and throws the system out of alignment, should the system detect the problem and notify the operator?

These types of issues are obviously far-reaching and sensor-dependent, however, some basic research in this area may affect sensor design to address these issues.

Use of Simulation to Test Sensor Design and Algorithm Implementation

Due to safety and the number of combinatoric roadway scenario possibilities, simulation of collision warning sensors may prove invaluable in the sensor design and algorithm implementation process. For example, one roadway scenario which was not tested as part of this program is the near-range cut-in. In this scenario an adjacent lane vehicle would enter the host vehicle's lane at a range of less than 5 meters. This scenario poses problems for an automotive radar with limited field-of-view. This scenario was not tested in this program due to safety concerns for the drivers. However, appropriately modeled simulation programs could address this and other dangerous scenarios and allow for sensor performance evaluation.

Human Factors and Response to Nuisance Alarms

Work related to the acceptable level of nuisance or false alarms would provide a valuable threshold benchmark to which automotive radar systems could be designed.

Human Factors and Response to Avoidance Maneuvers

To take collision safety to the ultimate level, collision sensors may someday initiate avoidance maneuvers. Basic research on the types and severity of maneuvers which are acceptable to the vehicle operator is necessary before any such system is implemented.

APPENDIX A. RADAR SYSTEM MODEL

This appendix has been included to provide a framework for the discussion in the body of this report and the remaining appendices; it covers some of the fundamentals regarding the operations of a Frequency Modulated Continuous Wave (FMCW) radar. The TRW Forward-Looking Automotive Radar (FLAR) used for this evaluation program operates on the FMCW principles outlined here. Much of the material in this appendix was taken from a two-day automotive radar course developed by ERIM for the National Highway Traffic Safety Administration.

This appendix contains the following information:

- Description of Radar Functions
- Components of a Radar System
- Object Reflections
- FMCW Radar Operating Principles

A.1 DESCRIPTION OF RADAR FUNCTIONS

The functions that a radar sensor provides to a larger system, whether it is collision avoidance or adaptive cruise control, can be broken down into three basic functions and two more advanced functions, as outlined below:

- Basic Functions:
  - ***Detection:*** determining whether or not an object is present in the vicinity of the radar sensor
  - ***Ranging:*** reporting the linear radial distance from the radar sensor to a detected object
  - ***Relative Range Rate (aka Relative Radial Velocity):*** reporting changes in range of detected objects as a function of time
- Advanced Functions:
  - ***Positioning:*** determining the location of an object with respect to the radar in terms of range and direction
  - ***Tracking:*** the ability to uniquely identify detected objects and maintain a time-history of their position (implemented as a control algorithm in the processor which may/may not affect actual radar operations-for example, antenna control)

The basic functions are provided by direct analysis of the radar return signals. The advanced functions require more complex processing which may require consideration of radar signal history or interfacing with electronics other than the radar itself.

The "detection" function is normally achieved by comparing the radar energy reflections captured by the receive antenna to some threshold level. When an object generates returns within the radar receiver which are sufficient in amplitude, the object is "detected" by the radar.

The "ranging" function is normally carried out by measuring the time delay corresponding to the elapsed time between the transmission of radar energy and reception of the radar energy reflected back by that object. FMCW radars, like the FLAR, use a modulation technique on the transmitted signal to determine the time delay.

The "'relative range rate" function can be achieved by two different methods. The first and most direct is to measure the "Doppler" shift induced on the transmitted radar energy by the movement of the object off which the radar energy reflects. The Doppler shift causes the frequency of the transmitted

waveform to be shifted either up or down, depending upon the target's movement. The second method is range differentiation, which uses the difference between two consecutive range measurements to determine the rate at which the range is changing. The FLAR uses the range differentiation method to calculate relative range rate.

The "positioning" function requires knowledge of the radar's antenna beam pattern and the current direction in which the antenna is pointed. By scanning an antenna beam across a scene and correlating returns to the beam's direction, the radar sensor can position the target with respect to the radar. The TRW FLAR uses a beam-switching mechanism to point the beam in three different directions. (Another method of positioning is the use of "'Monopulse Radar" which is beyond the scope of this appendix.)

The "tracking" function is achieved by having the radar internal processing electronics identify and maintain a time-history of the location of objects detected in the scene.

Figure A-l illustrates the role of a radar in an overall system like collision warning. The radar itself is a source of data input to the higher level system. From the radar developer perspective, the partition between the radar signal processing electronics and higher level system processing can be drawn in various locations, as indicated by the dotted line in Figure A-l.

With respect to the diagram in A- 1, this program evaluates the raw radar signal that connects the transmit/receive electronics to the signal processing electronics within the "Radar Sensor" box. To a lesser degree, the program also evaluates the TRW proprietary algorithms which define the signal processing performed on the raw radar signal.

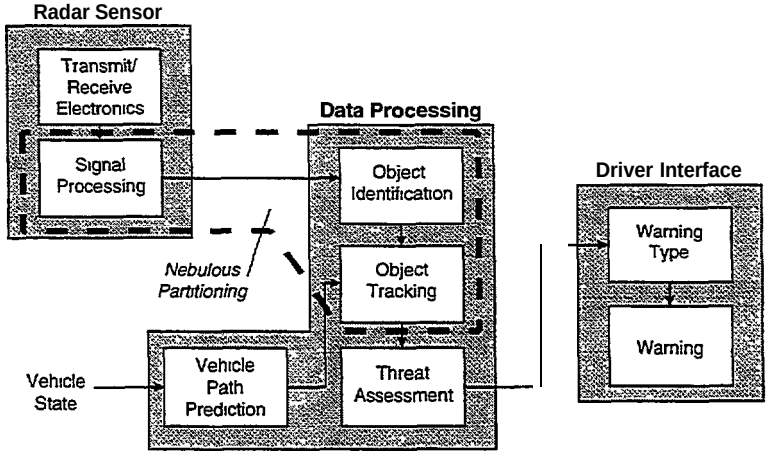

Figure A-l. Radar as Part of a Collision Warning System

A.2 COMPONENTS OF A RADAR SENSOR

Briefly, a radar is a device which emits electromagnetic energy (radio waves) and receives reflections of the emitted energy from objects within the radar's field-of-view. The field of view is defined by the antenna pattern(s). In the case of the FLAR, the emitted energy is in the 94 GHz region.

Figure A-2 shows a block diagram of a "generic" radar sensor. Table A-l lists the purpose for each of the components of the block diagram.

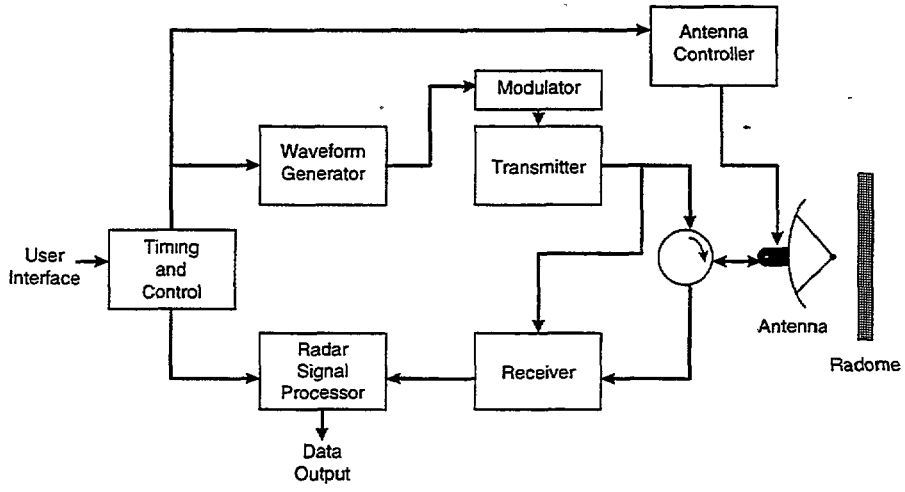

Figure A-2. A Generic Radar

Table A-1. Generic Radar Components

Component	Purpose
Waveform Generator	Controls the modulation of the transmitted waveform
Modulator	Controls the transmitter in terms of turning it on and off and dictating the frequency which is transmitted
Transmitter	Controls the power level of the emitted radio wave energy
Antenna/Controller	Concentrates and directs the emission of the radio energy
Receiver	Amplifies, filters, translates/demodulates the reflected energy, and formats it for use by the processing electronics
Signal Processor	Performs functions on the received signal to extract detection, range, and range rate info
Timing and Control	Synchronizes the operation of the other radar components

A.3 OBJECT REFLECTIONS

Different materials reflect radar energy to differing levels. Conductive surfaces such as metals reflect radar energy very well. Non-conductive surfaces reflect radar energy to varying degrees, based on their dielectric constant. Figure A-3 illustrates that when radar energy strikes an object, three things can happen: (1) the energy can be reflected, (2) the energy can be absorbed by the material, and (3) the energy can pass through the material. The degree to which any of these three possibilities occurs is dependent upon the dielectric constant, object geometry, and the angle at which the radar energy strikes the object (i.e., the incident angle).

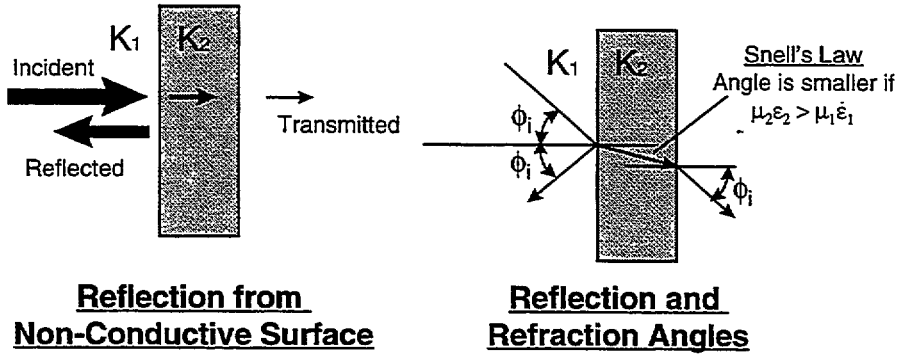

Figure A-3. Radar Energy Reflection and Refraction

Figure A-4 indicates what happens to the radar energy based on the incident angle. Reflection is similar to the optical reflection observed in a mirror. Refraction occurs when the radar energy gets "bent" as it passes through the interface between two mediums with different dielectric constants.

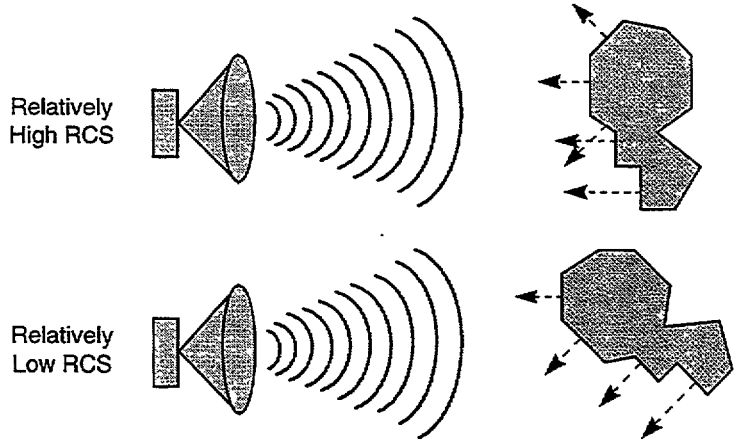

Figure A-4. Radar Returns and Orientation

Besides its material, the object's orientation also dictates how much energy is reflected back toward the radar. Figure A-3 shows an object which in one orientation causes a large return in the radar, while in another orientation causes a relatively low level return in the radar.

The amount of energy reflected back toward a radar by a particular object at a given orientation with respect to the radar is quantified by a parameter known as "Radar Cross Section" (RCS). The formal definition for RCS is given by the equation:

$$\text{sigma} = 4 * \pi * \frac{\text{Reflected power / Unit solid Angle}}{\text{Incident power / Unit area}}$$

RCS is typically measured in square meters or the decibel equivalent "dBsm," which is referenced to 1 square meter.

A more intuitive definition for RCS is illustrated in Figure A-5. Shown are two similar theoretical test setups. The first setup shows the object for which the RCS is to be determined, in this figure, a car. The second shows a theoretical scoop which captures energy and sends it to an isotropic antenna (i.e., an

antenna which emits an equal amount of energy in all directions). The size of this scoop can be changed to any required size. **The RCS of the object is equal to the size the scoop must be in order to induce the same level of return in the radar.** For example, suppose the car induces a 1 volt signal in the radar's receiver, and the scoop must be sized to 3 square meters to induce a similar 1 volt signal. Then the RCS for the car is 3 square meters (or 4.8 dBsm).

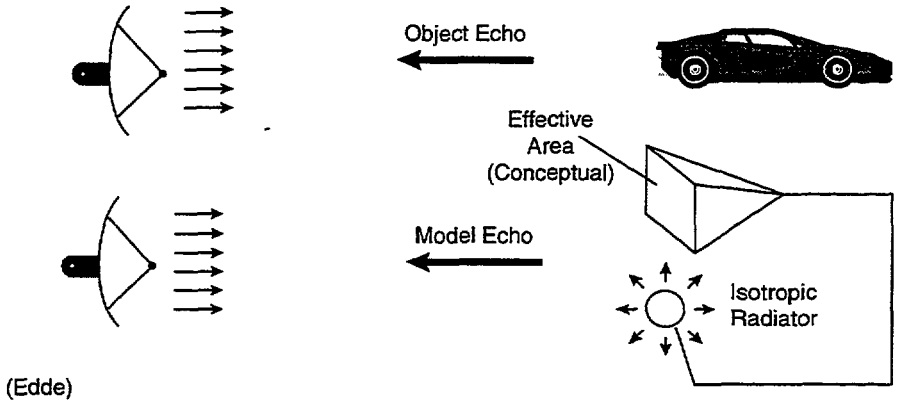

Figure A-5. Radar Cross Section Illustrated

In summary, it is a complex combination of reflection, refraction, absorption, transmission, and geometric directivity which defines how a particular object is viewed by a radar sensor. A parameter for measuring the "size" of an object from the radar's perspective is called the radar cross section, which indicating how much energy will be reflected back to the radar.

A.4 FMCW RADAR OPERATING PRINCIPLES

FMCW radar operation follows the following basic principles:

- The transmit signal is frequency modulated (normally a linear modulation—chirp)
- The modulation of the received echo is compared to the modulation of the transmitted signal to determine time delay and therefore range
- Range rate is determined by range differentiation or Doppler processing

Graphical representations in both the time and frequency domains for a chirp waveform are provided in Figure A-6. The linear frequency modulation of a chirp is applied to the transmit frequency in an FMCW radar. In the case of the FLAR, the transmitted waveform is modulated over a 375 MHz bandwidth centered at 94 GHz.

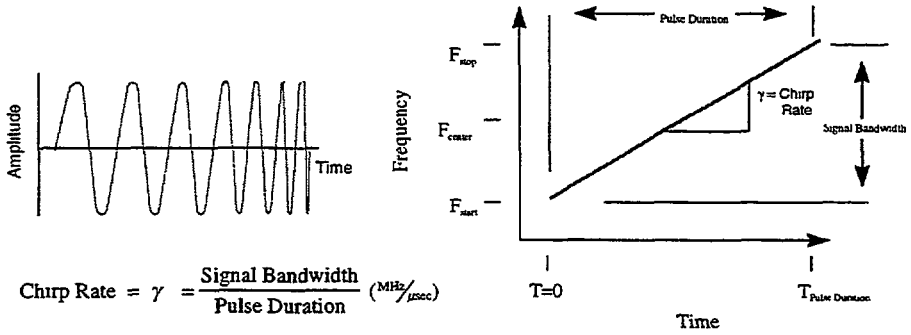

Figure A-6. Time and Frequency of a Chirp Waveform

The key to FMCW operation is that the shape of the waveform which returns to the radar after reflecting off objects is the same shape as the transmitted waveform. Figure A-7 illustrates how an FMCW radar can compare the transmitted and received signals to determine time delay.

The transmitted signal is emitted from the radar at time T = 0. Some time later (T_{d1}), a reflection back from an object is received by the radar. During the time of flight of the reflected signal, the transmitted signal frequency has increased as dictated by the chirp rate. Therefore, at any given instant of time after T_{d1}, there is a difference in frequency between the signal being transmitted and the one which was received. This frequency difference is proportional to the time of flight for the received signal (the proportionality constant is the chirp rate). Since radar energy travels through the atmosphere at a constant speed ($c = 3 * 10^8$ meters/second), the time of flight is therefore proportional to the range to the object which reflected the energy (the proportionality constant is c/2). This is the principle by which an FMCW radar measures range.

Obviously, the radar can receive reflected signals from many objects at different ranges within its field of view. The physical means of comparing the transmitted and received signal frequencies is performed by a passive component called an RF Mixer. The transmit and received signal are input to this component, and the output is the difference between the two. The output of the mixer is referred to as the intermediate frequency or IF. **The plots of the "raw radar signal" provided in this report actually map the IF signal from the FLAR sensor.**

By capturing the IF signal from the FLAR and analyzing it with frequency domain processing techniques, an evaluation for how the radar is responding to its environment can be made.

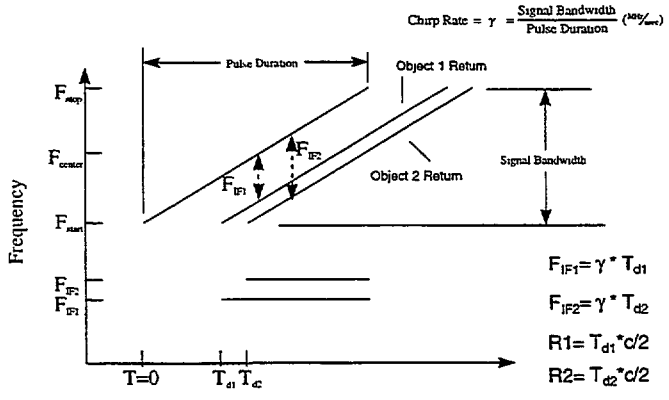

Figure A-7. Determining Time Delay

APPENDIX B. MATERIAL AND ENVIRONMENTAL DATA

B.1 MATERIALS TESTS-SUMMARY

B.1 .1 Purpose

The intent of the following tests was to quantitatively assess the effect on the quality of the received radar signal when the radar's "view" of a target is obstructed by various materials found on a car or in a roadway situation.

B.1.2 Procedure

The FLAR was placed approximately I meter off the ground on a level surface. A 5 dB comer reflector was then placed 20 meters away from the FLAR, at about the same height on a Styrofoam pillar. A reading of the comer reflector without any obstruction was taken to get a baseline from which all other tests could be compared. About 1.5 seconds of data were collected (about 200 samples) using ERIM's Data Collection Software. The baseline test was verified, as were all others, by recording the test with a SVHS camera.

The next step was to test the effect of individual materials on the FLAR sensor. A large piece of the material to be tested was placed in the beam of the sensor. Another 1.5 seconds of data were collected using the ERIM Data Collection Software. The tests were repeated using the following pieces of material:

glass, Plexiglas, epoxy glass, thin cardboard, thick cardboard (about l/3" thick), TPO (a plastic material often used in automotive bumpers), plywood, and RAM (radar absorbing material).

After the tests were completed, the data was analyzed on the ERIM Analysis PC using the ERIM's FUR Analysis Software. The AGC attenuation values were recorded and a Matlab script was written to analyze and average the return levels. Outputs from the Matlab analysis are attached.

The plot in Figure B-l (from the analysis PC) shows the return from a 5 dBsm comer reflector located just over 20 meters from the radar. The automatic gain control (AGC) setting is given below the plot. The AGC is a variable gain amplifier used in the radar receiver circuit to increase the dynamic range of the A/D converters. The AGC setting must be compensated for when comparing relative return levels. The attenuation value (in dB magnitude) associated with the AGC setting is also provided for each plot. The level of attenuation is referenced to the maximum gain of the amplifier.

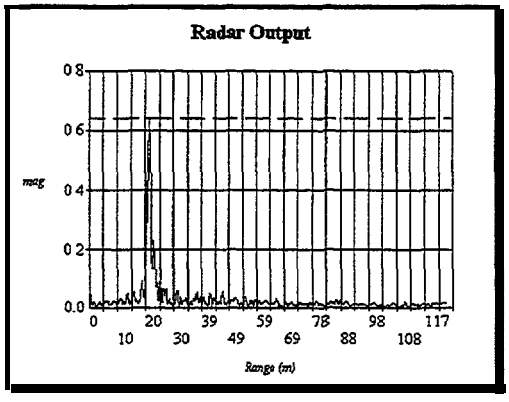

AGC: 4.15391 volts
Attenuation: 19.90 dB

Figure B-l. Baseline Test

The plot in Figure B-2 shows the return from a 5 dBsm comer reflector located just over 20 meters from the radar, with a sheet of glass placed about 1 meter from the RADAR at an angle of about 15 degrees from vertical. The automatic gain control (AGC) setting and corresponding magnitude

attenuation is given below the plot. The reflected signal from the glass can be seen in Figure B-2 as the smaller of the two spikes.

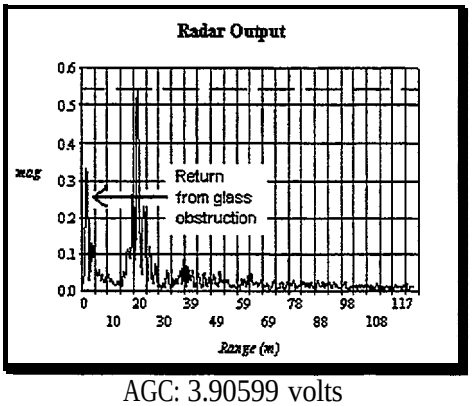

AGC: 3.90599 volts
Attenuation: 3.63 dB

Figure B-2. Glass (15 degree angle)

B.1.3 Results

Three effects were observed during the material obstruction tests: (1) target signal strength attenuation, (2) direct reflection from the material being tested, and (3) creation of multipath returns. Each of these effects are discussed below. A rudimentary discussion of reflection and refraction mechanisms is provided at the end of this section.

Attenuation

Table B-l summarizes the attenuation results of the material tests. The return levels and AGC settings for each collection are provided. These measured parameters were used to calculate the "AGC adjusted voltage" values which are then compared to determine the attenuation levels. The "Baseline" measurement was used as the reference for each attenuation calculation. Note that the attenuation levels provided are for "two-way" propagation. In other words, the radar signal passed through the material under test twice--once on transmission, and once after it was reflected off of the target in the scene.

Figure B-3 illustrates the relative attenuation levels listed in Table B-l . The materials are listed from lowest attenuation level to highest. Note that the RAM attenuation level represents the maximum attenuation level for the given test set-up (e.g., size and distance of target)- Returns from the reference reflector placed in the scene were always observable in the radar data except for tests with the RAM. Even in tests with the plywood as the obstructing material, the FLAR was still capable of detecting the 5 dBsm reference target at 20 meters.

Table B-1. Attenuation

Material Description	Measured Return Volts	AGC Control Setting (v)	AGC Mag. Attenuation (dB)	AGC Adjusted Return Volts	Two-Way Power Attenuation (dB)
Baseline	0.458	4.154	-19.9034	1.4403	0.0
Clear Plexiglas	0.405	3.956	-5.9292	0.5698	8.1
Thin Cardboard	0.4	3.906	-3.6324	0.4930	9.3
Windshield Glass (15 degrees)	0.381	3.906	-3.6324	0.4696	9.7
Epoxy Glass	0.343	3.906	-3.6324	0.4228	10.6
Thick Cardboard (corrugated)	0.188	3.906	-3.6324	0.2317	15.9
TPO	0.17	3.906	-3.6324	0.2095	16.7
TPO (15 degrees)	0.163	3.906	-3.6324	0.2009	17.1
Plywood (.75")	0.056	3.906	-3.6324	0.0690	26.4
RAM	0.05	3.906	-3.6324	0.0616	27.4

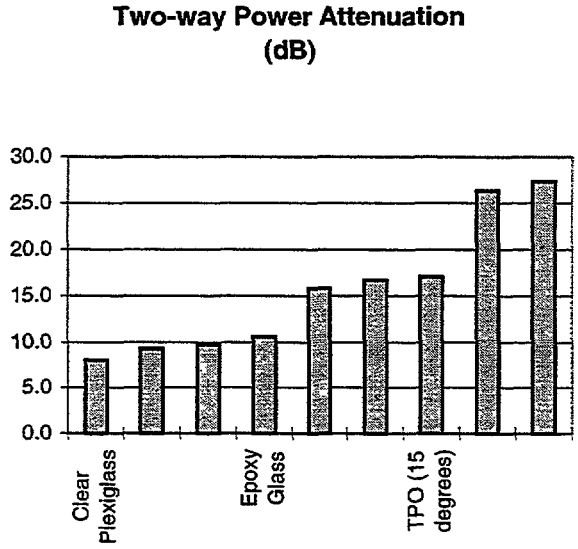

Figure B-3. Attenuation Levels

The two-way attenuation levels vary from 8.1 dB for the clear plexiglas to over 17 dB for the TPO (a plastic-type material commonly used for bumpers and facia styling) to over 26 dB for the plywood.

Reflections

In addition to attenuating the return levels from the reference reflector, many of the materials produced a direct radar signal return (i.e., the material reflected the radar energy. The materials producing the largest reflections were the windshield glass and TPO materials. Note that these reflection levels were highly dependent upon the orientation between the FLAR and the material sample. The plots

at the end of this section indicate that these reflection levels can be nearly equal to the return level from the reference reflector. Of course the material samples were at a much closer range than the reference reflector—1 to 2 meters for the material samples versus 20 meters for the reference reflector.

Much lower direct reflections were observed from the cardboard, plexiglās and plywood materials. While these reflections were clearly evident, they were not much above the noise floor of the FLAR.

Multipath

In addition to the reflections and signal attenuation, several of the material samples were observed to produce multipath returns from the reference reflector. Figure B-4 shows a diagram of how an obstructing material can cause a multipath return. Some level of energy is refracted by the material and directed along an indirect path to the target. Since the distance the radar signal must travel the indirect path is longer than that along the direct path, the resulting range reading from the radar will be greater than the actual direct range to the target.

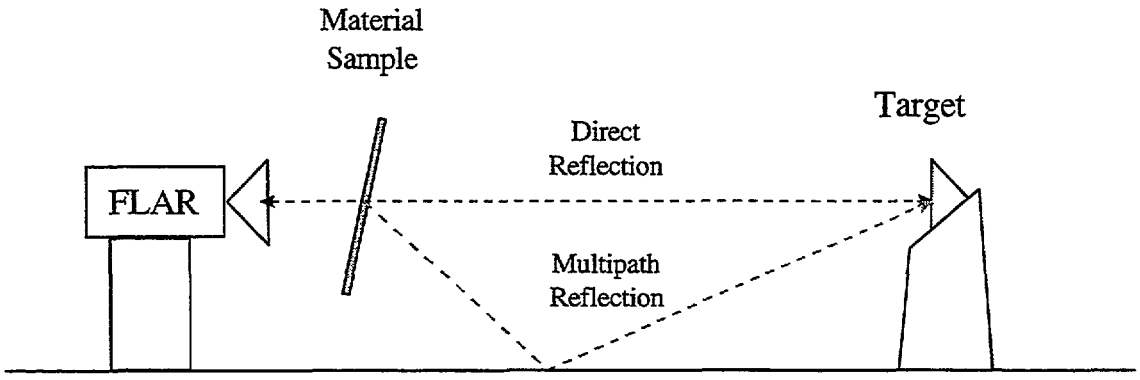

Figure B-4. Multipath Reflection

Figure B-5 shows the radar returns collected with a TPO material sample oriented 15 degrees off vertical. The multipath returns from the reference reflector are clearly evident. These effects were also observed for other materials tested. The effect of this phenomenon is that the peak level return from the reference reflector is decreased and false returns are produced. See the plots attached for more multipath examples.

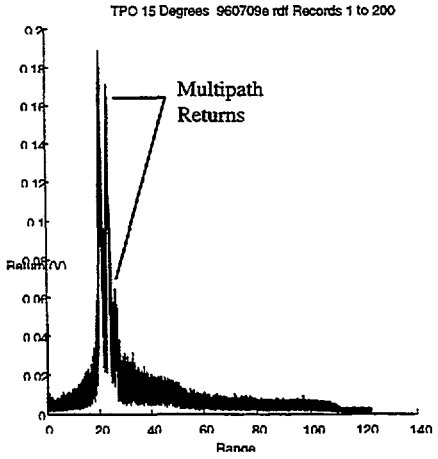

Figure B-5. Multipath Returns From TPO Material at 15 Degree Incident Angle

B.1.3.1 Reflection and Refraction Mechanisms

Radar signals are reflected by two different forms of media: conducting and non-conducting. When a wave strikes a conducting medium, the electric field of the wave induces an inverse electric field in the medium. This electric field then radiates a wave back at the radar sensor, as a returned signal.

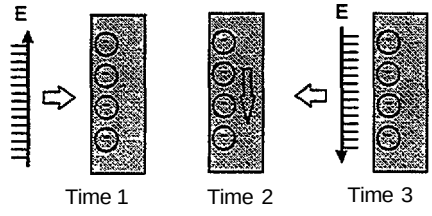

Figure B-6. Reflection From Conductive Surface

A non-conducting medium also reflects RADAR signals, but not always all of it. The amount of the signal that is reflected back at the sensor depends on the ratio of the dielectric constants (K_c) of the two media (in this case we use air as a medium). The dielectric constant of a medium determines the division between the electric and magnetic fields of a wave. When the RADAR signal enters a new medium the dielectric constant readjusts the wave's electric and magnetic field ratio. In order to do this, some of the signal must be reflected.

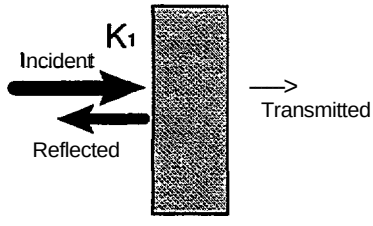

Figure B-7. Reflection From Non-Conductive Surface

If the angle of incidence (θ_1) is greater than zero when a wave enters a new region with a different dielectric constant, then the wave is deflected, otherwise known as refraction. The deflection increases the angle of incidence of the wave proportional with the ratio of the dielectric constant of the two media.

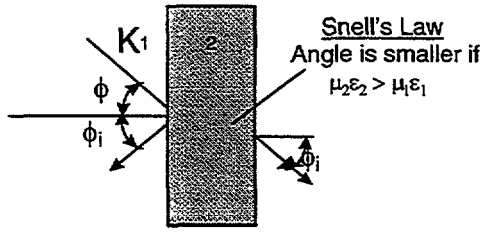

Figure B-8. Reflection and Refraction Angles

The level of return of the reflected signal, also depends upon the orientation and shape of the object. The orientation and shape of the object determines the reflected signal's direction. Figure B-9 illustrates how orientation affects signal return level.

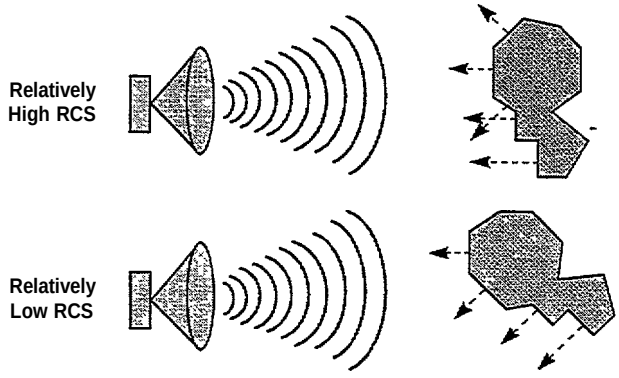

Figure B-9. Object Orientation Effect on Reflected Signal

B.1.4 Conclusions

The tests discussed in this section have evaluated the effects of various materials on the target return levels for a 94 GHz radar. Figure B-3 summarizes the test results. The power attenuation level is provided for each material tested. Again, these attenuation levels correspond to the effects on a 94 GHz radar, but similar results can be expected at 77 GHz Key observations of the test include:

- All materials tested allowed some portion of the radar signal to pass through the material and attenuated the RADAR signal to some degree.
- Except for the RAM material, the return from the reference reflector was still observable.
- Some materials reflected energy at certain orientations which was observable.
- Some materials produced multipath returns at certain orientations.

For styling, automotive radars will have to be integrated into the overall vehicle structure. This means the radar antennas will most likely be covered by some type of material, therefore knowledge of the absorption, trausmitivity, and reflection characteristics of various materials is critical to successful implementation of automotive radar sensors.

These materials tests identify issues which must be addressed to successfully integrate a radar into the automobile. First of all, if the radar antennas are to be concealed by some material, the signal attenuation resulting from the chosen material must be compensated for to maintain the required radar sensitivity. This can be easily done by increasing the transmit power of the radar. However, this may have serious cost implications. Therefore, the concealing material must be carefully selected. Typically suggested locations for automotive radars would place the sensors either behind the plastic material of the front facia or grill, or behind the glass of the windshield or headlights.

The quantitative data of these tests (see Figure B-3) indicate that placing the sensor behind a slanted windshield may produce less attenuation than placing it behind TPO-type plastic. An even better solution is to place it behind clear Plexiglas. Another option is to utilize specially fabricated material which exhibits very low attenuation, however, this could add cost to the system implementation.

In orienting the radar with respect to a concealing material, care must be taken not to produce a significant direct reflection which may saturate the radar receiver and "'blind" it to other objects. Also, and perhaps more serious from a threat assessment algorithm perspective, is the danger of having a concealing material generate numerous multipath returns. This could potentially place large burdens on the sensor processing electronics in terms of having to generate track files for objects which do not actually exist in the scene. Some level of multipath is inevitable just due to the complexity of the roadway environment, but inappropriately choosing and orienting a material in front of the radar sensor may severely compound the problem.

Another important issue regarding the attenuation characteristics of materials concerns accurately reporting range to roadway targets constructed from non-metal material. As vehicle manufacturers continue to reduce weights, the use of non-conductive plastic materials is expected to increase. As the results of these material tests indicate, use of non-conductive materials could severely decrease the overall radar cross-section of the vehicle.

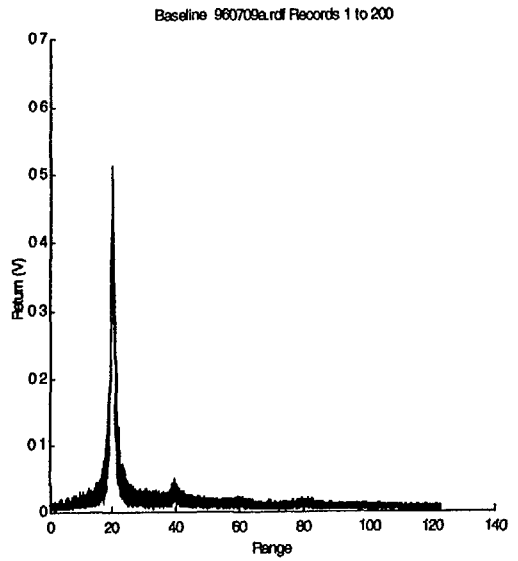
Baseline 960709a.rdf Records 1 to 200
Return (V)
Range
0
0.1
0.2
0.3
0.4
0.5
0.6
0.7
0
20
40
60
80
100
120
140

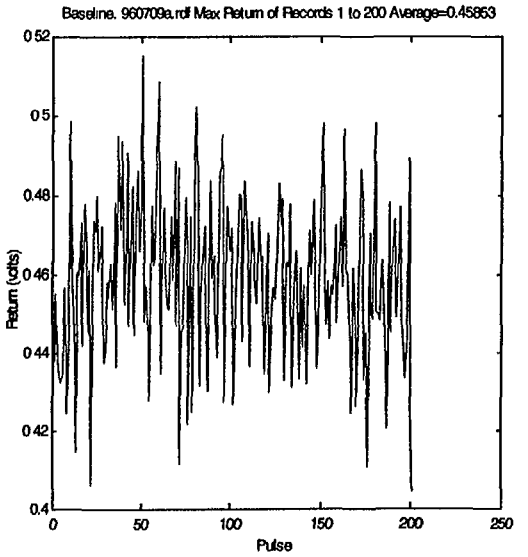
Baseline. 960709a.rdf Max Return of Records 1 to 200 Average=0.45853
Return (volts)
Pulse
0.4
0.42
0.44
0.46
0.48
0.5
0.52
0
50
100
150
200
250

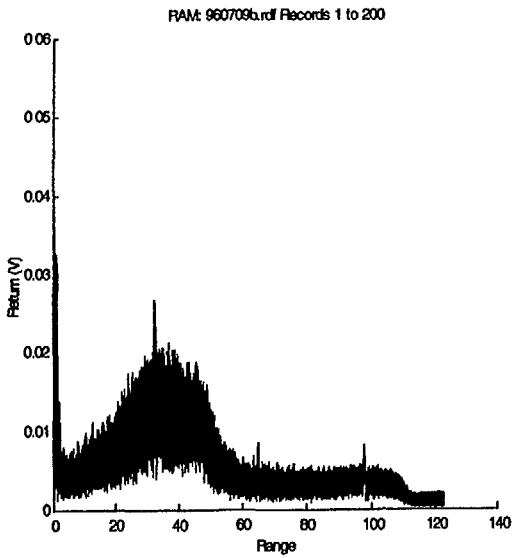
RAM: 960709a.rdf Records 1 to 200
Return (V)
Range
0
0.01
0.02
0.03
0.04
0.05
0.06
0
20
40
60
80
100
120
140

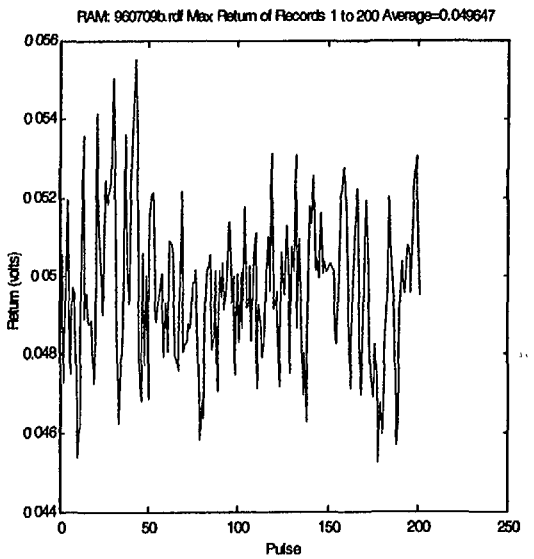
RAM: 960709a.rdf Max Return of Records 1 to 200 Average=0.049647
Return (volts)
Pulse
0.044
0.046
0.048
0.05
0.052
0.054
0.056
0
50
100
150
200
250

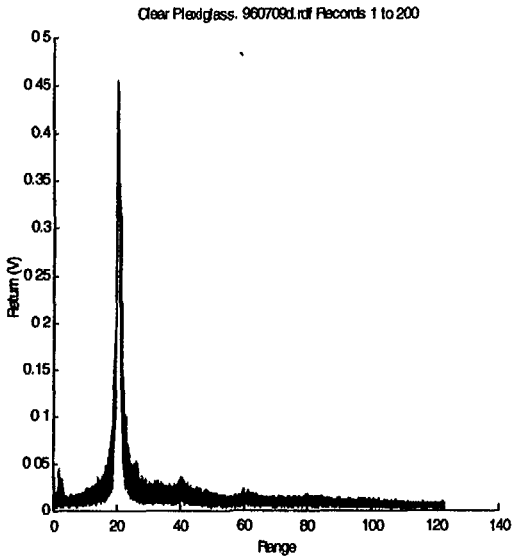
Clear Plexiglass. 960709d.rdf Records 1 to 200
Return (V)
Range

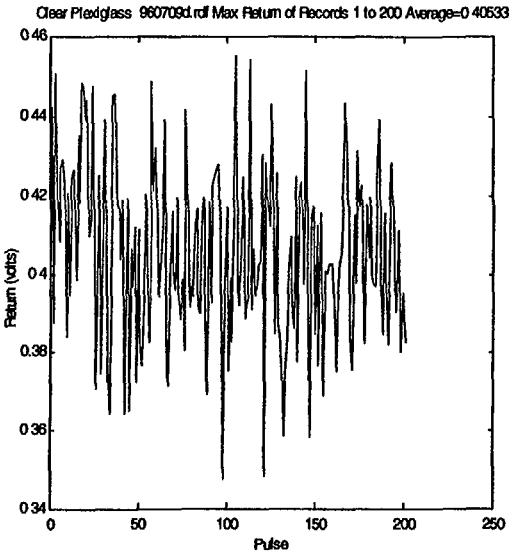
Clear Plexiglass 960709d.rdf Max Return of Records 1 to 200 Average=0.40533
Return (volts)
Pulse

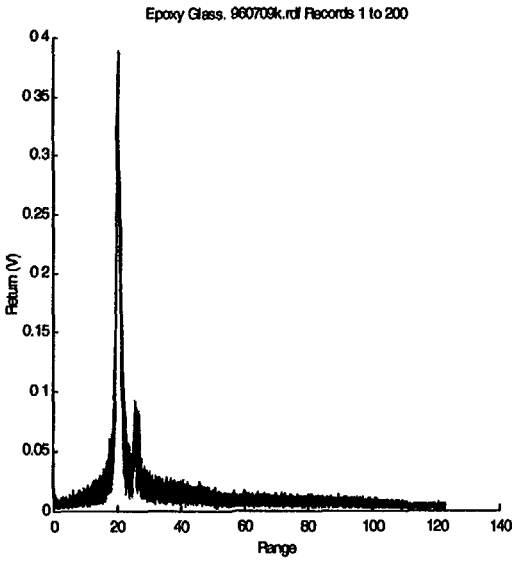
Epoxy Glass. 960709k.rdf Records 1 to 200
Return (V)
Range

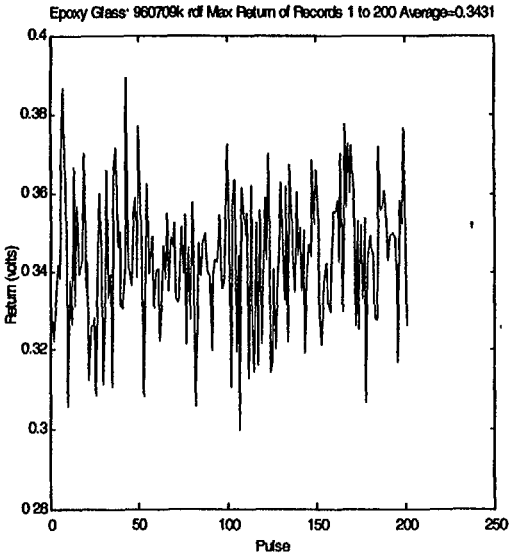
Epoxy Glass 960709k.rdf Max Return of Records 1 to 200 Average=0.3431
Return (volts)
Pulse

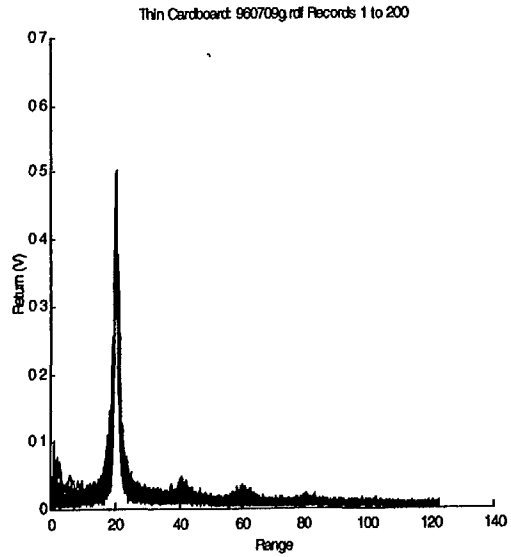
Thin Cardboard: 960709g.rdf Records 1 to 200
Return (V)
Range
0
0.1
0.2
0.3
0.4
0.5
0.6
0.7
0
20
40
60
80
100
120
140

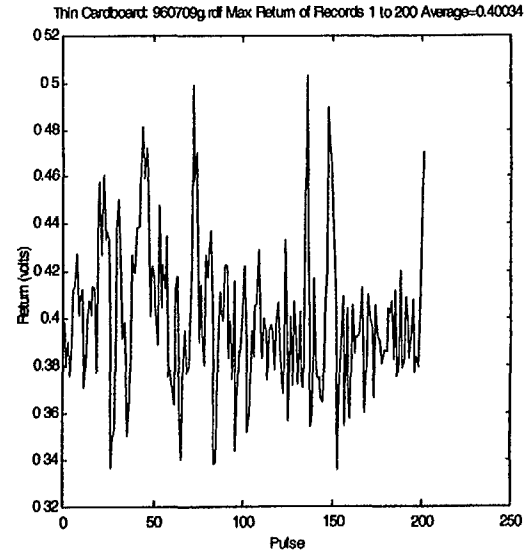
Thin Cardboard: 960709g.rdf Max Return of Records 1 to 200 Average=0.40034
Return (volts)
Pulse
0.32
0.34
0.36
0.38
0.4
0.42
0.44
0.46
0.48
0.5
0.52
0
50
100
150
200
250

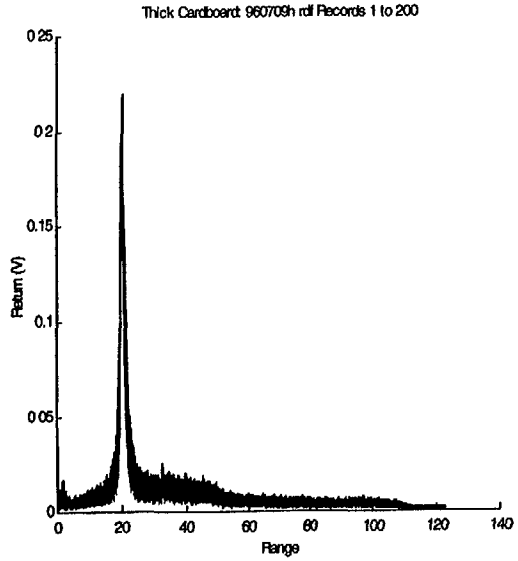
Thick Cardboard: 960709h.rdf Records 1 to 200
Return (V)
Range
0
0.05
0.1
0.15
0.2
0.25
0
20
40
60
80
100
120
140

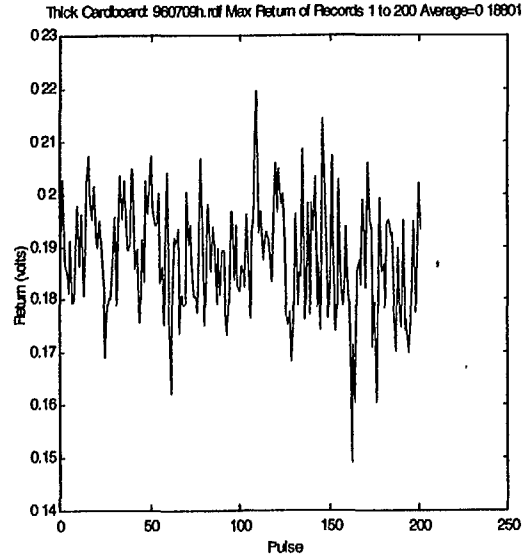
Thick Cardboard: 960709h.rdf Max Return of Records 1 to 200 Average=0.18801
Return (volts)
Pulse
0.14
0.15
0.16
0.17
0.18
0.19
0.2
0.21
0.22
0.23
0
50
100
150
200
250

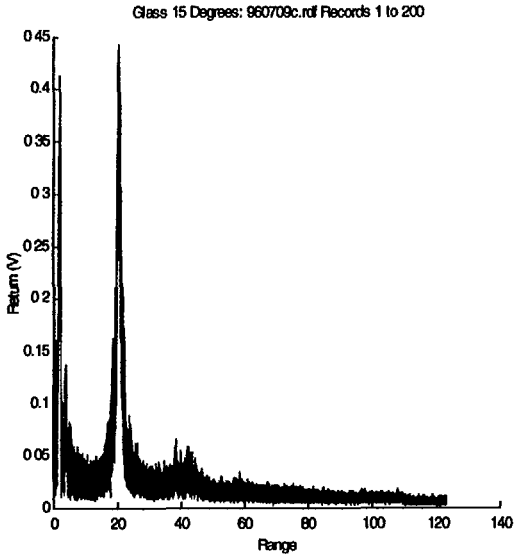
Glass 15 Degrees: 960709c.rdf Records 1 to 200
Return (V)
Range

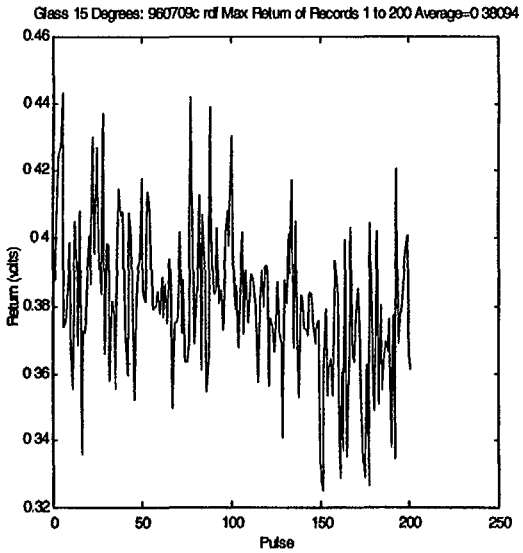
Glass 15 Degrees: 960709c rdf Max Return of Records 1 to 200 Average=0 38094
Return (volts)
Pulse

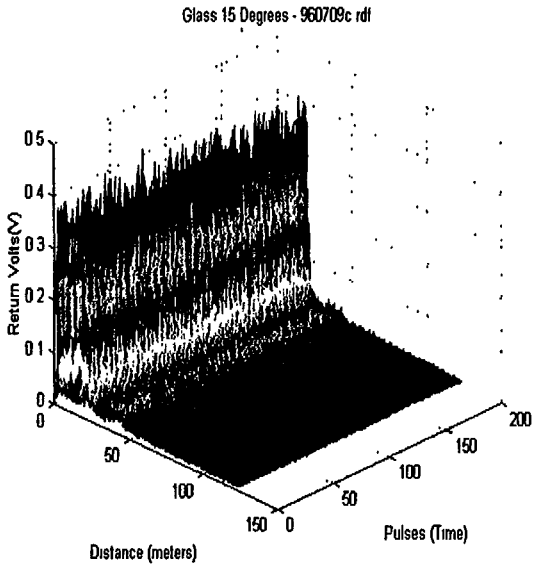
Glass 15 Degrees - 960709c rdf
Return Volts(V)
Distance (meters)
Pulses (Time)

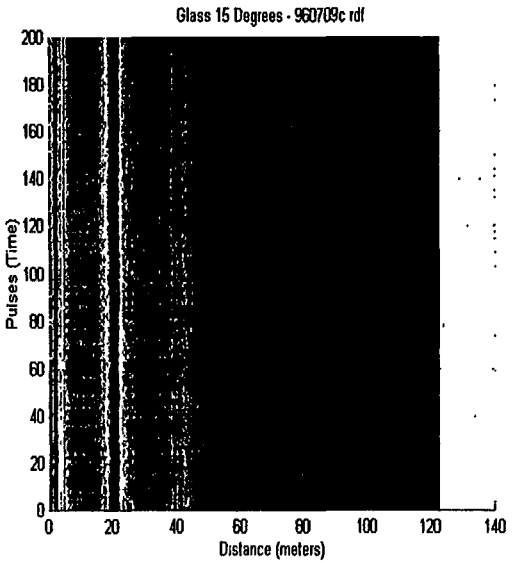
Glass 15 Degrees - 960709c rdf
Pulses (Time)
Distance (meters)

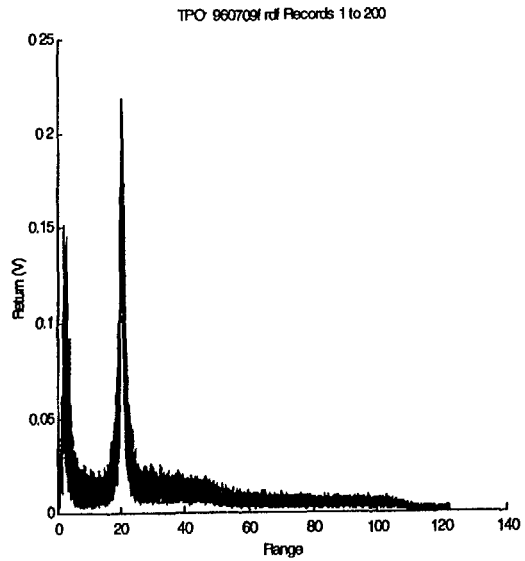
TPO 960709f rdf Records 1 to 200
Return (V)
Range

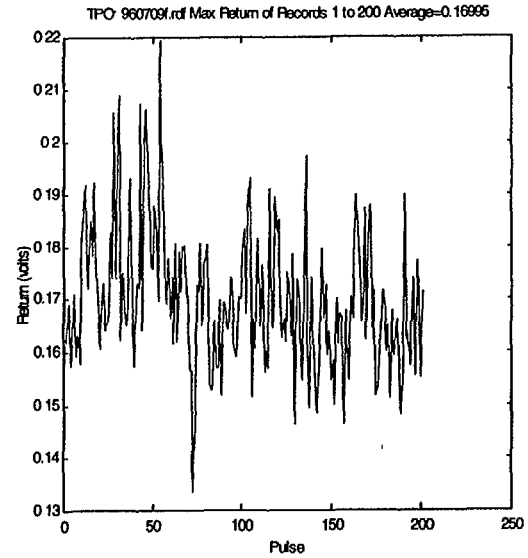
TPO 960709f.rdf Max Return of Records 1 to 200 Average=0.16995
Return (volts)
Pulse

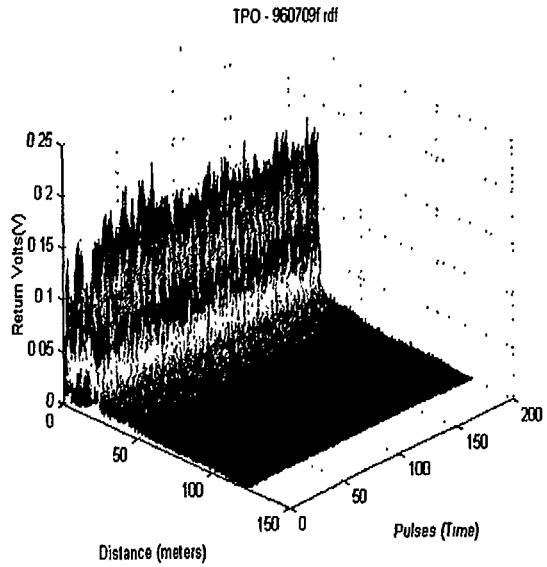
TPO - 960709f rdf
Return Volts(V)
Distance (meters)
Pulses (Time)

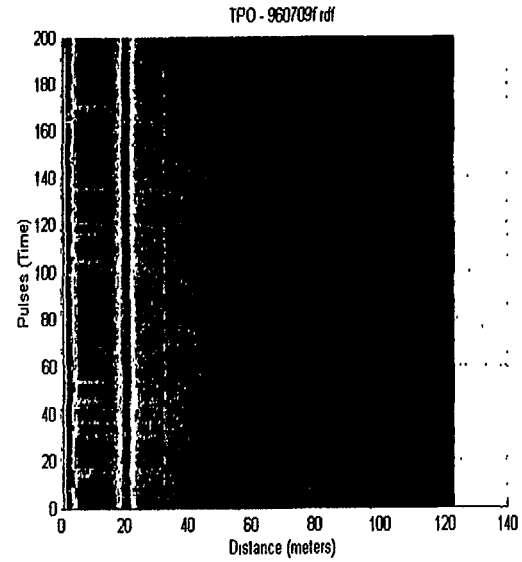
TPO - 960709f rdf
Pulses (Time)
Distance (meters)

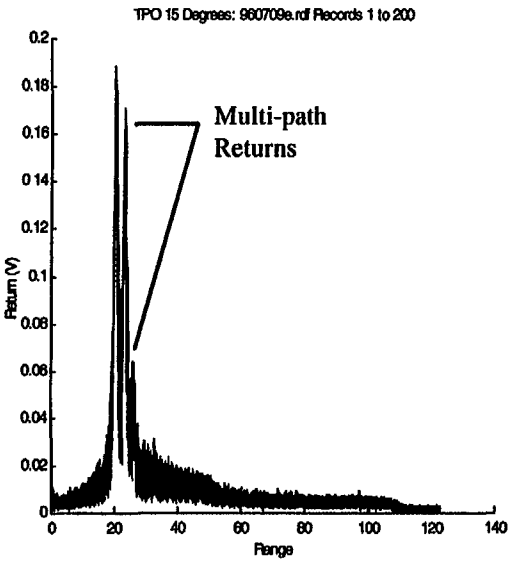
TPO 15 Degrees: 960709e.rdf Records 1 to 200
Multi-path
Returns
Return (V)
Range

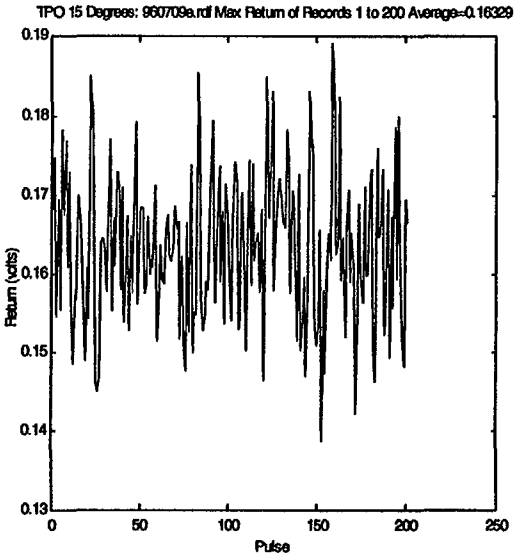
TPO 15 Degrees: 960709e.rdf Max Return of Records 1 to 200 Average=0.16329
Return (volts)
Pulse

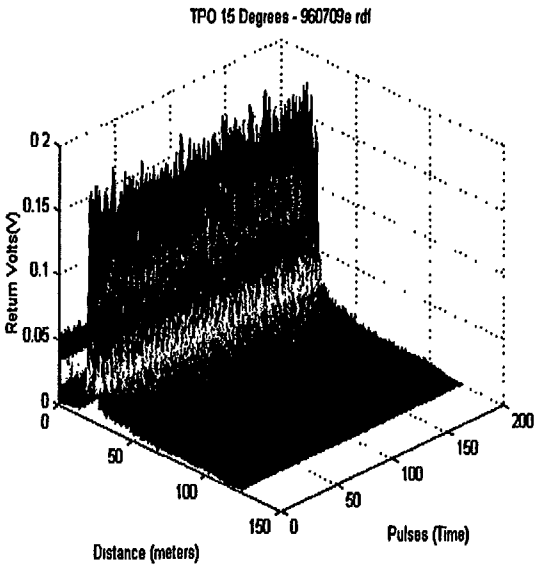
TPO 15 Degrees - 960709e rdf
Return Volts(V)
Distance (meters)
Pulses (Time)

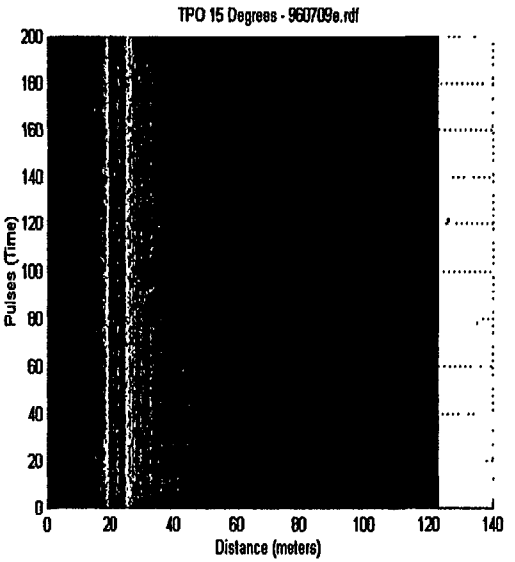
TPO 15 Degrees - 960709e.rdf
Pulses (Time)
Distance (meters)

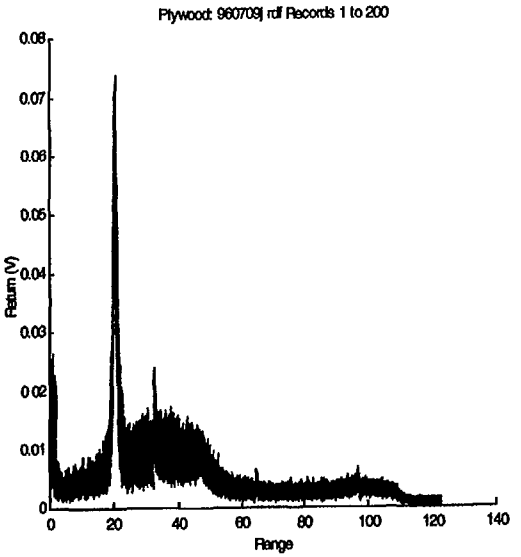
Plywood: 960709j rdf Records 1 to 200
Return (V)
Range

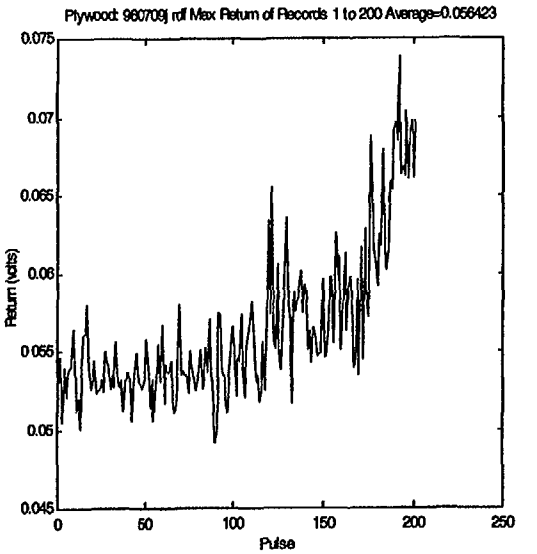
Plywood: 960709j rdf Max Return of Records 1 to 200 Average=0.056423
Return (volts)
Pulse

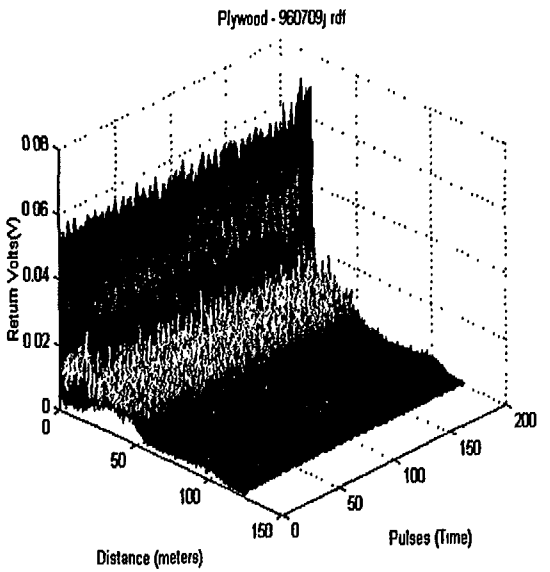
Plywood - 960709j rdf
Return Volts(V)
Distance (meters)
Pulses (Time)

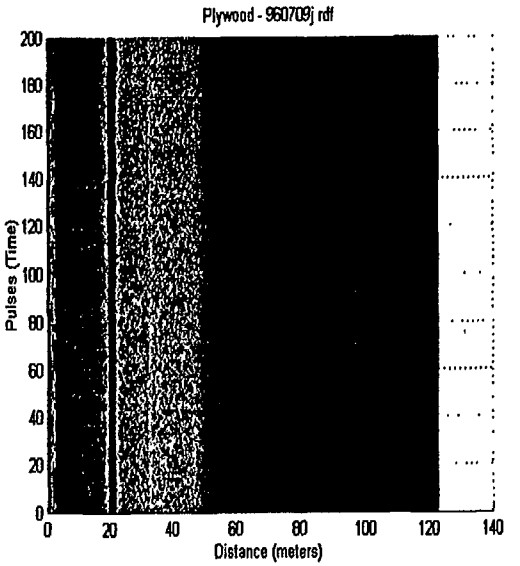
Plywood - 960709j rdf
Pulses (Time)
Distance (meters)

B.2 PRECIPITATION TESTS-SUMMARY

B.2.1 Purpose

The purpose of these precipitation tests was to evaluate the effects of snow, rain, and fog on the performance of the FLAR sensor.

B.2.2 Procedure

In general, the precipitation data collections were conducted as outlined below:

1. A reference target (either a vehicle or comer reflector) was placed within the FLAR's field-of-view at nominally a 10 to 20 meter range.
2. FLAR data was collected without any precipitation present, to provide a baseline for the specific collection.
3. Data was collected with varying degrees of precipitation rates present in the area between the FLAR and the target.
4. The data resulting from collections with precipitation present was compared to the baseline readings to determine the precipitation's effect on the performance. Return level averages and variances were used to quantify the effects.

Both natural and simulated precipitation tests were conducted to arrive at the results discussed below. The snow data was derived from natural snow precipitation only. The fog data was collected using an artificial fog machine. The rain data was collected using both natural rain and rain from a high-pressure washer to allow the precipitation rate to be more controlled.

B.2.3 Results

A set of representative plots summarizing the results of the tests are included at the end of this document. Note that data for these tests was collected during various periods and the results correlated fairly well from one collection scenario to another.

In general, the precipitation tested had little effect on the FLAR' s performance. In particular, the precipitation particles were not found to produce any significant returns to the F'LAR and the attenuation levels were very small.

Table B-2 shows the quantitative summary of the tests. The return levels and AGC settings for each collection are provided. These measured parameters were used to calculate the 'AGC adjusted voltage" values which are then compared to determine the attenuation levels. The "Baseline" for each collection was used as the reference for each attenuation calculation. Note that the attenuation levels provided are for "two-way" propagation. In other words, the radar signal passed through the precipitation-filled atmospheric medium twice--once on transmission, and once after it was reflected off of the target in the scene.

Table B-2. Precipitation Measurement

Precipitation Description	Target Range (m)	Measured Return Volts	AGC Control Setting (v)	AGC Mag. Attenuation (dB)	AGC Adjusted Return Volts	Two-Way Power Attenuation (dB)	Two-Way Power Attenuation (dB/10 m)
Light Rain	13	**0.492**	**3.906**	-3.6324	0.6064	-0.4	-0.29
Moderate Rain	13	0.441	3.906	-3.6324	0.5436	0.6	0.44
Heavy Rain	13	0.421	3.906	-3.6324	0.5189	1.0	0.75
Moderate Snow	22	**0.083**	**3.906**	**-3.6324**	**0.1023**	**-0.7**	**-0.30**
Heavy Snow	**22**	0.085	3.906	**-3.6324**	**0.1048**	**-0.9**	**-0.39**
Fog 1	**3**	0.366	**3.906**	**-3.6324**	**0.4511**	**0.3**	**1.05**
Fog 2	**3**	0.375	3.906	**-3.6324**	**0.4622**	**0.1**	**0.35**

Figure B-10 illustrates the attenuation levels produced from the various levels and types of precipitation. These attenuation levels have been normalized to 10 meter ranges. These values are considered insignificant since return levels from the FLAR during static collections with precision reference reflectors in a controlled environment have been observed to fluctuate by values similar to these. Note that negative attenuation levels indicate that the peak return from the target in the scene actually increased. This could potentially be due to the target getting wet aud causing more of the radar energy to be directed back in the direction of the FLAR or due to the ground between the radar and the target getting wet and causing a higher level of multipath return.

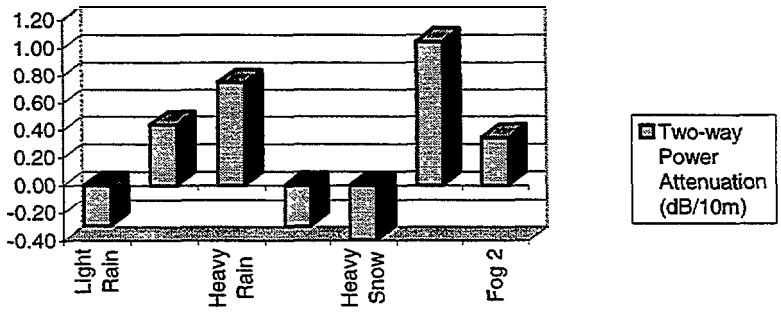

Figure B-10. Two-Way Power Attenuation (dB/10 m)

B.2.4 Conclusions

The primary conclusion of this test is that the FLAR performance was not observed to be significantly affected by the various levels and types of precipitation tested. In particular, the precipitation did not produce any observable return levels in the FLAR IF signal, and the attenuation levels were very low. However, the combination of a low RCS target at a far range during heavy rates of precipitation (or heavy fog) could cause a problem for an automotive radar.

The results achieved during this testing correlate well with those in the open literature. There are several papers which have been published on the attenuation of high frequency communication systems as a result of precipitation. In general, both theoretical and empirical attenuation levels -are stated to be about 10 dB per kilometer (one-way). Relating the information obtained in theopen literature to the operating ranges for automotive radars, one could expect power attenuation levels on the order of 1 to 3 dB at 100 meter ranges.

The measurements conducted as part of this program indicate that the actual attenuation levels may be somewhat higher than the 1 to 3 dB values mentioned above. More practical values could range from 2 to 10 dB of power loss at 100 meter ranges. Of course these values are highly dependent upon the rate of precipitation and also the particulate size of the precipitation. As the particulate size approaches r/4 wavelength of the radar frequency, the particulate will begin acting as an antenna.

In practical terms, the most important outcome of this test was the verification that the FLAR was capable of detecting targets witbm it field-of-view in the presence of significant precipitation. Except for the light rain collections, the target itself was visually obscured from the FLAR's location. During the heavy rain and fog tests, the target was frequently totally visually obscured. Despite the visual obscuration, return levels from the target were easily observed in the raw radar signal. These observations provide empirical support to those who site radar's all-weather performance advantage over infra-red or optical sensors for automotive applications.

The surprising phenomenon observed during the testing was the occasional <u>increase</u> in return levels in the presence of precipitation. This was observed during several collections. While the increase was not significant, it was measurable. Possible explanations for this phenomena are:

- As the precipitation fell, the ground between the radar and the target became wet and caused a larger multipath return to be produced. Theoretically, enhanced multipath returns can increase actual target returns over 10 dB given a particular geometry.
- As the precipitation particles landed in the target, they caused an increase in the non-specular returns due to increased refraction and energy scattering. For tests conducted with reference reflectors, the increase may have come from particles landing on the Styrofoam support pedestal.

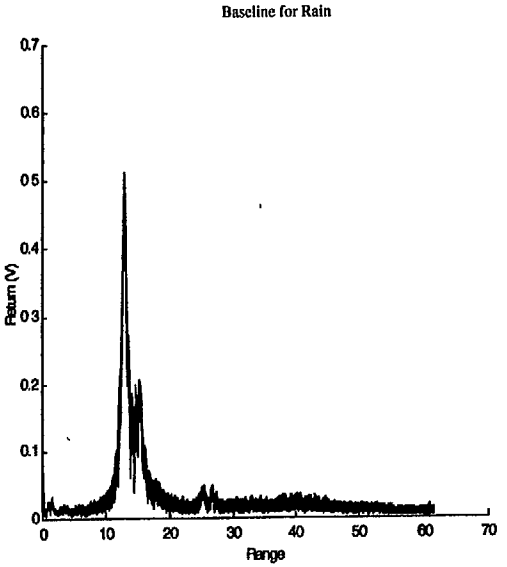
Baseline for Rain
Return (V)
Range
0.7
0.6
0.5
0.4
0.3
0.2
0.1
0
0 10 20 30 40 50 60 70

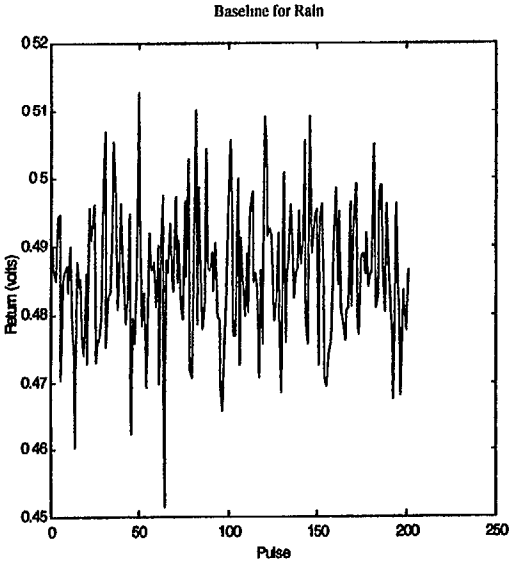
Baseline for Rain
Return (volts)
Pulse
0.52
0.51
0.5
0.49
0.48
0.47
0.46
0.45
0 50 100 150 200 250

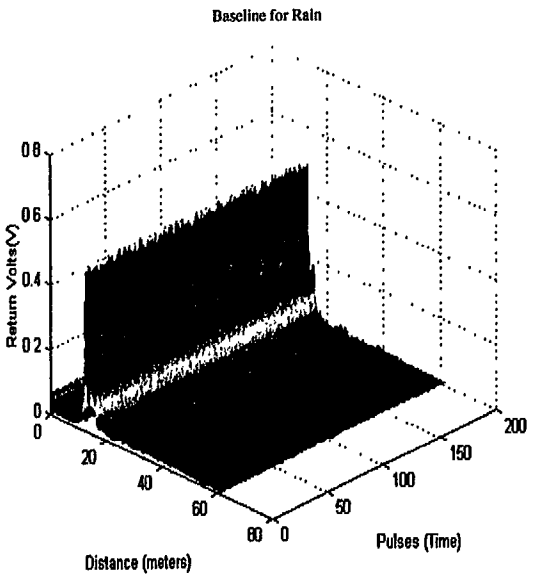
Baseline for Rain
Return Volts(V)
Distance (meters)
Pulses (Time)
0.8
0.6
0.4
0.2
0
0 20 40 60 80
0 50 100 150 200

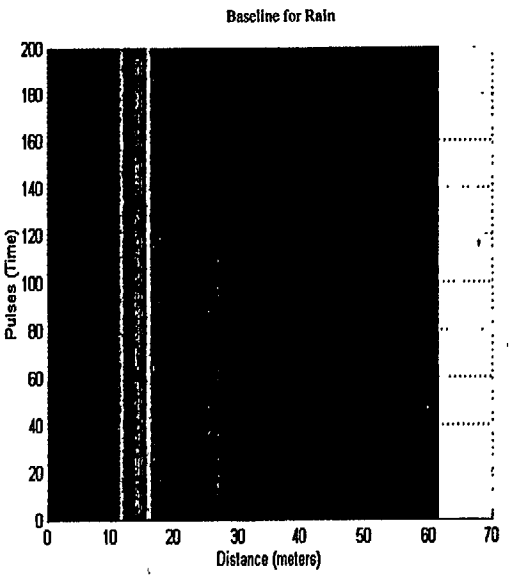
Baseline for Rain
Pulses (Time)
Distance (meters)
200
180
160
140
120
100
80
60
40
20
0
0 10 20 30 40 50 60 70

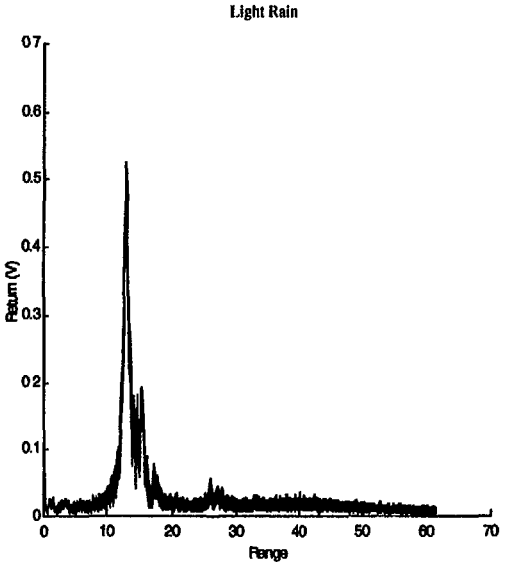
Light Rain
Return (V)
Range

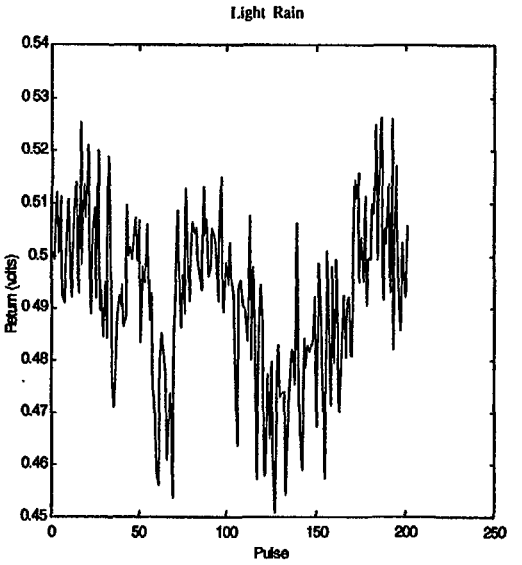
Light Rain
Return (volts)
Pulse

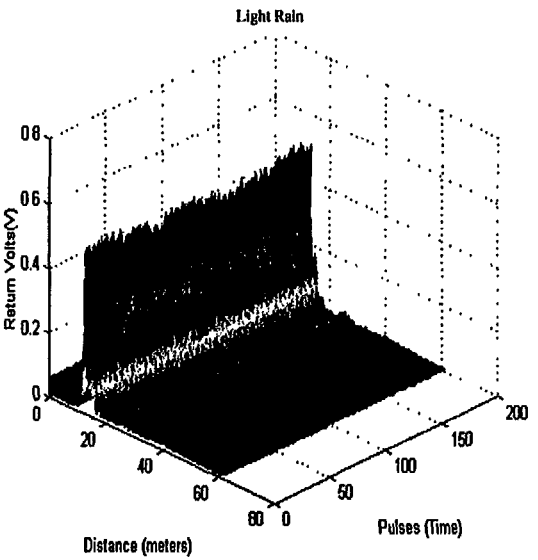
Light Rain
Return Volts(V)
Distance (meters)
Pulses (Time)

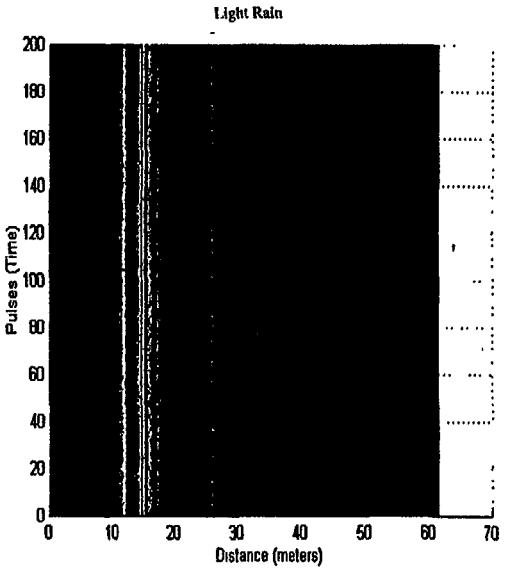
Light Rain
Pulses (Time)
Distance (meters)

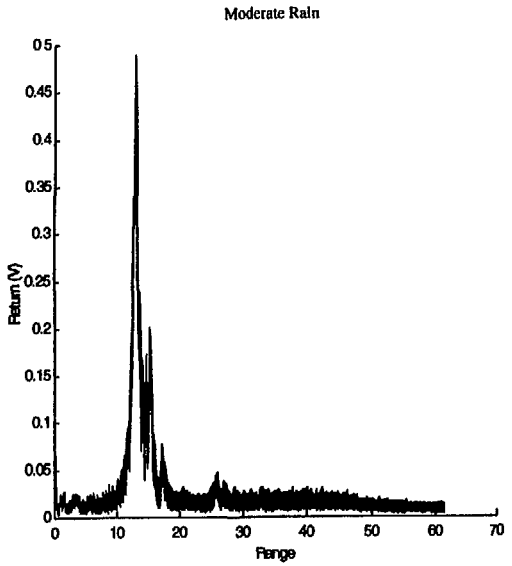
Moderate Rain
Return (V)
Range

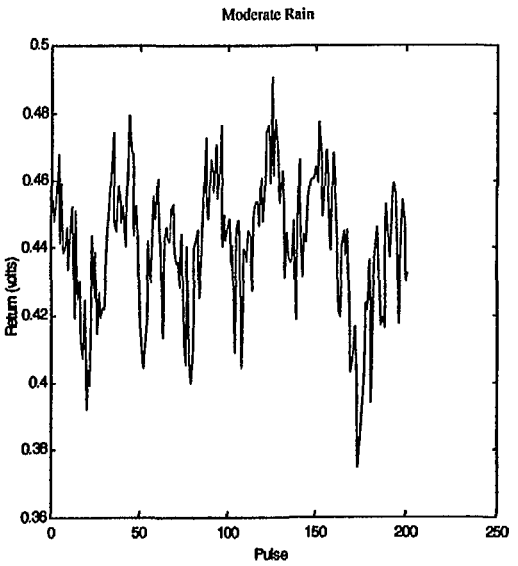
Moderate Rain
Return (volts)
Pulse

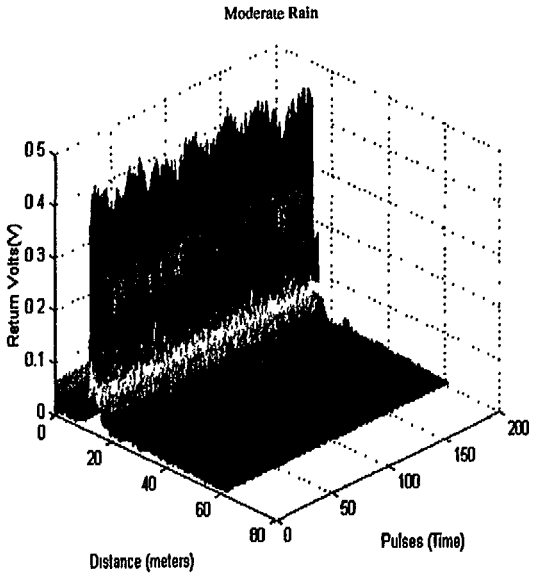
Moderate Rain
Return Volts(V)
Distance (meters)
Pulses (Time)

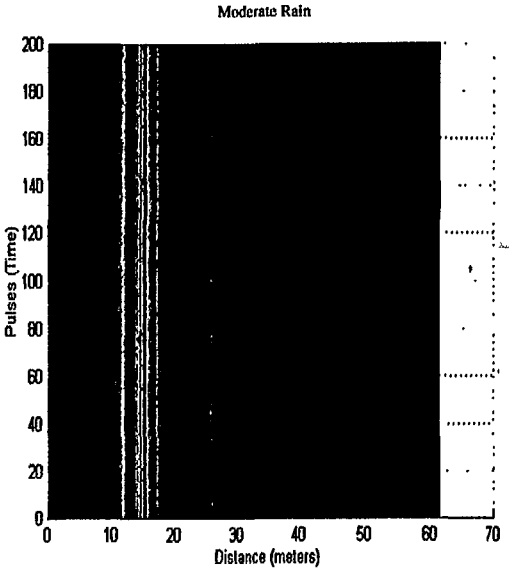
Moderate Rain
Pulses (Time)
Distance (meters)

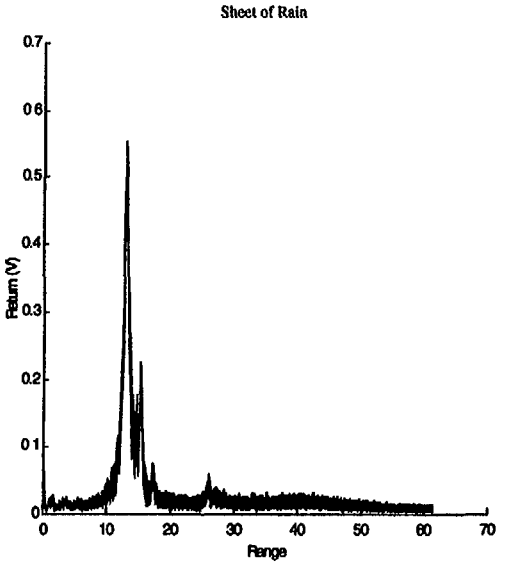
Sheet of Rain
Return (V)
Range
0.7
0.6
0.5
0.4
0.3
0.2
0.1
0
0
10
20
30
40
50
60
70

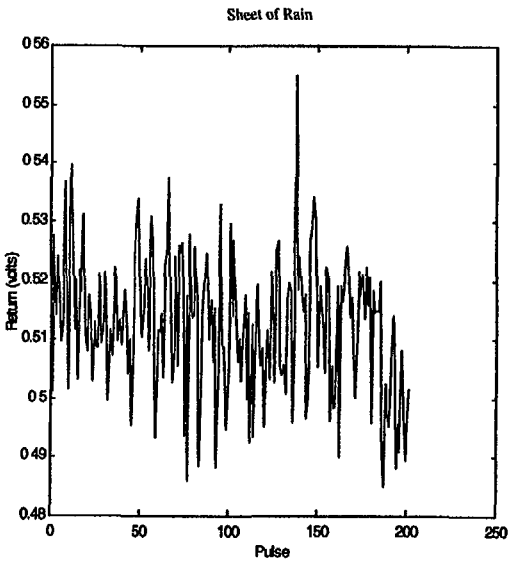
Sheet of Rain
Return (volts)
Pulse
0.56
0.55
0.54
0.53
0.52
0.51
0.5
0.49
0.48
0
50
100
150
200
250

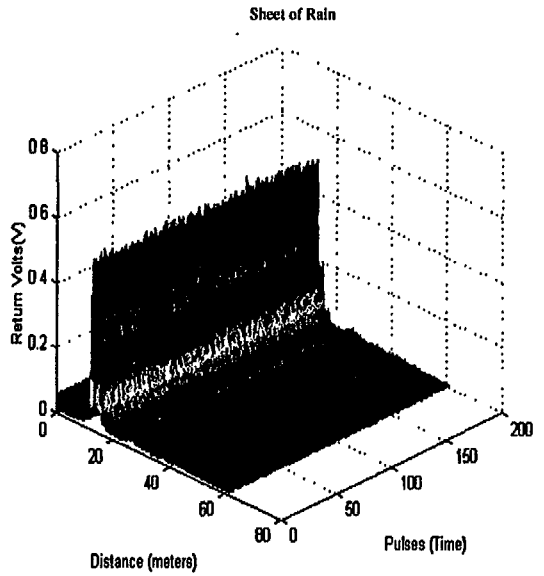
Sheet of Rain
Return Volts(V)
Distance (meters)
Pulses (Time)
0.8
0.6
0.4
0.2
0
0
20
40
60
80
0
50
100
150
200

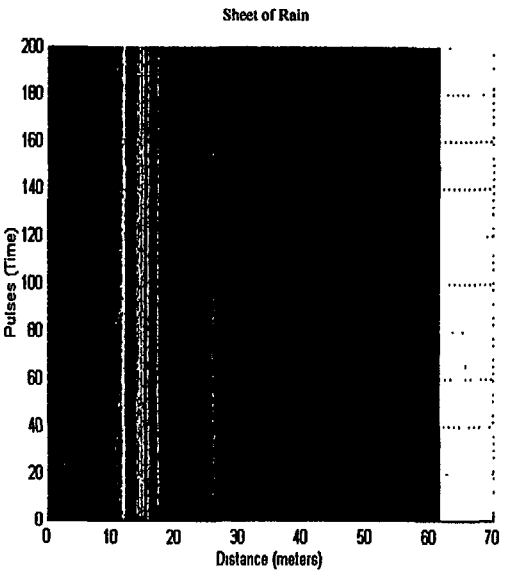
Sheet of Rain
Pulses (Time)
Distance (meters)
200
180
160
140
120
100
80
60
40
20
0
0
10
20
30
40
50
60
70

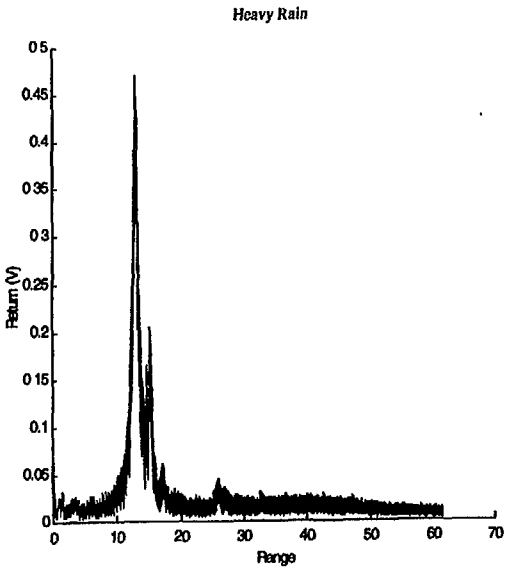
Heavy Rain
Return (V)
Range

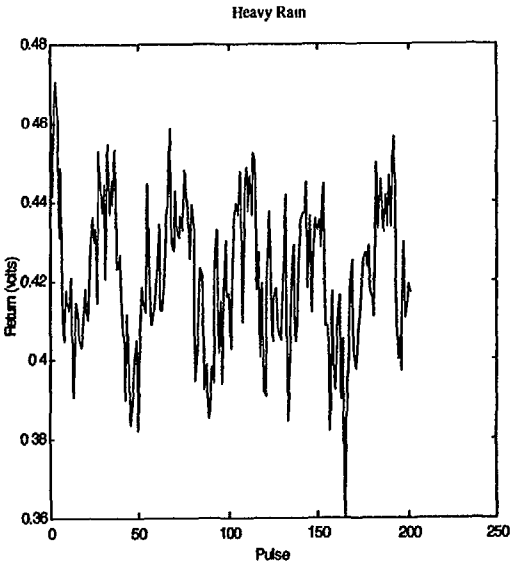
Heavy Rain
Return (Volts)
Pulse

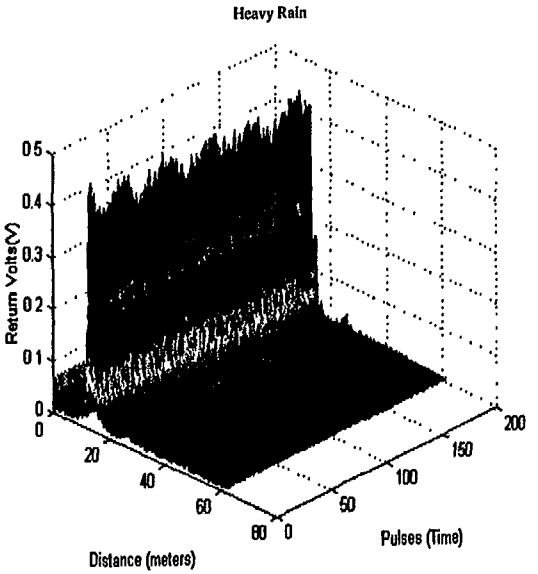
Heavy Rain
Return Volts(V)
Distance (meters)
Pulses (Time)

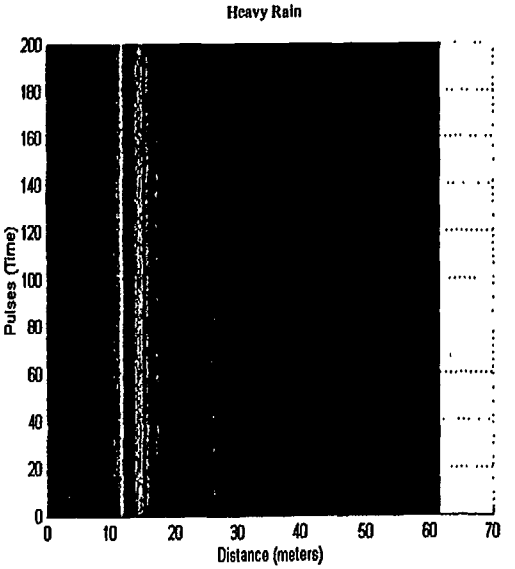
Heavy Rain
Pulses (Time)
Distance (meters)

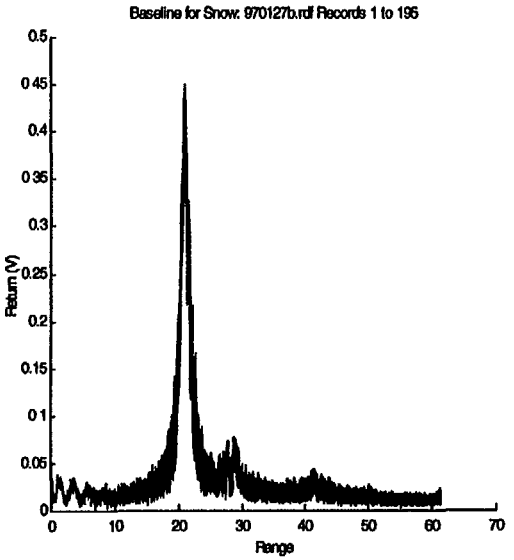
Baseline for Snow: 970127b.rdf Records 1 to 195
Return (V)
Range

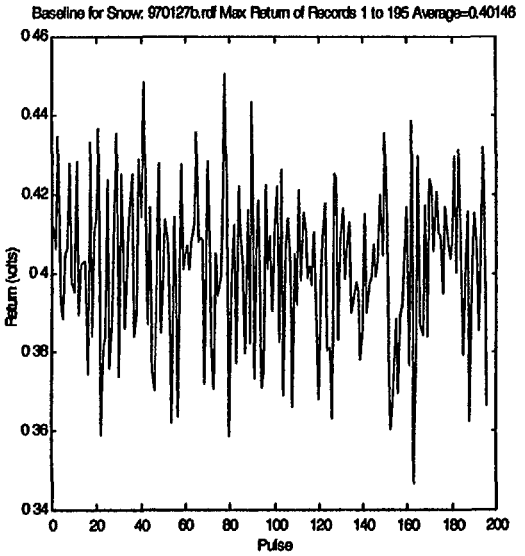
Baseline for Snow: 970127b.rdf Max Return of Records 1 to 195 Average=0.40146
Return (volts)
Pulse

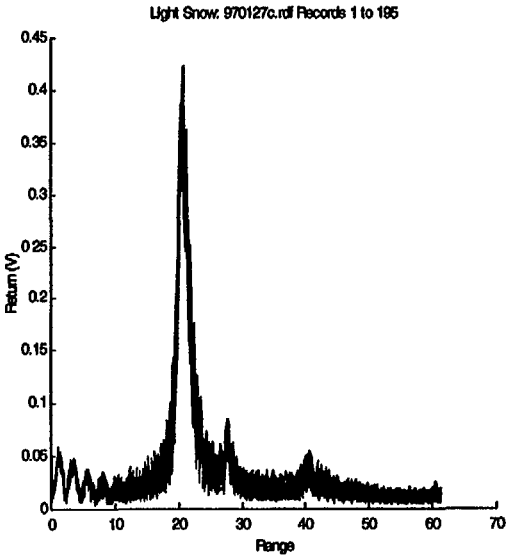
Light Snow: 970127c.rdf Records 1 to 195
Return (V)
Range

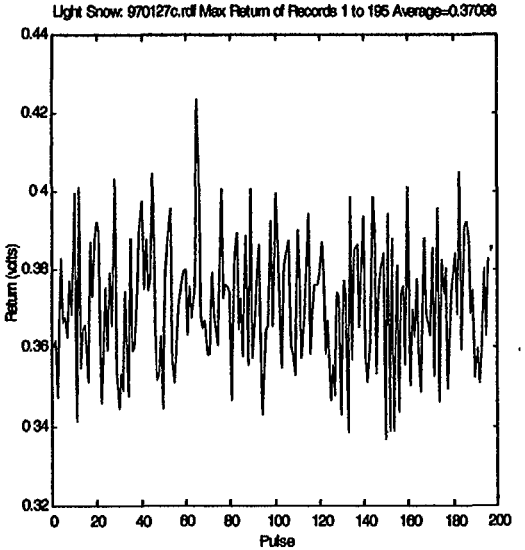
Light Snow: 970127c.rdf Max Return of Records 1 to 195 Average=0.37098
Return (volts)
Pulse

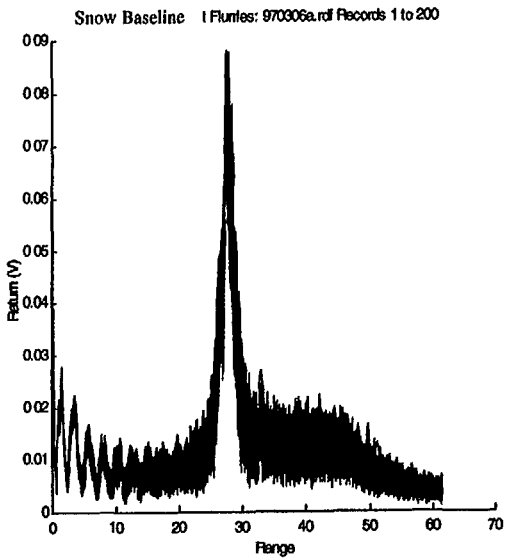
Snow Baseline
Return (V)
Range

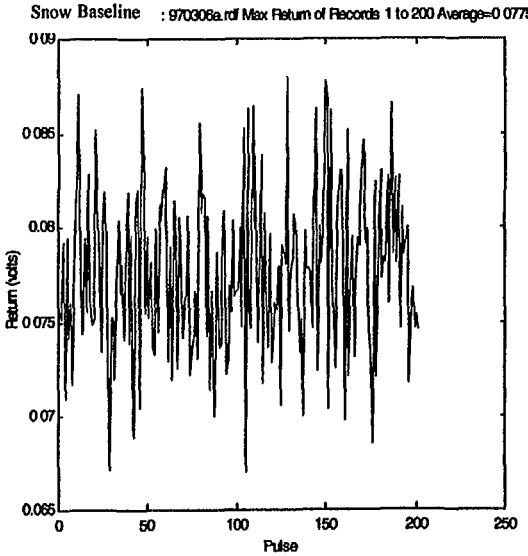
Snow Baseline
: 970306a.rdf Max Return of Records 1 to 200 Average=0 077564
Return (volts)
Pulse

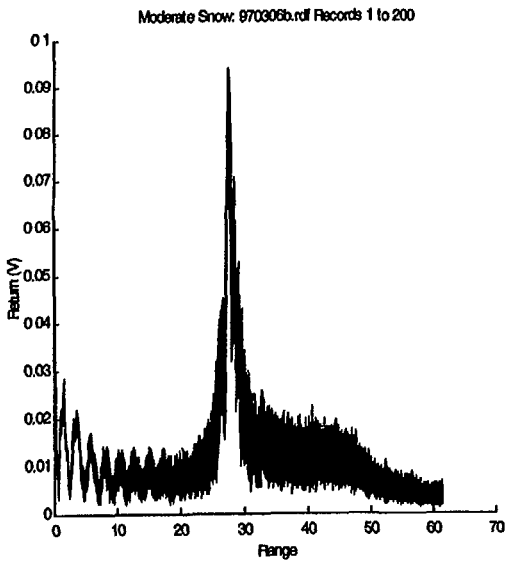
Moderate Snow: 970306b.rdf Records 1 to 200
Return (V)
Range

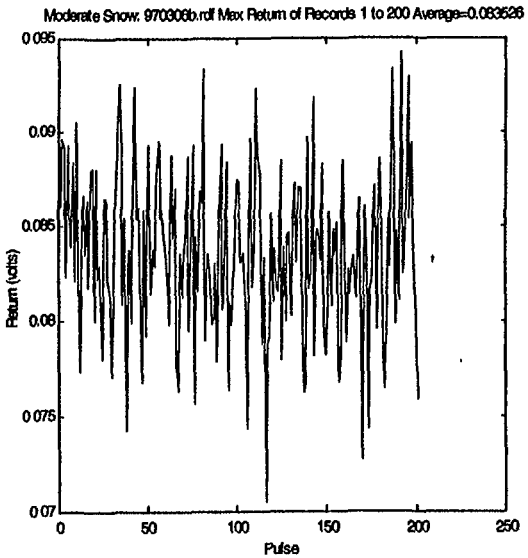
Moderate Snow: 970306b.rdf Max Return of Records 1 to 200 Average=0.083626
Return (volts)
Pulse

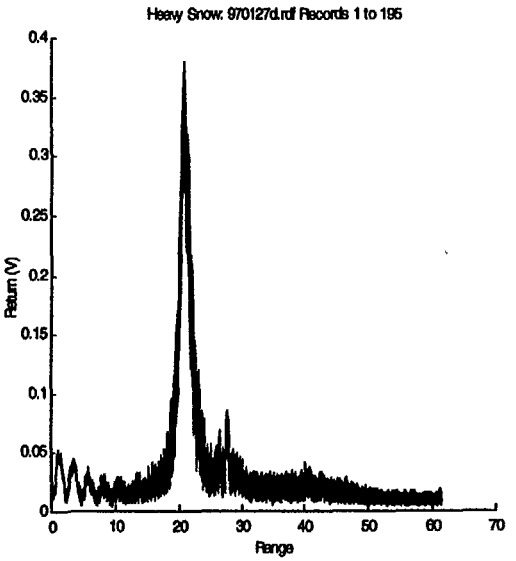
Heavy Snow: 970127d.rdf Records 1 to 195
Return (V)
Range
0.4
0.35
0.3
0.25
0.2
0.15
0.1
0.05
0
0
10
20
30
40
50
60
70

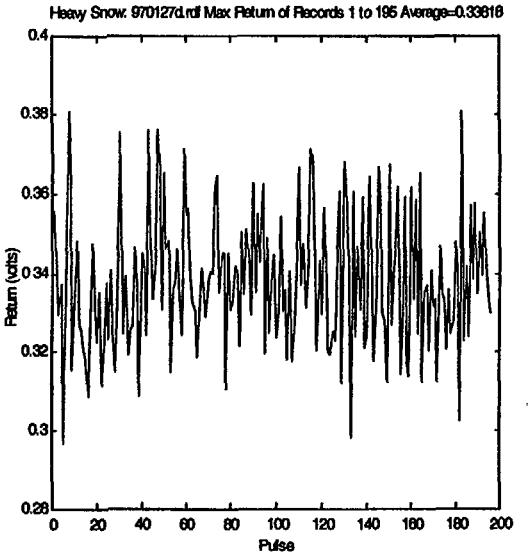
Heavy Snow: 970127d.rdf Max Return of Records 1 to 195 Average=0.33618
Return (volts)
Pulse
0.4
0.38
0.36
0.34
0.32
0.3
0.28
0
20
40
60
80
100
120
140
160
180
200

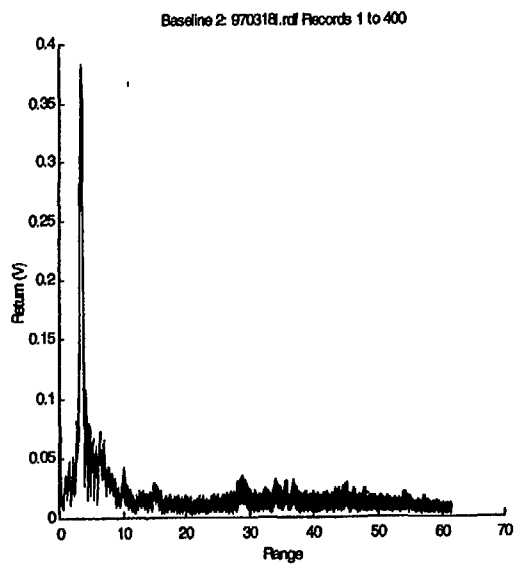
Baseline 2: 970318l.rdf Records 1 to 400
Return (V)
Range
0.4
0.35
0.3
0.25
0.2
0.15
0.1
0.05
0
0
10
20
30
40
50
60
70

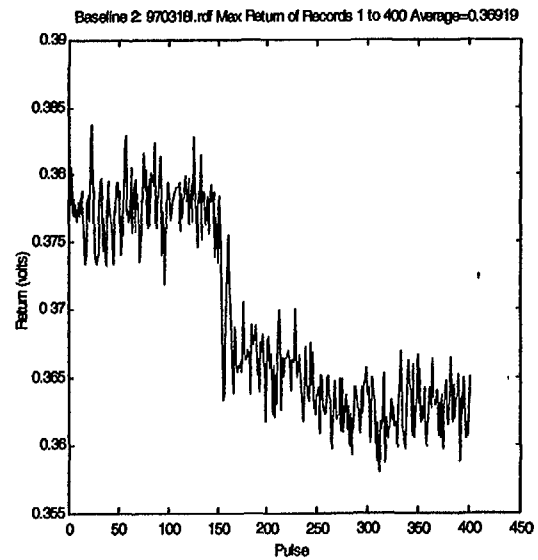
Baseline 2: 970318l.rdf Max Return of Records 1 to 400 Average=0.36919
Return (volts)
Pulse
0.39
0.385
0.38
0.375
0.37
0.365
0.36
0.355
0
50
100
150
200
250
300
350
400
450

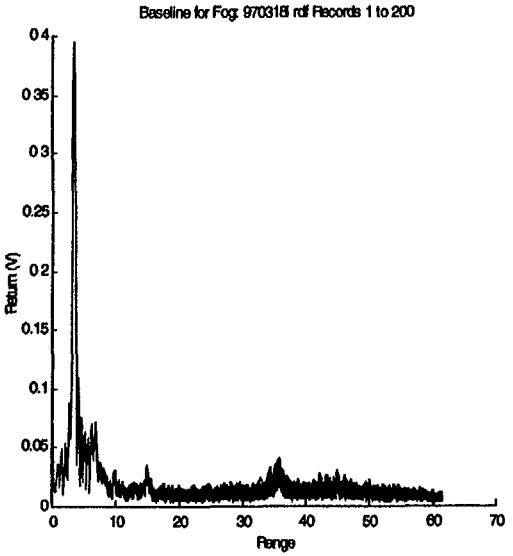
Baseline for Fog: 970318l rdf Records 1 to 200
Return (V)
Range

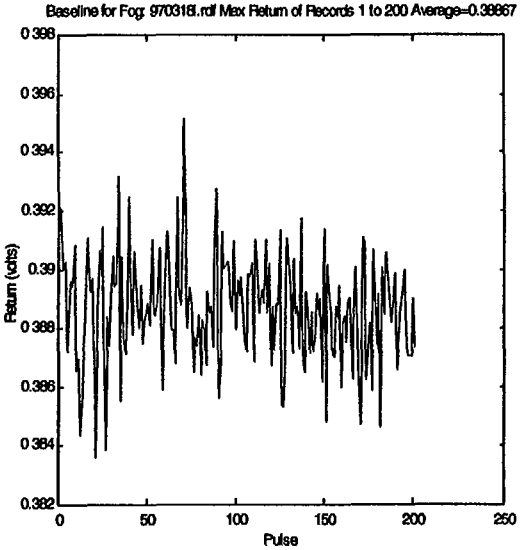
Baseline for Fog: 970318l.rdf Max Return of Records 1 to 200 Average=0.38867
Return (cnts)
Pulse

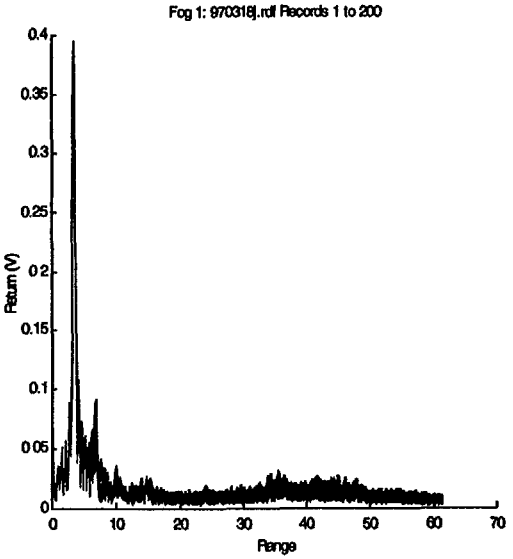
Fog 1: 970318j.rdf Records 1 to 200
Return (V)
Range

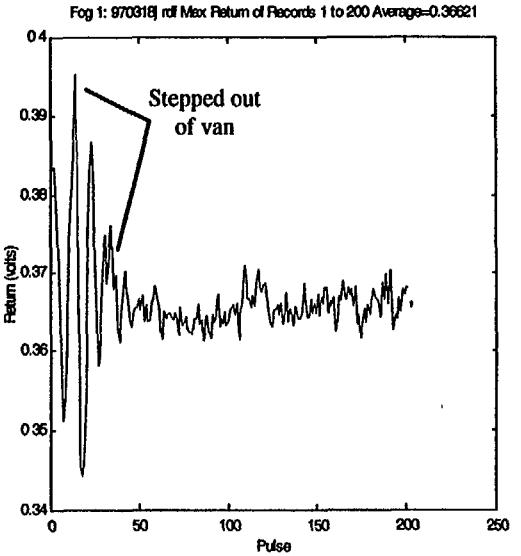
Fog 1: 970318j rdf Max Return of Records 1 to 200 Average=0.36621
Stepped out
of van
Return (cnts)
Pulse

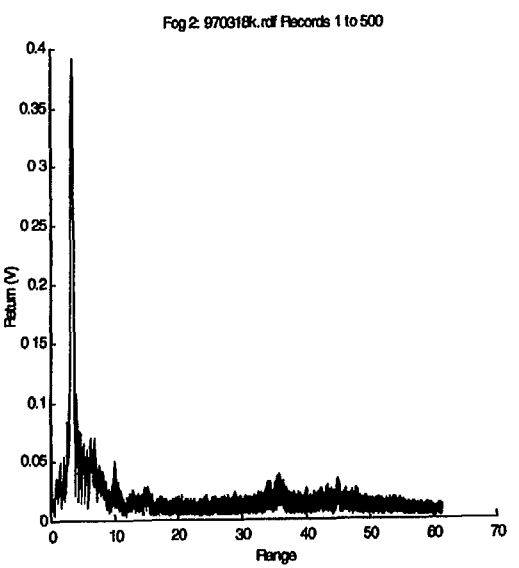
Fog 2: 970318k.rdf Records 1 to 500
Return (V)
Range
0.4
0.35
0.3
0.25
0.2
0.15
0.1
0.05
0
0
10
20
30
40
50
60
70

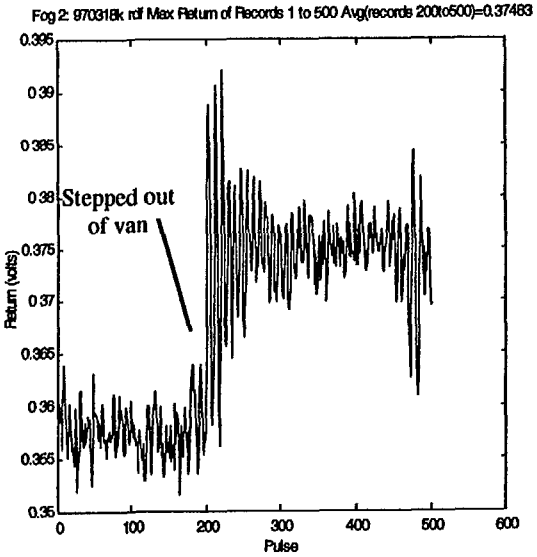
Fog 2: 970318k rdf Max Return of Records 1 to 500 Avg(records 200to500)=0.37483
Stepped out
of van
Return (volts)
Pulse
0.395
0.39
0.385
0.38
0.375
0.37
0.365
0.36
0.355
0.35
0
100
200
300
400
500
600

B.3 CONTAMINATION TESTS—SUMMARY

B.3.1 Purpose

The purpose of these contamination tests was to evaluate how dirt, moisture, and snow would effect the FLAR's performance. The "contamination" could occur either at the target location or at the sensor. For example, the target itself would be considered "contaminated" if it were snow covered, or the sensor could be "contaminated" if its antenna's were covered with mud.

B.3.2 Procedure

In general, the contamination data collections were conducted as outlined below:

1. A reference target (either a vehicle or corner reflector) was placed within the FLAR's field-of-view at nominally a 10 to 30 meter range.
2. FLAR data was collected without any contamination present, to provide a baseline for the specific collection.
3. The contaminating material was applied to either the target or the sensor. (Note that in the case of applying the contamination to the sensor, a glass plate was placed in front of the sensor during the baseline tests, and then the contaminate was actually applied to the glass plate. This was to simulate having the contaminate on the radome of the FLAR.)
4. FLAR data was collected with the contamination present.
5. The data resulting from collections with the contamination present was compared to the baseline readings to determine performance effects on the FLAR due to the contamination. Return level averages and variances were used to quantify the effects.

The following contamination scenarios were tested:

- Vehicle target contaminated with snow: In this scenario, the rear portion of the target vehicle (a Pontiac Sunbird) was partially (about 50 percent) with fairly dry snow.
- Vehicle target contaminated with water: In this scenario, the target vehicle (a small pick-up truck) was sprayed with water from a hose. Care was taken to perform the baseline test with already wet ground to isolate the vehicle contamination from multipath effects.
- FLAR sensor contaminated with snow: This scenario had approximately 1 inch of snow densely packed on the face of the FLAR sensor.
- FLAR sensor contaminated with semi-dry mud: The mud tests were divided into two levels of contamination. The first level had the glass plate covered with mud, but still visually translucent. The second level had the glass plate covered with thick so that it was visually opaque. This second level is referred to in the tests as "very muddy."

B.3.3 Results

A set of representative data plots summarizing the results of the tests are included at the end of this document.

The results of the contamination tests were not what was intuitively expected. Therefore, several data sets were collected/analyzed for each type of test and the results were found to be consistent.

Table B-3 shows the quantitative summary of the tests. The return levels and AGC settings for each collection are provided. These measured parameters were used to calculate the "AGC adjusted voltage"

values which are then compared to determine the attenuation levels. The "Baseline" for each collection was used as the reference for each attenuation calculation. Note that the attenuation levels provided are for "two-way" propagation.

Table B-3. Contamination Measurement

Material Description	Measured Return Volts	AGC Control Setting (v)	AGC Mag. Attenuation (dB)	AGC Adjusted Return Volts	Two-Way Power Attenuation (dB)
Water on Truck	0.514	3.906	-3.632	0.634	-0.5
Snow on Car	0.09	3.906	-3.632	0.111	-1.2
Translucent Mud at Sensor	0.197	3.906	-3.632	0.243	-0.7
Opaque Mud at Sensor	0.306	3.906	-3.632	0.377	-4.5
Snow Covered Sensor	0.02	3.906	-3.632	0.025	11.8

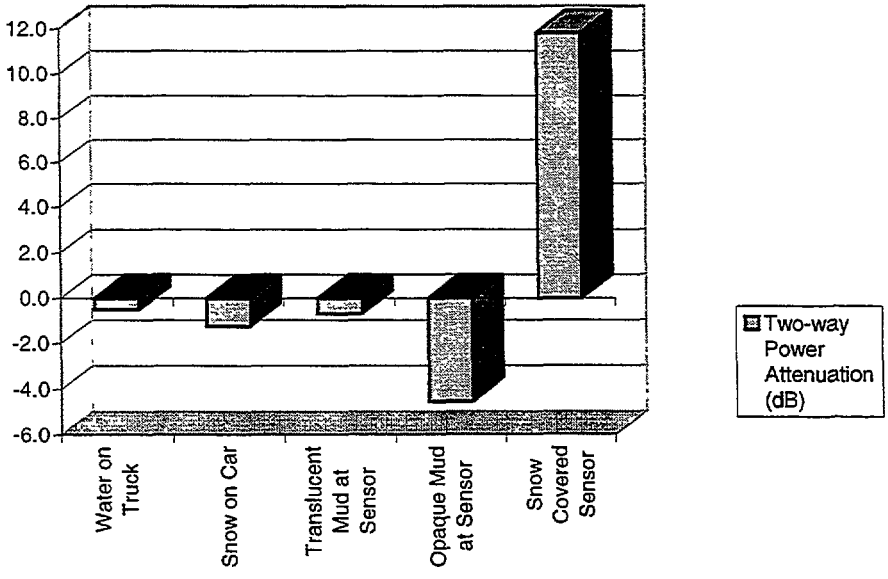

Figure B-11. Two-Way Power Attenuation (dB)

Figure B-11 above illustrates the attenuation levels produced from the various types of contamination. Note that negative attenuation levels indicate that the peak return from the target in the scene actually increased.

The contaminated vehicle test results correlate with some of the observations made during the precipitation tests. In these cases, a potential explanation is that the particulate contamination on the vehicle may be enhancing the return level by creating more scattering centers through refraction of the radar energy. Figure B-12 illustrates this concept.

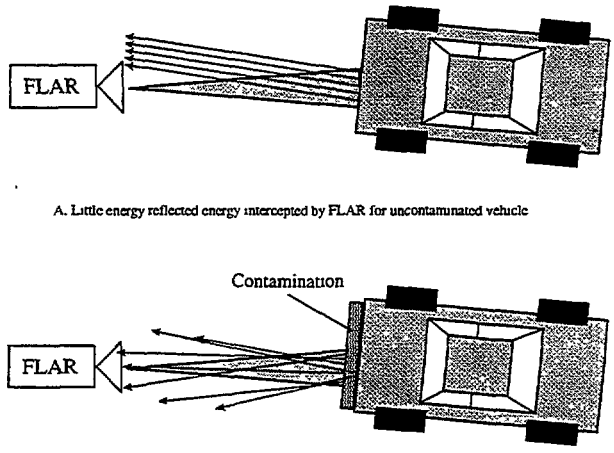

Figure B-12. Potential Cause for Contaminated Target Increased RCS

Figure B-12 shows how a contamination layer might cause reflected energy to become more diffused compared to the reflections from an uncontaminated target. While this diffusion process may cause the power density (mW/cm^3) of the reflected wave to decrease, the FLAR still intercepts more power per unit area (i.e., the receive antenna aperture). Note that this explanation is a hypothesis which should be verified through further testing which was beyond the scope of this project.

Similar to the contaminated target results were the results from the contaminated sensor testing using semi-dry mud. These tests again resulted in 'negative' attenuation, or an observed gain in peak return level. In analyzing the range profiles for the mud contamination tests, it was observed that the contaminated glass plate itself did NOT reflect energy back to the FLAR. The only difference between the baseline and contamination tests was the peak return level from the reference reflector. A potential cause for this phenomena could be an effect similar to that described above, except that the diffusion of energy occurs at the contaminated glass plate (approximately 1 meter in front of the sensor) rather than at the target. Again, this explanation is a theory requiring more stringent contamination testing for verification.

Finally, the result of the contamination test in which the FLAR sensor "caked" with 1 inch of wet snow indicates that the snow inhibited the sensor from detecting the reference target. Note that the 11 dB signal attenuation caused the reference target return to drop below the system noise level.

B.3.4 Conclusions

The analysis of the contamination tests have identified some phenomena which were unanticipated. The presence of contamination particulates at both the target and sensor have been observed to cause an increase in the peak return from reference targets in the FLAR's field of view. A potential mechanism for creating this phenomena is presented in the discussion of the test results given above. **It should be noted that this hypothesis has not been thoroughly tested and more research into the phenomena is required.** While the measurement equipment and procedures have been reviewed, the limited access to the FLAR electronics has severely limited the ability to rule a sensor specific response to the contamination scenarios which may be causing the unanticipated observations.

Not withstanding the explanation for the observed phenomena, the primary conclusion from these tests is that both target and sensor contamination from rain, snow, and mud may cause return levels from targets in the scene to actually increase. This would of course add to the robustness of the automotive

radar in detecting objects at non-specular aspect angles, however, the mechanism causing this phenomena needs to be more clearly understood.

Conversely, the snow-covered sensor tests indicate that certain contaminants could cause severe degradation in sensor performance to the point of missing significant targets within the scene.

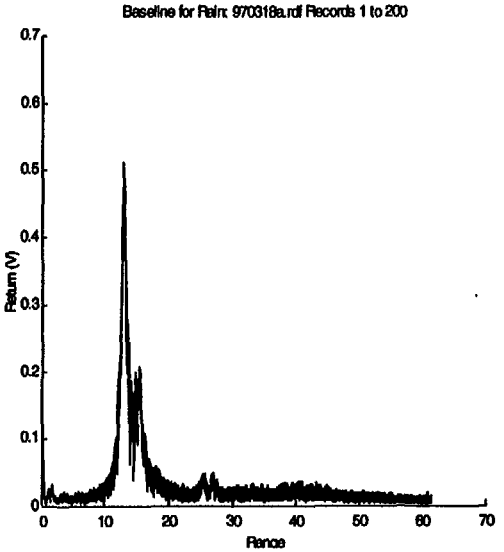
Baseline for Rain: 970318a.rdf Records 1 to 200
Return (V)
Range

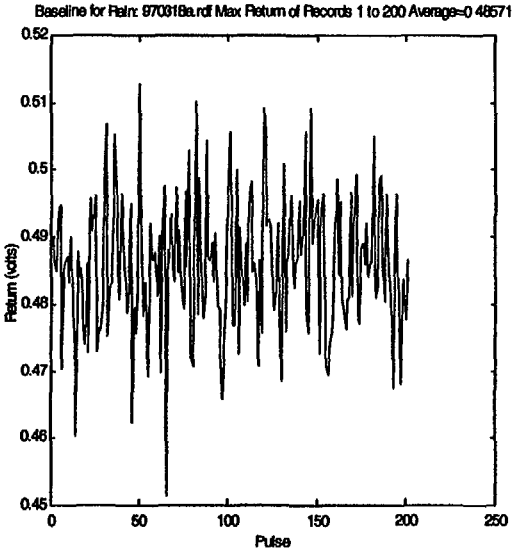
Baseline for Rain: 970318a.rdf Max Return of Records 1 to 200 Average=0 48571
Return (volts)
Pulse

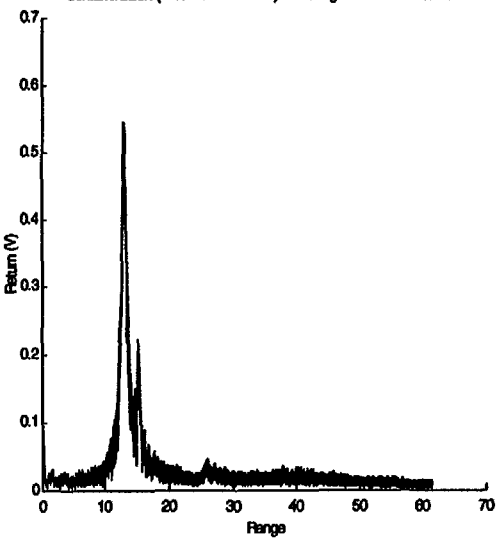
Contamination (Wet Truck-No Rain): 970318g.rdf Records 1 to 200
Return (V)
Range

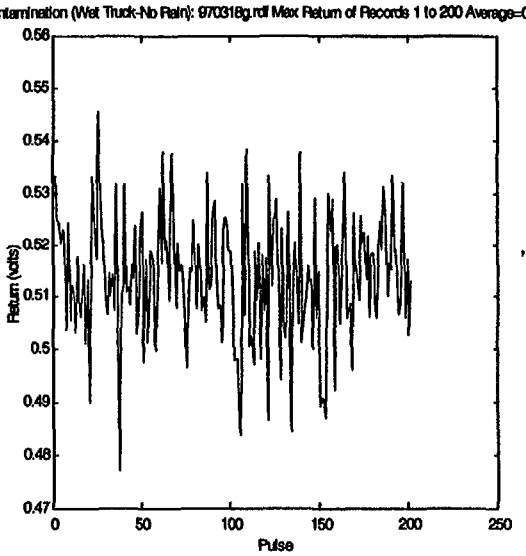
Contamination (Wet Truck-No Rain): 970318g.rdf Max Return of Records 1 to 200 Average=0.51406
Return (volts)
Pulse

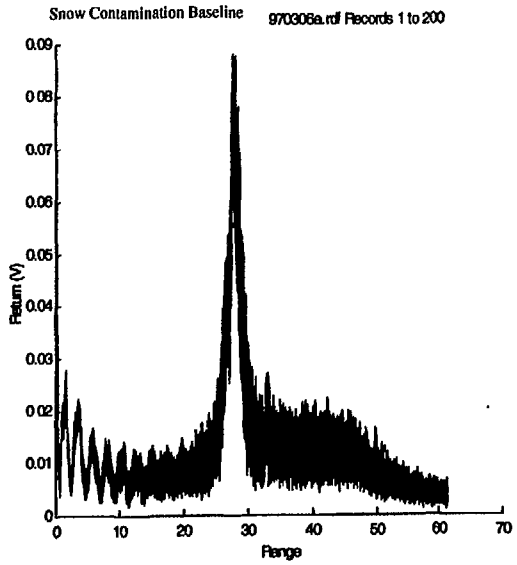
Snow Contamination Baseline
970306a.rdf Records 1 to 200
Return (V)
Range
0.09
0.08
0.07
0.06
0.05
0.04
0.03
0.02
0.01
0
0
10
20
30
40
50
60
70

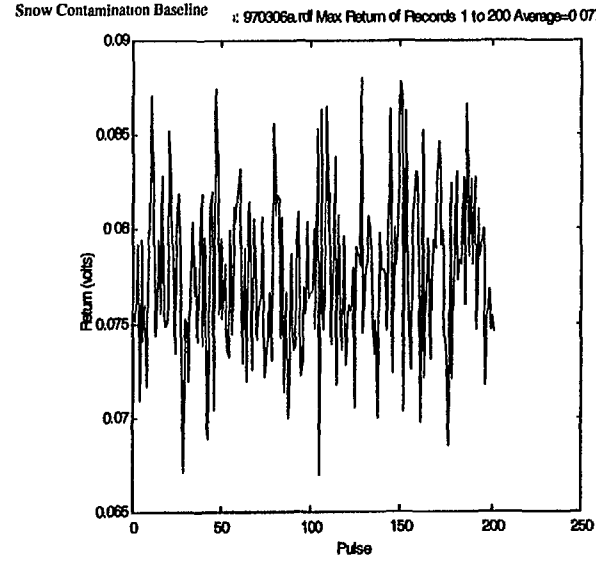
Snow Contamination Baseline
970306a.rdf Max Return of Records 1 to 200 Average=0 077564
Return (volts)
Pulse
0.09
0.085
0.08
0.075
0.07
0.065
0
50
100
150
200
250

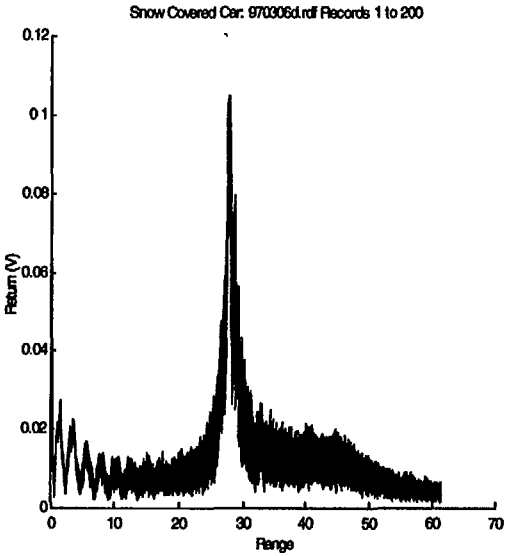
Snow Covered Car: 970306d.rdf Records 1 to 200
Return (V)
Range

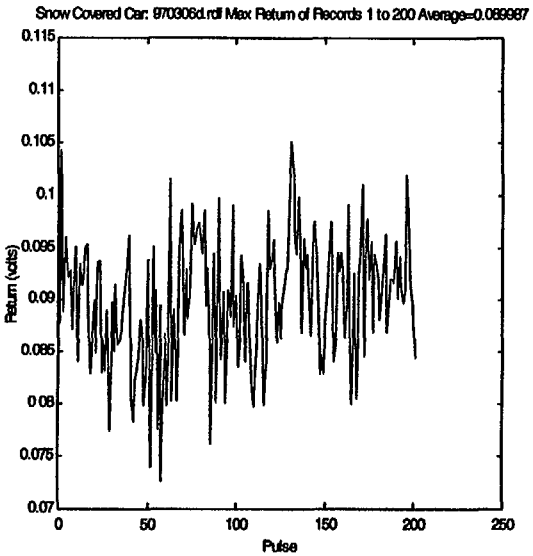
Snow Covered Car: 970306d.rdf Max Return of Records 1 to 200 Average=0.089987
Return (volts)
Pulse

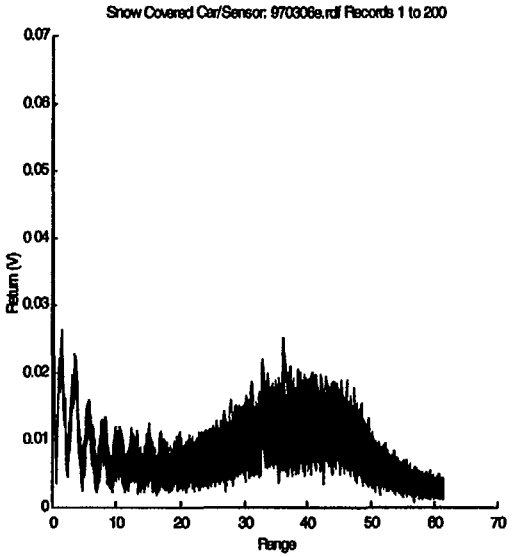
Snow Covered Car/Sensor: 970306e.rdf Records 1 to 200
Return (V)
Range

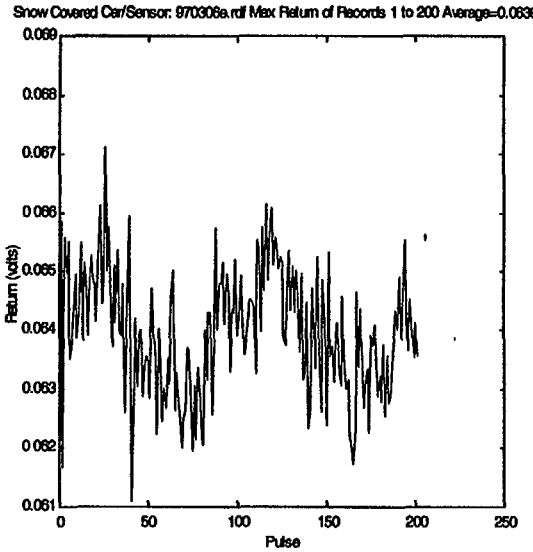
Snow Covered Car/Sensor: 970306e.rdf Max Return of Records 1 to 200 Average=0.063972
Return (volts)
Pulse

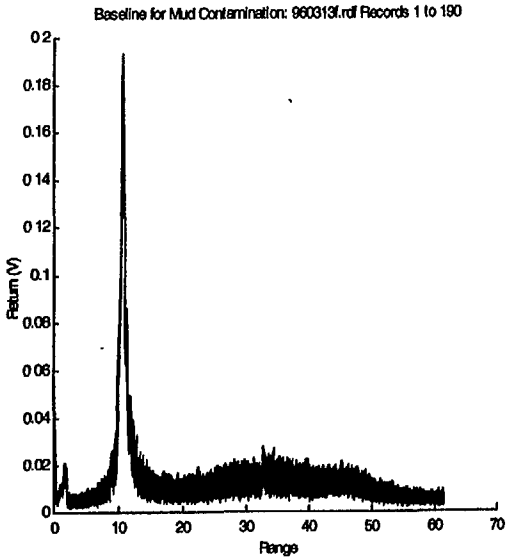
Baseline for Mud Contamination: 960313f.rdf Records 1 to 190
Return (V)
Range

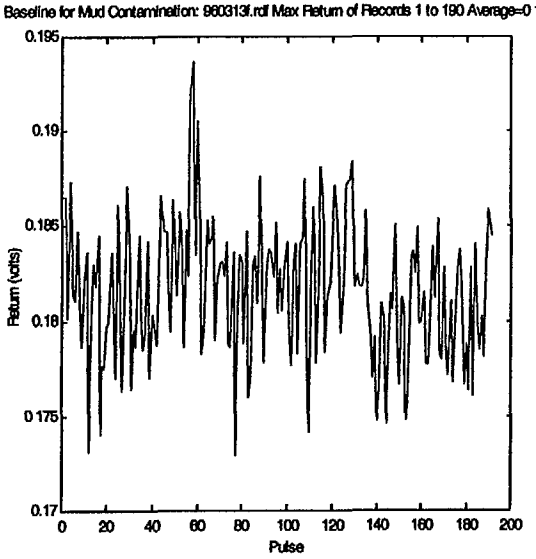
Baseline for Mud Contamination: 960313f.rdf Max Return of Records 1 to 190 Average=0 18165
Return (volts)
Pulse

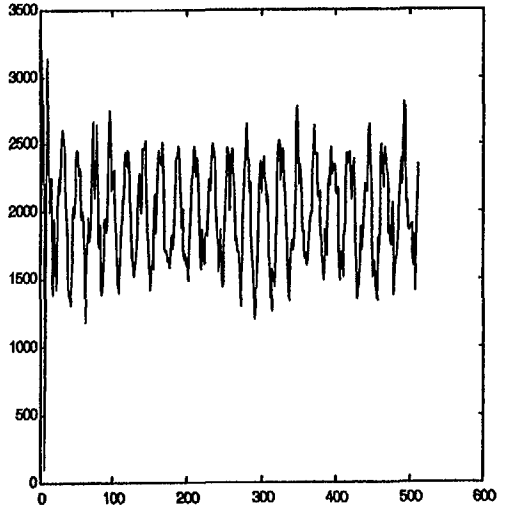

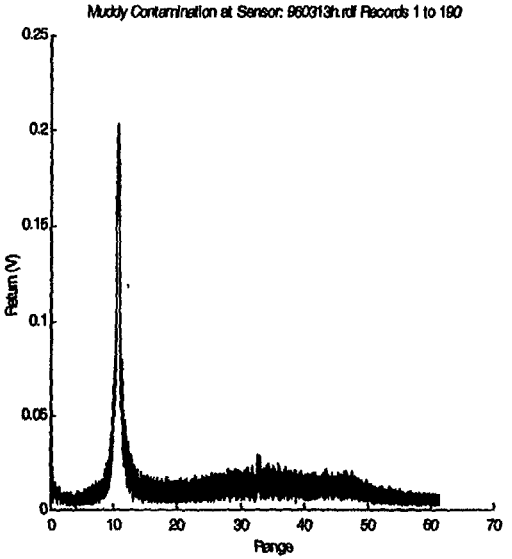
Muddy Contamination at Sensor: 960313h.rdf Records 1 to 190
Return (V)
Range
0.25
0.2
0.15
0.1
0.05
0
0
10
20
30
40
50
60
70

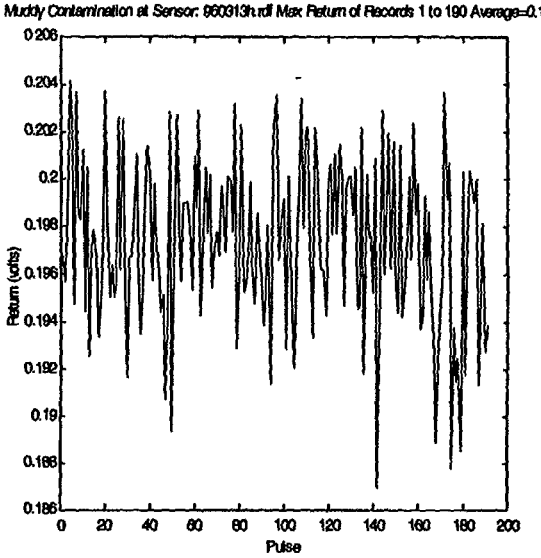
Muddy Contamination at Sensor: 960313h.rdf Max Return of Records 1 to 190 Average=0.1974
Return (volts)
Pulse
0.206
0.204
0.202
0.2
0.198
0.196
0.194
0.192
0.19
0.188
0.186
0
20
40
60
80
100
120
140
160
180
200

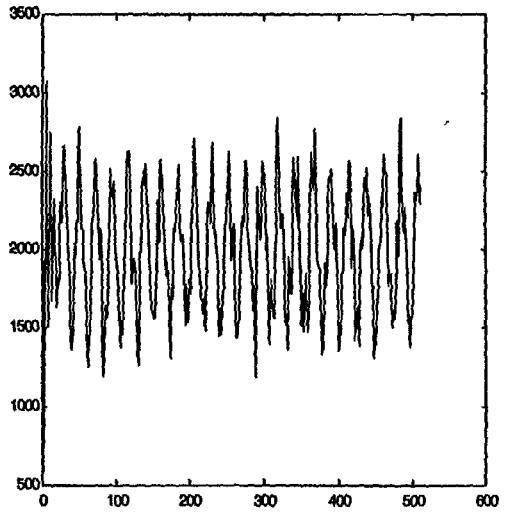
3500
3000
2500
2000
1500
1000
500
0
100
200
300
400
500
600

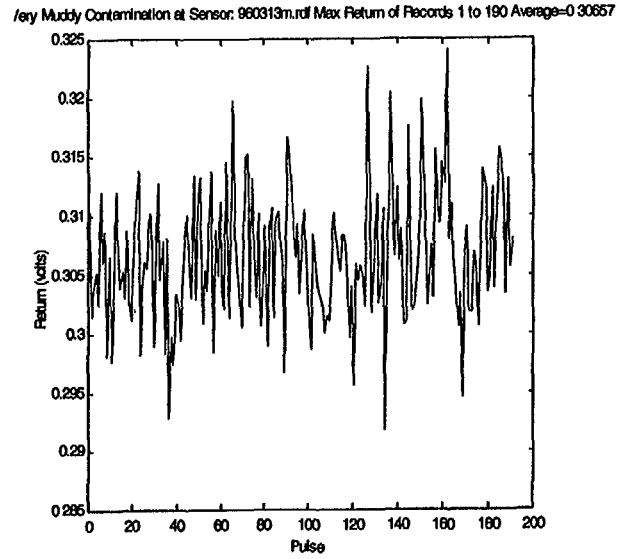
/ery Muddy Contamination at Sensor: 960313m.rdf Max Return of Records 1 to 190 Average=0 30657
Return (volts)
Pulse

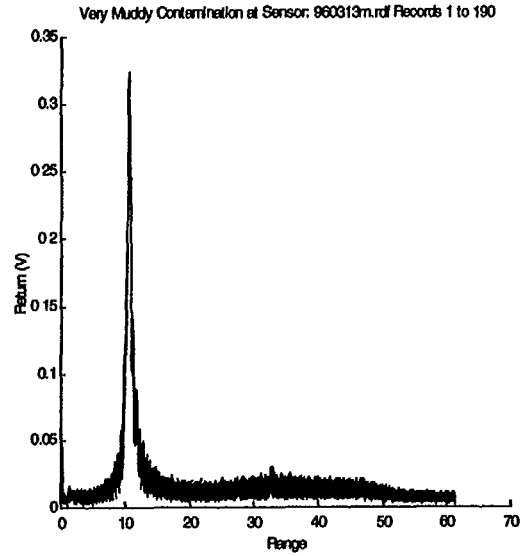
Very Muddy Contamination at Sensor: 960313m.rdf Records 1 to 190
Return (V)
Range

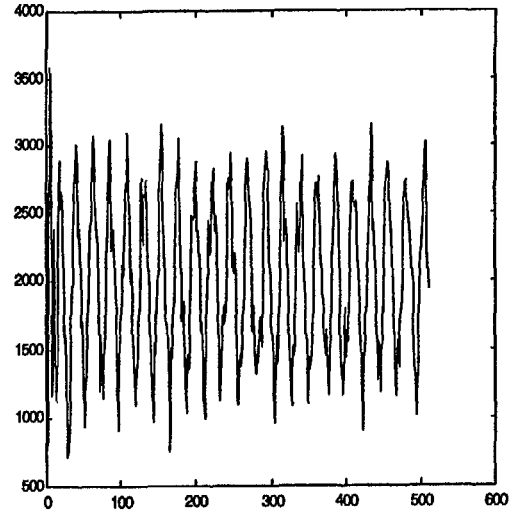

APPENDIX C. ERIM TESTBED VEHICLE AND DATA ANALYSIS SYSTEM

To support the evaluation of the TRW FLAR sensor in a true roadway environment, ERIM has developed an ITS Testbed System (TBS). ERIM's ITS Testbed System consists of two major components: (1) the Data Collection System (DCS), and (2) the Data Analysis System (DAS). The primary functions of the Testbed System are:

- Sensor data capture (both raw and processed data)
- Roadway environment monitoring to provide ground truth data
- Data reduction and analysis

The ERIM Testbed System was designed to be extremely flexible to support the future development and evaluation of sensors and algorithms for Advanced Vehicle Safety Systems. The remainder of this appendix will not go into detail on how the testbed vehicle was developed, but rather concentrate on its data collection and analysis capabilities, including the type of data collected, the DCS's limitations, the variety of processing techniques, indexing, and data reduction options.

This appendix is divided into three sections:

- C.1 Data Collection System,
- C.2 Data Analysis System, and
- C.3 ERIM Processing Software.

C.1 DATA COLLECTION SYSTEM

The first component of the ERIM Testbed System is the Data Collection System which acquires the test data and stores it for later use in the Data Analysis System.

C.1.1 Instrumentation Block Diagram

The Data Collection System (DCS) instrumentation is physically housed in a full-size van referred to as the Testbed Vehicle (TBV). Pictures of the TBV and instrumentation rack are shown in Figure C-1. The TRW FLAR sensor is mounted to the platform extending out from the front grill and bumper. A block diagram of the DCS instrumentation is provided in Figure C-2.

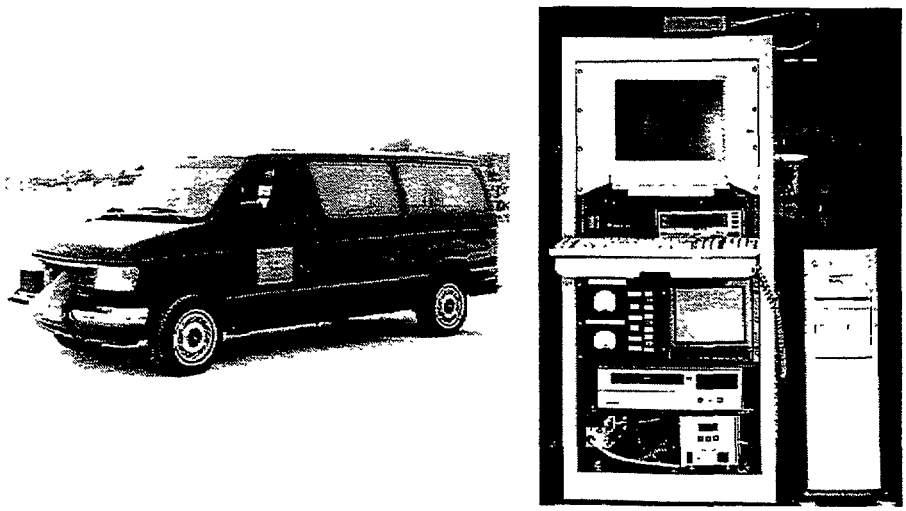

Figure C-1. Testbed Vehicle and Instrumentation Rack

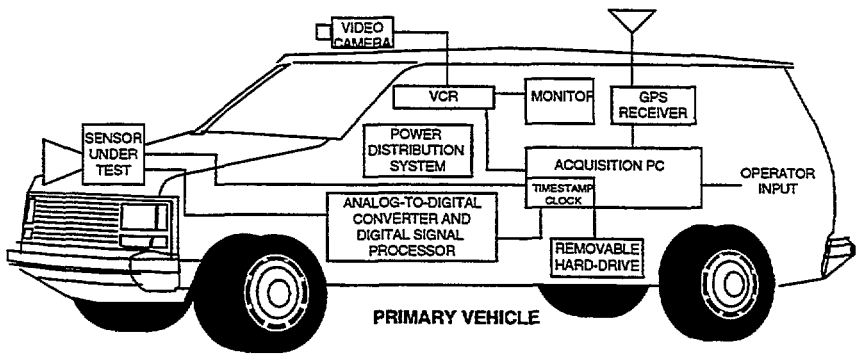

Figure C-2. Data Collection System Instrumentation Block Diagram

A 1300 Watt Power Inverter is used on board the TBV to convert the 12 volt DC vehicle power to 120v 60 Hz power. The 120v 60 Hz power is isolated from the vehicle and provides power to all the DCS instrumentation.

A Gateway I486 66MHz EISA-bus PC functions as the primary controller for the DCS instrumentation. A PC-based architecture was used so that the system can be easily expanded in the future. The collection PC has a precision time-stamp board which is synchronized to GPS time. Data from the time-stamp board is used to tag each set of data which gets recorded to disk by the PC. The collection PC also has a removable hard drive which is used to transfer data files between the Data Collection System and the Data Analysis System.

The interface between the collection PC and the raw TRW FLAR output is a high speed A/D converter and a programmable digital signal processing (DSP) board. The A/D converter runs at 10 MHz to provide ample oversampling of the FLAR 2 MHz IF signal. The DSP option provides a way to experiment with new processing techniques in real time. Under normal conditions, no DSP is performed and the raw data is recorded by the collection PC for later analysis. The A/D board, which is dual channel, also records the analog AGC signal. Knowledge of the AGC signal value is critical for properly interpreting the return signal levels intercepted by the FLAR. In addition to capturing the raw FLAR data, it is necessary to record the processed TRW data for analysis purposes. The collection PC

uses an RS232 data link as a means of transferring the TRW processed data from the FLAR to the collection PC memory.

To capture a visual representation of the roadway environment, a video camera is mounted in the front windshield of the TBV. The video data is recorded on a video cassette recorder and displayed to the DCS operator on a 9" monitor. The video cassette recorder has an on-board clock which timetags each frame. This enables later reconstruction of the roadway testing on the Data Analysis PC.

The final piece of instrumentation on the TBV is a Global Positioning System (GPS) receiver and associated antenna. The GPS receiver serves two functions. First, the highly accurate GPS clock and 1 pulse-per-second output provides the time reference for synchronized time-tagging of data collected by the PC and the video cassette recorder. Second, the GPS position data is used as a rough truthing mechanism for the FLAR sensor evaluation. By placing another GPS receiver in a lead vehicle, the position data from each vehicle can be used to help identify errors in the reported FLAR range data.

C.1.2 Basic Collection Capabilities

A summary of the DCS capabilities is provided below:

- Record a 12-bit digital version of the unprocessed FLAR IF signal on a pulse-by-pulse basis
- Perform some digital signal processing (e.g., FFTs) on the FLAR IF signal in real time, to quickly test new processing algorithms in the field
- Record video images of the roadway environment during data collection experiments
- Record GPS location information in both the TBV and a secondary lead vehicle for range truthing purposes
- Time tag all radar, GPS position, and video data so it can be synchronized during playback on the Data Analysis System
- Store all radar data on a removable hard drive and video data on a VHS cassette, for transportability and archiving

The real value of the DCS is realized by its ability to capture raw FLAR IF data corresponding to a specific roadway scenario, as represented by the video images. Since the IF data is stored in a computer file, a host of different processing algorithms can be applied to the raw data and the resulting sensor performance compared. Without the DCS, the developer would have to re-create the roadway scenario in order to compare algorithm techniques—an extremely difficult task. However, since the DCS stores the pertinent data for each scenario, a particular scenario can be replayed again and again on the Data Analysis System (described below) with any combination of processing algorithms.

As previously mentioned, the DCS architecture was designed to be as flexible as possible. This flexibility will allow for the future incorporation of new sensors and equipment. The primary issues for interfacing to new sensors are the data rates and frequencies of the signals to be collected. If the combination of these parameters exceeds the current limitations of the 10 MHz A/D board in the collection PC, the system can be upgraded with a new off-the-shelf data acquisition or custom hardware can be designed as necessary.

Other expansion possibilities include is monitoring brake, throttle, and steering angle to begin investigating human factors issues associated with automotive radar. There is also potential for tying the FLAR system to the testbed vehicle's cruise control, anti-lock braking, and supplemental restraint systems.

C.1.3 Enhanced Collection System Capabilities

C.1.3.1 New Sensor Head

A new three beam FLAR sensor head (Model # AICC-3B-02) was received from TRW. The new sensor represented the next generation of packaging technology, combining more functions (e.g., ability to select one of three beams in azimuth) in a smaller package. This new sensor was mounted on the ERIM Testbed System with a swivel mount that allowed the sensor to be aligned with the vehicle centerline without having to drill new mounting holes or use shims.

The new sensor head was tested against a known target to verify correct installation and performance.

C.1.3.2 Beam Select Switch

A beam select switch was provided by TRW. This switch was installed inside the testbed vehicle and allows the user to override the beam select signals sent from the DSP. That is, it allows the user to control which beam the FLAR is using independent of the radar operating mode.

C.1.3.3 Real Time DGPS Link

The Global Position System (GPS) is a satellite-based navigation system operated and maintained by the U.S. Department of Defense. GPS consists of a constellation of 24 satellites providing world-wide, 24 hour coverage. GPS provides the most accurate positioning of any currently active system. Being a satellite-based system it also does not suffer from degradation due to weather or limited coverage. Position accuracy is 100 Meters Circular Error Probability (CEP) for non-differential operation. That is, the reported position is within 100 meters of the actual position 95 percent of the time. Position accuracy improves to 5 meters CEP when operating in Differential GPS (DGPS) mode.

GPS is used in the ERIM TBS to provide truthing of vehicle positions during dynamic testing. One GPS unit is installed in the Testbed System and another in the target vehicle. The relative position of the two vehicles can be determined by post-processing the data from the two DGPS units. Each GPS unit receives the same correction data for the given set of satellites via the differential link. This being the case, the relative accuracy of the two units should be much better than the 5 meters absolute accuracy specified for each unit.

The differential unit installed in the Testbed System is a Trimble Navigation SVeeSix PLUS XT DGPS. The unit consists of a receiver module and a magnetic mount antenna. The system is integrated with the Data Collection System as shown in Figure C-3.

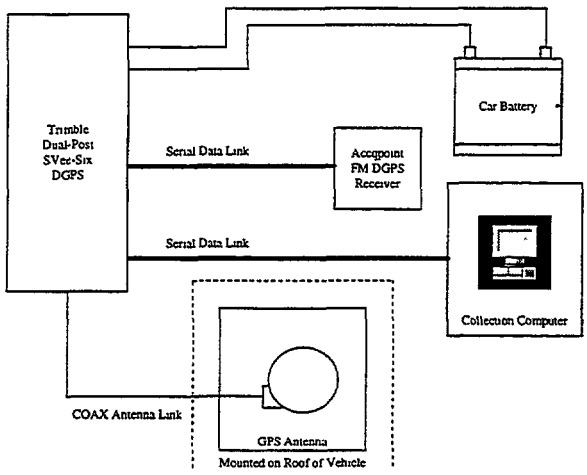

Figure C-3. The DGPS System

Upon power-up the GPS unit starts to search for satellites. The unit is designed to ensure that at least three satellites are found within the first two minutes of power-up. As soon as three satellites are found the unit starts to calculate an initial position fix. Typically the first position fix will occur in less than 5 minutes.

Differential operation is provided via an ACC-Q-POINT FM subcarrier receiver. The ACC-Q-POINT data is provided by a subscription service which ERIM has acquired. Upon power-up, the differential receiver module starts a search for correction data from an FM radio station that, as a subscription service, carries the differential correction parameters in a sub-band. The receiver then decodes the correction data and then transmits the data via a serial data link to the Trimble S-Vee-Six GPS receiver. If no differential correction sub-bands are found the unit defaults to a non-differential operating mode.

Position data (latitude and longitude in WGS-84 datum) is output to the collection computer twice per second (2 Hz). Velocity data is also output to the collection computer at a 2 Hz rate. Both the velocity and position data are time stamped with GPS time and store on the collection computer hard disk. GPS time stamps differ from Universal Coordinated Time (UTC) by a slowly varying constant. The equation describing this difference is:

$$UTC = GPS(time) — GPS/UTC(offset)$$

The GPS/UTC(offset) was 10 seconds as of August 1994. This offset increases by 1 second approximately every 18 months.

A duplicate GPS/DGPS system is located in a secondary vehicle and the location is recorded on a laptop PC. This secondary vehicle is used in conjunction with the testbed vehicle to run orchestrated tests. The GPS information from each vehicle is then used to provide truthing data against which the FLAR performance can be compared. See Appendix D for more on DGPS truthing.

C.1.4 Collection Software

The collection PC runs a DOS-based application that collects data from all the devices shown in Figure C-2. The DOS-based application runs in real-time and provides a menu-driven user interface. The operator has complete control over the data collection parameters. The operator also has options which allow for system as well as FLAR performance testing. This allows verification of system operation and FLAR baselining characterization before and after each collection run.

The flow diagram in Figure C-4 describes the data collection software processes. Once all the devices have been properly configured and the data acquisition board has been synchronized to the FLAR operation, the software enters the main loop of the data collection process. The main loop consists of capturing and time-tagging each radar pulse IF signal in a seven pulse frame. At the end of each frame, the TRW processed data is time-tagged, data integrity checks are made, and the entire set of data for that frame is written to disk. The main loop continues to execute until halted by the operator.

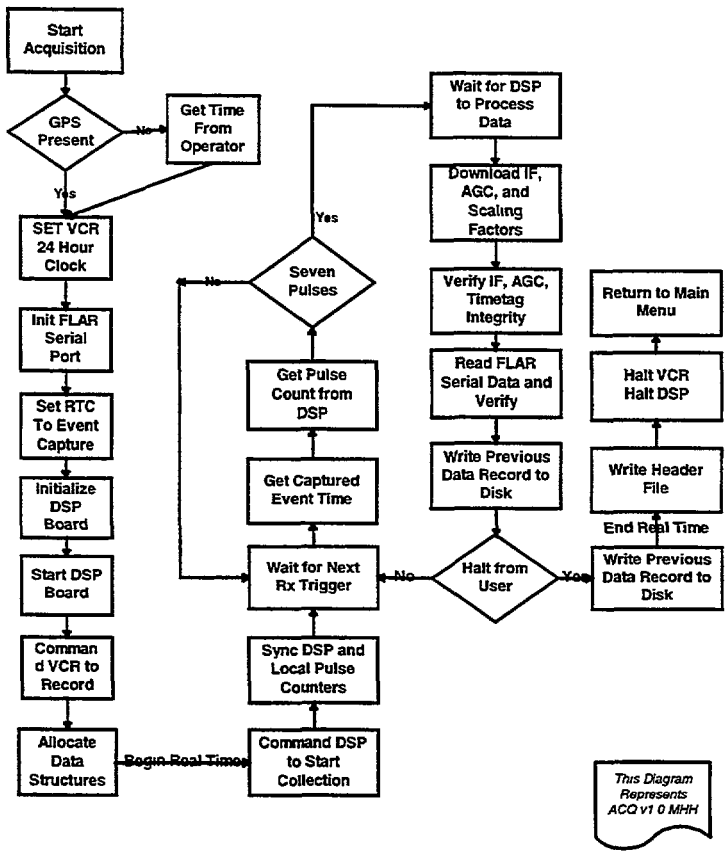

Figure C-4. Collection Software Flow Diagram

C.2 DATA ANALYSIS SYSTEM

The second component of the ERIM Testbed System is the Data Analysis System (DAS). The DAS is designed to accept data from the Data Collection System and give the operator the means of analyzing and reducing the data. The concept for the Data Analysis System is illustrated in Figure C-5. The DAS is hosted by a 90 MHz Pentium PC. Other equipment includes the removable hard drive which, allows data to be transferred from the collection PC to the analysis PC, and a VCR with time-stamp indexing capability.

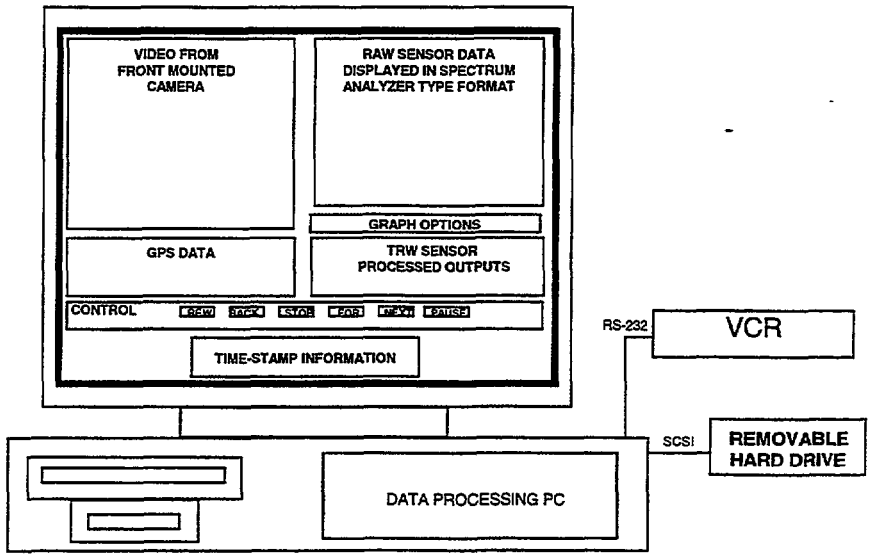

Figure C-5. Data Analysis Concept

C.2.1 Operator Interface

The data analysis software is a windows-based application developed with Microsoft Visual C++. This provides a user-friendly graphical interface to the DAS controls. Once a data file has been specified, the analysis program's VCR-like controls allow the operator to run the collected data backward and forward as desired. The current position within the data set is indicated by the time-stamp information displayed at the bottom of the screen. Video data and raw radar data corresponding to the current time stamp are displayed in the two large windows at the top of the screen. This allows the operator to visually analyze how the radar is responding to the given roadway environment.

The TRW-processed range, range rate and other information are displayed just below the plot of the raw radar data. The operator can now visually analyze how the TRW processor is interpreting the raw radar data and how it corresponds to objects in the scene. The GPS truthing information is also displayed when available.

C.2.2 Analysis Capabilities

The first step in the data analysis process is to pre-process the data using the ERIM generated FlarPP program. This program merges the radar data with the auxiliary data both provided by the FLAR sensor via the removable disk of the collection PC. The output is then sent to the data analysis software.

A summary of the DAS capabilities is provided below:

- Operator can replay collected data forward and backward via VCR-like controls
- Operator can quickly index through a data set by designating a specific time-stamp OR performing a video search to find a specific roadway event
- Data files can be segmented into smaller "specific scenario" subfiles by designating time-stamp information
- The beam pattern of the FLAR can be displayed on the video screen as a visual queue to the operator
- Various radar data processing algorithms can be applied to the same set of data and results compared

Combining the capabilities listed above into a single analysis package provides a powerful tool in performing data reduction, event searches, and data analysis. As previously mentioned, the real value of the Testbed System lies in its ability to perform various processing operations on a single set of data which corresponds to a particular roadway scenario. This offers developers an efficient way to refine algorithm implementation and meet functional requirements.

C.2.3 Matlab Analysis Software

Matlab routines allow independent analysis of the raw sensor data. These programs were developed for two reasons. First they allow the ERIM developed software to be checked independently of the TRW sensor. Second, they allow characterization of the FLAR sensor solely as a radar sensor, not as a radar sensor tailored to automatic cruise control applications. In other words, the Matlab software allows analysis of the raw data without any FLAR DSP calculations added in.

Individual radar pulses may be observed and processed, or multiple radar pulses may be averaged, in order to reduce the effect of random noise. Figure C-6 shows the results of averaging the FFTs of six radar returns. The dotted line shows the FFT of one radar return. The solid line shows the average of six returns. The averaging has the effect of smoothing out and lowering the average noise power.

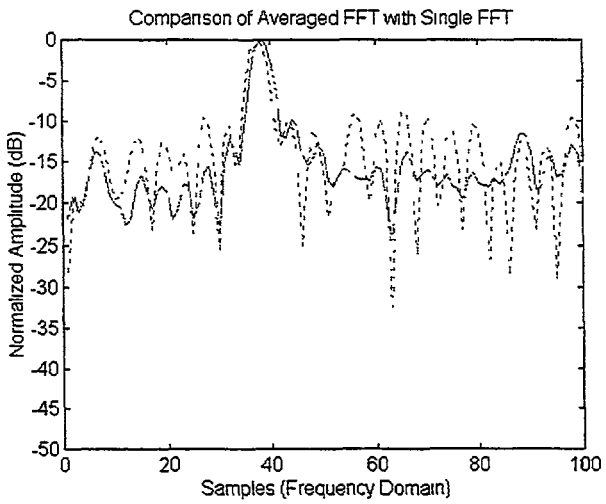

Figure C-6. Averaging Six Radar Returns

C.3 ERIM PROCESSING SOFTWARE TECHNICAL DESCRIPTION AND VERIFICATION TESTS

C.3.1 ABSTRACT

This section will present a description of the ERIM processing software used to verify the operation of the TRW Forward Looking Automotive Radar (FLAR). The ERIM hardware and software was verified using a synthesizer generated sine wave of known frequency and amplitude. The sine wave was recorded and processed through the data processing chain and also verified via independent analysis.

C.3.2 ERIM HARDWARE/SOFTWARE VALIDATION

This battery of tests was designed to check out the ERIM-specific hardware and software. Specifically it checks out the A/D converter board in the data acquisition computer and the FLAR Preprocessor (FlarPP) software.

C.3.3 TEST SETUP

An HP 3325A Synthesizer/Function Generator was connected directly to the Acquisition Computer A/D board. The input sine wave was measured using a Tektronics 475 oscilloscope to establish a baseline. The collected data was then processed using a custom Matlab program and the FlarPP program. The data from all three sources was compared to verify the correct operation of the collection and preprocessor systems. The following list shows the primary frequencies and voltages injected into the collection system.

1. 10 mVolts P-P, 100 KHz.
2. 1 Volt P-P, 100 KHz
3. 10 mVolts P-P, 1 MHz
4. 1 Volt P-P, 1 MHz

Other frequencies were injected in order to find the A/D converter foldover frequency. The frequency exactly matched the theoretical frequency. Therefore none of the plots will be presented.

The FLAR PreProcessor (FLARpp) program calculates the Fourier Transform of the raw radar returns and acts as the bridge between the FLAR sensor/collection system and the Data Analysis System (DAS). The FLARpp program accepts as input the radar data file (*filename*.rdf) and the radar header file (*filename*.hdr) and outputs a processed data file (*filename*.ppr) formatted to be used by the DAS. Each individual return of 512 real time domain samples is zero padded (i.e., zeros are added to the end of the sequence) to a length of 1024 and Fourier Transform by a radix 2 FFT routine. The output of the FFT routine is 1024 complex data samples of which only the first 512 are unique. The first 512 samples are converted from complex to magnitude samples and scaled by Eq. (C-1).

$$X(n) = \frac{4}{N}\sqrt{I(n)^2 + Q(n)^2} \qquad \text{(C-1)}$$

where $X(n)$ is the n^{th} output sample

N is the size of the FFT

I is the real component of the n^{th} complex sample

Q is the imaginary component of the n^{th} complex sample

The factor of four in the numerator is different than the factor of two that is usually in the numerator because of the scaling effect of zero padding on the FFT routine. Had the data been transformed without the zero padding, then the number in the numerator would have been two.

The custom Matlab program calculates the FFT of the radar returns much like the FLARpp program, with two exceptions. First, the Matlab program zero pads by a factor of four to a total length of 2048 points. This does not affect the spectrum, but it does give finer gradations in the frequency domain. Second, it averages six consecutive pulses in the frequency domain. This reduces the noise power in the spectrum; in fact, a signal-to-noise ratio (SNR) improvement of about 8 dB is realized. This is closer to the algorithm implemented by the FLAR processing software than the FLARpp output is. The result is then output in a graphical format.

C.3.4 TEST RESULTS

Tests verified that the A/D converter is a 12 bit converter that has an input voltage range of ± 1 Volt (i.e., 2 Volts P-P). The A/D converter samples at a 10 MHz rate. The collection software saves every other sample (i.e., it down-samples the data by a factor of two) without any anti-alias filtering. This process is considered valid as the input data is band limited to approximately 2 MHz. However some fold-over is inevitable, due mainly to the noise power which is spread equally over all frequencies.

Figures C-7 through C-11 show the results of the Matlab runs on both the raw radar data and the FlarPP processed data. The plots show very consistent results between the FlarPP data and the raw data processed independently through Matlab. The peak frequencies in the FlarPP generated plots are slightly different from the raw data Matlab plots because the FFT size is such that there is no bin at exactly the input frequency. The Matlab plots were generated using an FFT size twice as large as that used by the FlarPP, and thus the frequency resolution is greater.

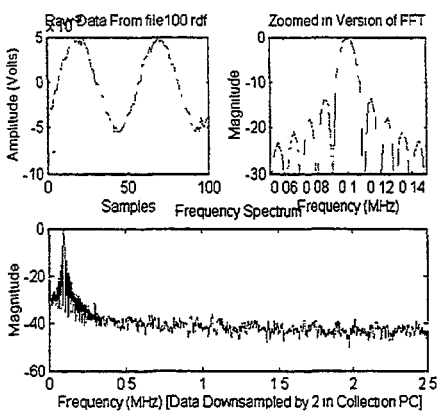

Figure C-7. Matlab Processed Data

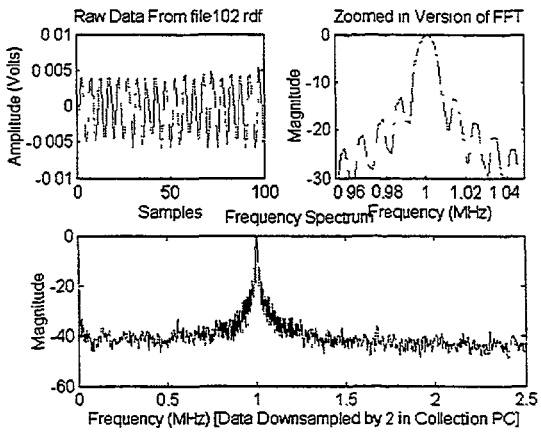

Figure C-8. Matlab Processed Data

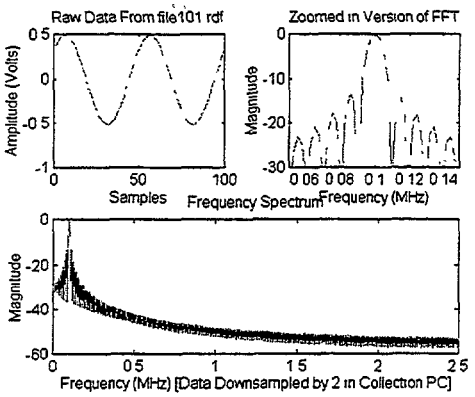

Figure C-9. Matlab Processed Data

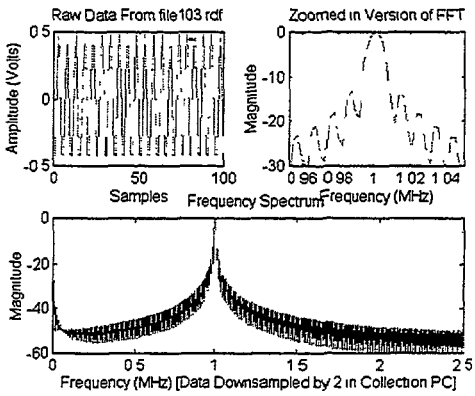

Figure C-10. Matlab Processed Data

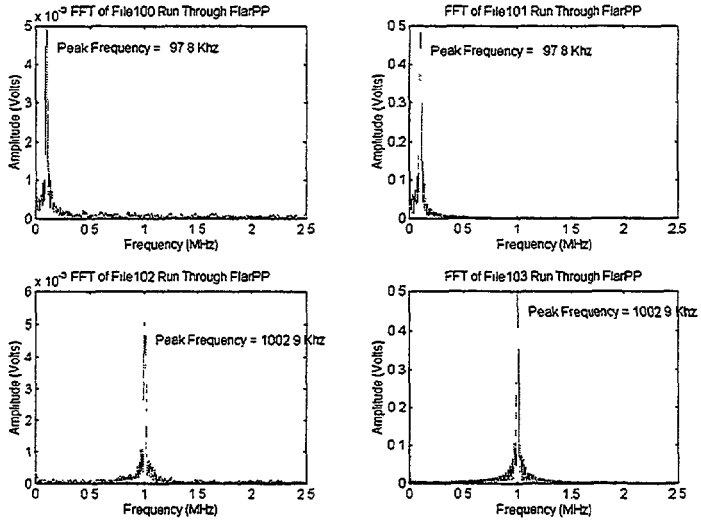

Figure C-11. Data Processed Using FLARPP Software

C.3.5 CONCLUSIONS

This test verified the operation of the ERIM constructed portion of the FLAR testbed system. Known test signals were input and followed throughout the system in order to verify the correct operation of the FLAR testbed.

APPENDIX D. DIFFERENTIAL GPS TRUTHING

D.1 INTRODUCTION

A Differential GPS (DGPS) system was used as a truthing mechanism for assessing the range and range rate accuracies of forward-looking automotive radars, or other range, and range rate measurement systems, when the automobiles undergo dynamic maneuvers. The typical test scenario involves two vehicles, each equipped with GPS receivers. The primary vehicle was the ERIM testbed vehicle hosting the radar sensor under test. The secondary vehicle represented a typical vehicle that would be observed by the host vehicle during typical roadway driving. The proposed DGPS system provided an independent measurement of the "truth" trajectory, that is, the true range and range rate, between the primary and secondary vehicles. The proposed DGPS system must provide an accurate trajectory during vehicle accelerations in order to thoroughly assess the effects of vehicle dynamics on the radar signal. This appendix describes a test sequence to evaluate the accuracy of the proposed DGPS system during vehicle dynamics and demonstrates that such a system has sufficient accuracy for this application.

The truthing concept configuration consists of two vehicles equipped with GPS receivers that collect GPS data as the vehicles execute a test maneuver. At the same time, a basestation GPS located near the test site is also collecting GPS data. These data, which are intrinsically synchronized in time, are then processed off-line to produce an independent measurement of the range and range rate between the two test vehicles. Comparing the GPS-derived range and range-rate measurements with those produced by the radar sensor-under test provide an accurate assessment of the radar's range and range-rate measurement performance. This procedure was used during many of roadway tests conducted with the TRW FLAR sensor. Appendix F of this report contains a number of "GPS Range versus Radar Range" plots used to assess the performance of the FLAR sensor.

The post-processing of the GPS and radar data is performed by three software. The PNAV DGPS processing software is a commercial package provided by Ashtech. This software produces differentially corrected position and velocity data for each vehicle. These data are then processed by software developed by ERIM to produce the independent range and range-rate measurements of the vehicle pair. The final software module, also developed by ERIM, combines the two pairs of measurements to produce numerical and graphical comparisons of the data.

Before accepting the DGPS solution as a valid truthing mechanism, ERIM conducted experimental dynamic runs to assess the quality of the DGPS solution. These experiments were conducted with the ERIM Motion Measurement System (MMS). A high quality inertial navigation system, such as the MMS, can accurately measure relatively high frequency (that is, much greater than Schuler frequency) acceleration and can serve as the sensor to measure the "truth" trajectory during high dynamics if initial position and velocity errors are canceled. A high accuracy strapdown inertial navigation/Kalman filter algorithm is used to combine the DGPS position data with the inertial data to align the inertial platform and estimate the inertial navigation position and velocity errors and inertial sensor biases during periods of low vehicle dynamics. Prior to an applied acceleration or turn, the inertial navigation/Kalman filter algorithm is switched to the free inertial mode. In the free inertial mode the DGPS data is not applied to the inertial data, rather, the free inertial trajectory is calculated by integrating accelerometer data into inertial velocity and position. The free inertial trajectory is then compared with the DGPS trajectory during vehicle dynamics.

D.2 TRUTHING REQUIREMENTS

The performance requirements of vehicle-based radar systems vary depending upon the particular application (such as intelligent cruise control, lane change aid, forward collision warning, etc.). Table D-1 lists the proposed nominal requirements for an FCW system.

Table D-1. FCW System Performance Requirements

Measured Parameter	Performance
Range Accuracy	0.5 to 1 m
Range Rate Accuracy	0.3 to 1 m/s
Update Rate	10 Hz

These parameters relate to the required performance of the DGPS truthing system being proposed. A desirable truthing system would provide measurements of range and range rate that are an order of magnitude more accurate than the measurements of the system under test. The remainder of this appendix describes the results of a sequence of tests aimed at evaluating how well a DGPS system can meet the truthing system requirements.

DGPS performance can be categorized based on the combination of GPS observables which are combined to form the DGPS solution or trajectory. Five observables are available: the Coarse Acquisition or CA code on the L1 carrier frequency, the Precise or P code on the L1 carrier frequency, the P code on the L2 carrier frequency, the L1 carrier phase, and the L2 carrier phase. The carrier phase information can be continuously integrated to provide a fine measurement of change of range, or the rate of change of carrier phase can be used as a measure of range rate and used to smooth the code ranges. Three categories of DGPS performance were considered for the truthing system evaluation. The first category is a DGPS solution using all the observables with dual frequency continuously integrated carrier phase which requires a dual frequency receiver. The second category is a DGPS solution using the CA code and a single frequency carrier integrated phase. The third category is a DGPS solution using CA code with carrier smoothing. In general, the cost, complexity and performance decrease from the first to third categories.

D.3 DESCRIPTION OF TEST

The ERIM ITS testbed van is a 1994 Ford Club Wagon full-size van. The van has been modified to function as a data collection platform for evaluating radar-based and electro-optical-based automotive sensors. The instrumentation includes a Pentium-based PC, high-speed AD converters, video capture equipment, and supplemental environmental sensors.

Three 2-Hz GPS receivers were selected and installed in the van for the experiment. They included a Trimble 4000SE single frequency receiver, an Ashtech Z12 dual frequency receiver and an Ashtech DNS12 single frequency receiver. The three antennas were mounted on the roof of the van above the driver/passenger compartment area.

A 2 kilometer, roughly East/West, straight stretch of road with a 90 degree North bound turn at the East end served as the site for the experiment. An Ashtech Z12 ground reference receiver and a Trimble 4000SE ground reference receiver were set up on two known survey points approximately 150 meters from the 90 degree turn in the road. The Z12 ground reference receiver provides the differential correction for the Z12 and DNS12 rover receivers.

The following scenarios were selected for the experiment:

1. Maximum acceleration to a specified velocity, constant velocity for several seconds, then maximum braking to a stop;
2. High speed lane change;
3. Straight segment, 90 degree turn, then straight segment.

The maximum braking test represents a scenario in which the radar-equipped vehicle detects a leading vehicle in the same lane or adjacent lane that suddenly executes a panic stop. The lane change test represents a passing vehicle suddenly moving into the same lane ahead of the radar-equipped vehicle (i.e., a rapid "cut-in"). The hard turn test represents an radar-equipped vehicle that must track and sort vehicles and roadside targets while heading into and through a turn.

The ERIM Motion Measurement System (MMS) provides the reference or truth data for the evaluation of the DGPS system during high acceleration. The MMS, described in Reference D-2, was originally developed to provide highly accurate trajectory measurement of the airborne platforms used in the formation of inverse SAR imagery. It consists of a Honeywell H770 RLG INS modified to provide outputs of delta-theta and delta-velocity at 1200 Hz, a Datum 9250-5730 Time/Frequency Reference (atomic clock), and appropriate control and recording electronics. Some of the significant sensor error specifications are listed in Table D-2. As an example, an accelerometer bias of 50 micro-g would result in an position error of 24 millimeters after 10 seconds. An accelerometer scale factor error of 100 parts/million and an applied acceleration of 0.75 g for 4 seconds would result in a position error of 6 millimeters. The gyro error contributions are at least an order of magnitude less for these same time periods. Extensive testing, described in Reference D-2, has verified the performance of the INS. The MMS has been used in several other SAR programs. The MMS has recently been installed in the van where it was used to record the motion of the van for a SAR experiment involving ground moving target detection. The INS was mounted on the floor of the van, approximately in the center of the cargo area. The atomic clock provides the time tagging for the inertial data. The atomic clock is synchronized to GPS time by means of its own internal GPS receiver.

Table D-2. MMS Inertial Sensor Error Specifications

Error Source	Specification
Accelerometer Bias	50 ug
Accelerometer Scale Factor	100 ppm
Gyro Drift	0.007 deg/hr
Gyro Random Walk	0.002 deg/rt-hr

All data from the inertial navigation unit, the GPS receivers and the reference GPS receivers were recorded for post processing. The Ashtech data was processed using Ashtech PNAV software, the Trimble data was processed with both Trimble POSTNAV II and FLYKIN software. GPS data was processed to create several DGPS trajectories of position and velocity. Each trajectory covers the duration of the day's experiment. Several trajectories could be created from each receiver pair. For example, the Ashtech Z-12 data was processed to produce trajectories using several combinations of observables, including All Observables, CA Code plus L1 Carrier Integrated Phase, and CA Code with Carrier Smoothing. By selecting subsets of the five observables available in the Z12 data the second two trajectories can be created and used to emulate single frequency receivers. The advantage of the emulation of the single frequency receivers is to compare the three categories of trajectories with data recorded from the same rover antenna and L1 pre-amplifier. The single frequency DNS12 data and

Trimble 4000SE data were processed to provide trajectories using CA Code plus L1 Carrier Integrated Phase, and CA Code with Carrier Smoothing

The inertial data was processed with the Advanced Navigation Processor (ANP), a high accuracy strapdown navigation/Kalman filter algorithm developed under the MMS program. The ANP uses the 1200 Hz delta-theta and delta-velocity data to provide a 50 Hz navigation trajectory output of position, velocity, and attitude. The ANP Kalman filter is processed at a 1 Hz rate. The ANP Kalman filter can use position data from any of the DGPS trajectories to align the inertial platform and estimate the inertial system errors (this process is called aiding). The lever arm vectors from the INS reference point to the phase center of each GPS antenna were carefully measured. In the ANP, the position measurements from the selected DGPS trajectory are translated to the INS reference point for use in the ANP Kalman filter calculations. The 50 Hz inertial trajectory is translated back to the selected GPS antenna point for direct comparison to the DGPS trajectory. All DGPS and ANP trajectories for this experiment were referenced to a rectangular coordinate frame which is centered at the survey point occupied by the Ashtech ground reference receiver, with x-axis aligned with East, y-axis with North, and z-axis with the Up or vertical direction.

The experiment began with the set-up of the ground reference receivers. After positioning the receiver antennas over the survey points, data logging to laptop computers was initiated. The equipment in the van was turned on several minutes before the test began in order to allow enough time prior to the first run for the MMS to align. Each run executes one of the three scenarios described in the introduction. Data was collected continuously for the duration of the experiment. After several minutes of stationary data had been collected, the driver began the first run. A few minutes of stationary data collection was planned between each run to allow several minutes of data between each maneuver for inertial alignment. Data was collected on two days, July 9, 1996 (GPS day 191), and July 11, 1996 (GPS day 193).

The inertial data was initially processed to create one trajectory for the duration of the day's experiment. The beginning of each dynamic maneuver was identified from the inertial position, velocity, and attitude trajectories. The time for the beginning of the free inertial trajectory for each dynamic maneuver was selected to be approximately 1-2 seconds prior to the beginning of the maneuver. The inertial data and corresponding DGPS position data was then reprocessed in the ANP for each maneuver. The beginning of the aided portion of each ANP trajectory was selected to include at least four minutes of data prior to the free inertial time and long enough to include a 180 degree turn of the van/platform in order to refine the Kalman filter estimates of some of the inertial error states such as the accelerometer bias states and the platform tilt error states.

D.4 RESULTS

The results presented in this appendix come from the July 11 experiment; the data presented is from the Ashtech Z-12 receiver. All GPS data is referenced to the same rover antenna. Three DGPS trajectories are presented, including: all observables (labeled "0 All Observables"), CA Code plus L1 Carrier Integrated Phase (labeled "X CA Code+Integrated Carrier"), and CA Code with Carrier Smoothing (labeled "+ CA Code w/ Smoothing"). The time scale on each plot is referenced to the beginning of free inertial mode. The Ashtech DGPS trajectories were processed using both the automotive dynamics and aircraft dynamics selection in PNAV. No significant differences were evident between the two dynamics modes. The DGPS trajectories described in this paper were processed with the aircraft dynamics mode. The ANP Kalman filter used the All Observables DGPS position for the aided inertial mode.

The first series of plots come from Run 1, Eastbound maximum braking. The van was moving at a speed of approximately 45 m.p.h., 20 meters/sec, when a panic stop was initiated. Figure D-1 shows a 10 second span of the East position; Figure D-2 shows the corresponding East velocity data. From the inertial velocity data, the braking begins at approximately t = 1.2s and ends at about t = 4.5s. The rocking motion of the van on its suspension can be seen in the inertial velocity data from about t = 4.5s to t = 6s. At t = 6s the driver had released the brake and begun to slowly pull off to the side of the road (due to occasional traffic on the road). Note that the CA Code with Carrier Smoothing has a significant overshoot in position and velocity. Figures D-3 and D-4 show East position and velocity with an expanded time scale. The CA Code with Carrier Smoothing trajectory reaches a maximum error of 2.5 meters in position and velocity errors of 7 m/s relative to the inertial trajectory. The All Observables and the CA Code with Carrier Integrated Phase trajectory positions follow the inertial position closely. There is a bias of 0.25 meter between the All Observables and the CA Code with Carrier Integrated Phase trajectories, which is probably due to the difference in the number of observables used in the solution. The All Observables and the CA Code with Carrier Integrated Phase velocities are nearly identical and both exhibit a time lag relative to the inertial data.

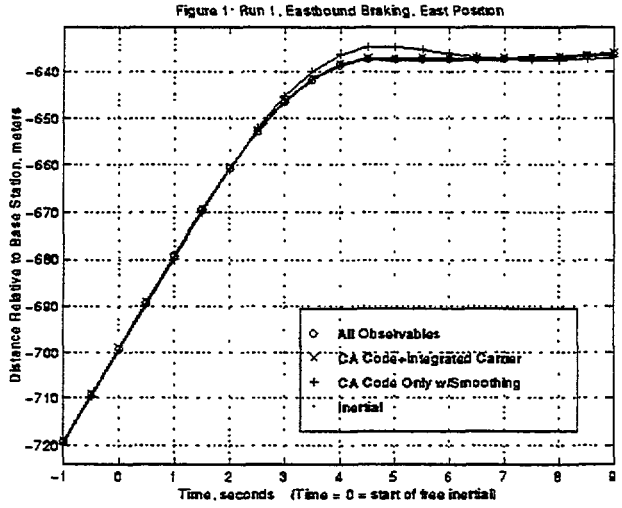

Figure D-1. Run 1, Eastbound Braking, East Position

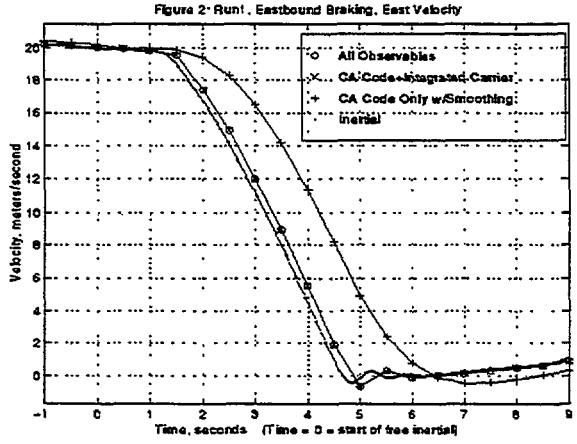

Figure D-2. Run 1, Eastbound Braking, East Velocity

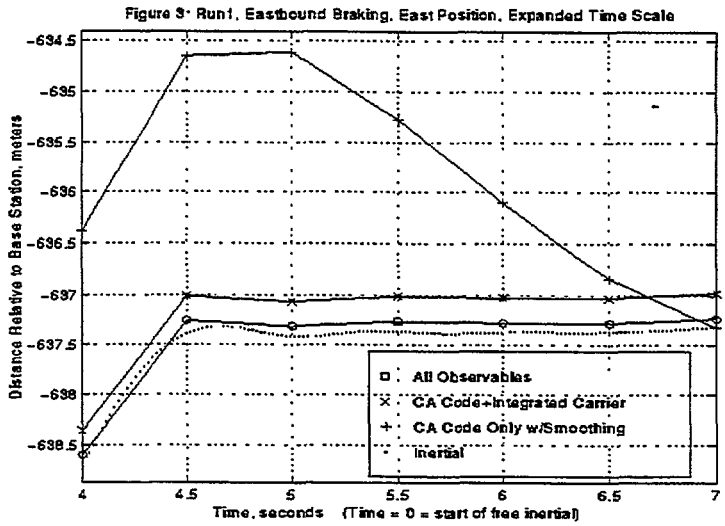

Figure D-3. Run 1, Eastbound Braking, East Position, Expanded Time Scale

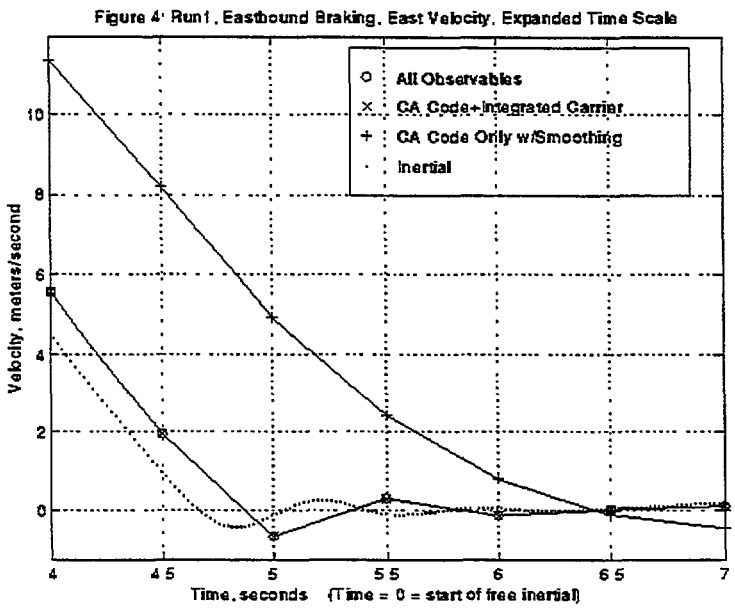

Figure D-4. Run 1, Eastbound Braking, East Velocity, Expanded Time Scale

Figure D-5 shows the Up position for the Eastbound Braking, Run 1. The plot shows that there could be a noticeable difference in DGPS trajectories using All Observables and one using the CA Code and a single frequency Carrier Integrated Phase. This example shows a difference of 1.75 meters. The CA Code with Carrier Smoothing position trajectory shows a curious response which can be more easily seen in the velocity data in Figure D-6. This velocity trajectory reaches a peak of 0.3 m/s vertical velocity. The vertical velocity of the other DGPS solutions appear to follow the inertial data with the same data lag observed in the horizontal velocity. As a side note, the slight negative velocity seen in the vertical velocity while the van is still moving is real. According to the local terrain survey data, the road is not level; it decreases in elevation about 3 meters going from West to East over the 2 kilometer stretch.

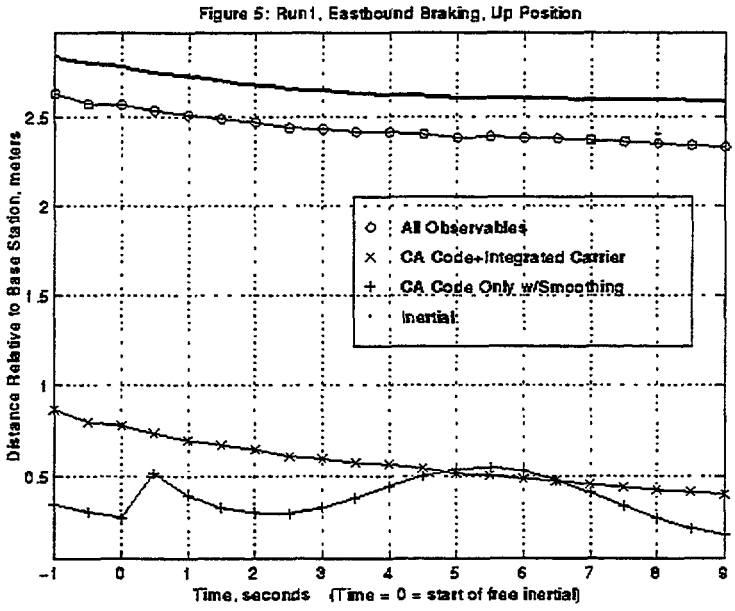

Figure D-5. Run 1, Eastbound Braking, Up Position

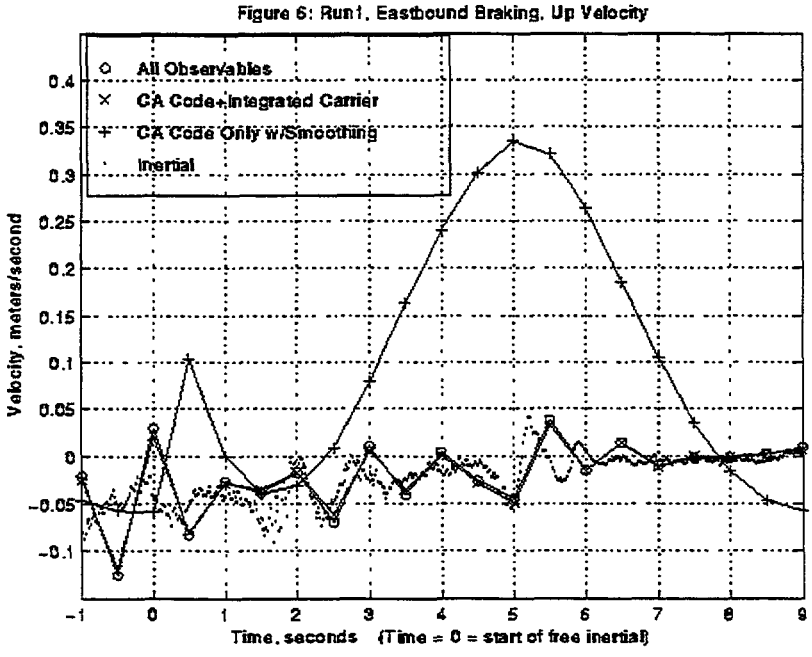

Figure D-6. Run 1, Eastbound Braking, Up Velocity

The next series of plots come from Run 3, the Eastbound Lane Change. Figure D-7 shows the North position, once again showing that a bias exists between the All Observables and the CA Code with Carrier Integrated Phase trajectories. The data indicates that the road is not precisely East/West. Figure D-8 shows the North velocity. In this plot, it can be seen that the sudden lane change is too fast for the filter in the CA Code with Carrier Smoothing trajectory. Figures D-9 and D-10 show the North position and velocity with an expanded time scale. The DGPS solutions using continuously integrated carrier phase follow the dynamics closely, with the All Observables solution exactly following the free

inertial solution and the CA Code with Carrier Integrated Phase solution showing about a 0.9 meter bias relative to the free inertial trajectory.

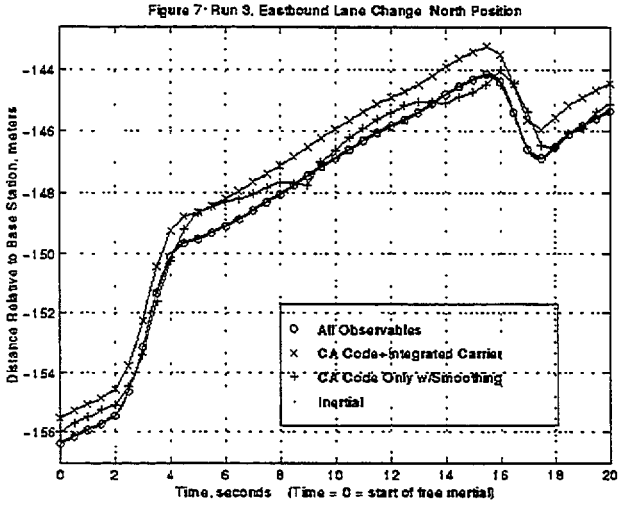

Figure D-7. Run 3, Eastbound Lane Change, North Position

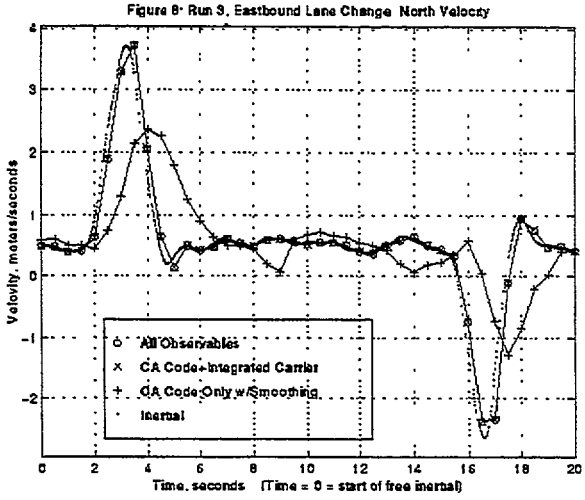

Figure D-8. Run 3, Eastbound Lane Change, North Velocity

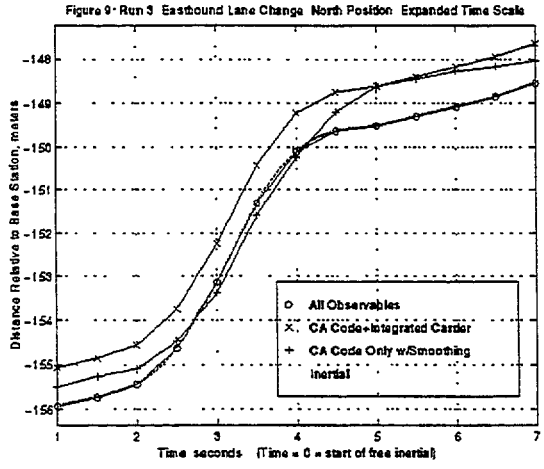

Figure D-9. Run 3, Eastbound Lane Change, North Position, Expanded Time Scale

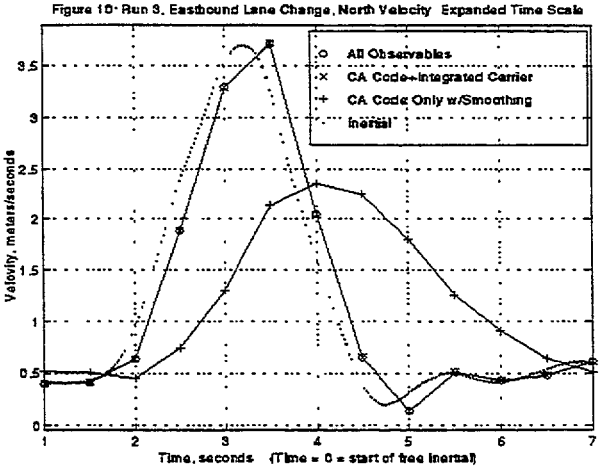

Figure D-10. Run 3, Eastbound Lane Change, North Velocity, Expanded Time Scale

The next series of plots come from Run 6, the East to North turn. Figures D-11 and D-12 show the East and North position while Figures D-13 and D-14 show the East and North velocity. At the beginning of free inertial time, t = 0s, the van is slowing and begins to brake prior to the turn at t = 4s. The van is in the turn from about t = 7s to t = 12s, as can be seen from the velocity data. At t = 12s the van is out of the turn and begins accelerating back up to 20 meters/second. Once again, the data shows that the CA Code with Carrier Smoothing has errors on the order of a few meters in position and several meters/second relative to the inertial data during the turn. The All Observables and CA Code with Carrier Integrated Phase trajectories show good response during the turn in comparison to the inertial data.

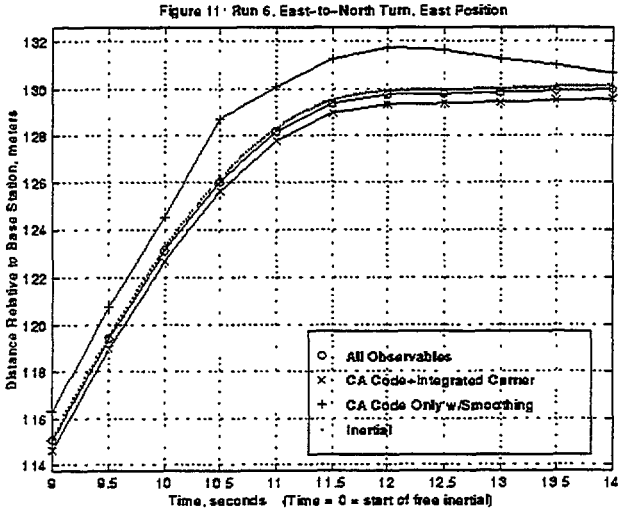

Figure D-11. Run 6, East-to-North Turn, East Position

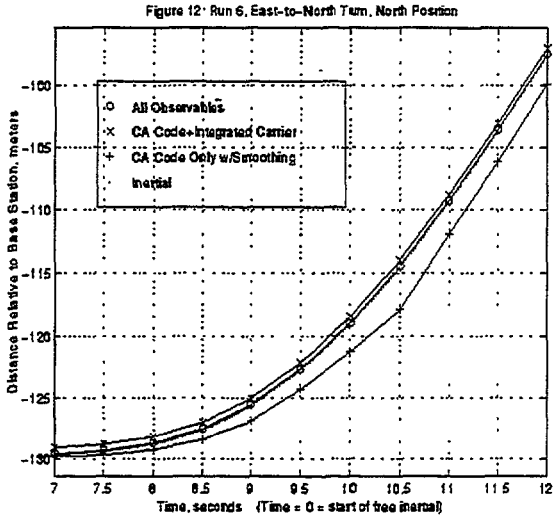

Figure D-12. Run 6, East-to-North Turn, North Position

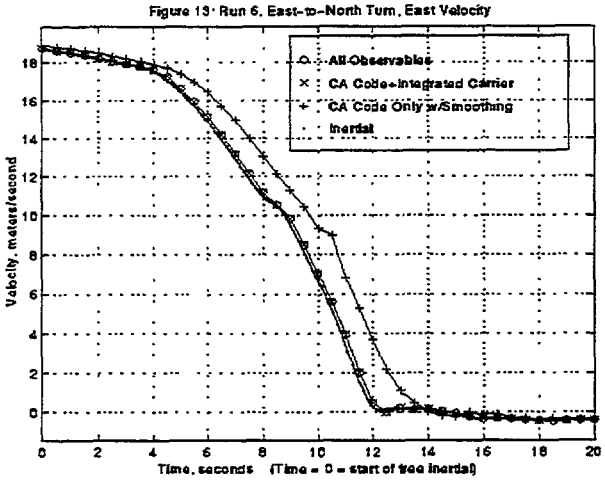

Figure D-13. Run 6, East-to-North Turn, East Velocity

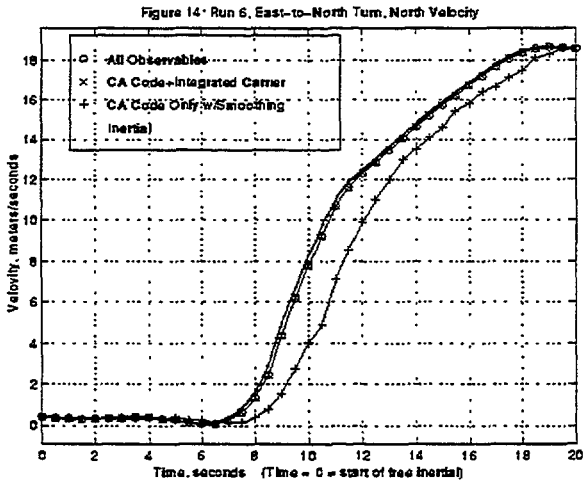

Figure D-14. Run 6, East-to-North Turn, North Velocity

D.5 CONCLUSIONS

The data presented in this appendix are obtained from the same Ashtech Z-12 rover receiver and processed in different combinations of observables to represent dual frequency carrier integrated phase DGPS solution, a CA Code with single carrier integrated phase DGPS solution, and a CA Code only with carrier smoothing solution. In this manner, the results are all referenced to the same rover antenna. The DNS-12 receiver and the Trimble 4000SE receiver are both single frequency receivers. The data from those receivers were processed to obtain trajectories corresponding to the CA Code with Carrier Integrated Phase and CA Code with Carrier Smoothing. After correcting for the different lever arm vectors from the inertial reference point and the phase center of the other two antennas, results similar to

the CA Code with Integrated Phase and CA Code with Carrier Smoothing were obtained. This shows that the emulation of these systems is valid and the conclusions are also valid.

The DGPS solutions using continuously integrated carrier phase observables have been shown to significantly improve accuracy relative to CA Code with Carrier Smoothing during the scenario dynamics. This is when radar signals from FCW systems will exhibit significant range, range rate, and Doppler modulation. By continuously integrating the DGPS carrier phase, the DGPS solution accurately follows the dynamics expected for the FCW radar system evaluation. This can be understood by realizing that the continuously integrated phase measurement is a delta-position or integrated velocity measurement that is similar to the delta-velocity measurement obtained by an inertial navigation system.

The selection of a single frequency receiver that is capable of continuously integrated carrier phase DGPS offers cost savings over a dual frequency receiver. However, the testing demonstrated that noticeable position errors can exist in the single frequency solution. The continuously integrated carrier phase observables provide a fine measurement of change of position, but the CA code and the two P code measurements provide an estimate of the integer ambiguities inherent in the carrier phase measurements and help control the residual absolute position error if used in a complementary filter implementation. It seems reasonable that the standard deviation of that residual position error is larger for the single frequency solution using only the CA code observable. Also, the time to reach an accurate estimate of the integer ambiguities can be significantly longer for the single frequency receiver because it does not have the benefit of the wide-lane ambiguity processing that is available with two frequency data. Figure D-15 shows an example of the settling time of the dual frequency carrier integrated phase solution and the single frequency carrier integrated phase solution. The plot shows the North position of the van in which the van began moving 135 seconds after data recording was initiated. The CA Code with Carrier Integrated Phase solution differs by approximately 1 meter relative to the All Observables solution while the van is still stationary. Once the van begins moving, the error relative to the All Observables solution reaches as much as 5 meters. The solutions appear to converge after several minutes of data. A single frequency DGPS solution would require a programmed settling time built into each FCW evaluation test each time data-logging is initiated. The dual frequency receiver system can reduce this time to a minimum and also reduce the time needed to reacquire and correct for cycle slips after the periods of signal blockage that can be expected in a ground vehicle application. A dual frequency receiver using differential carrier integrated phase processing with all observables would contribute to increased efficiency and simpler operation of the truthing system in the FCW radar evaluations.

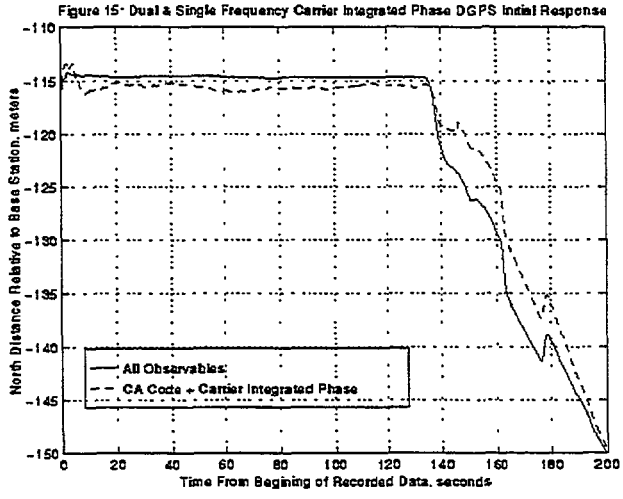

Figure D-15. Dual and Single Frequency Carrier Integrated Phase DGPS Initial Response

D.6 ACKNOWLEDGMENTS

This project was sponsored by ERIM through its Internal Research and Development funds. This appendix is an edited version of the paper "Dynamic Testing of a DGPS System used as a Truthing

Mechanism for Collision Avoidance Radar Evaluation," authored by John W. Sisak and Paul K. Zoratti. The paper was presented at The Institute of Navigation's National Technical Meeting in San, Jose, CA, 14-16 January 1997. The authors wish to thank all their ERIM colleagues who contributed effort to this project. In particular, the authors wish to thank Tom Blessing, Bob Hrabec, Eric Batzdorfer and Tom Chaplin for equipment installation, site preparation, and assistance during the test. Thanks also go to William Hanna, Mike Harrison, and Tom McQuade for their help in processing the inertial data and GPS data.

D.7 REFERENCES

D-1. "System and Parametric Trade-Offs of Forward Looking Automotive Radar Systems," Walter Nagy, Joseph Wilhelm, IEEE 1996 National Radar Conference, Ann Arbor MI, 13-16 May, 1996.

D-2. "High Accuracy, Short Term Trajectory Measurement of an Airborne Vehicle for Control of Inverse Synthetic Aperture Radar Image Formation," John W. Sisak & members of the ERIM Staff, 16th Biennial Guidance Test Symposium, Holloman AFB, NM, 5-7 October, 1993.

APPENDIX E. EVALUATION OF SENSOR-ROADWAY DYNAMICS TEST PLAN

E.1 OVERVIEW

The tests that will be executed in accordance with this plan are part of a Discretionary Cooperative Agreement with the National Highway Traffic Safety Administration (NHTSA Grant DTNH22-94-Y-17016), "Characterization and Evaluation of a Forward-Looking Automotive Radar Sensor." TRW is providing a prototype forward-looking automotive radar that is intended for Intelligent Cruise Control applications, and is the focus of these tests. TRW is also supporting the test and evaluation efforts. The tests range from very controlled laboratory settings to the evaluation of the FLAR in actual driving situations that can not be controlled in the classical laboratory manner. In the following sections, the tests are defined in terms of the setting, the data that will be collected and the analyses to be performed.

E.1.1 Purpose

This document serves two purposes. First, it presents a plan for testing a TRW prototype Forward-Looking Automotive Radar (FLAR) intended for ICC applications. The tests will be executed at two levels of evaluation: (1) as a radar sensor (i.e., as a remote sensing measurement device that can provide range, range rate and azimuth measurements of objects within the sensor's measurement field of regard); and (2) as an FLAR for ICC. Second, this plan provides the basis for developing detailed test procedures.

E.1.2 Products

Within the restrictions of time, funding and the capabilities of the physical resources, these tests will produce quantitative measures of performance that will characterize the FLAR under a variety of test scenarios, both synthetic and representative of actual driving conditions. The most quantitatively accurate results will be obtained under controlled test conditions, such as those found at test tracks. Test tracks, however, do not fully capture the real-world setting offered by freeways with varying levels of traffic. Within the limits imposed by safety and practicality, the tests conducted under test track conditions will be duplicated on freeways. The freeway tests can not be controlled to produce highly accurate measurements of vehicle positions, orientations and velocities, but these conditions will test the FLAR's ability to accommodate complex background and traffic conditions when functioning as an ICC sensor. Quantitative results will be presented in either tabular or graphical form, whichever is most appropriate. The freeway test results will be more descriptive in nature. For each test there will be a qualitative discussion and interpretation of the results with a concluding statement about the findings.

E.1.3 Limitations

These tests are being conducted with a forward-looking automotive radar (FLAR) that is a prototype-production radar for Intelligent Cruise Control (ICC). As such, it imposes certain limitations on what can be learned from these tests. It is intended as a commercial product, not a scientific instrument. TRW has, however, provided ERIM with access to low-level radar data that can be used to assess the performance of the radar prior to the implementation of the ICC-related functions. With this understanding, useful data and information can be acquired through carefully designed and executed tests.

There is a second limitation that must be addressed. Not all possible combinations of the test parameters will be examined as part of the testing performed under the current Cooperative Agreement. The goal will be to sample a wide range of conditions that will test the FLAR in such a manner that the maximum variation in performance is measured. For example, not all combinations of road type (e.g., straight, curved), surface material (concrete, asphalt) and backgrounds (e.g., bridges, guard rails) need to be explored to determine the range of performance. Many combinations will produce very similar results, or won't be of any interest for the ICC application. To limit the testing to a manageable size, such judgments have been applied in the development of this plan.

E.2 TEST DEFINITIONS

There will be five (5) types of tests that are briefly described below. Each Test Type will generally be composed of several sub-tests. For each test, the plan will define the test's purpose, Setting, Measurements and Data Analysis Products. The Setting will define the test location, all the test elements (e.g., vehicles, background objects) and their initial geometrical arrangement. Measurements will define the data to be collected and vehicle paths when appropriate. Data Analysis Products will define how the data will be reduced and presented.

Static

The Static tests are intended to characterize the FLAR in a stand-alone, non-ICC setting. These tests will verify that the FLAR is basically functioning by measuring key parameters such as radiated power, antenna beam pattern, system timing and outputs (e.g., range, range rate). These tests will also verify that the FLAR is ready for higher-level testing. The test site will be restricted to a controlled, non-roadway setting.

Environment and Materials

The Environment tests will be limited to three conditions: dry, wet (raining) and contamination of the radome. Various levels of rain must be considered. Two parameters associated with precipitation are of interest. First, precipitation density is somewhat proportional to rate of precipitation, which is easier to measure. Any degradation in sensor performance will be directly related to precipitation density. The second parameter is particle (i.e., rain drop) size. As the size of the particle approaches the wavelength of the radiated energy, approximately 3 mm for the FLAR, appreciable reflection can be expected. Dirt, sludge and salt residue will be tested for their effects on sensor performance, particularly as contaminants on the radome. The tests will be conducted in a static, off-roadway setting because the primary affect of the environment is to reduce the quality of the received signal. Typical materials found in a roadway setting will be evaluated in terms of their RF reflection, absorption and transmission.

Background

The Background tests will be conducted on local freeways, but during times without any traffic. The intent is to characterize the non-traffic component in the radar return from typical roadway objects that will appear in any forward-looking radar's field-of-view. Signs, bridges, tunnels, Jersey barriers, guard rails and the like will be included in these tests. Both the unprocessed and processed returns will be captured for the purpose of characterizing the background and false-alarm rates, respectively.

Test Track

As the title implies, this will be the collection of all tests that will be performed in a Test Track setting. Most of the scenarios will be repeated as part of the Freeway Tests, but Test Track tests will be more controlled in terms of vehicle geometries, and thus provide the more quantitative accurate measurements. The road surface materials and background will be varied as appropriate for a specific Test Scenario, but these parameters will not be exhaustively examined. The number of vehicles will also be limited. This removes an element of reality, but again permits more accurate measurements of the FLAR's basic performance.

Freeway

The Freeway tests will fall into two (2) major sub-categories, orchestrated and non-orchestrated. The Orchestrated tests will be performed only when ERIM can significantly control the prevailing traffic (i.e., all other vehicles will be provided by ERIM and they will follow a prescribed scenario). These tests will, for the most part, be a repeat of the Test-Track tests, but with realistic roadway backgrounds. The Non-orchestrated tests will be performed with whatever traffic is available, although ERIM will select the time of day, and thus the prevailing traffic density. The intent is to determine how well the FLAR performs in acquiring the vehicle to be tracked and maintaining track in a varying clutter environment. The host vehicle will be driven on the local freeways in such a manner to test the FLAR's ability to acquire an appropriate secondary vehicle and maintain track for the same scenarios used for the Orchestrated tests.

E.3 STATIC TESTS: RADAR-SENSOR EVALUATION

These tests will be restricted to a single off-roadway setting in which all objects, the FLAR and targets, are stationary. These tests are intended to characterize the FLAR in a stand-alone, non-ICC setting. These tests will verify that the FLAR is basically functioning by measuring key sensor parameters. Baseband, time-domain data (i.e., before any TRW signal processing such as the FFT), will be collected and stored for off-line analysis. Using the sensor calibration data from Task 2, FLAR Sensor Characterization, the raw data will be processed to produce measures of the parameters discussed in the following sections. These results will be compared with the actual values for the parameters, such as range from the FLAR to the corner reflector. The actual values will be obtained by independently measuring the target positions relative to the FLAR. This can be easily accomplished because the entire test setting is static. The comparisons will be presented in either a graphical or tabular form, whichever is most suitable.

E.3.1 Range Accuracy

The FLAR's range accuracy will be determined by placing corner reflectors, with different radar cross-sections (RCS), along the antenna boresight at several ranges between the specified limits of performance. This test will compare the measured ranges with known ranges and obtain the deviations, and also determine the minimum and maximum detectable ranges.

E.3.2 Range Resolution

The FLAR's range resolution will be determined by measuring its ability to resolve two stationary scatterers at different ranges. Two reflectors (corner reflectors, vehicles, and background objects), of approximately equal RCS, will be placed back-to-back along the antenna boresight. We will move one reflector further (closer), in small steps of approximately 0.5 meter until two distinct returns can be

observed in the return and perform this measurement at several ranges between the specified limits of performance and in both directions along the antenna boresight.

E.3.3 Field of View

The FLAR's angular extent as a function of range for each of the three beams will be determined by placing a single corner reflector, with an RCS of approximately 10 dBsm, along each beam's boresight and moving the reflector off-boresight in fractional degree increments until the reflector response is negligible. This measurement will be obtained at several ranges between the specified limits of performance

E.3.4 Step Response

The FLAR's new target acquisition time will be determined by unveiling a corner reflector within the FLAR's field-of-view and measuring the time if taken for the target to appear in the output. This measurement requires time synchronization between the input event and the measurement.

E.4 ENVIRONMENT AND MATERIALS TESTS

These tests are essentially a continuation of the Static Tests, in that they will be performed in a controlled, off-roadway setting in which all the test objects are stationary. The intent of these tests is to quantitatively assess the effect of the environment in which the systems will be deployed and of typical materials used in cars and roadway construction on the quality of the received signal. Baseband, time-domain data (i.e., before any TRW signal processing), will be collected and stored for off-line analysis. These tests have been grouped into the following categories: Materials, Target Contamination, and Precipitation.

E.4.1 Materials: Reflection, Absorption and Transmission

The following materials will be evaluated: glass, plastic composite, Plexiglas, cardboard and rubber. The material under test will be placed approximately 3 meters from the FLAR and corner reflector will be placed at approximately 20 meters. The measured values will be compared with handbook values and correlated with the di-electric constant for the material.

E.4.2 Target Contamination

The following contaminants will be evaluated: wet mud, dry dirt, water droplets, snow (on target), ice, and salt residue. A Plexiglas substrate will be used to "hold" the contaminant. The design will take into consideration the fact that reflections can occur whenever a di-electric difference exists between two materials. The tests and data analysis will then the follow the same procedures as described in Section E.4.1.

E.4.3 Precipitation

Varying levels of density, or rate, will be considered for fog, rain, and snow. The two-way attenuation will be determined using a corner reflector placed approximately 20 meters from the FLAR.

E.5 BACKGROUND TESTS

The Background tests will be conducted on local freeways, but during times without any traffic. The intent is to characterize the non-traffic component in the radar return from typical roadway objects that will appear in any forward-looking radar's field-of-view. The tests will be conducted by driving the Testbed Vehicle on freeways in the greater Ann Arbor area on routes selected for their variety of backgrounds. The freeway route between ERIM in Ann Arbor facilities and GM's in Warren provides a side range of backgrounds varying from grassy medians to urban canyons. Baseband, time-domain data (i.e., before any TRW signal processing) and the standard FLAR outputs will be collected and stored for off-line analysis.

The baseband data will be analyzed for characterizing the background returns and diagnosing any false alarms in FLAR outputs. Under these test conditions, the FLAR should not attempt to track any objects in the roadway scene. Any attempt to measure range, or range-rate, will be considered a false alarm. The background returns will be plotted as a function of distance along the freeway. The plots will be annotated with roadway features of interest (e.g., bridge abutment, guard rail).

E.6 TEST-TRACK TESTS

The following series of tests have been designed to evaluate the FLAR's performance in a number of roadway settings that are typical of every day driving. The primary variables are: (1) roadway geometry (straight and curved); (2) background clutter (e.g., stationary vehicles, Jersey barriers); and vehicles on the roadway. An independent measurement technique(s) will be used to determine vehicle positions as a function of time. The measurements based on FLAR data, and tracking data produced by the FLAR will be compared with the independent measurements to provide a measure of the FLAR's performance. Because the Measurements and Data Analysis Products are very common across all the tests, they are described once at the end of this Section.

Throughout the following descriptions, the Primary vehicle is the one equipped with the FLAR and data acquisition electronics. The Secondary vehicle(s) is an unequipped vehicle that is being tracked, or represents vehicle clutter. All Secondary vehicles will all be of a similar type, medium-sized sedans, unless stated otherwise.

F.6.1 Vehicle Induced False Alarms—Straight Roadway

The purpose of the following two tests is to determine the Primary vehicle's ability to ignore an out-of-lane Secondary vehicle on a straight section of roadway. In one case the vehicle is parked on the roadside shoulder and in the second case it is traveling in an adjacent lane in front of the Primary vehicle. Only the Primary and Secondary vehicles will be present on the roadway.

Vehicle on Shoulder

The Secondary vehicle will be parked on the roadside shoulder approximately 1/4 of a mile in front of the Primary vehicle. The Primary vehicle will accelerate to freeway speeds and pass the Secondary vehicle, completing the test.

Plan View of Test Setting

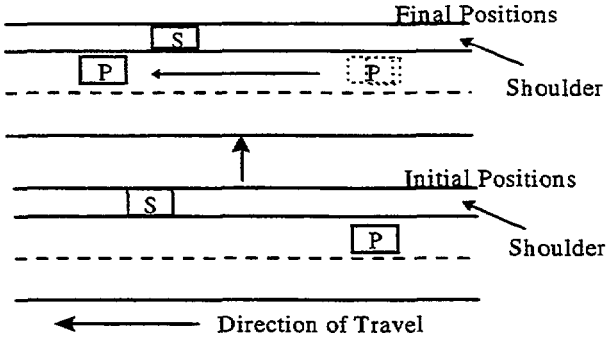

Vehicle in Adjacent Lane

The Primary and Secondary vehicles will be traveling at freeway speeds in adjacent lanes and in approximately the same positions at the start of the test. The Primary vehicle will maintain a constant speed and the Secondary vehicle will accelerate for a short period of time until it has reached a specifiedistance in front of the Primary vehicle. At this time, the Secondary vehicle will reduce its speed to that of the Primary vehicle and both vehicles will maintain this headway for a specified time. The test will terminate after the two vehicles have traveled at the constant headway for the required time.

Plan View of Test Setting

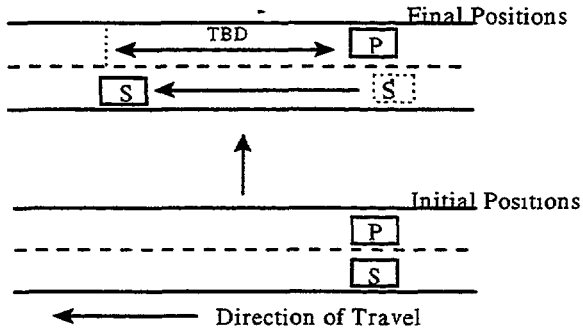

E.6.2 Braking Secondary Vehicle—Straight Roadway

The purpose of this test is to determine the Primary vehicle's response to a Secondary vehicle braking after the Primary vehicle had been tracking the Secondary vehicle. The test begins after the Primary and Secondary vehicles are maintaining a constant headway and speed. The Secondary vehicle will then brake moderately. The test will terminate after the Primary vehicle has reduced headway by a predetermined amount.

Plan View of Test Setting

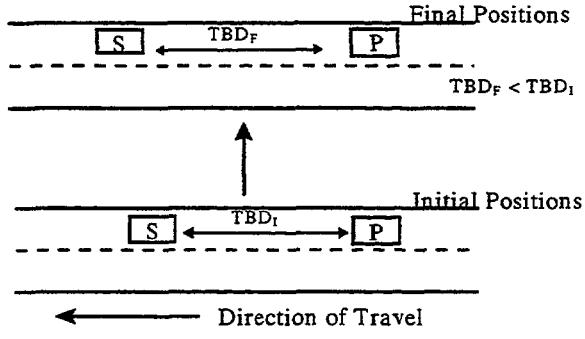

E.6.3 Out-of-Lane Vehicle Clutter—Straight Roadway

The purpose of this test is to determine the Primary vehicle's ability to track the in-lane Secondary vehicle when there is an out-of-lane Secondary vehicle that should be ignored. The test begins with the Primary vehicle maintaining a constant headway from the in-lane Secondary vehicle, and an out-of-lane Secondary vehicle next to the Primary vehicle. The Primary and Secondary vehicles maintain their lane positions throughout the test. The Primary and in-lane Secondary vehicles maintain their initial headway. The out-of-lane Secondary vehicle then accelerates to a position in front of the Primary vehicle and then maintains this position for the remainder of the test. The test will terminate after the out-of-lane Secondary vehicle has maintained a stable headway.

Plan View of Test Setting

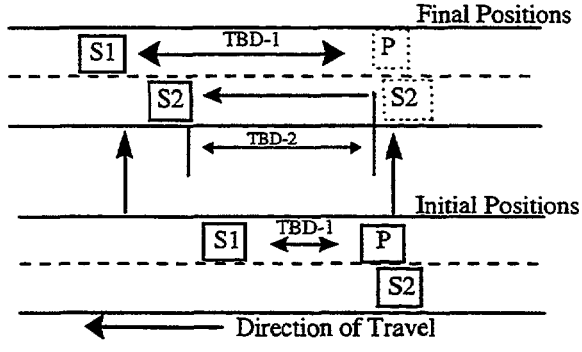

E.6.4 Intentional Lane Changes—Straight Roadway

The purpose of this test is to determine the Primary vehicle's ability to detect changes introduced by vehicle lane changes. Response time is also an important performance parameter that will be monitored. Only the Primary and Secondary vehicles will be present on the freeway. In the first test, the Primary vehicle changes its lane to pass the Secondary vehicle. In the second test, the Secondary vehicle moves out of the Primary vehicle's lane.

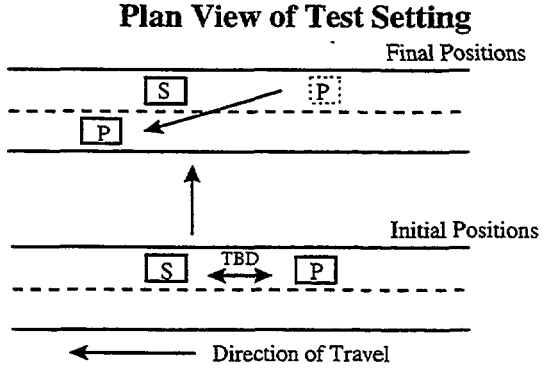

Primary Passes Secondary

The test begins with the Primary vehicle maintaining a constant headway from the in-lane Secondary vehicle. The Primary vehicle then accelerates moderately and changes its lane to pass the Secondary vehicle. The test will terminate after the Primary vehicle passes the Secondary vehicle.

Secondary Leaves Lane

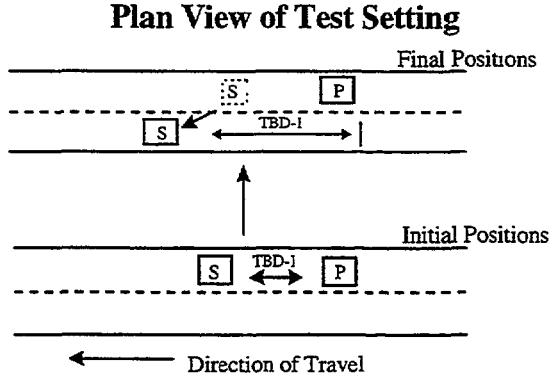

The test begins with the Primary vehicle maintaining a constant headway from the in-lane Secondary vehicle. The Secondary vehicle accelerates moderately and changes its lane, then decelerates so that its final headway in the adjacent lane is the same as before. The test will terminate after the Secondary vehicle has achieved and maintained the original headway.

E.6.5 Tracking New Secondary—Straight Roadway

The purpose of this test is to determine the Primary vehicle's ability to detect changes produced by a vehicle leaving its path and exposing a new vehicle in the Primary vehicle's path. The test begins with the Primary vehicle maintaining a constant headway from the first Secondary vehicle, and the first Secondary vehicle maintaining a constant headway from the second Secondary vehicle. The headways will be selected so that their sum is well within the maximum range performance of the FLAR. The Primary and second Secondary vehicles maintain a constant speed throughout the test. The first Secondary then accelerates, changes its lane and assumes its final position in the adjacent lane, in front of the second Secondary vehicle. The test will terminate when the first Secondary vehicle has achieved its final position.

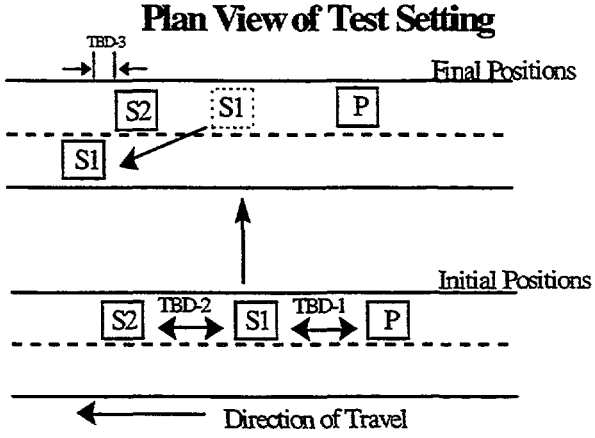

E.6.6 Tracking With a Cut-in-Straight Roadway

The purpose of this test is to determine the Primary vehicle's ability to detect changes produced by a vehicle entering its path. The test begins with the Primary vehicle maintaining a constant headway from the first Secondary vehicle, with the second Secondary vehicle adjacent to the Primary vehicle and traveling at the same speed. The headway will be selected that is within the FLAR's maximum operating range, large enough that a third vehicle can safely enter and operate in it. The Primary and first Secondary vehicles will maintain their relative positions throughout the test. The second Secondary vehicle will accelerate and move into the right-hand lane between the other two vehicles. The final headways will be selected for safe operation within the FLAR's minimum operating range. The test will terminate when the three vehicles have achieved the designated headways.

Plan View of Test Setting

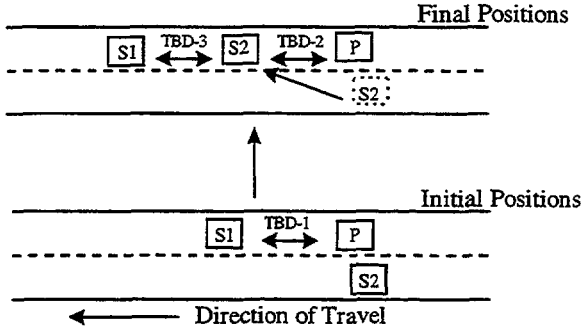

E.6.7 Strong Vehicle Clutter in Range—Straight Roadway

The purpose of this test is to determine the Primary vehicle's ability to acquire and maintain track on a fixed Secondary vehicle (i.e., the in-lane vehicle) in the presence of another in-lane Secondary vehicle, but at a greater range. This tests the FLAR's ability to discriminate vehicles in the same lane, but with varying RCS and range. The closer Secondary vehicle will be a motorcycle. The clutter vehicle will have a radar cross-section significantly greater than that of the motorcycle. The FLAR should detect and maintain track on the motorcycle and ignore the presence of the clutter vehicle. The test begins with the motorcycle and clutter Secondary vehicle in the adjacent lane to the Primary, with all the vehicles traveling at the same speed. The motorcycle then accelerates and moves into the Primary vehicle's lane in front of the Primary vehicle. The clutter Secondary vehicle then accelerates, moves into the same lane in front of the motorcycle. The headways will be selected for safe operation the maximum operating range of the FLAR. The test will terminate after the three vehicles have maintained the indicated positions for a specified time.

Plan View of Test Setting

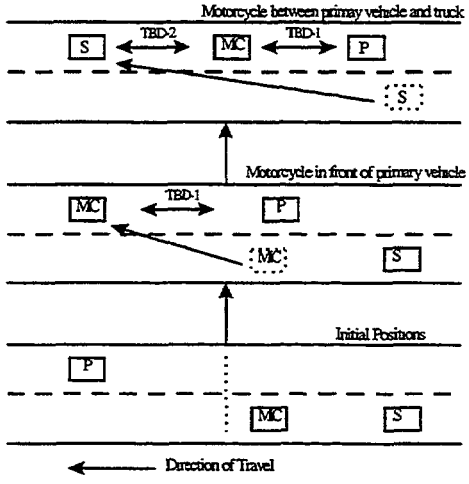

E.6.8 Vehicle Clutter in Azimuth—Straight Roadway

The purpose of this test is to determine the Primary vehicle's ability to maintain track on a fixed Secondary vehicle in its lane within a vehicle-cluttered environment (i.e., vehicles in adjacent lanes). This tests the FLAR's ability to discriminate between in-lane and out-of-lane vehicles. The two out-of-lane Secondary vehicles will be selected to have radar cross-sections slightly greater than that of the in-lane Secondary vehicle. The test begins with the Primary vehicle maintaining a constant headway from the in-lane Secondary vehicle, out-of-lane Secondary vehicles adjacent to the Primary vehicle and traveling at the same speed. The out-of-lane Secondary vehicles then accelerate until they are adjacent to the in-lane Secondary vehicle. They maintain this position, and then decelerate until they are again adjacent to the Primary vehicle. The test will terminate when the initial, relative vehicle positions have been achieved.

Plan View of Test Setting

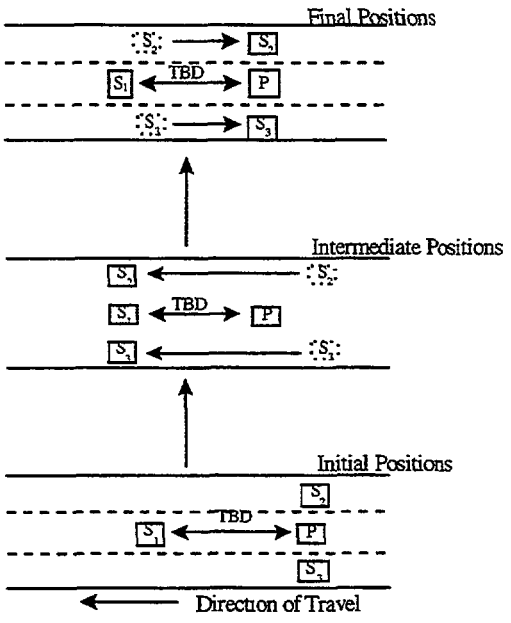

E.6.9 Merging Traffic—Straight Roadway

The purpose of this test is to determine the FLAR's response to merging traffic from a freeway entrance lane. The test begins with the Primary vehicle maintaining a constant headway from the in-lane Secondary vehicle, while the merging Secondary vehicle is on the entrance ramp. The merging Secondary vehicle accelerates so that it is between the Primary and Secondary vehicles, but still in the merging lane. The merging Secondary vehicle will stop accelerating when it is in front of the Primary vehicle; the Primary and Secondary vehicles will maintain a constant speed and headway, then the merging Secondary vehicle will decelerate and merge behind the Primary vehicle. At this point the test is complete.

Plan View of Test Setting

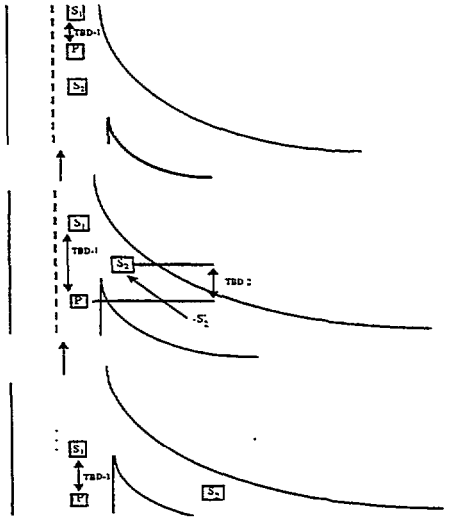

E.6.10 Vehicle Induced False Alarms—Curved Roadway

The purpose of the following two tests is to determine the Primary vehicle's ability to ignore an out-of-lane Secondary vehicle on a curved section of roadway. In one case the vehicle is parked on the roadside shoulder and in the second case the Secondary vehicle is traveling in an adjacent lane in front of the Primary vehicle. Only the Primary and Secondary vehicles will be present on the roadway.

Plan View of Test Setting *

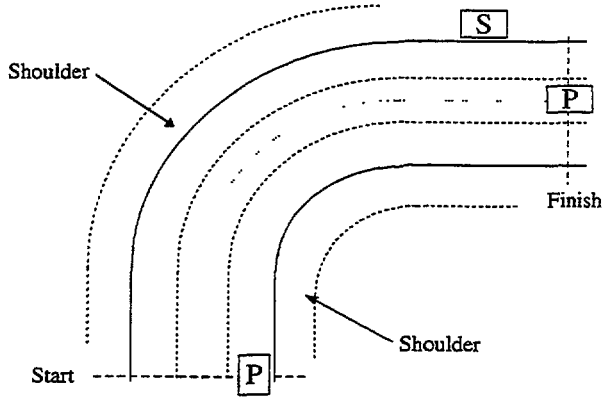

* Curve accentuated for illustratrative purposes

Vehicle on Shoulder

The Secondary vehicle will be parked on the roadside shoulder approximately 1/4 of a mile in front of the Primary vehicle. The Primary vehicle will accelerate to freeway speeds and pass the Secondary vehicle completing the test.

Vehicle in Adjacent Lane

The Primary and Secondary vehicles will be traveling at freeway speeds in adjacent lanes and in approximately the same positions at the start of the test. The Primary vehicle will maintain a constant speed and the Secondary vehicle will accelerate for a short period of time until a predetermined distance ahead of the Primary vehicle. At this time, the Secondary vehicle will reduce its speed to that of the Primary vehicle and both vehicles will maintain this headway. The test will terminate after the two vehicles have traveled at the constant headway for the specified time.

Plan View of Test Setting *

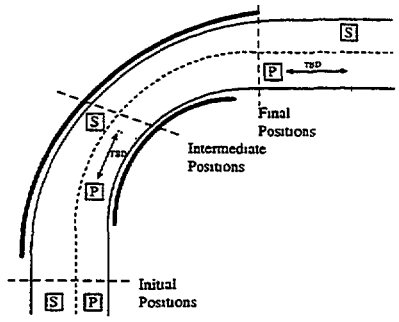

* Curve accentuated for illustratrative purposes

E.6.11 Tracking Through a Curve

The purpose of this test is to determine the Primary vehicle's ability to track a Secondary vehicle through a standard freeway curve on a dry, flat section of roadway. The test will be performed under good driving conditions. Roadway will be selected so that guard rails, Jersey Barriers and signs are in the scene, but tested separately.

The test will commence when the Primary is tracking the Secondary vehicle in a straight section of roadway prior to entering a curve. Both vehicles will be traveling at the posted speed limit and attempt to maintain those speeds and the initial separation distance throughout the test maneuver. The test will terminate when both vehicles are again on a straight section of roadway. The test will be performed at several radius of curvatures that are intended to encompass those found in typical freeway settings.

Plan View of Test Setting *

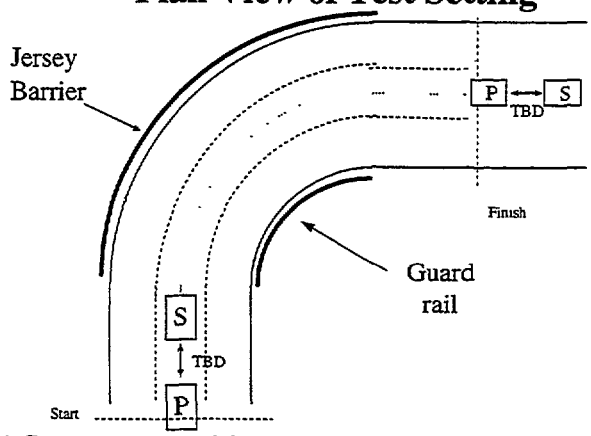

* Curve accentuated for illustratrative purposes

E.6.12 Vehicle Clutter in Azimuth—Curved Roadway

The purpose of this test is to determine the Primary vehicle's ability to track a fixed Secondary vehicle in its lane within a vehicle-cluttered environment (i.e., vehicles in adjacent lanes). This tests the FLAR's ability to discriminate between in-lane and out-of-lane vehicles on a curved section of roadway. The two out-of-lane Secondary vehicles will be selected to have radar cross-sections slightly greater than that of the in-lane Secondary vehicle. The test begins with the Primary vehicle maintaining a constant headway from the in-lane Secondary vehicle, with the out-of-lane Secondary vehicles adjacent to the Primary vehicle and traveling at the same speed. The out-of-lane Secondary vehicles then accelerate until they are adjacent to the in-lane Secondary vehicle. They maintain this position, then decelerate until they are again adjacent to the Primary vehicle. The test will terminate when the initial, relative vehicle positions have been achieved once the vehicles are on a straight section of roadway.

Plan View of Test Setting

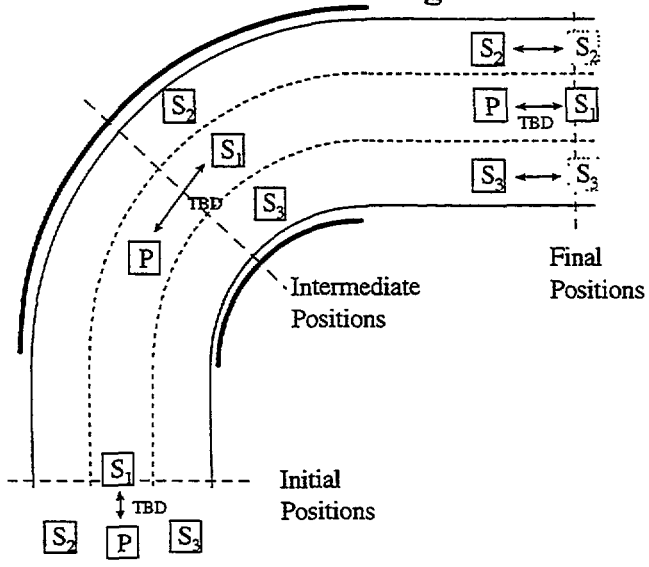

* Curve accentuated for illustratrative purposes

E.6.13 Measurements

The same basic set of measurements will be made for all the above tests. The data acquired on the Testbed Vehicle will all be time tagged to support the reduction and analysis of the data. The data to be collected is:

1. Baseband, time-domain data (i.e., before any TRW signal processing such as the FFT);
2. FLAR processed data, range, range rate, and various sensor status information;
3. Video data of the forward scene; and
4. Site survey data of all marker locations used to define maneuver positions.

E.6.14 Data Analysis Products

The analyzed results from each test will be compared with the independent measurements for assessing the FLAR's performance. There are two basic types of tests: detections and (position, relative velocity) measurements. The detection tests will examine two cases: false positives (declaring that a vehicle is in-lane when it is not); and misses (not detecting a vehicle when it is in-lane). These tests will be repeated a number of times to provide some statistical data. The majority of the tests involve the evaluation of the FLAR as a measurement device to support ICC applications. For these tests, plots and tabularized data will be presented to compare actual measurements against the true values obtained through independent measurements.

E.7 FREEWAY TESTS

The Freeway tests will fall into two (2) major sub-categories, orchestrated and non-orchestrated. The Orchestrated tests will be performed only when ERIM can significantly control the prevailing traffic (i.e., all other vehicles will be provided by ERIM and they will follow a prescribed scenario). These tests will, for the most part, be a repeat of the Test-Track tests, but with realistic roadway backgrounds. The Non-orchestrated tests will be performed with whatever traffic is available, although ERIM will select the time of day, and thus the prevailing traffic density. The intent is to determine how well the FLAR performs in acquiring the vehicle to be tracked and maintaining track in a varying clutter environment. The Primary vehicle will be driven on the local Freeways in such a manner to test the FLAR's ability to acquire an appropriate Secondary vehicle and maintain track for the same scenarios used in the Orchestrated tests.

E.7.1 Orchestrated Tests

The following Test Track Tests should be repeated, but with the indicated modifications. Every reasonable attempt should be made to perform these tests at times when non-ERIM vehicles are not likely to be on the road. The primary intent is to determine the impact of actual freeway backgrounds on the FLAR's performance. Tests involving vehicle maneuvers will be avoided.

Vehicle Induced False Alarms—Straight Roadway

Background should include guard rails.

Out-of-Lane Vehicle Clutter—Straight Roadway

Down-range background should contain bridge abutments.

Intentional Lane Changes—Straight Roadway

Down-range background should contain bridge abutments.

Tracking New Secondary—Straight Roadway

Down-range background should contain bridge abutments.

Strong Vehicle Clutter in Range—Straight Roadway

Down-range background should contain bridge abutments.

Merging Traffic—Straight Roadway

Background should include guard rails, signs and any other typical roadway clutter.

Tracking Through a Curve

Background should contain a Jersey barrier, or other strong radar reflective objects.

E.7.2 Non-Orchestrated Tests

The above tests should be repeated, but conducted under three traffic conditions: (1) light—where there is an occasional non-ERIM vehicle in the adjacent lane; (2) medium—where there is always one adjacent lane occupied by a non-ERIM vehicle and an occasional passing vehicle; and (3) heavy—typical rush-hour traffic.

APPENDIX F. TEST-TRACK RESULTS

F.1 VEHICLE INDUCED FALSE ALARMS—STRAIGHT ROADWAY

F.1.1 Purpose

The purpose of the following two tests ("Roadside Vehicle" and "Adjacent Lane Vehicle") is to determine the Primary vehicle's ability to ignore an out-of-lane Secondary vehicle on a straight section of roadway. In one case, the Secondary (target) vehicle is parked on the roadside shoulder; in the second it is traveling in an adjacent lane in front of the Primary (or host) vehicle. Only the Primary and Secondary vehicles will be present on the roadway.

These tests were designed to measure the return levels, if any, observed in the raw radar return signal from the "non-threatening" secondary vehicle. We refer to these "non-threatening" vehicles as "clutter," that produce returns which are not of primary interest to the radar system. In the automotive radar application, the Secondary vehicles in these tests are clutter because they are not located in the operating lane of the Primary vehicle and therefore, do not constitute a collision threat under normal driving conditions.

F.1.1.1 Roadside Vehicle

Procedure

The Secondary vehicle was parked on the roadside shoulder approximately 1/4 of a mile in front of the Primary vehicle. The Primary vehicle accelerated to freeway speeds and passed the Secondary vehicle, completing the test.

This test procedure was repeated a number of times using both a Honda Accord and a Semi-Tractor/Trailer as the Secondary vehicles. Also, runs were made with the FLAR sensor's center beam active. The center beam has a 3 degree azimuth and 3 degree elevation beamwidth.

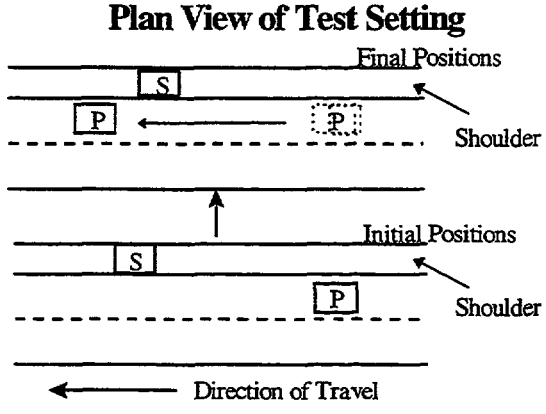

Results

Data from these tests was screened using the ERIM Analysis PC software to identify data sets for further analysis. Several data sets were selected and the raw radar returns (prior to any digitization in the FLAR) were processed using custom Matlab scripts.

The Matlab processing of data from both the Honda Accord runs and Semi-Tractor/Trailer runs showed evidence that the FLAR raw data detected these roadside vehicles. The Semi-Tractor/Trailer vehicle provided a stronger return under the geometric conditions of the test than the Honda Accord. The data from one of the test runs with the Semi-Tractor/Trailer as the Secondary vehicle will be used to illustrate these findings.

Figure F-1 shows the FLAR signal returns for one of the test runs. The returns resulting from the roadside vehicle are annotated in the figure. As expected, the radar initially detects' the target at a long range. As time progresses and the Primary vehicle approaches the Secondary vehicle, the range of the radar returns correspondingly decreases and their amplitude increases. Finally, the radar returns from the Secondary vehicle fall off sharply and are not evident above the baseline returns of the system.

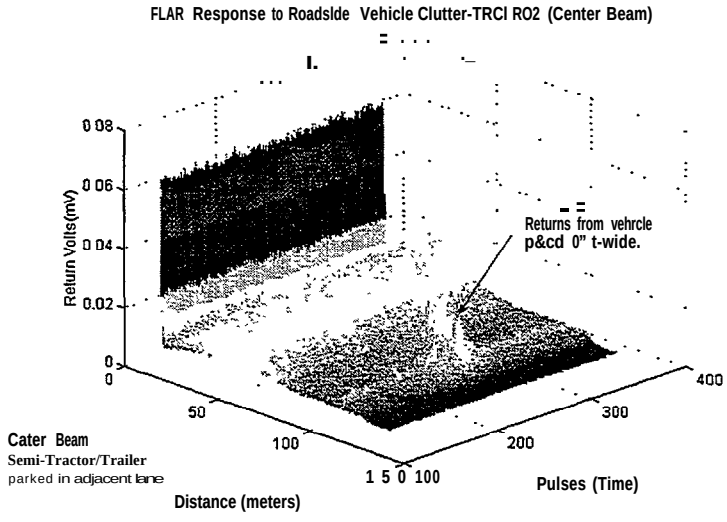

Figure F-1. FLAR Response to Roadside Vehicle Clutter

Quantitative analysis indicates that for the given geometries in this test, the tractor/trailer RCS levels varied from -3 to +3 dBsm. These levels are highly dependent on the orientation between the radar and the target, and also the positioning of the target within the illuminating radar beam pattern as discussed below.

The range at which the Secondary vehicle was first detected was approximately 90 meters and the range at which the returns fell off was approximately 50 meters. Figure F-2 illustrates the geometric orientations which induced the radar returns. Simple trigonometric anaIysis indicates that the roadside vehicle produced radar returns during the period at which it was at an azimuthal heading of 1.3 to 2.3 degrees (referenced to the Primary vehicle's radar beam boresight).

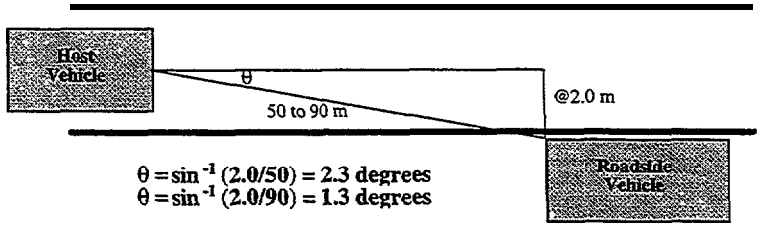

Figure F-2. Object Orientation Roadside Clutter Analysis

'Throughout the discussions in this report, the term "detects" refers to the observable presence of radar returns from a particular object in the radar's raw IF signal. This is different than stating that the FLAR "locked-on" and tracked a target. The term "locked-on" refers to the fact that the FLAR (and its internal TRW-proprietary processing algorithms) identified and tracked the object.

Results

As in the roadside vehicle experiments, data from these tests was screened using the ERIM Analysis PC software to identify data sets for further analysis. Several data sets were selected and the raw radar returns (prior to any digitization in the FLAR) were processed using custom Matlab scripts.

For test runs with the radar's center beam active, the adjacent lane tests showed that returns from the Secondary adjacent lane vehicles were not present. While this result does not appear consistent with the roadside vehicle tests, the difference can be attributed to slightly different geometric orientations, which resulted in the Secondary vehicle being located outside the mainlobe of the center beam.

For test runs with the radar's left beam active, the adjacent lane vehicles produced clear radar returns. By having the left beam active, the FLAR's effective field-of-view is skewed to the left by approximately 2.7 degrees. This multiple beam approach, to increase the FLAR's overall field-of-view, was employed primarily to support tracking vehicles while the primary vehicle was in a curve. From this test, it is evident that this multiple beam approach can help detect vehicles in an adjacent lane.

Figure F-4 is an example run with a semi-tractor/trailer as the Secondary vehicle. Here we see that the radar detected the Secondary vehicle at ranges varying from approximately 45 to 65 meters. These return levels are lower than one might expect with the Ieft beam being active, however considering that the orientation and shape of the semi-tractor/trailer, it is reasonable to assume that a large portion of the ener,v is being reflected away from the FLAR receiver. Quantitative analysis indicated that for the given orientations, the truck returns correlated to a target with an RCS of approximately -5 dBsm. Tests run with the Accord resulted in similar RCS measurements.

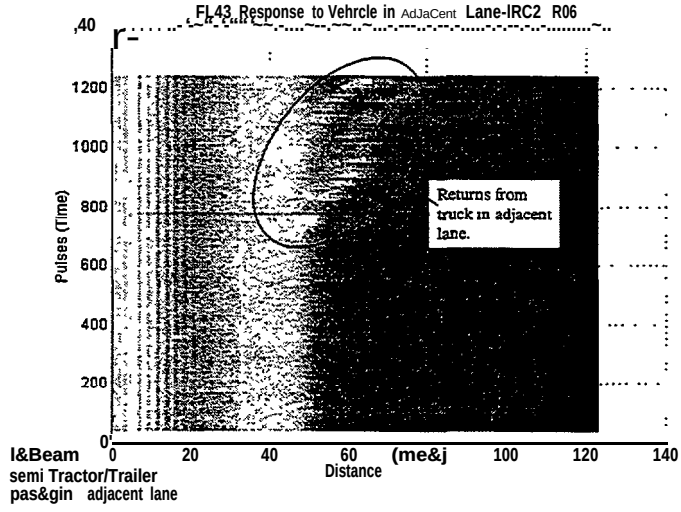

Figure F-4. FLAR Response to Vehicle in Adjacent Lane

This figure also illustrates another interesting phenomena -- the radar has detected two separate groups of scatterers on the same vehicle, which appear as two totally separate returns. Analysis of the collected data determined that the first return (the lower return in the figure) is coming from a scatterer located on the front part of the Secondary vehicle, probably the front set of wheels. The second return (the top return in the figure), which is separated from the first by approximately 55 feet, is coming from the rear portion of the vehicle, probably the rear set of wheels.

Figure F-5 illustrates the geometric orientation corresponding to the range over which the Secondary vehicle was detected by the left beam. These are consistent with the measured beam patterns of the FLAR as shown in Figure F -6. The range of azimuth angle over which the vehicle in the adjacent lane

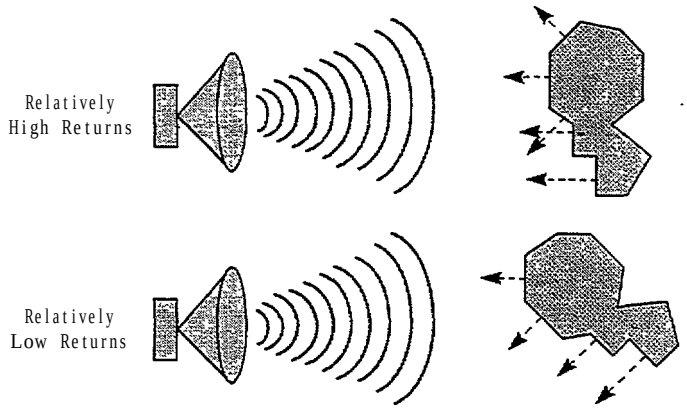

Figure F-7. **How Target Orientation Affects Return Levels**

Conclusions

Conclusions derived from the experiments are summarized below.

- Some automotive radar system designers have used a 3 degree 3 dB beamwidth since it covers one lane width at approximately 100 m (the specified detection range). These test show that large RCS objects outside the stated beamwidth will produce returns in the radar sensor.
- Even though automotive radars may have an extended FOV (either through beam switching or scanning), the orientation and shape of vehicles in the adjacent lanes can produce return levels much lower than expected.
- While the return levels from the Secondary vehicles in these tests are relatively low, the specific orientation and structure of roadside/adjacent lane clutter can produce relatively high return levels. Quantitatively speaking, the geometries and orientations of the experiments resulted in observed RCS levels from both the Accord and tractor/trailer on the order of -5 to 0 dBsm.
- The radar would interpret returns witnessed in these experiments an object in the direct path of the primary vehicle.
- Threat algorithms must take into account returns from objects located outside the stated beamwidth of the antenna (3 dB width)
- The results indicate that some form of azimuth resolution, at least half a lane width, would be highly beneficial for collision avoidance systems.

F.2 BRAKING SECONDARY VEHICLE-STRAIGHT ROADWAY

F.2.1 Purpose

The purposeof this test is to evaluate the Primary vehicle's response to a target vehicle which braked after the Primary vehicle had been tracking it. Events of interest are loss of target tracking and the return levels from target vehicle.

Procedure

During the test, the Primary vehicle maintained a constant speed (45 MPH), while the target vehicle accelerated and braked to vary the range between the two vehicles. The range was varied from approximately 20 to 50 meters. The test took place on a closed test track with only the primary and secondary vehicles present. Only the FLAR center beam was active during the test. The center beam has a 3 dB beamwidth of 3 degrees in both azimuth and elevation.

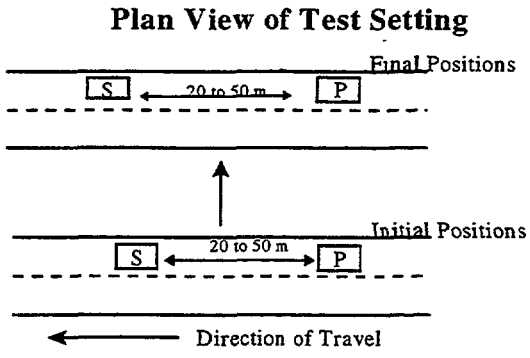

Results

Several runs were made following the procedure described above. The results were found to be consistent from run to run. Plots from one run will be used in the discussion below to illustrate the results.

Figure F-8 illustrates the raw (IF) radar return signals received by the FLAR system. Figure F-8(a) shows that in this fairly low clutter environment, the return signal levels from the target vehicle were clearly visible above the noise floor of the system for most of the time (note that the signal level shown in the plot consists of integrating the energy from six consecutive radar pulses). The dynamics between the host and target vehicles are easily seen in Figure F-8(b). The target vehicle continuously approached and receded from the host vehicle in a sinusoidal pattern.

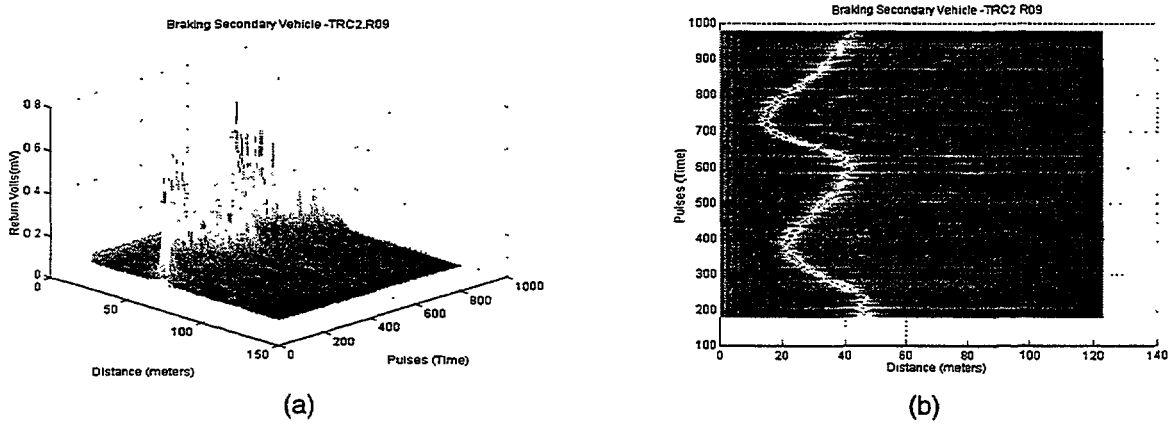

Figure F-8. Braking Secondary Vehicle

Return Levels

The return signal levels followed a pattern which would be expected from the experiment dynamics. As the range to the target vehicle decreased, the return levels increased and as the range to the target vehicle increased, the return levels decreased. A plot showing the peak return level for each group of processed radar pulses is provided in Figure F-9.

Quantitative analysis showed that the target vehicle, a Honda Accord exhibited average radar cross section (RCS) values ranging from +3 to +8 dBsm. Average RCS must be emphasized, because short term (pulse-to-pulse) variations in the calculated RCS were observed to vary by as much as 10 dB.

These short term variations in exhibited RCS levels can be attributed to scintillation and directive reflectivity effects. The scintillation effects are caused by the interaction of the electromagnetic waves reflected by individual radar scatterers which are distributed across the target vehicle. Due to the very short wavelength of the energy emitted by the FLAR, minute changes in the distance between the radar and the various scatterers causes the reflected waves to interact in constructive and destructive manners. When the waves add together constructively, the return 1evel increases; when they interact destructively, the return levels decrease.

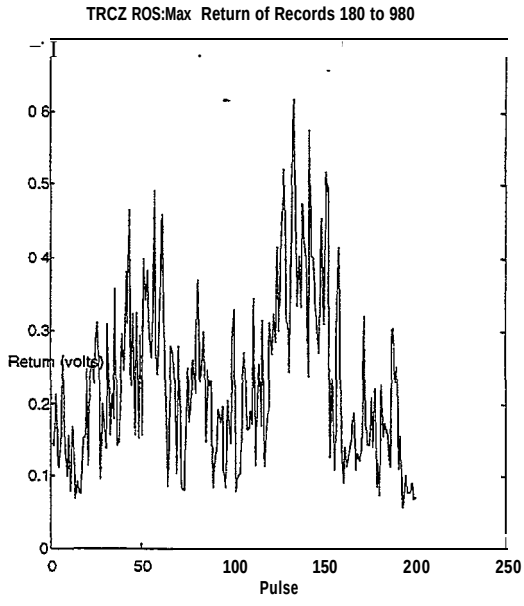

Figure F-9. Peak Return Levels

Directive reflectivity simply refers to the level at which a scatterer directs energy back at the illuminating radar. As the orientation between a complex shaped scatterer and an illuminating radar varies, the amount of energy reflected back at the illuminating radar can change drastically. A simple example of this effect is the glint of the sun off of a mirror.

Ability to Maintain Lock on Target Vehicle

Fortunately, these short term variations average out aud simple processing techniques will allow the radar sensor to maintain a consistent lock on the target, provided the target's average RCS results in return levels sufficiently above the sensor's noise floor.

In analyzing the processed outputs of the FLAR (which utilizes TRW's proprietary algorithms), it was found that the sensor did maintain a consistent lock on the target vehicle throughout the test collections. It should be noted though, that even the lowest returns from the target vehicle were above the baseline noise floor of the FLAR.

Accuracy of FLAR Tracking

In addition to evaluating the return levels and the ability of the FLAR to maintain lock on the target vehicle, a differential GPS (DGPS) truthing mechanism was utilized to evaluate the accuracy with which the FLAR reported the range to the target vehicle. During the tests, the reported range outputs from the FLAR were recorded. These ranges were calculated by TRW's proprietary processing algorithms and updated by the FLAR every 50 milliseconds.

Figure F-10 shows the results of the DGPS truthing analysis. Comparing the DGPS 'true' range with the range reported from the FLAR indicates that the FLAR was able to track the target vehicle to within 1 meter for the particular scenarios created during the test runs. This accuracy meets the reported specification of the FLAR.

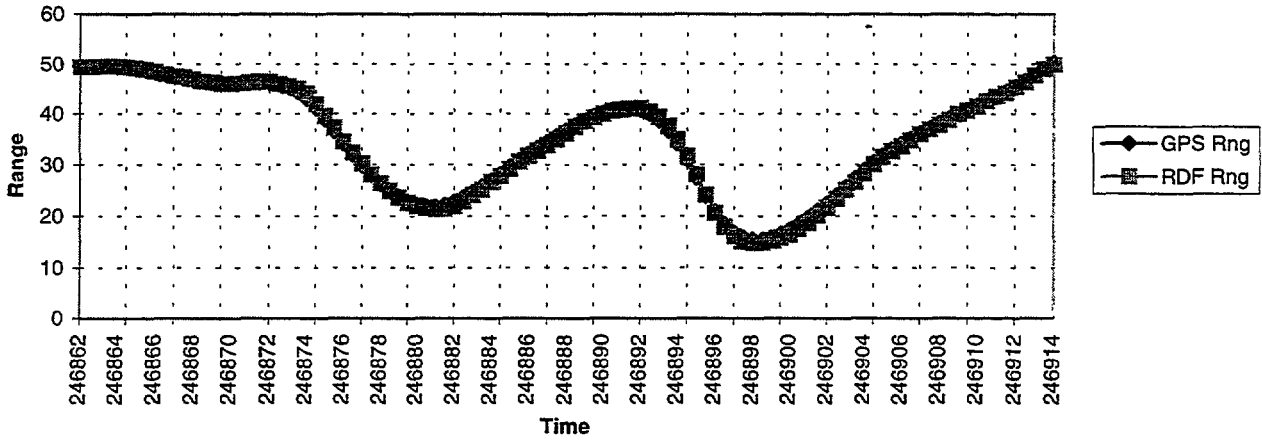

R9 w/ Analysis S/W Range Offest Implemented

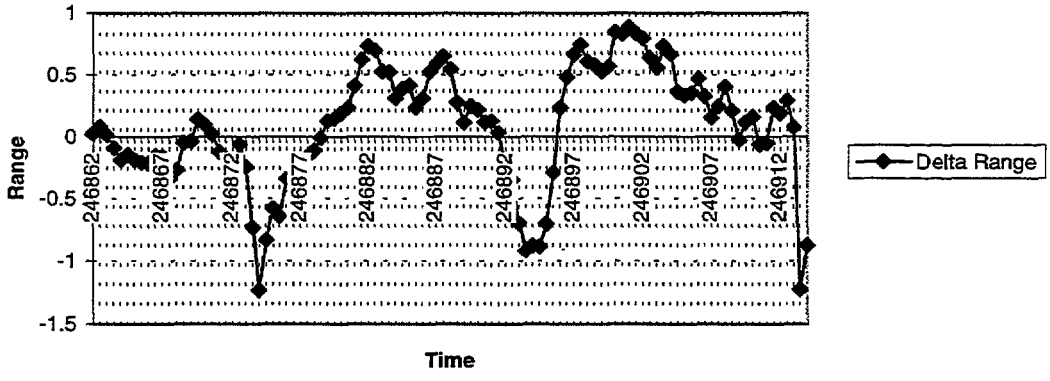

Figure F-10. GPS Truth for R9

Conclusions

The braking target vehicle test analysis did not produce any unanticipated results. In the relatively simple environment created during these tests, the radar returns accurately depicted the dynamics of the target vehicle.

The actual RCS levels were seen to vary by over 10 dB over the short term (500 msec), but tended to average out to a +3 to +8 dBsm RCS for the target vehicle (a Honda Accord). These levels are well correlated to the RCS measurements made on similar vehicles as part of this program. The variations in signal levels observed in this test can be expected to occur to differing degrees for most objects an automotive radar will encounter on the roadway.

Scintillation and directive reflectivity characteristics play a key role in the variations of the signal return levels seen by the radar sensor, as a result of the simple dynamics between the host and target vehicles. In many cases, these effects will actually help automotive radar detect low RCS targets by

sporadically generating relatively high level returns as a result of glint and constructive wave interactions.

Finally, the DGPS truthing mechanism was found to have a very high degree of correlation with the reported range values from the FLAR sensor. In fact, during the braking target vehicle tests, the FLAR was found to be accurate to within 1 meter for the duration of the collections.

F.3 OUT-OF-LANE VEHICLE CLUTTER—STRAIGHT ROADWAY

Purpose

The purpose of this test is to determine the Primary vehicle's ability to track the in-lane target vehicle when there is an out-of-lane "clutter" vehicle that should be ignored. These tests begin to address the issue of "clutter" vehicles interfering with the returns from target vehicles and causing errors in the reported ranges of the target vehicles. Events to watch for in this test are loss of lock on the target vehicle, returns from the clutter vehicle, and errors in reported range to the target vehicle.

Procedure

The test begins with the Primary vehicle maintaining a constant distance of approximately 30 meters from the in-lane target vehicle, (S1) and an out-of-lane "clutter" vehicle (S2) next to the Primary vehicle. The Primary and target vehicles maintain their lane positions throughout the test. The out-of-lane clutter vehicle accelerates to a position approximately 50 meters in front of the Primary vehicle and maintains this position (in the outside lane) for the remainder of the test.

A Honda Accord was used a the target vehicle and a semi-tractor/trailer was used as the clutter vehicle.

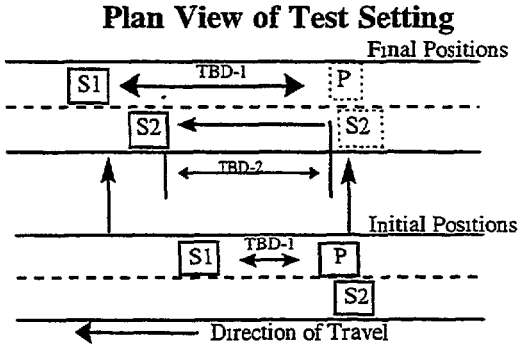

Results

Several test runs were made using the procedure described above. Test runs were made with both the center beam and left beams active. Figure F-11 is a data plot resulting from a run in which the left beam of the FLAR was active and will be used here to summarize the results of these tests.

As was the case in all the test runs, returns from the target vehicle were always observable in the raw radar data. Also, the TRW-proprietary algorithms used in the FLAR always maintained lock on the target vehicle whether the center or left beam was active.

Analysis of the DGPS data indicated that the presence of the clutter vehicle did not cause any erroneous range data to be reported

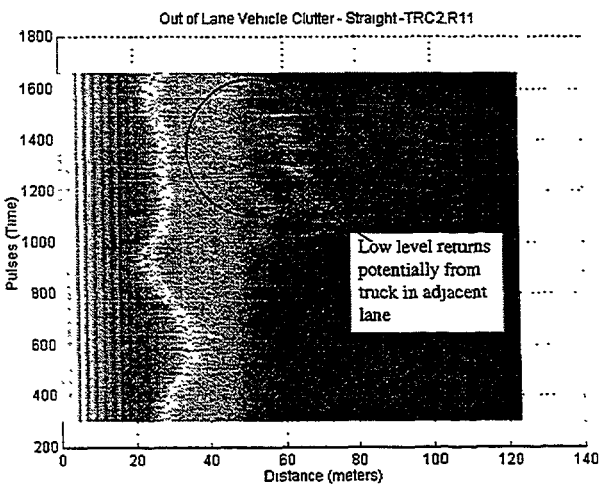

Figure F-11. Out of Lane Vehicle Clutter—Straight

by the FLAR for the given scenario. Likewise, no sudden shifts in IF frequency were observed in the raw radar data; this would have indicated some multipath interference induced by the clutter vehicle.

Returns from the clutter vehicle were only evident during runs in which the left beam was active. The annotations in Figure F- 11 highlight the returns attributed **to** the clutter vehicle; they are consistent with those observed during tests with the semi-tractor/trailer in a similar orientation. These returns were of a very low level and barely rose above the radar system noise floor.

Upon analyzing the video data which was collected along with the radar data, it was observed that the target vehicle had actually drifted to the right portion of its lane during the period when the returns from the clutter vehicle were present. Geometric analysis of the vehicle locations with respect to the radar during the collection show that the radar's field of view provided by the left beam was limited to roughly the left-most portion of the lane occupied by the Primary vehicle. Therefore, the clutter vehicle was being "occluded" by the target vehicle when the target vehicle was in the left or center portion of its lane. However, as the target vehicle drifted to the right, the clutter vehicle was being illuminated by the radar and thus provided the returns observed in Figure F-l 1.

Conclusions

For the given test scenarios, no significant effects from clutter vehicles on a straight roadway were observed. However, observations do lead to the conclusion that different scenarios may produce somewhat different results. In particular, target vehicles located at longer ranges than those tested in these experiments would allow the FLAR's left beam to more intensely illuminate the clutter vehicle, producing higher level returns. It is unlikely, at least on straight roadways, that these clutter returns would compete with or those from the target vehicles.

Unfortunately, the infinite combinations of vehicle positions could not be tested in this program. As a result, another potential effect of adjacent lane vehicle clutter which was not exhaustively tested for was that of multipath. Certain geometries between the radar, the target vehicle, and the clutter vehicle may produce returns resulting from "indirect" reflections off the vehicles. For example, the transmitted radar ener-7 may first reflect off the target vehicle toward the clutter vehicle, and reflect off the clutter vehicle and return to the radar. The result would be a return which would appear to come from the target vehicle, but at a longer range. It is suggested that more testing, to address empirical or simulated, to address multipath effects be conducted in the future.

These tests also provide some insight into results which could be expected for automotive radars which employ scanning antenna technology and larger field of views. As the antenna is directed towards the edges of its FOV, it will probably pick up returns from clutter vehicles in adjacent lanes. The scanning antenna mechanism will give system designers the ability to employ algorithms to help discriminate and identify clutter target returns based on the antenna's position within the scanning range.

F.4 INTENTIONAL LANE CHANGES-STRAIGHT ROADWAY

Purpose

The purpose of this test was to determine the radar's response to vehicle lane changes. Response time is an important performance parameter that was monitored.

Procedure

Only the Primary and target (Secondary) vehicles were present on the freeway. Two different types of lane changes were evaluated. In the first test, the Primary vehicle changed its lane to pass the target vehicle. In the second test, the target vehicle moved out of the Primary vehicle's lane.

Primary Passes Target

The test began with the Primary vehicle maintaining a constant distance to the target vehicle. The Primary vehicle then accelerated moderately and changed its lane to pass the target vehicle. The test terminates after the Primary vehicle passes the target vehicle.

Plan View of Test Setting

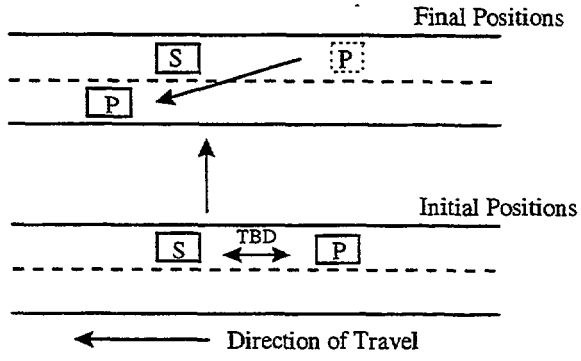

Target Leaves Lane

The test began with the Primary vehicle maintaining a constant distance to the target vehicle. The target vehicle accelerated moderately and changed its lane, then decelerated to approximately the same distance as at the beginning of the test. The test terminated after the Secondary vehicle had achieved and maintained the original headway.

Plan View of Test Setting

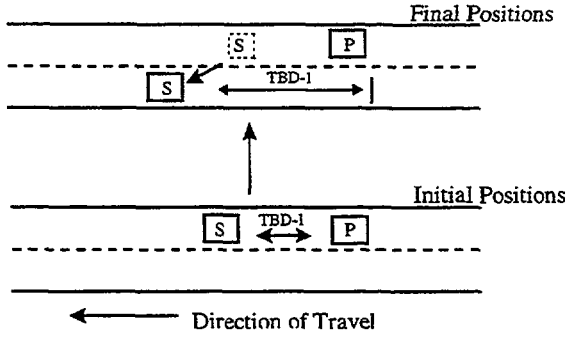

Results

In general, the radar sensor performed very well under the low-clutter environment created during these tests. The response time for the radar to react to the lane change appeared to be very good based on analysis of the video data, raw radar data, and GPS data. The analog video collection system limited the amount of quantitative analysis that could be done in terms of absolute response times, but the raw radar data and dynamic movements captured by the video system appeared to correlate to within a second. Performance was consistent over all the tests conducted and no significant differences were observed between the host lane change and target lane change dynamics.

A set of collection data taken during a host vehicle lane change maneuver will be used to summarize the results. The data plots in Figure F-12 are from a run in which the Primary vehicle was following a Honda Accord, and the Primary vehicle made a lane change. Figure F-12(a) illustrates the typical return characteristics as the Primary vehicle approaches the target vehicle, namely, the return levels increase as range decreases. The Accord measured to be approximately 3 to 7 dBsm through the run.

Procedure

The test began with the Primary (host) vehicle maintaining a constant distance to the first target vehicle (S1), with the second target vehicle adjacent to the Primary vehicle and traveling at the same speed. The second target vehicle then accelerated and moved into the right-hand lane between the other two vehicles. The distance between vehicles was selected for safe operation and to be within the FLAR's minimum operating range.

Plan View of Test Setting

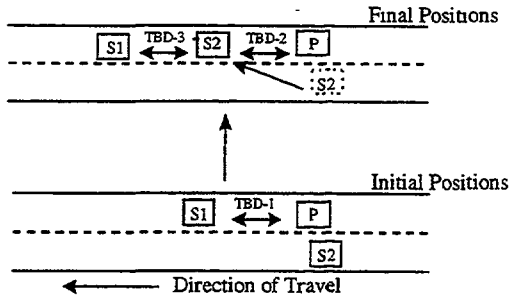

Results

The results of these tests parallel those described in the previous section, "Tracking New Target Vehicle—Straight Roadway." The primary difference was in the vehicle dynamics which produced the result. In the previous the first targeted vehicle departed from the Primary vehicle's lane, presenting the radar with a second target vehicle at a greater range than the first. In these tests, the second target cuts into the land and is presented to the radar at a range less than the first target vehicle by a maneuver.

The end result for both are similar in that the radar performed well. Sample data plots for one of the test runs conducted as part of this series of tests are provided below. The reader should refer to the discussion in "F.5: Tracking New Target Vehicle—Straight Roadway" for a more detailed discussion.

Figure F-16 plots the raw radar data collected throughout the duration of a test conducted using two Honda Accords as the target vehicles. Figure F-16(a) includes a time line of events and annotation indicating the sources of the respective returns. Figure F-16(b) shows the amplitudes of the relative return levels which correlate to an expected RCS of a Honda Accord of between +3 to +7 dBsm.

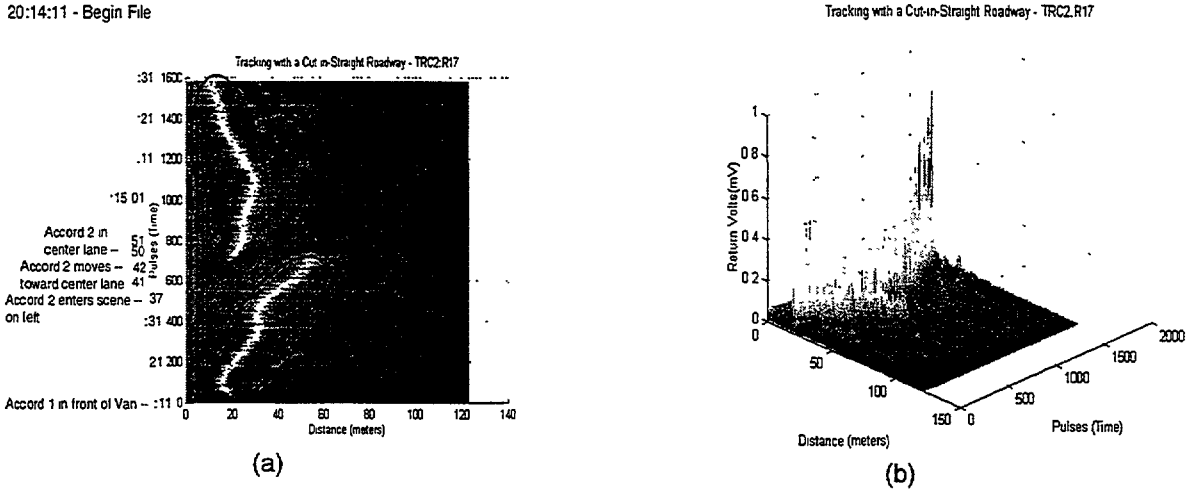

Figure F-16. Tracking With a Cut-In Straight Roadway

Figure F-17 is a plot of the GPS truth data and the FLAR reported range data. As in the lane departure tests, the FLAR produced no dropouts or jitter in the transition from one target vehicle to the other.

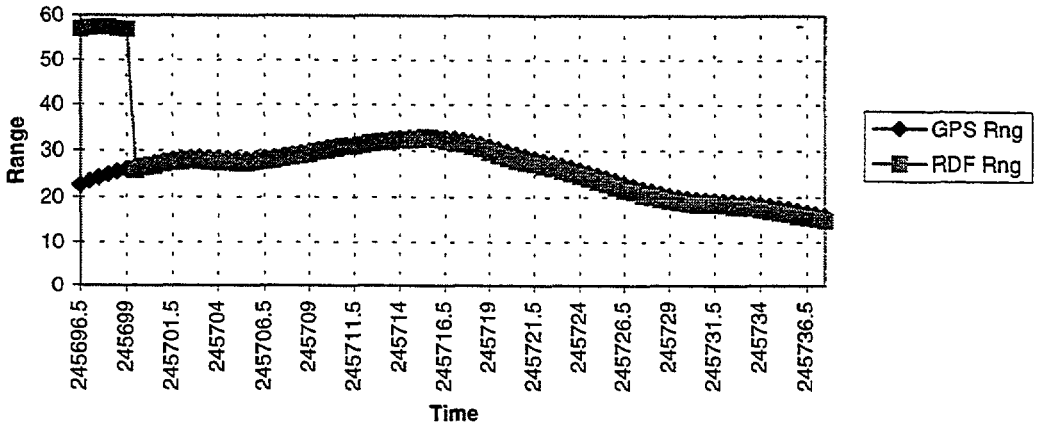

Figure F-17. GPS Truth for R17

Conclusions

The important issue to note in these tests is that during the cut-in process, the second target vehicle was actually in a position such that a collision could occur with the host vehicle, but the radar sensor would never "see" the target vehicle. Again this is a limitation of the FLAR's field of view.

Figure F-18 illustrates the problem in which the radar beam is not illuminating the target vehicle although the target vehicle is obviously within the primary vehicle's path. For the Adaptive Cruise Control Application, the operator may actually find himself accelerating into a collision with the undetected target vehicle. Two options for this situation are available. The first is to increase the field-of-view of the forward-looking sensor, and the second is to install simple supplemental sensors which work at close range but have a wide field-of-view. These supplemental near-range sensors could be strategically placed in areas near the edge of the vehicle, such as the headlight area.

Both of the solutions to this problem add both cost and complexity to the system and require a detailed trade-off analysis.

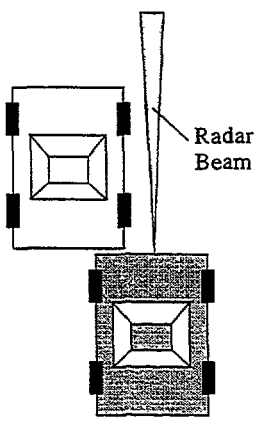

Figure F-18. Beam Illumination

F.7 STRONG VEHICLE CLUTTER IN RANGE—STRAIGHT ROADWAY

Purpose

The purpose of this test is to determine the radar's ability to acquire and maintain track on a fixed target vehicle in the presence of a relatively stronger (in terms of RCS), in-lane Secondary vehicle, but at a greater range. This will test the FLAR's ability to discriminate vehicles in the same lane, but with varying RCS and range.

Procedure

The nearer range target vehicle was a motorcycle (MC). The clutter vehicle was a semi-tractor/trailer with a radar cross-section significantly greater than that of the motorcycle. The FLAR's task was to detect and maintain track on the motorcycle and ignore the presence of the clutter vehicle. The test began with the motorcycle and clutter Secondary vehicle in the adjacent lane to the Primary, with all the vehicles traveling at the same speed. The motorcycle then accelerated, moves into the Primary vehicle's lane, and maintained a position in front of the Primary vehicle. The position of the motorcycle with respect to the primary vehicle was varied on a run-by-run basis. The clutter Secondary vehicle then accelerated, moved into the same lane, and varied its position from 5 to 80 meters in front of the motorcycle. The distances were selected for safe operation; their sum was less than the maximum operating range of the FLAR. The test continued for several minutes with the motorcycle varying its position within its lane.

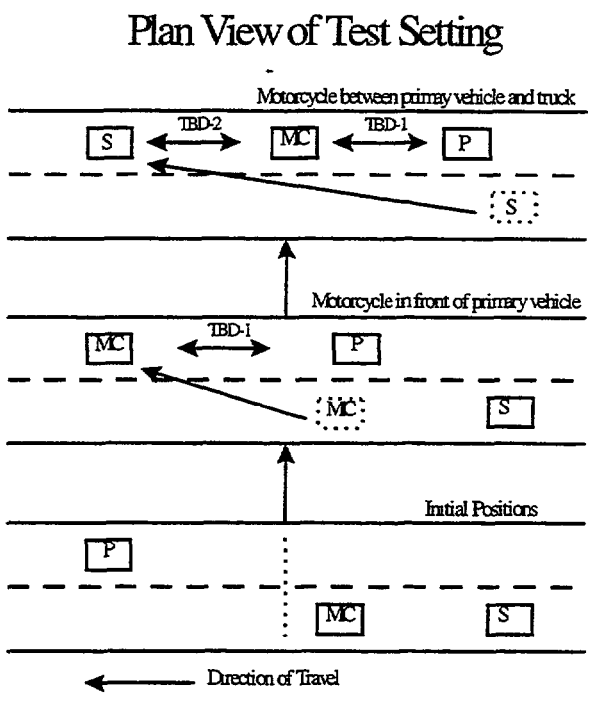

Results

These tests yielded some of the more interesting results in the program. Two separate data sets will be used to illustrate the effects of strong range clutter on the radar's response. Both data sets are taken from collections in which the motorcycle was located between the host vehicle and a semi-tractor/trailer.

Data Set #1: Radar Maintains Lock on Motorcycle

Figure F-19 is a plot of the radar return signals collected during the test. The figure also provides a time line of events which occurred during the collection and annotation of the respective sources which created the returns.

The motorcycle entered the primary vehicles lane approximately 10 seconds into the test and the radar's field of view approximately 13 seconds into the test. The initial range to the motorcycle was about 15 meters. The motorcycle continued accelerating until it reached a range of approximately 25 meters. This range was roughly maintained for the duration of the test. Approximately 30 seconds after the motorcycle entered the radar's field of view, the clutter vehicle (i.e., the truck) entered the lane in front of the primary vehicle. The radar returns generated by the truck are clearly seen on Figure F-19.

With both the motorcycle and truck with the radar's field of view, returns from both targets could be frequently observed. Occasionally, the motorcycle would be in a position such that it totally occluded the returns from the truck. This is observed in Figure F-19 at approximately 14:53:48 (or pulse 1500). The interesting point to note is that as the motorcycle drifted to the side of the lane, its return levels decreased, but were still observable, and those from the truck increased significantly. This is of course

due to the fact that as the motorcycle moved off of the radar beam's boresight, more of the energy illuminated the truck and less illuminated the motorcycle.

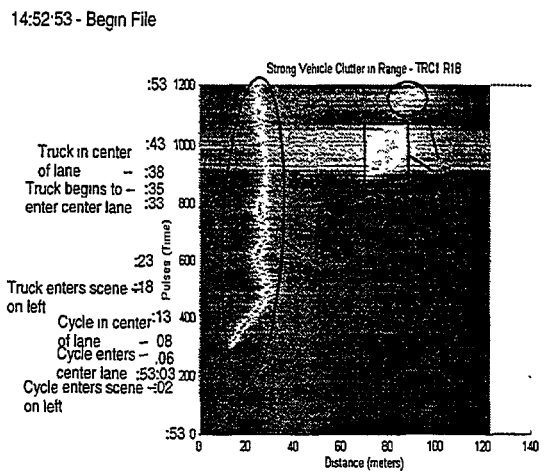

Figure F-19. Strong Vehicle Clutter in Range

The key performance attribute in this type of scenario is whether or not the radar can maintain lock on the motorcycle as it drifts to the edges of its lane, even in the presence of the truck returns. Based on the plot in Figure F-19, it is reasonable to conclude that a moderately robust tracking algorithm should be able to maintain lock on the motorcycle.

Figure F-20 shows that the FLAR and its TRW-proprietary processing algorithm did, in fact, maintain lock on the motorcycle. The line labeled "GPS Rng" in Figure F-20 corresponds to the measured range to the truck utilizing the DGPS truthing mechanism. The line labeled "RDF Rng" corresponds to the range reported by the FLAR. The TRW FLAR was designed to operate as an Adaptive Cruise Control sensor and, therefore, its primary function is to identify the target in front of the host vehicle and track its range. It is obvious from this plot that once the FLAR began tracking the motorcycle, it was able to maintain track throughout the test even in the presence of returns from the clutter vehicle which were stronger than that of the motorcycle.

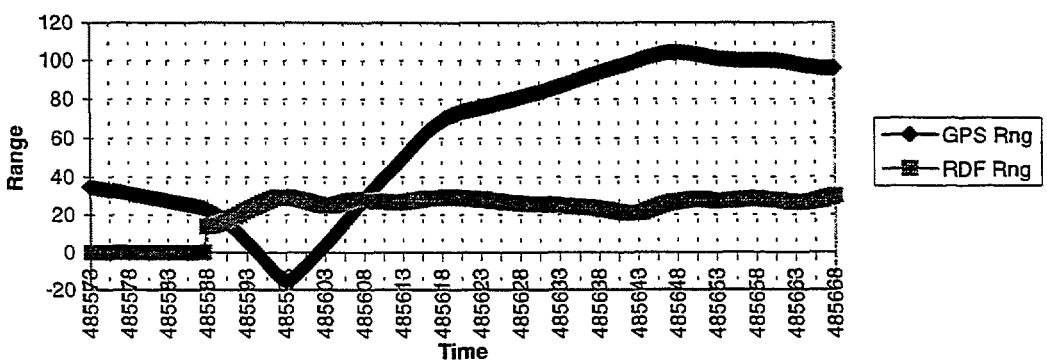

Figure F-20. GPS Truth for R18

Figure F-21 is another plot which contains the same data shown in Figure F-19; however, the differences in the relative return levels can be more clearly seen. MATLAB processing of this type of data allowed numerical analysis to estimate the radar cross-sections exhibited by both the motorcycle and the truck during the test.

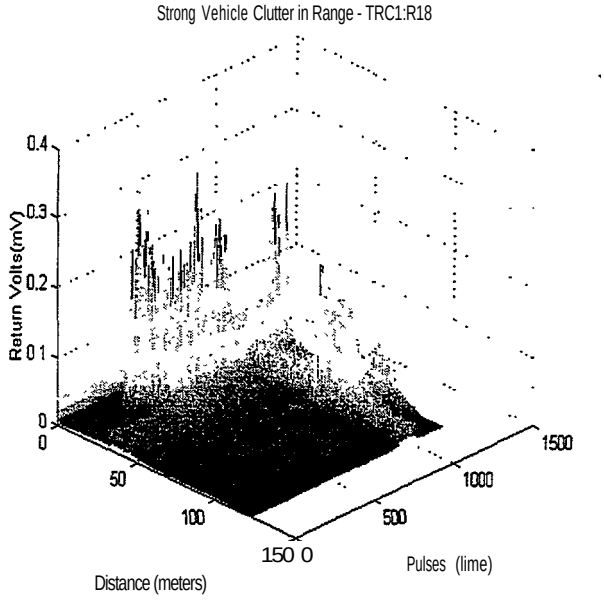

Figure F-21. Strong Vehicle Clutter in Range

Table F-1 summarizes the results of the radar cross section (RCS) analysis. The motorcycle was seen to vary from -6 to +3 dBsm depending upon its location within the lane. The truck exhibited RCS levels of 20 to 25 dBsm during periods when the motorcycle was positioned on the left side of the lane. As mentioned earlier, the motorcycle blocked nearly all of the truck returns when it was positioned in the center of the lane.

Table F-1. RCS Analysis Results

Target	Estimated RCS
Motorcycle in Center of Lane	0 to 3 dBsm
Motorcycle on Left Side of Lane	-6 to 0 dBsm
Truck with Cycle on Left Side of Lane	**20** to 25 dBsm

The RCS levels are quite consistent with the measurements taken during the "Roadway Object RCS Characteristics" phase of this program. The reader is referred to the "Catalog of RCS Characteristics for Common Roadway Objects" for more information on typical RCS levels. The catalog is available from both ERIM and NHTSA.

Data Set #2: Radar Loses Lock on Motorcycle

Figure F-22 is a plot of another test run made with the motorcycle and truck as the target vehicles. Again, a time line of events is provided in the figure and the source for the returns is annotated on the plot. Note **that** during pulses 1200 to 1400, both motorcycle and truck returns can be observed.

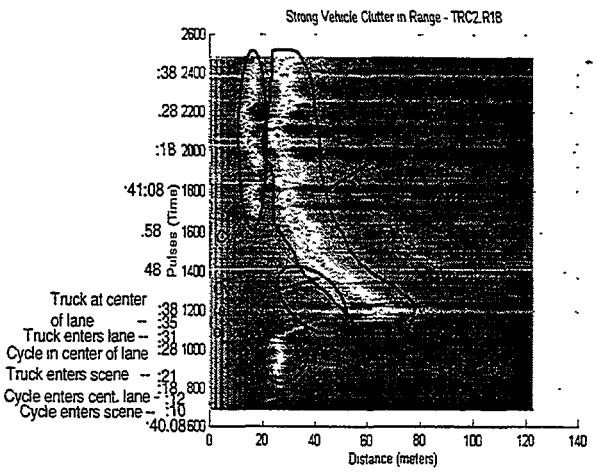

Figure F-22. Strong Vehicle Clutter in Range

Approximately 13 seconds into the test, the motorcycle enters the radar's FOV at a range of about 25 meters. The motorcycle then continues to accelerate as the truck enters the primary vehicle's lane. At about 30 seconds into the test (around pulse 1100), returns from both the motorcycle and the truck can be observed. The motorcycle is approximately 50 meters away, and the truck is 10 meters beyond the motorcycle. At this point, as expected, the returns from the motorcycle appear to be relatively low compared to that of the truck.

As both the truck and motorcycle decelerated with respect to the primary vehicle, the motorcycle was observed to drift to the left side of the lane. The plot in Figure F-22, illustrates that for a substantial period of time (about 15 seconds), the motorcycle returns were no longer observable. Subsequently, the motorcycle drifted back toward the center of the lane and was once again detected by the radar. The motorcycle stayed fairly close to the center of the lane, with some small deviations, for the duration of the collection.

The results of this test run contrast to those described for the previous data set in that the truck returns remained much more prominent throughout the run. In fact, once the truck entered the primary vehicle's lane, there were only several short periods during which the truck was fully occluded by the motorcycle.

As was the case with the previous data set, the critical performance parameter from the radar standpoint is whether or not the a consistent lock on the motorcycle can be held. Observing the raw radar returns indicates that there are two periods of time during which the radar may have had trouble maintaining a lock on the motorcycle. The largest gap occurs from 15:40:48 to 15:41:02 (pulses 1400 to 1650 in Figure F-22). The smaller gap occurs from 15:41:10 to 15:41:12 (pulses 1820 to 1900 in Figure F-22).

Figure F-23 is the corresponding GPS truthing plot to the test run. The truck range is represented by the line labeled "GPS Rng" and the reported FLAR range is represented by the line labeled "RDF Rng". It is clearly evident in the plot that the FLAR (utilizing the TRW-proprietary processing algorithms) did in fact lose lock on the motorcycle during the larger of the two gaps mentioned in the preceding paragraph. During this period, the FLAR began tracking the truck rather than the motorcycle. The transitions from tracking one vehicle as opposed to the other were not gradual transitions, but rather abrupt, in that the report range showed no residual effects from the previously tracked vehicle's position.

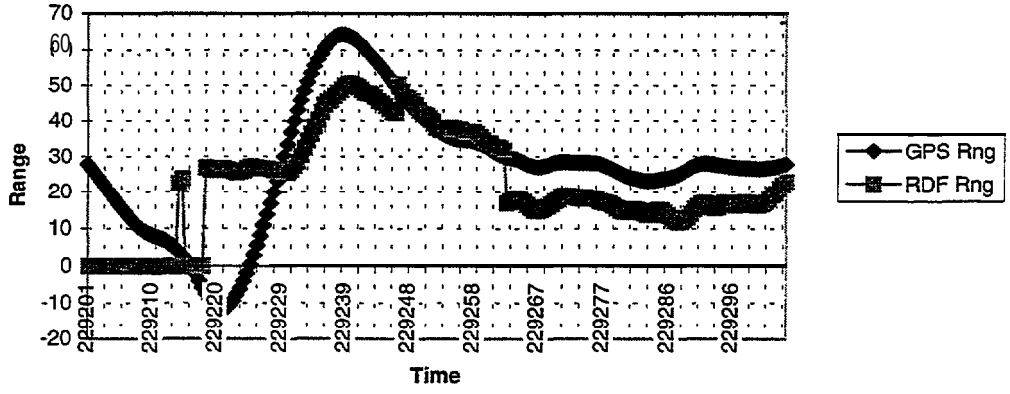

Figure F-23. GPS Truth for R18

Figure F-24 provides a better view of the relative return levels seen in the raw radar data during the collection. Peak level returns were evaluated to estimate the radar cross section (RCS) exhibited by each of the vehicles. These levels were found to be consistent with those listed in Table F-1,as expected.

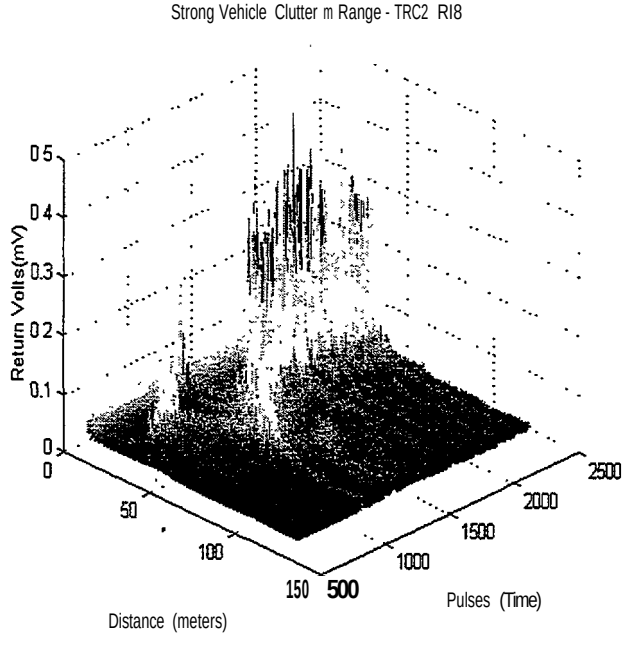

Figure F-24. Strong Vehicle Clutter in Range

Conclusions

The empirical data discussed in this test report indicate that automotive radar designs must carefully address the scenario of having a relatively small target located between the host vehicle and a relatively large target. Motorcycles and narrow cars pose the worst problems because they allow much of the radar energy to illuminate the large target located in front of them.

It was frequently observed in the empirical data that returns from both the motorcycle and truck targets within the host vehicle's lane were present. Furthermore, as the motorcycle drifted within its lane, its returns could actually dissipate to the point where the FLAR began tracking the truck which was at a greater range than the motorcycle. Obviously, this series of events could-have disastrous consequences in an ACC application. The driver could find himself accelerating to achieve a set headway behind the truck while colliding with the motorcycle.

These results emphasize the need for some form of scanning beam, in order to increase the radar's field of view and concentrate the highest gain portion of the beam across the path of the host vehicle.

One final issue of concern for this scenario deals with the use of automatic gain control (AGC) in the radar receiver circuitry. AGC implementations may be used to increase the effective dynamic range of a radar receiver and also protect it from saturation. However, there is a risk that a large vehicle, like the truck, may cause the AGC circuitry to reduce the sensitivity of the receiver to low level returns like those generated by the motorcycle.

The raw radar data in these tests was analyzed for AGC activity. The truck was found to induce a decrease in the FLAR receiver sensitivity by reducing the gain in the AGC circuitry. However, further analysis showed that the decrease in sensitivity did not, in and of itself, cause the loss of lock on the motorcycle. Instead, the primary cause for loss of track on the motorcycle was its position within the radar's beam.

F.8 VEHICLE CLUTTER IN AZIMUTH-STRAIGHT ROADWAY

Purpose

The purpose of these tests were to evaluate the radar's response to "clutter" vehicles positioned in azimuth (i.e., in adjacent lanes) while tracking a target vehicle located in the host vehicle's lane. This tests the FLAR's ability to discriminate between in-lane and out-of-lane vehicles.

Procedure

The FLAR's center beam (3 dB width of 3 degrees in azimuth and elevation) was activated during these tests.

The two out-of-lane Secondary vehicles (S2 and S3) had radar cross-sections equal to or greater than that of the in-lane Secondary vehicle. The test began with the Primary vehicle maintaining a constant distance from the in-lane target vehicle; the out-of-lane clutter vehicles were adjacent to the Primary vehicle and traveling at the same speed. The out-of-lane clutter vehicles then accelerated until they were adjacent to the in-lane Secondary vehicle. They maintained this position for several seconds and then decelerated until they were again adjacent to the Primary vehicle. The test terminated when the initial, relative vehicle positions had been achieved.

Plan View of Test Setting

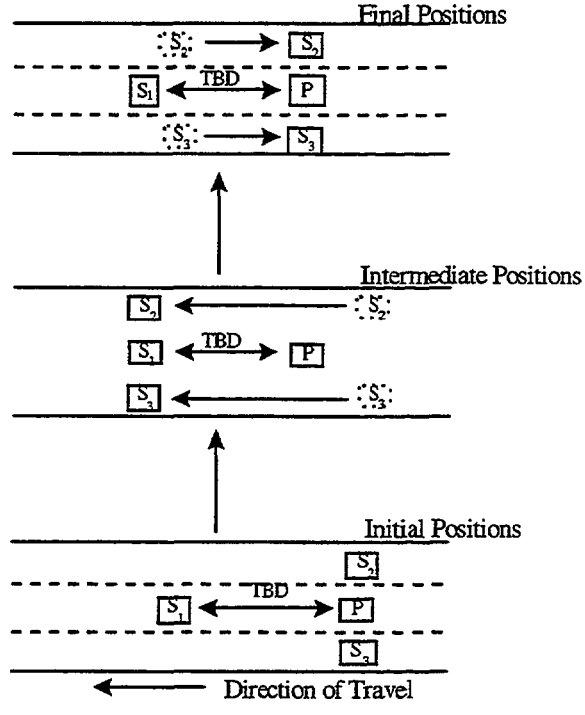

Results

The results for this test scenario are provided in the next section.

F.9 MERGING TRAFFIC-STRAIGHT ROADWAY

Another version of this test was conducted using a single clutter vehicle in the adjacent lane to simulate the situation frequently observed near a freeway entrance ramp. The vehicle dynamics are similar detailed in Section F.8 "Vehicle Clutter in Azimuth—Straight Roadway" tests described above.

Results

The results of both sets of tests were found to be very benign. Over six different test runs of varying target vehicle ranges up to 50 meters, the clutter vehicles never invoked a response in the raw radar data or the FLAR processed outputs. The plots in Figure F-25 summarize the empirical data collected in the tests.

The radar data accurately tracked the target vehicle's location throughout the test. The return levels from the Honda Accord target vehicle consistent with measurements made during other tests (at 3 to 7 dBsm).

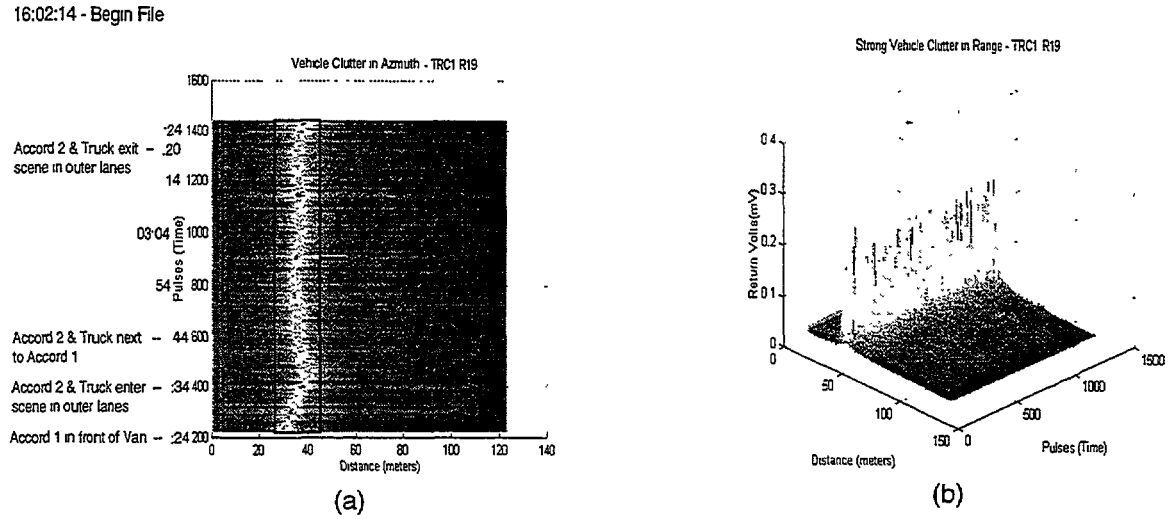

Figure F-25. Vehicle Clutter in Azimuth

Conclusions

For ranges up to 50 meters, vehicles in adjacent lanes do not appear to affect the raw returns of the radar sensor, given the 3 degree beamwidth of the FLAR. These tests did not extend to ranges beyond 50 meters, and further testing should be conducted.

F.10 VEHICLE INDUCED FALSE ALARMS—CURVED ROADWAY

F.10.1 Purpose

The purpose of the following two tests ("Stationary Target Vehicle on Shoulder" and "Moving Adjacent Lane Target Vehicle") is to evaluate the effect of guard rails and out-of-lane target vehicles located on a curved roadway. In one case the vehicle was parked on the roadside shoulder and in the other it was traveling in an adjacent lane in front of the Primary vehicle. Only the Primary and Secondary vehicles were present on the roadway.

These tests were designed to measure the return levels, if any, observed in the raw radar return signal from the "non-threatening" secondary vehicle and the guard rail.

F.10.1.1 Stationary Target Vehicle on Shoulder

Procedure

The Secondary vehicle was parked on the outside lane of a curved roadway which included a guard rail. The Primary vehicle began in the straight portion of the roadway, accelerated to freeway speed, passed the Secondary vehicle, and continued on until it exited the curved portion of the roadway completing the test.

This test procedure was repeated a number of times using both a Honda Accord and a Semi-Tractor/Trailer as the Secondary vehicles. Runs were also made with the FLAR sensor's center beam active. The center beam has a 3 degree azimuth and 3 degree elevation beamwidth.

Results

The ERIM Analysis PC software was used to screen the data and identify the data sets worthy of further analysis. Several data sets were selected and the raw radar returns (prior to any digitization in the FLAR) were processed using custom Matlab scripts. Several of the MATLAB output plots will be used here to illustrate the results. A complete set of plots from all MATLAB processed tests are included at the end of this document.

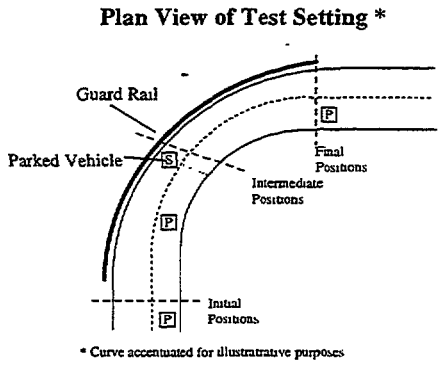

In general, radar returns form both the roadside guard rail and target vehicles were observed in the MATLAB processed data. The signal levels were well above the noise floor as will be illustrated below. Interestingly, the FLAR processed data (i.e., the TRW processing algorithm within the FLAR) never "locked-on" and tracked the returns from the guard rail or parked target vehicles for any significant period of time.

F.10.1.2 Characteristic Return From Guard Rail

Figure F-26 illustrates the characteristic return from a guard rail located on a curved section of roadway. As the primary vehicle approaches the curve, the radar beam remains fixed on a single section of guard rail which is located directly in front of the vehicle. Therefore, the reflection from the guard rail "appears" to the radar as a stationary object located directly in front of the radar, and approaching the radar at a rate equal to the vehicle's velocity. This portion of the guard rail characteristic is illustrated by the returns occurring during pulses 2100 to 2200 in Figure F-26.

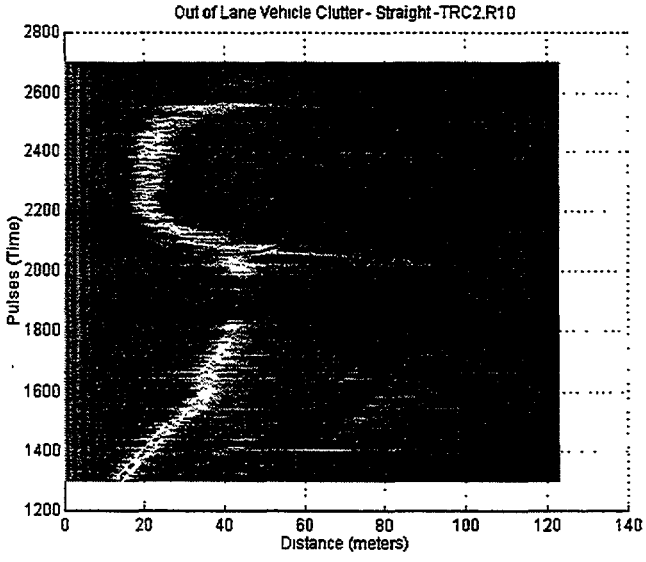

Figure F-26. Out of Lane Vehicle Clutter—Straight

Once the vehicle itself enters the curve, the radar beam begins traveling along the horizontal extent of the guard rail as the vehicle's heading constantly changes. Therefore, provided that the guard rail and roadway have similar curvatures, the portion of the guard rail being illuminated by the radar remains at a constant range as the vehicle proceeds through the curve. The guard rail returns of this type are observed for pulses 2200 through 2500 in Figure F-26.

Just prior to exiting the curve, the radar beam illuminates portions of the guard rail that do not have a similar curvature to that of the roadway. These portions of guard rail are actually straight. Therefore, as the vehicle exits the curve, the distance to the guard rail rapidly increases until the radar beam is no longer illuminating the guard rail, but instead is directed down the lane occupied by the host vehicle. This is illustrated during pulses 2500 and up in Figure F-26.

This dynamic sequence of events (see Figure F-27) creates the characteristic "C-shaped" return from the guard rail. Analysis of the guard rail experiments conducted under this program have resulted in RCS values for guard rails on the order of 0 to 5 dBsm. Of course these values are heavily dependent upon specific configuration of the guard rail, but it is evident that these RCS levels can compete with those from vehicles, pedestrians, and other roadway objects (see Section 3 of the final report for a description of RCS measurements on common roadway objects).

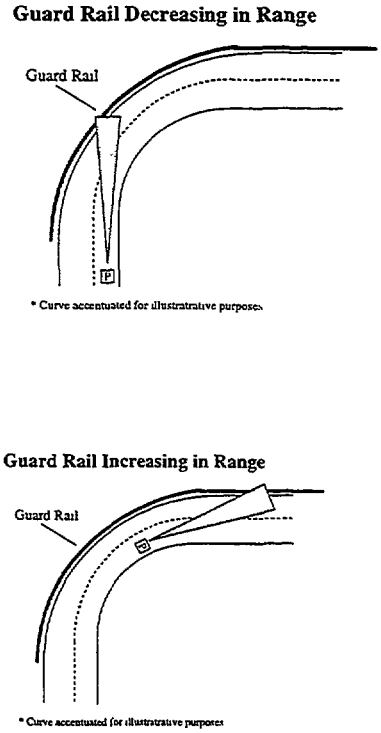

Figure F-27. Sequence of Guard Rail Returns

The final observation from the guard rail return is that due to the radar footprint which illuminates the curved portion of the rail, the returns indicate that the target has significant range extent. This attribute may be the cause for the FLAR's inability to "lock-on" and track the target as mentioned above.

F.10.1.3 Returns from Stationary Honda Accord

Figure F-28 shows are plots taken from experiments run with the Honda Accord used as the stationary target vehicle. The return from the Accord is annotated in Figure F-28(a). The return from the vehicle is brief due to the radar illumination beam sweeping horizontally through the scene as the host vehicle proceeds through the turn (see Figure F-27 for illustration of beam dynamics). Figure F-28(b) illustrates the relative return level from the Accord as compared to the guard rail and noise floor.

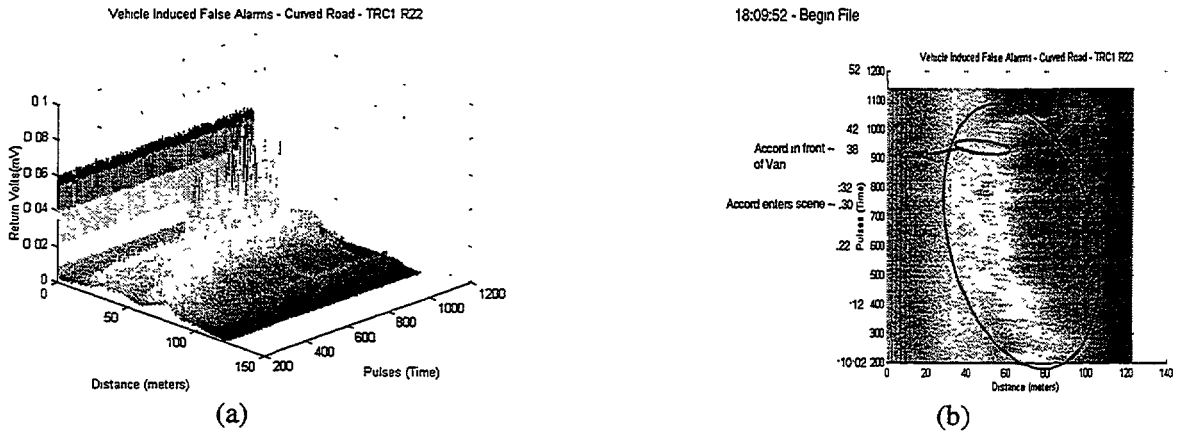

Figure F-28. Vehicle Induced False Alarms—Curved Road

Quantitative analysis of the returns from the Accord result in an RCS measurement of 2 to 3 dBsm. The value for the Accord correlates well to the RCS measurements made on similar vehicles in this program. This return level is slightly above that of the guard rail itself. During this test, the FLAR itself, utilizing the TRW processing algorithms, sporadically "locked-on" and tracked the returns from the guard rail for very brief periods of time (less than 500 msec). None of these brief "lock-on" periods corresponded to the returns from the Accord.

F.10.1.4 Returns from Stationary Tractor/Trailer

Figure F-29 shows plots taken from experiments run with the semi-tractor/trailer used as the stationary target vehicle. The return from the tractor/trailer is annotated in Figure F-29(a). The return from the vehicle is still fairly brief, but significantly longer than that from the Accord—approximately 1.25 second as opposed to 500 msec. The longer duration is due to the greater length of the truck compared to the Accord. This difference in length causes the horizontally sweeping radar beam to illuminate the truck for a longer period of time than it illuminated the Accord turn (see Figure F-27 for illustration of beam dynamics). Figure F-29(b) illustrates the relative return level from the Tractor/Trailer as compared to the guard rail and noise floor.

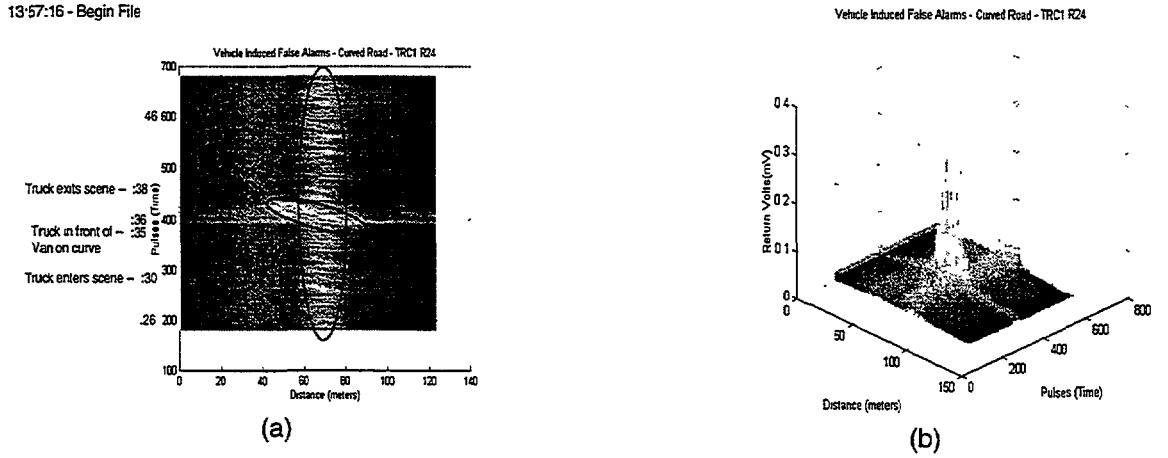

Figure F-29. Vehicle Induced False Alarms—Curved Road

Quantitative analysis of the returns from the tractor/trailer returns result in an RCS measurement of over 12 dBsm. The value for the tractor/trailer correlates well to the RCS measurements made on similar vehicles in this program. The truck's high RCS causes its return levels to rise substantially above those from the guard rail. During this particular test, the FLAR itself, utilizing the TRW processing algorithms, never "locked-on" and tracked the returns from the guard rail or the large brief return from the truck.

Conclusions for Stationary Target Vehicle on Shoulder

The test results discussed above illustrate how the dynamic movement of the radar through a typical roadway curve produces a characteristic return pattern (the 'C-shape') from a guard rail located on that curve.

Table F-2 provides quantitative information regarding the return levels observed in these measurements. Clearly, these levels of returns could certainly induce false alarms under specific scenarios.

Table F-2. Return Levels of Stationary Clutter

Description	Filename	RCSs (dBsm)
Guard Rail	TRC2:R10	0.9986449
Accord on Shoulder	TRC1:R22	2.5822699
Truck on Shoulder	TRC1:R24	12.37137

F.10.1.5 Moving Adjacent Lane Target Vehicle

Procedure

The Primary and Secondary vehicles were traveling at freeway speeds in adjacent lanes as they proceeded through the curve. A number of runs were made during which the range between the vehicles was held relatively constant. This range was varied from 10 to 70 meters on a per experiment basis. Runs were also made in which the range varied during the run. The Primary vehicle maintained a constant speed and the Secondary vehicle varied its speed to achieve the desired range profiles.

Plan View of Test Setting *

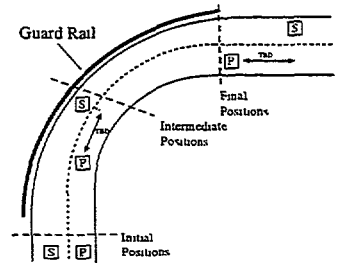

Multiple runs of this test were made using a Honda Accord and semi-tractor/trailer as the Secondary vehicle. Also, some runs were made with the FLAR center beam active, and some with the left beam active. Refer to the discussion on the FLAR antenna beam analysis for the description of these beam patterns.

Results

Data from these tests was screened using the ERIM Analysis PC software to identify the data sets worthy of further analysis. Several data sets were selected and the raw radar returns (prior to any digitization in the FLAR) were processed using custom Matlab scripts. Several of the MATLAB output

plots will be used here to illustrate the results. A complete set of plots from all MATLAR processed tests are included at the end of this document.

The plots provided in Figure F-30 are indicative of the results obtained with a moving target vehicle in an adjacent lane on a curved road. In this particular case, the secondary vehicle, a semi-tractor with trailer, provided a strong and consistent return throughout the majority of the curve maneuver,

For the given dynamics of this test, the raw radar return which was collected from the FXAR's center beam could be interpreted as though the host vehicle was directly behind the primary vehicle at a fairly consistent 40 to 50 meter range. For an ACC system, this would mean that the primary vehicle should track and maintain a specified headway to the secondary vehicle. However, this would of course be an operational error since the secondary vehicle is actually located in the adjacent lane.

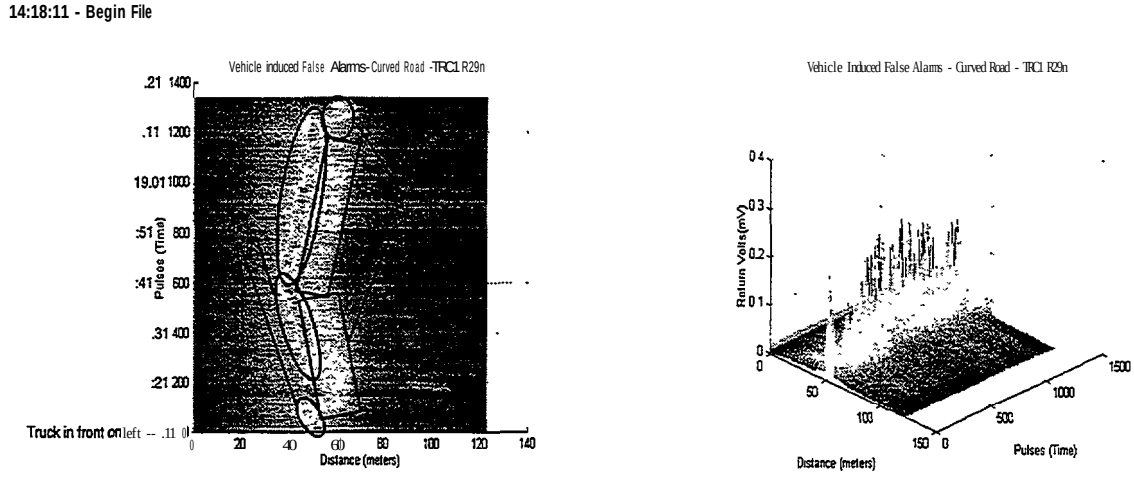

Figure F-30. Adjacent Lane Vehicle on Curve

Conclusions for Adjacent Lane Target Vehicle on Curve

The results of the adjacent lane vehicle tests have shown that without knowledge of the host vehicle dynamics or of the lane geometry in front of the host vehicle, it is very probable that a FLAR unit would incorrectly lock on to an adjacent lane vehicle. If additional information about the host vehicle's environment and activities were available, these could be utilized by the processing electronics to significantly decrease these types of false alarms.

For instance, an angular rate sensor on-board the host vehicle would provide information related to the current trajectory of the vehicle. If the radar system is aware that the vehicle is currently maneuvering through a curve, and the approximate curvature of the curve could be derived, then the radar data processing algorithm and threat assessment algorithm could use this information to filter out returns from adjacent lane vehicles based on the range and azimuthal location of the returns. This of course assumes that the radar system possesses the necessary azimuthal resolution.

F.1 1 TRACKING THROUGH A CURVE

Purpose

The purpose of this test was to determine the FLAR's ability to maintain track on a target vehicle through a standard freeway curve on a dry, flat section of roadway. The test was performed under good driving conditions. Roadway was selected that had guard rails in the scene.

Issues that were considered in these tests included the loss of returns from the target vehicle, and the returns induced by the guard rail around the curve.

Procedure

The test commenced when the Primary vehicle was tracking the target vehicle (a Honda Accord) in a straight section of roadway prior to entering a curve. Both vehicles were traveling at approximately the same speed, attempting to maintain those speeds and the initial separation of 10,40, and 70 meters throughout the test maneuver. The test terminated when both vehicles were again on a straight section of roadway.

As implied above, several tests were conducted, with the distance between the host and target vehicle being 10,40, and greater than 70 meters in individuaI runs.

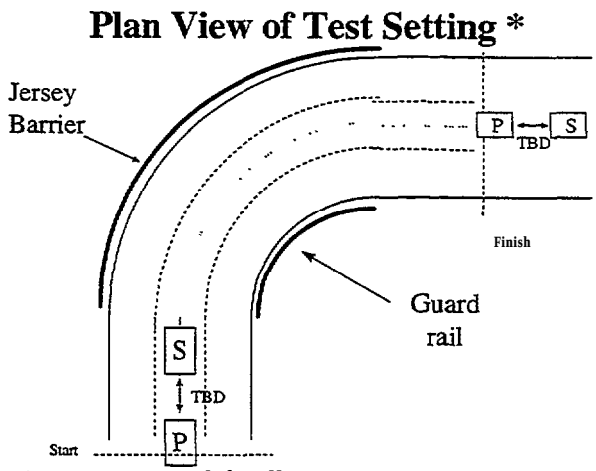

* Curve accentuated for illustratrative purposes

Results

The raw radar data plots for the mns conducted with target vehicles at 10,40, and 70 meters are provided in Figures F-3 1 and F-32. Figure F-3 1 is annotated to identify the source for each of the radar returns. Figure F-32 provides information on the relative return levels which can be used for more numerical analysis.

The remainder of this section will contrast the results from the three different test runs.

Ability to Maintain Track on Target Vehicle

The data plots shown in Figure F-3 1 clearly indicate that the return levels from the target vehicle were not impacted during the turn maneuver when the target vehicle was at a nominal 10 meter range [see Figure F-31(a)]. However, the reuim levels did exhibit significant impact when the target vehicle was at the nominal 40 and 70 meter ranges [see Figures F-31(b) and (c)]. At a 40 meter range, the target's vehicle's return levels were observed throughout the turn maneuver at a much lower level than on a straight roadway. At 70 meters, the target vehicle was not observed at all throughout the turn maneuver. For a more quantitative assessment of the impact on the return levels, see the analysis of the relative return levels provided below.

The radius of the curve used on these tests was approximately 238 meters which is a relatively tight turning radius at normal highway speeds. Table F-3 shows the angular departure from the radar antenna boresight at which the target vehicle is located, given the target vehicle range and a 780 feet radius curve. These values correlate very well with the observations. At a 10 meter range, the target vehicle is located 1.2 degrees off of the antenna boresight. This is within the 3 degree (1.5 degrees on either side of the boresight) PLAR center beam which was active on these tests.

Table F-3. Angular Departure for 238 Meter Radius Curve

Range to Target	**Angular Departure From Boresight**
10 meters	1.2 degees
40 meters	4.8 degrees
70 meters	8.5 degees

On the other hand, at 40 meters the target vehicle is 4.8 degrees off the boresight. As explained in 'Section F. 1: Vehicle Induced False Alarms-Straight Roadway," the real antenna beam extends beyond the 3 degree specification with much lower gain. Therefore, it makes sense that the target vehicle is still visible at 40 meters, but at much lower levels.

At 70 meters, the vehicle is located 8.5 degrees off of the antenna boresight. At this level of departure, the antenna beam gain is extremely low and the target vehicle is effectively out of the radar's field of view. As Figure F-31(c) ilhtstrates, radar returns from the target vehicle given this scenario were not evident.

This data leads to the conclusion: The ability of an automotive radar to maintain lock on a target vehicle is dependent upon the range to the target vehicle and the radius of the curve. In evaluating the raw radar returns under this test scenario, one could conclude that a radar should be able to track the vehicle at 10 meters, may be able to track the vehicle at 40 meters, and probably could not track the vehicle at 70 meters.

The GPS truthing plots provided in Figure F-33 correspond to the data plots from the three tests runs. The range to the target vehicle is represented by the curve labeled "GPS Rng" and the reported range from the FLAR (using the TRW-proprietary algorithms) is represented by the curve labeled "RDF Rng".

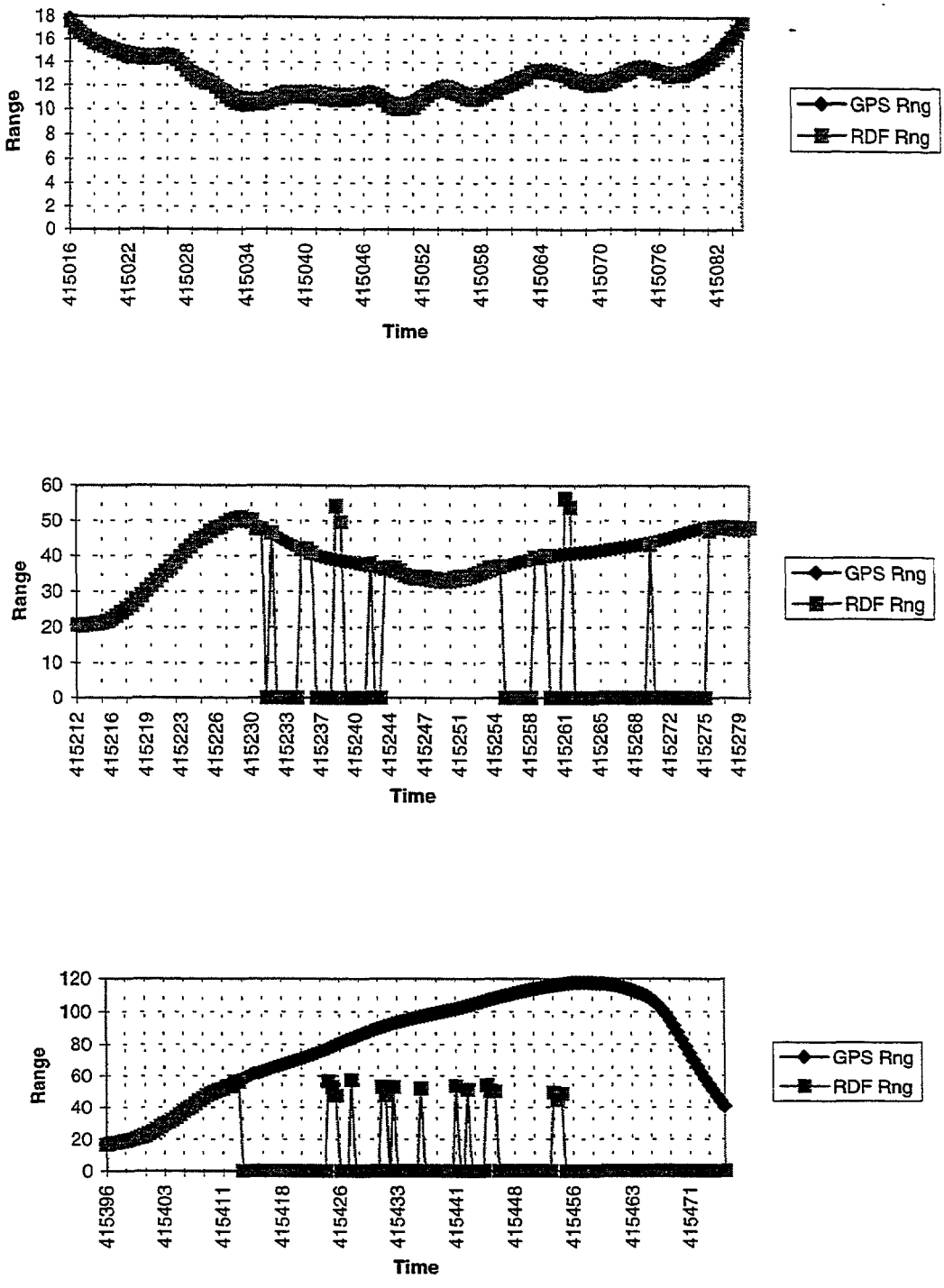

Figure F-33. GPS Truth for R30r, R31r, and R32r

As expected, the FLAR had no trouble tracking the target vehicle through the curve at a 10 meter range. Also as expected, the FLAR was unable to track the target vehicle at 70 meters once it entered the

curve. Between those two extremes is the test with the target vehicle at 40 meters. The middle plot in Figure F-33 clearly shows that when the range to the target dropped below 40 meters, the F'LAR was able to acquire and track the vehicle. However, as the target range exceeded 40 meters, the FLAR was very unreliable in providing an accurate measurement to the target vehicle.

The other interesting information contained in the plots of Figure F-33, is that the radar intermittently identifies the guard rail as a target to be tracked (indicated by the non-zero "RDF Rng" readings which do not correspond to "GPS Rng" values). It was originally expected that the radar would track the guard rail throughout the turn maneuver since the returns were consistently present. However, it is suspected that the TRW algorithms resident within the FLAR may have had difficulty identifying the centroid of the guard rail returns since they were spread over a 15 meter range.

Analysis of Relative Return Levels

The plots provided in Figure F-32 indicate the sizes of the relative return levels between the Honda Accord on the straight path, the Honda Accord around the curve, and the guard rail. Table F-4 summarizes the numerical analysis aimed at generating quantitative results on typical RCS values which can be expected in a scenario similar to the one tested here. Note again that this particular scenario used a curve with an approximately 238 meter radius.

Table F-4. RCS Numerical Analysis

Target	Empirically Estimated RCS
Accord on Straight Road	0 to 5 dBsm
Accord at 10 m Range on Curve	0 to 5 dBsm
Accord at 40 m Range on Curve	-3 dBsm and below
Accord at 70 m Range on Curve	No Returns Observed
Guard Rail on Curve	Typically 0 dBsm, 4 dF3sm peaks

The Accord on the straight roadway exhibited RCS levels consistent with those observed during other tests and measured during the RCS Characteristics task of this program. There was very little difference in the RCS of the Accord on a straight and at a 10 meter range on the curve. At the 40 meter range, the RCS of the Accord dropped significantly.

Characteristic Return from Guard Rail

The return from the guard rail was consistent throughout the curve maneuver, in that it was always present. The RCS averaged around 0 dBsm and occasionally peaked up near 4 dBsm. Comparison of these numbers shows that in terms of the magnitude, the guard rail can appear similar to a car.

The shape of the return from the guard rail (see Figure F-3 1) has significant range or depth to it. The radar returns from the guard rail are spread over approximateIy 10 to 15 meters in range. Figure F-34 shows how the incident radar energy will illuminate targets on curved roadways, such as guard rails.

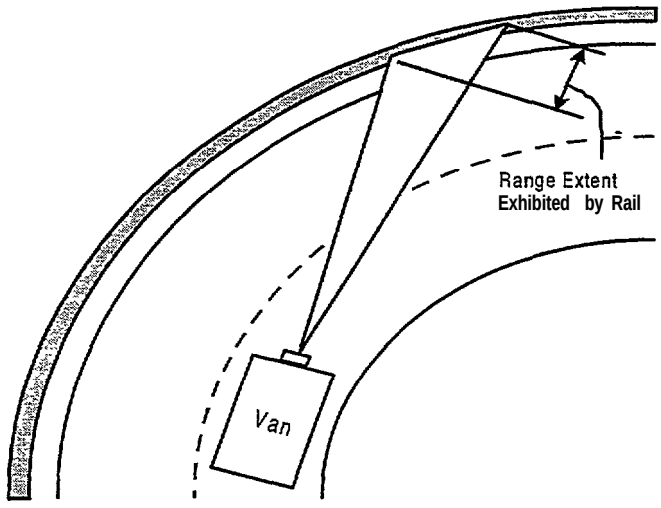

Figure F-34. illumination of **Targets on Curved Roadways**

The other interesting characteristic of the guardrail return is its "C-shaped" profile over time. The reason for this profile is discussed in detail in Section 6.10, "Vehicle Induced False Alarms-Curved Roadway.

Conclusions

The change in return levels from preceding vehicles on a straight roadway to those on a curved roadway is dependent upon the radius of the curve and the range to the vehicle. These tests showed that for a curve with an approximate 238 meter radius, vehicle ranges above 40 meters lead to a loss of track on the target (note that this is for an antenna beam with a 3 degree 3 dB width). The differences in return levels can be attributed to a combination of the target vehicle being located off of the antenna beam boresight, and the aspect angle being less than or greater than 180 degrees.

Guard rails located at the outer extent of the curved roadway were observed to exhibit RCS levels comparable to that of the vehicle tested. The vehicle tested was a Honda Accord with a 0 to 5 dBsm RCS characteristic for 180 degree aspect angle. Although returns from the guard rail were consistently observed in the radar raw data, the FLAR did not consistently track the guard rail as a target.

The results of these tests indicate the value that could be provided by lmowledge of the vehicle dynamics for a collision avoidance or ACC system. Knowing when a vehicle is in a curve, whether from yaw rate sensing or steering wheel angle, would be an important input to a system's threat assessment algorithm. The information could be useful in identifying certain returns as those from roadside objects, such as guard rails. The information could also be used to adjust the radar's field of view in the direction of the curve to aid in maintaining track on the preceding vehicle.

F.12 VEHICLE CLUTTER IN AZIMUTH-CURVED ROADWAY

Purpose

The purpose of this test was to determine the FLAR's ability to maintain track on a target vehicle through a standard freeway curve with other vehicles present in adjacent lanes. The test was performed under good driving conditions.

Issues considered in these tests included the loss of returns from the target vehicle, the FLAR's ability to discriminate between in-lane and out-of-lane target vehicles, and the returns induced by the vehicles in the adjacent lanes.

Procedure

For these tests, four different vehicles were used on a circular track with an approximate 500 foot radius. The primary vehicle (P) and target vehicle (Sl) were driven in the center lane of the circle. The two other vehicles were clutter vehicles (S2 and S3) driven in the inner and outer lanes of the circle. The two out-of-lane clutter vehicles were selected to have radar cross-sections similar that of the in-lane target vehicle. Actually, all three secondary vehicles were Honda Accords.

The test began with the Primary vehicle maintaining a constant distance from the m-lane target vehicle; the out-of-lane clutter vehicles were adjacent to the Primary vehicle and traveling at the same speed. The out-of-lane clutter vehicles accelerated until they were adjacent to the in-lane Secondary vehicle. They maintained this position for several seconds and then decelerated until they were again adjacent to the Primary vehicle.

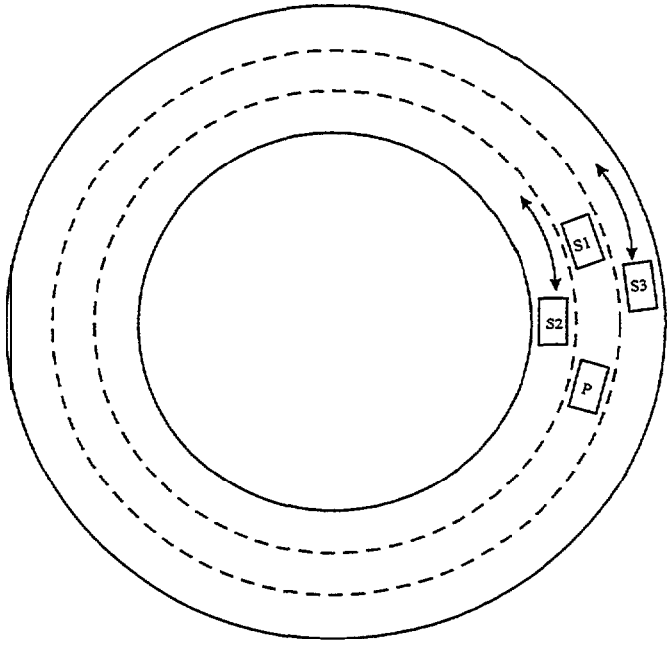

Figure F-35. Vehicle Clutter on Curved Roadway Scenario

These types of maneuvers were repeated several times during the course of a test run. Sometimes the clutter vehicles maneuvered together, and some times individually. The distance between the primary and target vehicles was varied during each test runs. Also, the FLAR's active beam (left, center, or right) was varied on separate runs.

Results

To illustrate and discuss the results of this series of tests, data from one of the test runs in which the FLAR's center beam was active will be used. Observations from test runs in which the left and right beam were active will also be discussed.

The series of plots shown in Figure F-36 are all from the same data set. Each plot consists of a different time interval of the test, which lasted for almost 5 minutes. The time sequence begins with the bottom plot in Figure F-36, proceeds up to the middle plot and then is completed with the top plot.

The returns which are visible in the data plots are annotated to indicate the vehicle which induced them. Accord 1 is the actual target vehicle located in the same lane as the host vehicle. Accord 2 was driving on the inside lane and Accord 3 was driving on the outside lane. The radius of curvature was approximately 500 feet in the middle lane.

To analyze these tests, extensive use was made of the ERIM Analysis Software which includes a video playback of the test which is synchronized to the radar data. Without the video playback, it is difficult to convey the exact vehicle maneuvers being conducted throughout the test. In an effort to convey the vehicle positions during the test to the reader, the line labeled "GPS Rng" in Figure F-37 indicates the range from the radar to the target vehicle throughout the test. The pulse number on the x-axis of Figure F-37 corresponds to the pulse number on the y-axis of the radar return plots in Figure F-36. Also, Table F-5 provides a sequence of events for the target and two clutter vehicles referenced to radar pulse number.

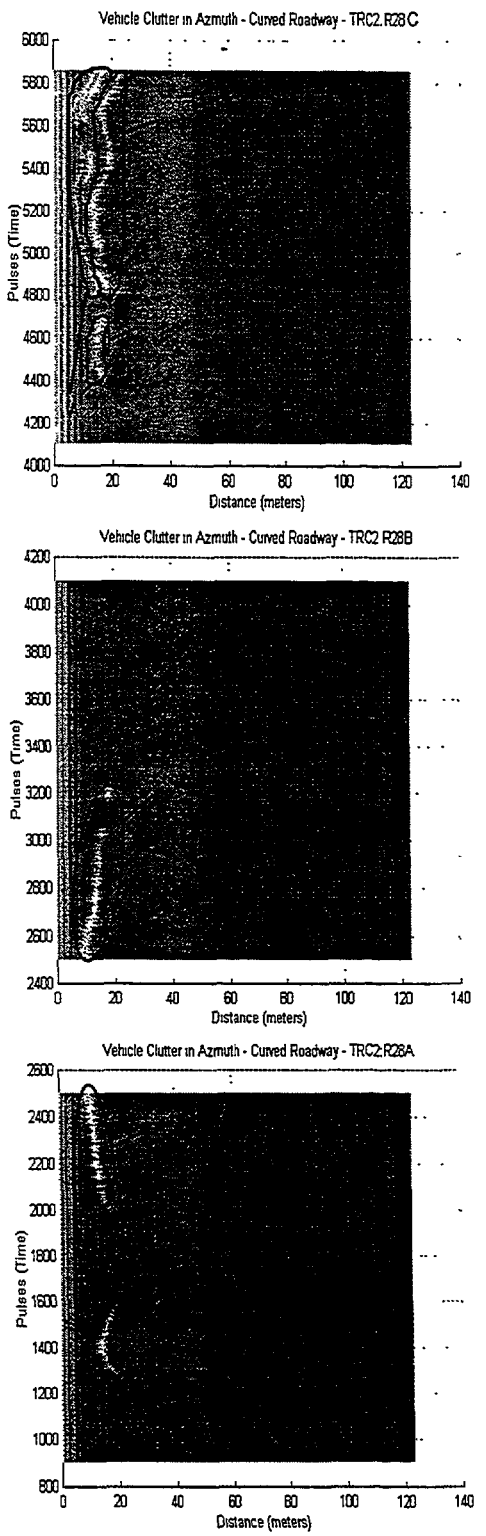

Figure F-36. Radar Data Curved —Roadway

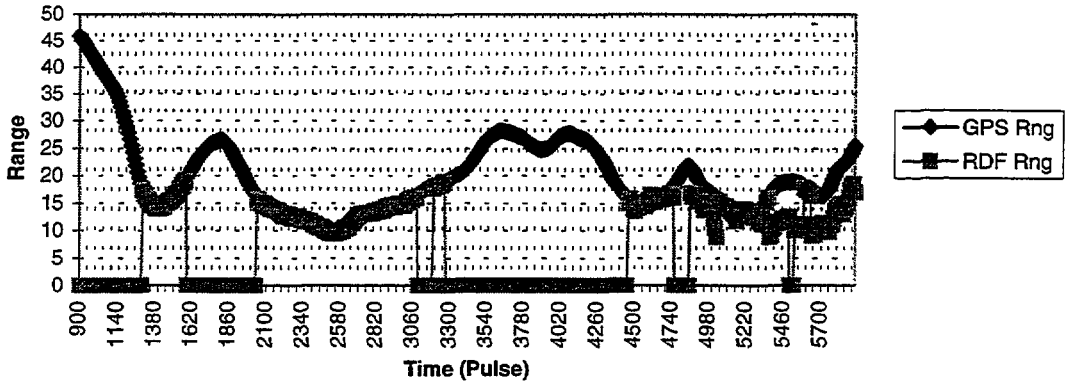

Figure F-37. GPS Truth for R28

Table F-5. Curved Roadway Test Analysis Summary

Pulse #	Vehicle Activity	Radar Response
900-2600	Accord 1 is only vehicle in scene	Radar ability to track Accord 1 position dependent upon range
2500-2700	Accords 2/3 enter scene and accelerate to positions adjacent to Accord 1	Accords 2/3 appeared to have no effect on raw radar data and ability of FLAR to track Accord 1
2700-3000	Accords 2/3 maintain positions adjacent to Accord 1	same as above
3000-3100	Accords 2/3 split-off and drop out of scene	same as above
3000-4200	Accord 1 is only vehicle in scene	Radar ability to track Accord 1 position dependent upon range
4200-4400	Accord 3 enters scene and accelerates to position in outside lane and 1 car length behind Accord 1	Accord 3 position has effect on raw radar returns. As Accord 1 and Accord 3 maneuver, returns from both vehicles are observed.
4400-end	Accord 3 maintains position in outside lane, 1 car length behind Accord 1	same as above

Correlation between the information in Figure F-36, Figure F-37, and Table F-5 is necessary to establish the cause and effect of vehicle maneuvers on the radar sensor. The third column in Table F-5 summarizes the radar response to the various events conducted during the test.

As observed in other tests conducted on curved roadways, the radar returns from preceding vehicles are dependent upon the radius of curvature in the roadway and the target vehicle's range from the radar. These two variables dictate whether or not the target vehicle position is located within the FLAR's field of view. Considering pulses 900 to 2600, where the only vehicle in the scene was Accord 1, Figure F-36 indicates that the vehicle both entered and withdrew from the FLAR's FOV. This information can be correlated with the GPS truthing information included in Figure F-37. The line labeled "GPS Rng" is the

actual range to Accord 1, and the line labeled "RDF Rng" is the FLAR's reported range to target vehicle output. It is clear that the FLAR's ability to track the target vehicle coincided with time intervals when the raw radar data indicates the vehicle was within the FOV.

The time period during which the returns from the target vehicle were not evident in the raw radar data correspond to intervals in which the target vehicle range exceeded more than 15 to 20 meters. Table F-6 shows at what angle from the antenna boresight a vehicle would be located on a 500 foot radius curve given a particular range to that vehicle. These numbers are in agreement with the configuration of the FLAR and the empirical observations made during this test.

Table F-6. Vehicle Location Versus Range to Vehicle

Range to Target Vehicle	Vehicle Location Off Antenna Boresight
10 meters	1.9 degrees
15 meters	2.8 degrees
20 meters	3.8 degrees

A plot of the FLAR's center beam pattern is provided in Figure F-38. A line has been drawn to indicate where in the beam pattern a target would fall if it was located four degrees off the antenna boresight.

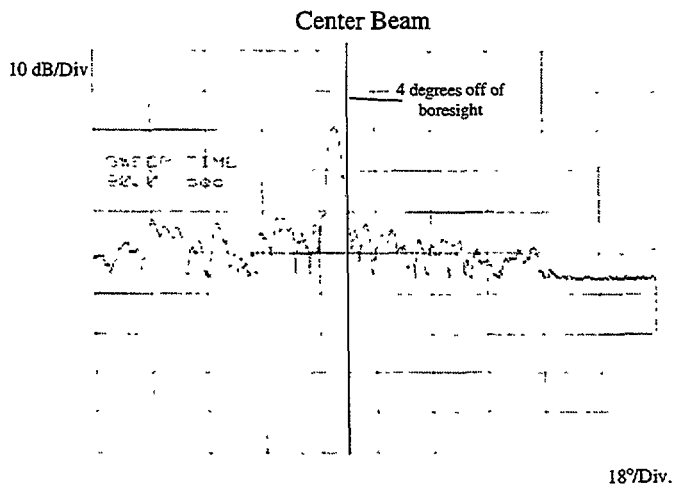

Figure F-38. Center Beam Patterns

It is obvious that the antenna gain in this region is extremely low. This explains why the returns from Accord 1 are not visible in the raw radar data when its range exceeds 15 to 20 meters on a 500 foot radius curve.

This also helps to explain why Accords 2 and 3 did not induce any returns in the radar during pulses 2500 to 3000. The data in Figure F-37 shows that the range to Accord 1 during that period was under 20 meters. Therefore, Accord 1's position prevented the radar beam from being reflected off any other objects, as pictured in Figure F-39. Here the radar beam is incident on Accord 1, but not on any other objects in the scene. This is verified by the raw radar plots in Figure F-36.

The observations and results made during pulses 3000 to 4200 are similar to those made during pulses 900 to 2600 described above.

From pulse 4200 to the end of the test run (pulse 5850), things start to get interesting. Here, the relative positioning of Accords 1 and 3 begins to have an effect on the raw radar returns and the ability of the FLAR to accurately track the target vehicle within its own lane.

The same dependency of the FLAR's ability to detect targets on radius of curvature and range to target still holds true. Figure F-38 shows that targets are still detected by the FLAR only when their range drops below 20 meters or so. The truthing information for pulses 4300 and up from Figure F-38 is reproduced in Figure F-40 for greater clarity.

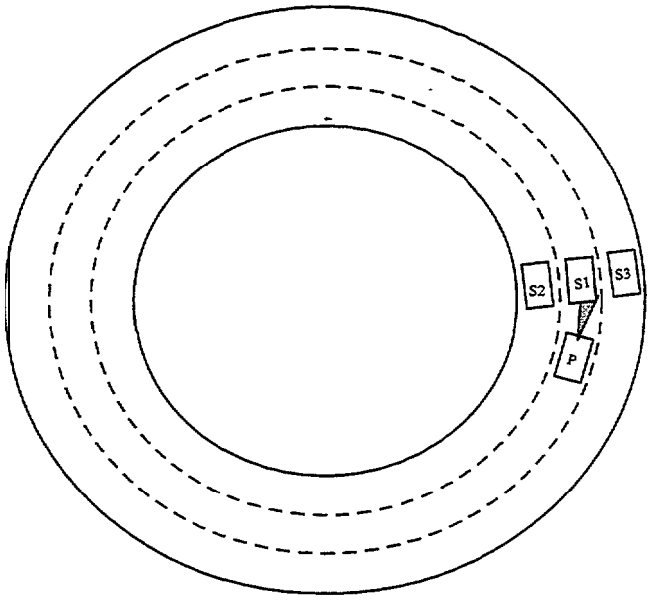

Figure F-39. Short Range Illumination

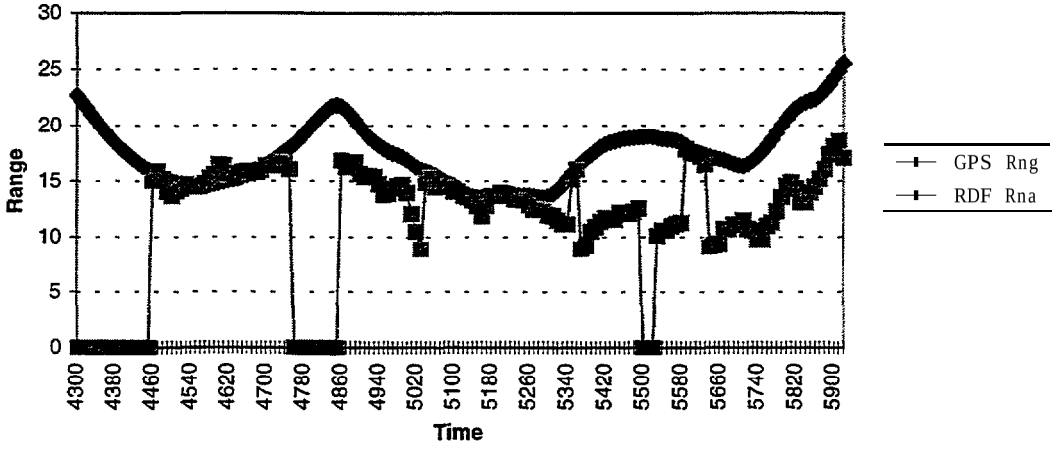

Figure F-40. GPS Truth for R28

The data in Figure F-40 shows that the FLAR (and the TRW-proprietary processing algorithm) detected an object inside the actual range of Accord 1. Comparison of this data in Figure F-40 with the raw radar data plots provided in Figure F-36 verifies that the FLAR is indeed tracking Accord 3. Figure F-41 shows a diagram of the situation.

Referring back to the top plot in Figure F-36, returns from both vehicles can be frequently observed. Due to the orientation of the vehicles, the returns from Accord 3 appear at a nearer range. Therefore, the FLAR treats this return as the **target to** be tracked. The FLAR has no knowledge of which lane Accord 3 is actually in.

Also referring to the raw radar plots in Figure F-36, it appears that returns are coming from different scattering centers located on Accord 3, perhaps the rear and front wheel wells.

The return levels observed from the Honda Accords during this test were typical of other tests with these vehicles. In general, the Accords exhibited a -2 to +5 dBsm radar cross section. This is slightly lower than tests conducted with the Accords on a straight roadway. The explanation for the difference lies in the orientation between the radar and the targets. On curved roadway less return is expected, since the relatively flat sides of the vehicle tend to reflect energy away from the radar.

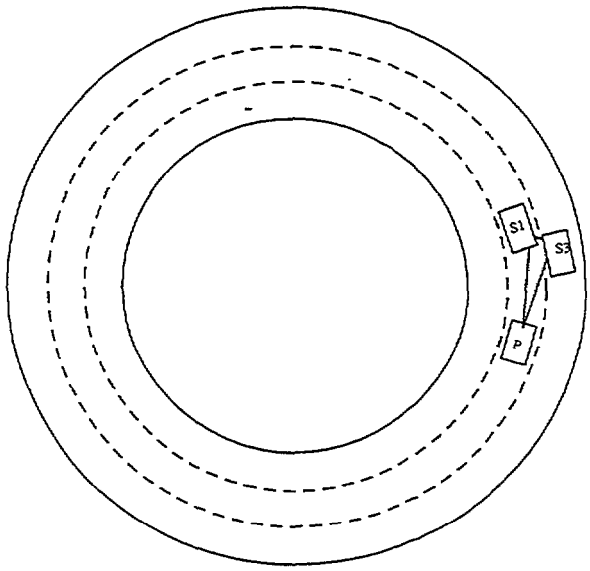

Figure F-41. Medium Range Illumination

The other collections made using this test scenario, but with the left or right beams activated, produced similar results in terms of the field-of-view limitations. It was found that collections with the left beam active allowed the FLAR to track the target vehicle out to a range of 40 meters versus the 20 meter limitation with the center beam. Also, neither Accord 2 or 3 was detected during the "left beam" tests.

On the other hand, "right beam" tests reduced the FLAR's ability to track the in-lane target vehicle down to around 10 meters. However Accord 3, located in the outside lane, could be tracked out to 35 meters or so. These "side beam" tests show how adjusting the FLAR's field of view will affect its performance, especially in curved roadway scenarios.

Conclusions

The empirical data in these tests showed that the ability of the FLAR to accurately track preceding vehicles in a curve depends on the curvature of the roadway and the range to the target vehicles. The diagrams provided the in the "Results" section of this document illustrate this dependency.

The FLAR center beam with its 3 degree 3dB azimuth width limited the detection range to the in-lane target vehicle to around 20 meters in a 500 foot radius curve. Given that 20 meters is not a very great distance, this limitation needs to be addressed by either steering the beam during a curve maneuver or increasing the radar's field of view by scanning the antenna across the scene. The tests conducted with the side beams indicates the gains that can be made in terms of increasing the detection ranges.

The results of these tests, combined with those from curved road tests with a guard rail present, indicate that it will be extremely difficult for an automotive radar to accurately assess the environmental dangers during a curve maneuver without other inputs into the system. Inputs such as yaw rate, steering wheel angIe, and any information regarding the azimuth positioning of objects in the scene would greatly enhance the robustness of the threat assessment algorithm. Yaw rate and steering wheel angle information could be easily gathered from sensors installed on the car. As for azimuthal positioning of objects, two options exist. The first is to create an even narrower **antenna** beam and scan it across the

scene. The other is to perform a data fusion function from a separate sensor such as an IR or optical camera to identify object positioning within the scene.

Obviously, adding another sensor beyond the radar for collision avoidance or ACC applications would make the system cost prohibitive. However, as night driving enhancement systems and lane sensing systems evolve, the possibility of sharing information among sensors becomes viable.

TEST TRACK DATA PLOTS

The following pages are selected raw data plots generated from the Test Track collections. The plots are presented by the test scenario being addressed as described in the test plan provided in Appendix E. Each plot is labeled with the appropriate test identification and annotation on the plots is provided where appropriate. The reader is referred to the test plan and test results descriptions in Appendices E and F, respectively.

These plots are provided to assist developers in quantitatively assessing the radar response to the scenarios tested. Of course these results are specific to the TRW FLAR sensor configuration (e.g., antenna gain and beam shape). The reader is referred to Section 4 of the final report which discusses the FLAR sensor characteristics in order to extrapolate the results to other configurations.

6.1 Vehicle Induced False Alarm - Vehicle At Roadside

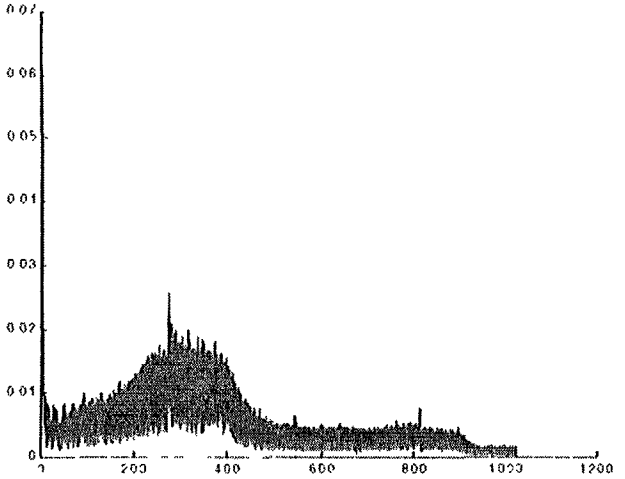

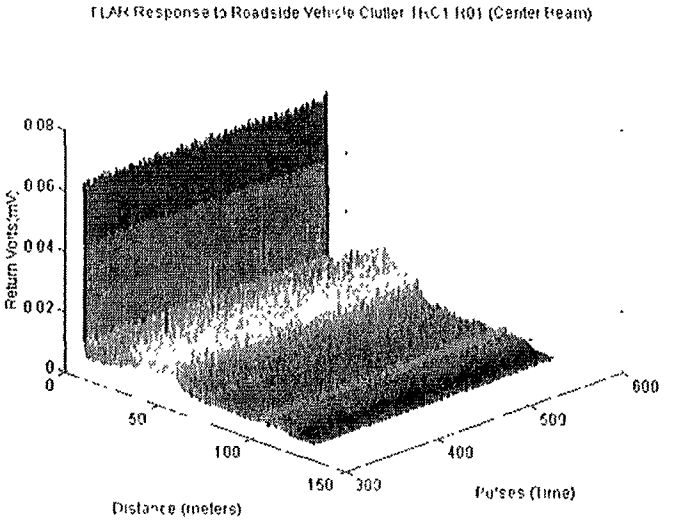

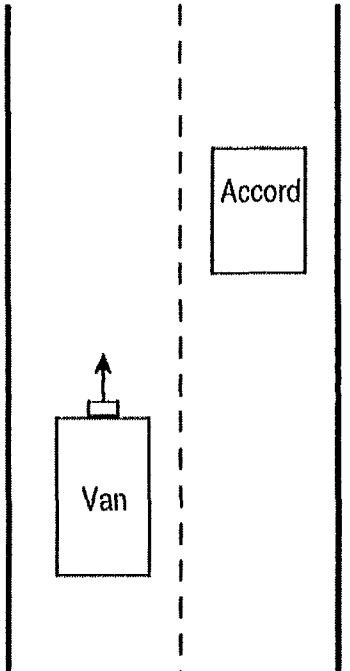

Center Beam
Honda Accord
parked in adjacent lane

6.1 Vehicle Induced False Alarm - Vehicle At Roadside

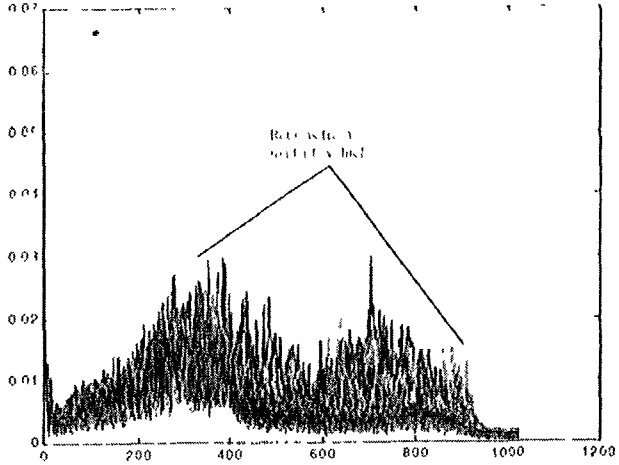

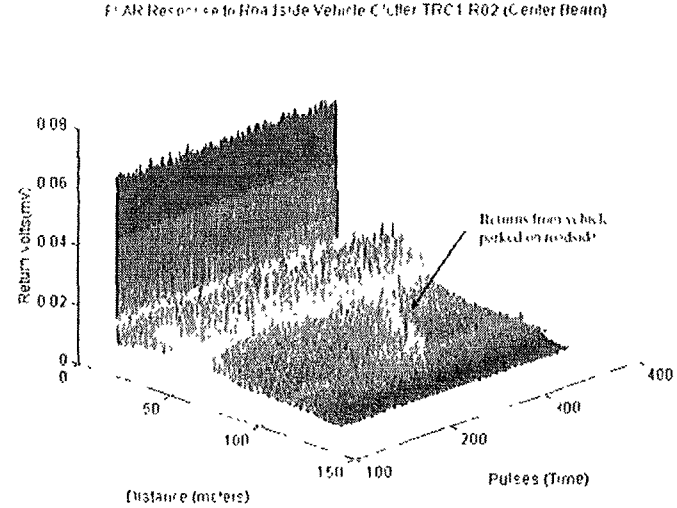

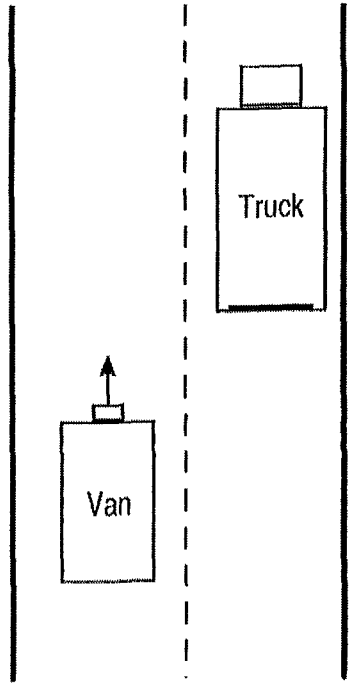

Center Beam
Semi-Tractor/Trailer
parked in adjacent lane

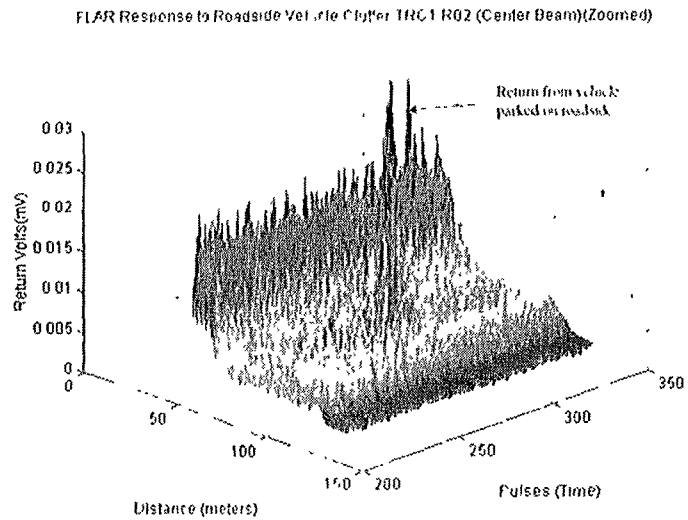

6.1 Vehicle Induced False Alarm - Vehicle At Roadside

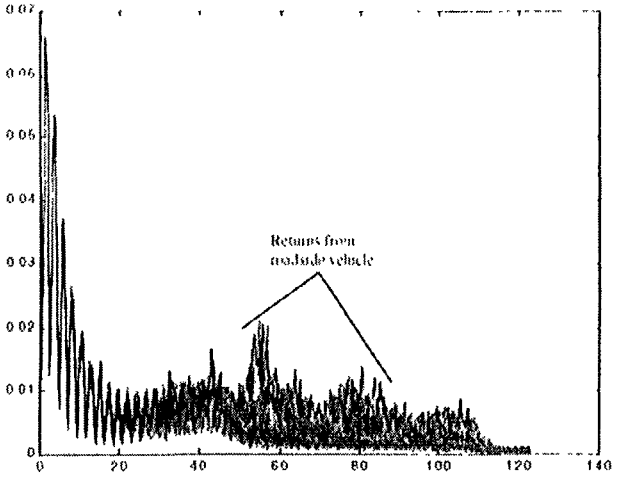

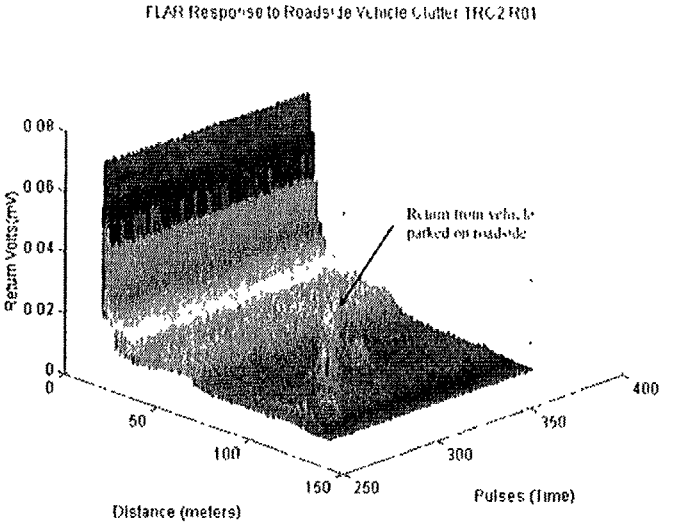

Center Beam
Semi-Tractor/Trailer
parked in adjacent lane

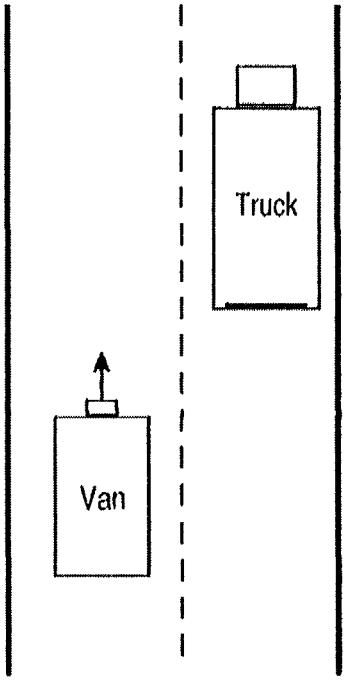

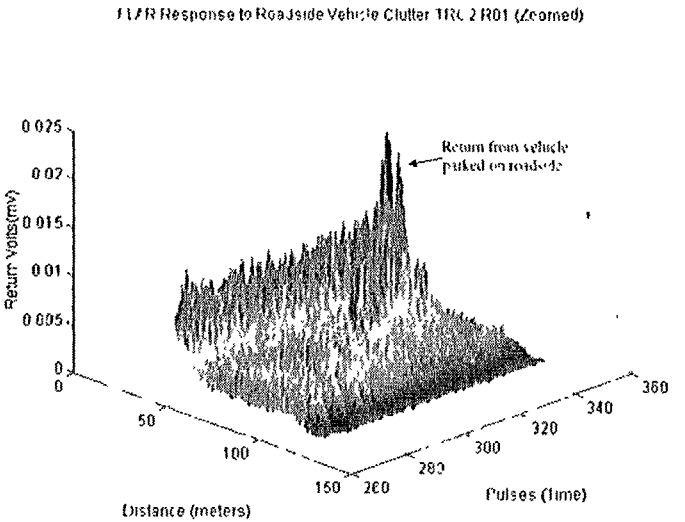

6.1 Vehicle Induced False Alarm - Vehicle At Roadside

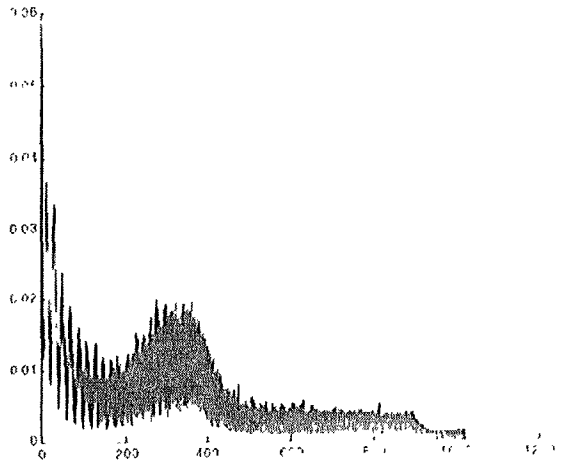

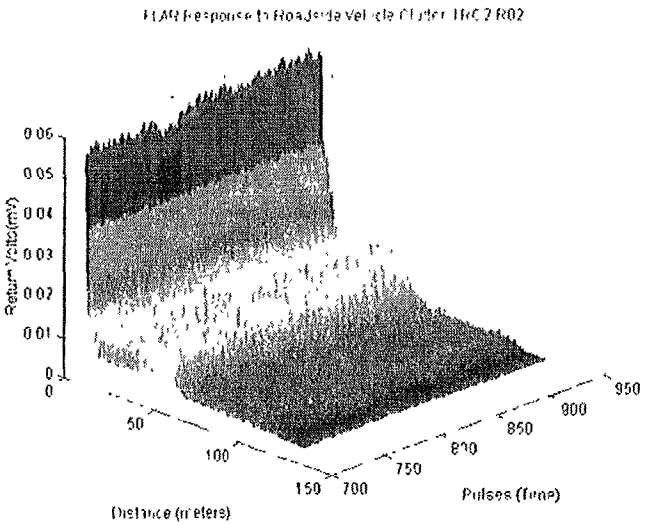

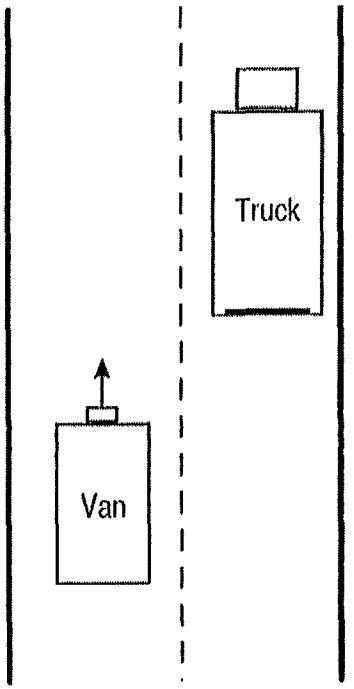

Right Beam
Semi-Tractor/Trailer
parked in adjacent lane

6.1 Vehicle Induced False Alarm - Vehicle At Roadside

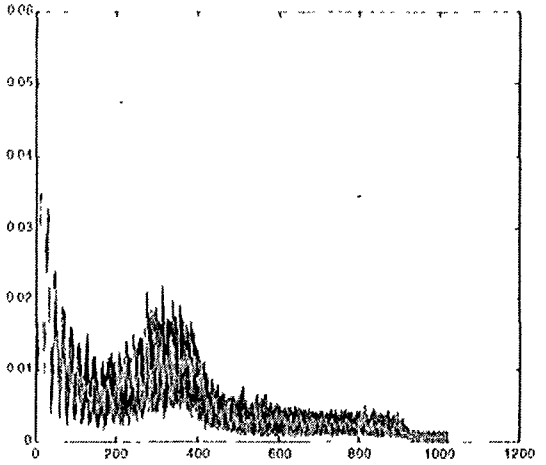

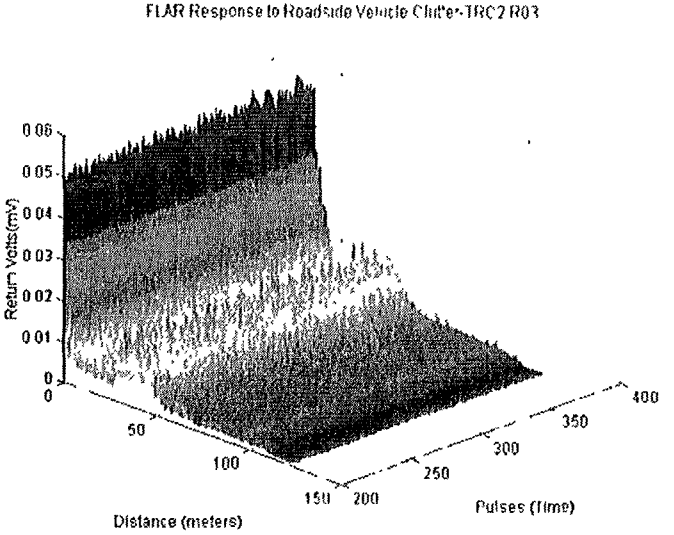

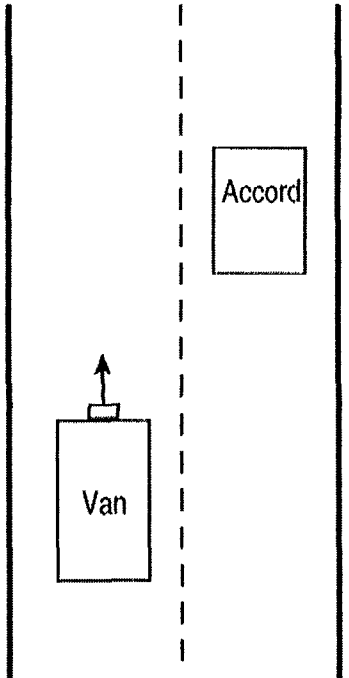

Center Beam
Honda Accord
parked in adjacent lane

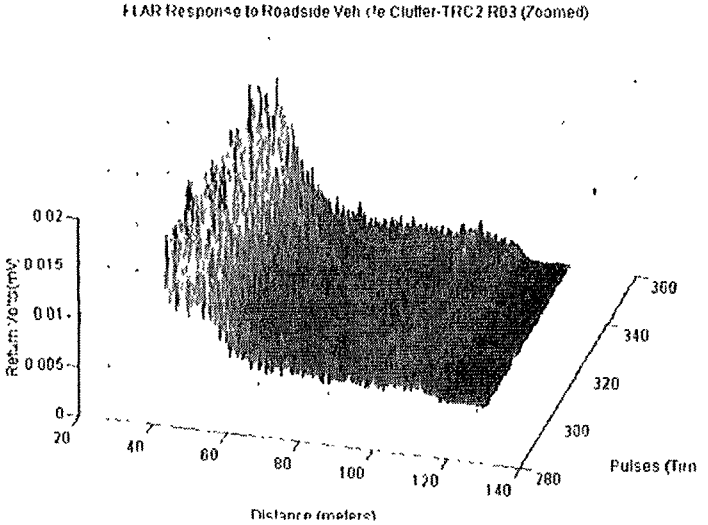

6.1 Vehicle Induced False Alarm - Vehicle At Roadside

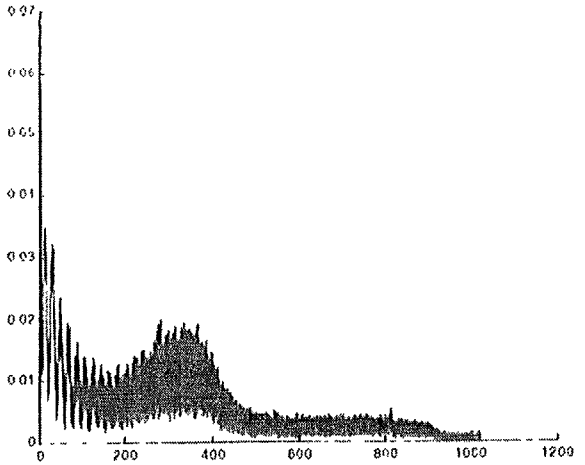

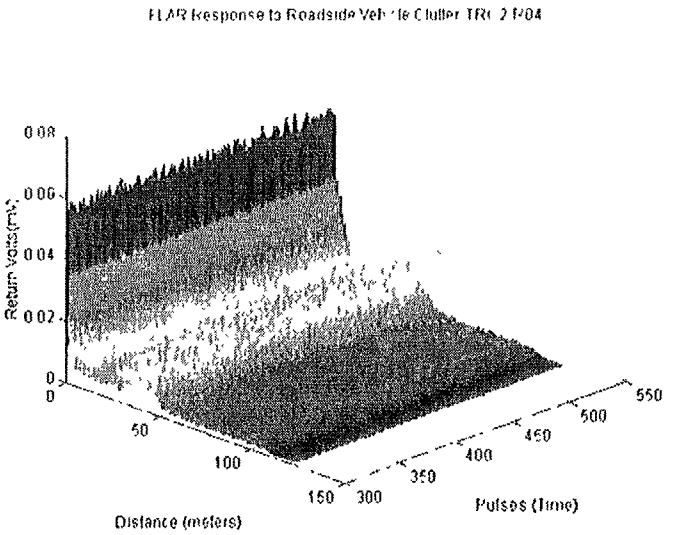

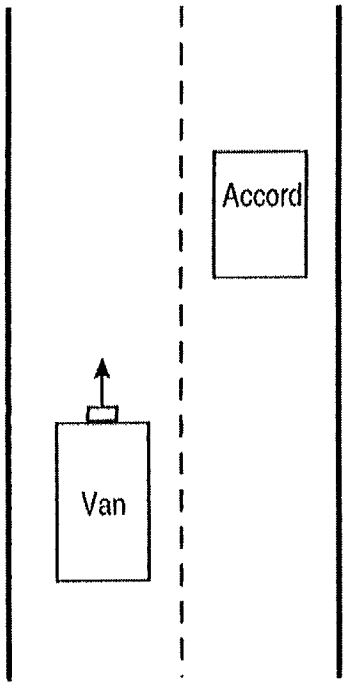

Right Beam
Honda Accord
parked in adjacent lane

Object Orientation Roadside Clutter Analysis

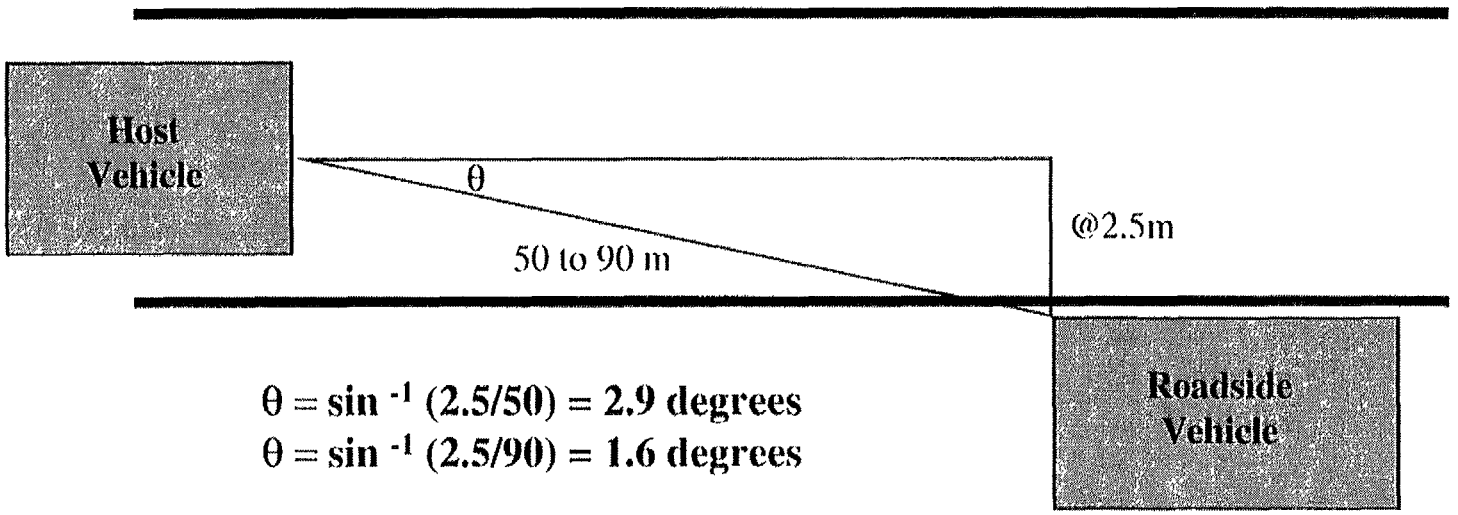

$\theta = \sin^{-1}(2.5/50) = 2.9$ degrees

$\theta = \sin^{-1}(2.5/90) = 1.6$ degrees

6.1b Vehicle Induced False Alarm - Vehicle in Adjacent Lane

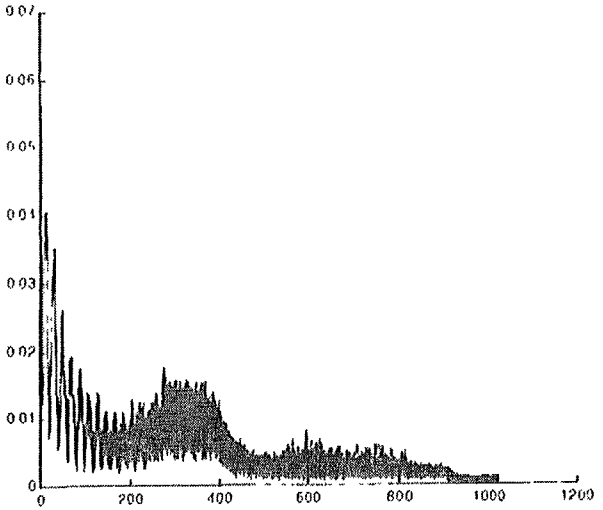

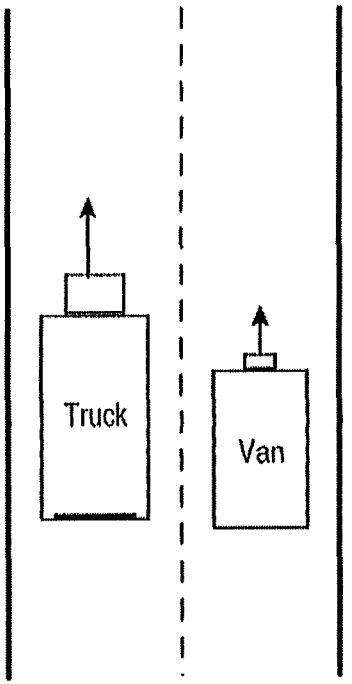

Center Beam
Semi Tractor/Trailer
passing in adjacent lane

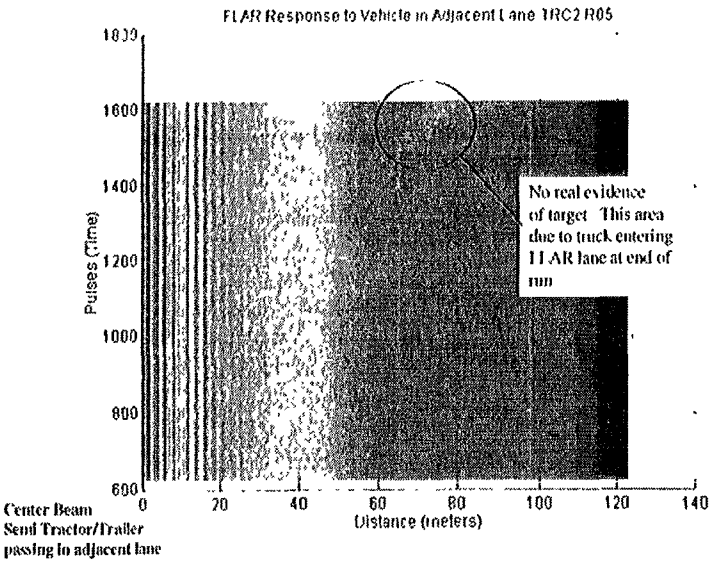

6.1b Vehicle Induced False Alarm - Vehicle in Adjacent Lane

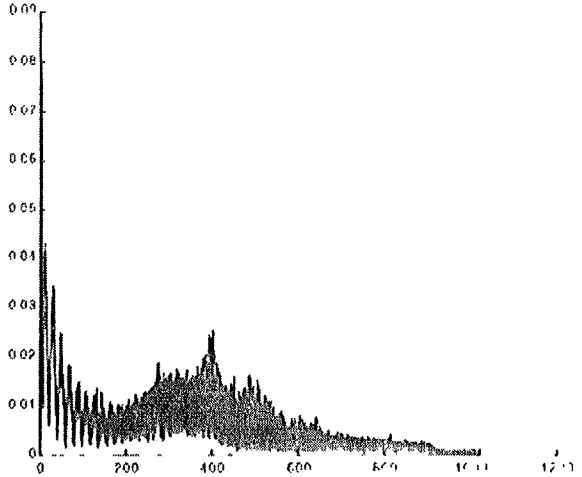

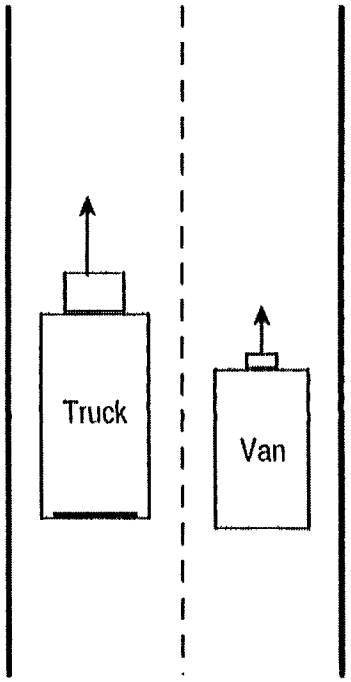

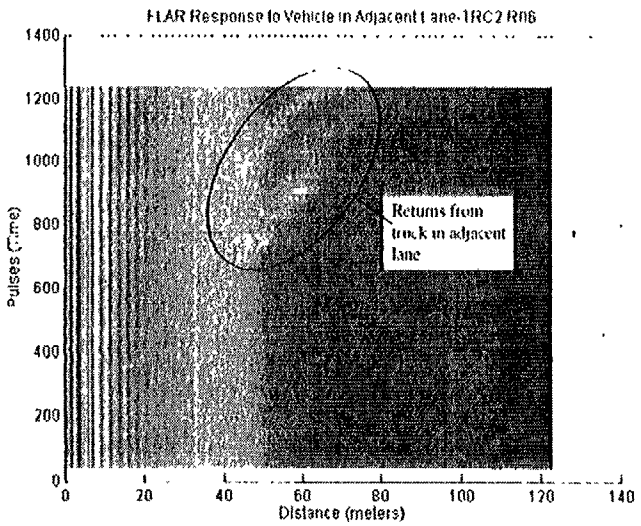

Left Beam
Semi Tractor/Trailer
passing in adjacent lane

6.1b Vehicle Induced False Alarm - Vehicle in Adjacent Lane

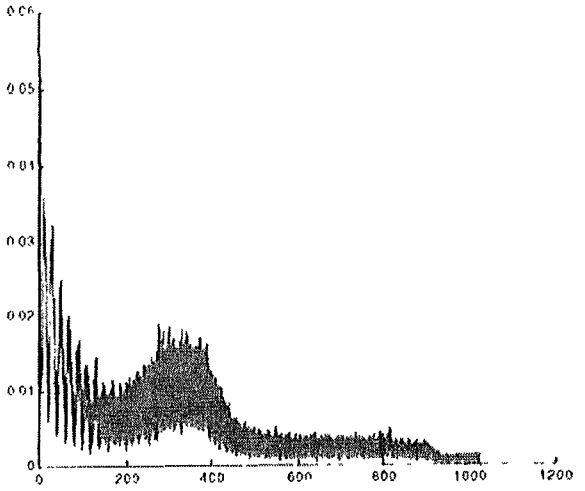

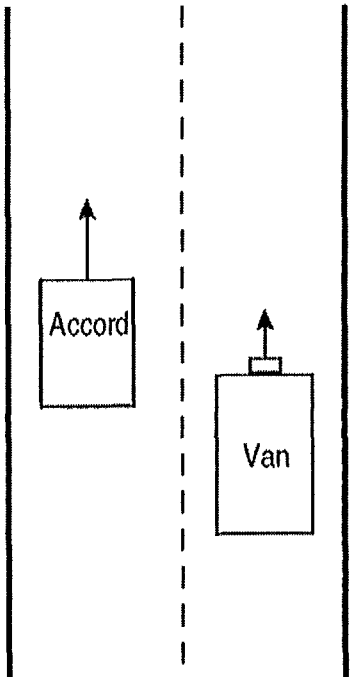

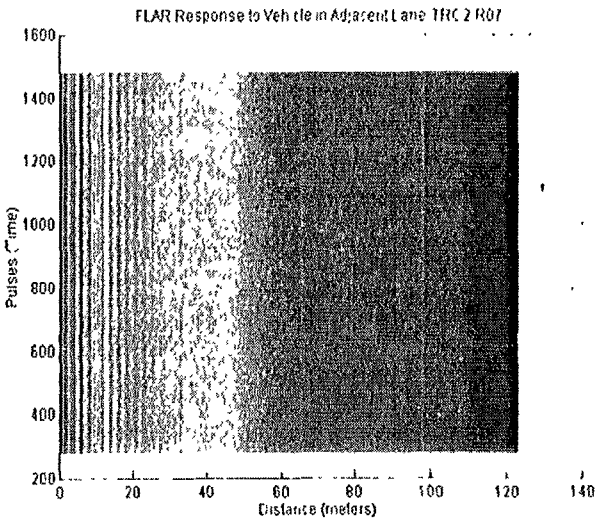

Center Beam
Accord
passing in adjacent lane

6.1b Vehicle Induced False Alarm - Vehicle in Adjacent Lane

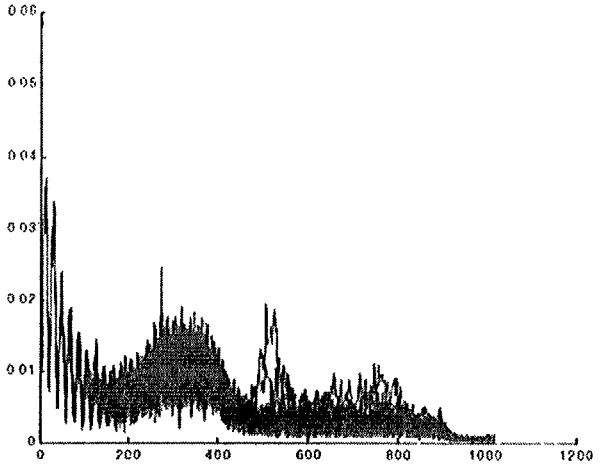

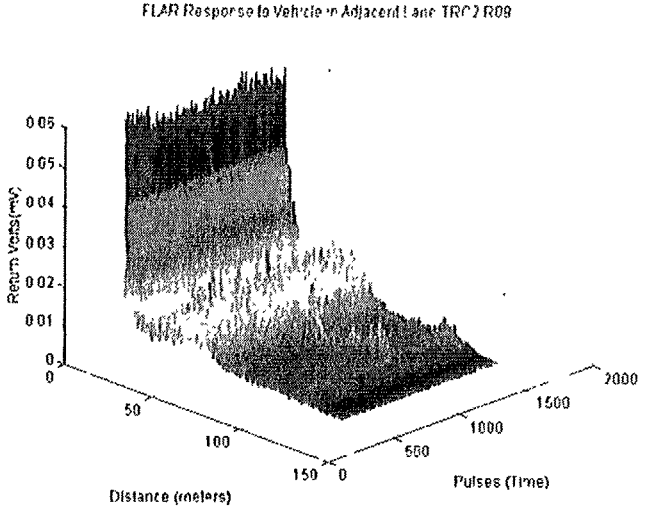

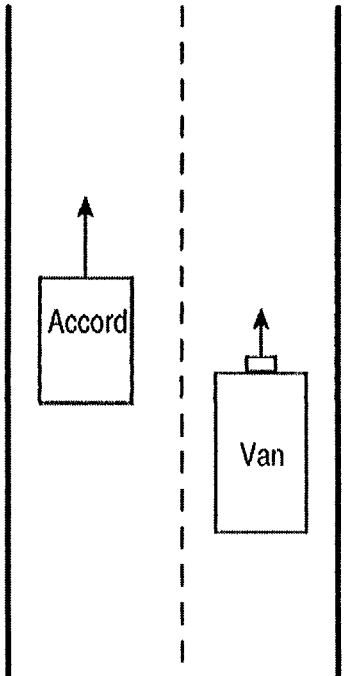

Left Beam
Accord
passing in adjacent lane

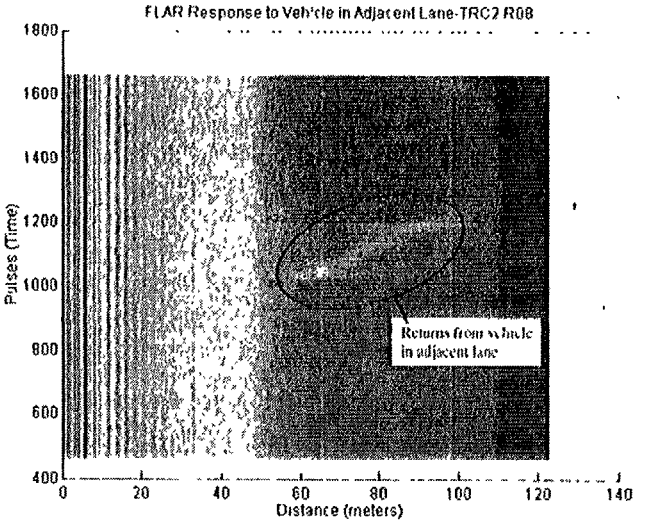

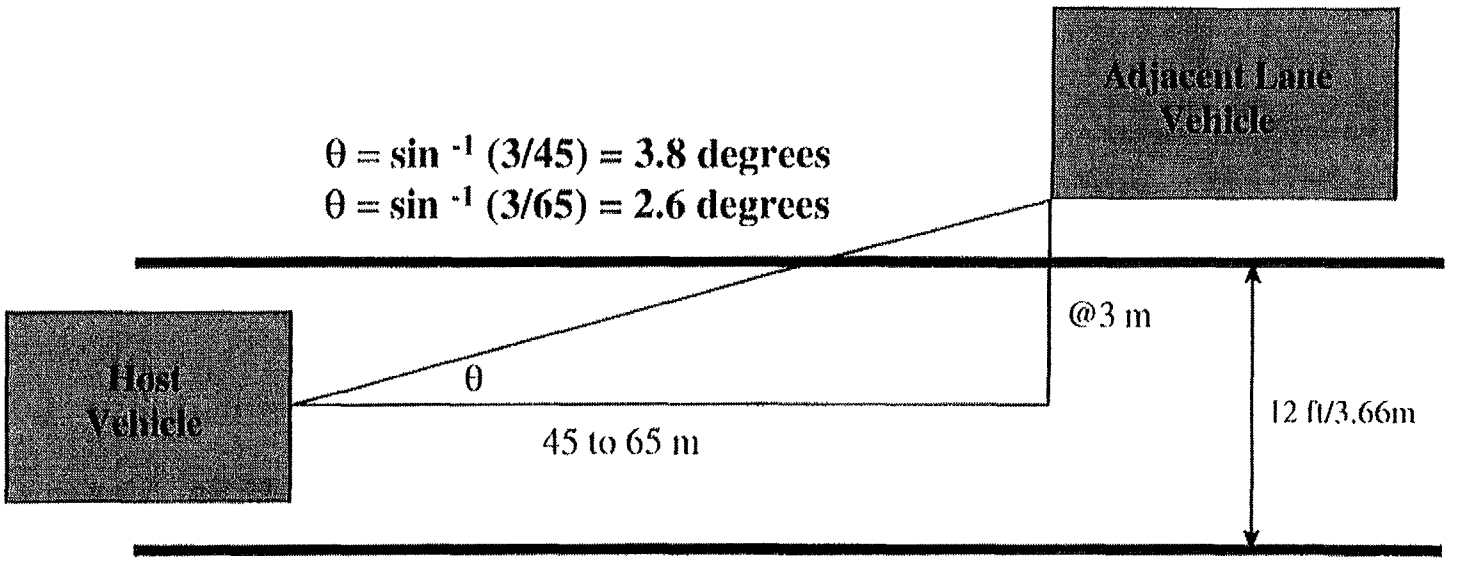

Object Orientation Adjacent Lane Clutter Analysis

6.2 Braking Secondary Vehicle - Straight Roadway

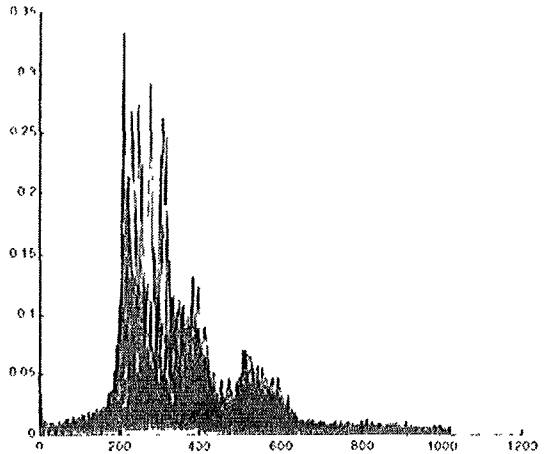

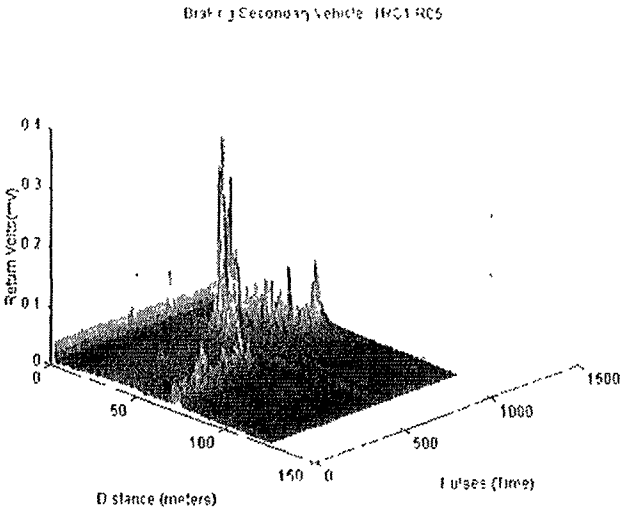

Center Beam
Braking Lead Vehicle
(Accord)
Straight Roadway

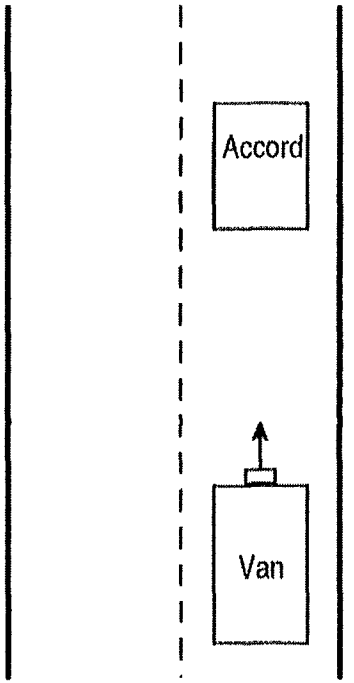

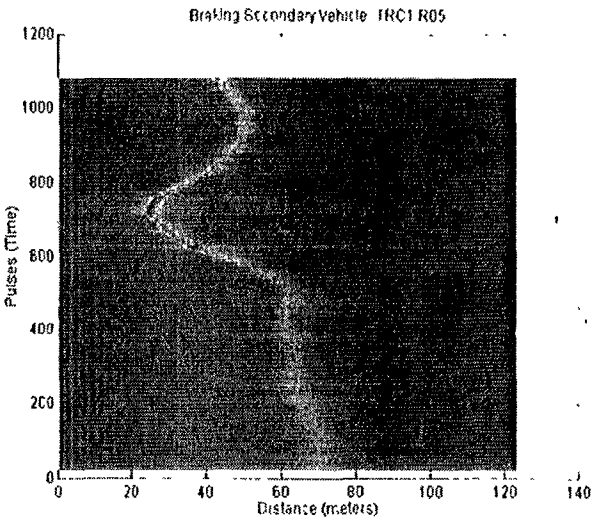

6.2 Braking Secondary Vehicle - Straight Roadway

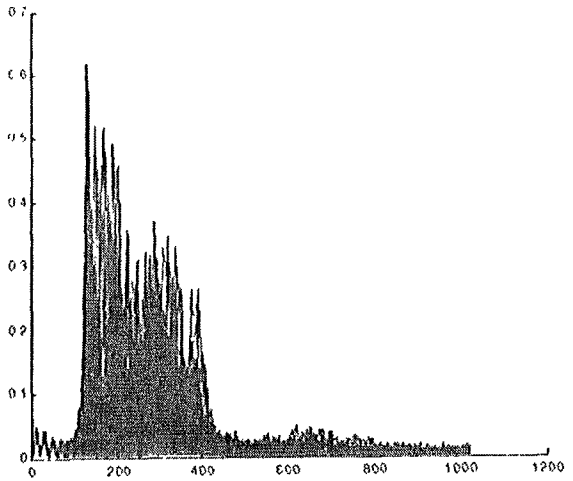

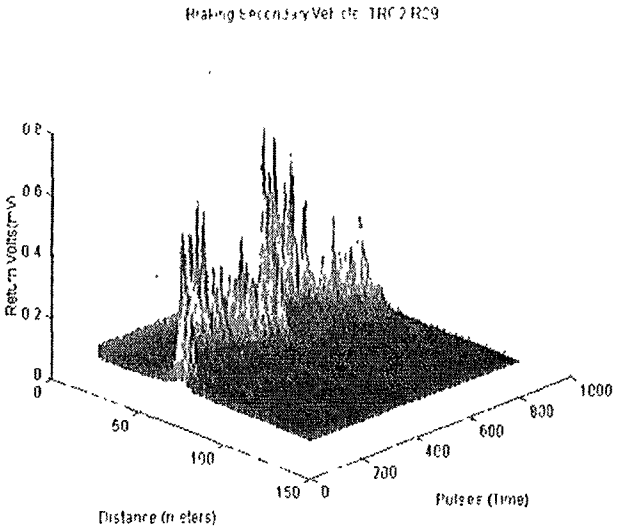

Center Beam
Braking Lead Vehicle
(Accord)
Straight Roadway

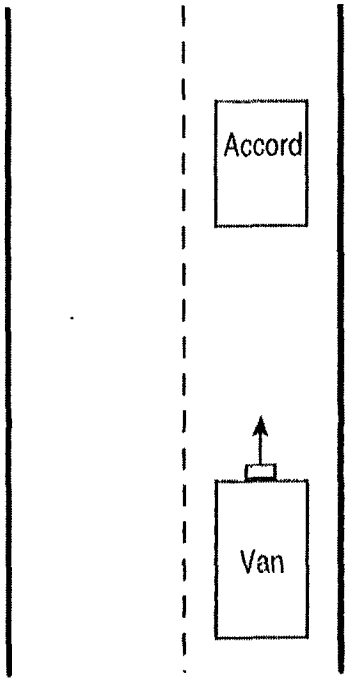

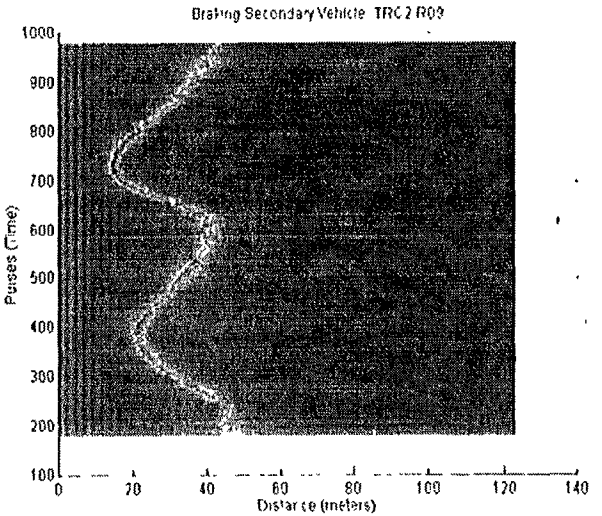

6.3 Out-of-Lane Vehicle Clutter - Straight Roadway

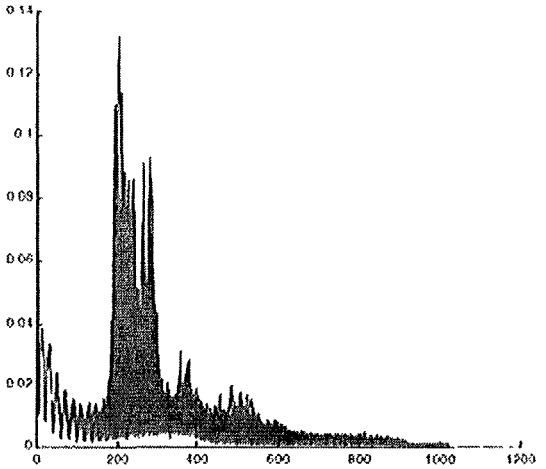

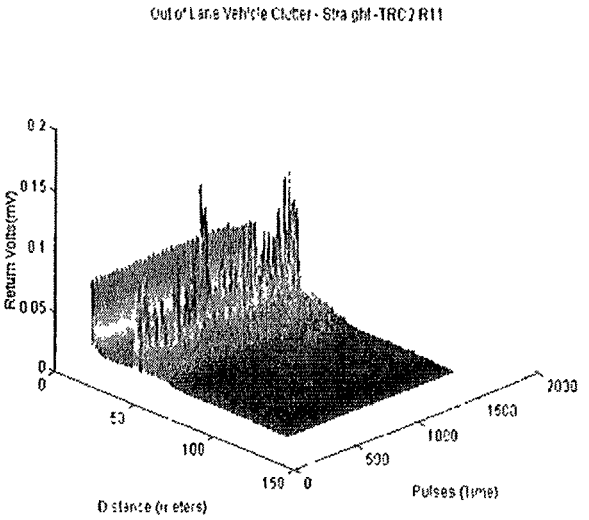

Left Beam
Accord Passed on Left
by Truck/Trailer
17:37:28 to 17:38:36

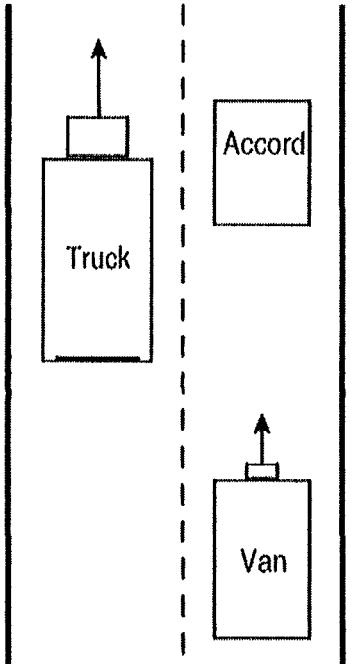

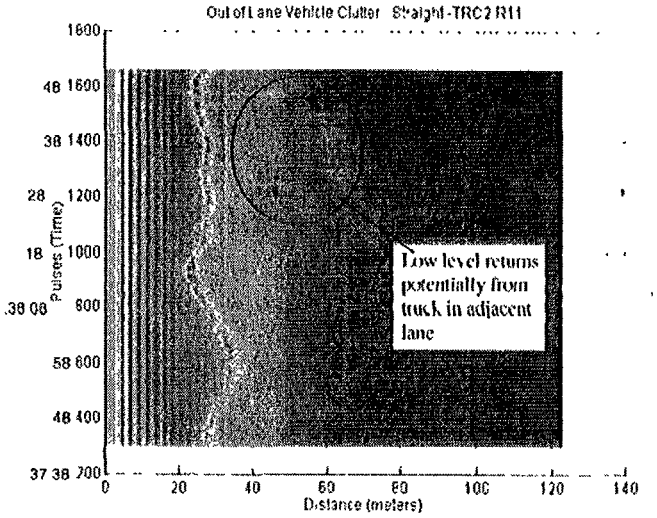

6.3 Out-of-Lane Vehicle Clutter - Straight Roadway

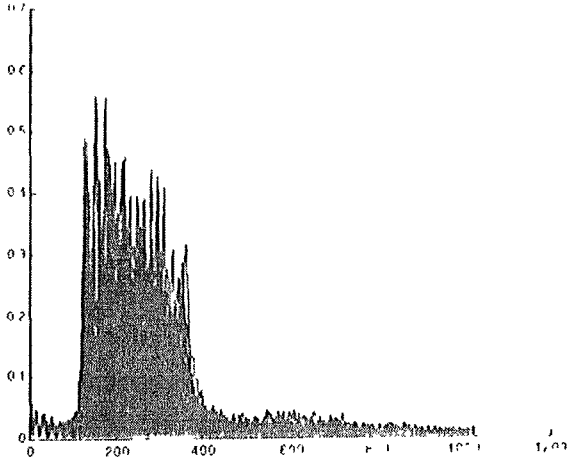

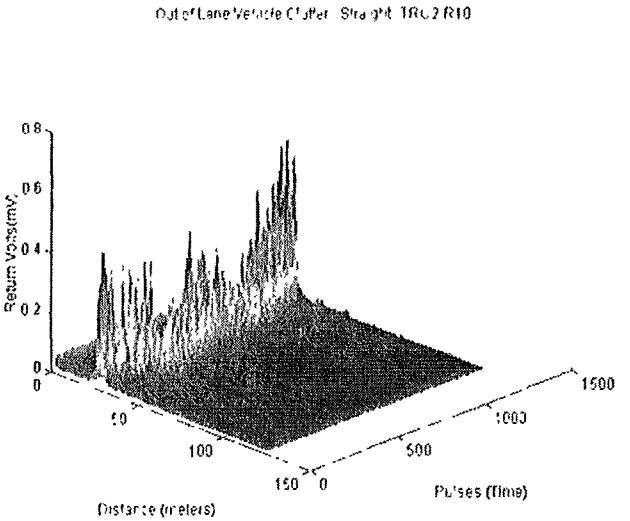

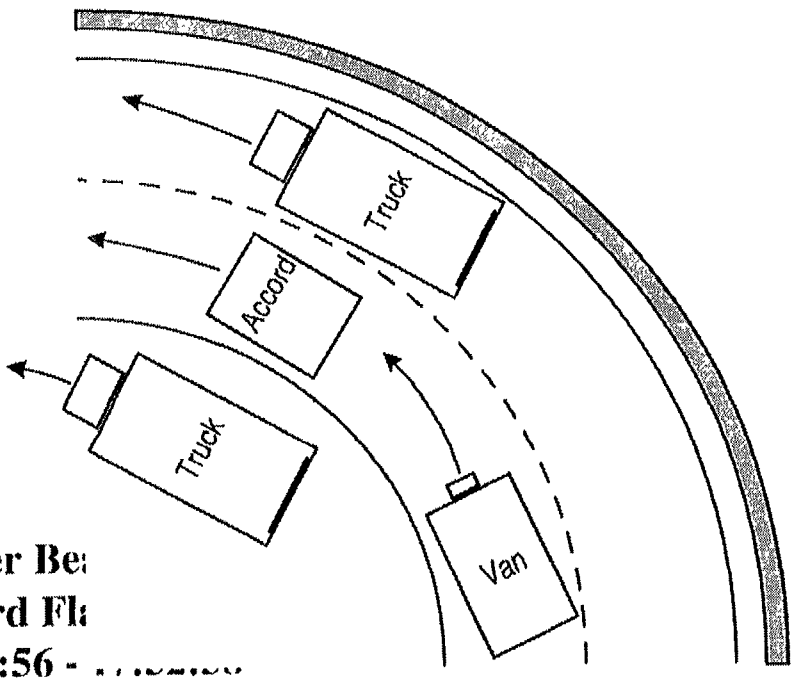

Center Be:
Accord Fl:
17:51:56 -

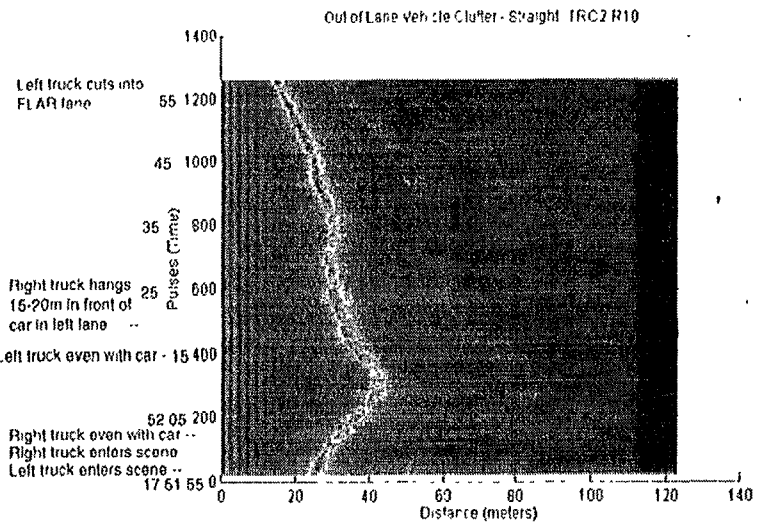

6.3 Out-of-Lane Vehicle Clutter - Straight Roadway

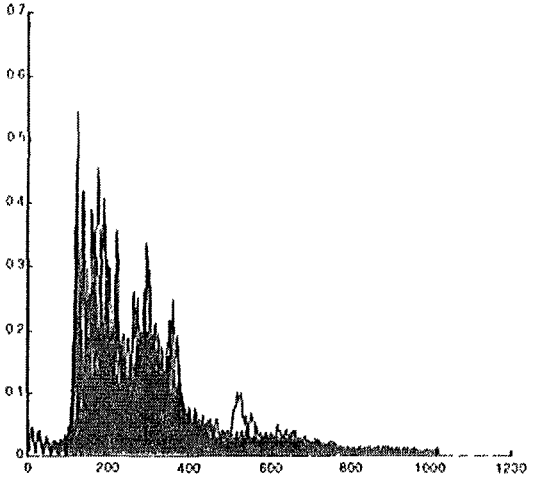

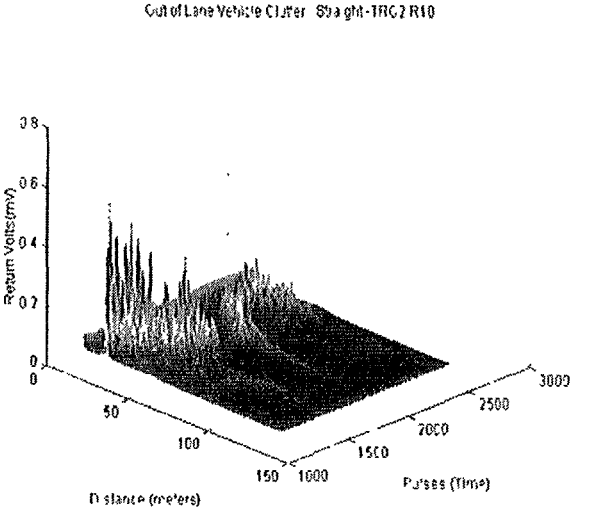

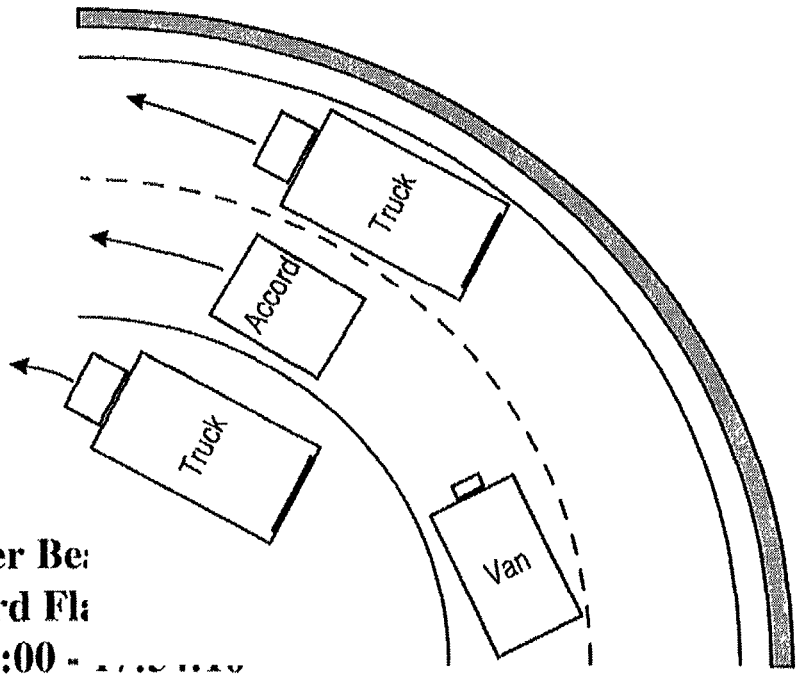

Center Be:
Accord Fl:
17:53:00 -

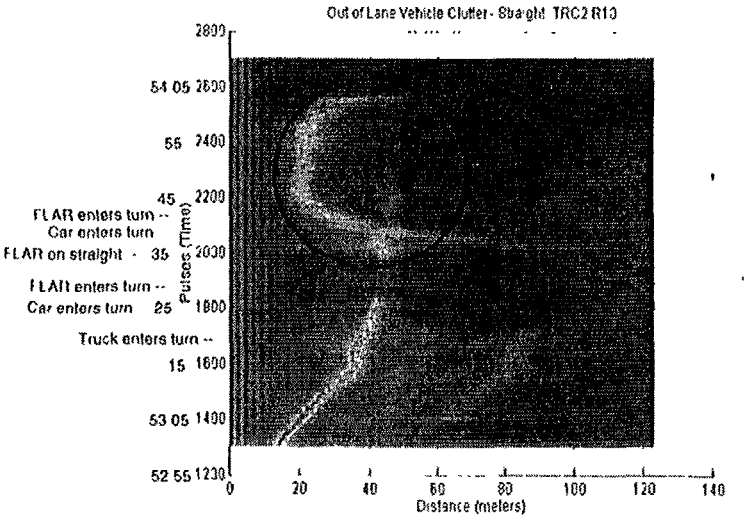

6.4 Intentional Lane Changes - Straight Roadway

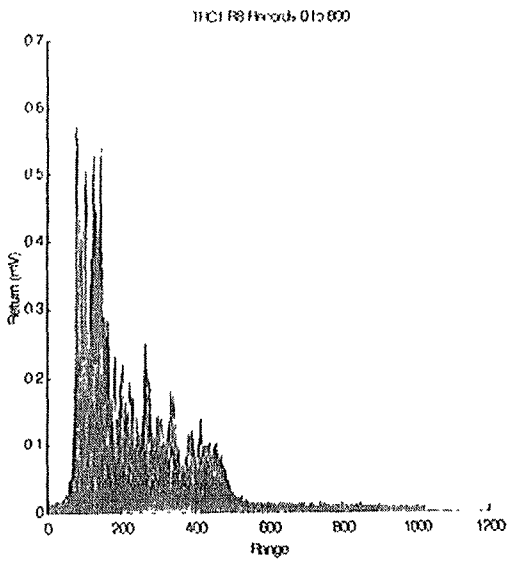

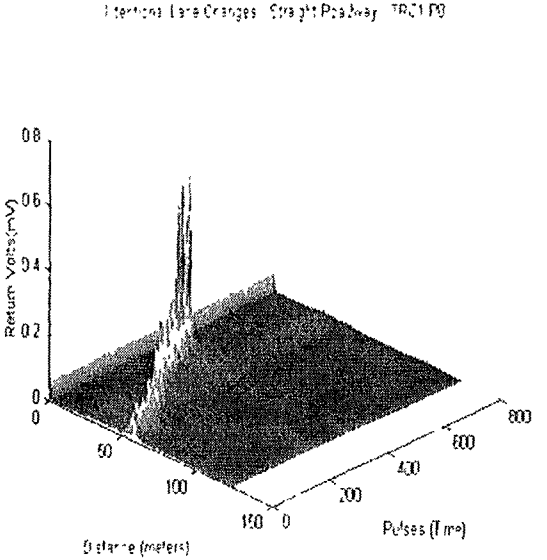

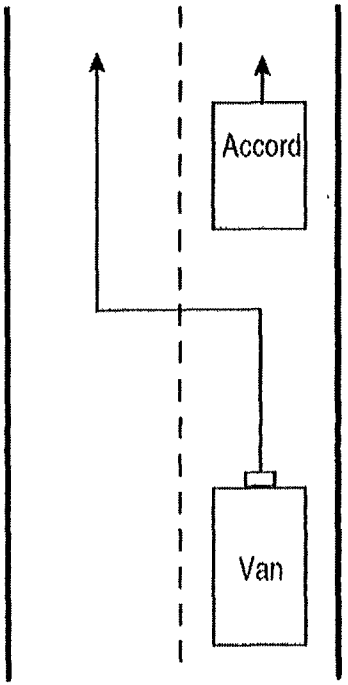

18:48:37 - Begin File

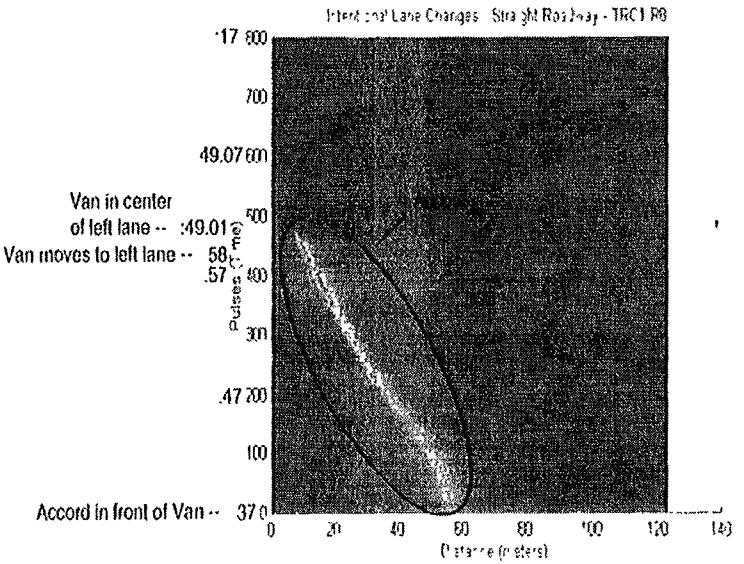

6.4 Intentional Lane Changes - Straight Roadway

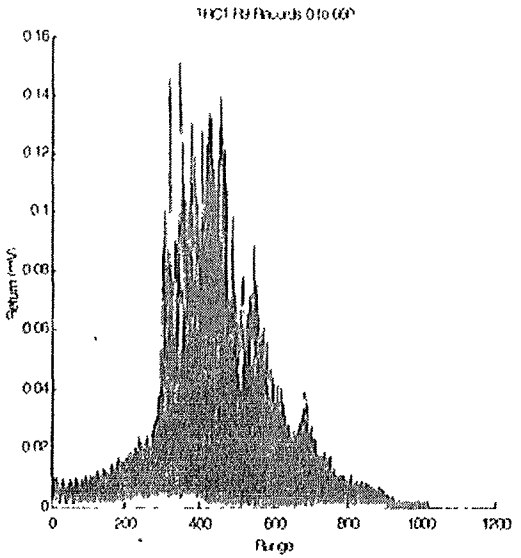

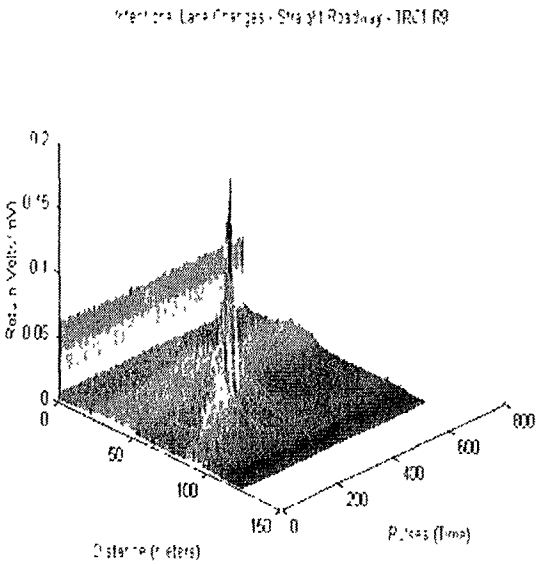

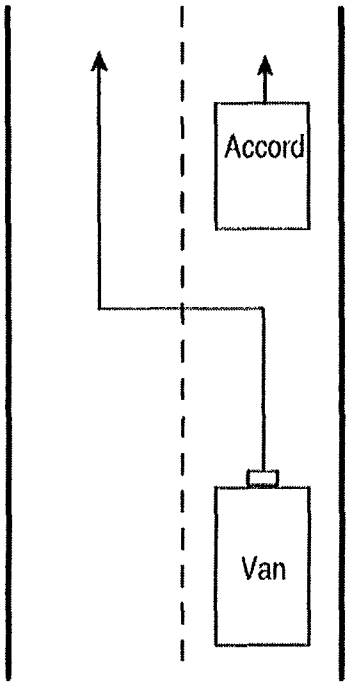

18:56:44 - Begin File

Accord exits scene -- :08

Van in center of -- :57.04
left lane

Van moves to left -- :57.01
lane

Accord in front of Van -- :44

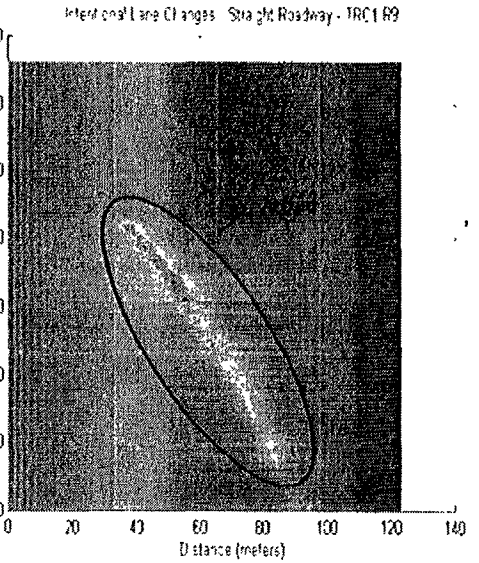

6.4 Intentional Lane Changes - Straight Roadway

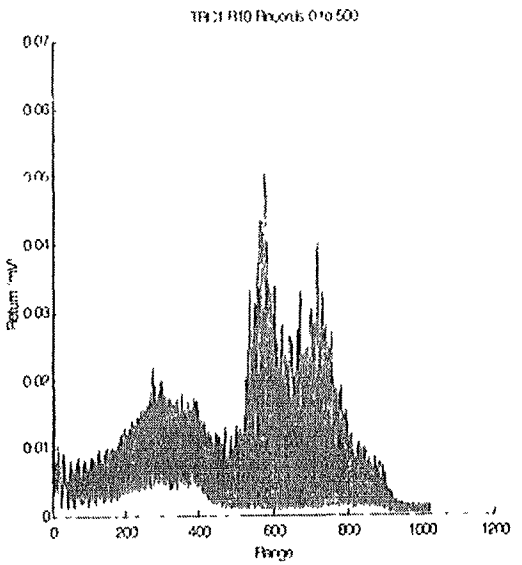

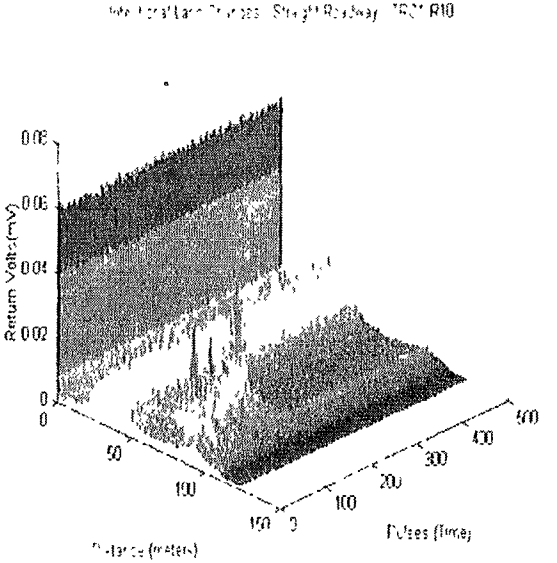

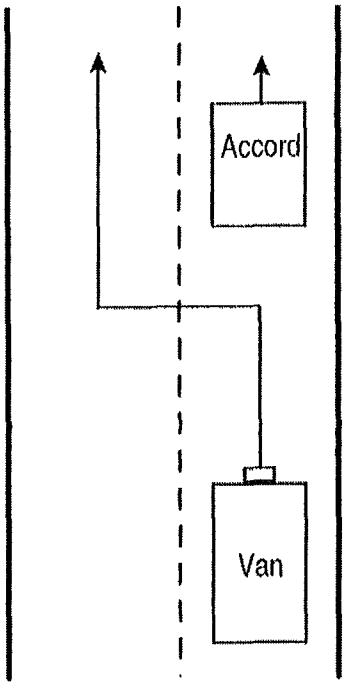

19:05:32 - Begin File

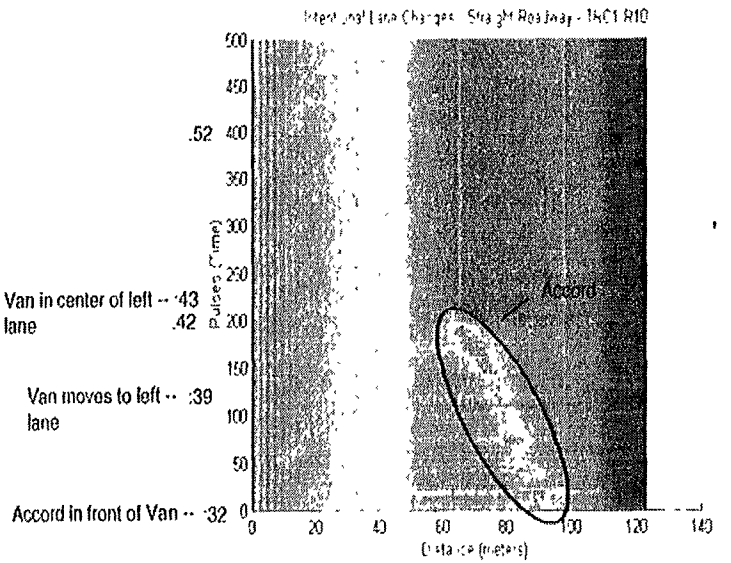

6.4 Intentional Lane Changes - Straight Roadway

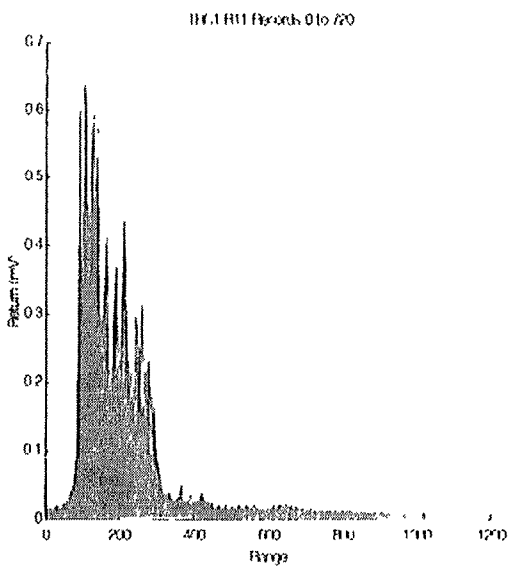

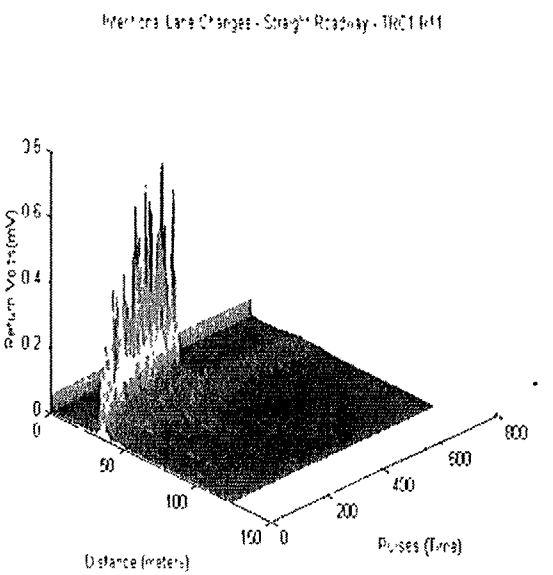

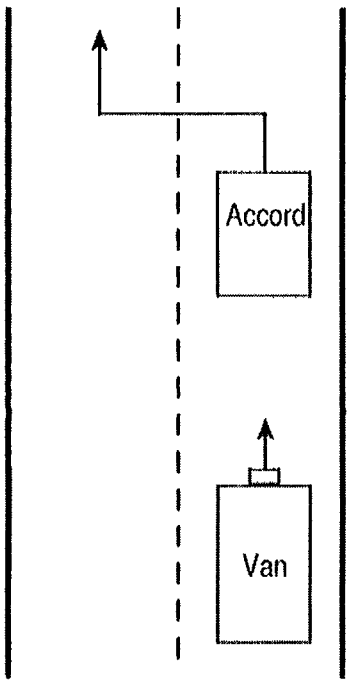

19.18:15 - Begin File

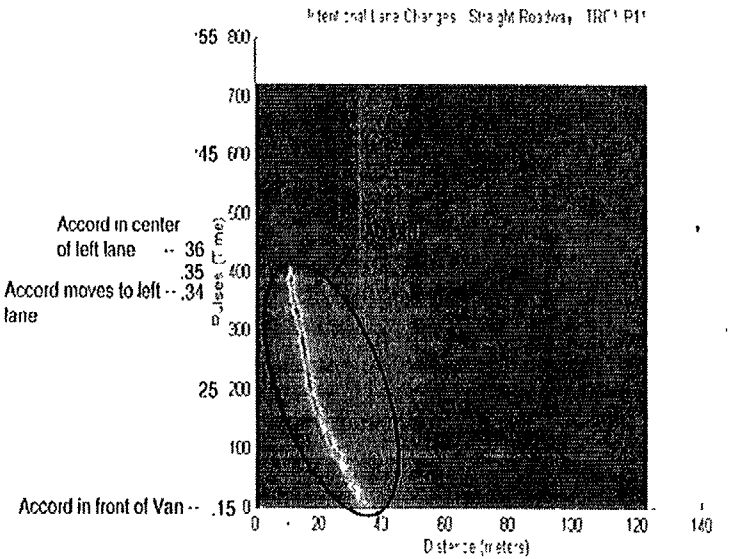

6.4 Intentional Lane Changes - Straight Roadway

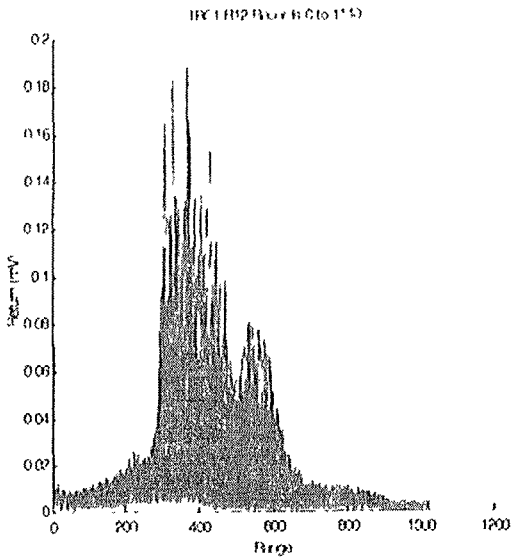

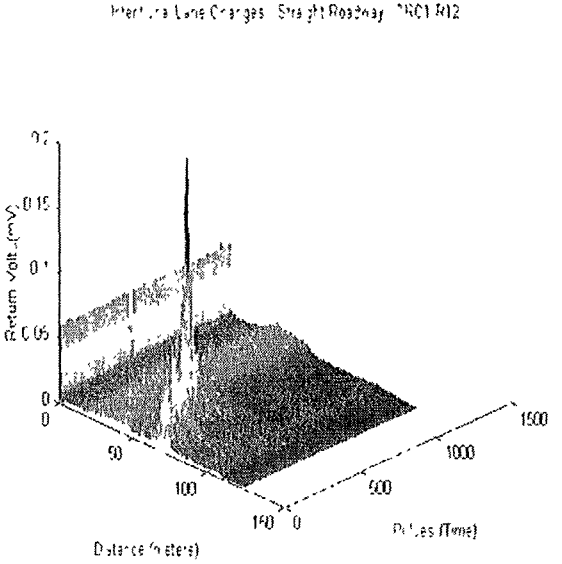

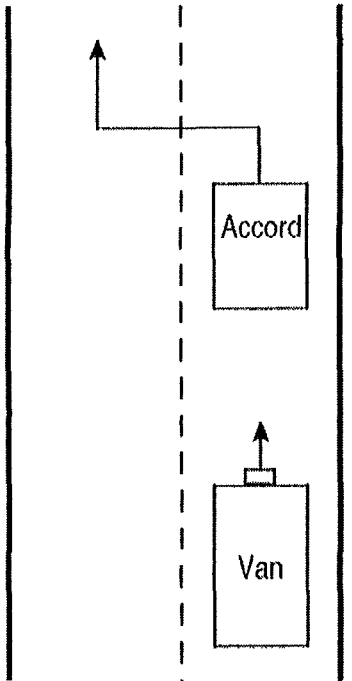

19:28:17 - Begin File

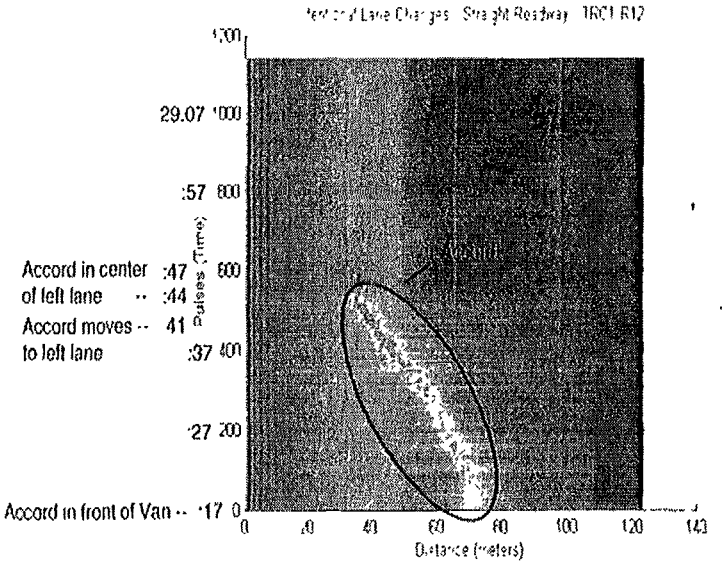

6.4 Intentional Lane Changes - Straight Roadway

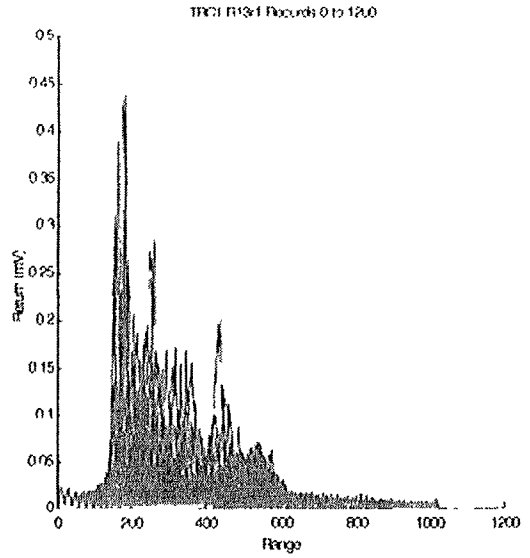

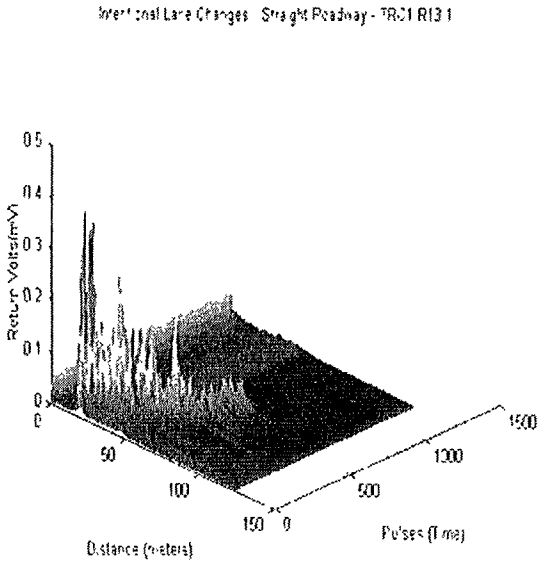

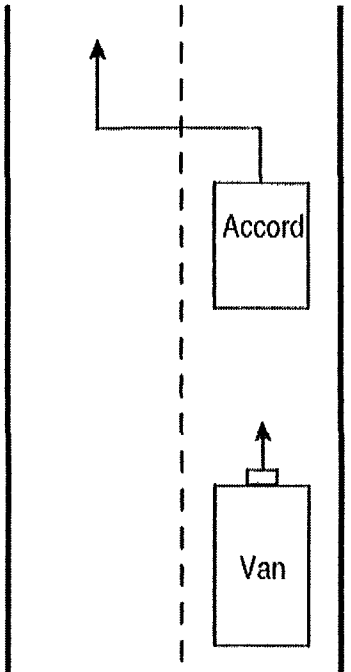

17:08:09 - Begin File

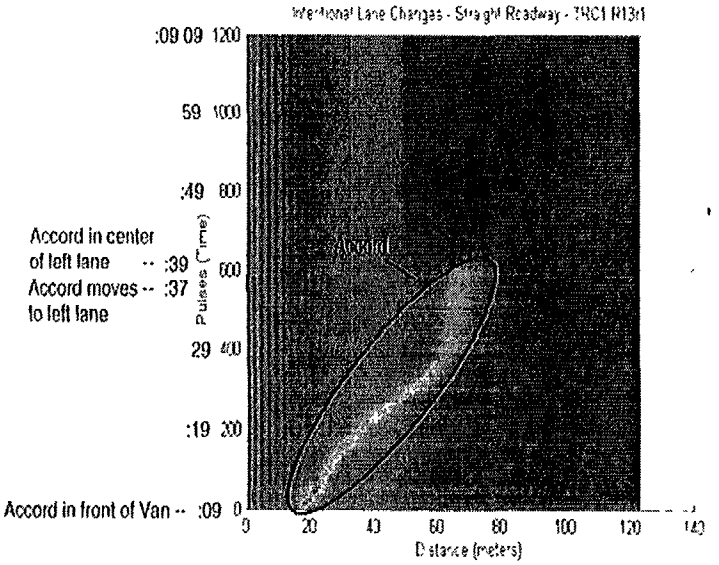

6.4 Intentional Lane Changes - Straight Roadway

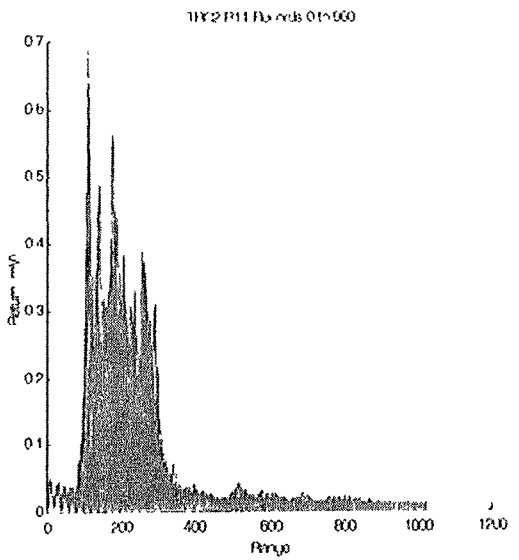

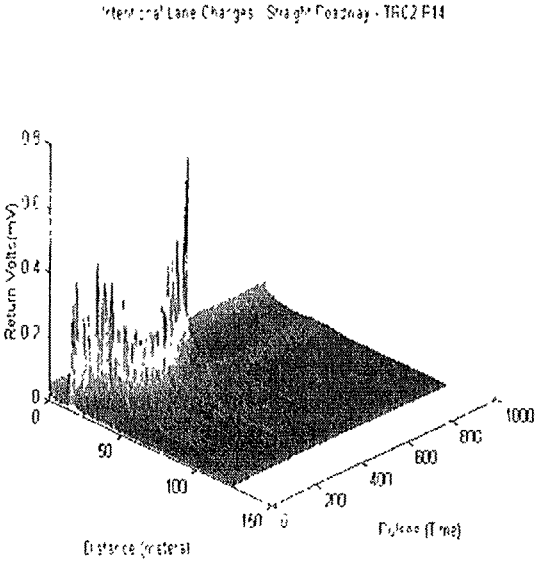

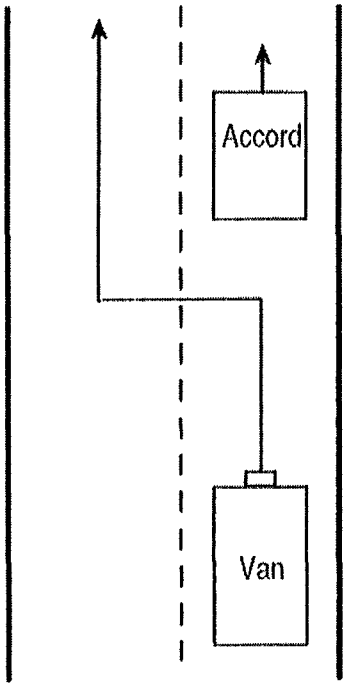

20:41:42 - Begin File

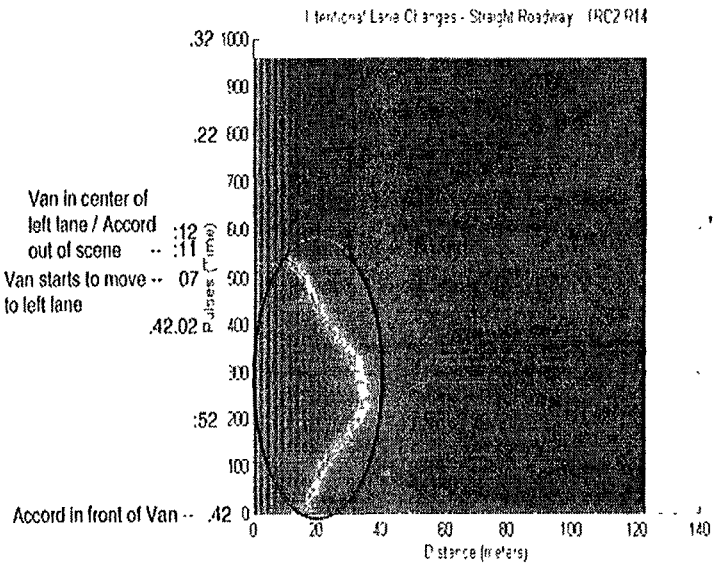

6.4 Intentional Lane Changes - Straight Roadway

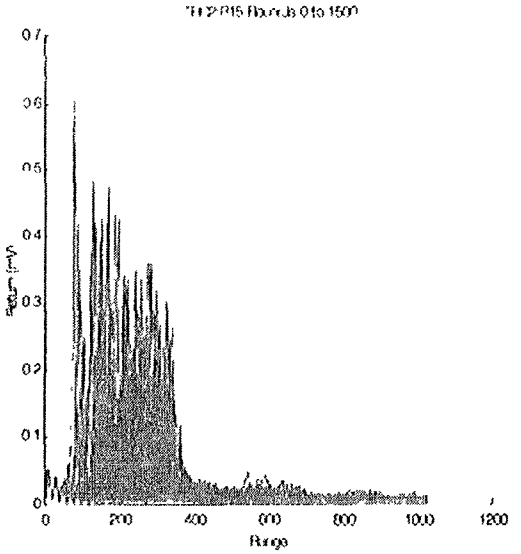

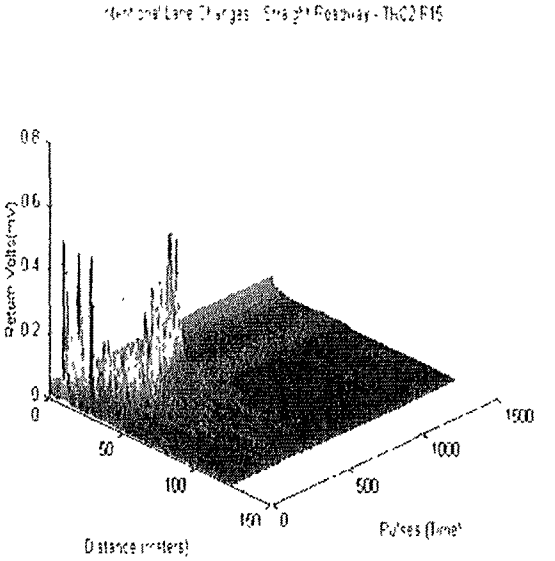

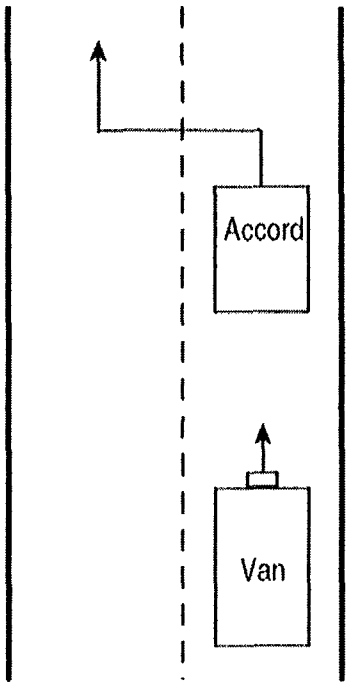

20:45:20 - Begin File

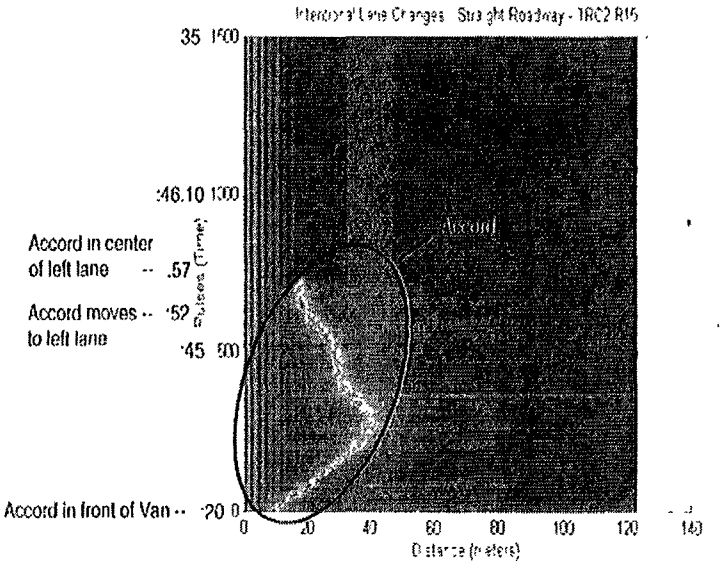

6.5 Tracking New Secondary - Straight Roadway

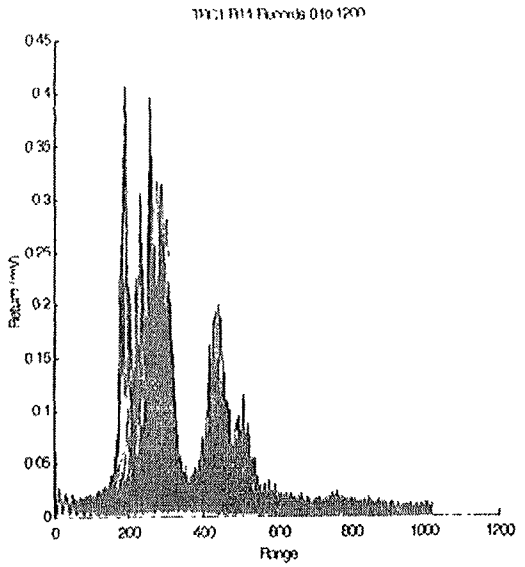

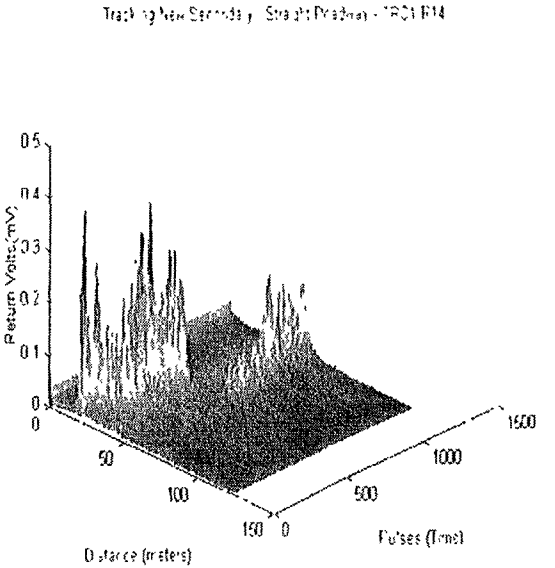

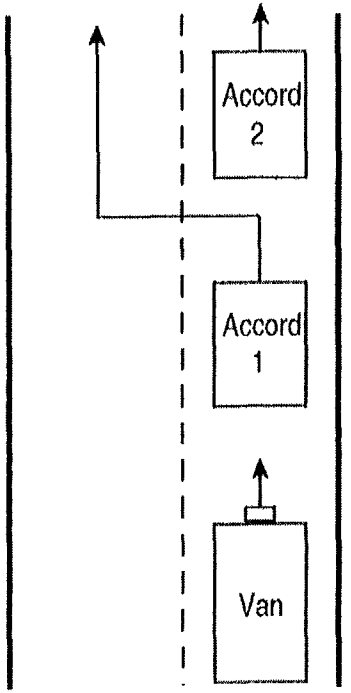

17:00:58 - Begin File

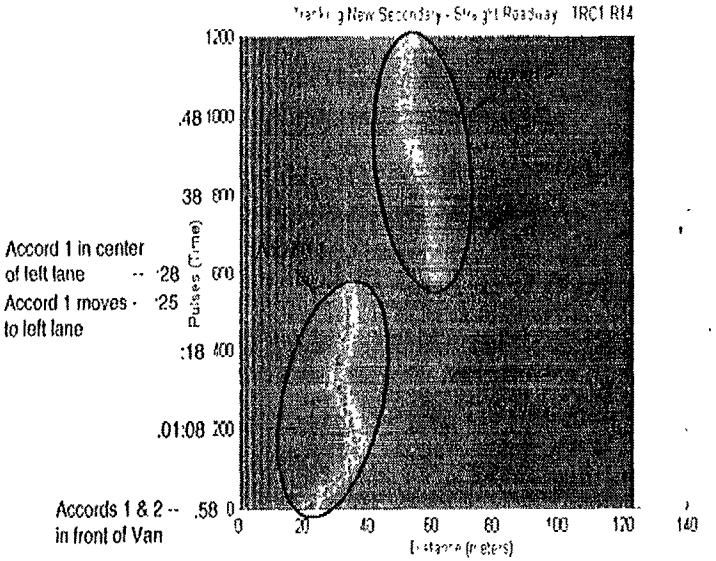

6.5 Tracking New Secondary - Straight Roadway

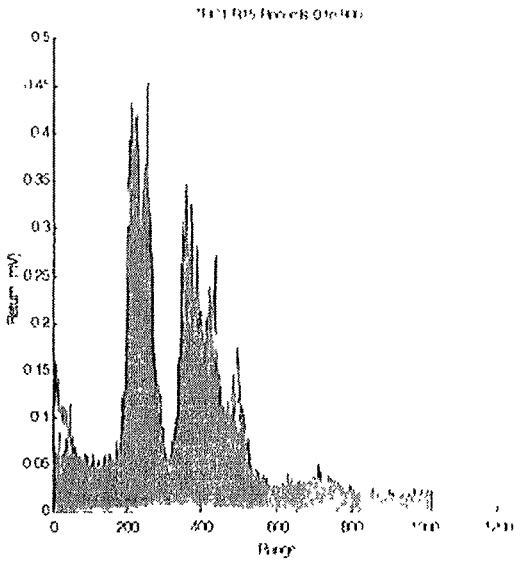

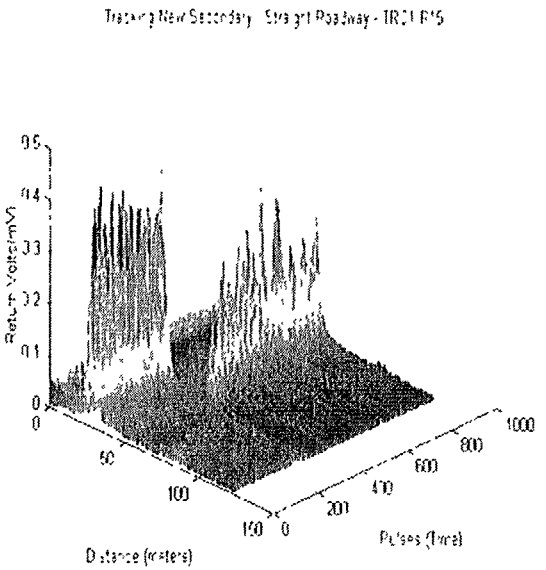

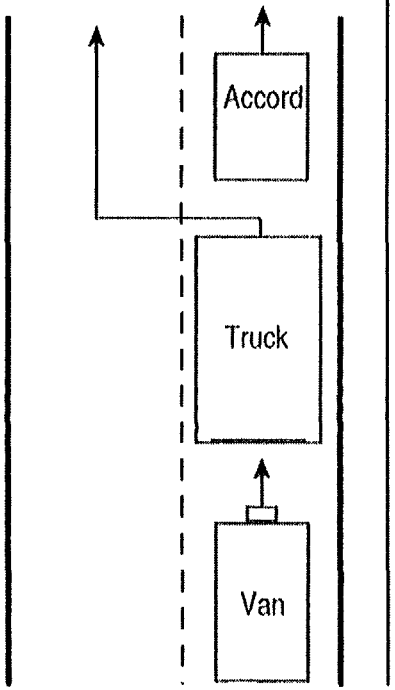

14:37:56 - Begin File

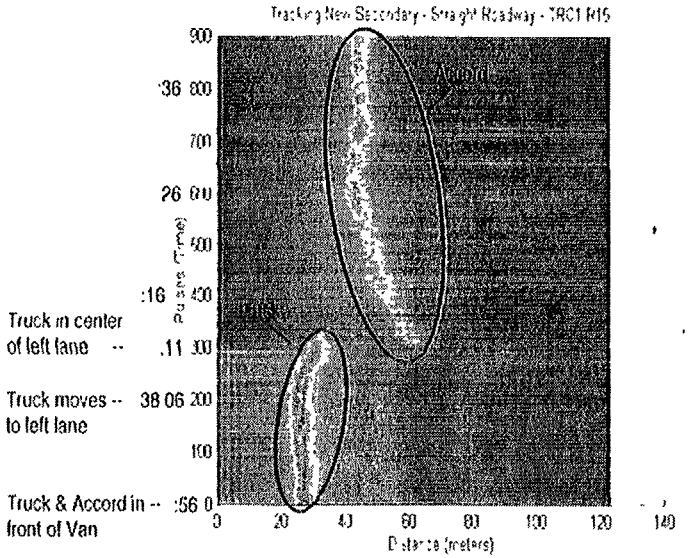

6.5 Tracking New Secondary - Straight Roadway

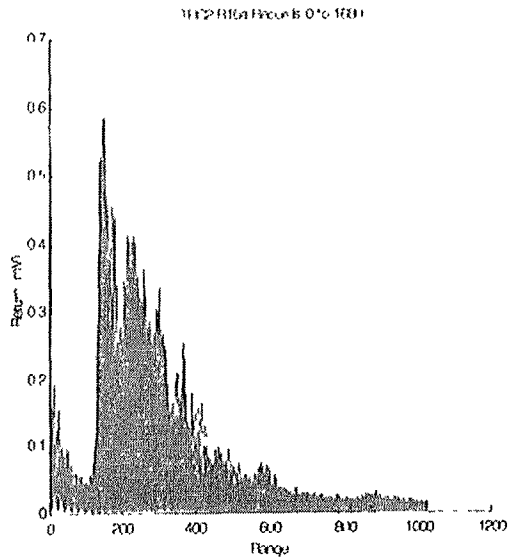

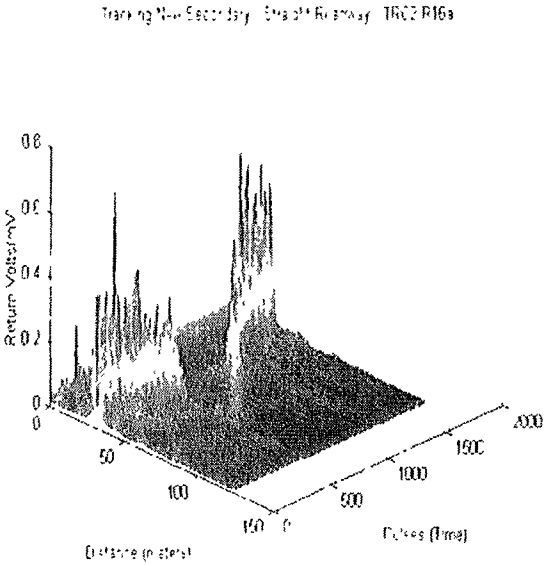

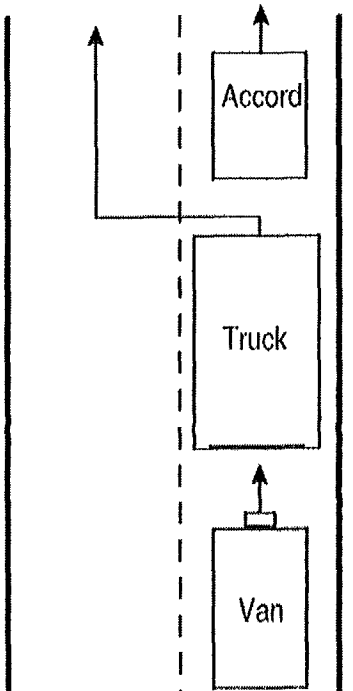

16:27:26 - Begin File

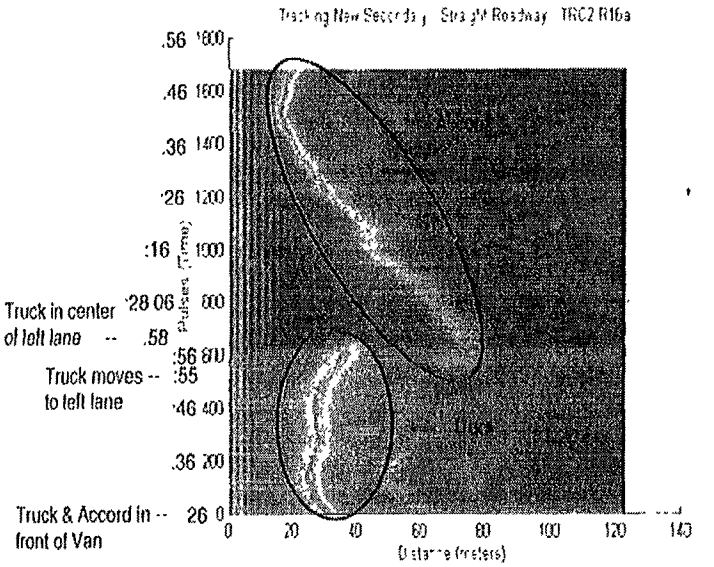

6.6 Tracking with a Cut-in-Straight Roadway

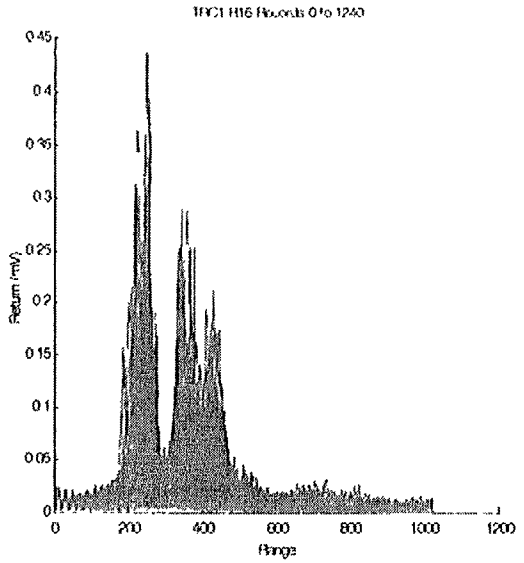

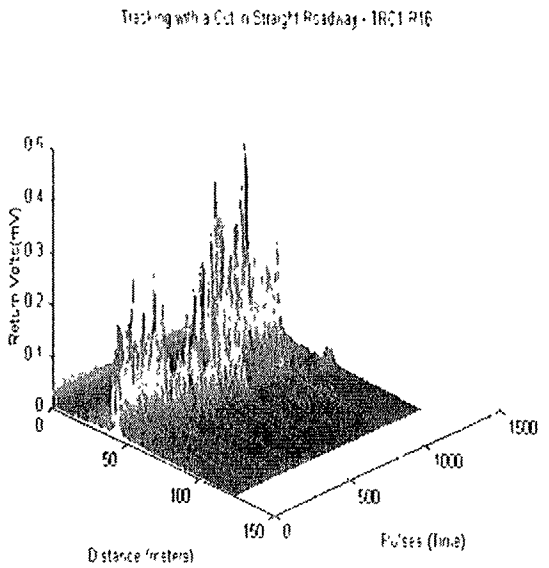

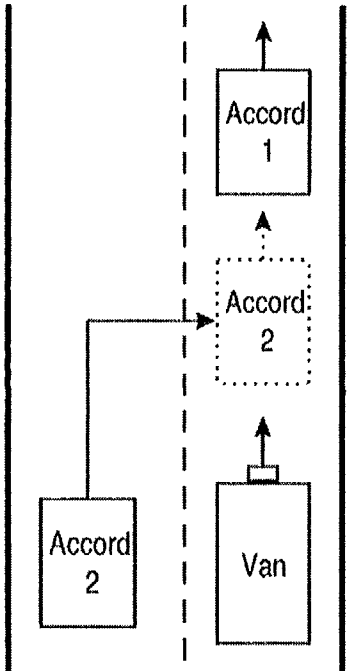

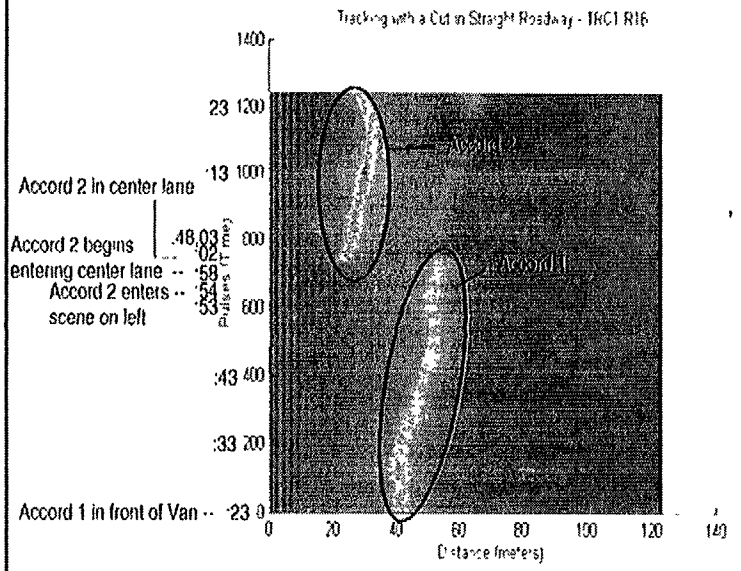

6.6 Tracking with a Cut-in-Straight Roadway

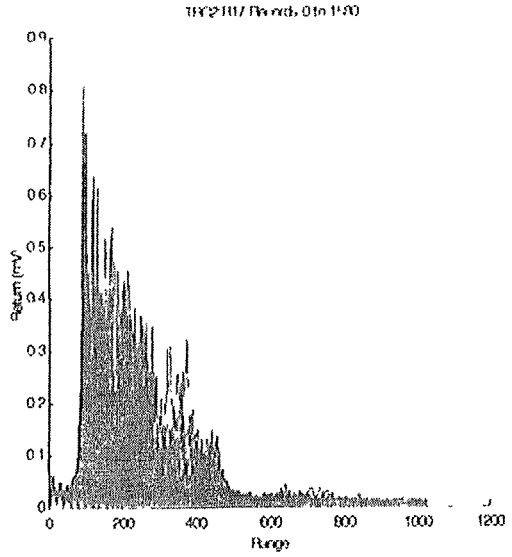

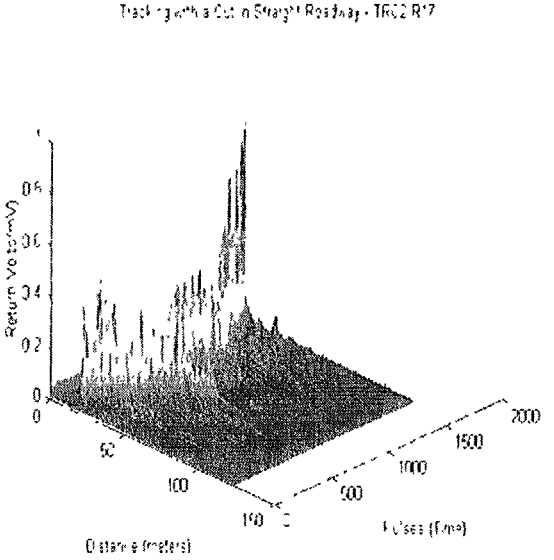

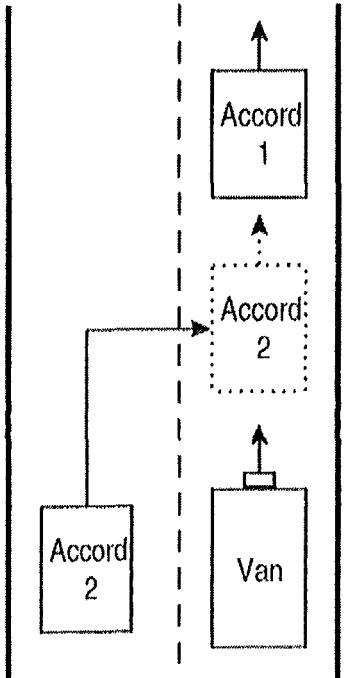

20:14:11 - Begin File

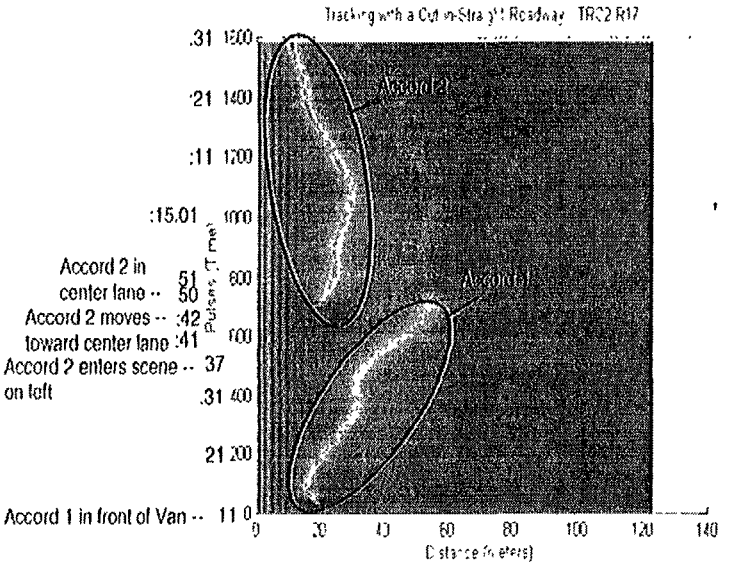

6.7 - Strong Vehicle Clutter in Range - Straight Roadway

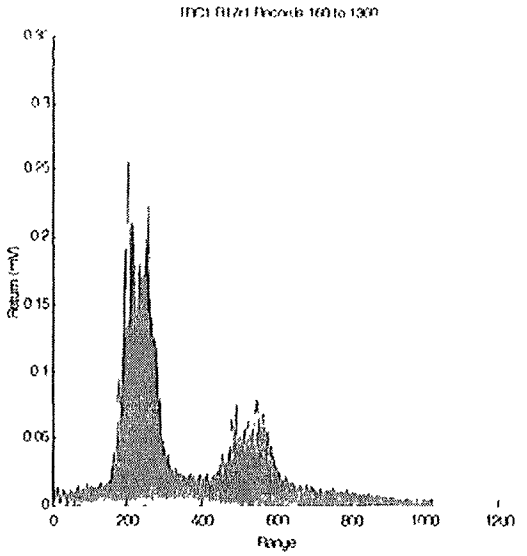

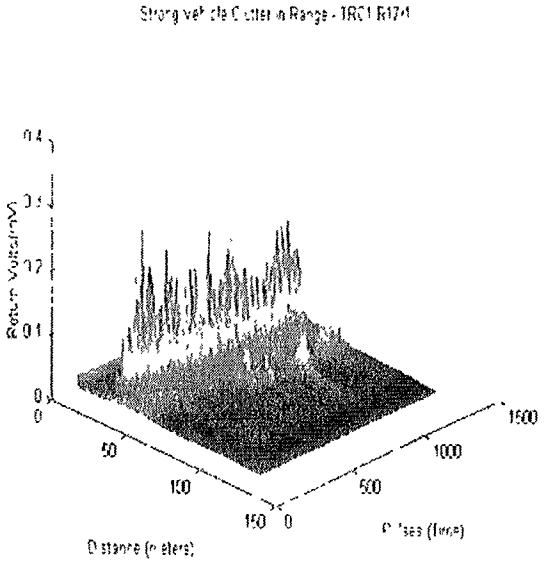

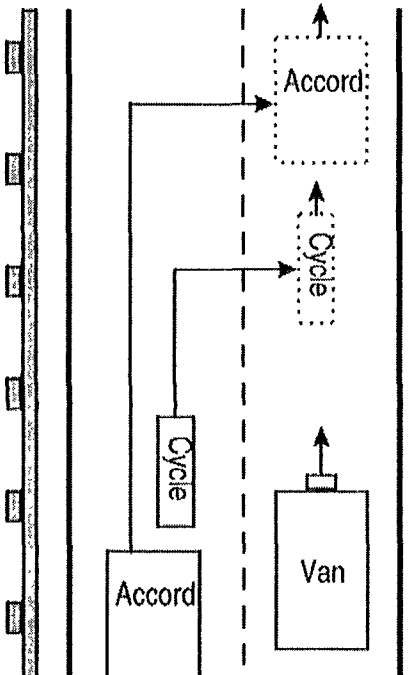

15:23:55 - Begin File

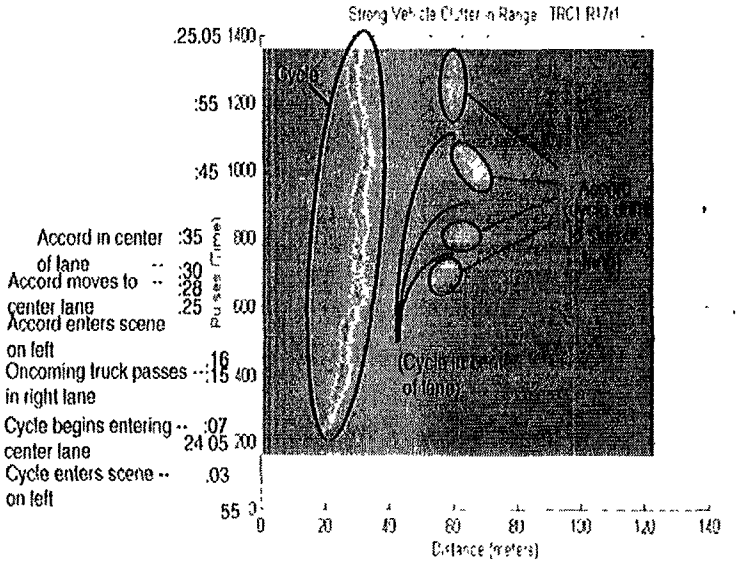

6.7 - Strong Vehicle Clutter in Range - Straight Roadway

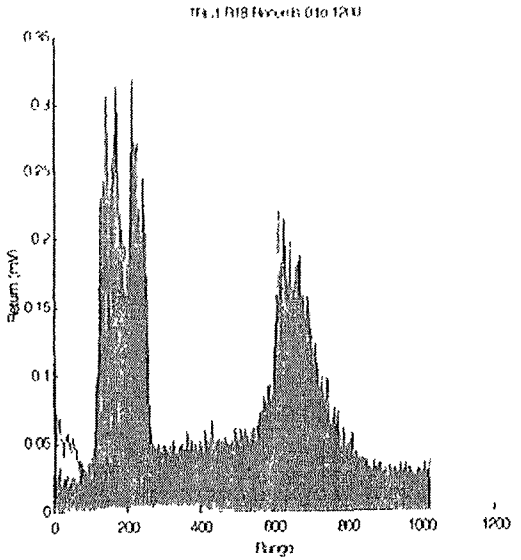

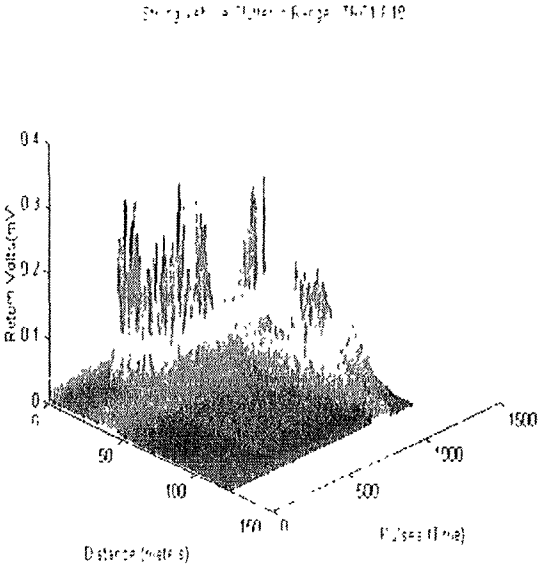

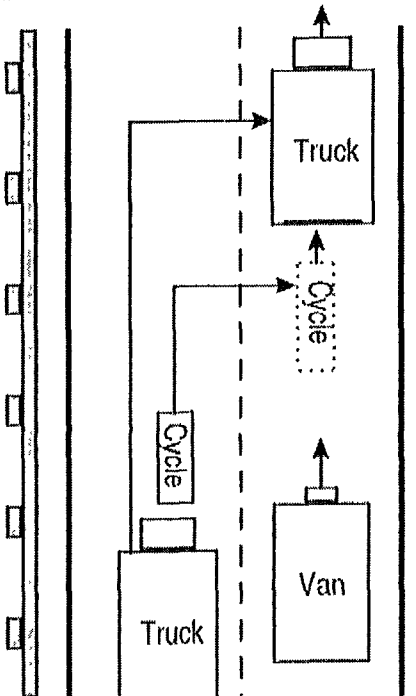

14:52:53 - Begin File

Truck in center of lane :43
Truck begins to enter center lane :38 :35 :33
Truck enters scene on left :23 :18
Cycle in center of lane :13 :08
Cycle enters center lane :06 :53.03
Cycle enters scene on left :02

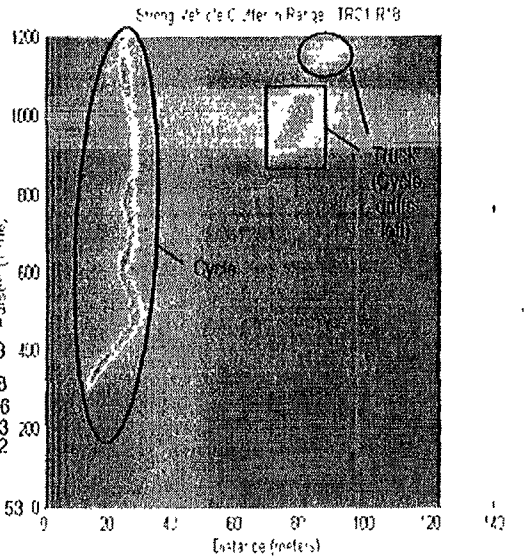

6.7 - Strong Vehicle Clutter in Range - Straight Roadway

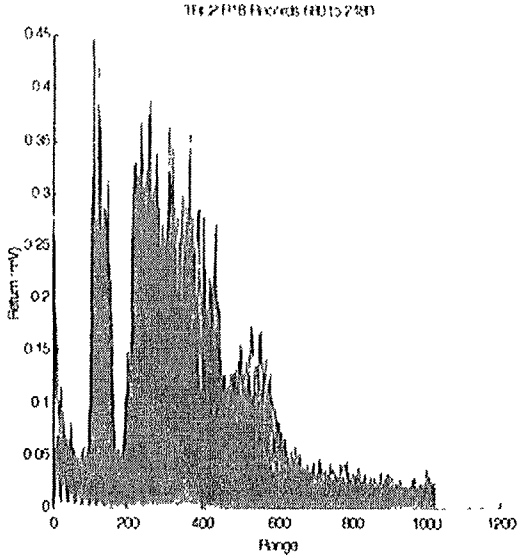

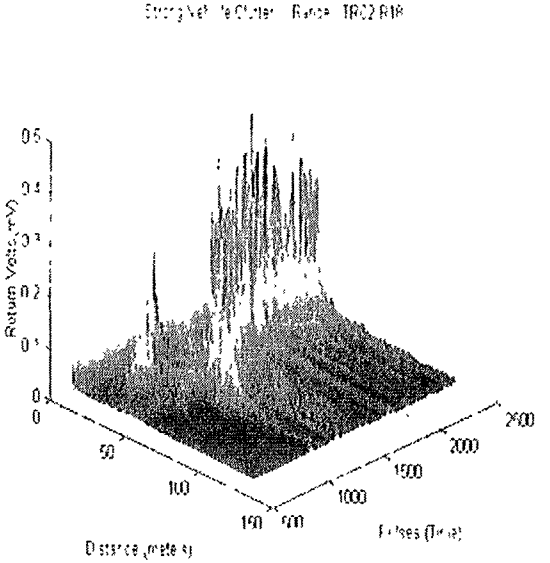

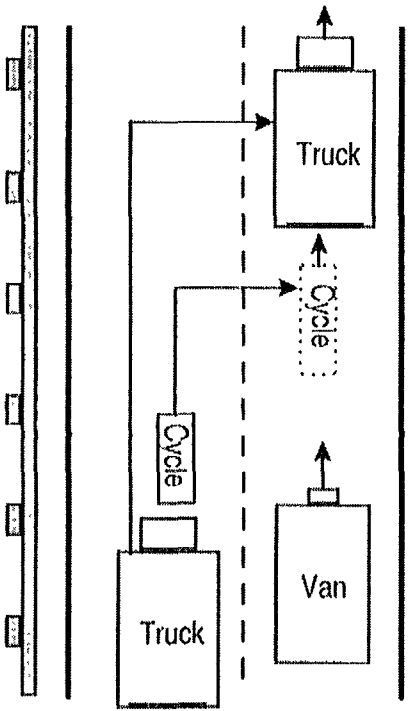

15:39:38 - Begin File

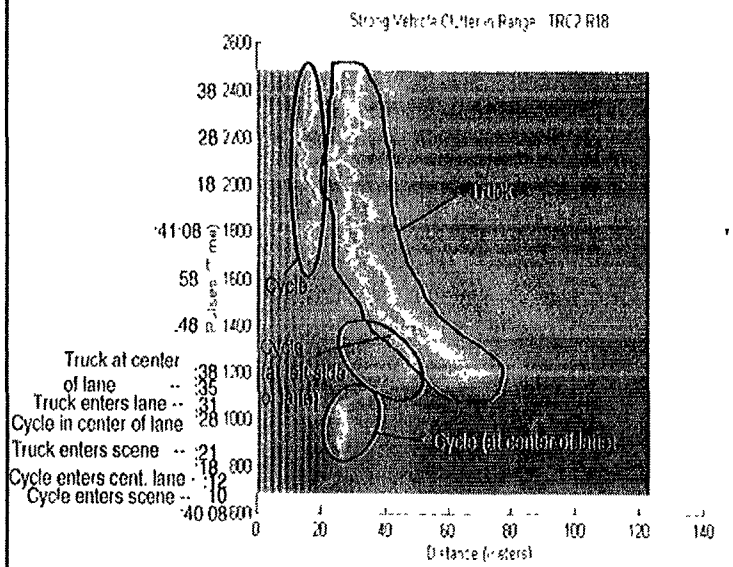

6.8 Vehicle Clutter in Azmuth

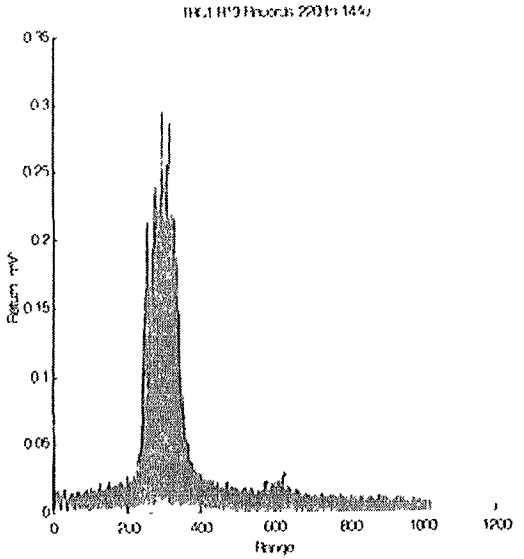

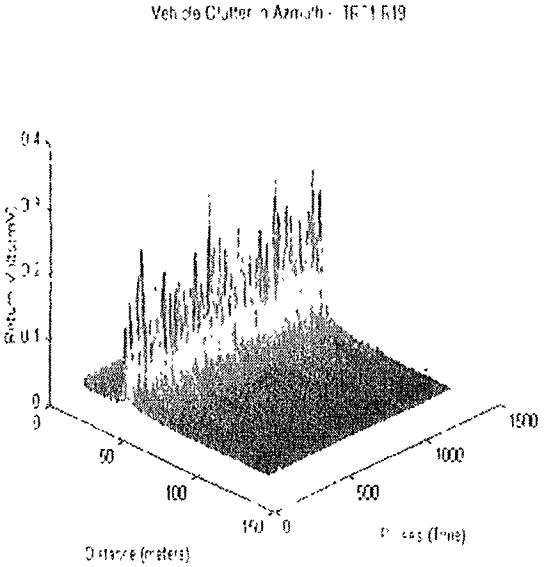

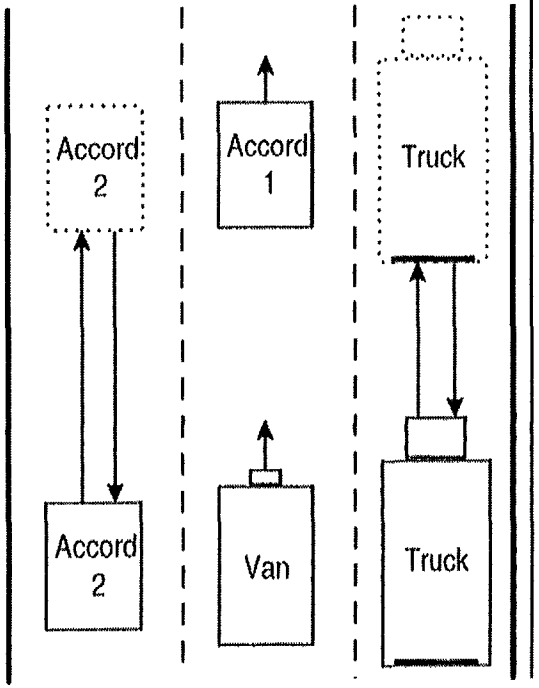

16:02:14 - Begin File

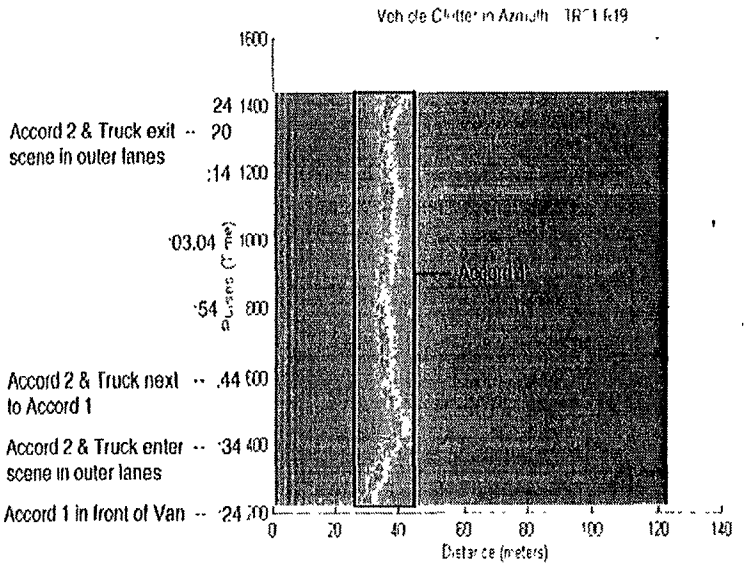

6.8 Vehicle Clutter in Azmuth

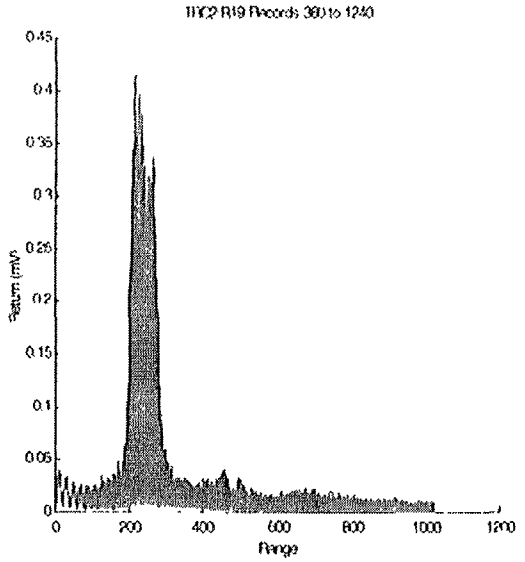

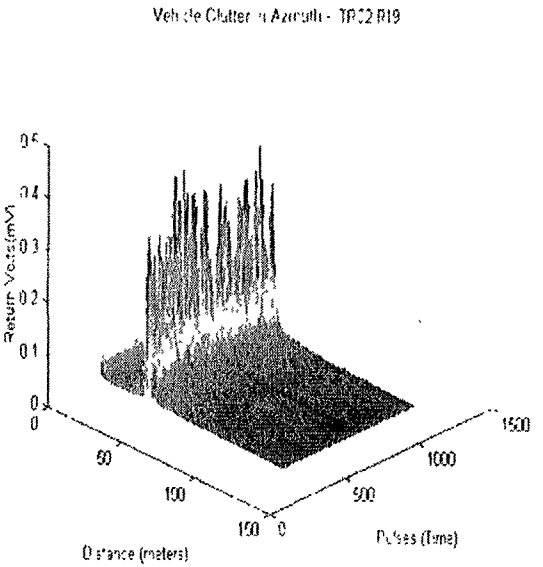

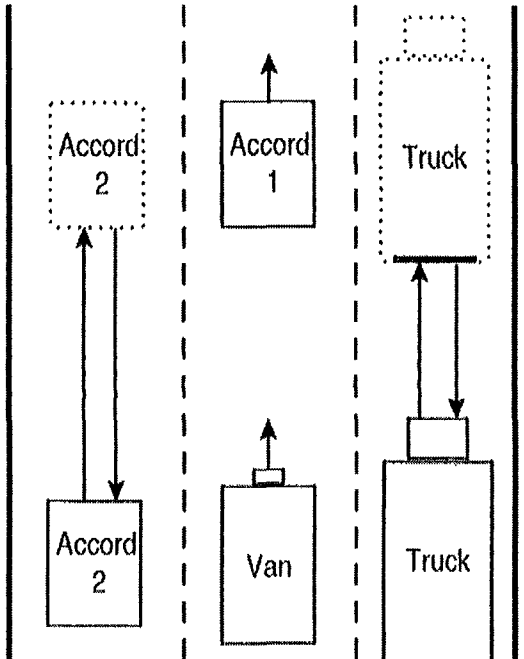

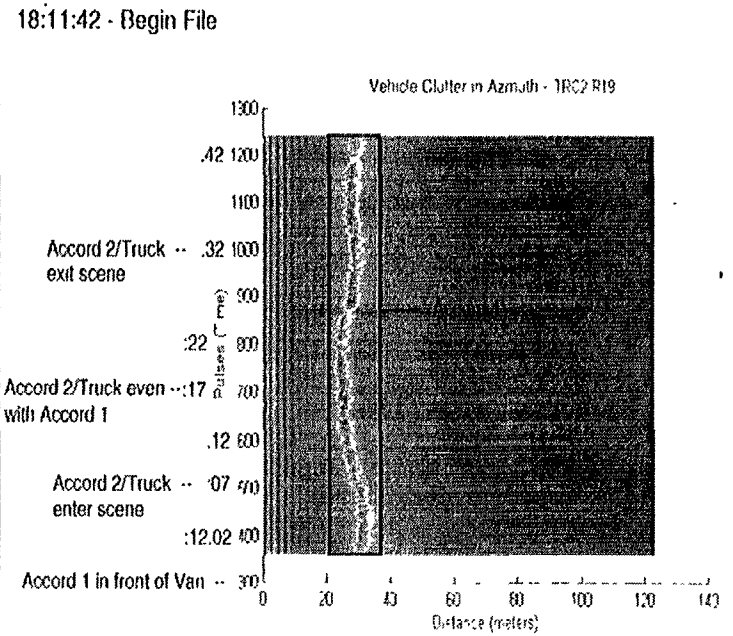

6.8 Vehicle Clutter in Azmuth

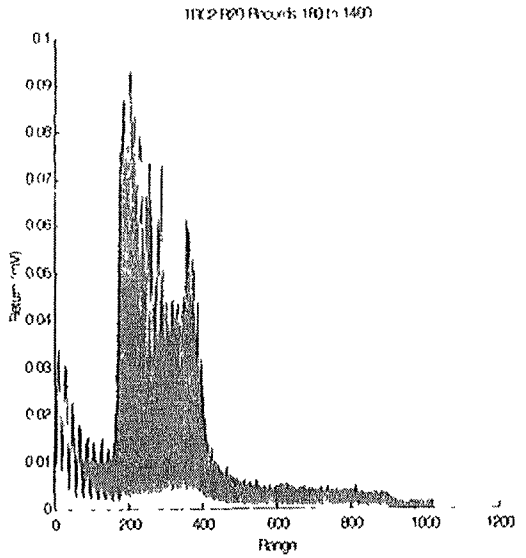

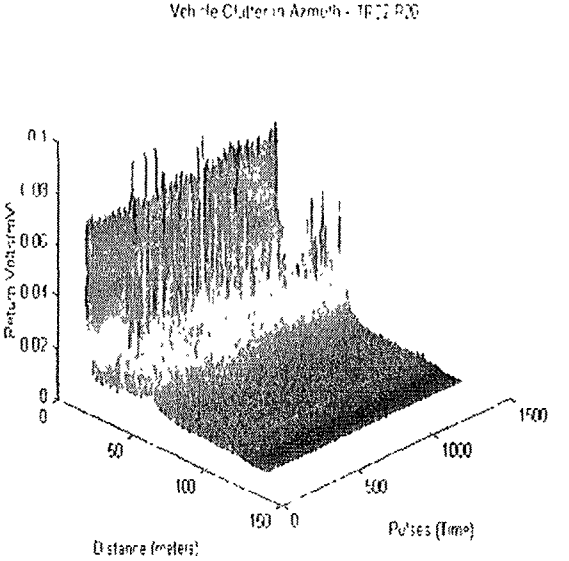

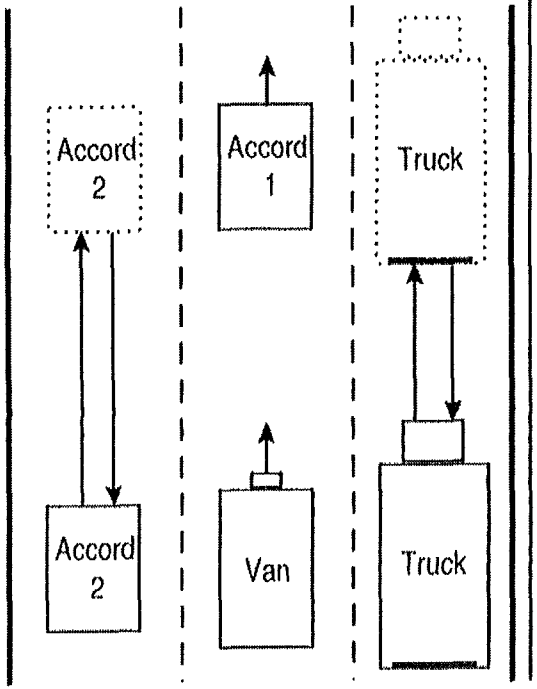

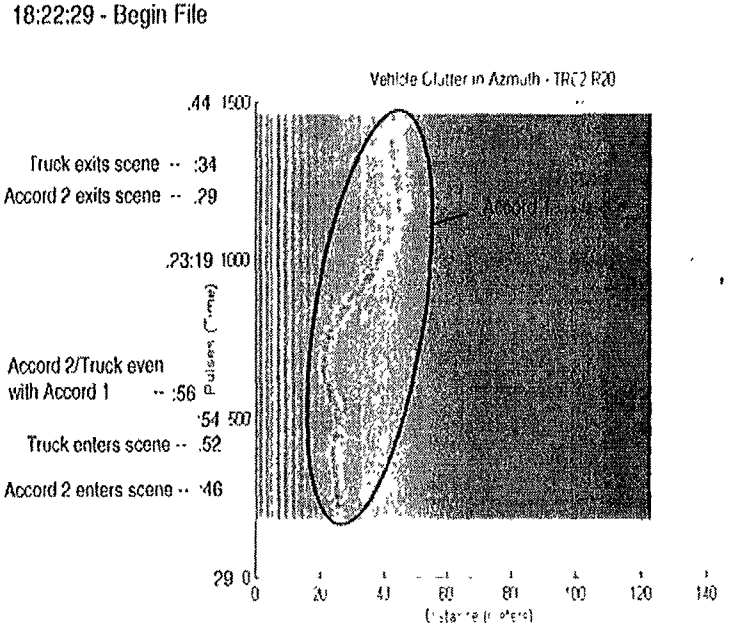

6.8 Vehicle Clutter in Azmuth

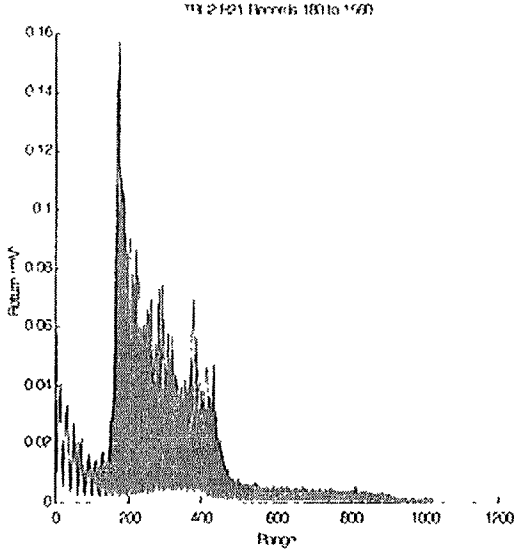

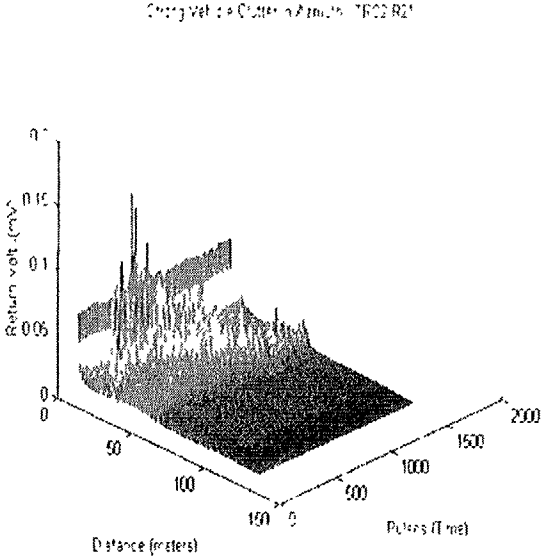

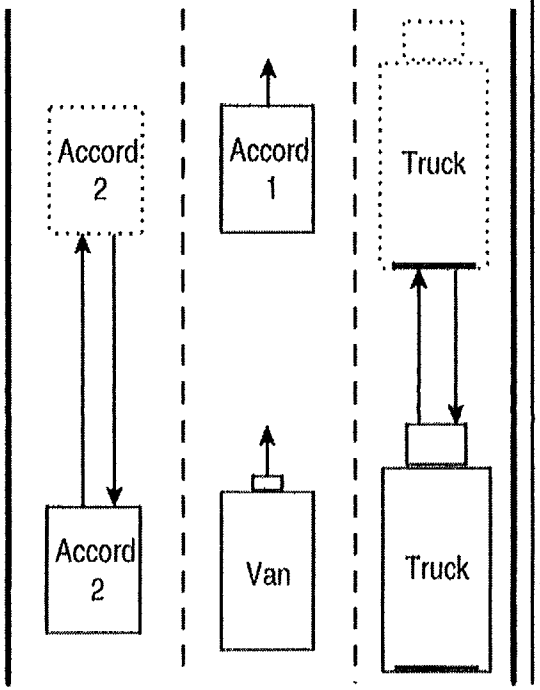

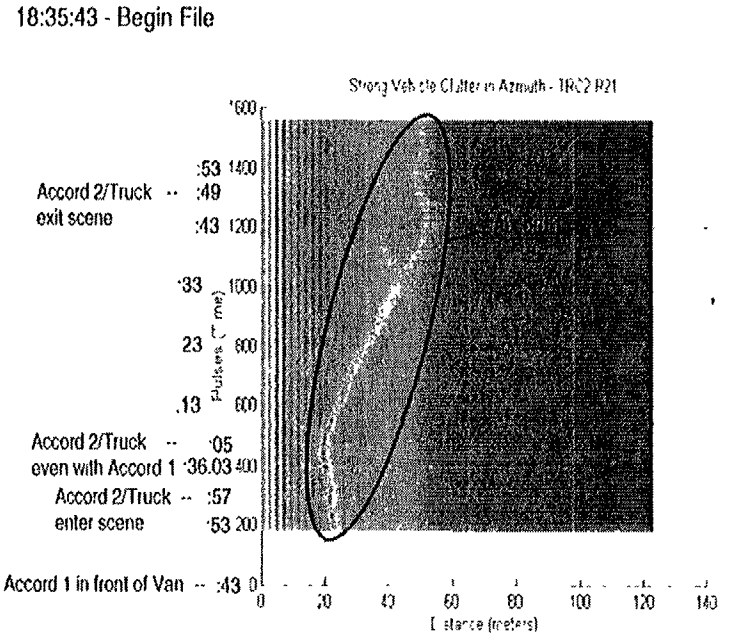

6.9 Merging Traffic - Straight Roadway

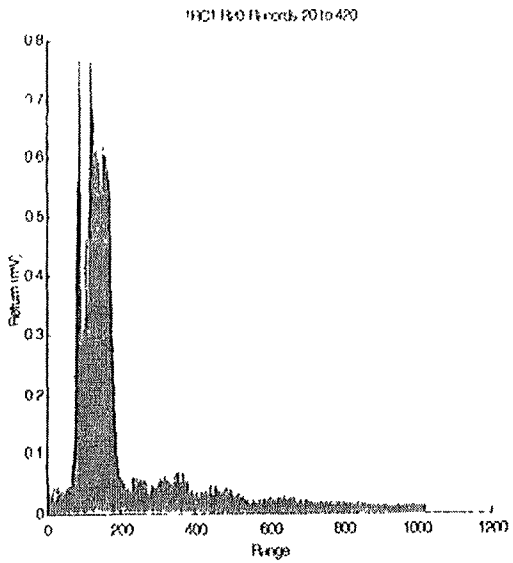

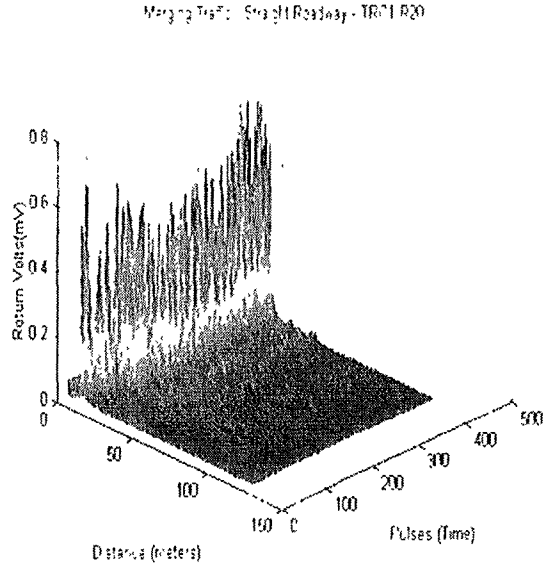

Accord 2 tries to merge between Van & Accord 1, but never does.

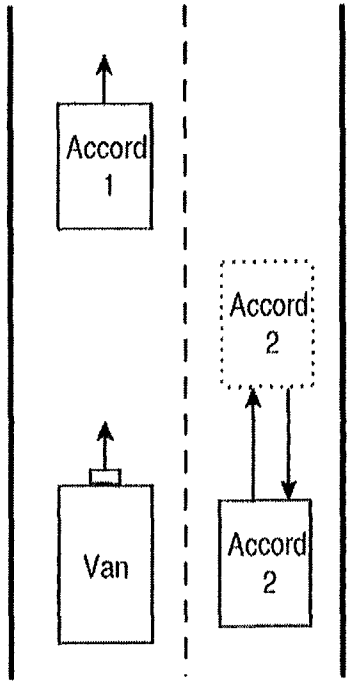

11:52:18 - Begin File

Accord 2 enters and exits scene from right -- :32

Accord 1 in front of Van -- :18

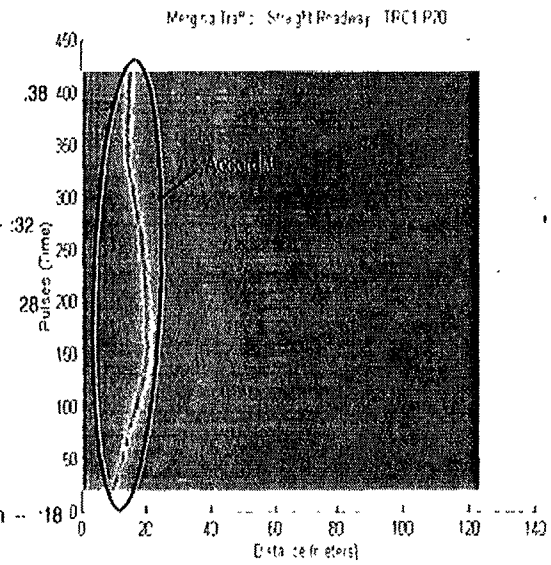

6.10 Vehicle Induced False Alarms - Curved Roadway

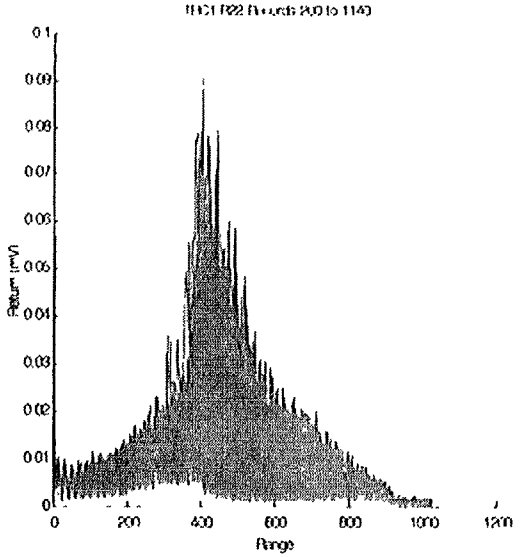

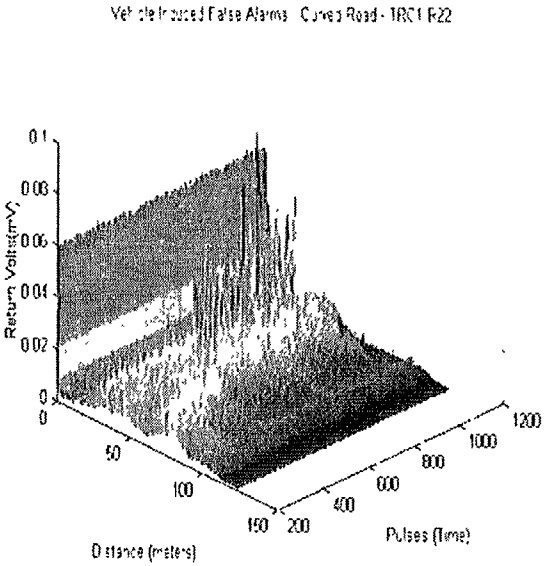

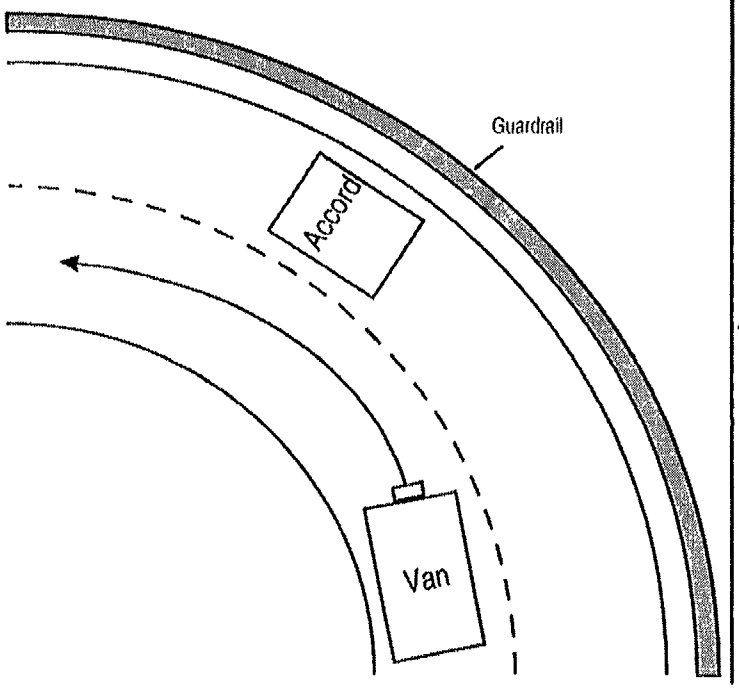

18:09:52 - Begin File

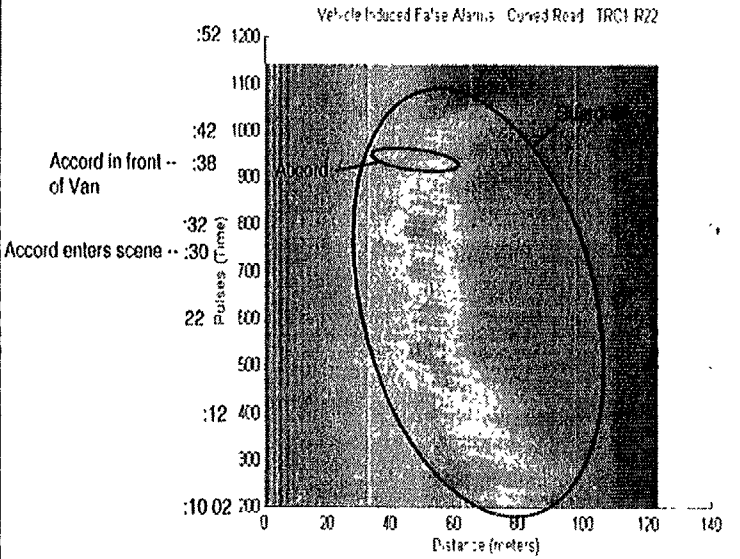

6.10 Vehicle Induced False Alarms - Curved Roadway

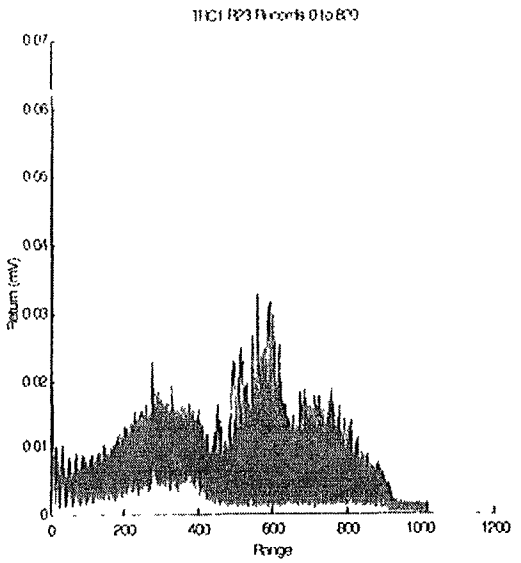

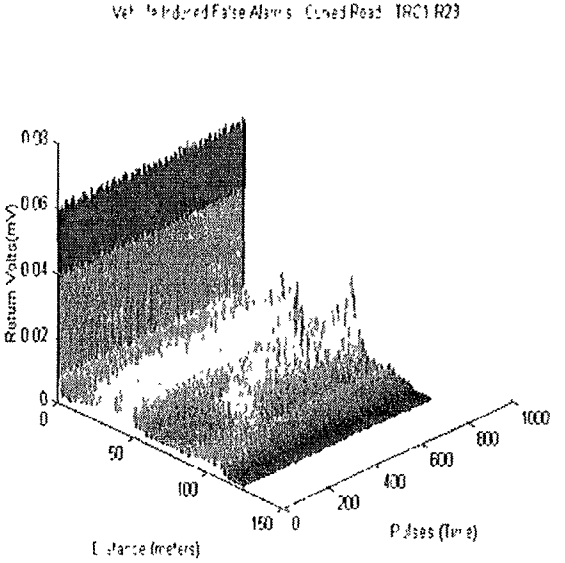

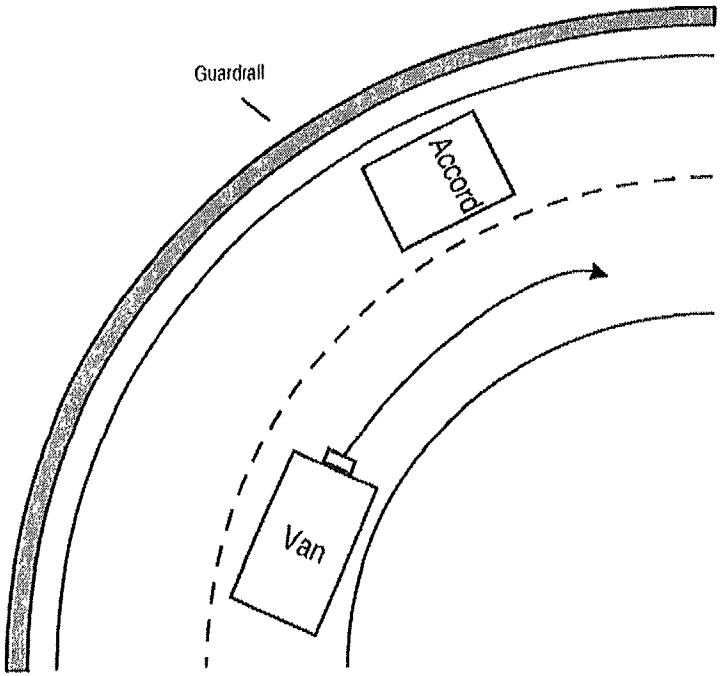

17:57:02 -Begin File

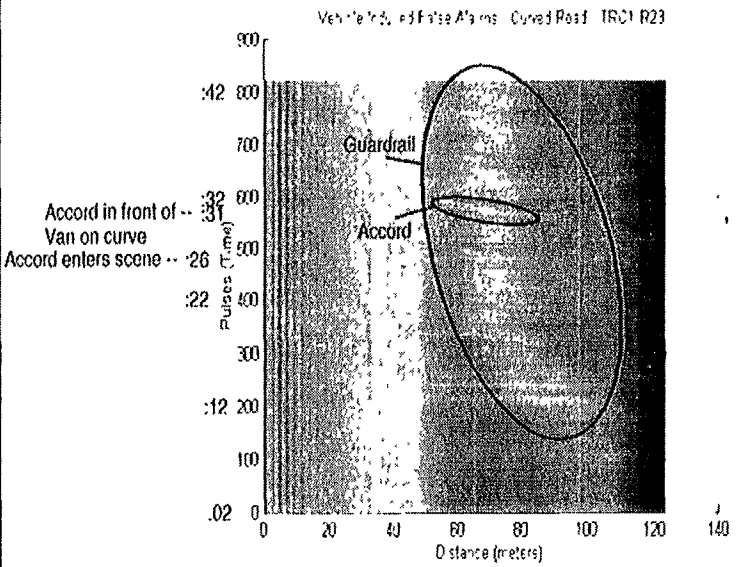

6.10 Vehicle Induced False Alarms - Curved Roadway

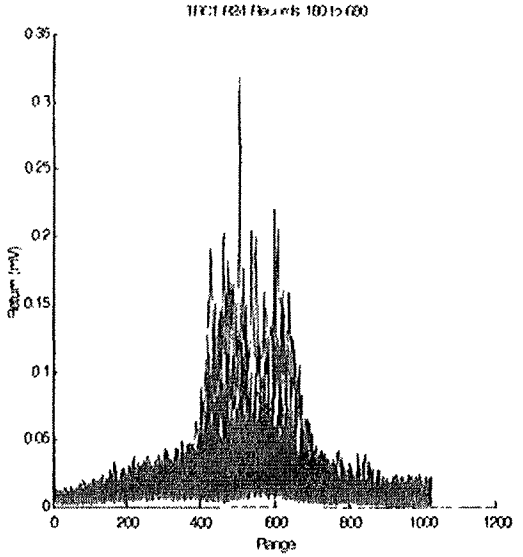

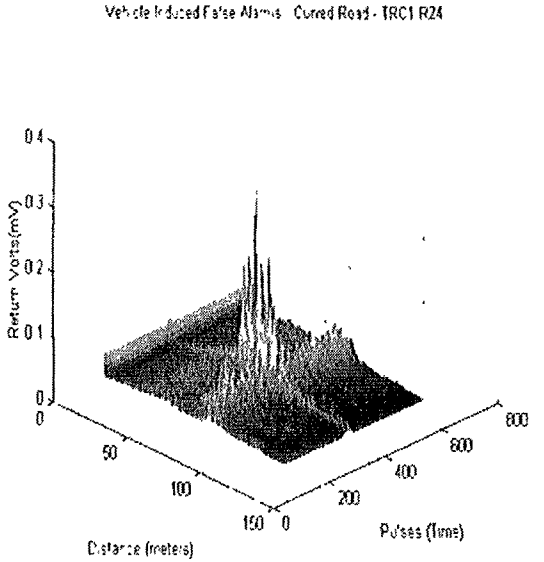

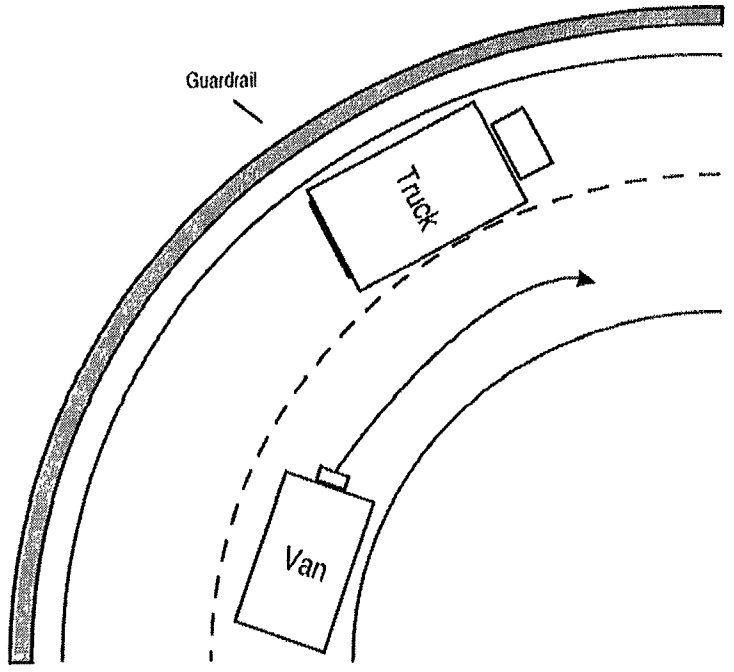

13:57:16 - Begin File

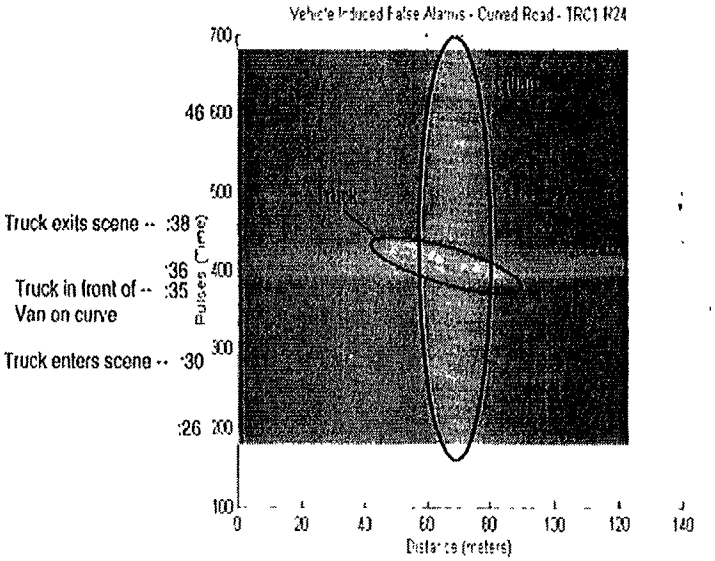

6.10 Vehicle Induced False Alarms - Curved Roadway

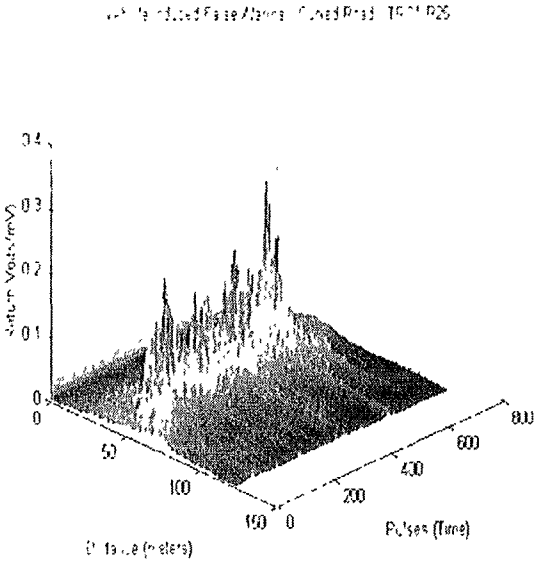

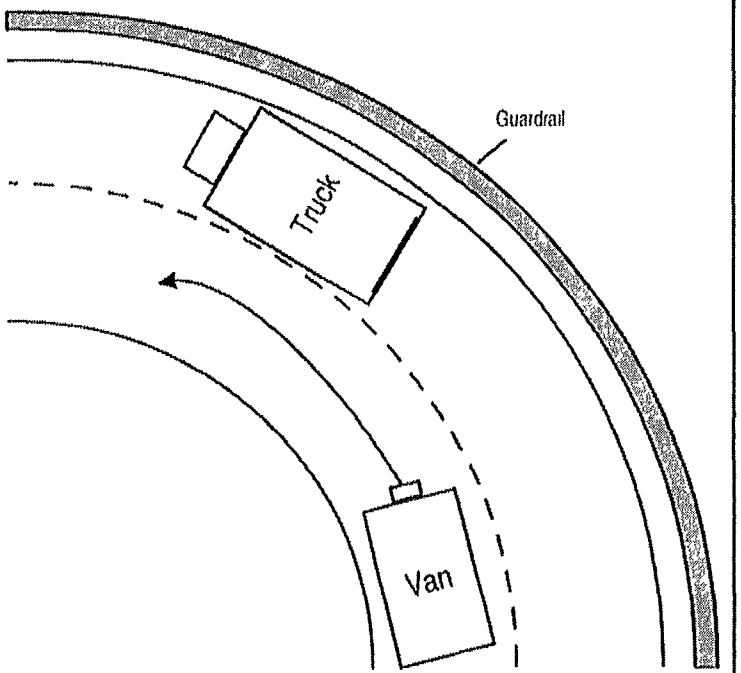

13:45:35 - Begin File

Truck in front of -- :00
Van on curve
Truck enters scene -- :55

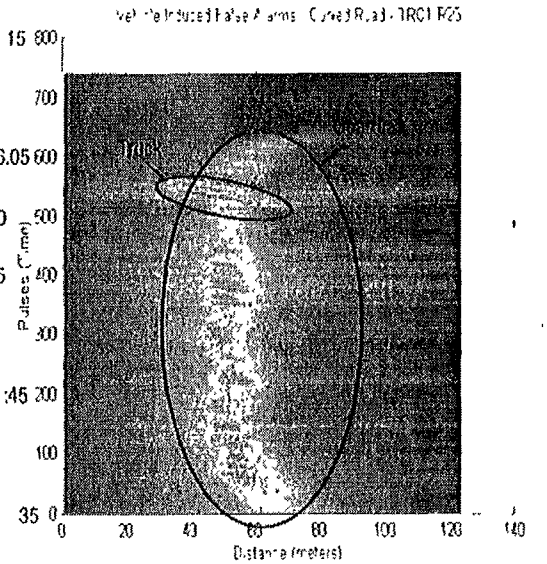

6.10 Vehicle Induced False Alarms - Curved Roadways

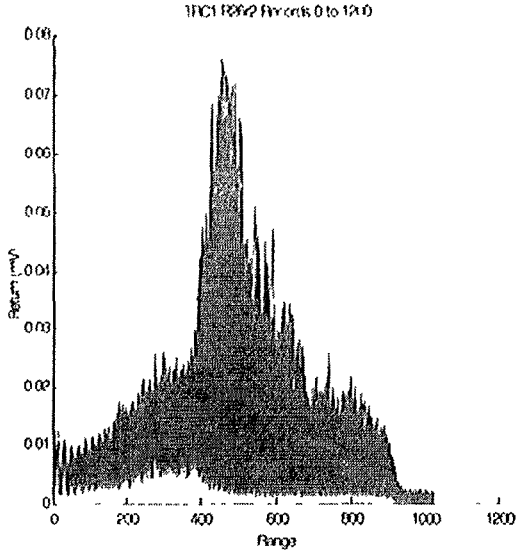

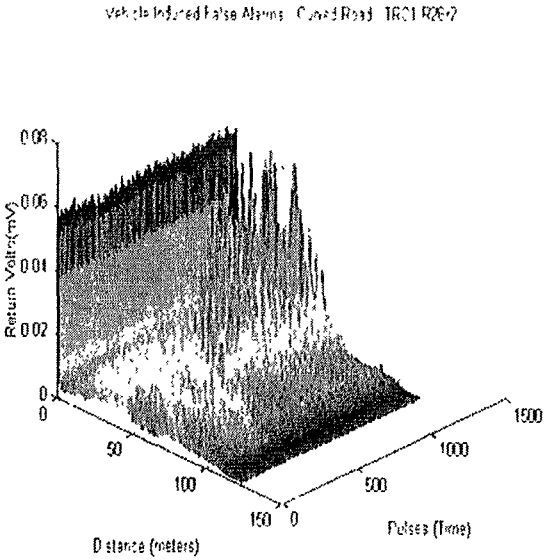

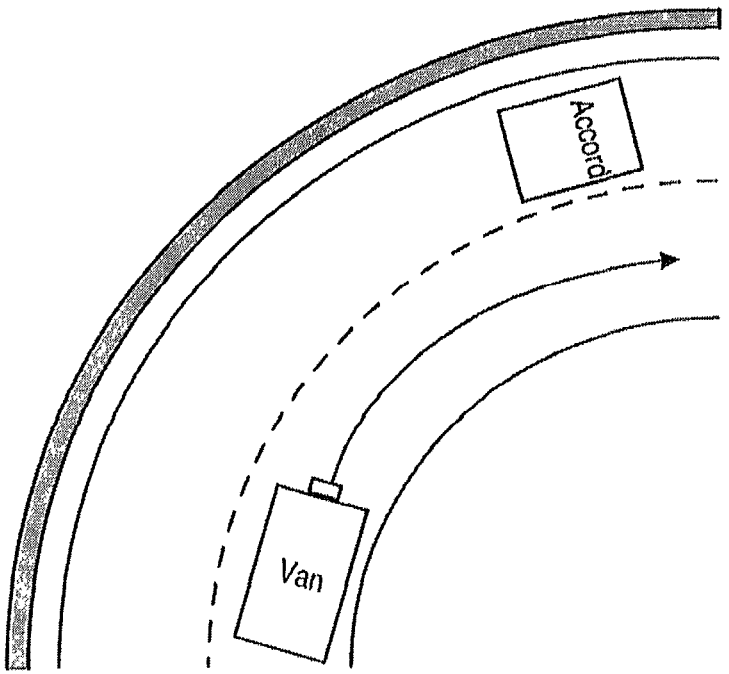

19:02:41 -Begin File

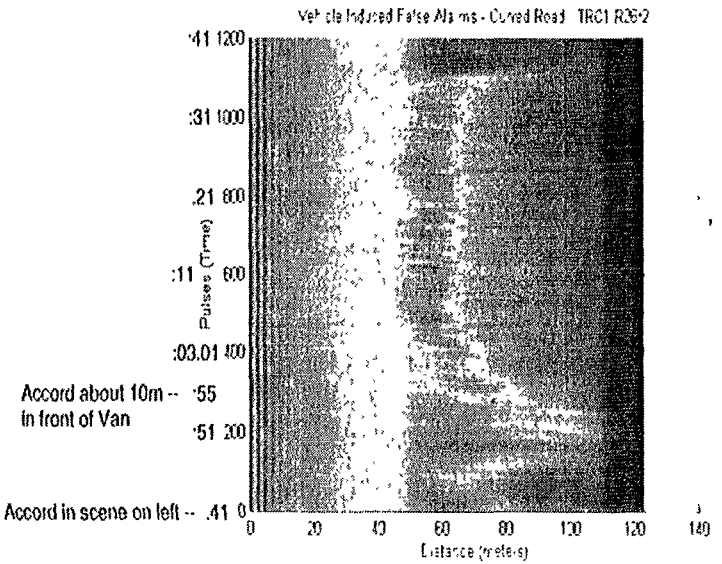

Accord about 10m -- in front of Van

Accord in scene on left --

6.10 Vehicle Induced False Alarms - Curved Roadways

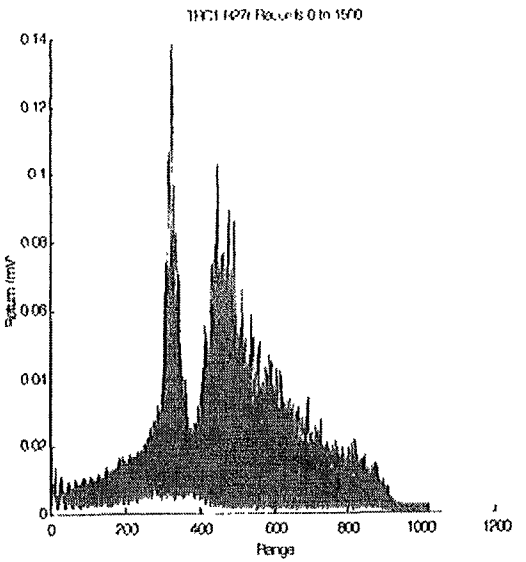

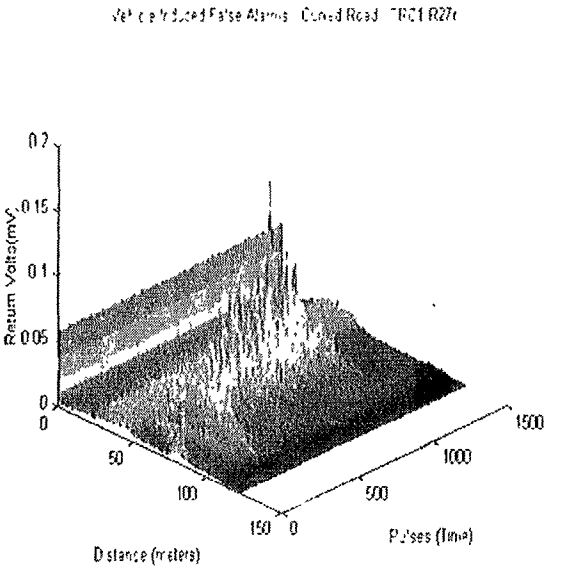

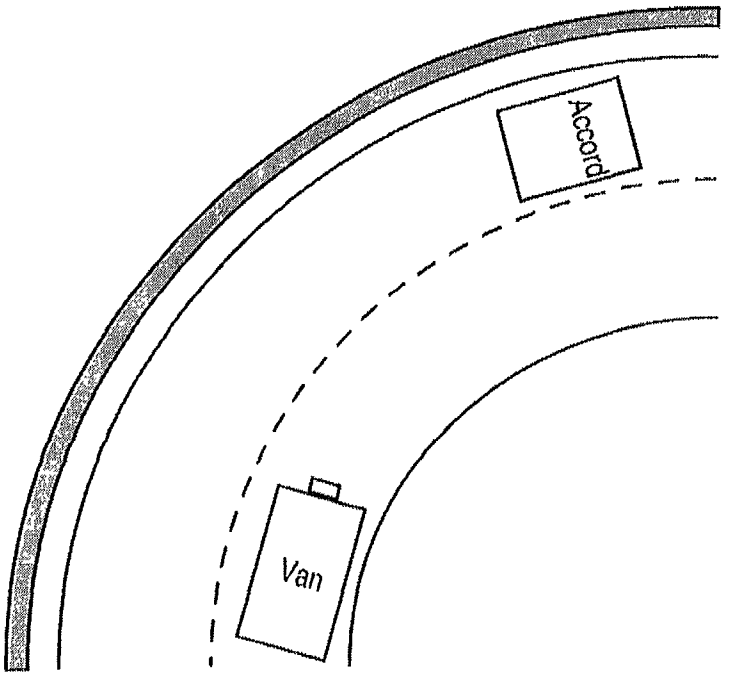

19:06:40 - Begin File

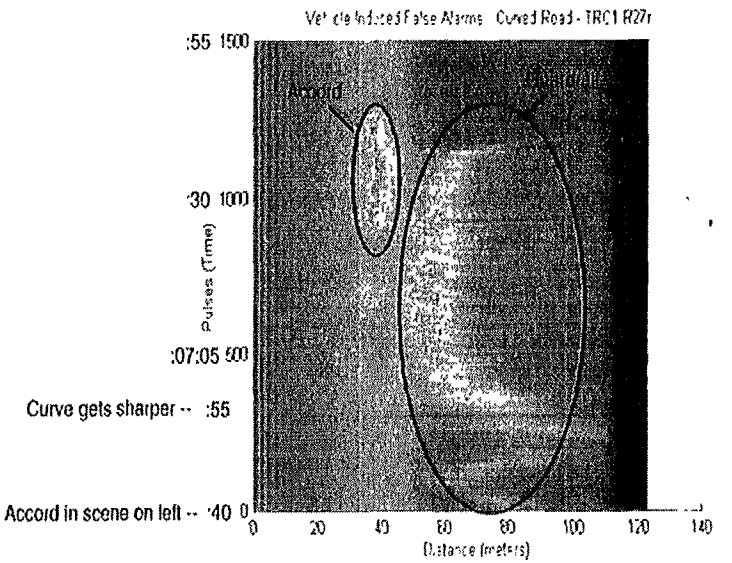

6.10 Vehicle Induced False Alarms - Curved Roadways

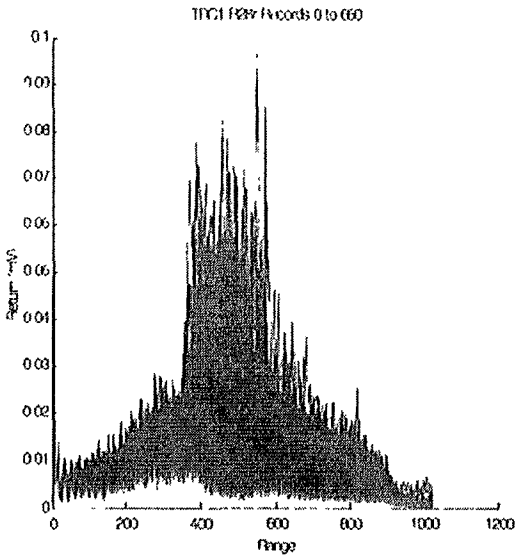

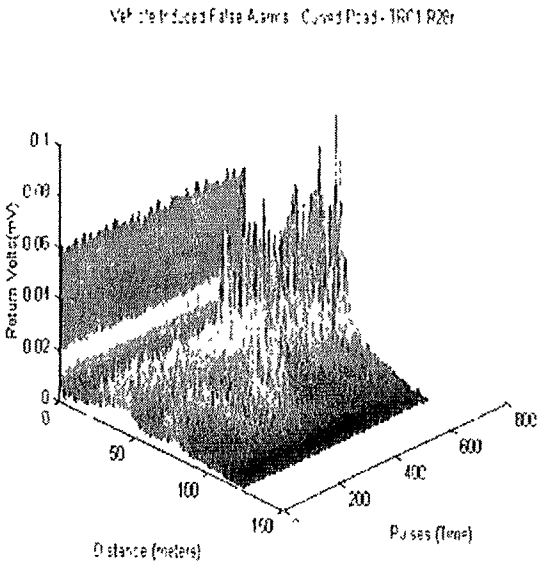

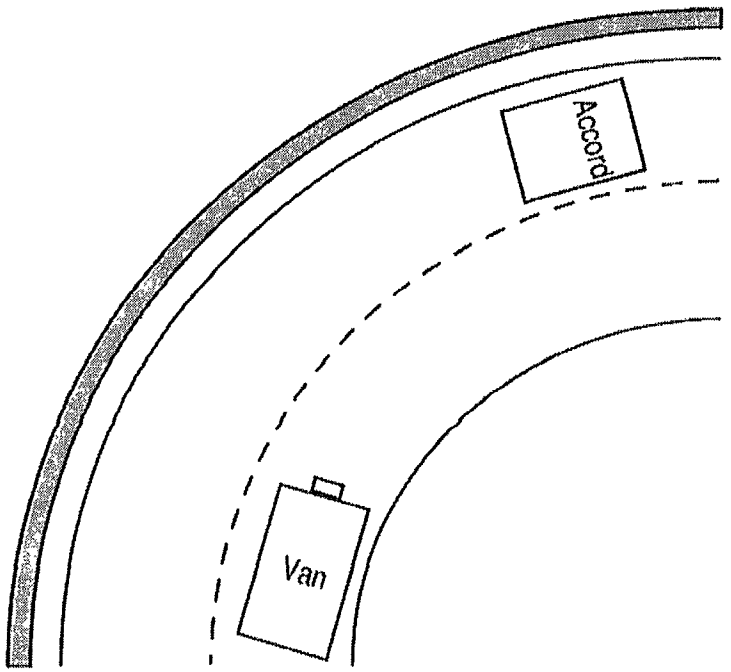

19:13:06 - Begin File

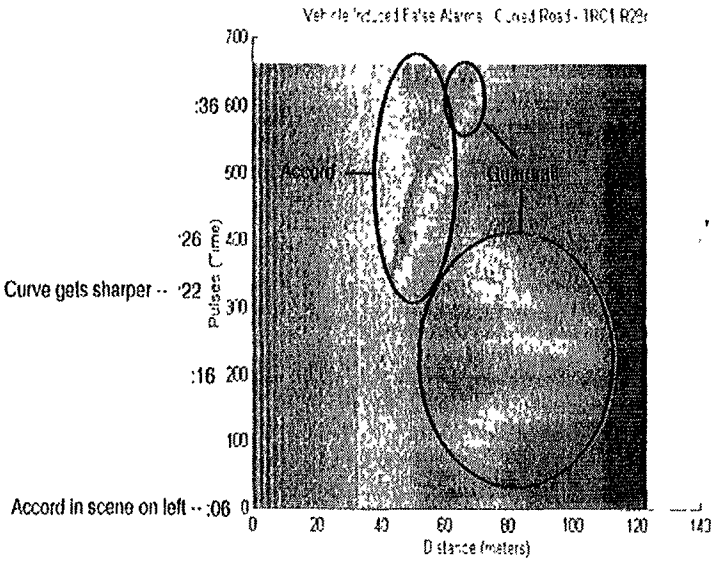

6.10 Vehicle Induced False Alarms - Curved Roads

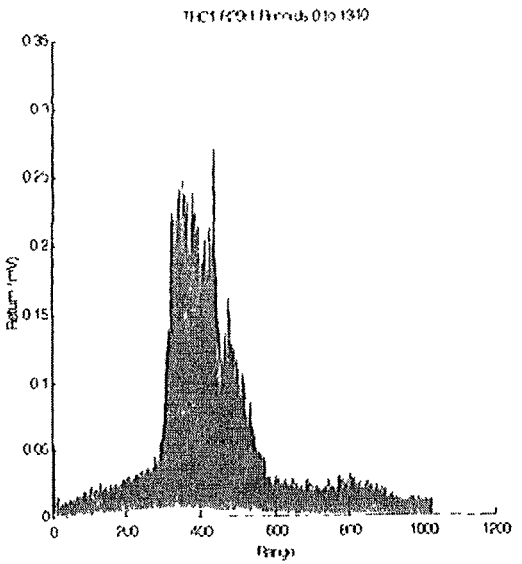

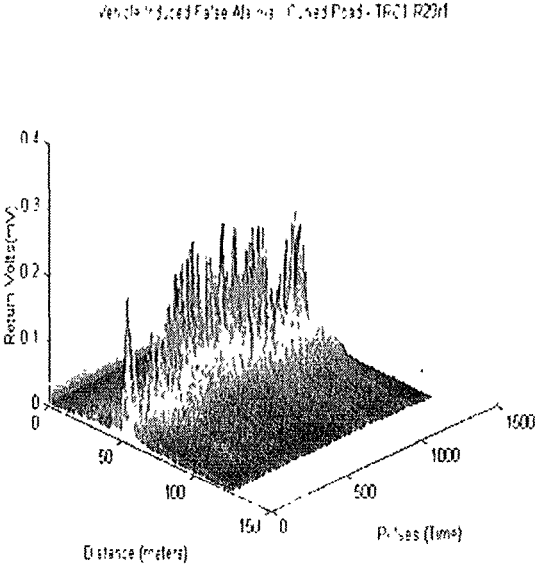

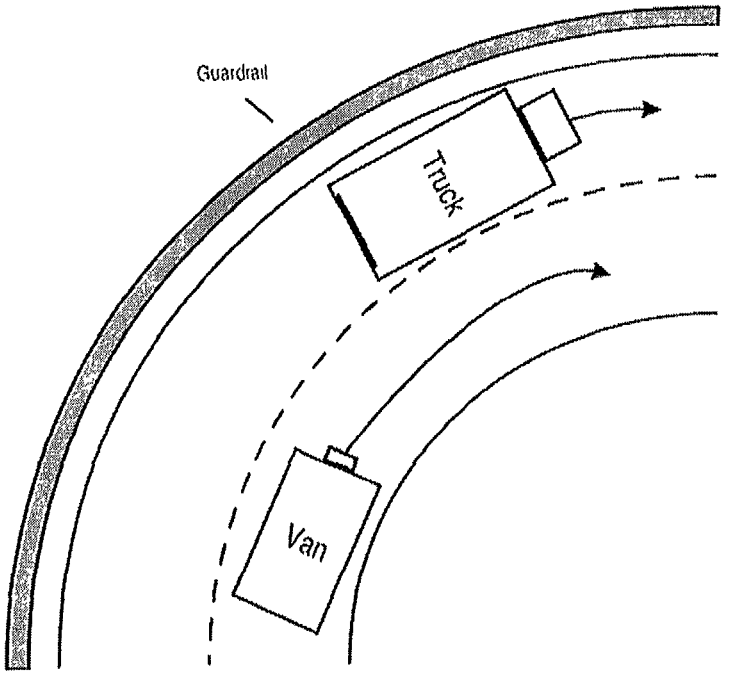

14:18:11 - Begin File

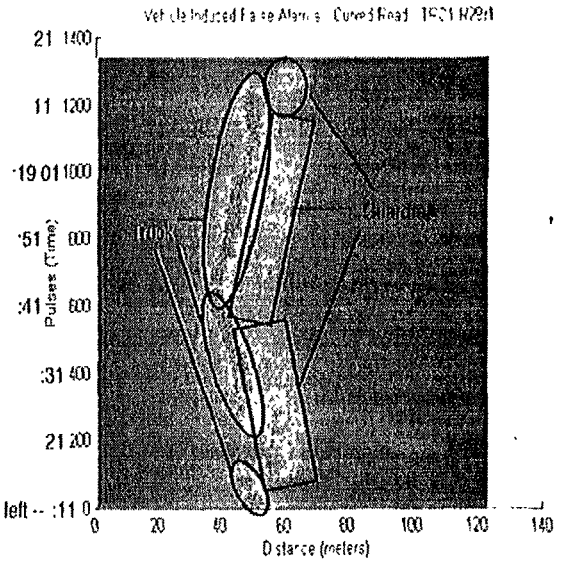

6.10 Vehicle Induced False Alarms - Curved Roads

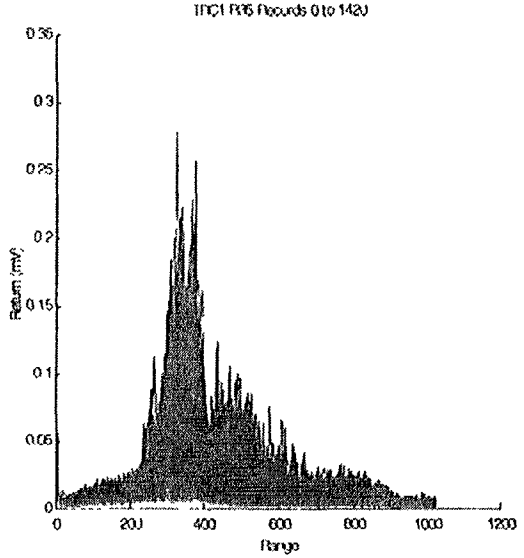

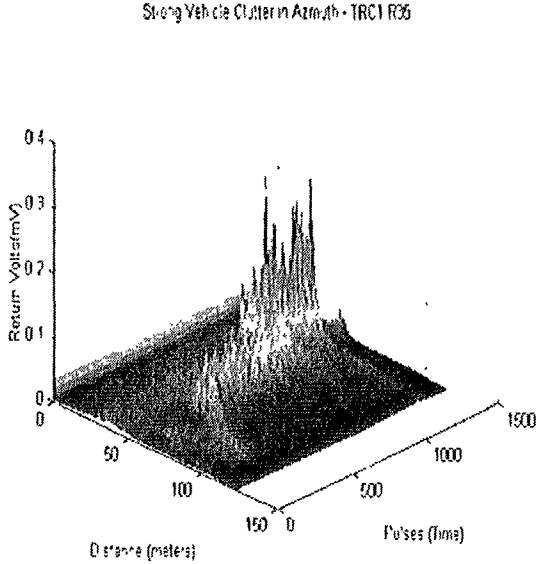

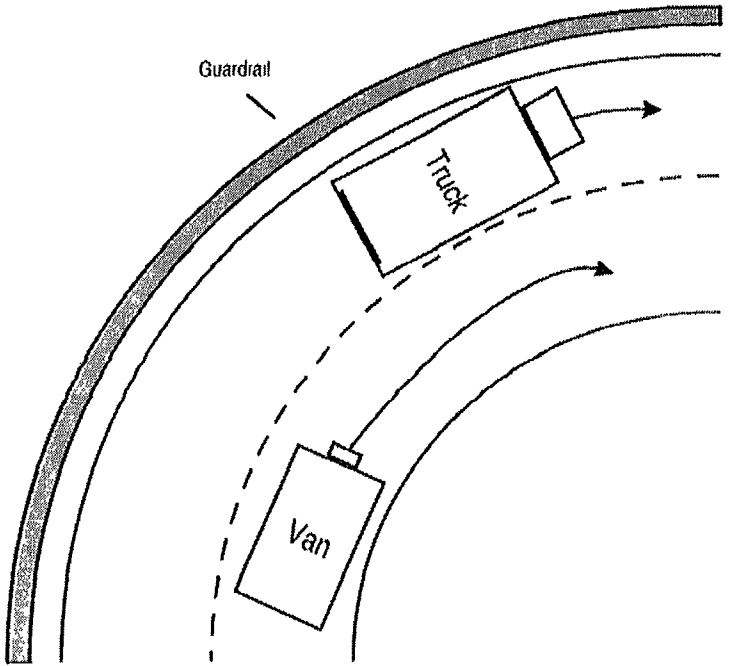

14:11:48 - Begin File

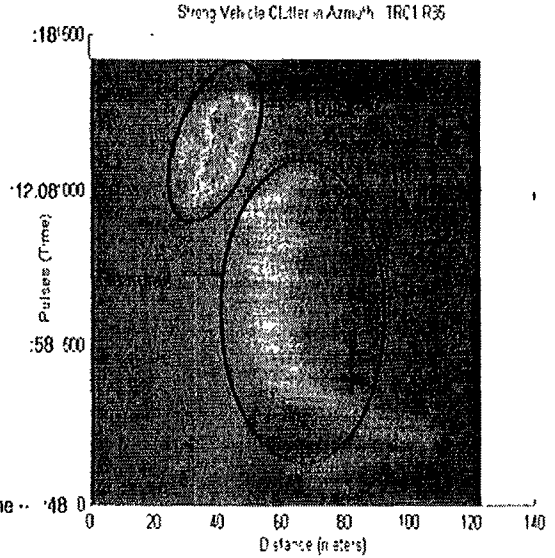

Truck in scene in left lane

6.10 Vehicle Induced False Alarms - Curved Roads

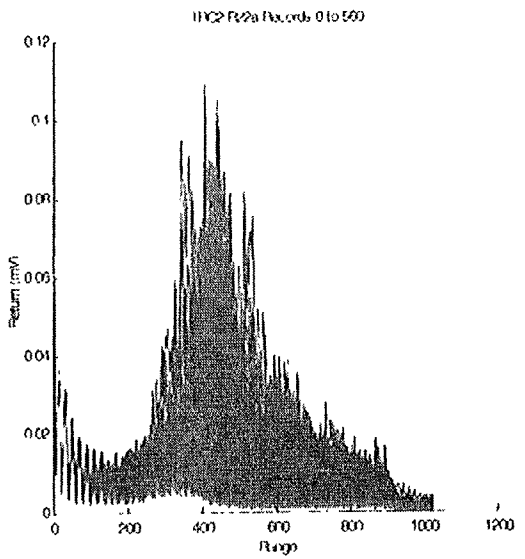

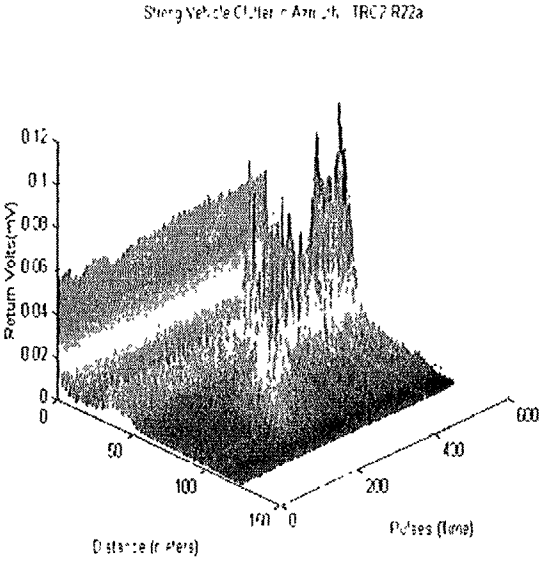

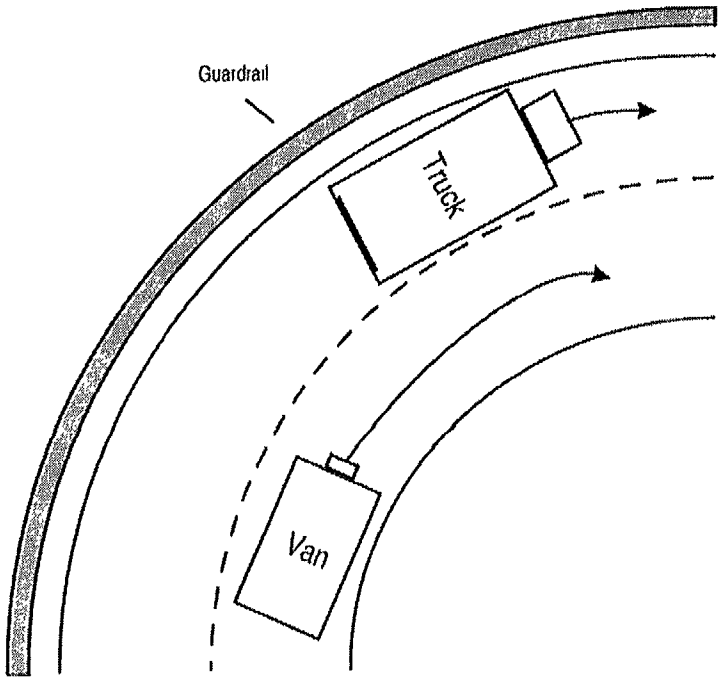

14:11:48 - Begin File

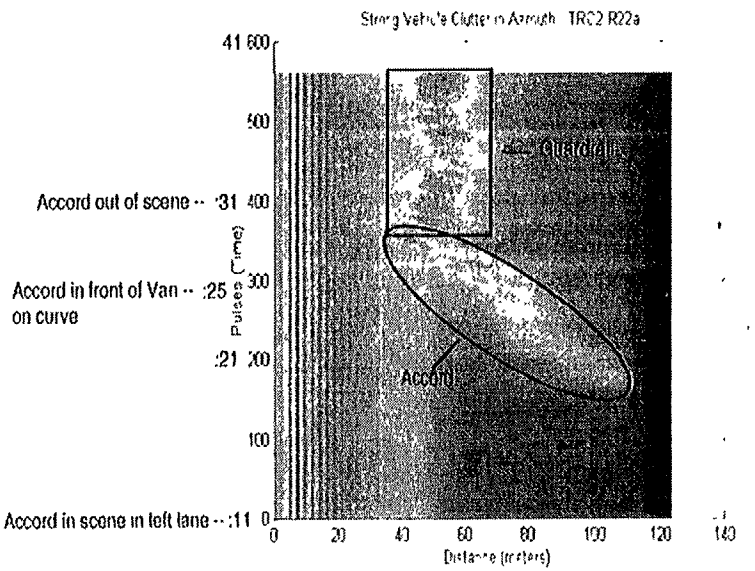

6.10 Vehicle Induced False Alarms - Curved Roads

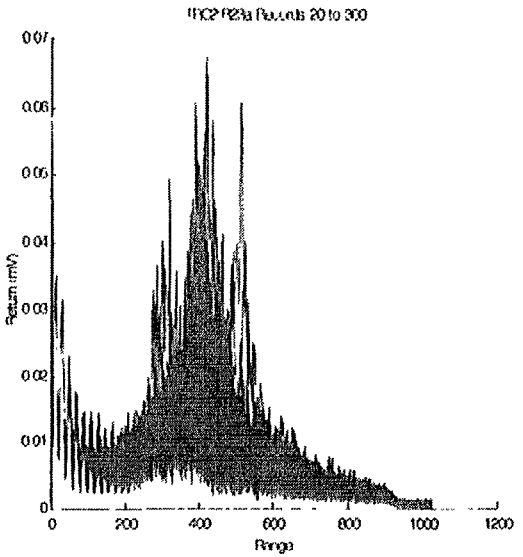

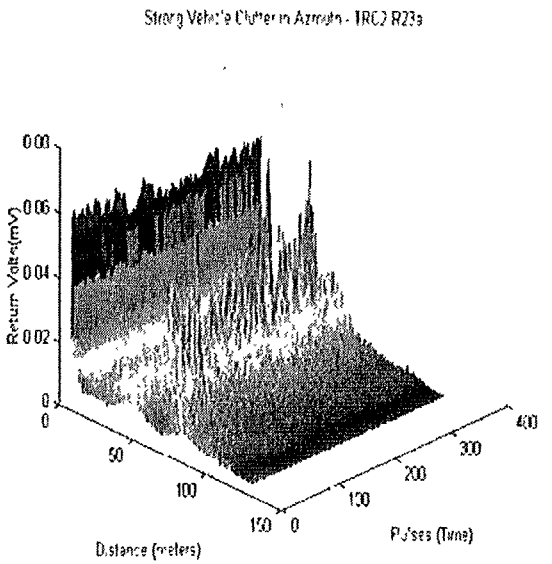

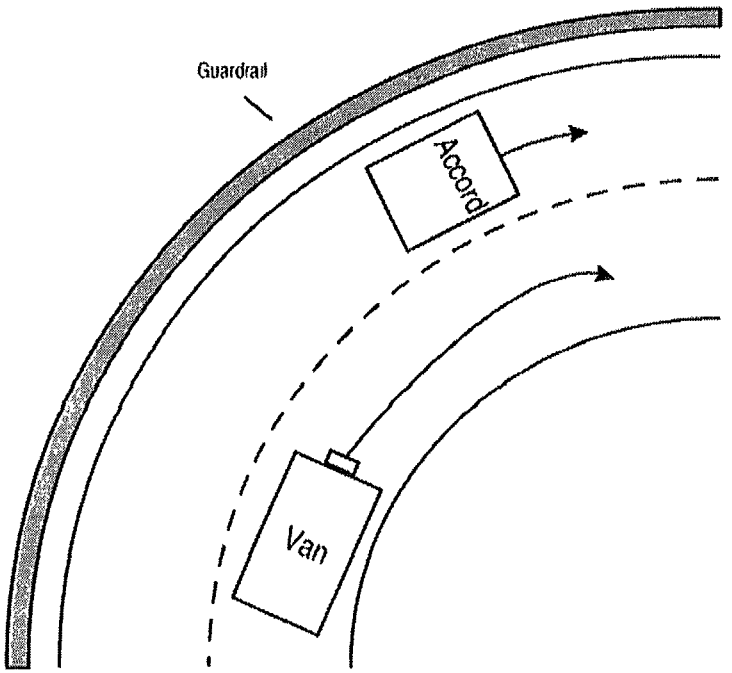

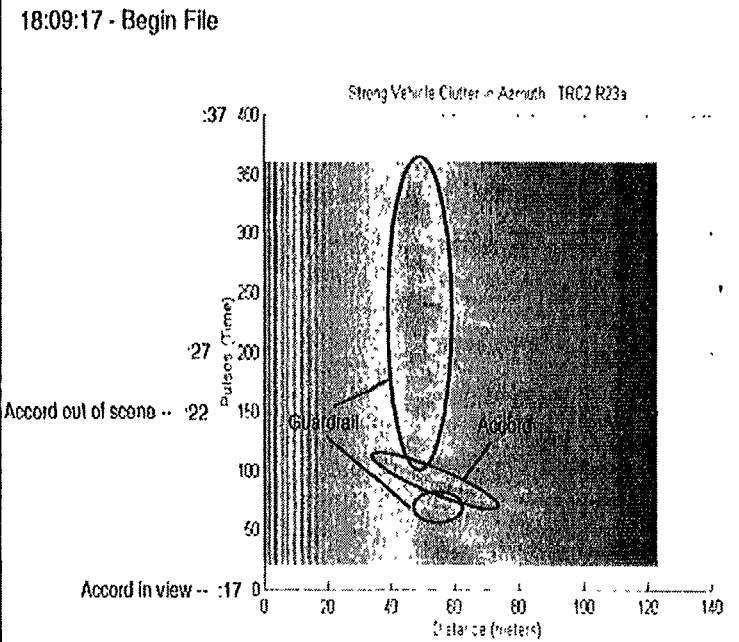

6.10 Vehicle Induced False Alarms - Curved Roads

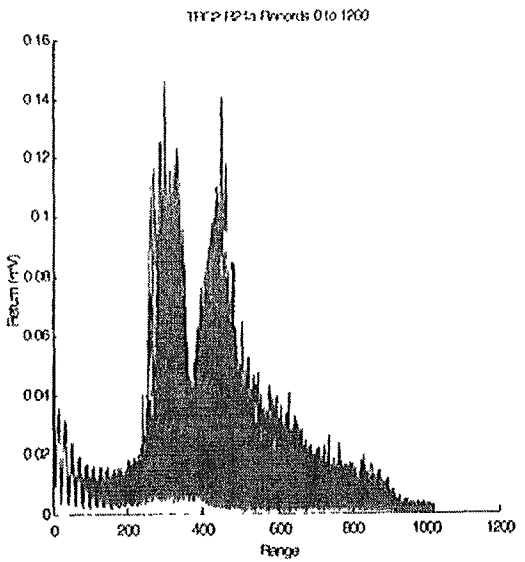

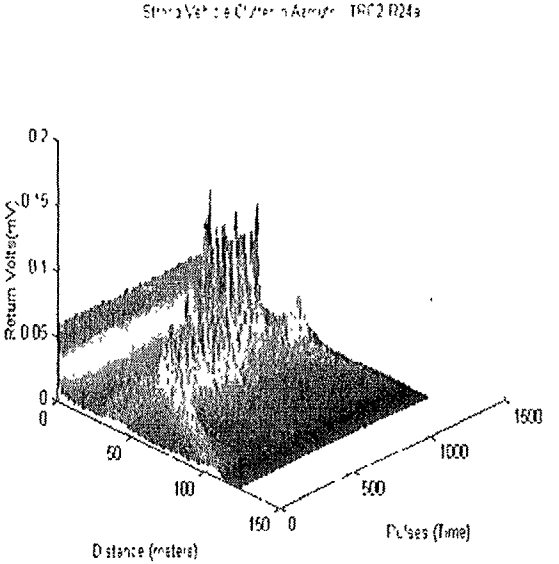

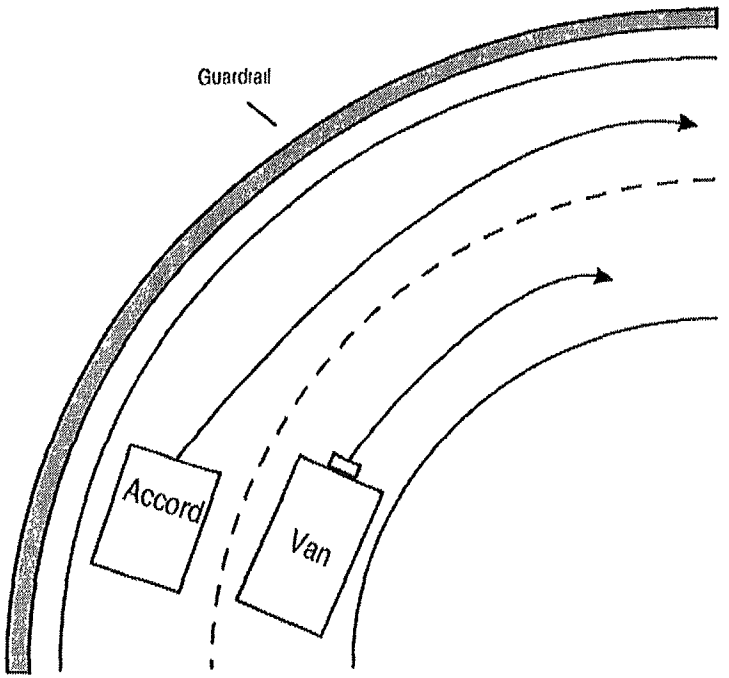

18:31:20 - Begin File

Accord enters scene --

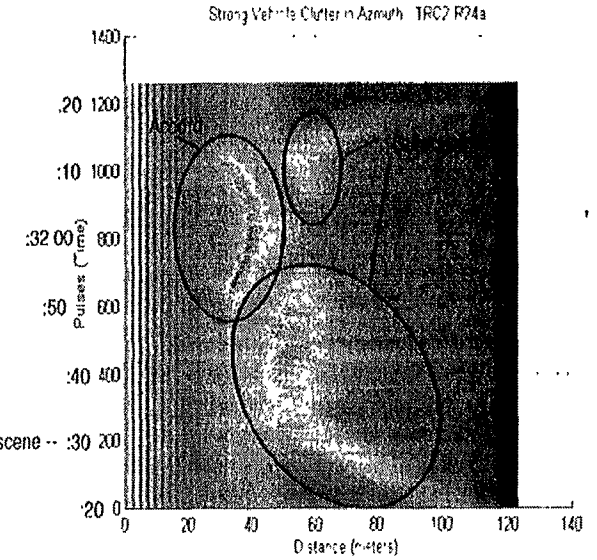

6.10 Vehicle Induced False Alarms - Curved Roads

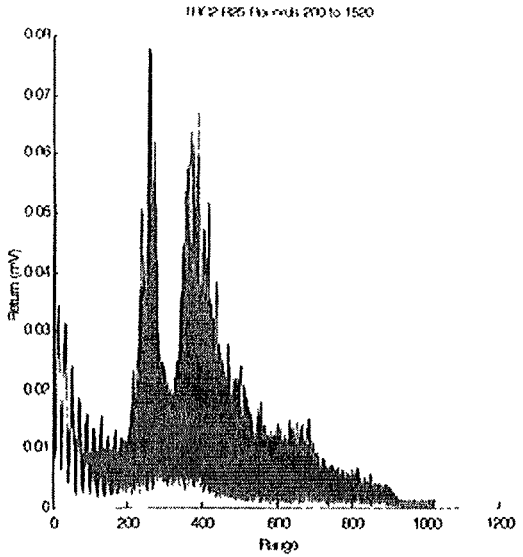

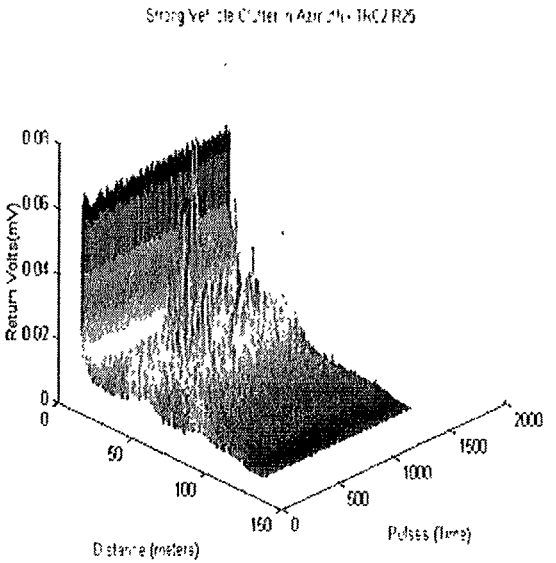

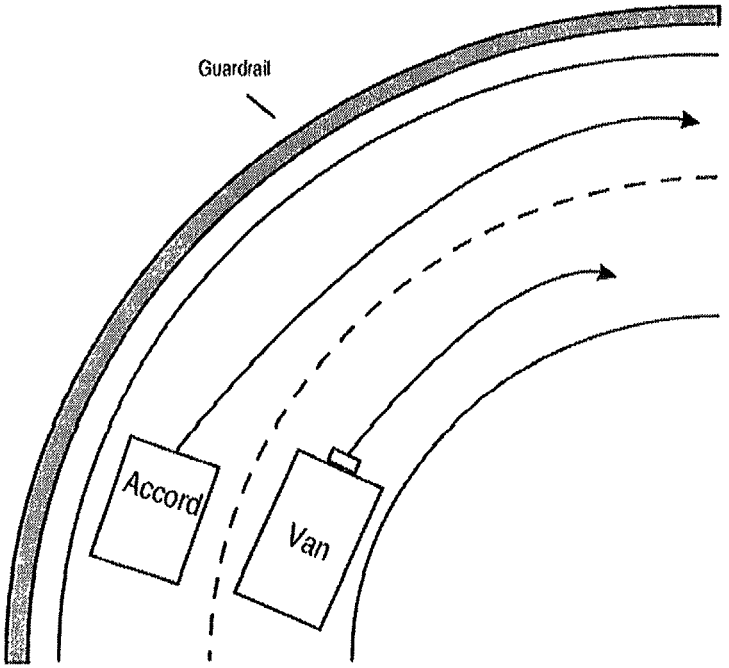

18:44:25 - Begin File

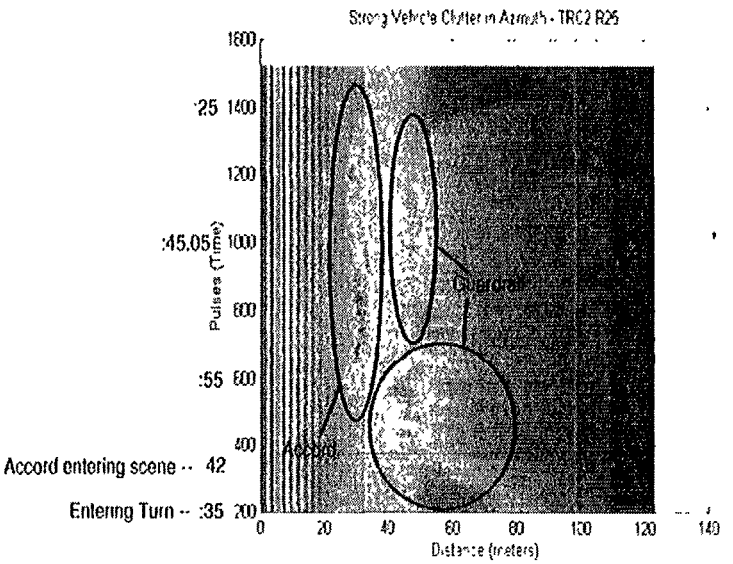

6.10 Vehicle Induced False Alarms - Curved Roads

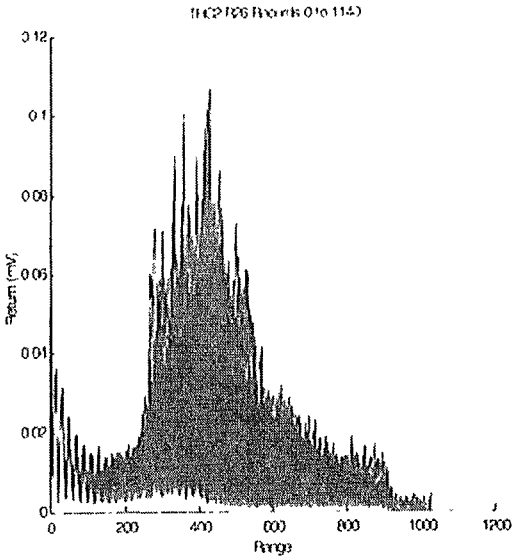

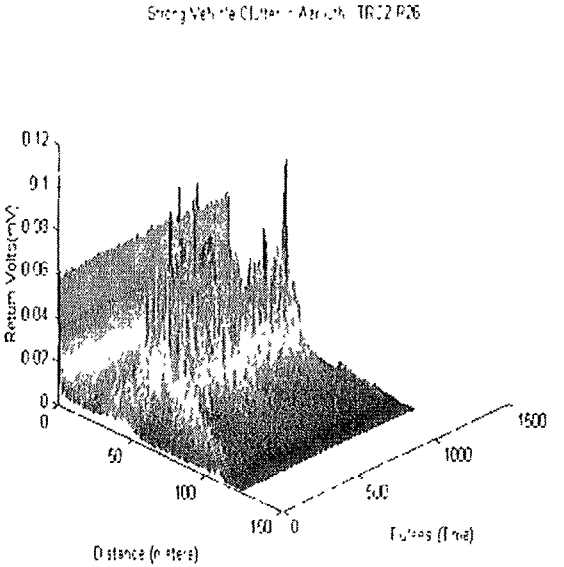

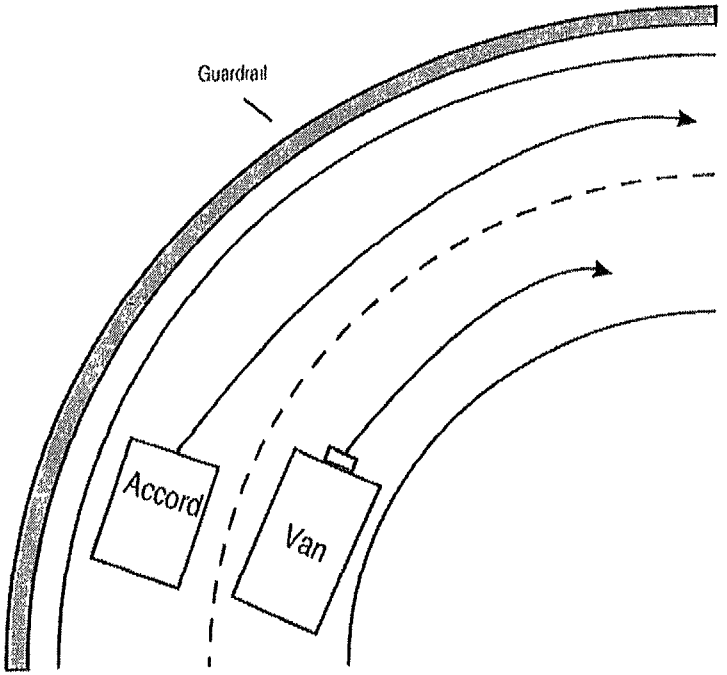

18:37:07 - Begin File

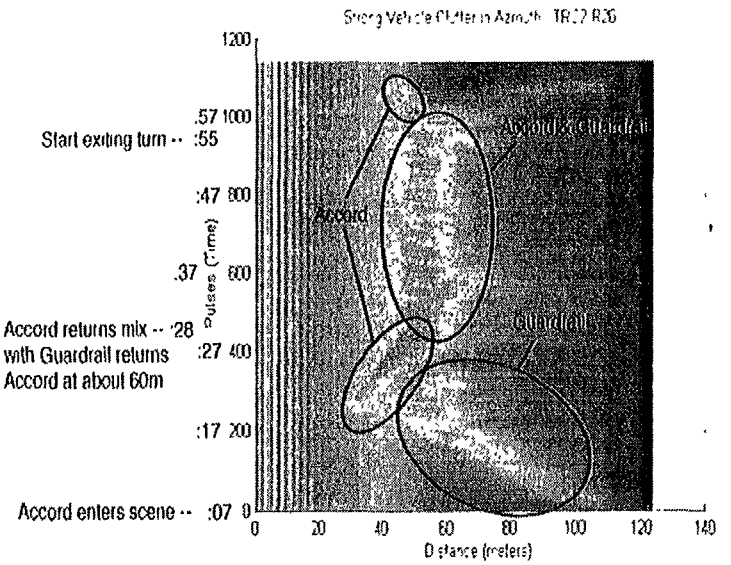

6.10 Vehicle Induced False Alarms - Curved Roads

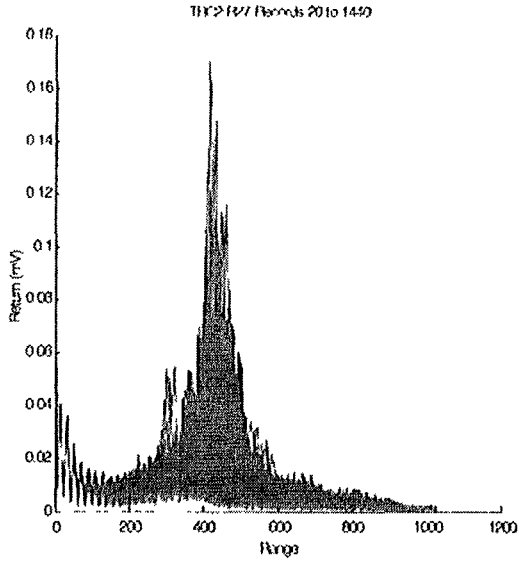

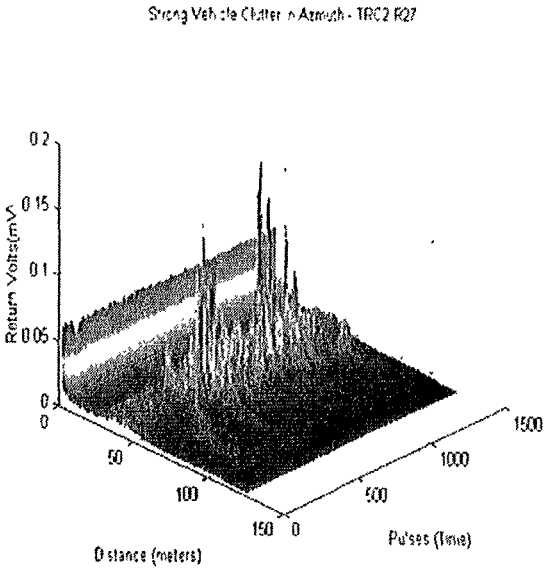

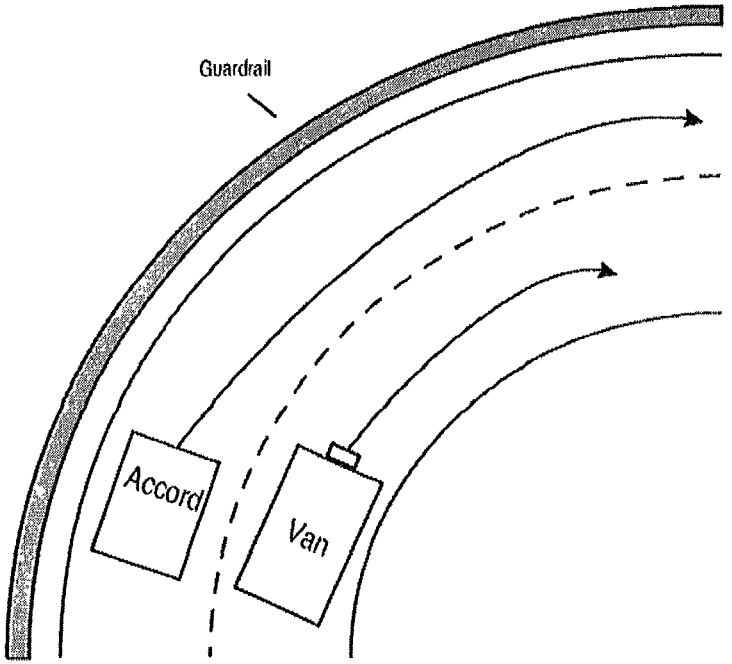

18:50:39 - Begin File

Accord enters scene -- :48

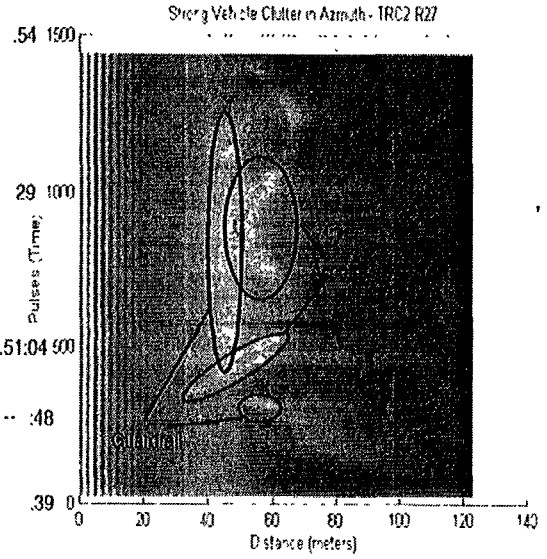

6.11 Tracking Through A Curve

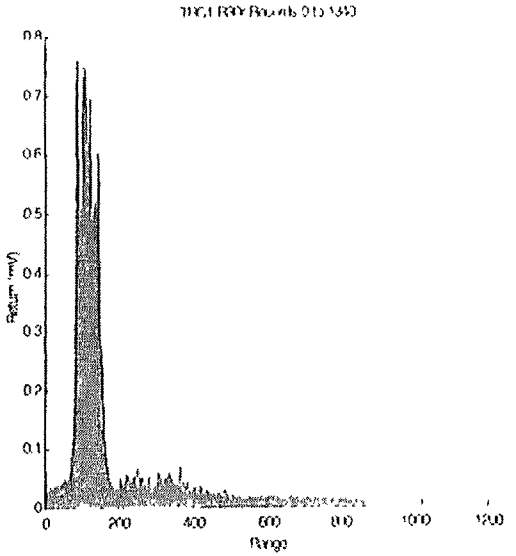

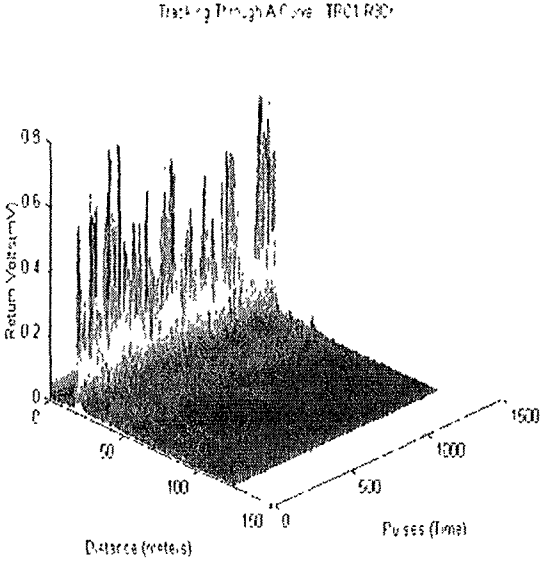

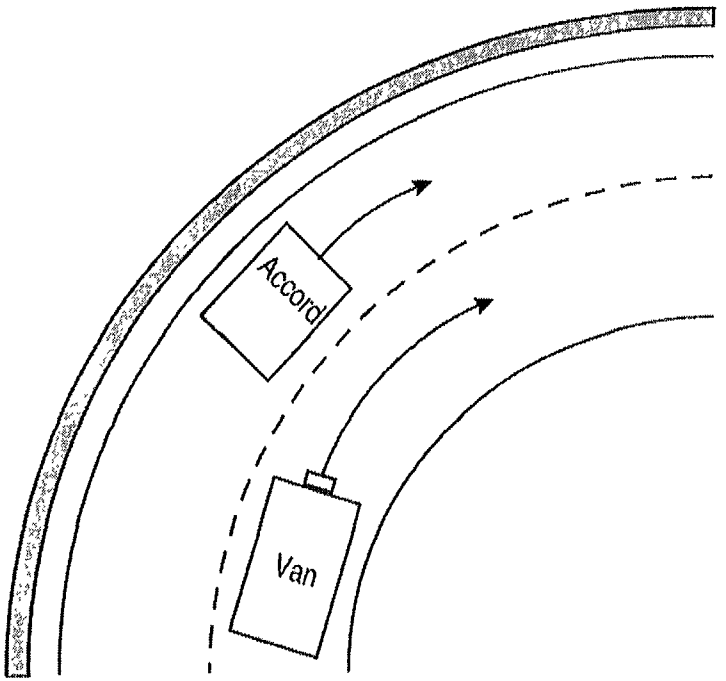

19:16:56 - Begin File

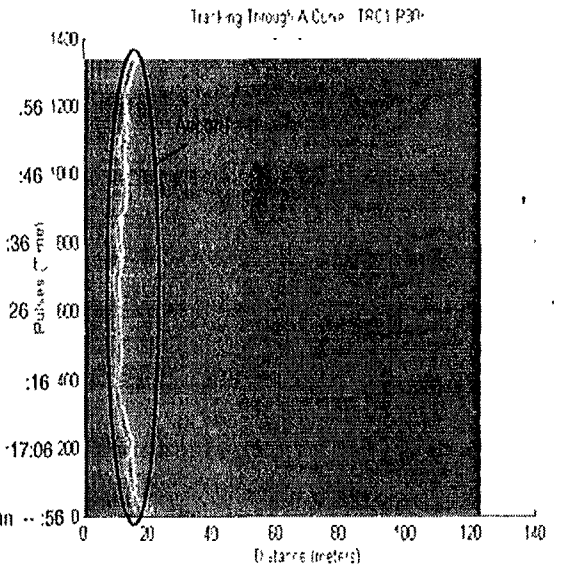

Accord 10m in front of Van -- :56

6.11 Tracking Through A Curve

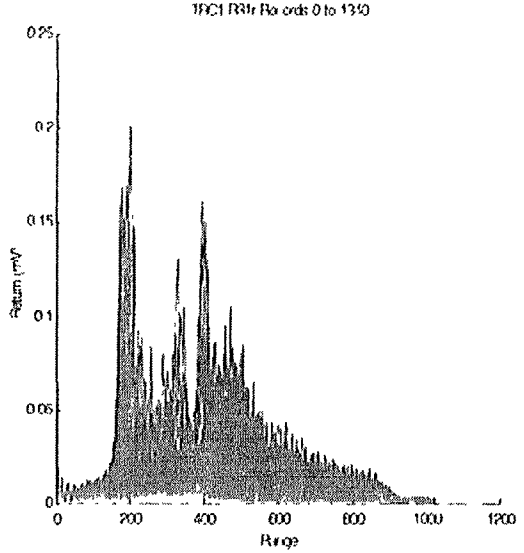

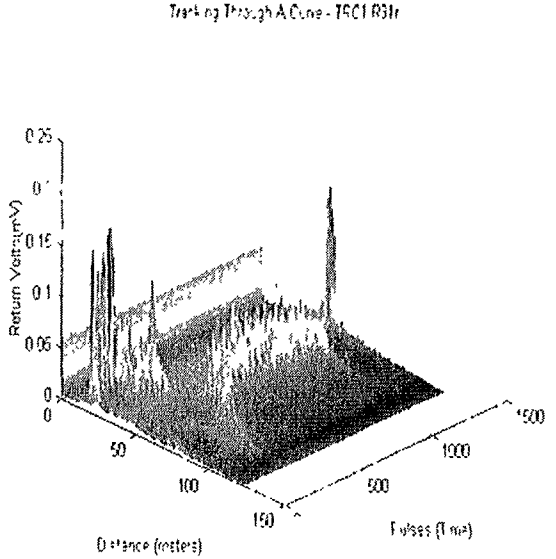

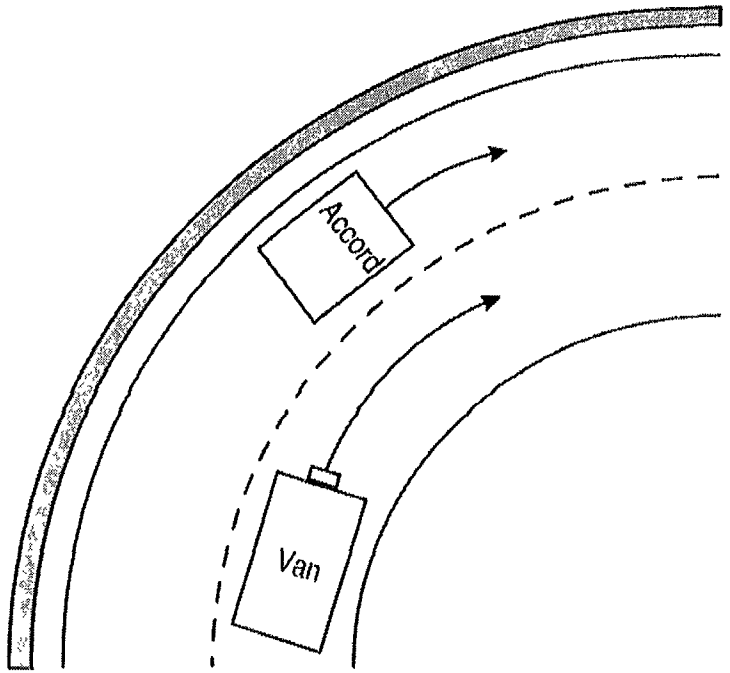

19:20:12 - Begin File

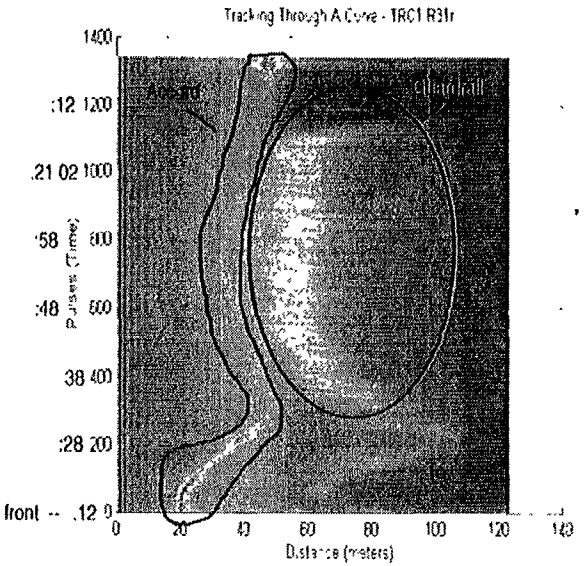

Accord 40m in front of Van

6.11 Tracking Through A Curve

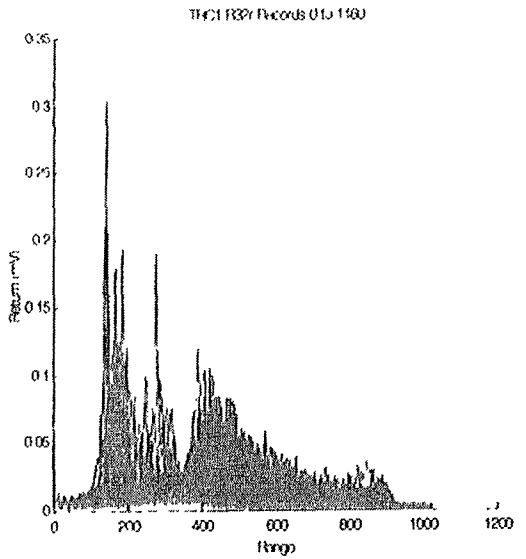

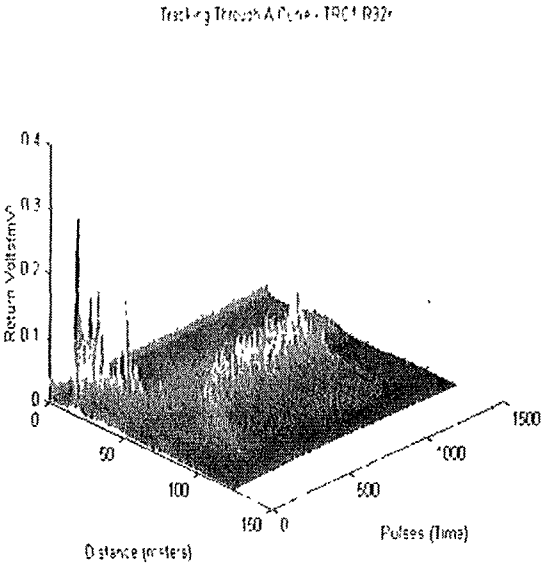

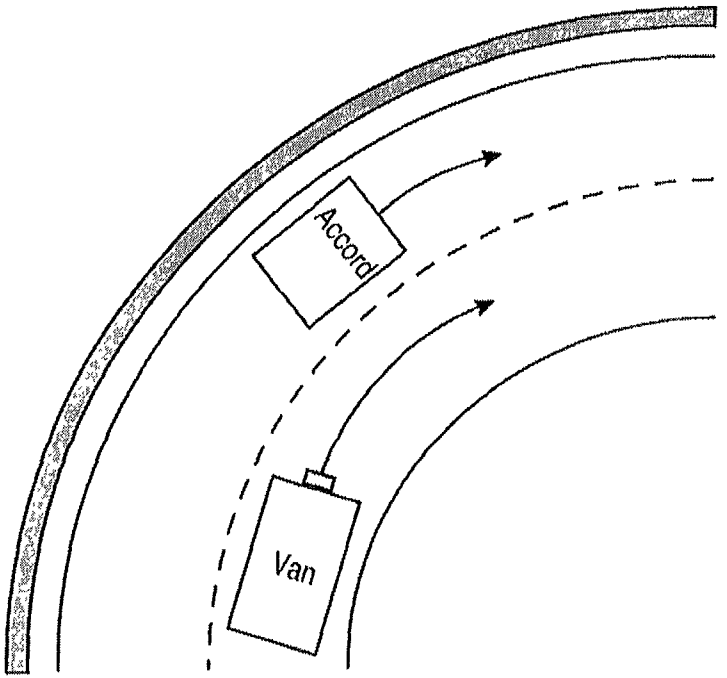

19:23:16 - Begin File

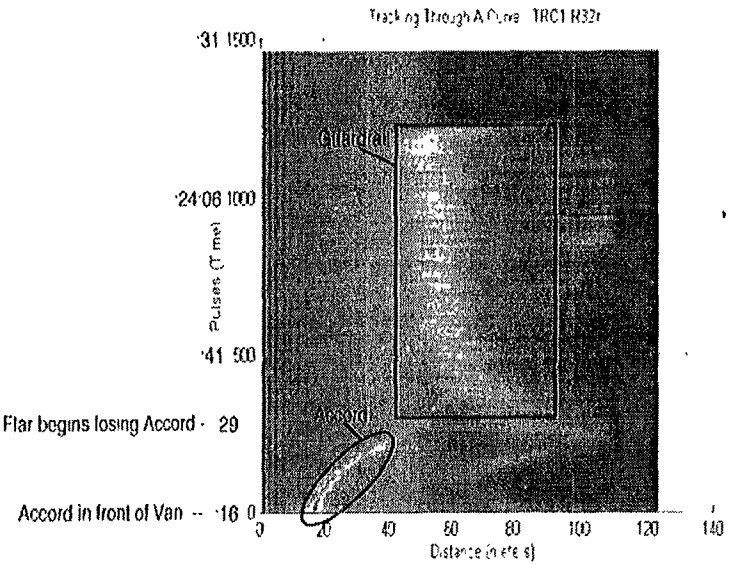

6.12 Vehicle Clutter in Azmuth - Curved Roadway

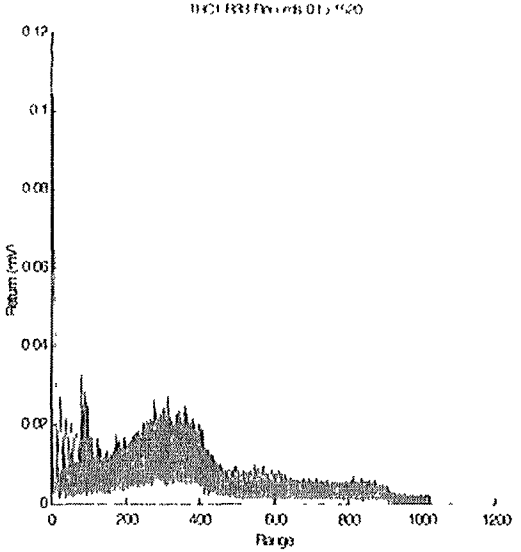

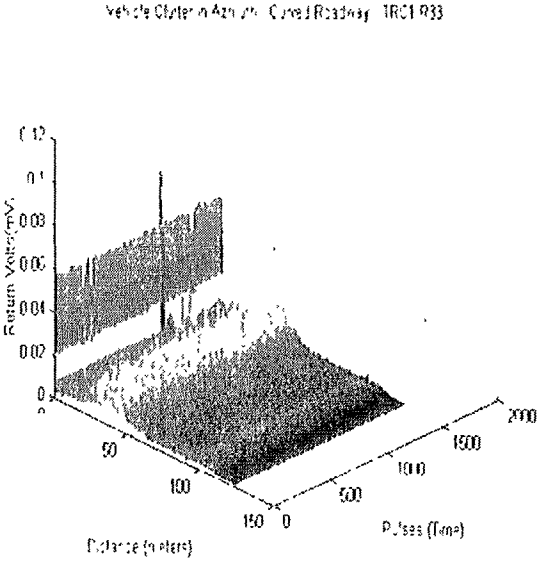

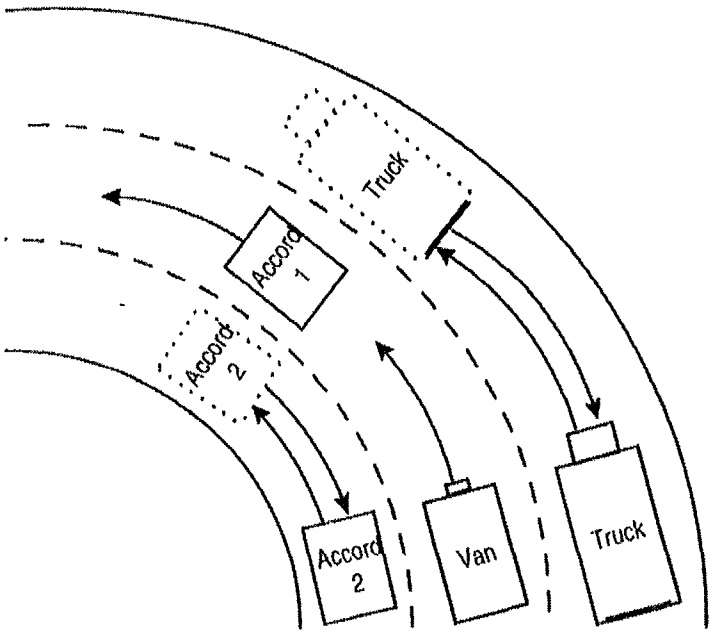

11:13:13 - Begin File

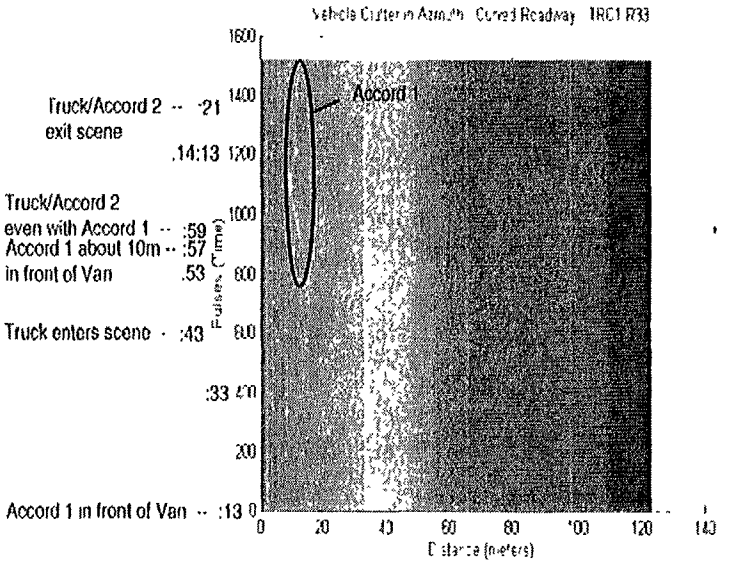

6.12 Vehicle Clutter in Azmuth - Curved Roadway

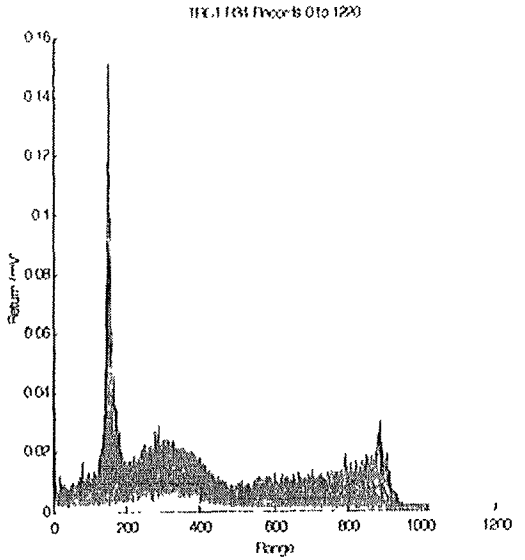

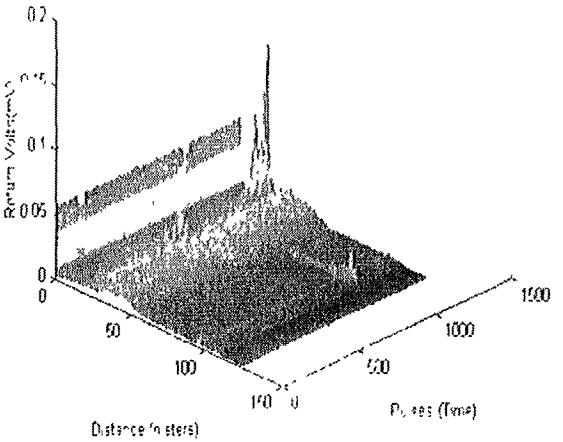

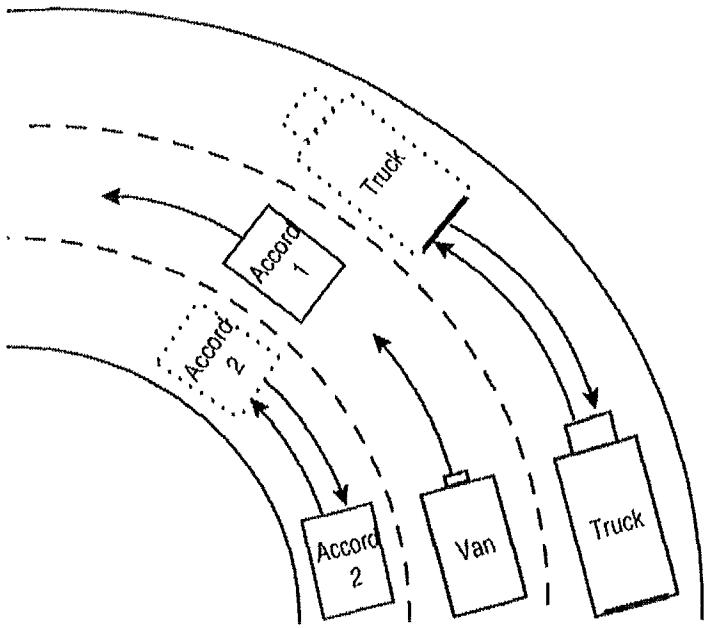

12:10:50 - Begin File

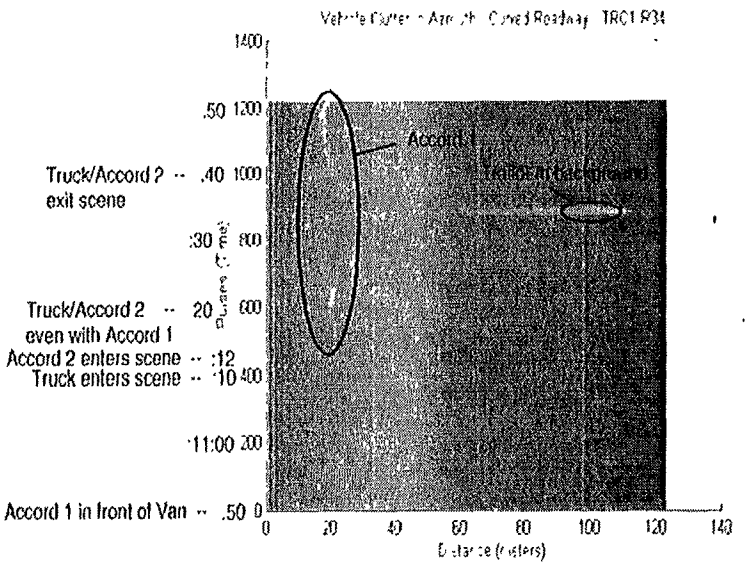

6.12 Vehicle Clutter in Azmuth - Curved Roadway

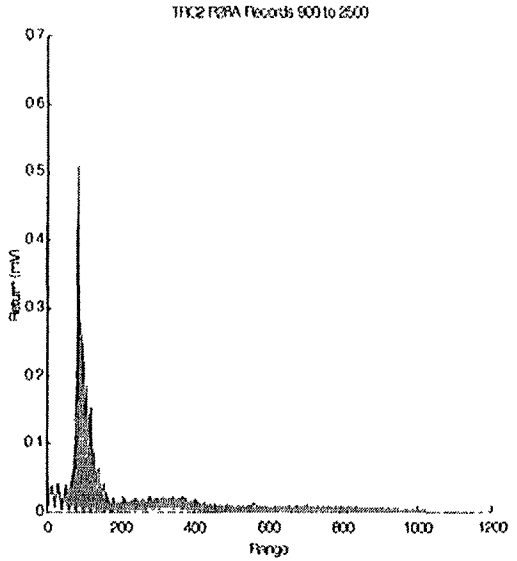

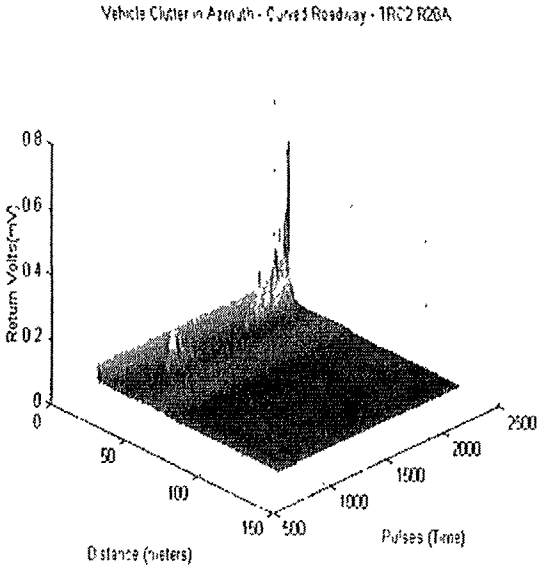

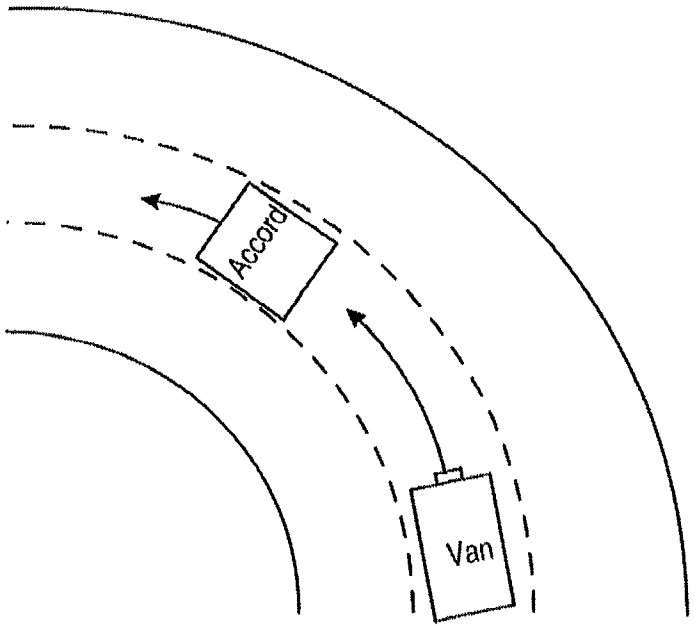

14:02:05 - Begin File

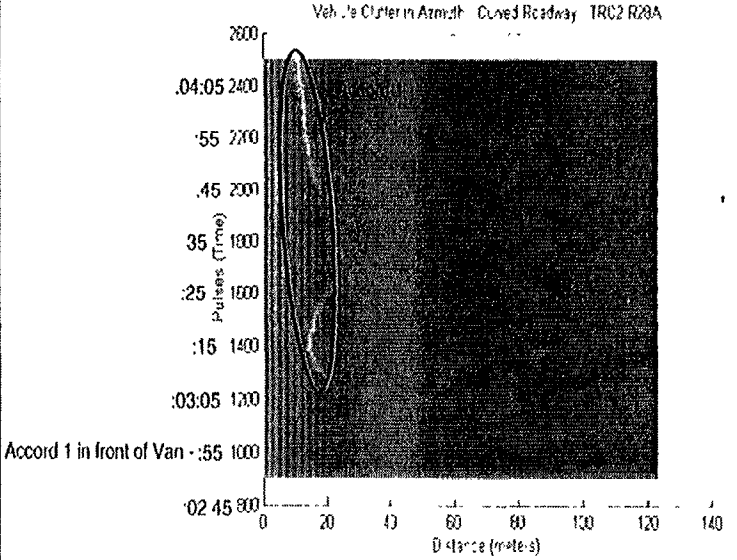

6.12 Vehicle Clutter in Azmuth - Curved Roadway

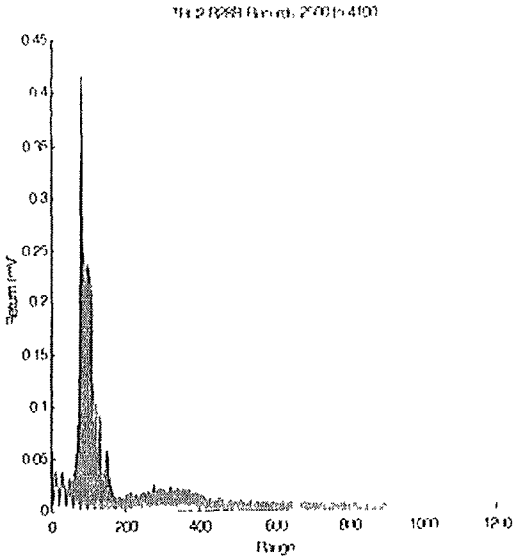

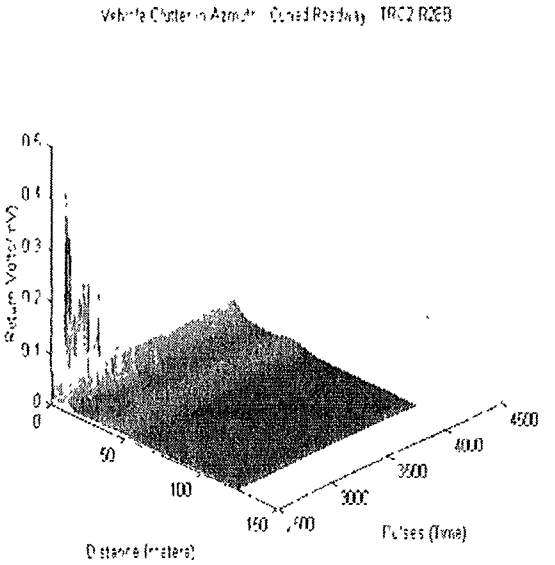

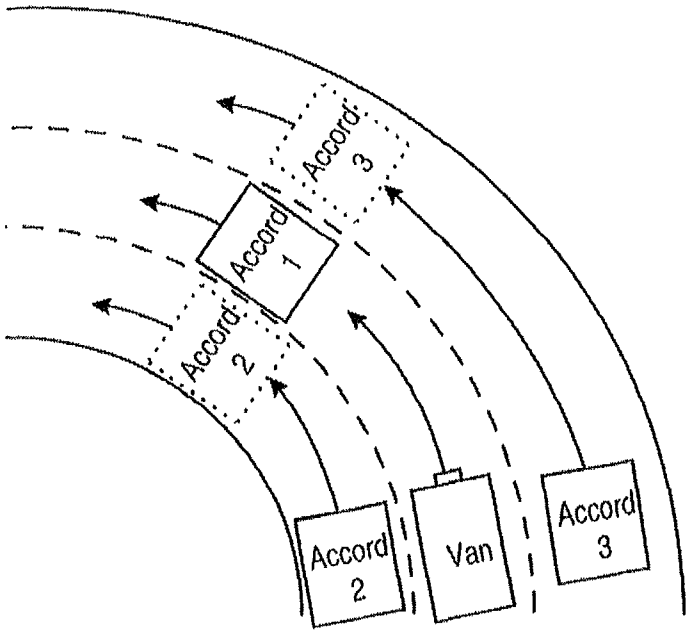

14:02:05 - Begin File

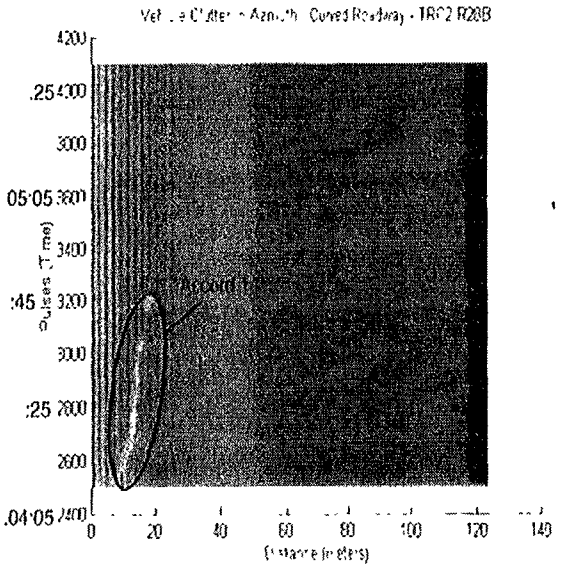

6.12 Vehicle-Clutter in Azmuth - Curved Roadway

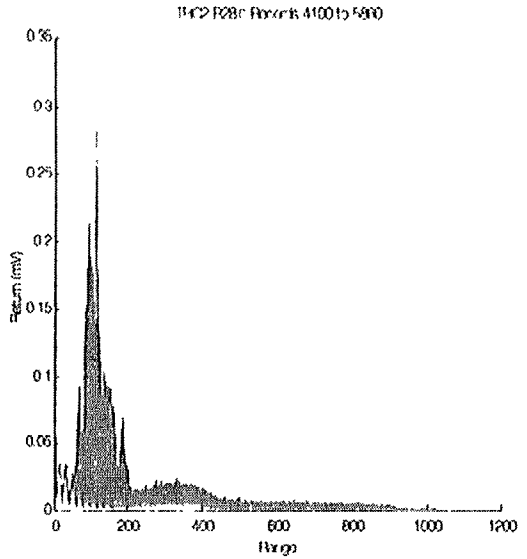

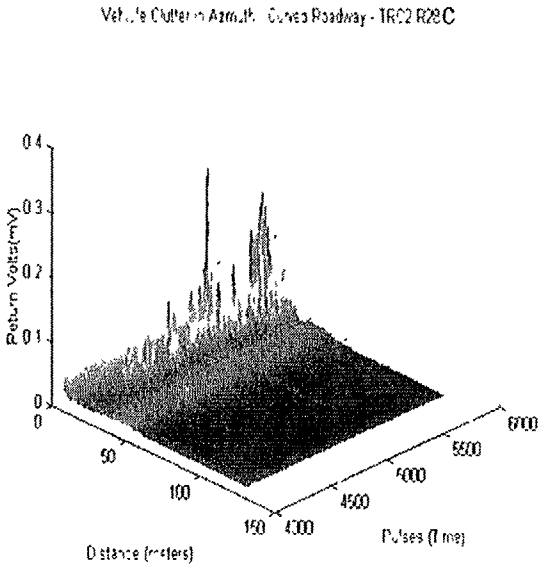

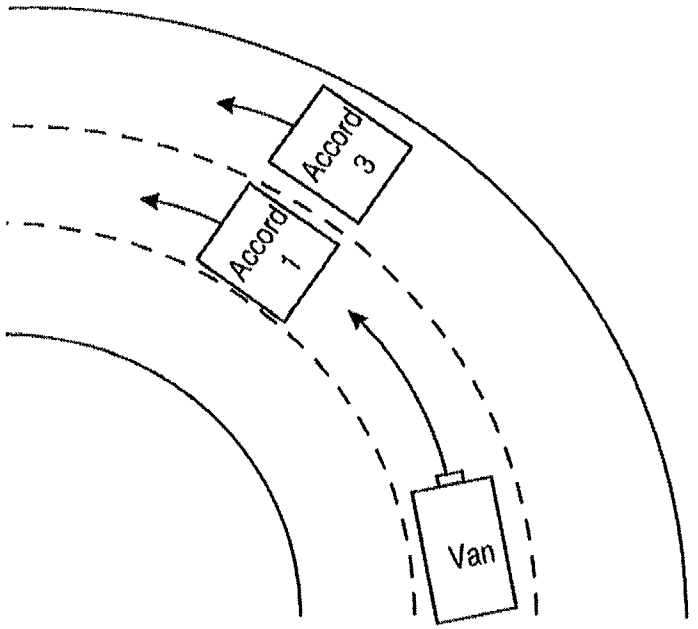

14:02:05 - Begin File

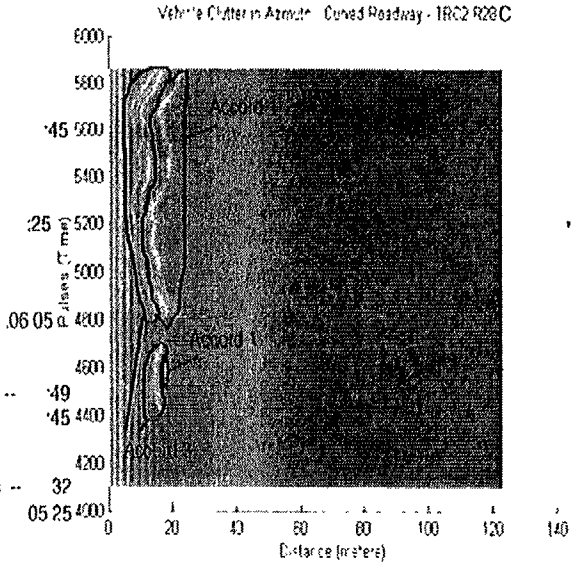

Accord 3 even with Accord 1

Accord 3 enters scene

6.12 Vehicle Clutter in Azmuth - Curved Roadway

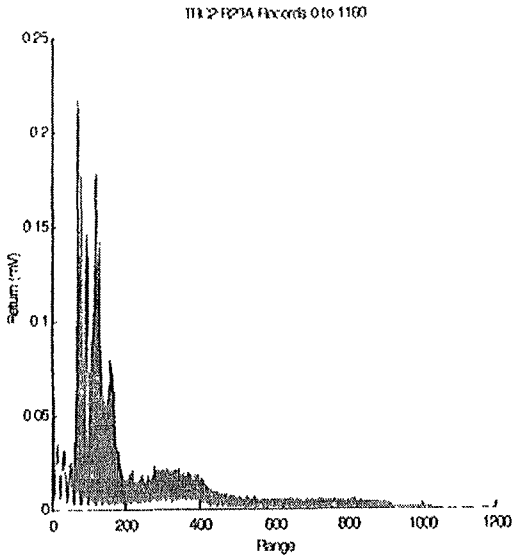

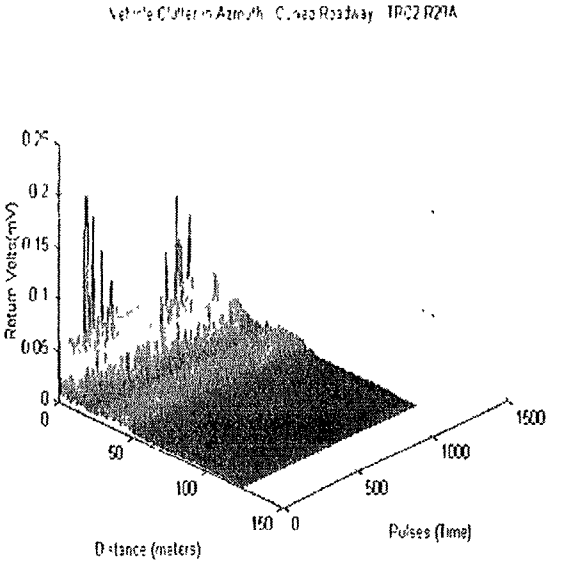

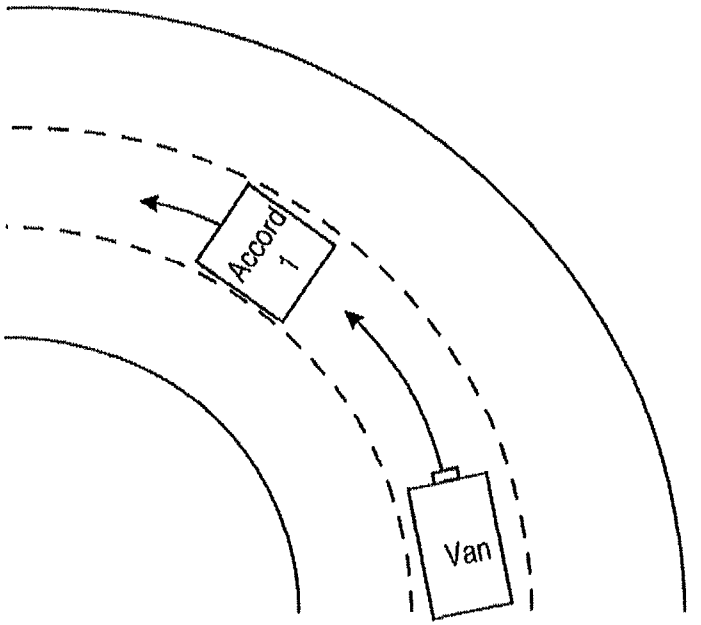

14:31:12 - Begin File

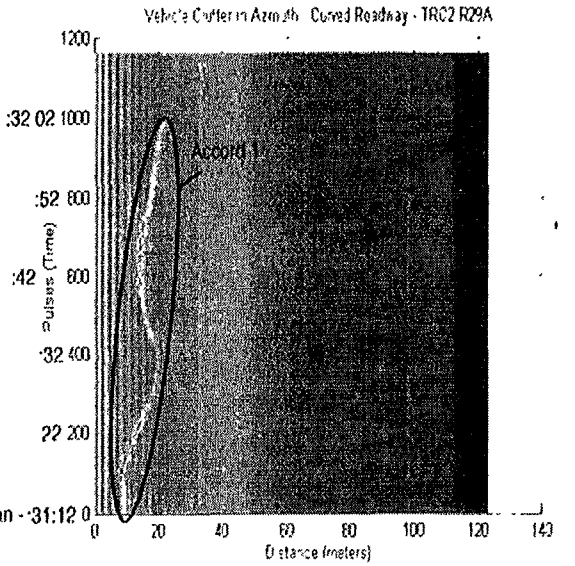

Accord 1 in front of Van - 31:12

6.12 Vehicle Clutter in Azmuth - Curved Roadway

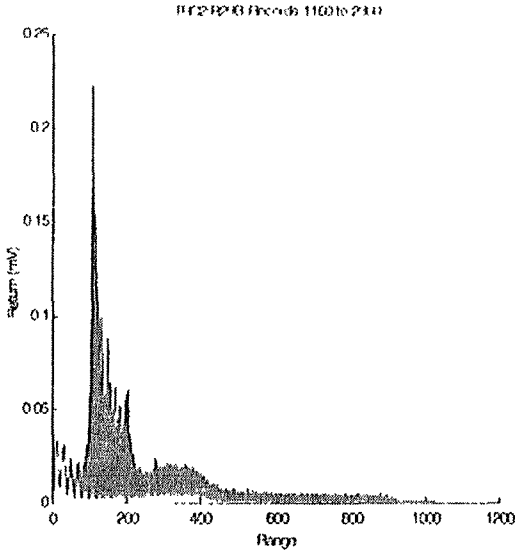

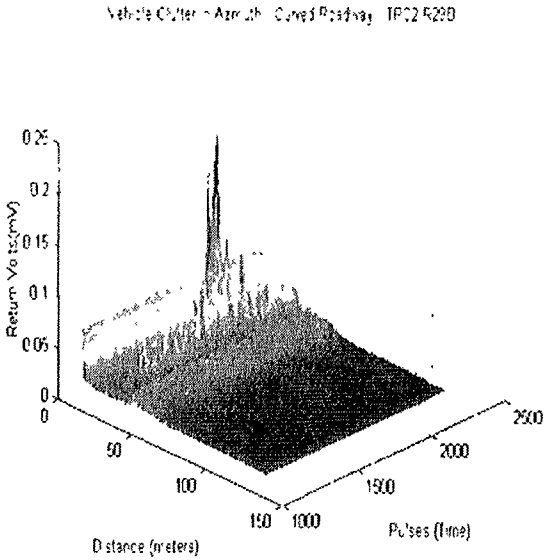

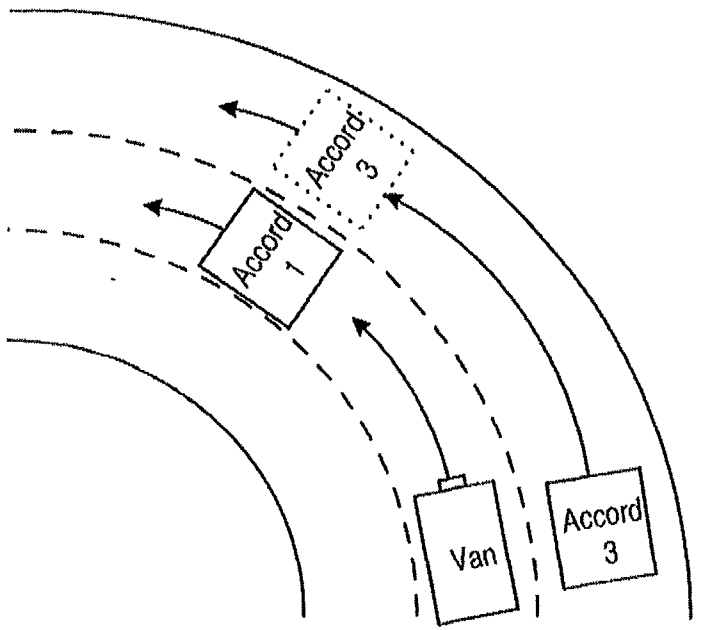

14:31:12 - Begin File

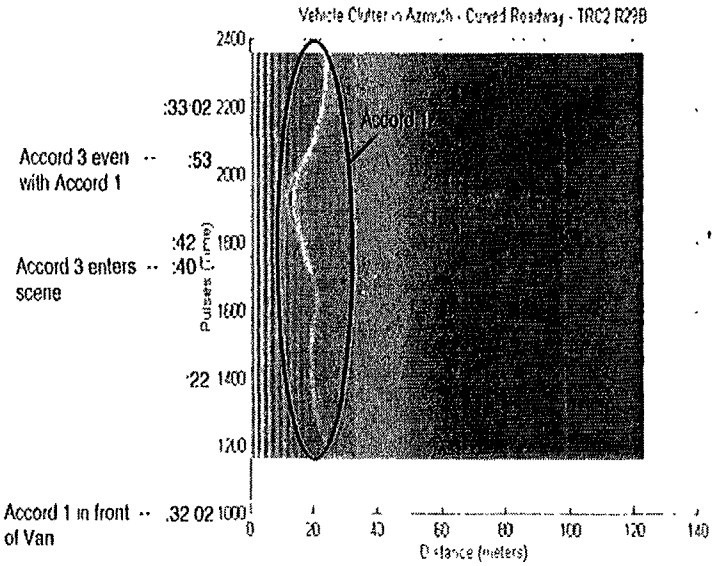

6.12 Vehicle Clutter in Azmuth - Curved Roadway

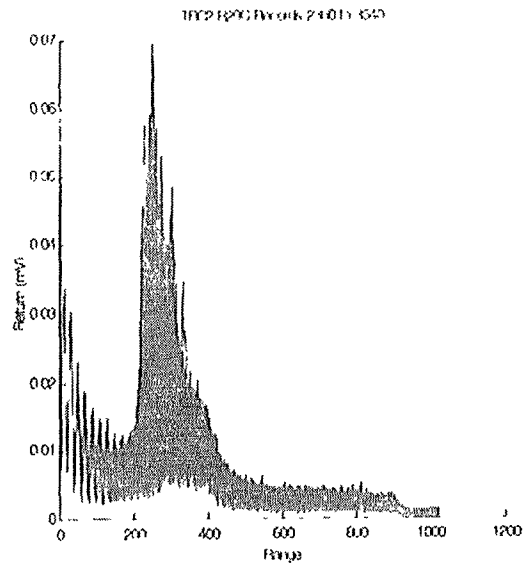

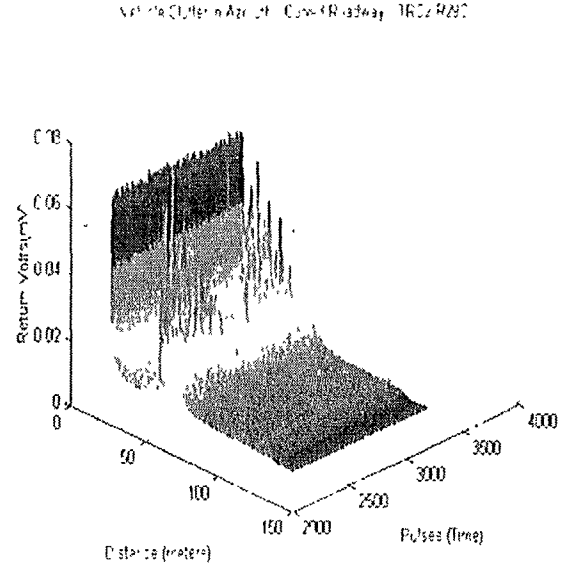

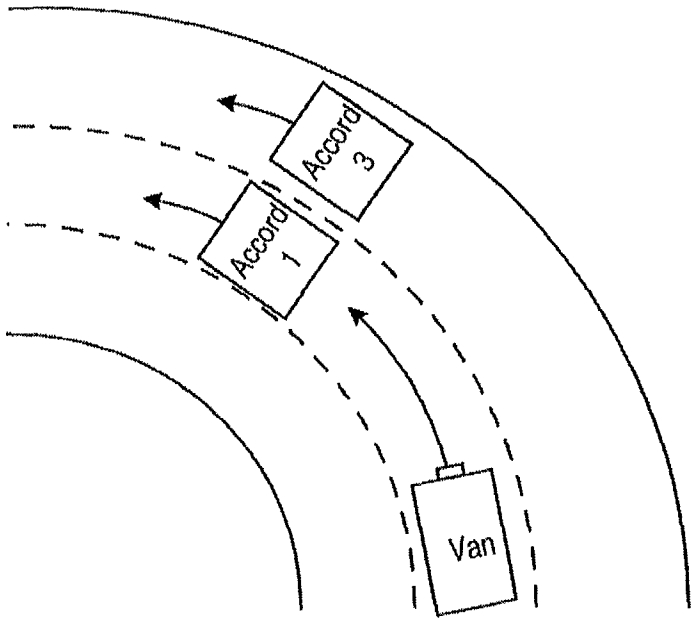

14:31:12 - Begin File

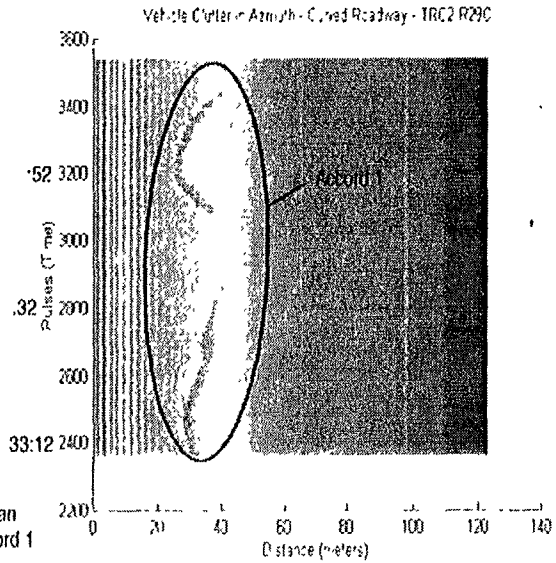

Accord 1 in front of Van
Accord 3 next to Accord 1

6.12 Vehicle Clutter in Azmuth - Curved Roadway

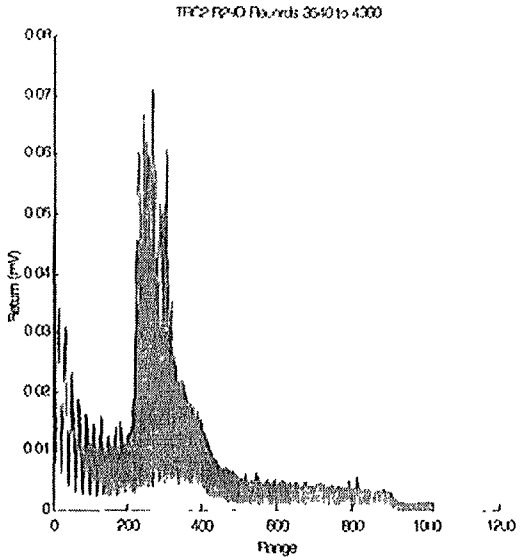

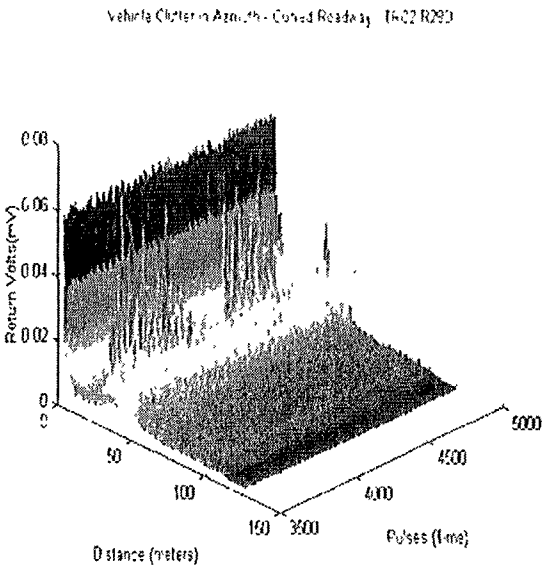

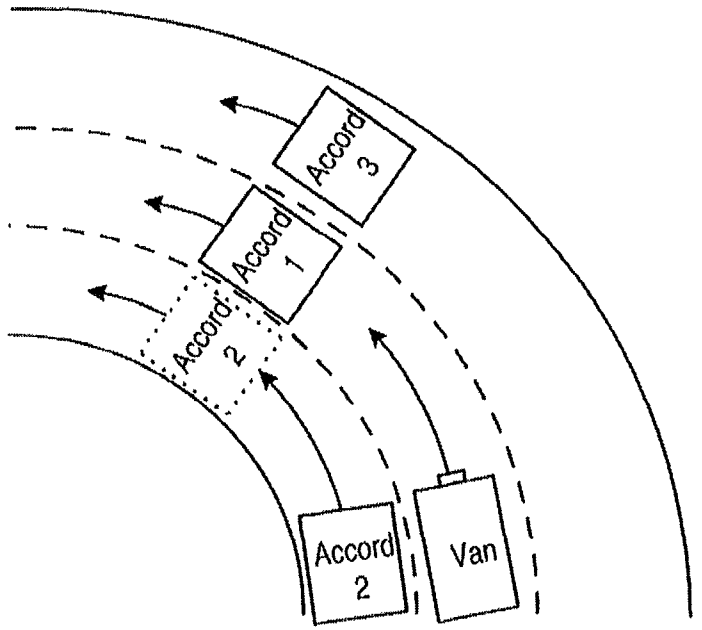

14:31:12 - Begin File

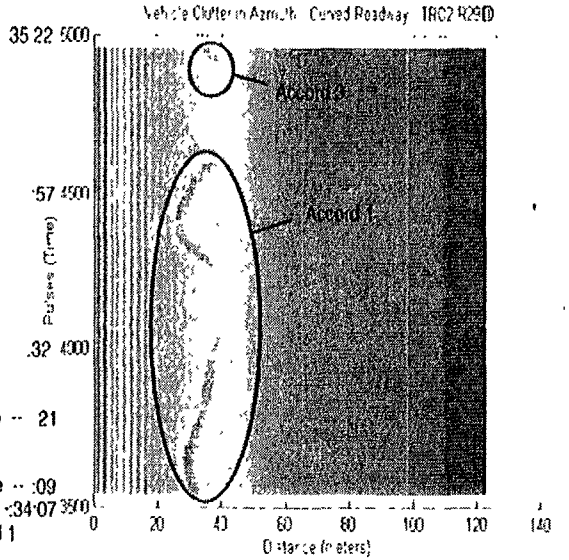

Accord 2 next to Accords 1 & 3 -- 21

Accord 2 enters scene -- :09

Accord 1 in front of Van -:34:07

Accord 3 next to Accord 1

6.12 Vehicle Clutter in Azmuth - Curved Roadway

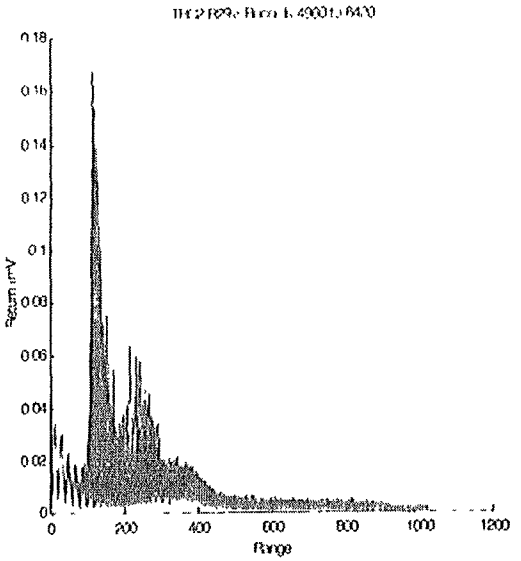

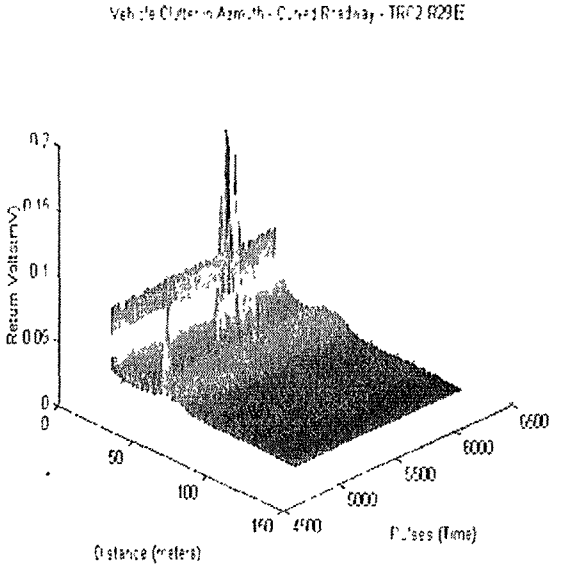

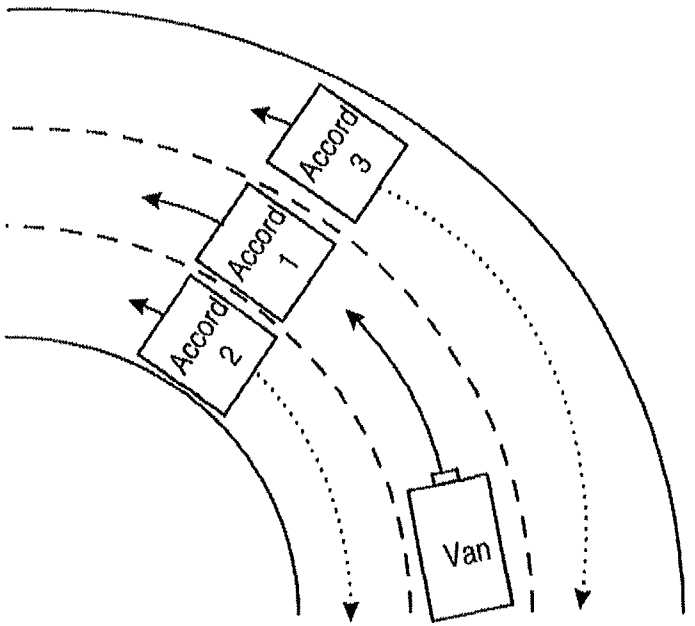

14:31:12 - Begin File

Accord 3 exits scene -- :41

Accords 1,2 & 3 -- in front of Van :35.22

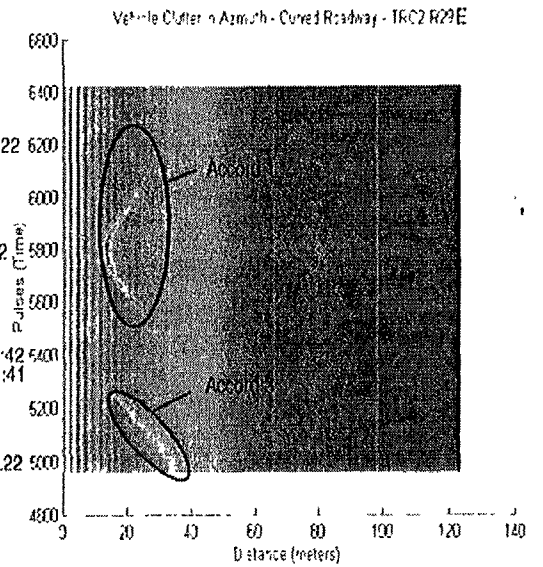

6.12 Vehicle Clutter in Azmuth - Curved Roadway

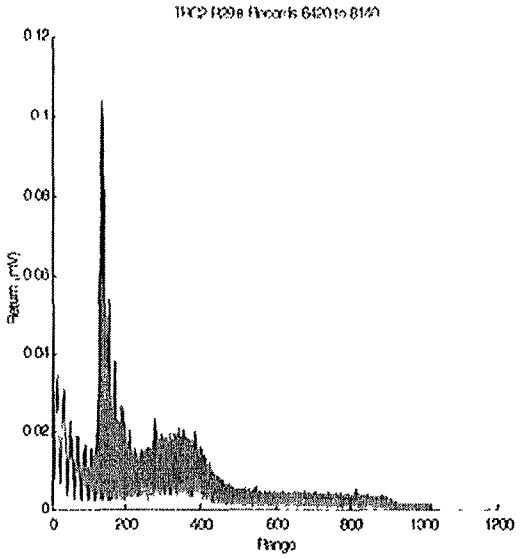

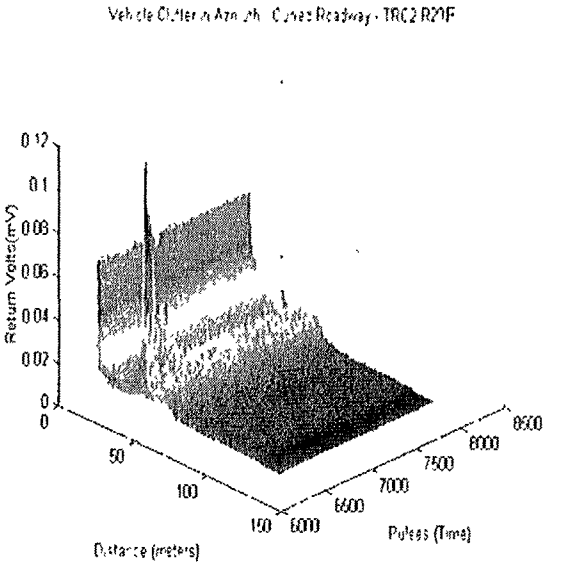

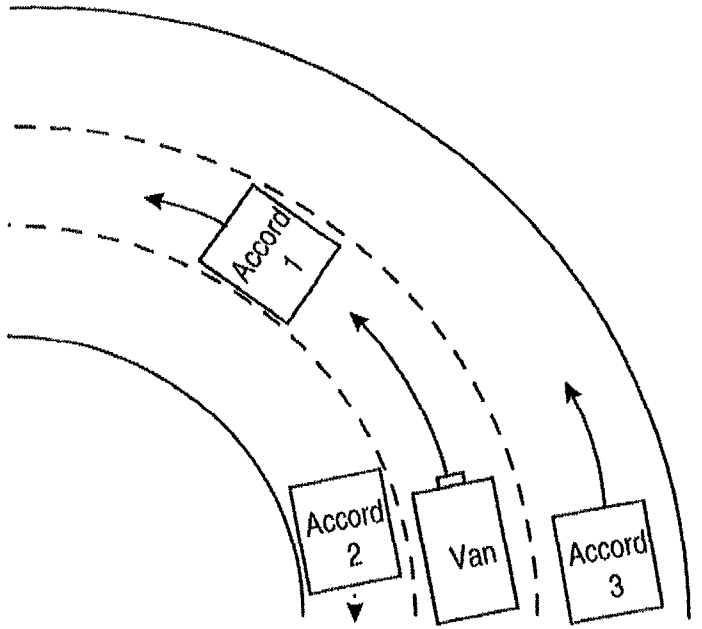

14:31:12 - Begin File

Accord 3 enters scene

Accord 1 in front

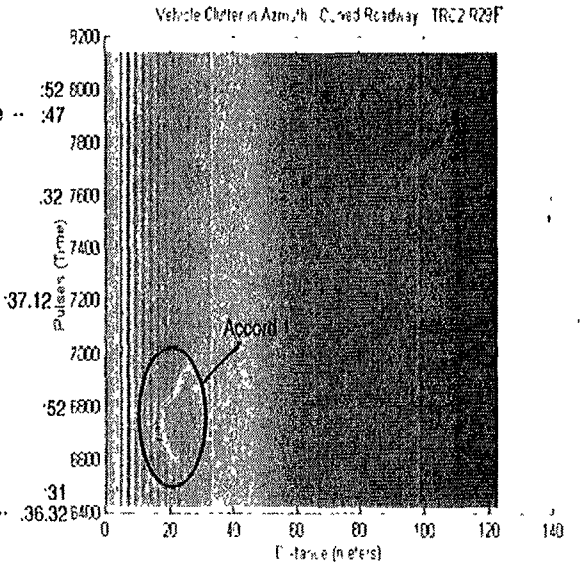

6.12 Vehicle Clutter in Azmuth - Curved Roadway

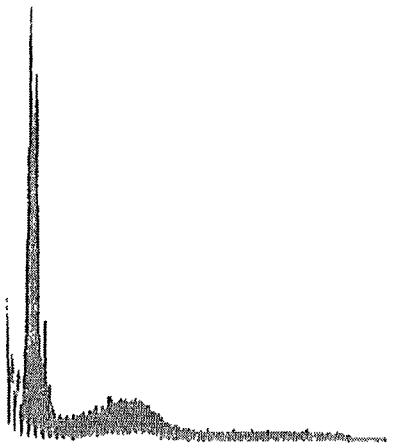

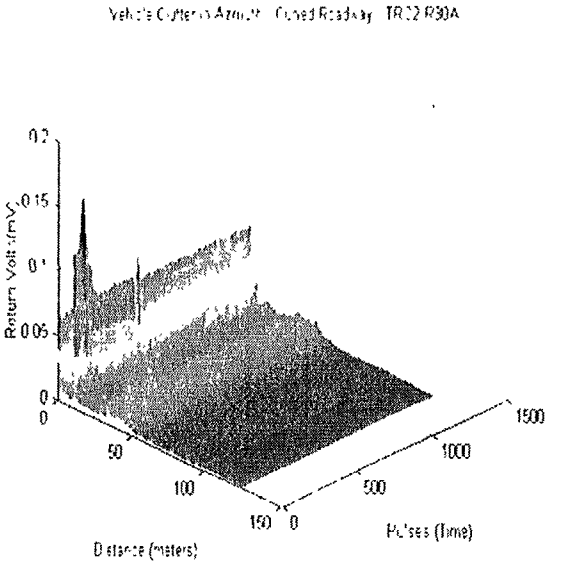

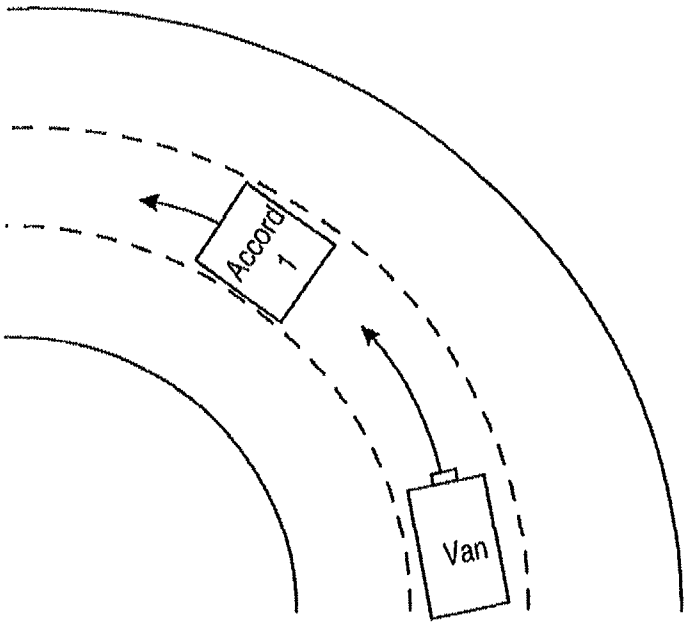

15:34:24 - Begin File

Accord 1 begins to move - :47

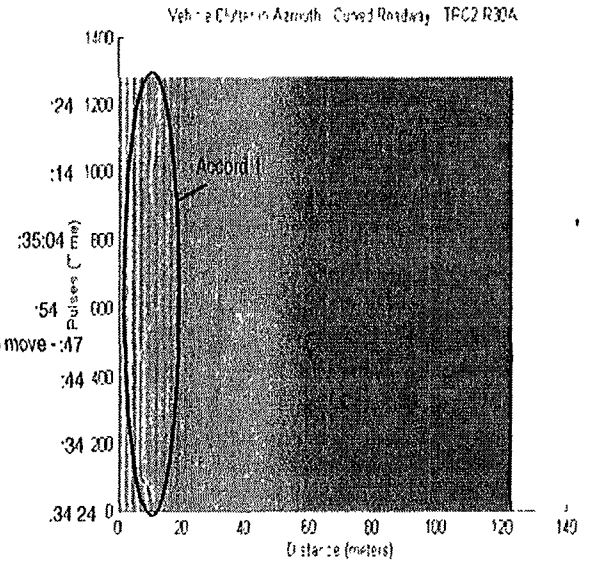

6.12 Vehicle Clutter in Azmuth - Curved Roadway

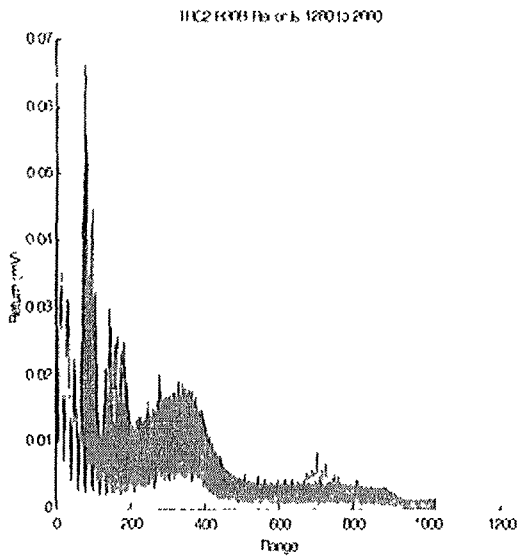

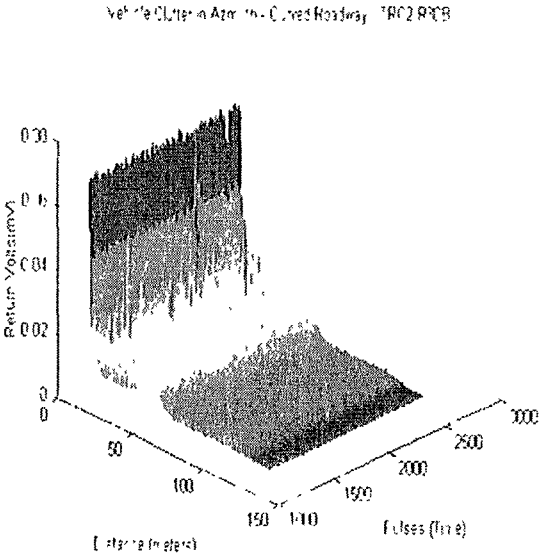

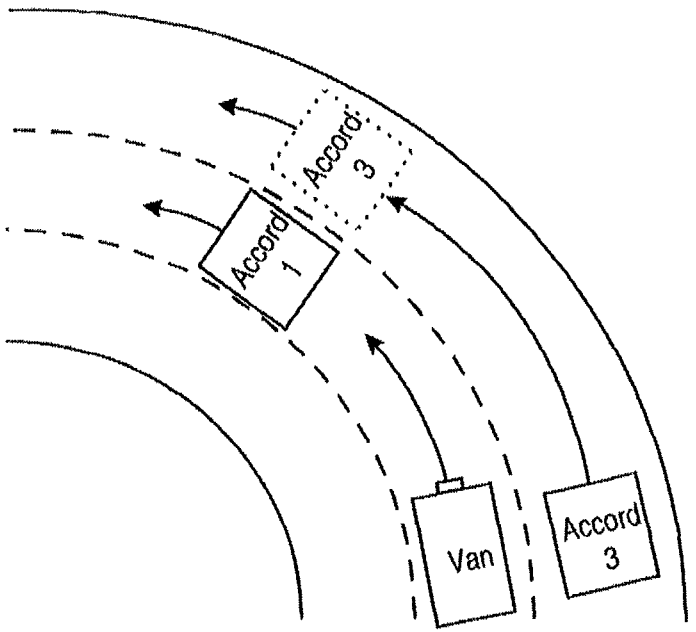

15:34:24 - Begin File

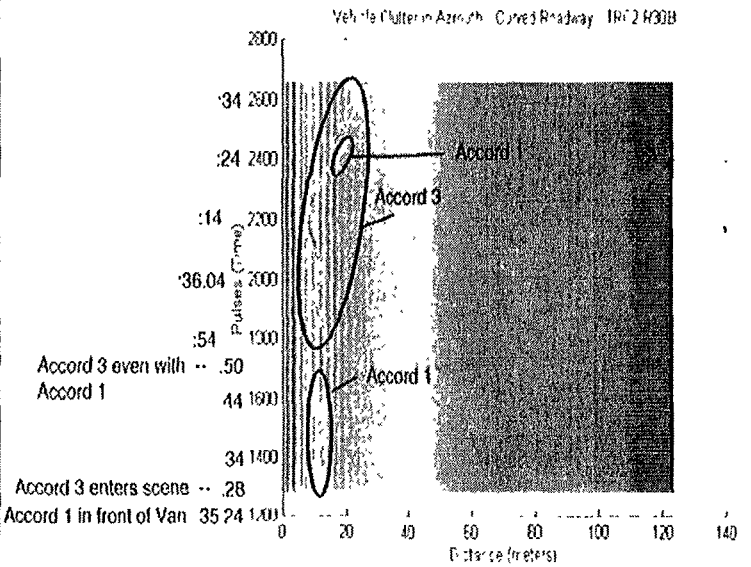

6.12 Vehicle Clutter in Azmuth - Curved Roadway

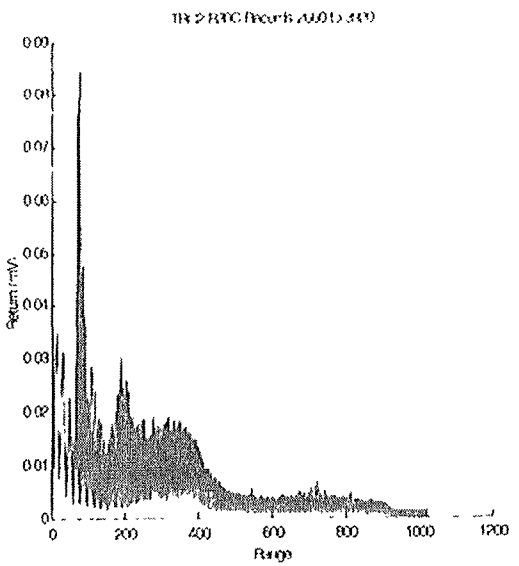

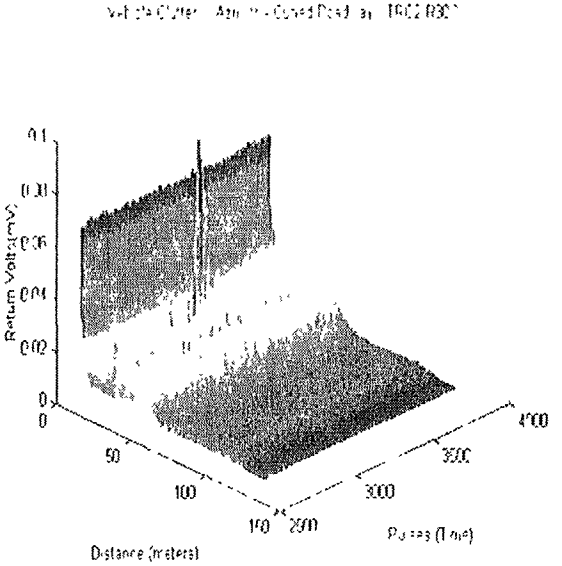

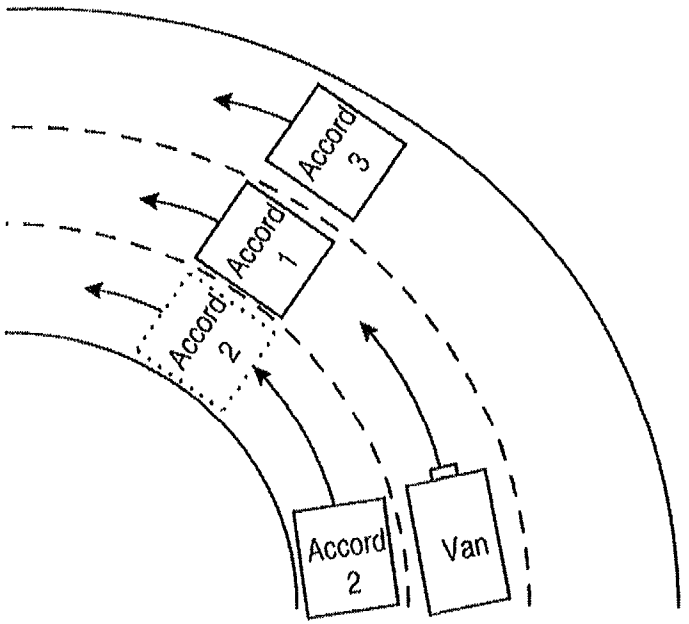

15:34:24 - Begin File

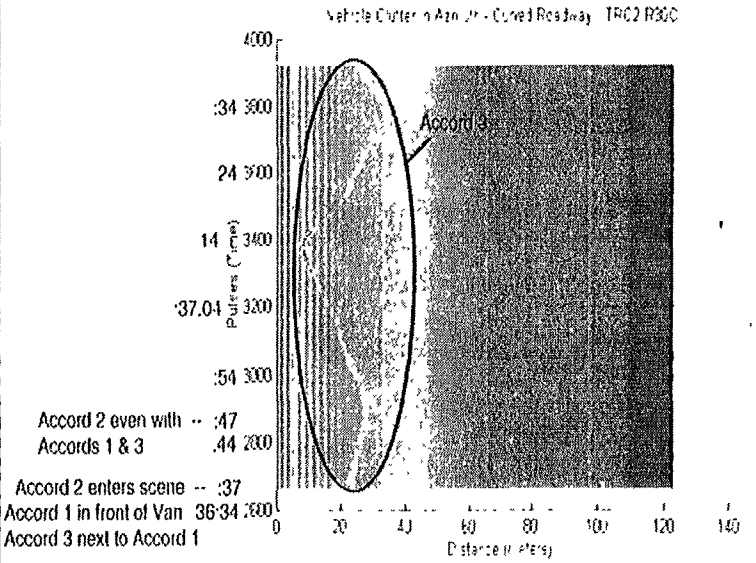

Accord 2 even with -- :47
Accords 1 & 3 .44

Accord 2 enters scene -- :37
Accord 1 in front of Van 36:34
Accord 3 next to Accord 1

6.12 Vehicle Clutter in Azmuth - Curved Roadway

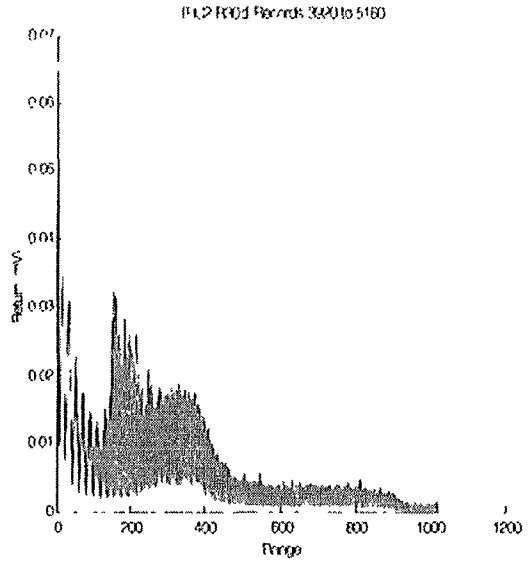

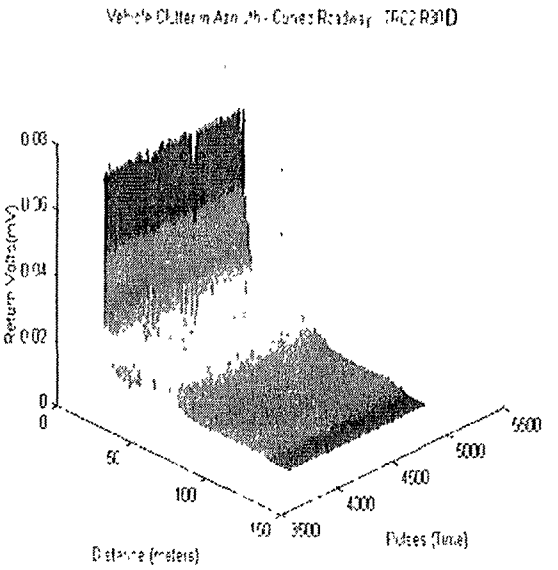

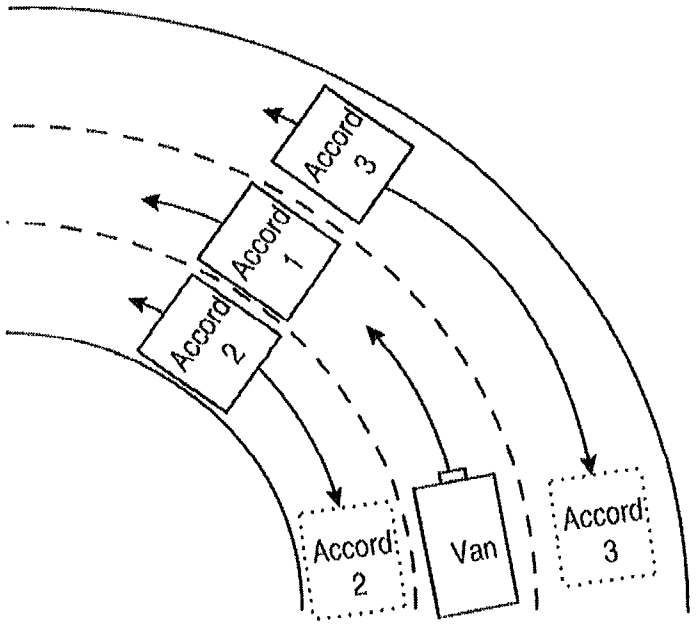

15:34:24 - Begin File

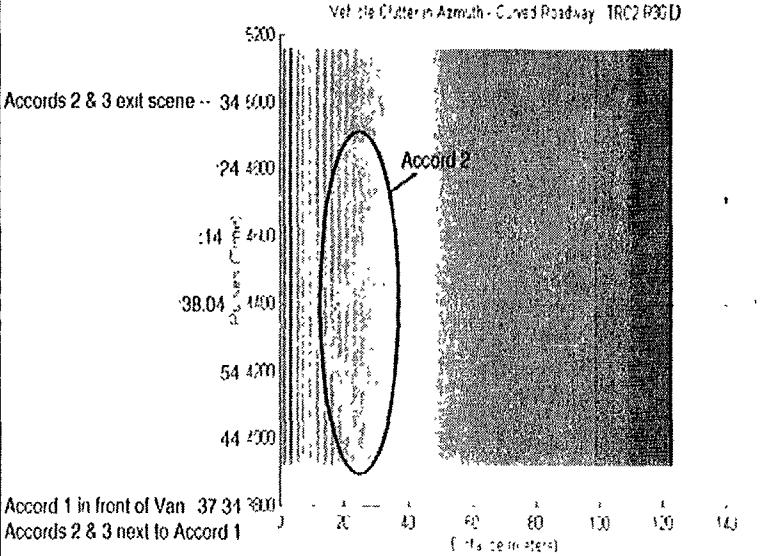

6.12 Vehicle Clutter in Azmuth - Curved Roadway

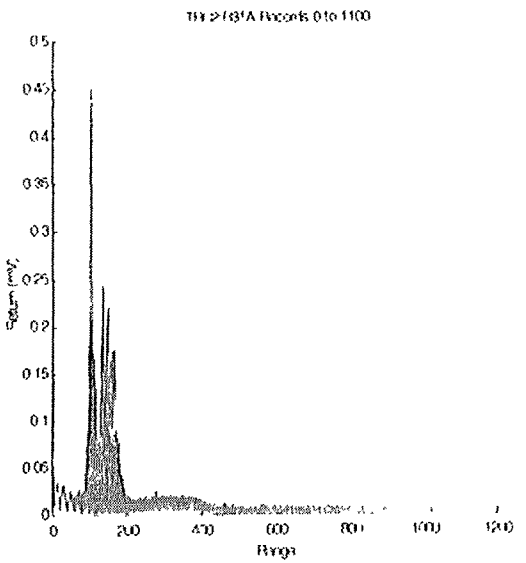

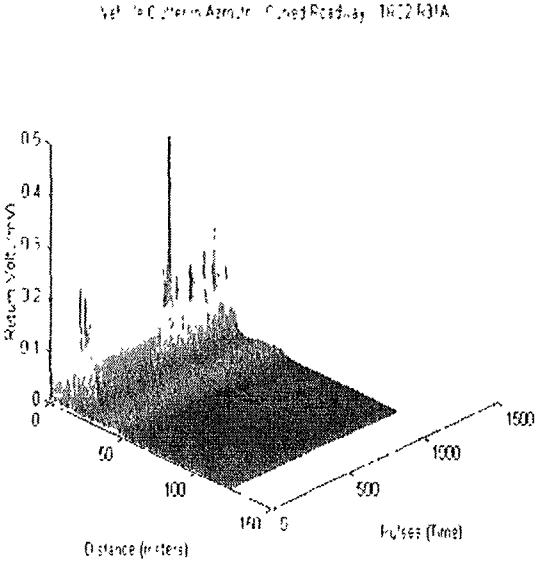

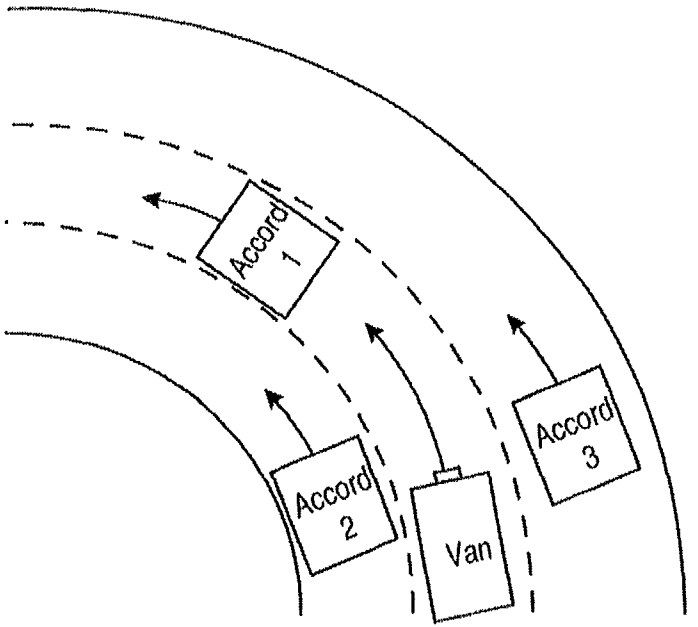

14:12:59 - Begin File

Accords 2 & 3 enter scene

Accord 1 in front of Van

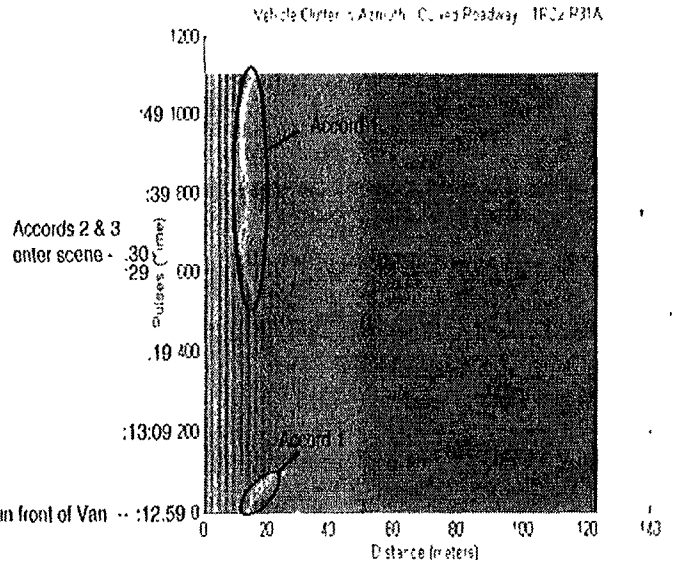

6.12 Vehicle Clutter in Azmuth - Curved Roadway

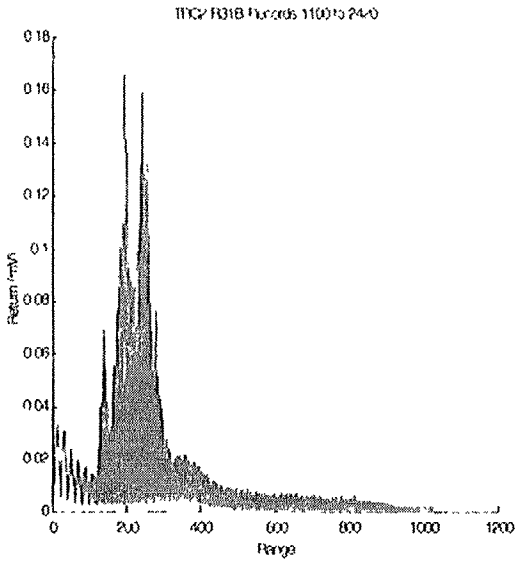

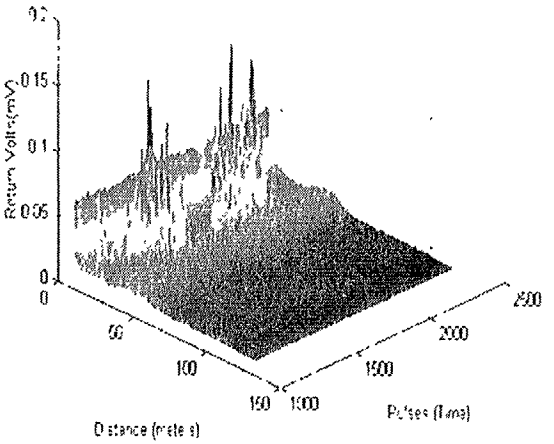

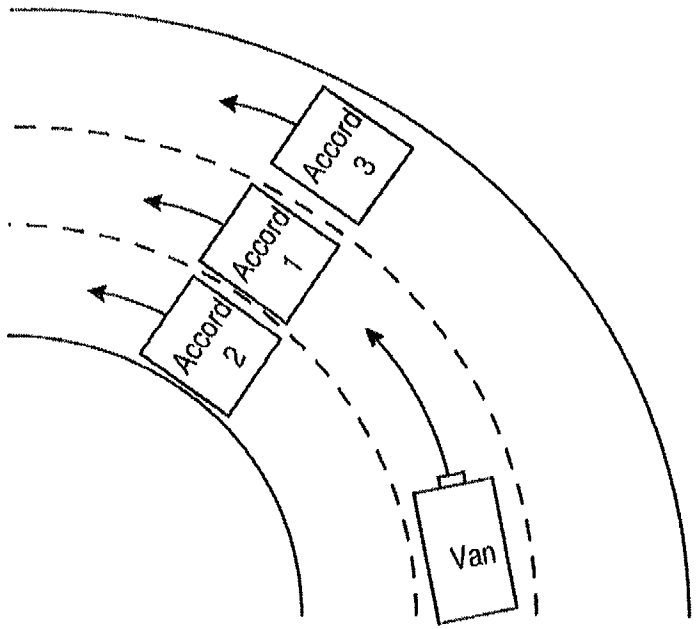

14:12:59 - Begin File

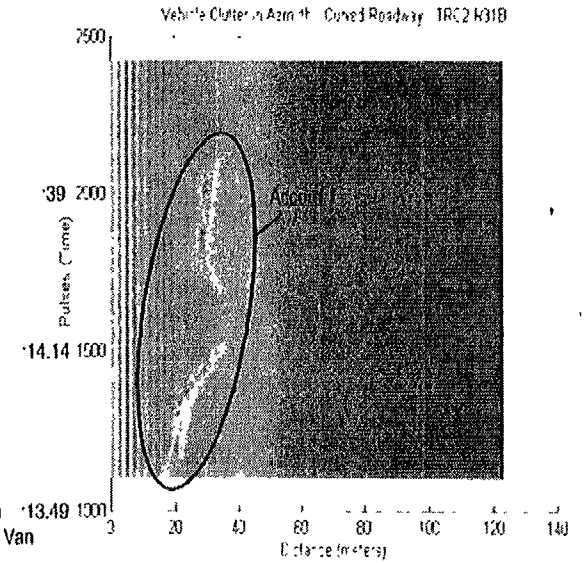

Accords 1,2,3 even
Accord 1 in front of Van

6.12 Vehicle Clutter in Azmuth - Curved Roadway

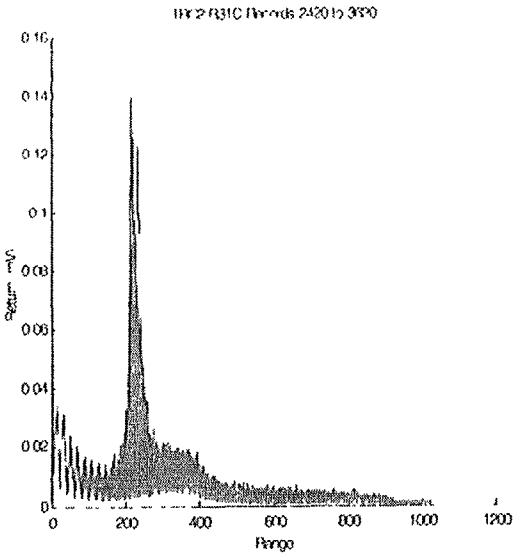

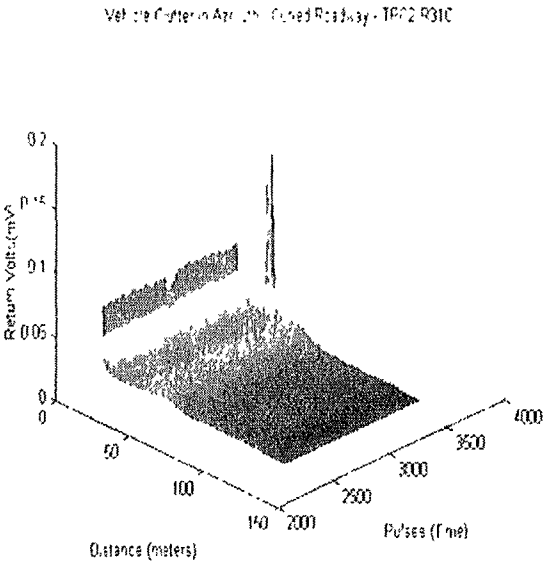

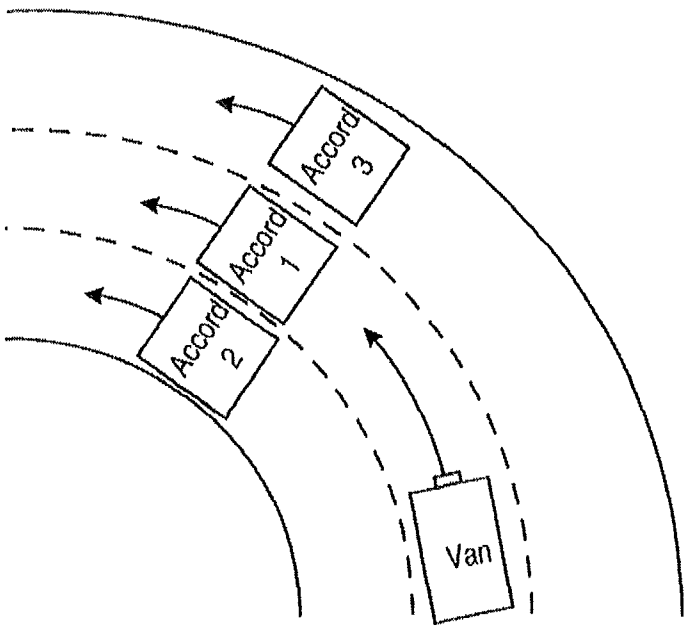

14:12:59 - Begin File

Accord 3 drifts 5m back - :52

Accords 1,2,3 even :14:59
Accord 1 in front of Van

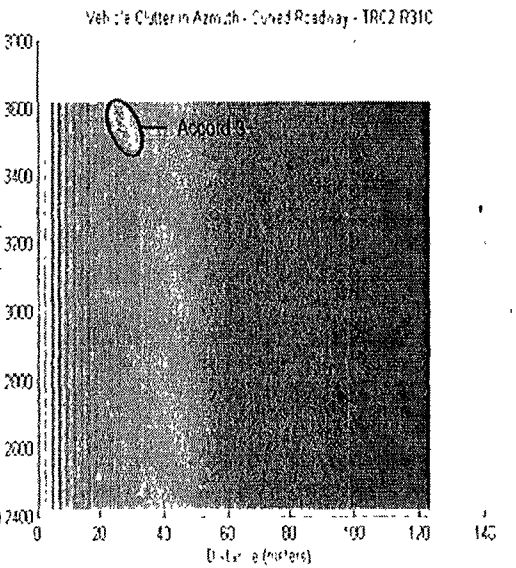

6.12 Vehicle Clutter in Azmuth - Curved Roadway

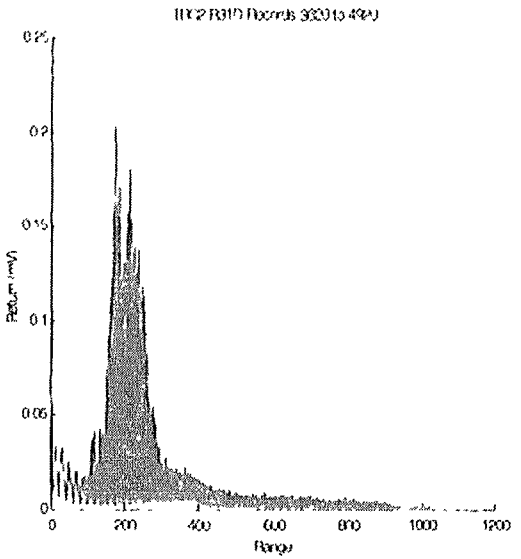

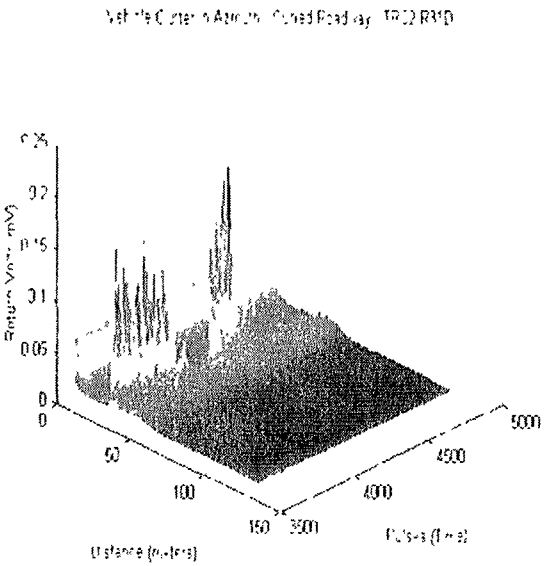

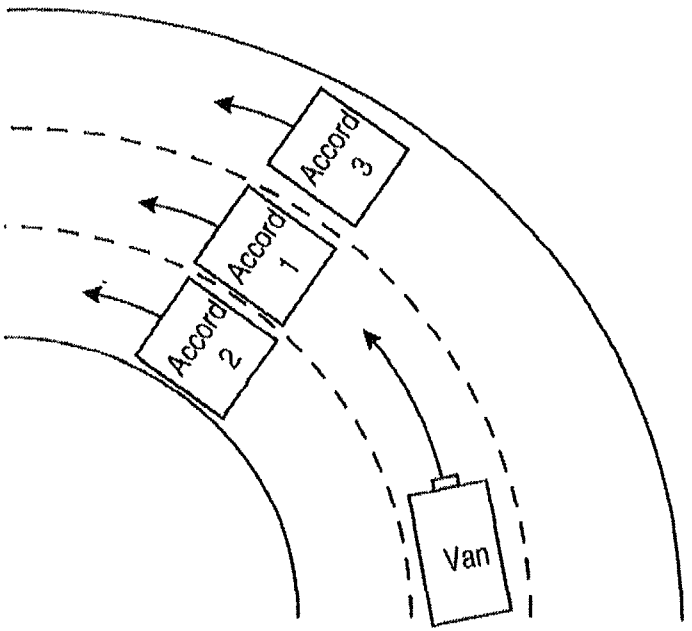

14:12:59 - Begin File

Accord 3 drifts back -- again from Accords 1,2

Accord 3 back in line -- with Accords 1,2

Accords 2,3 next to Accord 1
Accord 1 in front of Van

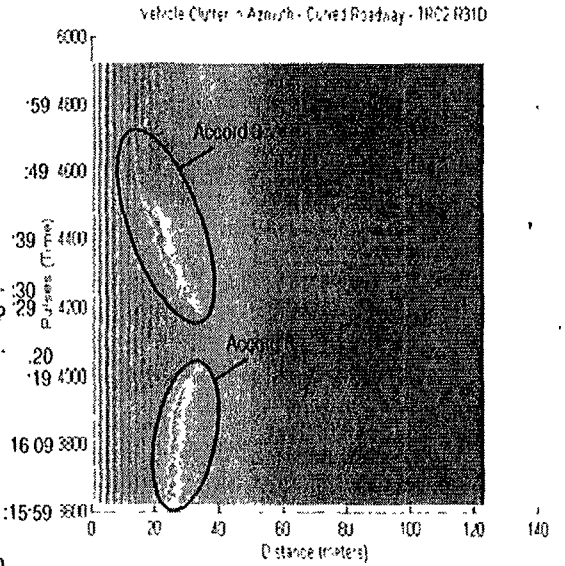

6.12 Vehicle Clutter in Azmuth - Curved Roadway

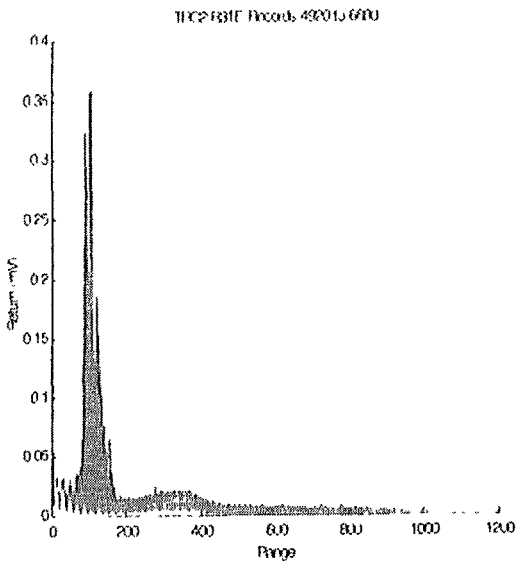

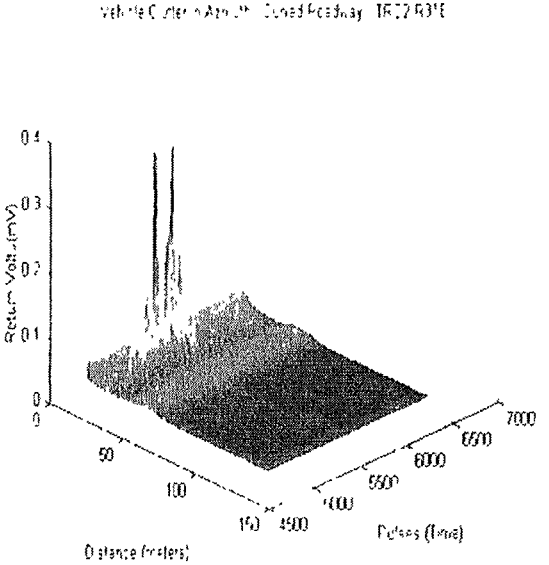

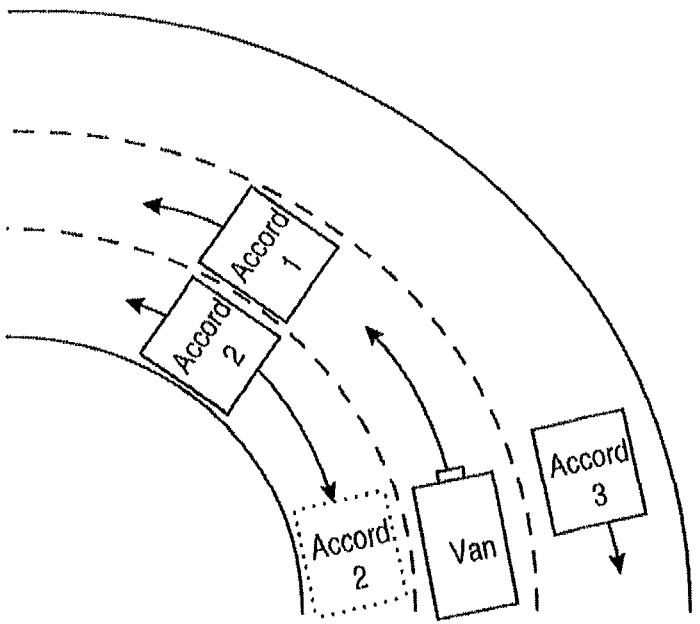

14:12:59 - Begin File

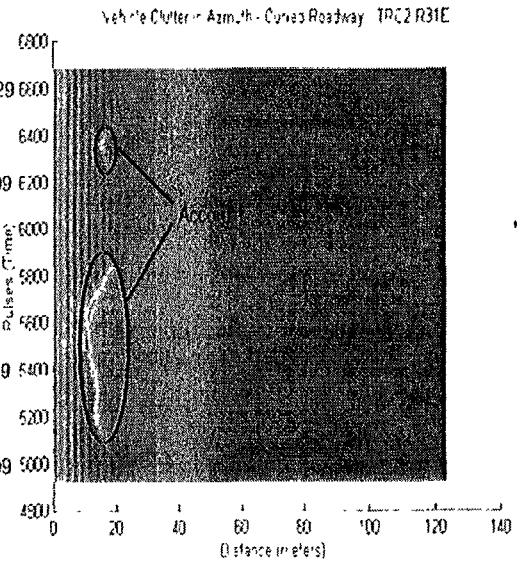

Accord 2 exits scene

Accord 3 exits scene
Accord 1,2 in front of Van

APPENDIX G. OPEN ROADWAY TESTS

This appendix summarizes the results of the FLAR program testing conducted on the open roadway. The open roadway tests are divided into two categories:

- Background Tests. Conducted with little or no traffic to assess the roadway background environment.
- Traffic Tests. Conducted with varying levels of traffic density.

G.1 BACKGROUND TESTS

The purpose of the background tests was to characterize the "non-traffic" component in the radar returns from common roadway objects that will appear within any forward-looking radar's field of view. The data for these tests were collected by taking the ERIM Testbed Vehicle on the roadways in the greater Ann Arbor area and identifying route segments with background attributes of interest. Data on the following types of roadway background were collected:

- Bridge Overpasses
- Different Road Types
- Guard Rails
- Roadside Signs
- Hills

A variety of data sets were collected on the roadway and analyzed using the ERIM FLAR Analysis Software. Data sets of interest were further processed using custom Matlab scripts to extract desired information from the raw radar data. The remainder of this section will summarize the results for the various background tests. Sample data plots will be used to illustrate results and diagrams provided where necessary.

G.1 .1 Bridge Overpasses

Bridge overpasses are of a particular concern to forward-looking radars because they extend over the entire roadway and, therefore, may appear as a stopped object within the primary vehicle's lane. This could occur even with radar's outfitted with the finest azimuthal resolution. Radar designers have approached this problem by limiting the antenna's beam width in the vertical plane in an effort to keep the overpass structures beyond the radar's field of view.

The TRW FLAR has a 3 dB elevation beam width of 3 degrees. The plot in Figure G-l shows the elevation plane 3 dB pattern for a 3 degree radar beam. Also, the plot includes reference lines for 12 and 14 foot bridges. Note that the beam height is 0.75 meters at a 0 meter range. This value corresponds to the mounting height of the TRW FLAR on the ERlM Testbed Vehicle.

Figure G-l shows that the 3 dB point of a 3 degree radar beam does not intersect with a 12 foot bridge until beyond a 100 meter range. This was an important factor in the selection of a 3 degree beam width in elevation. However, as the back of the vehicle is loaded with cargo, this beam pattern could be offset (i.e., tilted) up to several degrees. As the loading increases, the offset becomes more severe, and the antenna beam begins to illuminate the overpass structure. The tests described below were conducted to evaluate the extent to which an elevation offset in the radar beam would effect the returns in the raw radar data induced by bridge overpasses. These tests were conducted on US-23 under the Earhart Road bridge which is about 14 feet above the roadway.

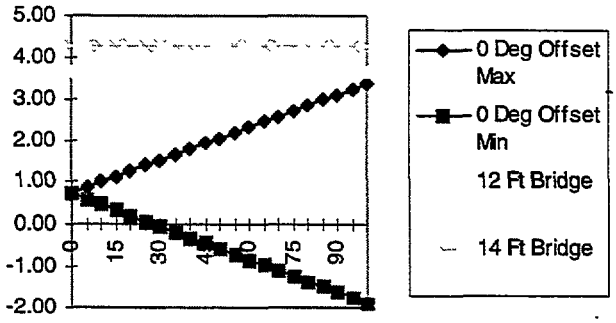

Figure G-1. Overpass Illumination—0° Offset

0 Degree Offset

Many runs under bridge overpasses have been made throughout the data collection phase of this program, and no evidence of returns from the overpass structures have been observed. As part of the bridge overpass tests, data collections were taken with a 0 degree offset under the Earhart Bridge on US-23 (14 feet above the road). A 10 dBsm corner reflector was placed on the top portion of the bridge for reference. The data was analyzed and no returns from the bridge overpass structure were observed.

1 Degree Offset

To simulate the loading of the ERIM Testbed Vehicle, the FLAR RF unit was tilted to a 1 degree offset. The plot in Figure G-2 shows the 3 dB illumination pattern for a 1 degree offset in the FLAR 3 degree antenna. Notice that the plot indicates an intersection of the beam pattern with the 14 foot bridge at about 80 meters. Therefore, one could expect that returns from the bridge overpass structure would be observable when the range to the bridge is between 80 and 100 meters.

Figure G-3 is the actual raw radar data collected during the test run. The returns from the bridge overpass structure are annotated on the plot. The returns from the overpass structure are observable from the time the bridge is 100 meters from the radar until it is nearly 60 meters from the radar. The reason the overpass was observed all the way down to 60 meters instead of being lost at 80 meters as depicted in Figure G-2 is that the plot in Figure G-2 is the illumination pattern for the 3 dB point on the antenna beam. The actual antenna beam provides gain (at a much lower level) beyond the 3 dB point and therefore, illuminates the bridge.

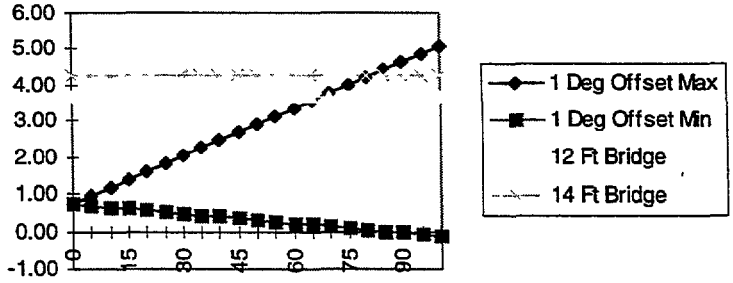

Figure G-2. Overpass Illumination—1° Offset

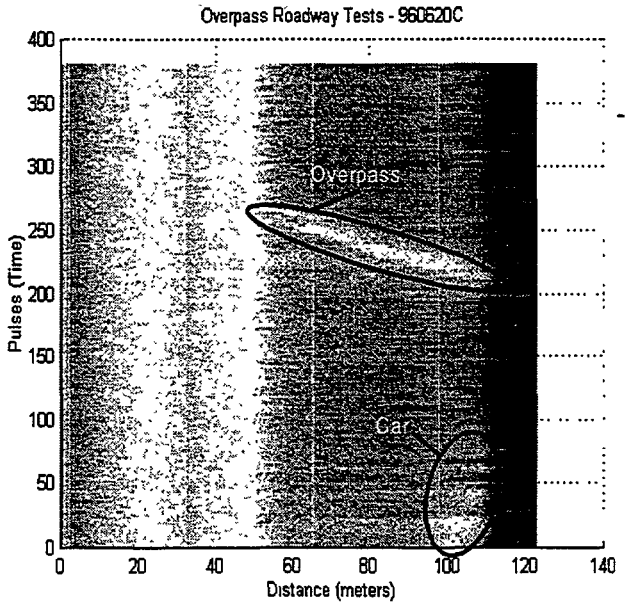

Figure G-3. Overpass Returns—1° Offset

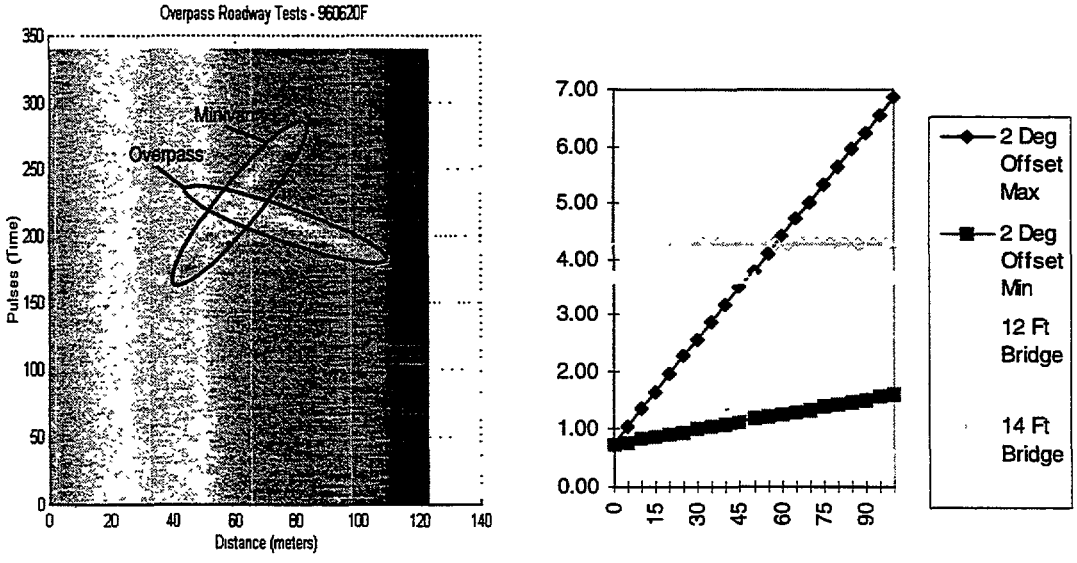

Figure G-4. 2 Degree Offset Data

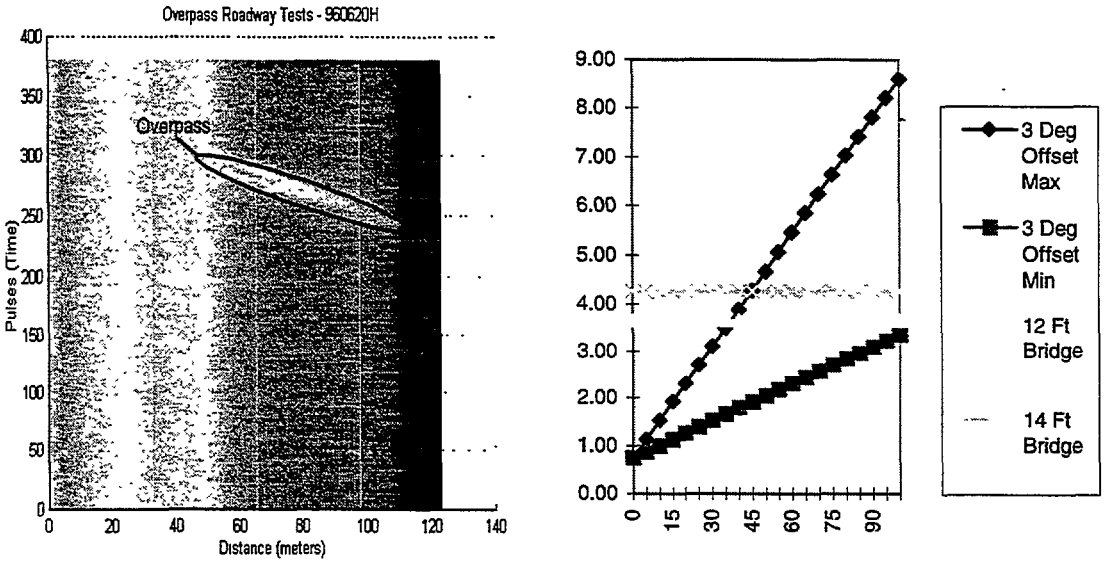

Figure G-5. 3 Degree Offset Data

2 and 3 Degree Offset

Test runs were made with the FLAR's angle of inclination at 2 and 3 degrees. The raw radar data and 3 dB antenna illumination plots corresponding to the 2 and 3 degree offset runs are shown in Figures G-4 and G-5, respectively. As the offset angle increases, the returns from the bridge overpass structure are observable at progressively nearer ranges. The raw radar data plot in Figure G-4 includes returns from a mini-van which was in the FLAR's field of view at the same time the bridge overpass returns were present.

It is interesting to note that in these test the FLAR, utilizing TRW-proprietary algorithms, did NOT lock-on and track the returns from the bridge overpasses. The FLAR did, however, briefly track the mini-van during the 2 degree offset test.

During the 2 and 3 degree offset tests, the maximum exhibited RCS value was -1 dBsm. It was determined that the 10 dBsm corner reflector placed on the TOP portion of the bridge structure was NOT contributing to the returns for these tests.

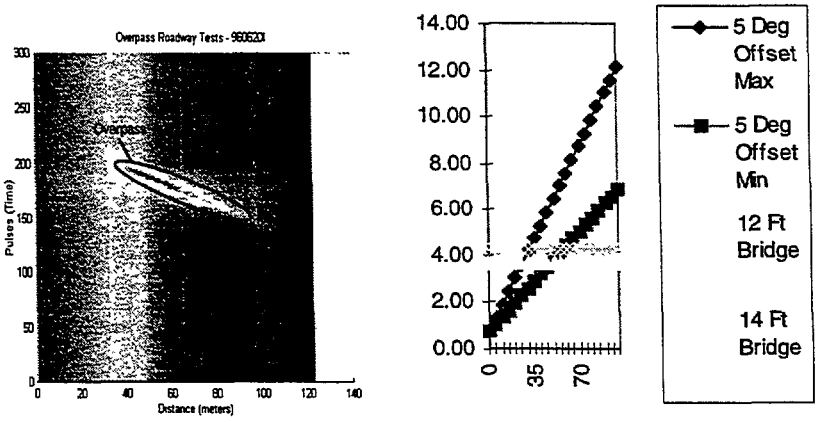

Figure G-6. 5 Degree Offset Data

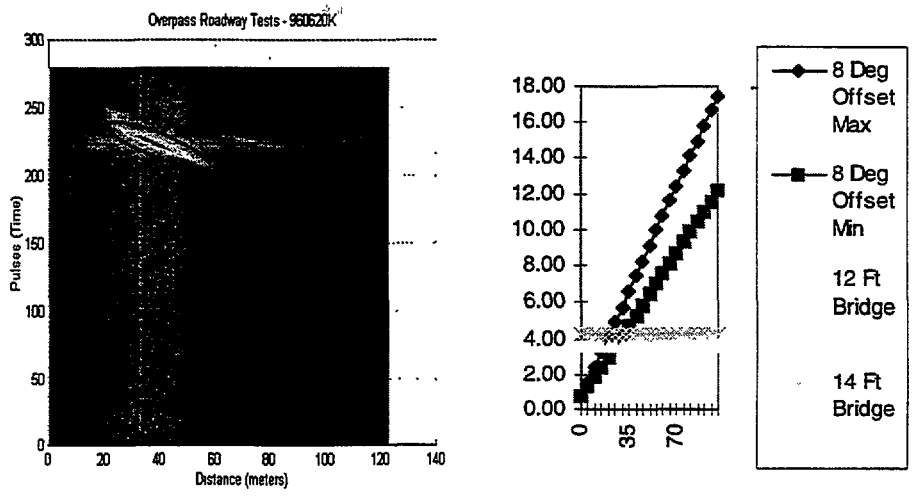

Figure G-7. 8 Degree Offset Data

5 and 8 Degree Offset

The raw radar data and illumination plots for the 5 and 8 degree offset tests are provided in Figures G-6 and G-7, respectively. As expected, the returns from the overpass structure increased in amplitude as the offset angle increased. The maximum exhibited RCS from the overpass structure was about 5 dBsm for the 8 degree offset collection. The 10 dBsm corner reflector which was placed at the top of the overpass structure was removed and subsequent collections were made to verify that the corner reflector was NOT contributing to the measured RCS values.

Suprisingly, the FLAR did not lock on and track the overpass structure returns in any of the tests. Without detailed knowledge of the TRW-proprietary algorithms within the FLAR unit, it is difficult to specify the exact reason that the FLAR seemed to ignore the overpass returns. However, since the FLAR was designed for ACC applications, and not collision avoidance, the threat assessment/tracking algorithm may have discarded the overpass returns based on their relative range rate and transient appearance in the raw data.

The 5 and 8 degree offset tests were seen to differ from the 1, 2, and 3 degree tests in that returns from the overpass structure were not observed until a range well under 100 meters. This is due to the beam illumination patterns as illustrated in Figures G-6 and G-7. Because of the elevation angle offset, the lower extent of the illumination pattern does not illuminate the overpass until ranges well under 100 meters.

Bridge Overpass Conclusions

The bridge overpass tests indicated that even a slight 1 degree change in the elevation angle of the FLAR resulted in the detection of overpass returns in the raw radar data. As this elevation offset angle is increased, the return levels from the overpass also increased. The table below summarizes the maximum RCS exhibited by the overpass structure for a given elevation offset angle.

Table G-1. Overpass RCS

Elevation Angle Offset	Maximum Overpass RCS
0 degrees	No returns
1 degree	-10 dBsm
2 degrees	-8 dBsm
3 degrees	-1 dBsm
5 degrees	2.5 dBsm
8 degrees	7 dBsm

The fact that the FLAR did not track (i.e., report) the range to the bridge overpass indicates that the ACC application optimized algorithms within the FLAR may not perform well for collision warning applications.

G.1.2 Road Types

The FLAR sensor was exposed to a number of different road types during the data collection phase of this program. These road types included concrete, asphalt and dirt roads. The tests described here were conducted to evaluate the effects of the various roadways on radar response as a result of returns produced by reflections from the roadway itself. The results from the "Road Type" tests are summarized in Figure G-8.

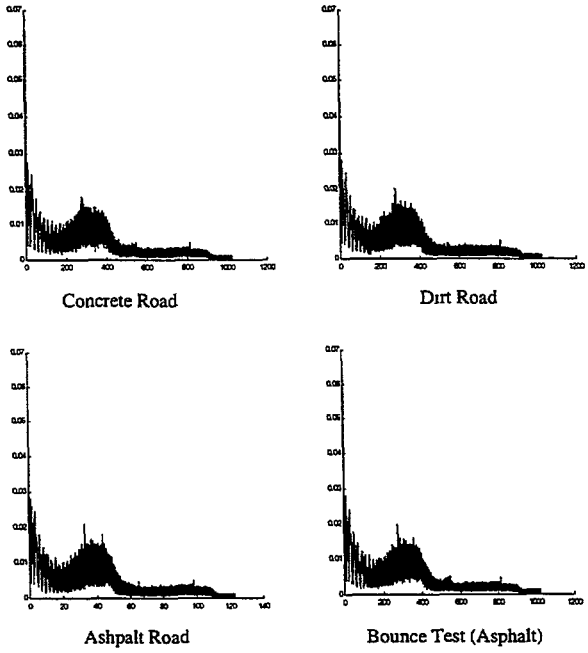

Figure G-8. Returns From Various Road Surfaces

The plots in Figure G-8 are range profile plots taken over several hundred radar pulses. The data was collected with the ERIM Testbed Vehicle moving down a road segment with no other targets within the radar field of view. The issue with the various road types was whether or not their relative roughness

would induce different responses in the radar sensor. As illustrated in Figure G-1, the 3 degree elevation beam width of the FLAR radar intersects with the ground at about 30 meters. Analyzing the data in the plots indicates that there are no significant changes in radar returns resulting from the type of roadway.

The "hump" in the range profiles which appears from 20 to 50 meters was initially thought to be caused by returns from the intersection with the ground surface. A "bounce test" was conducted (see plot 4 in Figure G-8) in which the front portion of the vehicle was bounced up and down in an attempt to change the hump's profile. However, as seen, the bounce tests had no effect on the characteristic hump. The hump and nearer range return levels are part of the baseline operating characteristics of the FLAR sensor. See section 4 in the body of the report for further discussion of baseline performance characteristics.

The conclusion from these tests is that the returns from the radar beam illumination of the ground surface is insignificant with respect to the noise floor of the FLAR sensor. Even the very bumpy dirt road used in these tests failed to produce any observable changes in radar response.

One other issue which deserves further study is the difference in multipath effects which are due to various road surfaces. Surface moisture should also be included in further studies. Evidence of multipath off the road surface were observed on several occasions during the road testing. Multipath off of the roadway surface can actually allow the transmitted radar energy to pass under a preceding vehicle. Furthermore, this energy can be reflected off of objects in front of a preceding vehicle, allowing the radar to "see" objects not in its direct field of view.

G.1.3 Guard Rails, Signs, and Hills

Figure G-9 shows raw radar returns collected during some S-curve maneuvers on a 2-lane roadway. The returns in the plot were induced by guard rail and metal sign posts located on the roadway. The guard rail resulted in a much more significant return than the signs. A detailed description of guard rail return characteristics is provided in Section 10 of Appendix F.

The return levels induced by the signs were generally found to exhibit an RCS characteristic level somewhere between 0 and 3 dBsm. For the roadway dynamics corresponding to the data in Figure G-9, the radar returns from the signs were very transient and had a very high range rate associated with them.

The FLAR and its TRW-proprietary algorithms did not report on (i.e., track) any of the road signs encountered during the roadway tests.

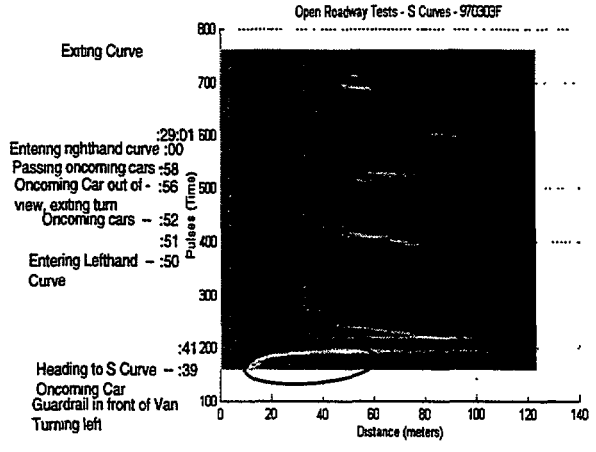

Figure G-9. Returns on Curved Roadway

Similar to the various roadway type tests described previously, the hill tests conducted on various roadway showed no signs of significant radar response due to the hill itself. The effect the hills did have on the radar sensor were all related to loss of track on target vehicles as they departed from the radar's field-of-view due to passing over a hill in the roadway. Again, the hills themselves did not induce any response in the radar.

G.1.4 Traffic Tests

The traffic tests conducted under this program were aimed at qualitatively evaluating the open roadway environment. On the open roadway, a forward looking radar is exposed to numerous types of objects with diverse dynamic characteristics. The object-rich environment in which the radar must operate consists of other moving vehicles and roadside "stuff". We have categorized this "stuff" as background objects. These background objects include bridge overpasses, signs, guard rails, and so forth. The response to these background types of objects has been discussed previously. This section will focus on qualitatively examining the returns from other moving vehicles. The following three areas will be addressed in this section:

- Complexity of Road Environment
- On-coming Traffic Characteristics
- "Non-standard" Vehicles

G.1.5 Complexity of Roadway Environment

To evaluate the FLAR response to other moving vehicles, a number of collections were made in various traffic densities. While higher traffic densities would seem to constitute a much more difficult environment for the FLAR, it is important to remember that the sensor's field of view limits the number of targets which generate returns to the radar. Figure G-10 illustrates how the radar's FOV limits the number of objects which can be tracked. The lightly shaped target in the left lane of Figure G-10 will not cause a return to be induced in the radar. This indicates that the traffic density present outside of the radar's FOV has little effect on its performance.

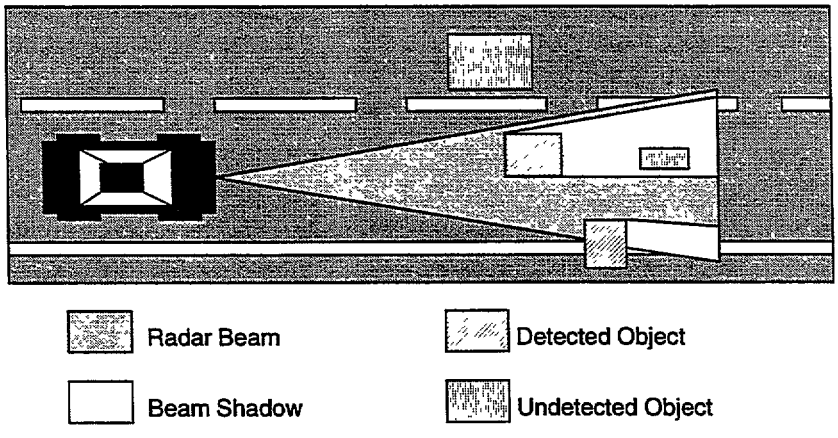

Figure G-10. FOV and Occlusion Limitations

Another factor related to the FLAR's performance in various levels of traffic density is occlusion of the radar energy. Referring to Figure G-10, one can see that the object within the host vehicle's lane and furthest in range does not induce a return to the radar because the radar energy has been occluded (blocked) by another object. (It is important to note that under certain geometries and roadway

configurations that the FLAR can actually see vehicles beyond a preceding vehicle due to multipath effects of the radar energy under the preceding vehicle.)

These two factors, sensor FOV and energy occlusion, result in the FLAR performance being less sensitive to traffic density than one might intuitively expect. The largest impact of traffic density on the FLAR performance is related to the dynamic movements between the FLAR host-vehicle and surrounding vehicles.

Figure G-l 1 illustrates the FLAR performance in a heavy traffic scenario. The text along the left side of Figure G-l 1 describes the various vehicle movements and locations along the collection timeline. Two general observations, both fairly intuitive, were made during the roadway tests with varying traffic densities:

1. As traffic density increased from light (2 to 3 cars within 100 meter stretch of road) to moderate, significantly less of the background returns were observed in the radar output. The returns which were observed were almost always from another moving vehicle.
2. As traffic density increased from moderate to heavy, similar types of returns were observed but at increasingly nearer ranges.

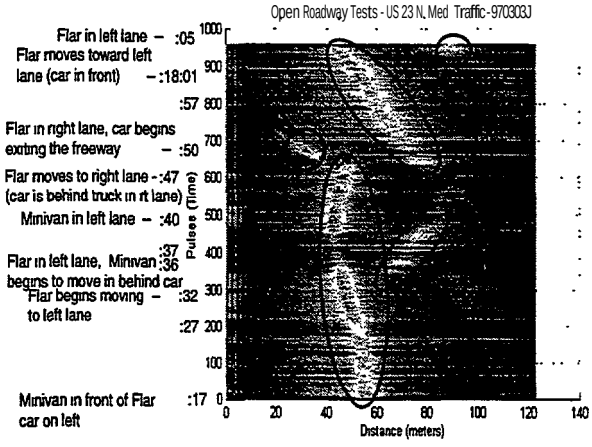

Figure G-l 1. Collection in Heavy Traffic

The first observation may actually result in the moderate traffic density scenario being easier for the threat assessment algorithm to handle than the light traffic scenario. This is due to the fact that many of the "extraneous" returns from background objects, which have high motion dynamics relative to the host vehicle, are not evident in the raw radar returns. There are reasons the background returns are no longer observable in the raw radar data. The first reason is that the increased number of vehicles are occluding the background objects. The second reason is that the returns from the vehicles (i.e., their RCS) is generally higher than that of the background objects. The automatic gain control of the FLAR is adjusted to avoid saturation from the vehicle returns, thereby reducing the sensitivity of the FLAR receiver. Therefore, the relatively weaker returns from the background objects are no longer observable.

The second observation indicates that under heavy traffic scenarios, the threat assessment algorithm has much less time to warn the operator of a potential impending crash. In addition to having less time, the algorithm may also have much less data. Due to the rapid detection and loss of track on the surrounding vehicles due to dynamic movements (see Figure G-l l), the threat assessment algorithm may end-up with significantly less of a time-location profile (i.e., track) of an object under heavy traffic conditions.

In conclusion, qualitatively speaking from a pure sensor perspective, traffic density does not have as much of an effect on sensor performance as one may intuitively expect. Field-of-view and occlusion effects play significant roles in limiting the number of returns to the radar sensor regardless of traffic density. It is important to note that their are secondary effects of higher traffic density such as multipath which can induce returns in the sensor. From a collision avoidance or ACC application perspective, the biggest impact traffic density has is related to the average time a threat assessment algorithm has to react to a particular scenario. By definition, the spacing between vehicles in high density traffic is lower and therefore reaction times are decreased.

G.1.6 Oncoming Traffic Characteristics

Several data collections were made while on a a-lane, non-divided highway on which oncoming traffic was present. The raw radar data plot in Figure G-12 summarizes how the returns from oncoming traffic manifests itself with respect to the radar sensor. The specific returns from the oncoming traffic are annotated in the figure. These returns are very transient in nature and while there are clearly evident above the sensor's noise floor, they are relatively low (on the order of -10 to -2 dBsm) when compared to typical returns from a preceding vehicle located in the host vehicle's lane.

The reason for the lower return levels is that the orientation between the radar and the oncoming vehicle is such that the vehicle is located at the edge of the radar antenna pattern. This data was collected on a straight roadway and the results are similar to those for the test track experiments conducted with a vehicle located at the side of the roadway.

This traffic scenario may cause large problems for an automotive radar designed for collision warning/avoidance. The problem is that the vehicle has a high closing rate and appears to be located within the host vehicle's lane. The high closing rate is evident in Figure G-12 by the wide almost horizontal return lines from the oncoming traffic. Also evident in the figure is that the oncoming vehicle exits the sensor's field of view at around 40 meters. Note that the FLAR's FOV for these tests was based on a 3dB beamwidth of 3 degrees. At 40 meters, an object closing at 100 MPH (assuming 50 MPH for each vehicle) has less than 1 second to impact.

The parameters of the threat assessment and warning algorithms must be set such that the false alarms from oncoming traffic is minimized. In the case of on-coming traffic on a straight-away, this would mean that the warning time would have to be set to less than 1 second, or the processing algorithms may chose to ignore oncoming traffic based on the relative speeds of the objects. Obviously ignoring objects which are approaching the host vehicle at speeds greater than its own ground speed would minimize false alarms, but would also have an impact on the number of crashes the system would be effective in mitigating.

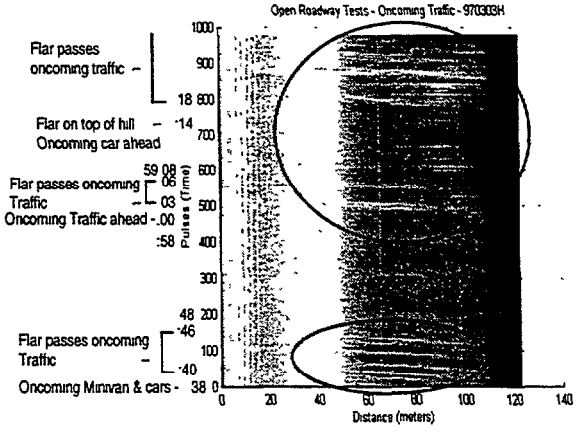

Figure G-12. Returns From On-Coming Traffic

G.1.7 Non-Standard Vehicles

Another issue regarding the data collected on the open roadway is related to the variety of vehicles on may encounter. These types of vehicles range from small sports cars, to large tractor trailers, to towed home-made wood trailers, to towed fiberglass boats, and so on. The point is that one encounters a large number of "non-standard" vehicles on the roadway.

Figure G-13 shows the FLAR radar returns resulting from following an empty automobile carrier vehicle. This vehicle is irregularly shaped and constructed primarily from metal. The plot in Figure G-13 shows how the return signature from the single vehicle is range dependent. At near ranges, there appears to be individual scattering centers located at the rear of the vehicle along with another set of scatterers towards the front of the vehicle. This second set of scatterers is located somewhere within the carrier trailer. As the range to the vehicle increases, the return from the vehicle changes in that the returns from the second set of scatterers fades away and the individual scattering centers from the rear of the vehicle blend together.

This empirical data does not indicate that the car carrier would cause any particular problems to the FLAR in terms of detection and tracking of the vehicle. However, if a FLAR implementation and processing begins to rely on particular vehicle signatures for classification or performs some sort of centroid processing to locate and track targets, these "non-standard" returns from the carrier vehicle may pose problems.

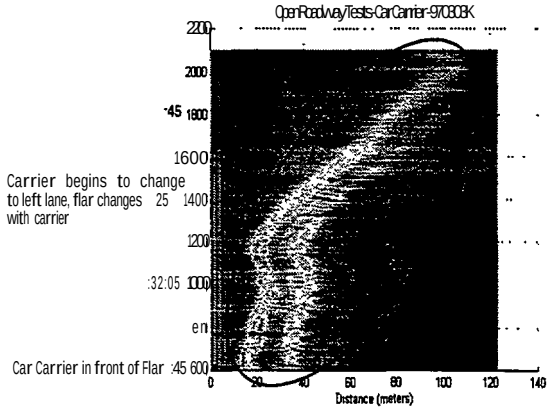

Figure G-l 3. Returns From Car Carrier Vehicle

OPEN ROADWAY DATA PLOTS

The following pages are selected raw data plots generated from the Open Roadway collections. These plots were selected to provide a reasonably sample of the type of data collected on the open road. Each plot is labeled with the appropriate test identification and annotation on the plots is provided where appropriate along with a description of the roadway environment. The reader is referred to the test results descriptions in Appendix G.

These plots are provided to assist developers in quantitatively assessing the radar response to the scenarios tested. Of course these results are specific to the TRW FLAR sensor configuration (e.g. antenna gain and beam shape). The reader is referred to Section 4 of the final report which discusses the FLAR sensor characteristics in order to extrapolate the results to other configurations.

960620 - Overpass Roadway Tests

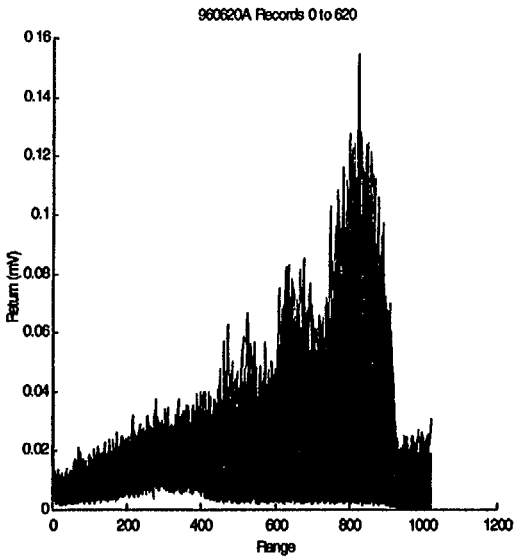

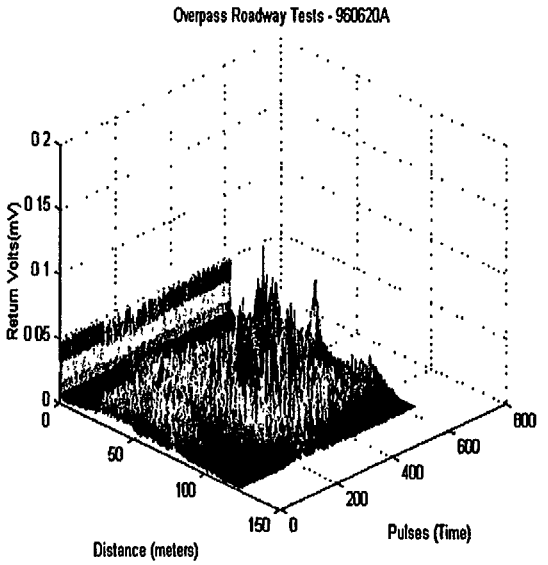

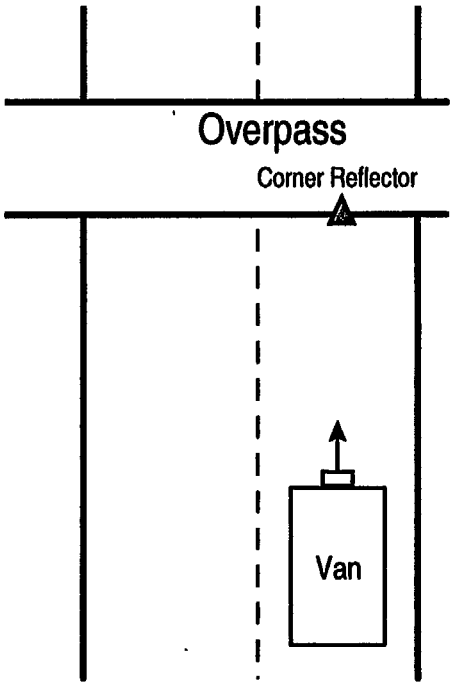

09:20:16 - Begin File
0 degree offset

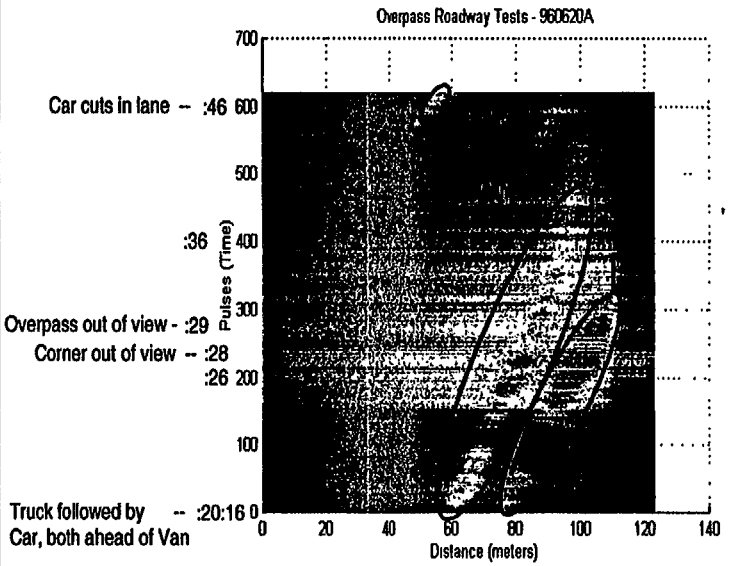

960620 - Overpass Roadway Tests

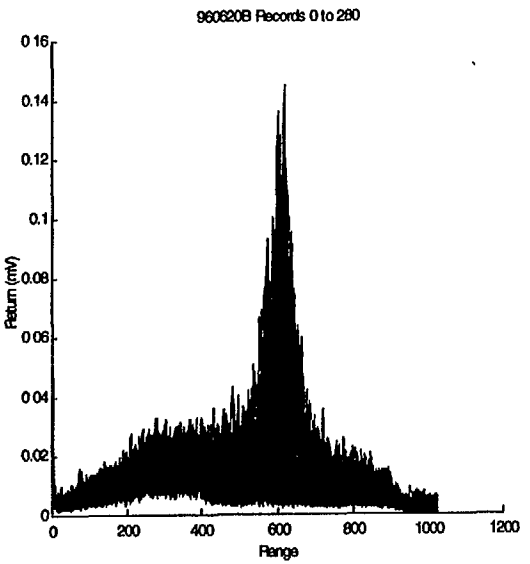

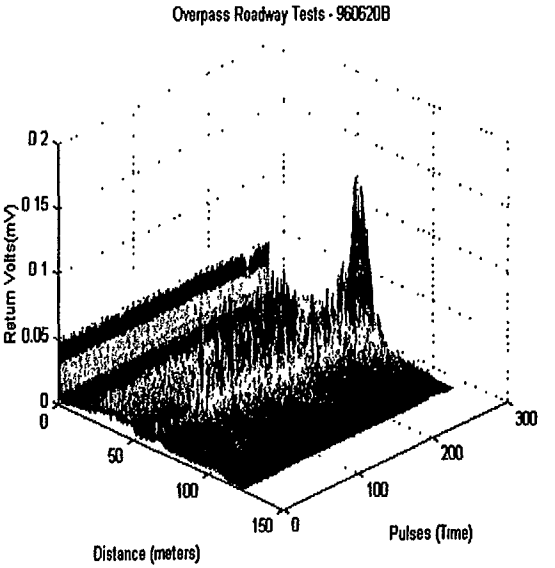

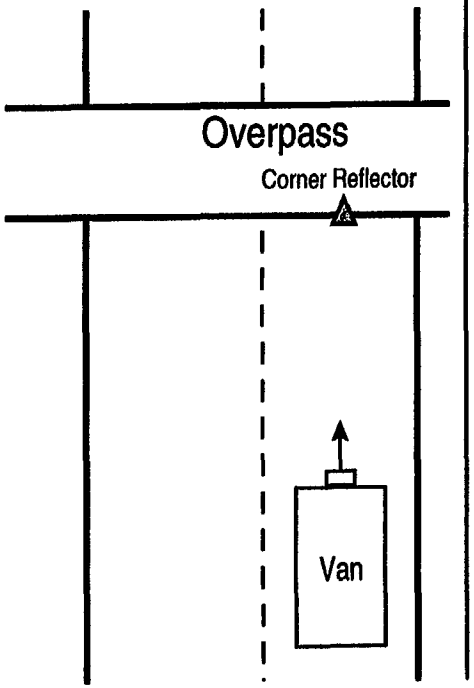

09:28:17 - Begin File
0 degree offset

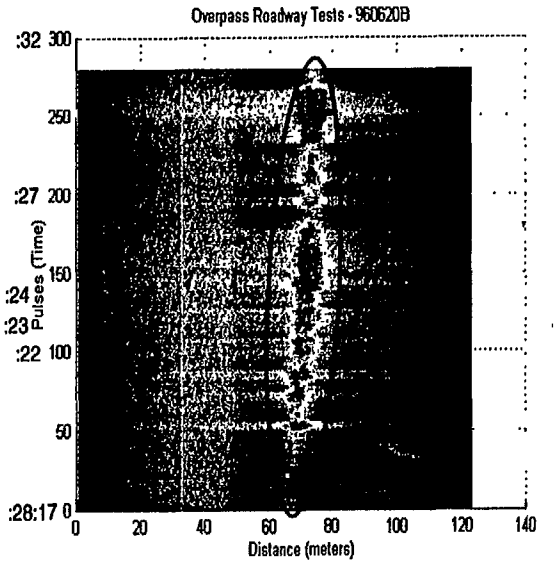

Overpass out of view -- :24
Corner out of view -- :23
Car in front of Van -- :28:17

960620 - Overpass Roadway Tests

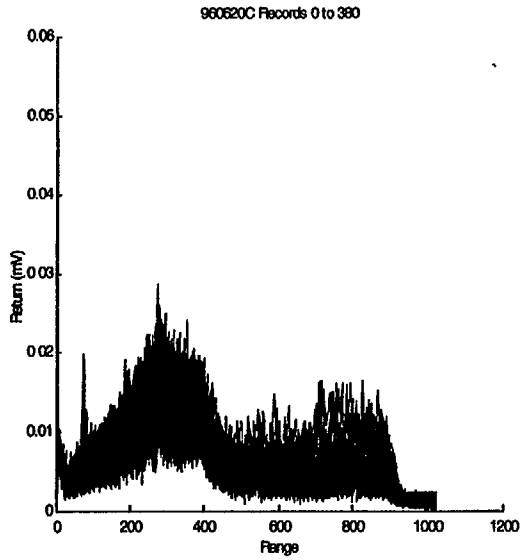

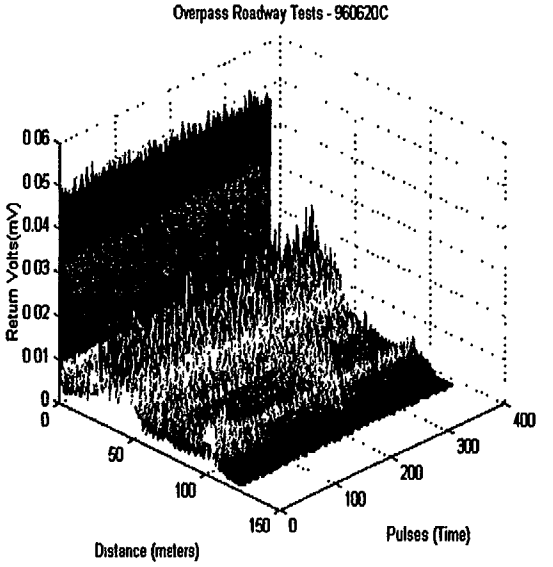

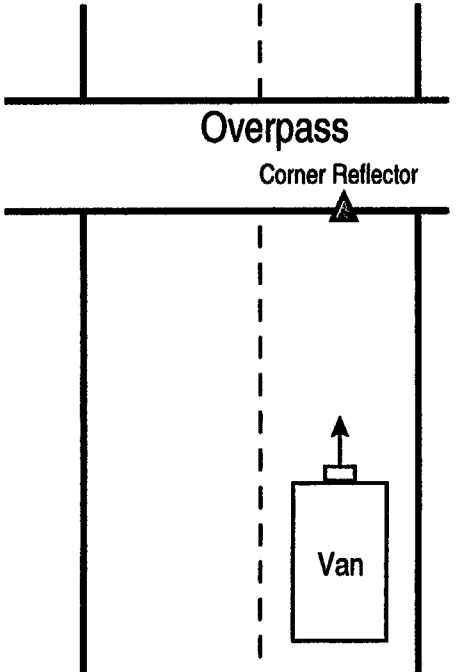

09:36:18 - Begin File
1 degree offset

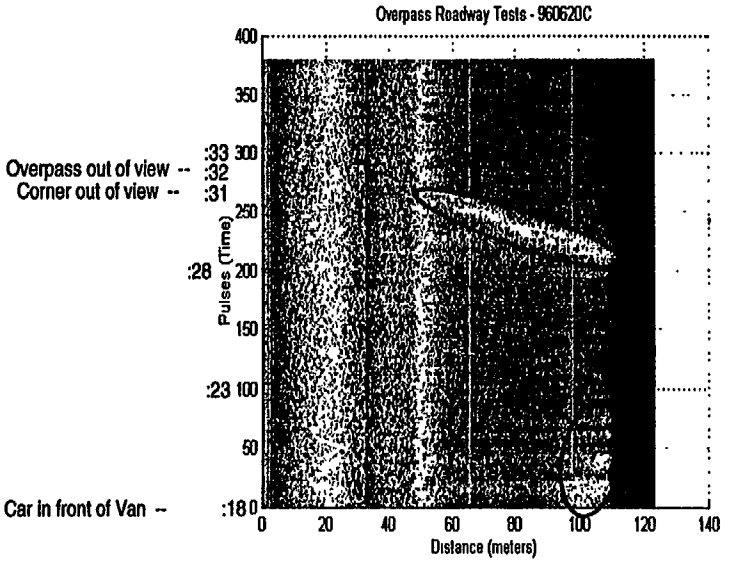

960620 - Overpass Roadway Tests

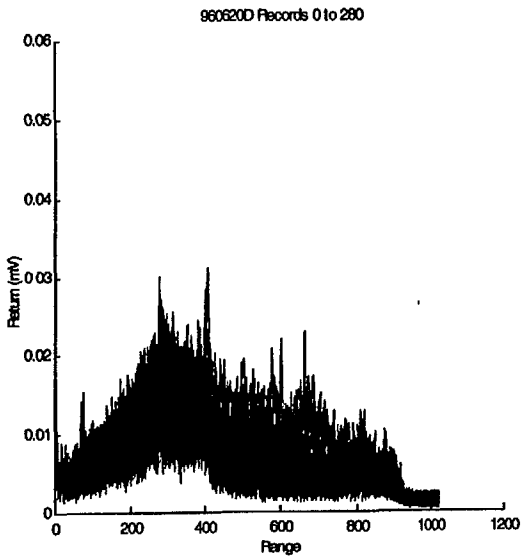

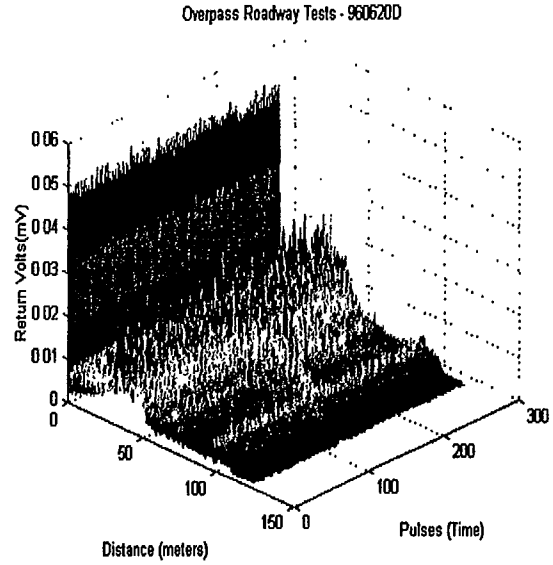

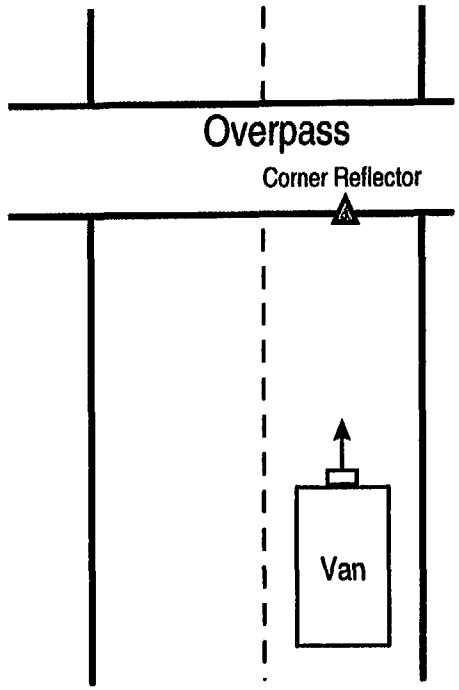

09:40:51 - Begin File
1 degree offset

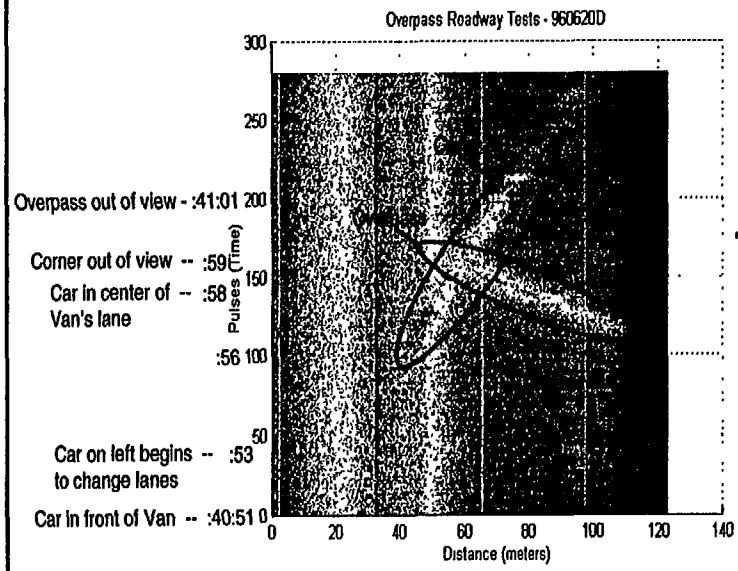

960620 - Overpass Roadway Tests

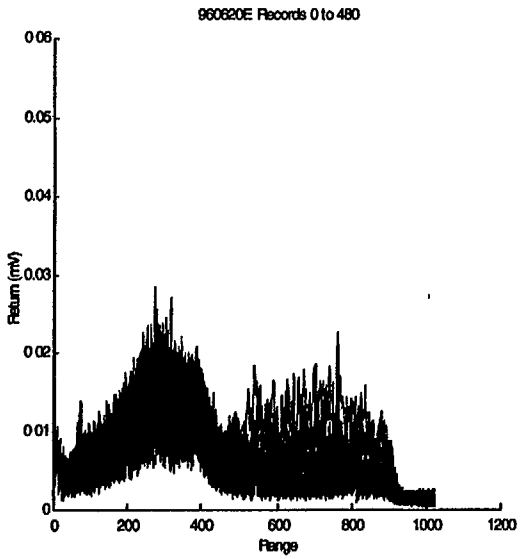

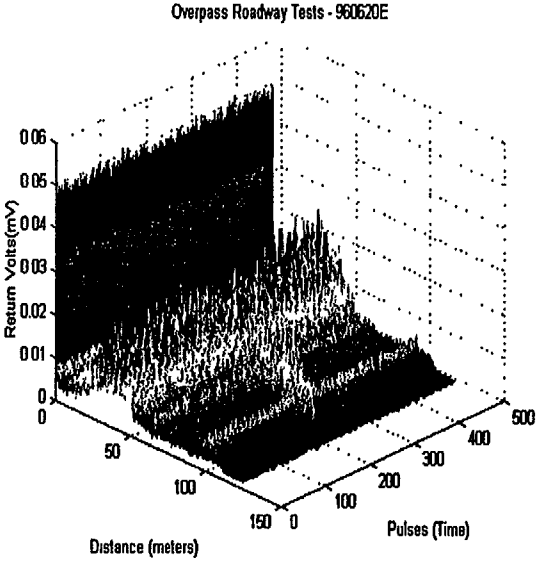

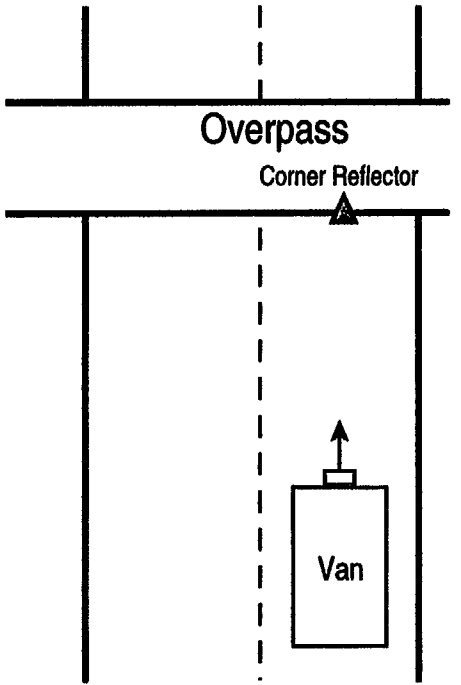

09:50:16 - Begin File
2 degree offset

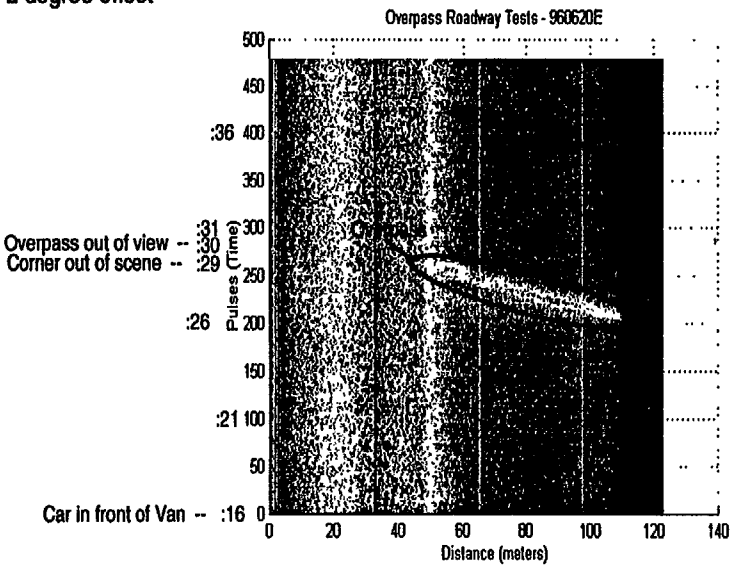

960620 - Overpass Roadway Tests

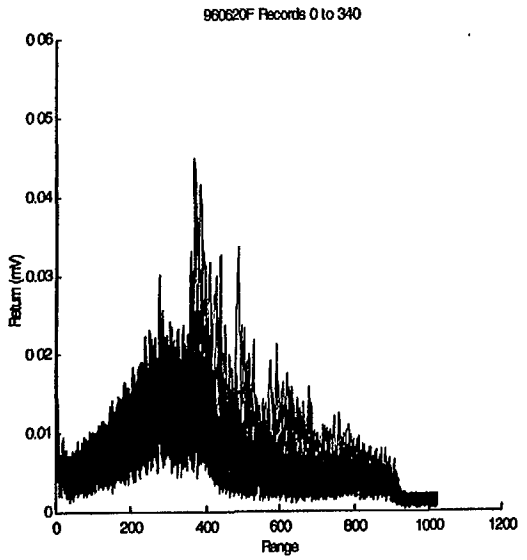

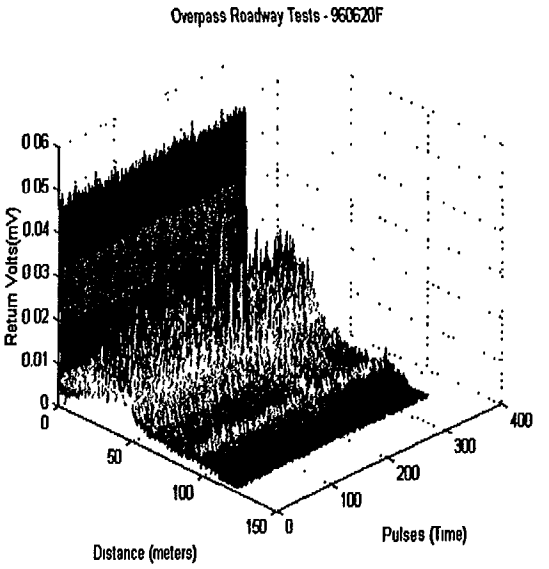

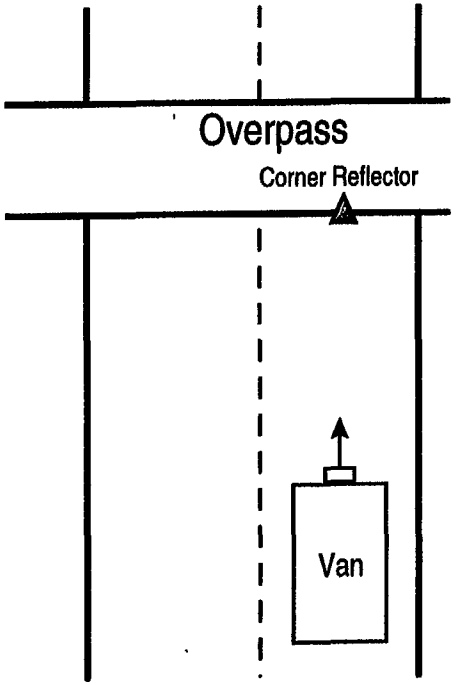

09:53:55 - Begin File
2 degree file

Overpass out of scene -- :07
Corner out of scene -- :06
:05

Minivan in center -- :02
of lane

:54:00

Minivan begins to cut -- :59
in front of Van

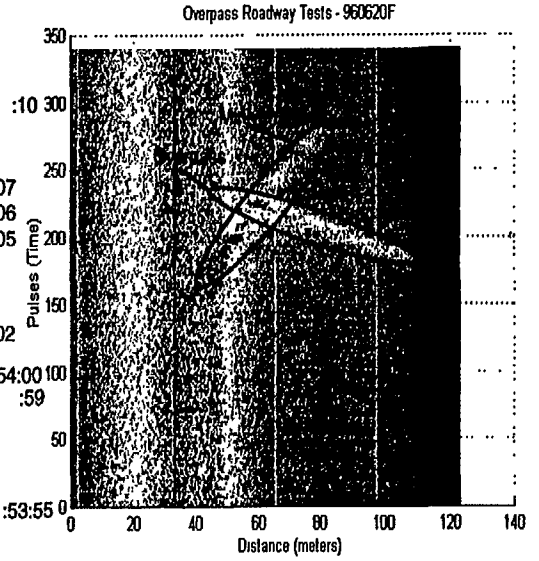

960620 - Overpass Roadway Tests

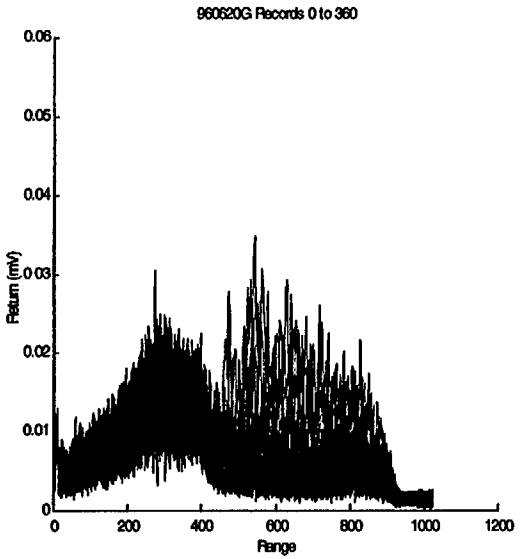

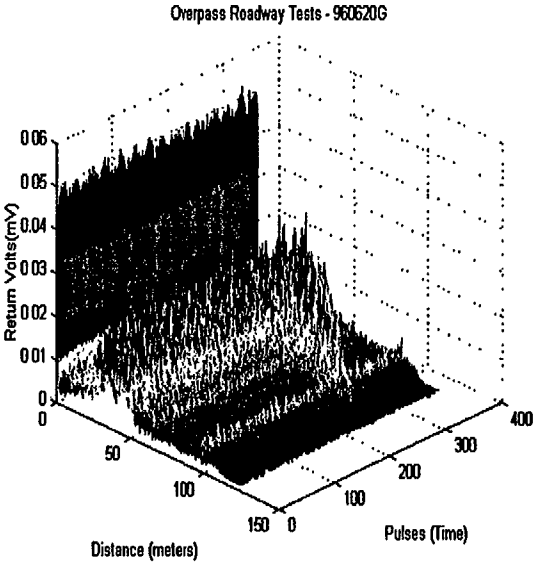

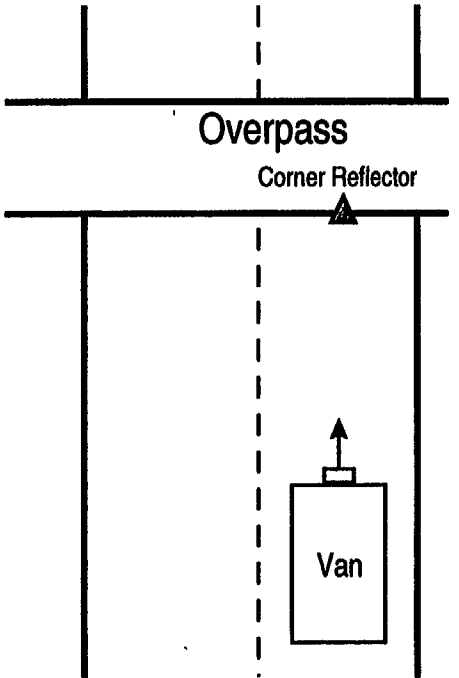

10:01:18 - Begin File
3 degree offset

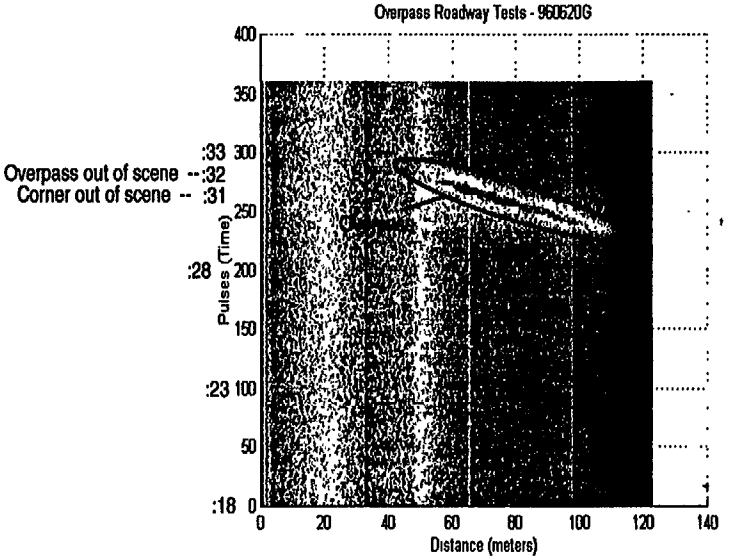

960620 - Overpass Roadway Tests

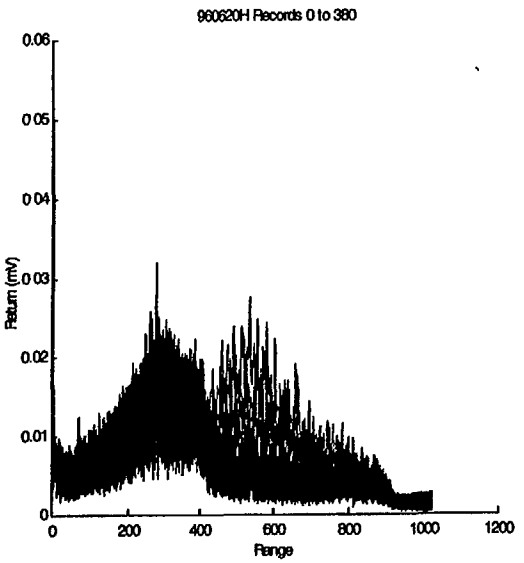

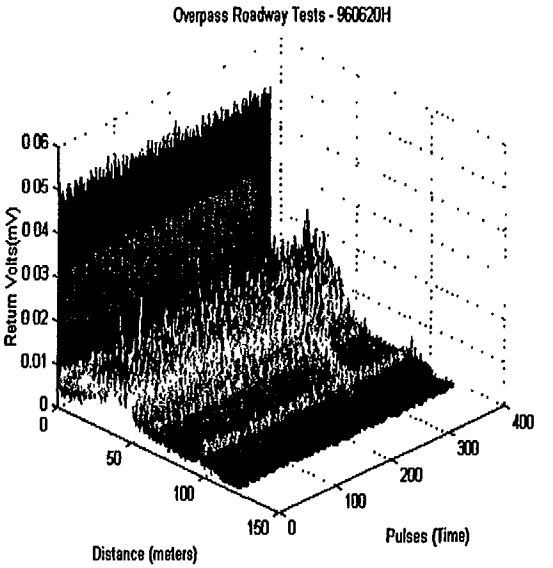

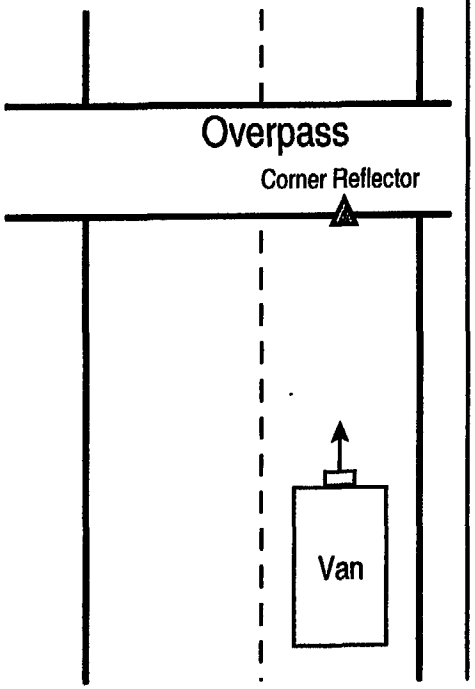

10:05:05 - Begin File
3 degree offset

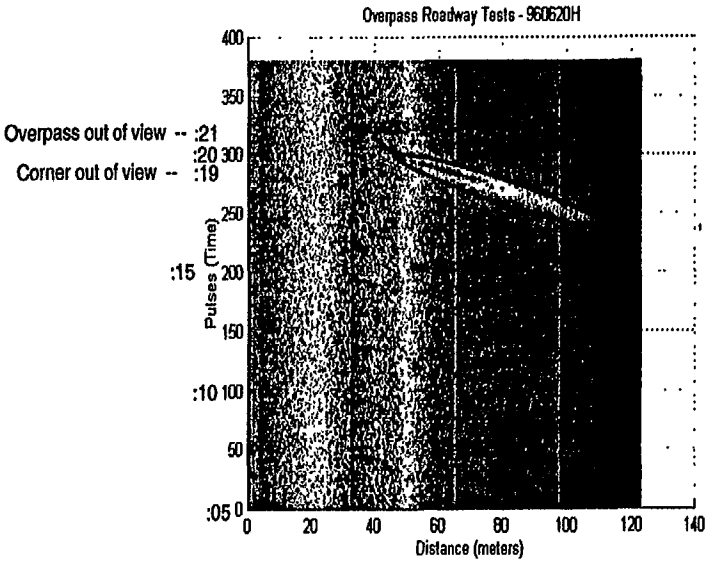

960620 - Overpass Roadway Tests

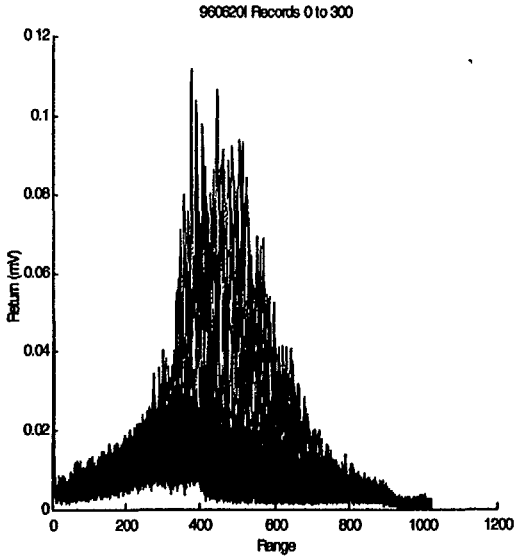

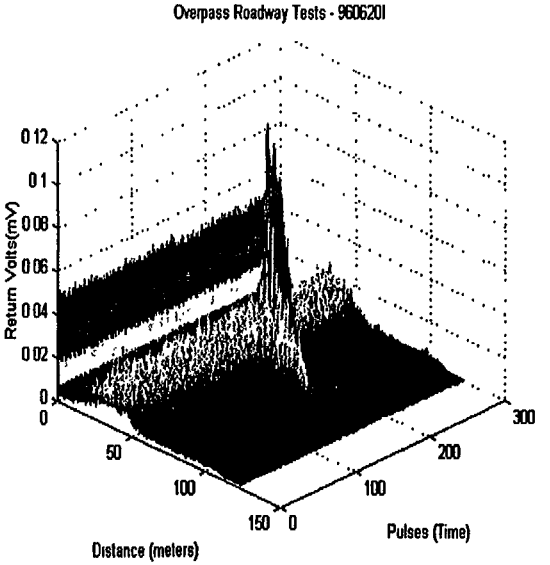

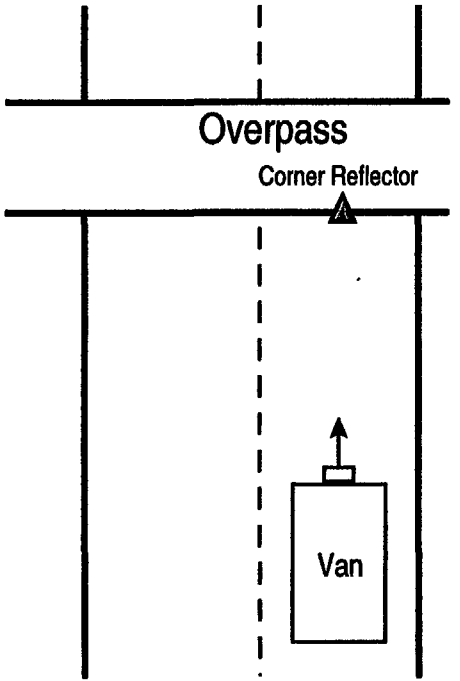

10:14:19 - Begin File
5 degree offset

Overpass out of scene -- :29
Corner out of scene -- :28

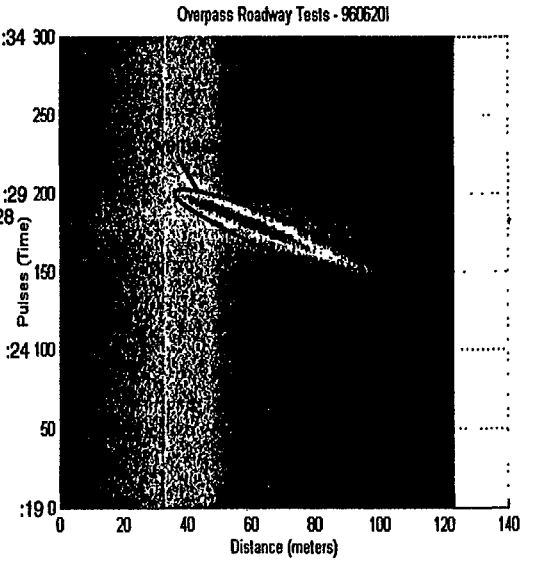

960620 - Overpass Roadway Tests

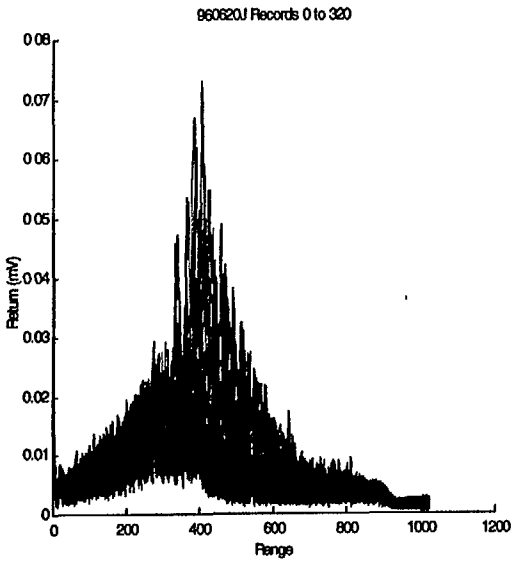

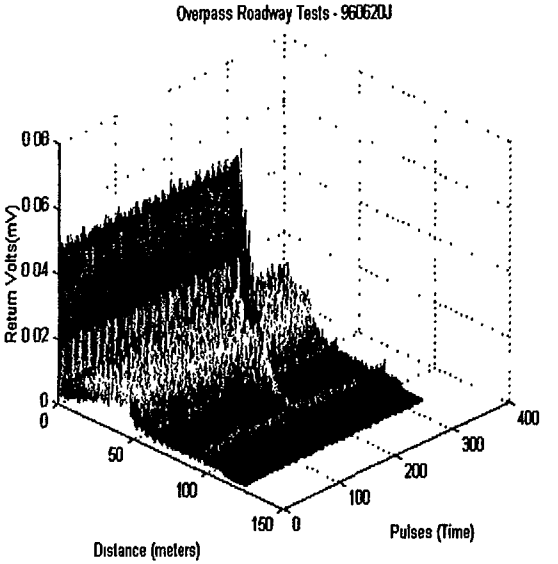

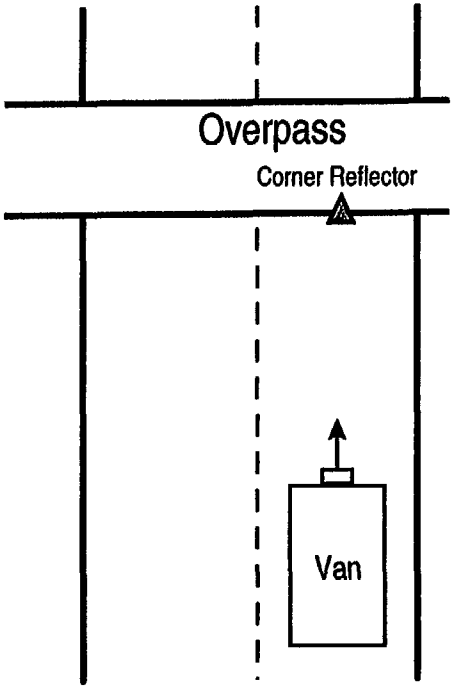

10:18:31 - Begin File
5 degree offset

Overpass out of scene - :41
Corner out of scene -- :40

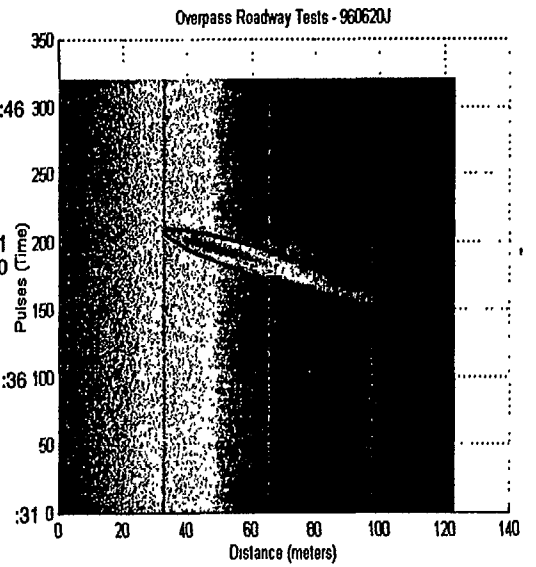

960620 - Overpass Roadway Tests

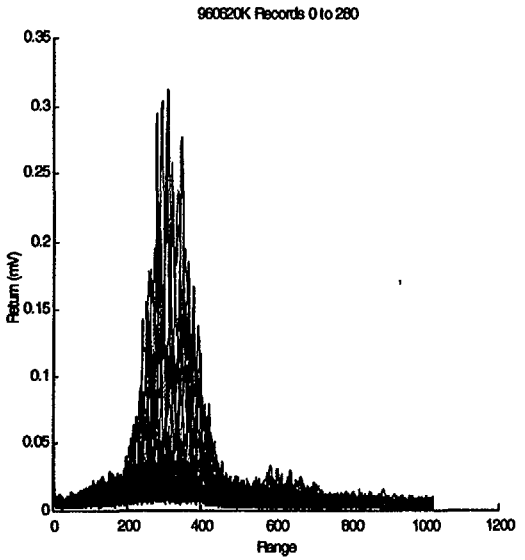

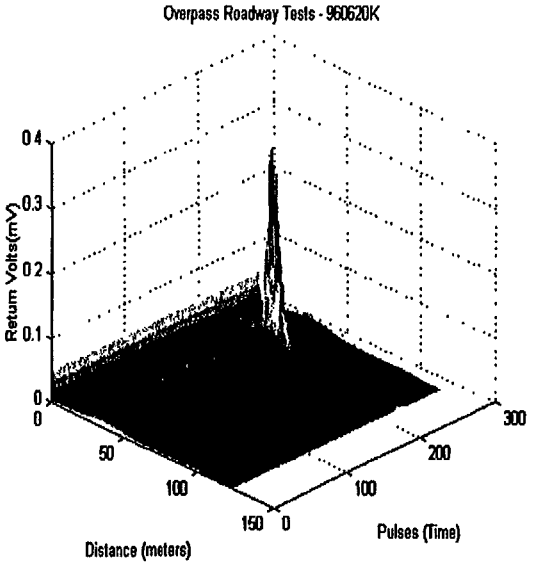

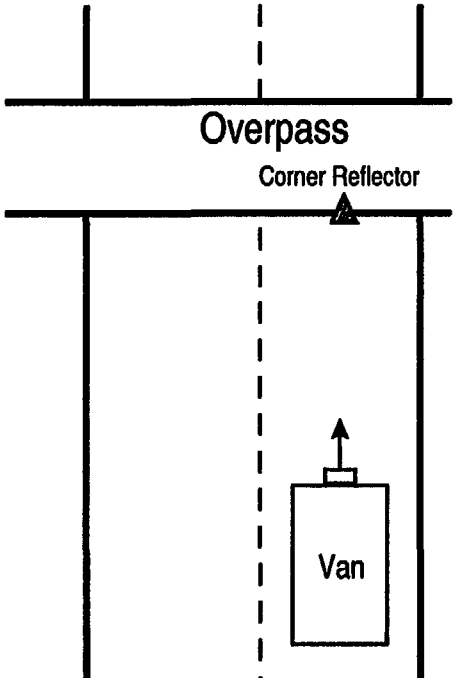

10:25:11 - Begin File
8 degree offset

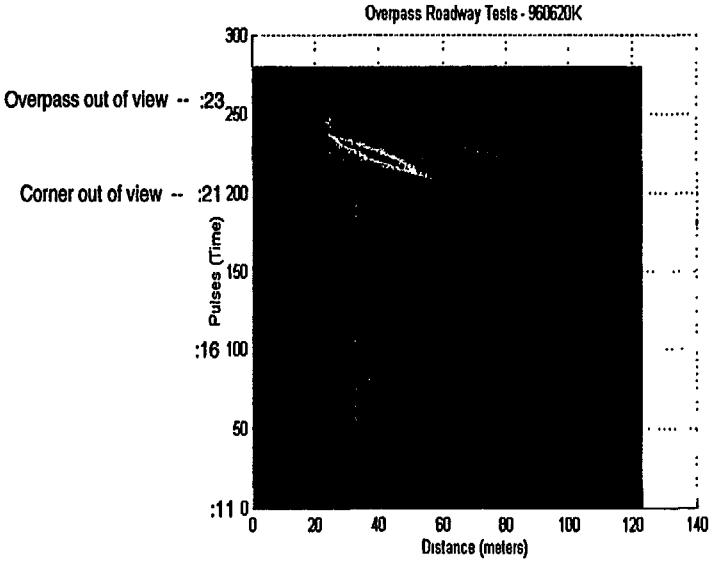

960620 - Overpass Roadway Tests

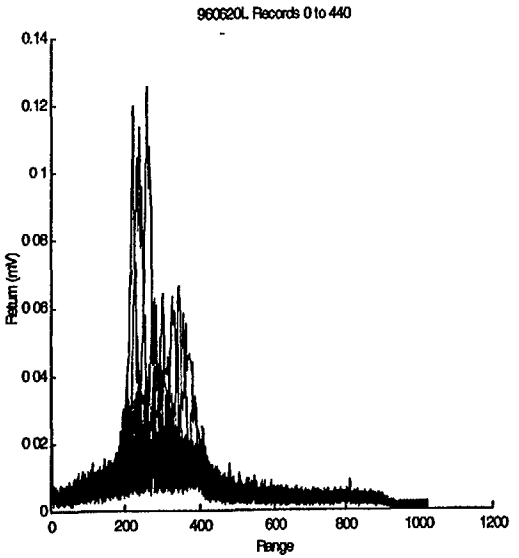

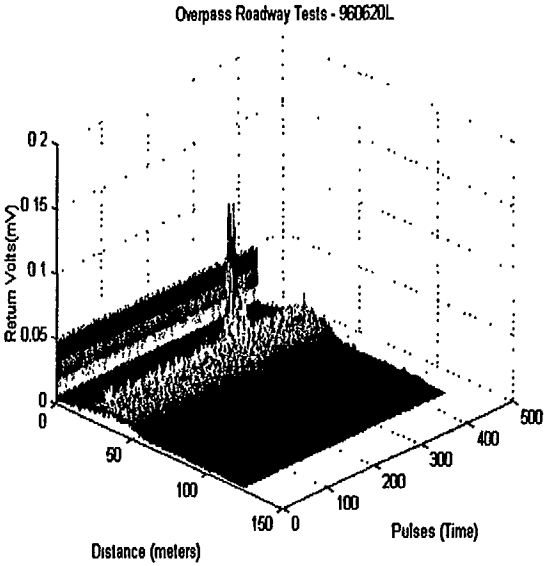

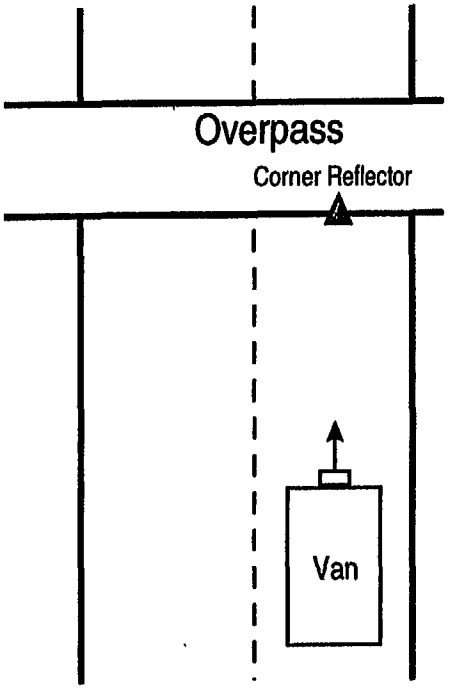

10:28:33 - Begin File
8 degree offset

Overpass out of view -- :47
Corner out of view -- :46

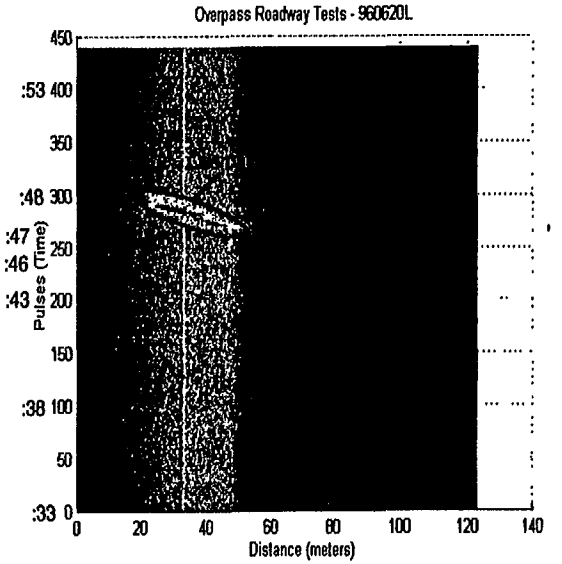

960620 - Overpass Roadway Tests

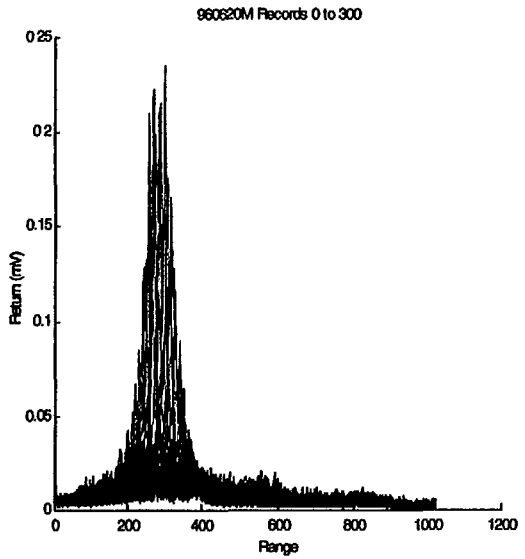

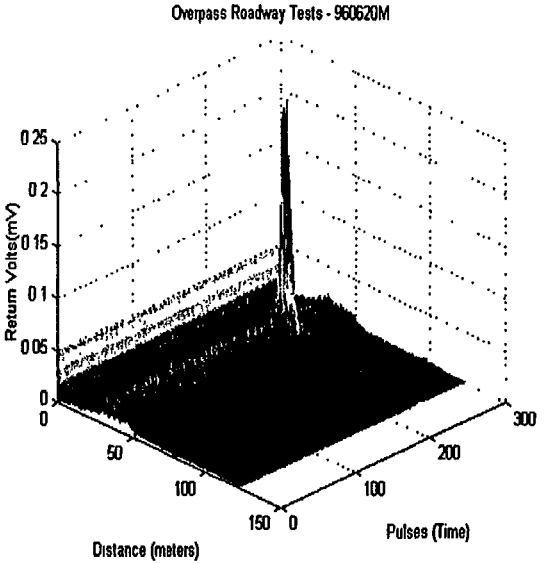

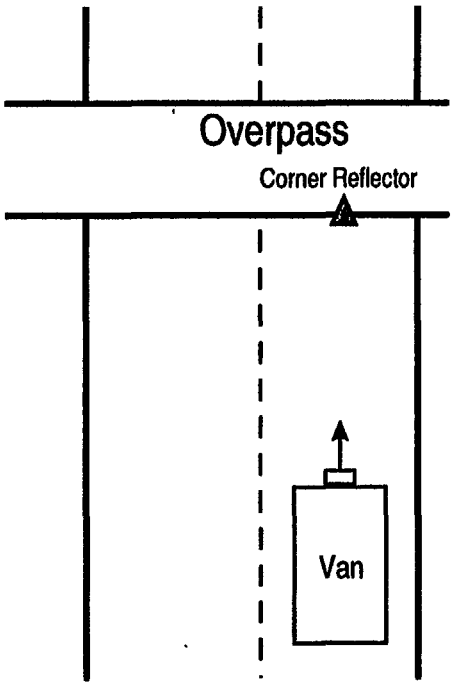

10:33:05 - Begin File
8 degree offset
* no corner present

Overpass out of view -- car cuts in

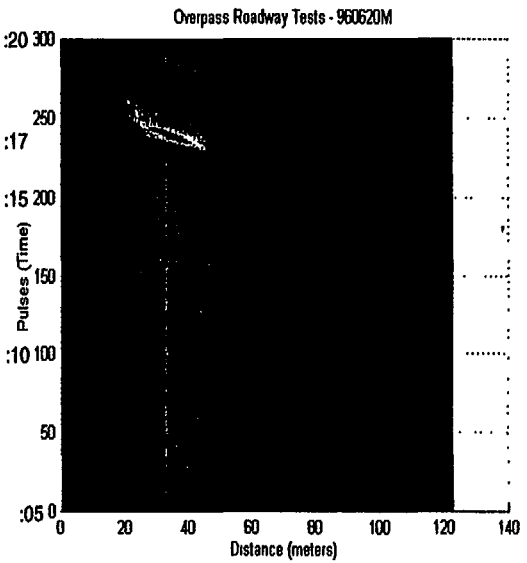

970301 - Roadway Backgrounds

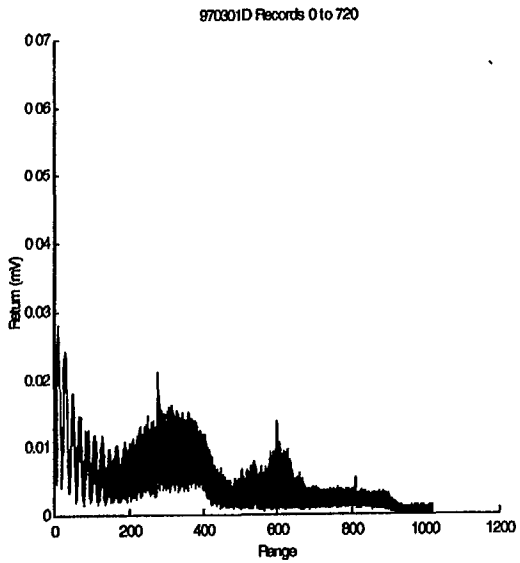

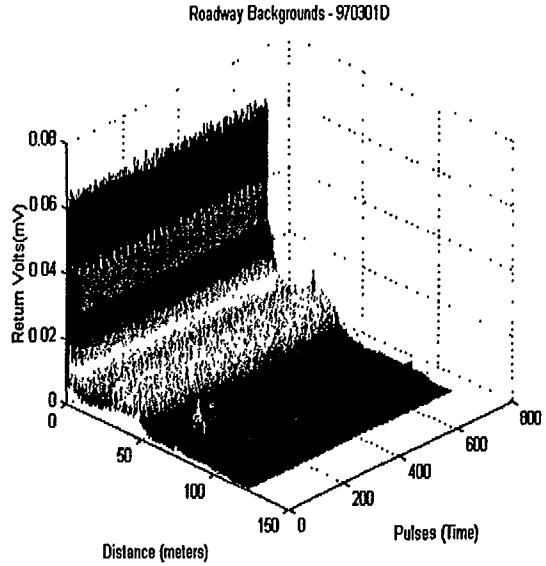

19:02:34 - Begin File

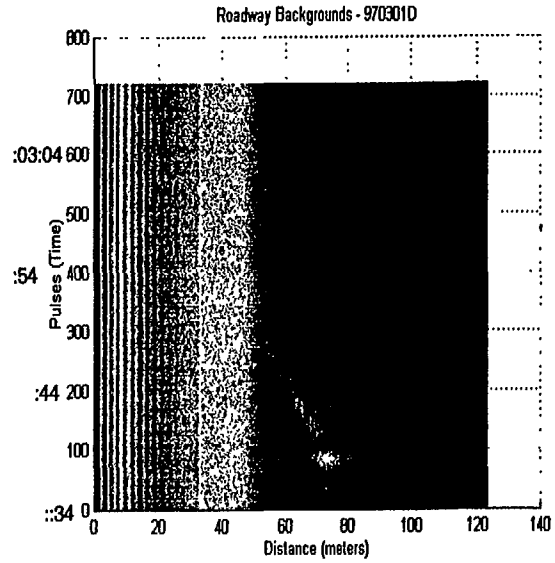

970301 - Roadway Backgrounds

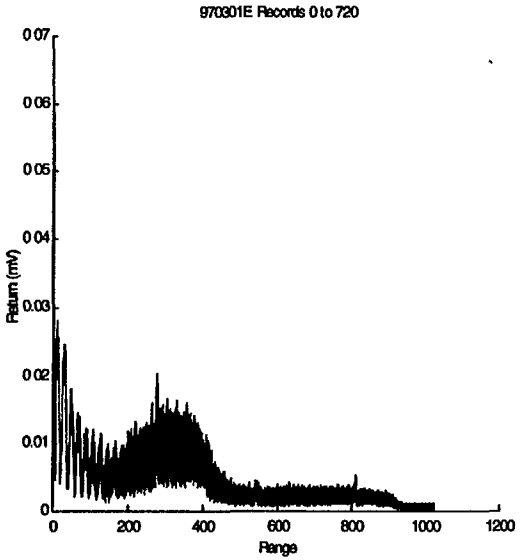

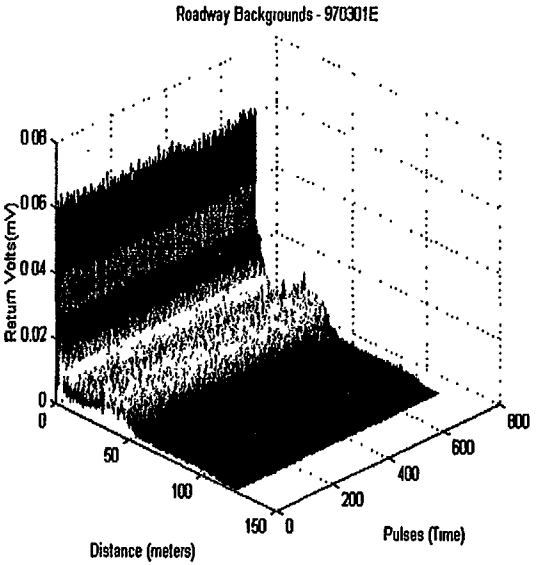

19:06:29 - Begin File

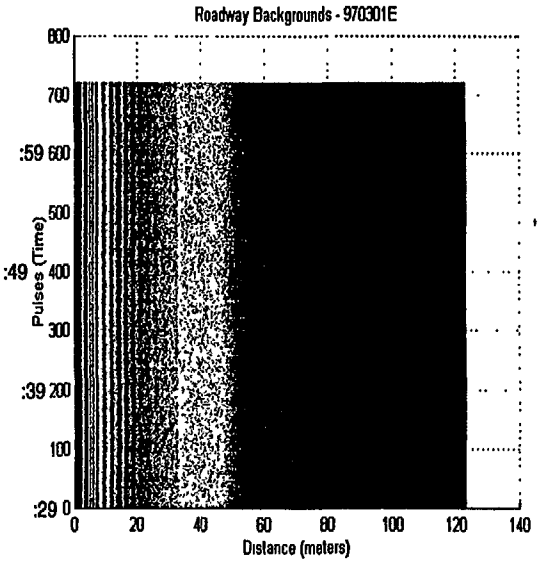

970303 - Open Roadway Tests

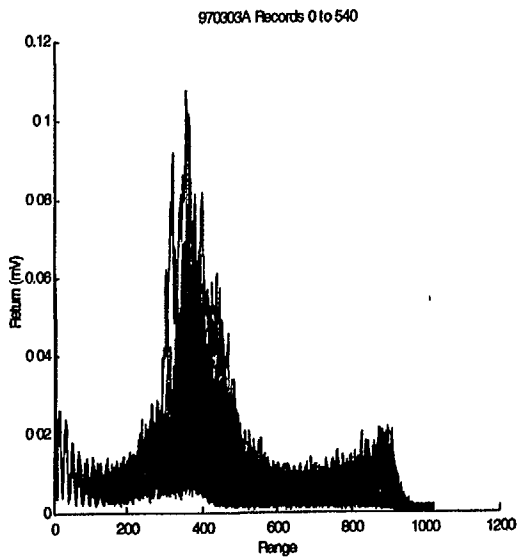

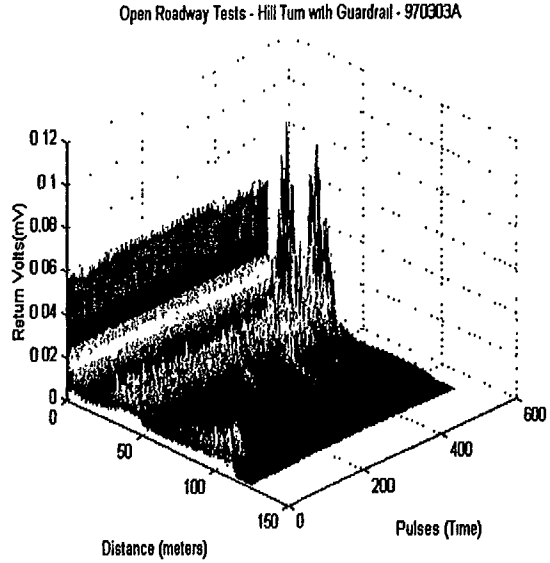

Hill & Turn with Guardrail
Two lane highway
Center Beam

19:22:45 - Begin File

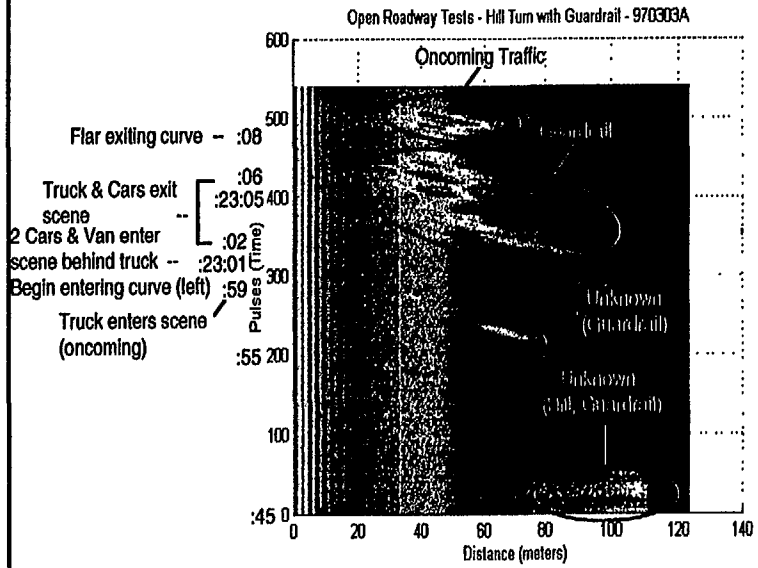

970303 - Open Roadway Tests

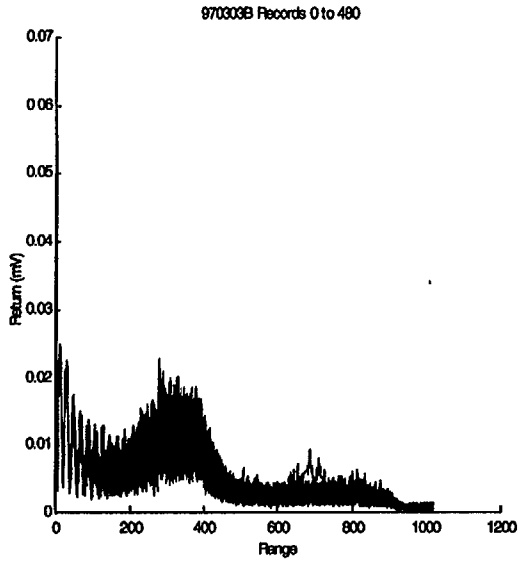

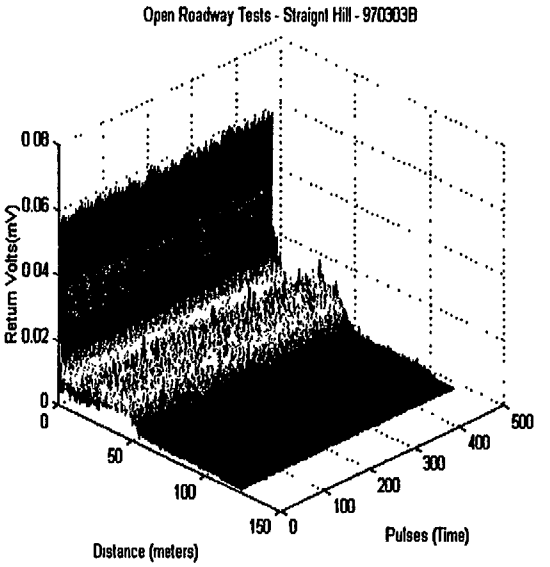

Straight Hill
Two Lane Highway
Center Beam

19:43:43 - Begin File

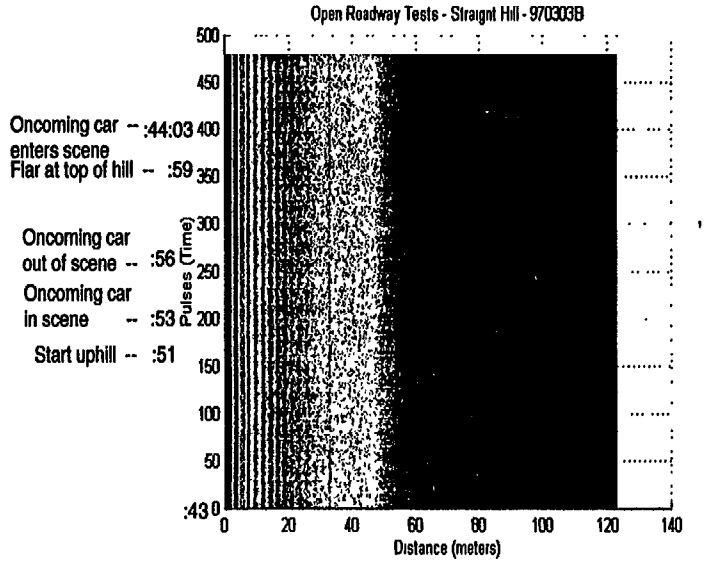

970303 - Open Roadway Tests

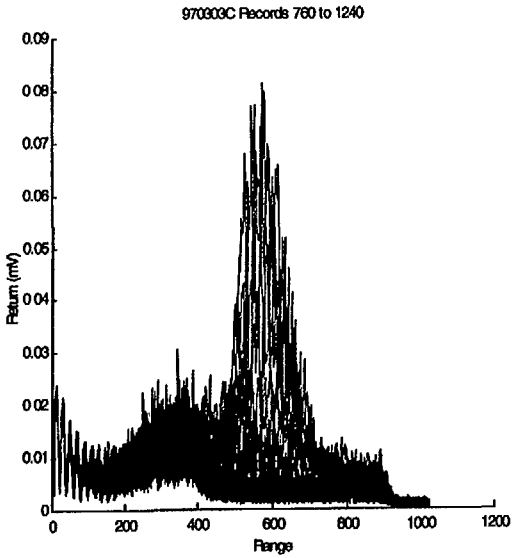

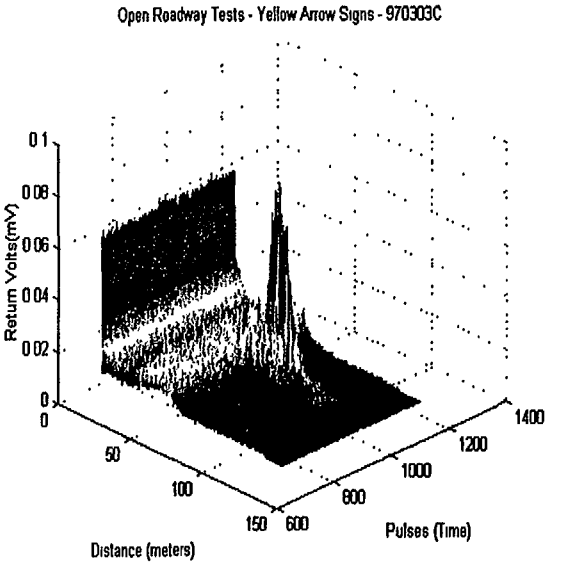

Yellow Arrow Signs on Curve
Two Lane Highway
Center Beam

19:59:27 - Begin File

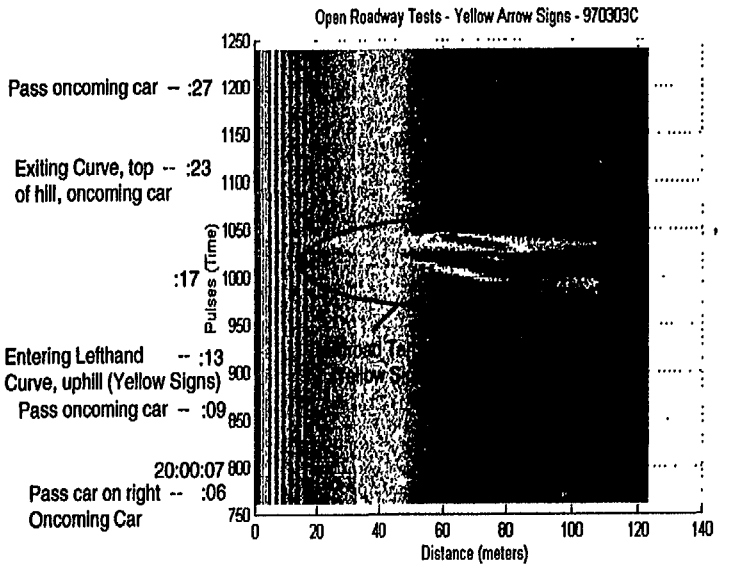

970303 - Open Roadway Tests

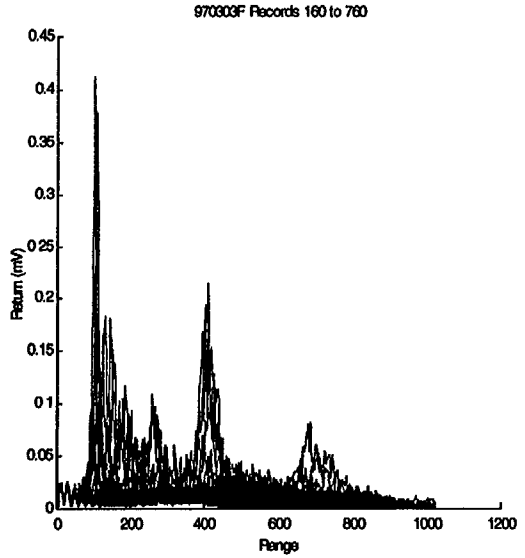

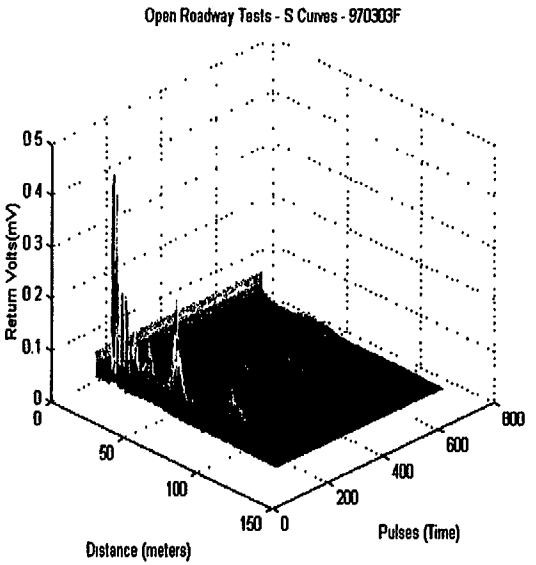

S Curves
Two Lane Highway
Center Beam

20:28:31 - Begin File

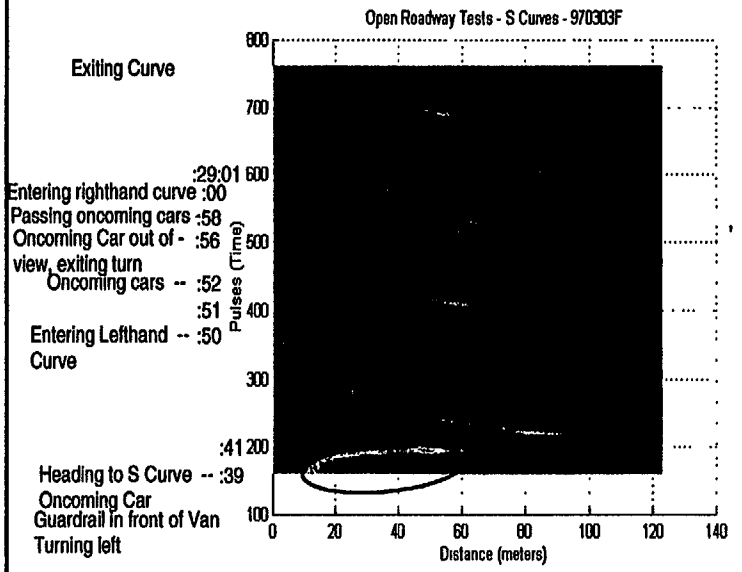

970303 - Open Roadway Tests

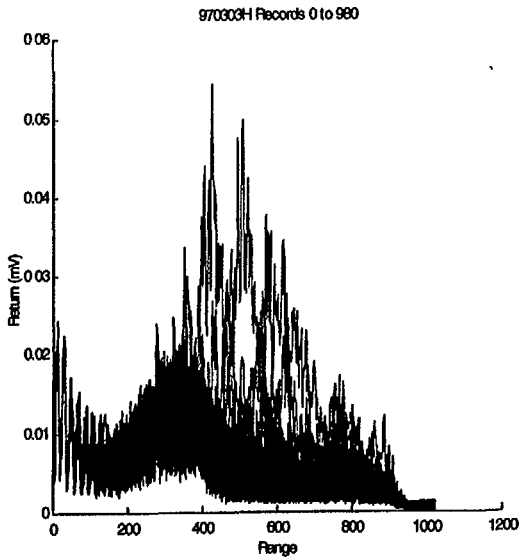

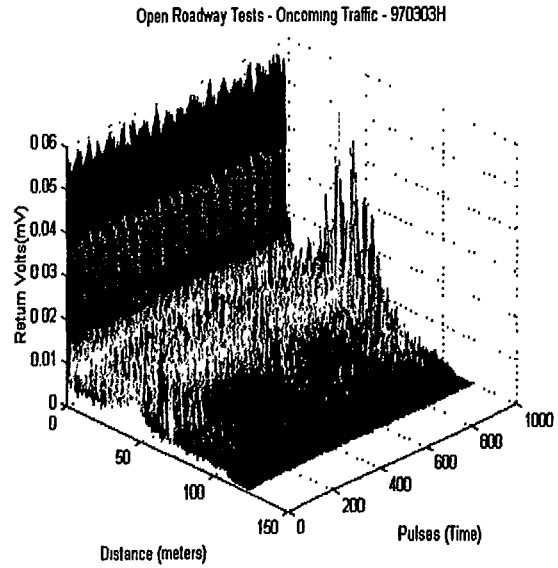

Oncoming Traffic
Two Lane Highway
Left Beam

20:58:38 - Begin File

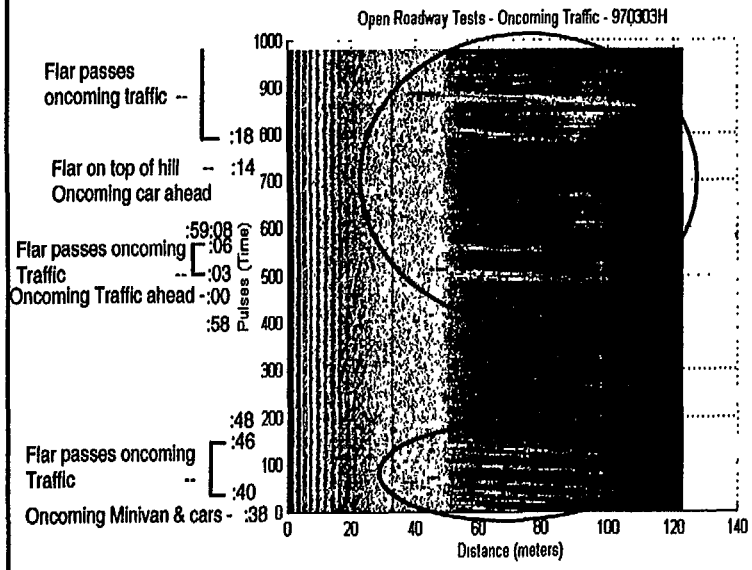

970303 - Open Roadway Tests

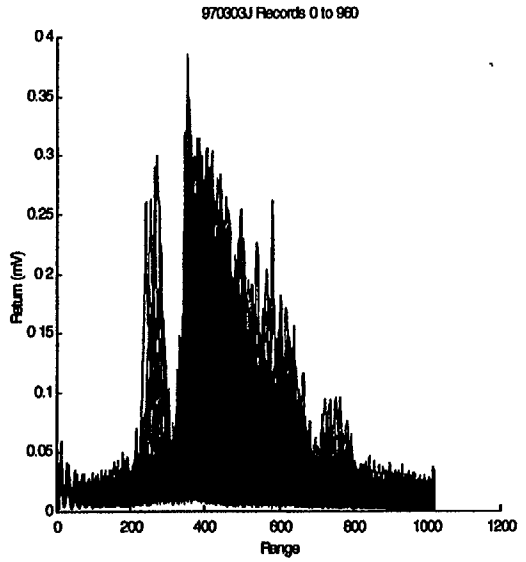

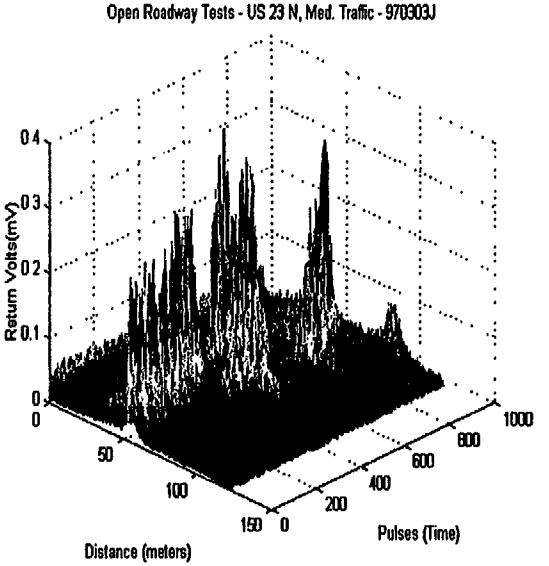

US 23 North - Medium Traffic
Divided Freeway
Center Beam

21:17:17 - Begin File

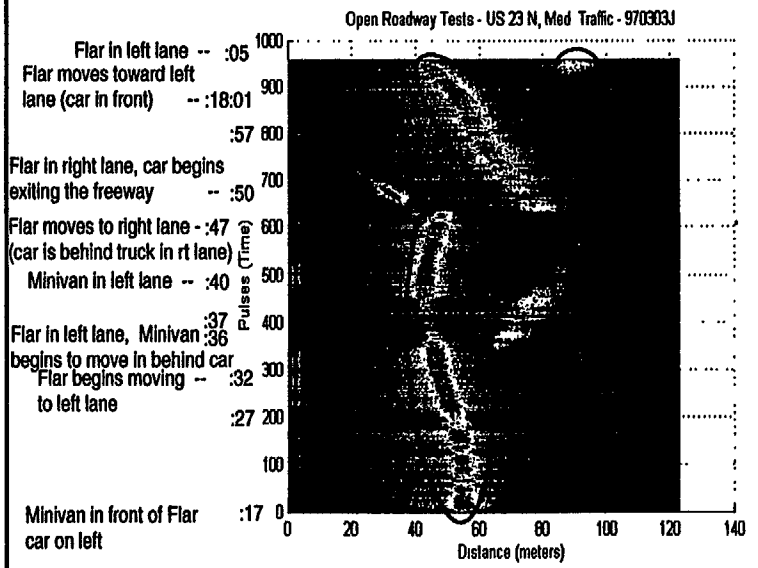

970303 - Open Roadway Tests

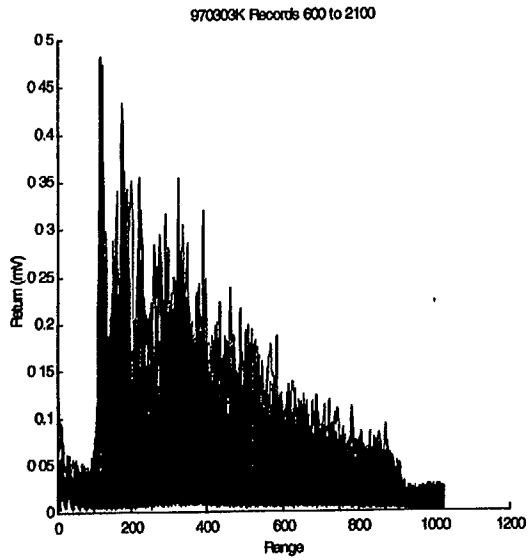

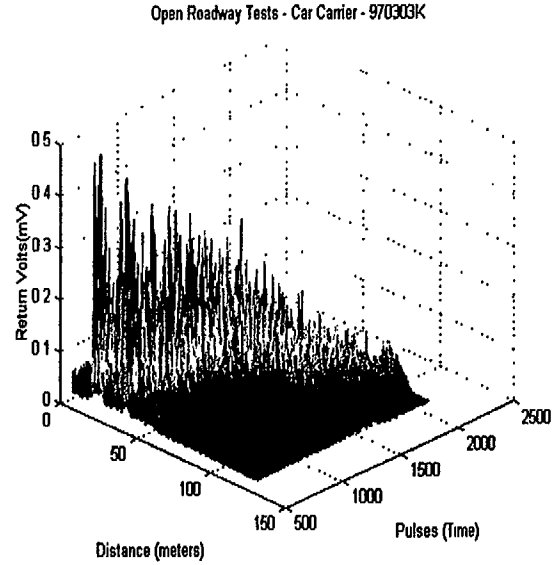

Car Carrier
Divided Freeway
Center Beam

21:31:15 - Begin File

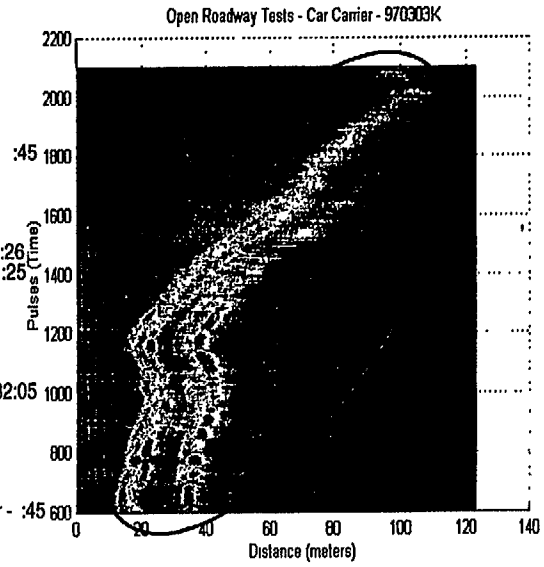

Carrier begins to change - :26
to left lane, flar changes :25
with carrier

:32:05

Car Carrier in front of Flar - :45

970303 - Open Roadway Tests

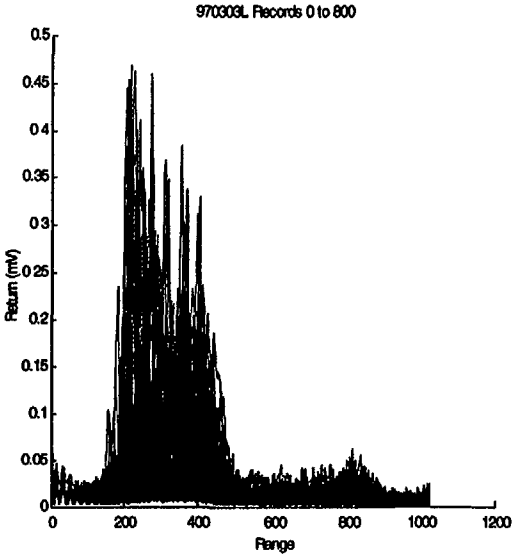

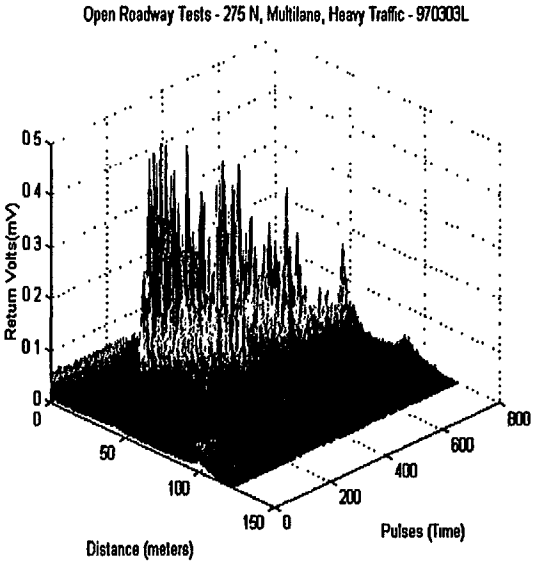

275 N, Multilane, Heavy Traffic
Divided Freeway
Center Beam

21:36:25 - Begin File